GEOCHEMISTRY AND MINERALOGY OF MID-ARCHEAN TO MID-PROTEROZOIC SEDIMENTS FROM THE KAAPVAAL CRATON, SOUTHERN AFRICA: SOURCE-AREA PROVENANCE, WEATHERING, TECTONIC SETTING AND CRUSTAL EVOLUTION

by

David J. Wronkiewicz

Submitted in Partial Fulfillment
of the Requirements for the Degree of
Doctor of Philosophy in Geochemistry

New Mexico Institute of Mining and Technology
Socorro, New Mexico, USA
March, 1989

The file of men reached the Ridge-of-White-Waters, which later settlers would call Witwatersrand, where the Old Seeker hoped to find evidence that gold existed, but the more carefully he explored . . . the more disappointed he became. Here the telltale signs, which in the lands about Zimbabwe indicated gold, were missing; there was no gold, and it became obvious that the exploration had been fruitless, but on the evening of their last day of tramping the hills the Old Seeker discovered what he was looking for. It was an ant hill, eleven feet high, and he rushed to it, breaking it apart with a long stick and fumbling through the fine-grained soil.

'What are you looking for?' Nxumalo asked, and the old man said, 'Gold. These ants dig down two hundred feet to build their tunnels. If there's gold here, they bring flecks to the surface.'

At this site there were none, and reluctantly the Old Seeker had to admit that he had taken this long journey to no avail: 'I didn't come to see your father. I didn't come for rhino horn. Son, when you have a multitude of targets, always aim for the one of merit. I came seeking gold, and I'm convinced there's gold here.'

--James A. Michener--The Covenant

Table of Contents

APPENDICES

LIST OF TABLES

LIST OF FIGURES

Figure Page

Figure Page

Figure Page

ACKNOWLEDGMENTS

Sincere thanks are bestowed to Dr. K.C. Condie, who's insight and guidance made this project possible. I also wish to thank the members of my committee, Drs. G.S. Austin, A.J. Budding, W.X. Chavez, P.R. Kyle, J.R. MacMillan and D.I. Norman, who during their various visits to the States, have provided assistance for this project.

Thanks go to Nick Lindsey, Ian, and Russ Myers for providing a place to hang my hat, the Blind Pig and some generally good times in Johannesburg.

D.L. Garnett, A.M. Killick and E. Kinloch of Johannesburg Consolidated Investment Co., Ltd. and G. Borthwick of Anglo American Corp., provided assistance and access to drill-core samples. N. Laskowski and A.O. Fuller provided samples from their personal collections, greatly increasing our sample coverage of the Pongola and Witwatersrand Supergroups, respectively. D.R. Hunter, A.H. Wilson, T.S. McCarthy, T. Hewitt, K. Palmer, R. Myers, L. Robb, D. Lowe and P. Camden-Smith led various field excursions which greatly improved my understanding of South African geology.

Clay Crow, Mark Boryta, Pat Bowling and especially Mike Knoper are thanked for computer assistance and many stimulating geoloic discussions. The many patient hours Penny Taylor spent entering correlation data has not gone unnoticed. Charlie Harmon and crew at Sandia National Laboratories and Chris McKee of New Mexico Tech are thanked for their analytical assistance.

Sections of this paper have been greatly improved through critical reviews of three papers submitted to Geochimica et Cosmochimica Acta. K.A. Eriksson, C. Frost, D.L. Garnett, D.R. Hunter, A.M. Killick, S.M. McLennan and G.N. Phillips are thanked for their efforts in these reviews.

Finally, I wish to thank the support of Maribeth and Payton, who put up with all these years of neglect and abject poverty. And a warm thanks to all South Africans who made my stay a pleasant one.

This research was supported by NSF grant EAR-8742013 (to Dr. K.C. Condie).

ABSTRACT

Approximately 300 pelites from Precambrian sediments deposited on the Kaapvaal craton have been analyzed to study secular geochemical changes of the mid-Archean to early Proterozoic upper-continental crust. Pelites from the Pongola Supergroup (3.0 Ga) have mean REE and HFSE contents, negative Eu anomalies (Eu/Eu*=0.69), and La/Yb ratios ($\sim$13) that are similar to those of the Phanerozoic North American Shale Composite (NASC). Cr/Zr ratios range from 1-3, whereas concentrations of Ni (30-300 ppm) and Cr (100-800 ppm), as well as Th/U (3-4) and Th/Sc ratios (0.4-1.0) are intermediate between those of NASC and pelites from the Moodies successions (3.2 Ga). Deeply weathered pre-Pongola paleosols, high pelite Cr/Ni ratios and Co-Mg depletion are features that suggest a portion of these sediments were derived from highly weathered komatiitic rocks. Overall geochemical characteristics suggest an evolved (felsic-rich) source for the Pongola relative to the more primitive (mafic-rich) signature exhibited by Moodies pelites.

Pelites from the Witwatersrand Supergroup (2.8-2.7 Ga) are depleted in REE and HFSE, and enriched in Ni, Cr and Co relative to NASC. Proportions of granite, basalt and komatiite increased upsection at the expense of tonalitic sources for these sediments. Contributions from basalt and komatiite peaked during deposition of Booysens pelites as evidenced by enriched Ni (200-700 ppm), Cr (400-1600 ppm)

and MgO (5-12 %) contents, and elevated Cr/Zr ratios (4-16). Contributions from granitic rocks increased upwards through deposition of the K8 pelite unit. These pelites have high REE and Th (~10 ppm) contents, La/Yb ratios (~14), as well as NASC-like Eu anomalies (Eu/Eu*=0.67). Elevated contributions from both felsic and komatiitic sources in the upper Witwatersrand coincide with deposition of paleo-placer gold and uranium ores, suggesting a dual provenance (granite and komatiitic greenstones) for these deposits.

Pelites from the Ventersdorp Supergroup (~2.6 Ga) are unusual, in that they exhibit well-developed negative Eu anomalies (Eu/Eu*=0.61) and high La/Yb ratios (20), yet retain high Ni (~300 ppm), Cr (600 ppm) and MgO (~5%) concentrations. These pelites are similar to the Witwatersrand-Booysens unit in that they appear to be derived from large proportions of both granite and komatiite. Transvaal sediments (~2.3-2.1 Ga) record the progressive erosion of increasingly evolved crustal regions. Lower Transvaal pelites have high Eu/Eu* (0.73-0.85) and Cr/Zr (3-4) ratios, high Ni (100-300 ppm) and Cr (~400 ppm) contents, and relatively low La/Yb ratios (7-12), features which reflect significant contributions from primitive sources. Pelites from upper Transvaal, Waterberg (~1.8 Ga) and Soutpansberg sequences (~1.8-1.7 Ga) have NASC-like Eu/Eu* (~0.65), La/Yb (13-21) and Cr/Zr (0.4-1.1) ratios, low Ni (30-90 ppm) and Cr (110-180 ppm), and high Th (16-22

ppm) contents, indicating derivation from evolved sources containing large proportions of granite.

A minimum of three primitive to evolved crustal cycles are recorded in the compositions of Kaapvaal pelites. Each sedimentary cycle reflects evolution of exposed crust, from mafic- and komatiitic-rich to relatively felsic-rich components (chiefly granite). Initiation of each cycle coincides with major deformational events along the perimeter of the Kaapvaal craton. Such a correspondence suggests a cause and effect relationship between arc or microcontinent accretion and Kaapvaal sedimentary cycles. Following each deformation event, new mafic-komatiitic sources were exposed in accreted terranes, leading to the initiation of a new sedimentary cycle. Continued uplift of these regions progressively unroofed granitic rocks leading to more felsic signatures in derivative sediments. Alternatively, these cycles may be related to pulses of granitic magmatism associated with evolution of the Kaapvaal craton. Individual sedimentary cycles also are superimposed on a long-term (3.2-2.1 Ga) primitive to evolved crustal transition. These observations suggest that the upper Kaapvaal crust evolved in a complex series of punctuated events over a time span greater than 1.1 Ga.

INTRODUCTION

Notable increases in rare earth (REE) and large ion lithophile element (LILE) contents, negative Eu anomalies, and Th/U ratios are proposed to occur in sediments across the Archean-Proterozoic boundary (Taylor and McLennan, 1981). These changes are interpreted to reflect fundamental differences in the composition of exposed upper-continental crust caused by voluminous additions of granitic magma during the late Archean (McLennan and Taylor, 1982, 1988; Taylor and McLennan, 1983). These changes may reflect a transition from an exposed Archean crust, which overall is of a more mafic composition than the post-Archean upper crust. The shift in sediment composition related to the Archean-Proterozoic boundary, while episodic regionally, is proposed to occur over a protracted period worldwide (3.2-2.5 Ga; McLennan et al., 1983). In South Africa, the break in sedimentary REE patterns reflecting this crustal transition may occur at about 3.0-2.8 Ga (McLennan and Taylor, 1988). Gibbs et al. (1986) suggest that these crustal transitions are an artifact of a tectonic sampling bias, whereby the majority of Archean sediments examined are representative of mafic-rich greenstone successions and post-Archean samples are largely from continental margin or intracratonic successions. By reversing the typical sampling pattern, and comparing pelites from Proterozoic

greenstones with Archean continental margin sediments, these authors note that reversed age-composition sedimentary relationships can be documented.

The transition from primitive to evolved upper-continental crust is believed to be diachronous between different cratons (Hunter, 1974; Taylor and McLennan, 1983; Nesbitt, 1987). Thus, to examine the evolution of cratons, a study should be made from a single geographic region which contains a continuum of well-preserved strata occurring across the Archean-Proterozoic boundary. The southern African Kaapvaal craton is unique in this respect because cratonic platform sediments (sandstones + shales +/- carbonates) are deposited here in close proximity, over a time span ranging from 3.2 to 1.7 Ga (Fig. 1). The sediments are generally well-exposed, relatively undeformed and subjected to maximum regional metamorphic conditions characterized by mid-greenschist facies.

Clastic sediments provide an important source of information on the composition, tectonic setting and evolutionary growth of the early continental crust. Pelites or shales are preferred for geochemical provenance studies due to their homogeneity and impermeability. Quartzites are less desirable for provenance studies due to their low trace element contents, pre-lithified permeability, and hydraulic segregation of sand-sized particles during transport. However, to evaluate the overall effects of

Figure 1. Simplified Precambrian stratigraphy and chronology of the Kaapvaal, Zimbabwe and Limpopo provinces, southern Africa. Modified after Tankard et al. (1982).

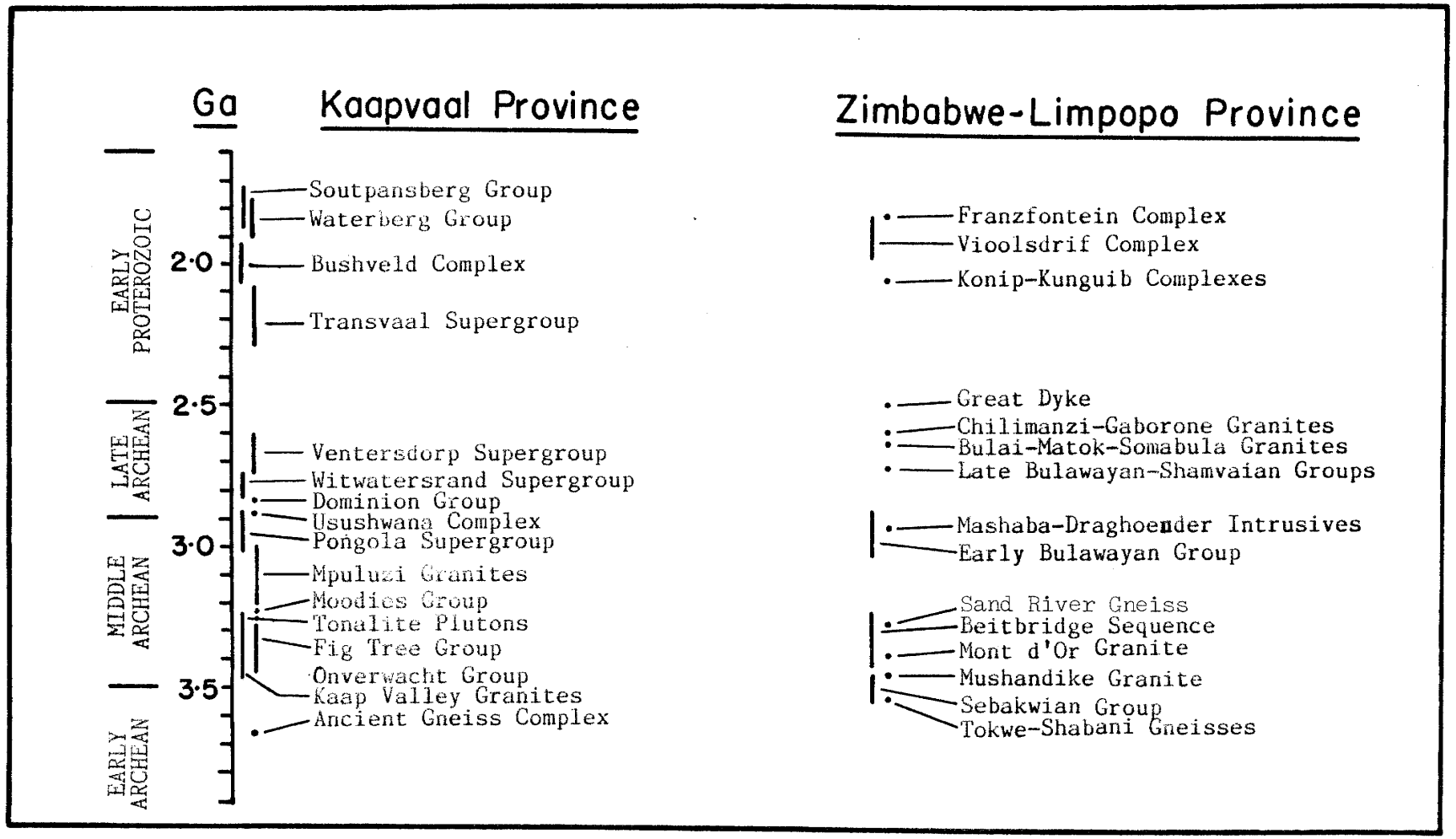
Ga
Kaapvaal Province
Zimbabwe-Limpopo Province
EARLY PROTEROZOIC
LATE ARCHEAN
MIDDLE ARCHEAN
EARLY ARCHEAN
2·0
2·5
3·0
3·5
Soutpansberg Group
Waterberg Group
Bushveld Complex
Transvaal Supergroup
Ventersdorp Supergroup
Witwatersrand Supergroup
Dominion Group
Ushushwana Complex
Pongola Supergroup
Mpuluzi Granites
Moodies Group
Tonalite Plutons
Fig Tree Group
Onverwacht Group
Kaap Valley Granites
Ancient Gneiss Complex
Franzfontein Complex
Vioolsdrif Complex
Konip-Kunguib Complexes
Great Dyke
Chilimanzi-Gaborone Granites
Bulai-Matok-Somabula Granites
Late Bulawayan-Shamvaian Groups
Mashaba-Draghoender Intrusives
Early Bulawayan Group
Sand River Gneiss
Beitbridge Sequence
Mont d'Or Granite
Mushandike Granite
Sebakwian Group
Tokwe-Shabani Gneisses

element fractionation in the sedimentary cycle, quartzites must be considered together with pelites. This study examines the composition and mineralogy of mid-Archean to mid-Proterozoic pelites and quartzites from the Kaapvaal craton in southern Africa. Data from approximately 300 pelite and 50 quartzite samples are compared with existing sedimentary data from the region and used to critically evaluate current ideas on crustal evolution. The principal objective of this study is to evaluate the composition of the Kaapvaal craton during the early Precambrian and discuss results in reference to changes across the Archean-Proterozoic boundary. In addition, results are discussed in terms of tectonic setting, paleoweathering, Ni-Cr distributions in Archean sediments, element transport and fractionation in the sedimentary cycle, and Witwatersrand gold genesis. Sample locations, collection, analytical methods (including preperation, detection limits, accuracy, precision and peak identification parameters) and geochemical results are given in Appendices A-C.

GEOLOGIC SETTING

PRE-CRATONIC HISTORY OF SOUTHERN AFRICA

Early Archean basement complexes of southern Africa's Limpopo, Kaapvaal and Zimbabwe provinces represent some of the oldest preserved fragments of the Earth's early continental crust (Fig. 2). Crustal segments of the Limpopo basement gneiss (3.3 Ga; Armstrong et al., 1987), Limpopo supracrustal Beit Bridge assemblage ($\leq$ 3.3 Ga), and Ancient Gneiss Complex (3.6-3.5 Ga; Kroner and Todt 1988) represent some of the earliest protocontinent remnants of the Kaapvaal craton. The Ancient Gneiss Complex is composed of tonalitic gneiss, amphibolite, and interlayered microcline gneiss and metasediment (Hunter et al., 1978). Gneisses appear to have developed in response to partial melting of hydrous basaltic lithosphere and are succeeded by widespread development of greenstone volcanics and sediments (Hunter, 1974; Tegtmeyer and Kroner, 1987; Kroner and Compston, 1988). Early greenstone episodes are represented by linear accumulations of the Barberton, Murchison, Pietersburg and Giyani greenstone belts (3.5-3.2 Ga) on the Kaapvaal craton, and Sebakwian (3.5 Ga) and Bulawayan greenstones (2.9-2.7 Ga) on the Zimbabwe craton (Anhaeusser, 1973; Nesbitt et al., 1981). These greenstones probably developed in tectonic environments analogous to modern island arc and/or continental rift environments (Anhaeusser, 1973; Hunter, 1974). Volcanic rocks from the Barberton greenstone

Figure 2. Generalized geologic map of southern Africa showing positions of the Limpopo Mobile Belt as well as the Kaapvaal and Zimbabwe cratonic provinces. Also shown are the middle Archean to early Proterozoic basins examined in this study. J, Johannesburg. After Tankard et al. (1982).

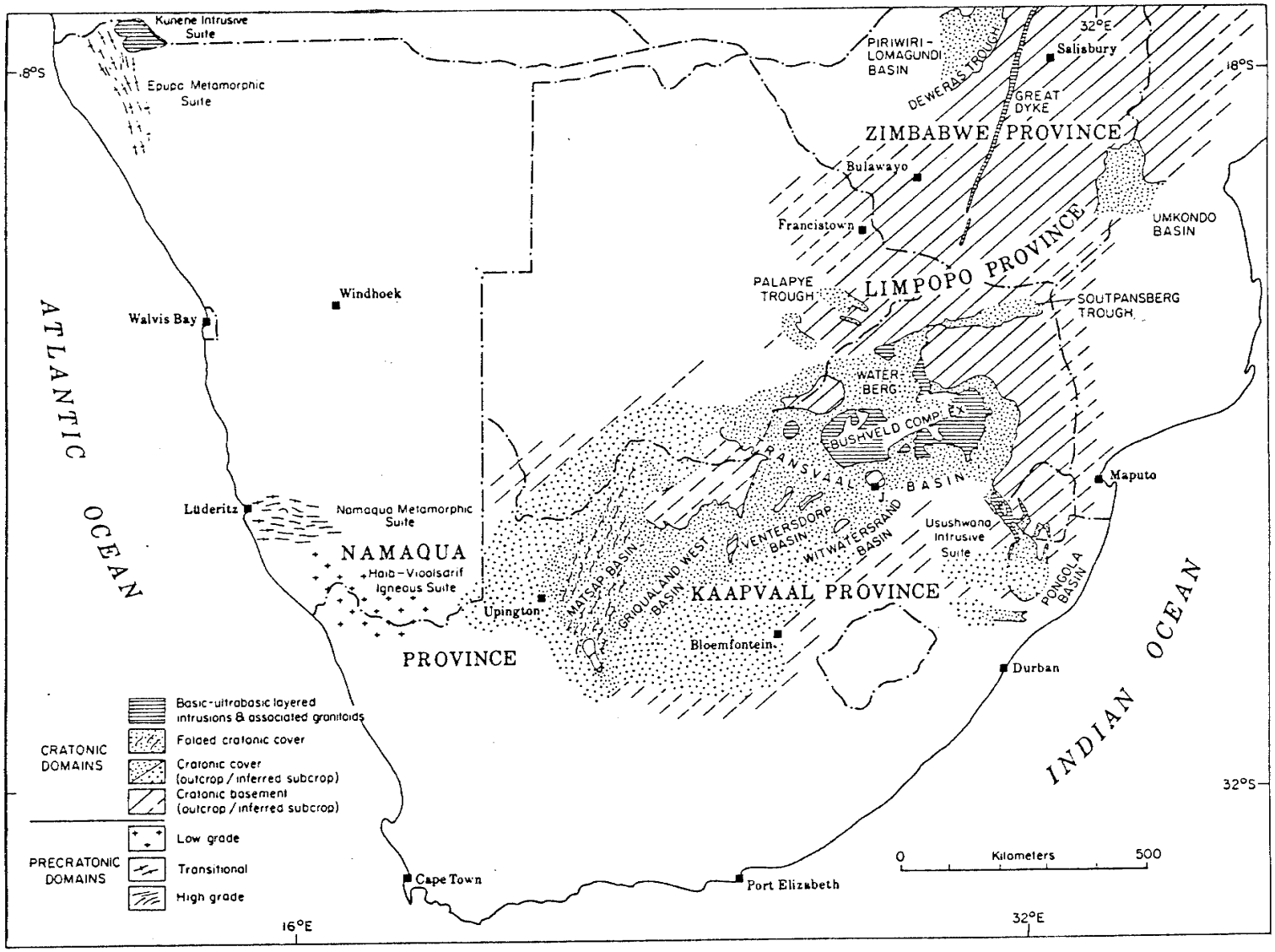
Kunene Intrusive Suite
Epupa Metamorphic Suite
8°S
18°S
32°E
PIRIWIRI - LOMAGUNDI BASIN
DEWERAS TROUGH
GREAT DYKE
Salisbury
ZIMBABWE PROVINCE
Bulawayo
Francistown
UMKONDO BASIN
LIMPOPO PROVINCE
PALAPYE TROUGH
SOUTPANSBERG TROUGH
Windhoek
Walvis Bay
ATLANTIC OCEAN
WATER-BERG
BUSHVELD COMPLEX
TRANSVAAL BASIN
Maputo
Lüderitz
Namaqua Metamorphic Suite
NAMAQUA
Haib-Vioolsarif Igneous Suite
VENTERSDORP BASIN
WITWATERSRAND BASIN
Usushwana Intrusive Suite
MATSAP BASIN
GRIQUALAND WEST BASIN
KAAPVAAL PROVINCE
PONGOLA BASIN
Upington
Bloemfontein
Durban
PROVINCE
INDIAN OCEAN
32°S
CRATONIC DOMAINS
Basic-ultrabasic layered intrusions & associated granitoids
Folded cratonic cover
Cratonic cover (outcrop / inferred subcrop)
Cratonic basement (outcrop / inferred subcrop)
PRECRATONIC DOMAINS
Low grade
Transitional
High grade
0
Kilometers
500
Cape Town
Port Elizabeth
16°E
32°E

typically are mafic to komatiitic in composition, but may include intermediate to felsic tuffs and breccias. Sediments include thick sequences of greywacke, with lesser chert, pelite, quartzite and conglomerate (Anhaeusser, 1973; Fig. 3).

Early thin, primordial crust underwent progressive thickening and stabiliztion at 3.2-3.0 Ga ago, allowing accumulation of the first cratonic sedimentary successions. Cratonic thickening may result from arc or sediment accretion along convergent continental margins, tonalite underplating, and/or widespread intra-crustal melting and emplacement of granites into the upper-continental crust (Anhaeusser, 1973; Davies and Allsopp, 1976; Condie, 1981; Taylor and McLennan, 1985). Granitoid emplacement in the Kaapvaal craton exhibits marked periodicity with magmatic cycles at 3.5, 3.2-3.0 and 3.2-2.5 Ga (Anhaeusser and Robb, 1981; Fig. 1). Intrusive events on the Zimbabwe craton are not well documented, but also appear to be episodic with major intrusions at 3.5-3.3, 2.9 and 2.6 Ga ago (Nesbitt et al., 1981; Fig. 1). Episodic granitic intrusions on both the Kaapvaal and Zimbabwe cratons may be related to primitive Wilson-Cycles, with periodicity caused by repeated collision and/or separation of land masses between 3.4-2.5 Ga (Light, 1982). Alternatively, these intrusive episodes may be related to mantle plume induced rifting episodes associated with greenstone-belt formation (Hunter, 1974).

Figure 3. Generalized geologic map and stratigraphic section of the Swaziland sequence, Barberton greenstone belt, southern Africa. After Anhaeusser (1973).

STRATIGRAPHIC COLUMN OF THE SWAZILAND SEQUENCE

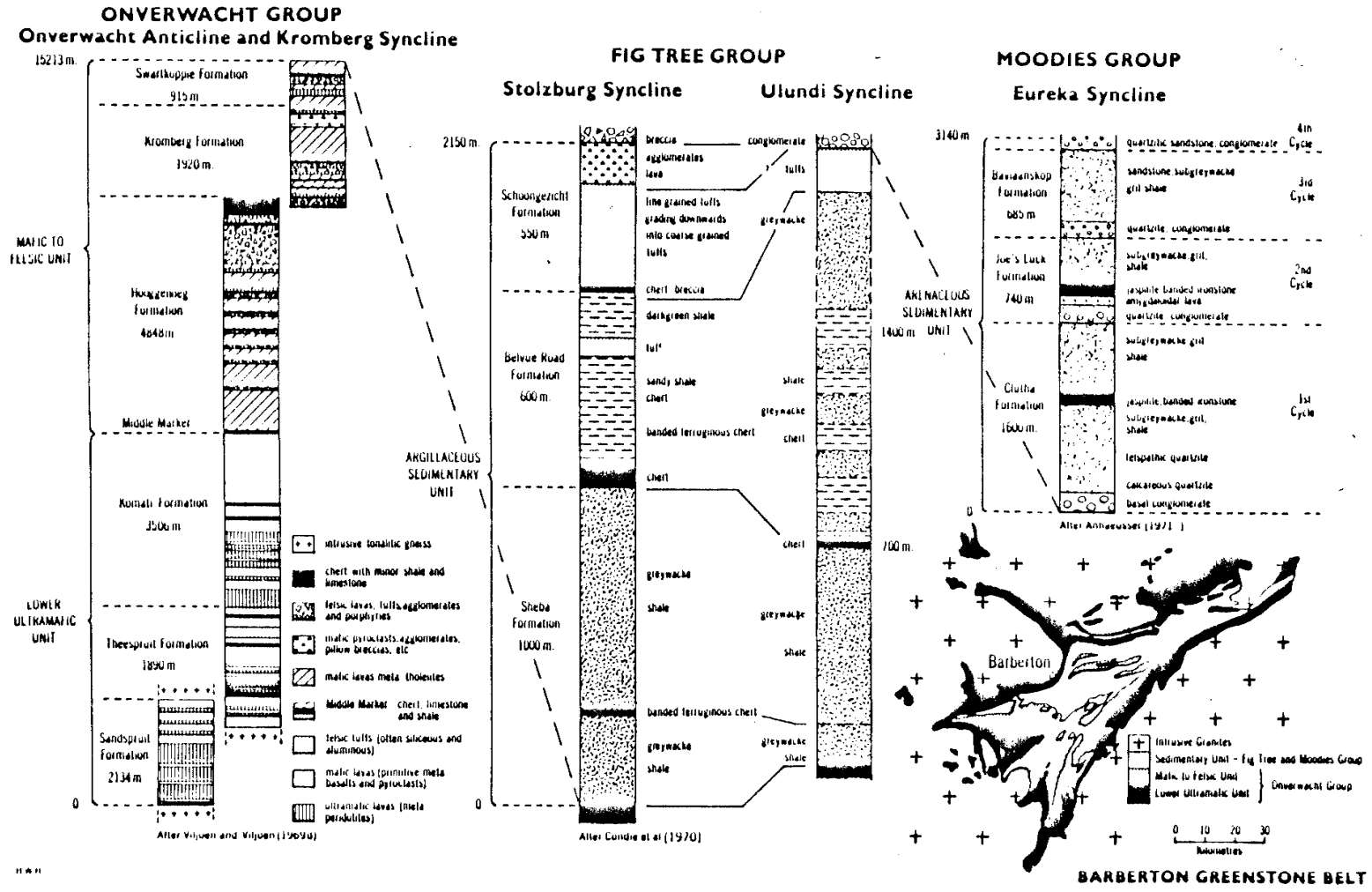

The present study is concerned with the onset of modern continental crust and basin development, beginning approximately 3.2 Ga ago, when the crust thickened sufficiently to permit the first accumulation of platform-type sediments of the Moodies Group. These sediments lie conformably to unconformably on older greenstone sequences and are composed of a 1.5-3.6 km thick section of conglomerate, quartzite, sub-graywacke, pelite, volcanics, and banded iron formation (Fig. 3). The Moodies Group is interpreted to be deposited in alluvial and marginal marine environments (Eriksson, 1977, 1978, 1979, 1980). Proportions of granitic rock fragments and K-feldspar increase upsection within the Moodies sediments, apparently recording increased exposure of granitic source rocks (Condie et al., 1970; Eriksson, 1980; Reimer et al., 1985).

PONGOLA SUPERGROUP

Scattered outcrops of the mid-Archean Pongola Supergroup are exposed along a 240 km north-south by 70 km east-west belt in eastern South Africa and Swaziland (Fig. 4). A minimum depositional area of 32,500 km^2 is inferred for this sequence by Button (1981), who notes that much of the original basin may be lost to erosional or igneous processes, or is overlain by younger sediments. Stratigraphic thicknesses increase from 2.5 km in the southern Wit-Mfolozi River inlier, to 14 km in the northern part of

Figure 4. Generalized geologic map and stratigraphic columns of the Pongola Supergroup. Also shown are outcrops of both pre- and post-Pongola intrusions. Geology after Button (1981a). MPR, Mozaan Piet Retief pelites; MWM, Mozaan Wit-Mfolozi pelites; NMP, Nsuze Mpongoza River pelites; NUWM, Nsuze Upper Wit-Mfolozi pelites; NLWM, Nsuze Lower Wit-Mfolozi pelites; NVS, Nsuze Vitshundi pelites. Inset map shows the location of the Pongola basin in reference to the Kaapvaal craton and the southern African continent.

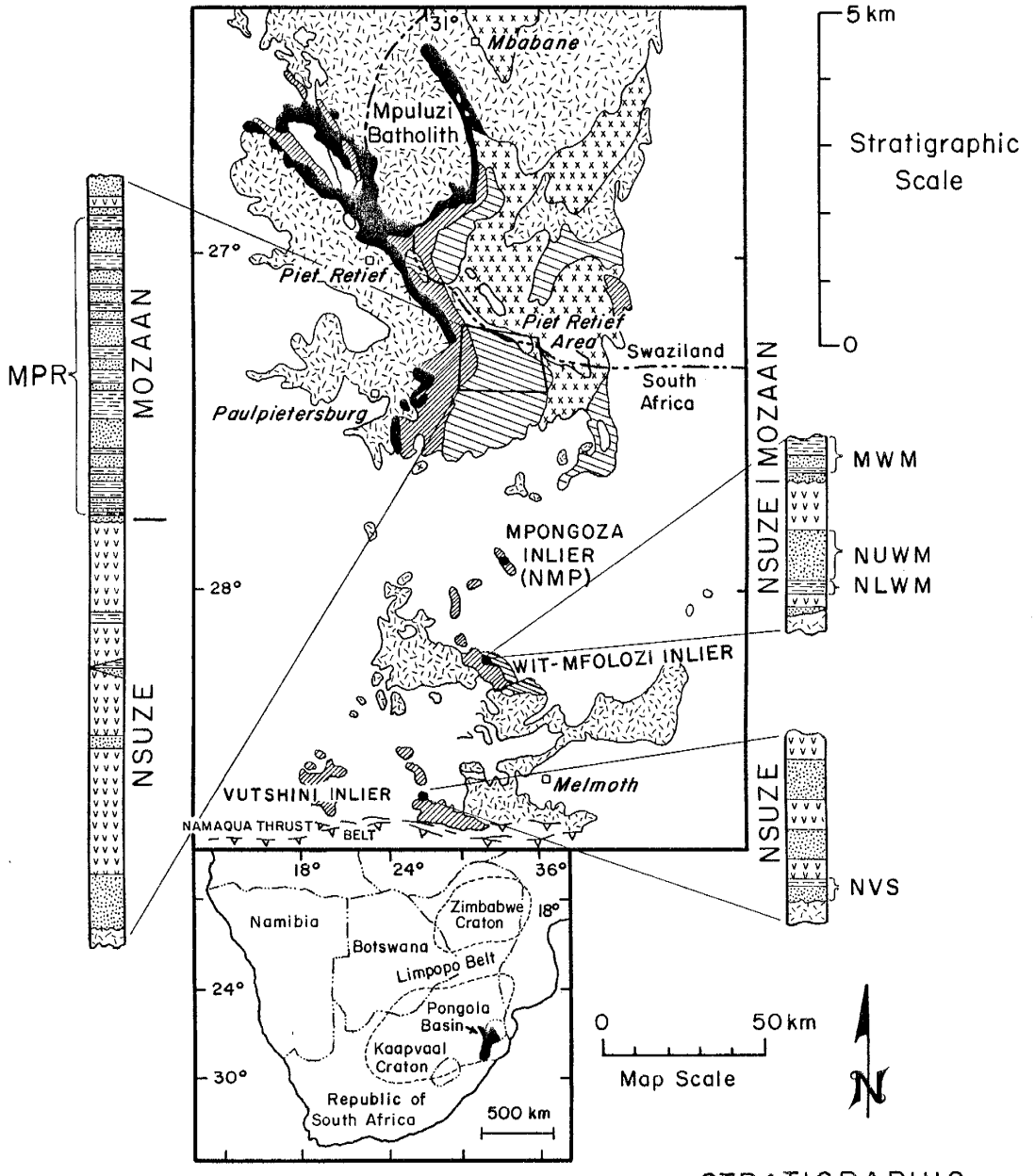

MAP KEY:

- Post-Pongola granites
- Usushwana Intrusive Complex
- Mozaan Subgroup
- Nsuze Subgroup
- Pre-Pongola granite — greenstone basement
- Political Boundary

STRATIGRAPHIC COLUMN KEY:

- Pelites
- Quartzites
- Volcanics
- Granite-greenstone basement
- Unconformity

the basin (Matthews, 1967; Armstrong et al., 1982).

The Pongola Supergroup is divided into the Nsuze (formerly Insuzi) and overlying Mozaan Groups (Fig. 4). The Nsuze Group rests nonconformably on 3.2-3.0 Ga granitic basement (homogenous hood granites), scattered remnants of greenstone belts, and the Ancient Gneiss Complex (3.6-3.5 Ga). Southern basement contacts are with freshly eroded biotite-microcline granite, whereas northern Nsuze strata rest on a well-developed paleoregolith composed of sericite, quartz, vermiculite and microcrystalline quartz (Matthews and Scharrer, 1968; Armstrong et al., 1982). This horizon apparently was produced during Archean weathering of pre-Pongola basement. The Wit-Mfolozi Nsuze sequence attains a maximum thickness of 1.9 km (Matthews, 1967). At this location, it commences with a thin basal layer of quartz arenite, conglomerate and arkose, which is overlain by lower and upper sequences of amygdaloidal and locally pillowed basalt, separated from each other by pelite, quartz arenite, calcareous sandstone and stromatolitic dolomite (Fig. 4). A 6-9 km thick section of Nsuze sediments and volcanics is exposed in the northern Piet Retief region, where basal sediments composed of arkosic arenite and quartz wacke are succeeded by quartz arenite and minor conglomerate. Overlying these sediments are subaereal to locally sub-aqueous lava and tuff, ranging in composition from mafic to felsic, with minor intercalated quartz arenite and pelite

(Watchorn and Armstrong, 1980; Armstrong et al., 1986).

The contact between the Mozaan and Nsuze Groups is gradational in the north (Watchorn, 1978), while the Mozaan section unconformably truncates successively lower Nsuze units when traced to the southeast (Button, 1981a). The Mozaan Group is 4-5 km thick in northern outcrops, while only 700m of strata are preserved in the Wit-Mfolozi section (Matthews, 1967; Armstrong et al., 1982). This sequence is composed of alternating layers of pelite and quartz arenite, with minor banded iron formation and conglomerate (Fig. 4). Sediments from both the Nsuze and Mozaan Groups are interpreted to reflect deposition in fluvial as well as tide-dominated, near-shore marine environments (Von Brunn and Hobday, 1976; Watchorn, 1980a).

The Pongola Supergroup is only mildly deformed into a number of gentle domes and basins, with folding apparently associated with intrusion of granites located to the east (Fig. 4; Button, 1981a). Most margins of the Pongola basin have been destroyed by intrusive activity; however, pene-contemporaneous normal and left-lateral strike-slip faulting and associated basin subsidence are reported in southern Pongola exposures (Matthews, 1967; Dix, 1984).

Various models are proposed for the tectonic evolution of the Pongola basin. Hegner et al. (1981) interpret the Pongola sequence as developing in a graben-like setting, representing the remnants of a failed greenstone belt.

Tankard et al. (1982, p. 74) suggest a volcanic arc setting for the Pongola volcanics, noting that granitic basement and basal arenites of the Nsuze Group favor a continental-type arc system. Bimodal silica contents of Nsuze volcanics, rapid lateral variations in thickness and character of sediments, shallow-water depositional environments, and basement-derived arkoses and conglomerates led Burke et al. (1985a) to suggest that the Pongola Group represents a continental rift succession. Age constraints from underlying Nsuze volcanics and Usushwana complex intrusives indicate that the >4600m of Mozaan sediments in the Piet Retief area (Matthews and Scharrer, 1968) were probably deposited in a time interval of <60 my. These results imply minimum Mozaan sedimentation rates of 0.08 m/1000 years, a value which is similar to that tabulated by Schwab (1986) for ancient aulacogen, rift-valley, foreland and successor basins. Actual rates of sediment accumulation may be greater because the upper portion of the Mozaan Group is eroded and because Mozaan sedimentation probably ceased prior to the Usushwana intrusive episode. Major and trace element studies of Nsuze volcanics indicate a compositional range from basalt to rhyolite with an abundance of lavas of intermediate composition (Armstrong et al., 1986; Crow et al., 1988). These data, as well as the absence of alkaline volcanism led Armstrong et al. (1986) to dispute the rift hypothesis, suggesting instead that the tectonic setting of

the Nsuze Group does not compare favorably with any Phanerozoic plate tectonic setting.

DOMINION GROUP

Dominion erosional remnants cover an area of ~16,000 km^2 in the southwest Transvaal and western Orange Free states of South Africa (Fig. 5). Sedimentary and volcanic rocks of the Dominion Group rest nonconformably on 2900 +/- 150 Ma granitic basement (Nicolaysen et al., 1962) and are interpreted to represent the protobasinal phase of the overlying Witwatersrand Supergroup (Watchorn, 1980b, 1981; Tankard et al., 1982; Fig. 6). The Dominion Group is divided, from oldest to youngest, into the Rhenosterspruit, Rhenosterhoek and Syferfontein Formations. These sequences are interpreted to be deposited in continental rift, continental arc and foreland basin tectonic settings (Burke et al., 1986; Tankard et al., 1982; Crow and Condie, 1987, respectively).

The Rhenosterspruit is composed of <120m of feldspathic to sericitic quartzite and basal comglomerate deposited as a valley-fill sequence over eroded basement surfaces (Fig. 6; Watchorn, 1980b). Gold and uranium have been mined intermittently in the past from basal conglomerates, which show mineralogical and depositional similarities to the more famous Witwatersrand deposits. These sediments differ from the Witwatersrand in having higher contents of Co, As, Ta and REE (Reimer, 1987). Conglomerate lithologies are

Figure 5. Generalized geologic map of the Dominion Group, southern Africa. Also shown are outcrops of pre-Dominion granites and overlying Witwatersrand Supergroup sediments. +BBS and +BSF indicate drill-core sample locations. Geology after Visser (1984).

Figure 6. (follwing page) Generalized stratigraphic section of the Dominion Group. Modified after Kent (1980a).

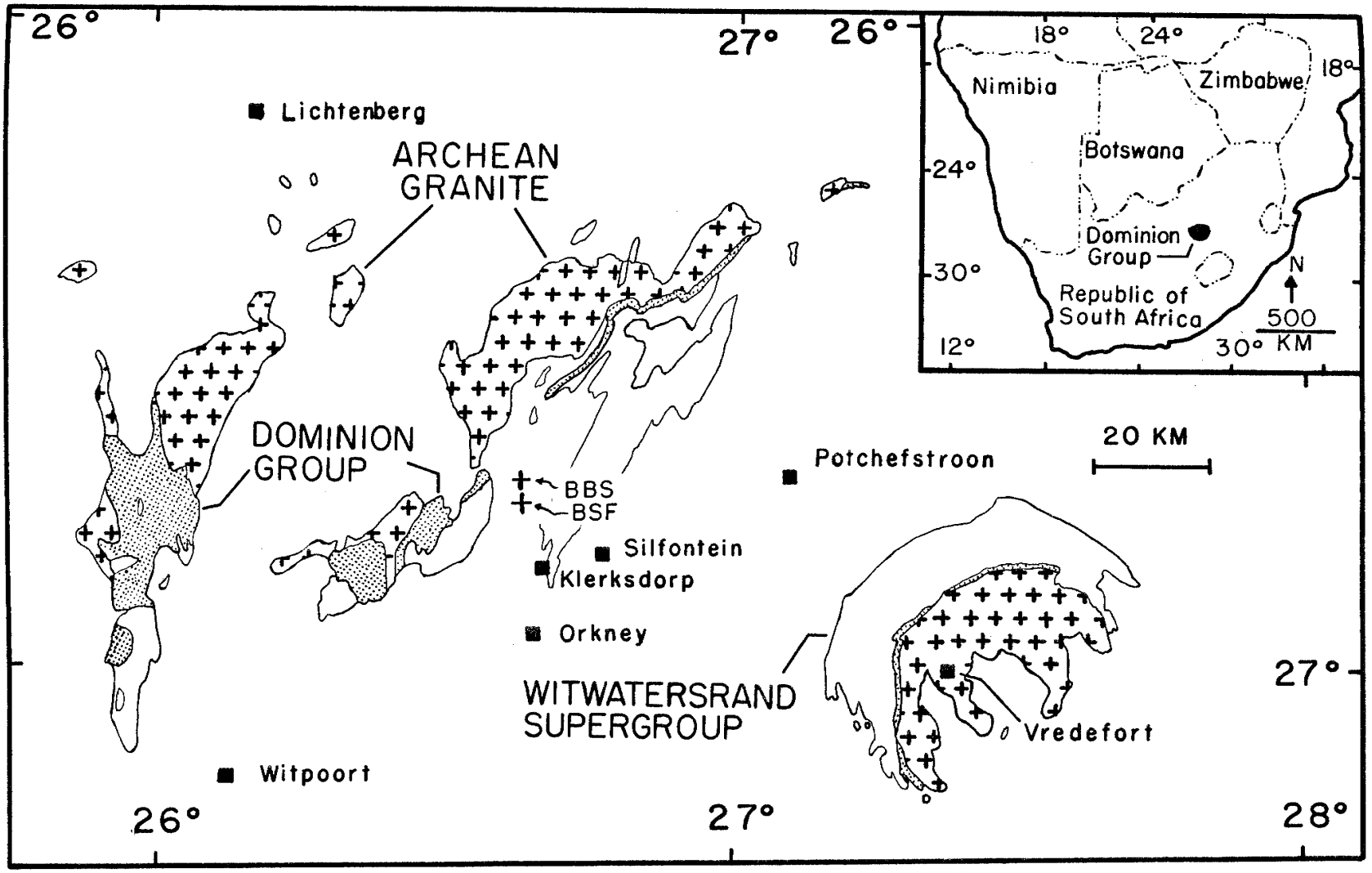
26°
27°
26°
Lichtenberg
ARCHEAN
GRANITE
DOMINION
GROUP
BBS
BSF
Silfontein
Klerksdorp
Orkney
Potchefstroon
20 KM
WITWATERSRAND
SUPERGROUP
Vredefort
Witpoort
26°
27°
28°
27°
18°
24°
18°
Nimibia
Zimbabwe
Botswana
24°
Dominion
Group
30°
N
Republic of
South Africa
500
12°
30° KM

FORMATION

Syferfontein Porphyry

Rhenosterhoek Andesite

Rhenosterspruit Quartzite

Archean Granite

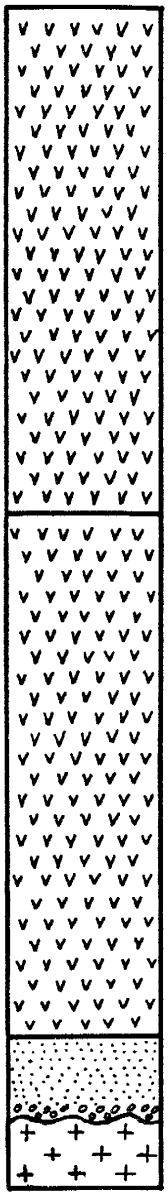

dominated by well-rounded quartzite pebbles set in a chloritic matrix. Heavy mineral detritus is enriched in pegmatitic minerals such as uraninite, monazite, zircon, cassiterite and columbite/tantalite as well as chromite, pyrite, zircon, cassiterite, various sulfide minerals and garnet (Viljoen et al., 1970; Reimer, 1987). Gold typically is authigenic and enriched in Cu and Ni. Deposition of these immature conglomeratic sediments is interpreted to have taken place predominantly in shallow braided dendritic stream systems occasionally dominated by emphemeral sheet wash (Tankard et al., 1982). Reimer (1987) estimates a source provenance for these sediments consisting of 80-85% granite and alkali-rich gneisses, 10-15% mafic to ultramafic greenstones, and <10% reworked arenites.

The Rhenosterhoek gradationally overlies the Rhenosterspruit and is composed of >1 km of subaerially deposited andesite, basaltic andesite lava, tuff and breccia, with lesser felsic porphyry and intercalated sediment (Fig. 6). Paleosols indicative of periodic exposure and weathering are described in the section by Button and Tyler (1981) and Grandstaff et al. (1986). The Syferfontein Formation conformably succeeds underlying Rhenosterhoek volcanics and is composed of ~1.5 km of quartz-feldspar porphyries with lesser basalt, andesite, felsic tuff and breccia.

WITWATERSRAND SUPERGROUP

The Witwatersrand Supergroup is deposited in an arcuate, oval shaped, 42,000 km^2 northeast-trending basin, which is fault-bounded along its northwestern margin (Pretorius, 1981a, 1981b; Fig. 7). The Witwatersrand sequence is divided into the lower West Rand and upper Central Rand Groups (Fig. 8), the former of which conformably overlies volcanics of the Dominion Group and nonconformably overlaps Archean basement granites. Stratigraphic thicknesses increase (830-7500m) towards the northwestern margin of the basin for the West Rand Group, whereas maximum thicknesses (2880m) of the Central Rand Group occur in the center of the basin, a pattern consistent with southeastern migration of the basin axis with time (Pretorius, 1976, 1981b). The Witwatersrand section exhibits two generations of open folds and is cut by late high-angle and thrust faults, some of which were reactivated as transcurrent faults (Pretorius, 1981b; Roering, 1986).

Extensive Au- and U-bearing sediments in the Witwatersrand Supergroup have been the subject of numerous studies (Pretorius, 1976, 1981a; Tankard et al., 1982). This deposit is generally interpreted as a paleoplacer (Pretorius, 1976) with mineralization occurring chiefly in conglomerates located in the upper half of the succession. The conglomerates and associated quartzites represent a more

Figure 7. Generalized geologic map of the Witwatersrand basin (After Robb and Meyer, 1985). Also shown are outcrops of pre-Witwatersrand granite-greenstone basement, major sediment transport directions into the Witwatersrand basin, and areas of sample collection. Inset map shows the location of the Witwatersrand basin in reference to the Kaapvaal craton and the southern African continent.

Figure 8. (following page) Simplified stratigraphic column of the Witwatersrand Supergroup, southern Africa (after Kent, 1980b; Robb and Meyer, 1985). Pelite horizons analyzed in this study also are noted.

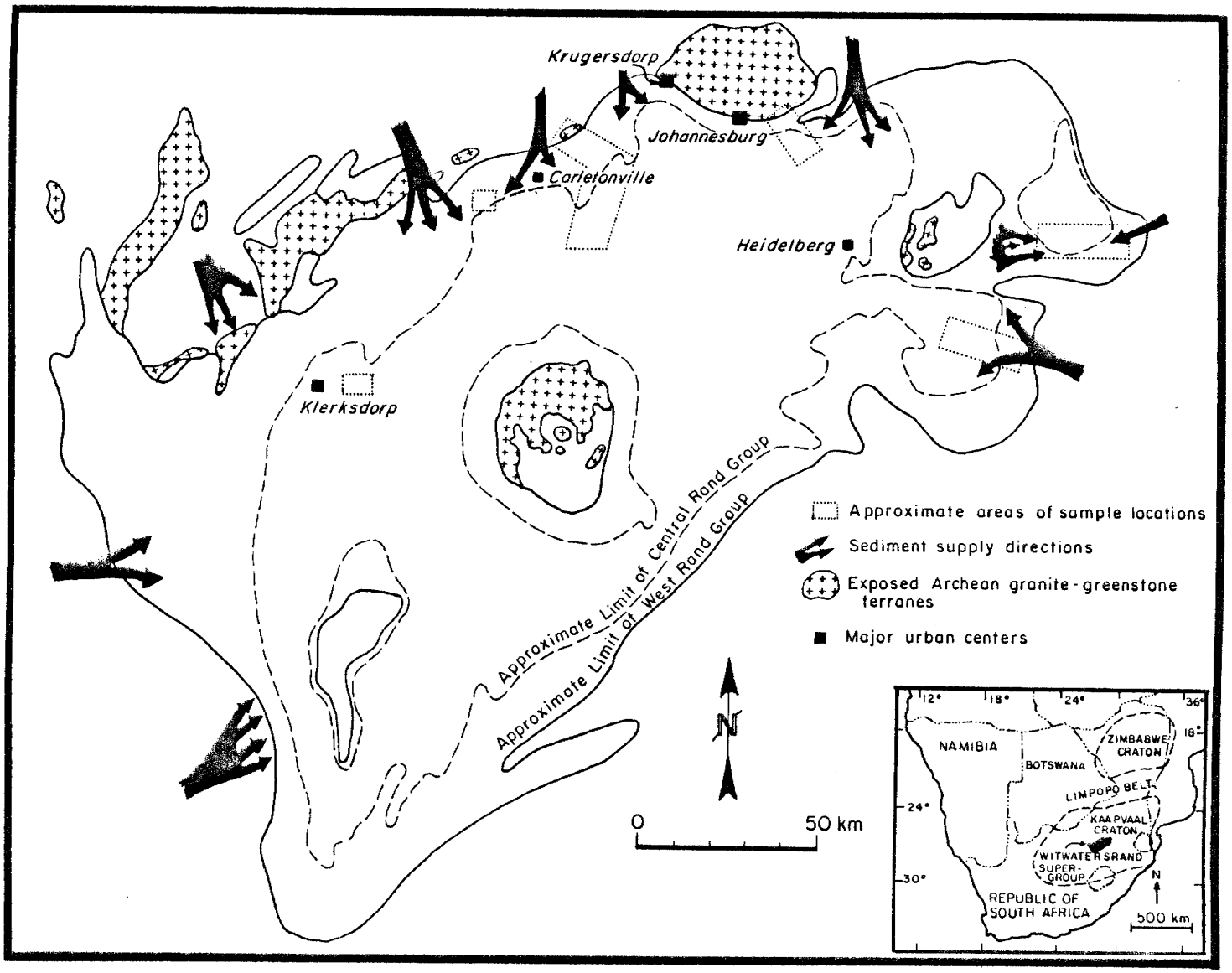
Krugersdorp
Johannesburg
Carletonville
Heidelberg
Klerksdorp
Approximate Limit of Central Rand Group
Approximate Limit of West Rand Group
Approximate areas of sample locations
Sediment supply directions
Exposed Archean granite-greenstone terranes
Major urban centers
N
0
50 km
12°
18°
24°
36°
18°
24°
30°
NAMIBIA
BOTSWANA
ZIMBABWE CRATON
LIMPOPO BELT
KAAPVAAL CRATON
WITWATERSRAND SUPER-GROUP
REPUBLIC OF SOUTH AFRICA
N
500 km

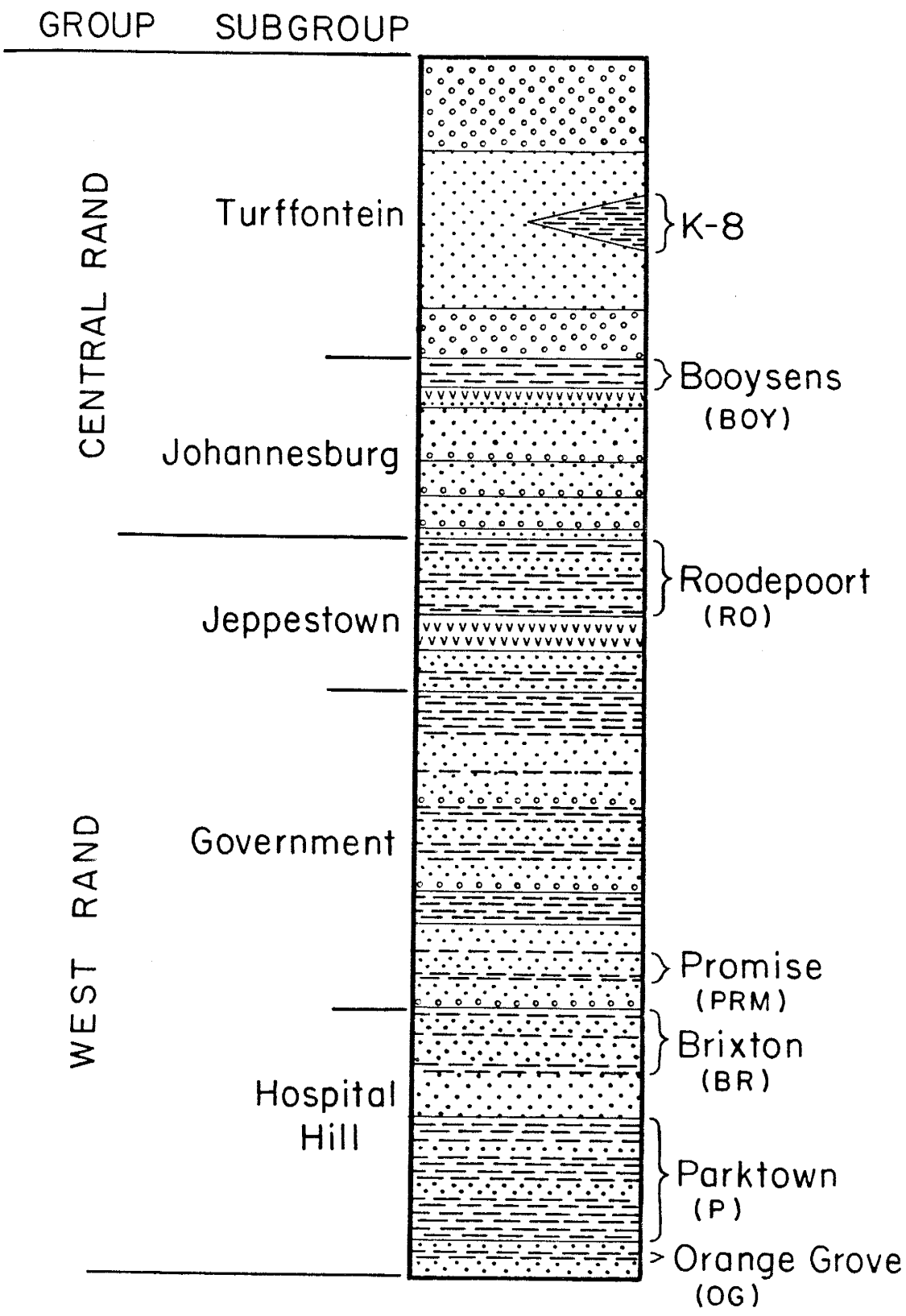
GROUP
SUBGROUP
CENTRAL RAND
Turffontein
K-8
Booysens
(BOY)
Johannesburg
Roodepoort
(RO)
Jeppestown
WEST RAND
Government
Promise
(PRM)
Brixton
(BR)
Hospital
Hill
Parktown
(P)
Orange Grove
(OG)

proximal high energy facies environment than underlying finer-grained West Rand sediments. Pebble compositions are dominated by quartz and chert with lesser quartzite and quartz porphyry in a matrix of muscovite and chlorite (Pretorius, 1976). Witwatersrand quartzites range from subgreywacke to mature quartz arenite compositions and are interpreted to be deposited in fluvial to shallow-marine fluvial fan settings, with extensive tidal and storm reworking (Eriksson et al., 1981). Pelites also are an important component of these sediments, comprising approximately 30% of the supergroup, and an even greater proportion of the West Rand Group (Pretorius, 1976).

In terms of tectonic setting, continental rift, periphrial foreland basin, and wrench-fault basin models are proposed for the Witwatersrand Basin (Pretorius, 1976; Burke et al., 1986; Stannistreet et al., 1986). Of these models, the foreland basin (+/- wrench-faulting) model is favored in terms of the abundance of quartzites and shales in the Witwatersrand Supergroup, a subduction-zone geochemical signature that characterizes volcanics of the underlying Dominion Group and overlying Ventersdorp Supergroup, and continent collisional episodes recorded in <2.9 Ga deformational events in the Limpopo belt to the north (Light, 1982; Schweitzer and Kroner, 1985; Crow and Condie, 1987). Compressional block faulting and folding of sediments in the Welkom goldfield are interpreted to be

similar to features characteristic of Laramide compressional events in western North America (Callow and Meyers, 1986). These deformation patterns support a foreland basin model for the Witwatersrand basin. Thrusting along the northern Witwatersrand basin margin is characterized by northward and eastward directed thrusts (Roering, 1986; Callow and Myers, 1986), a direction opposite to that which would be expected if the Witwatersrand formed as a result of compressional stresses generated in the Limpopo belt.

VENTERSDORP AND TRANSVAAL SUPERGROUPS

The Ventersdorp and Transvaal Supergroups occur in northeast-southwest trending basins covering areas greater than 200,000 and 500,000 km^2, respectively, in northern South Africa and southern Botswana (Fig. 9). The Ventersdorp sequence is up to 5 km thick, and is divided into the Klipriviersberg, Platberg and Pniel Groups, whereas the Transvaal Supergroup is divided into the Wolkberg, Chuniespoort and Pretoria Groups (Fig. 10). The largely volcanic Klipriviersberg and Platberg Groups, the chemical sediments of the Chuniespoort Group, and Transvaal aged sediments of the northern Cape region were not examined in this study.

The Pniel Group disconformably overlies older Ventersdorp strata and is divided into the sedimentary Bothaville and volcanic dominated Allanridge Formations

Figure 9. Generalized geologic map showing outcrop distributions of the Ventersdorp and Transvaal Supergroups, southern Africa (modified after Kent, 1980b; Coertze et al., 1980), as well as areas of drill-core (region within 100 km NW to SW of Johannesburg) and surface sample (region 100-200 km SE of Pietersburg) collection. Inset map shows location of Figure 9 in reference to the Kaapvaal craton and the southern African continent.

Figure 10. (following page) Simplified stratigraphic column of the Ventersdorp and Transvaal Supergroups, South Africa (modified after Coertze et al., 1980; Burke et al, 1985b). Pelite formations analyzed in this study and horizons discussed in the text also are noted.

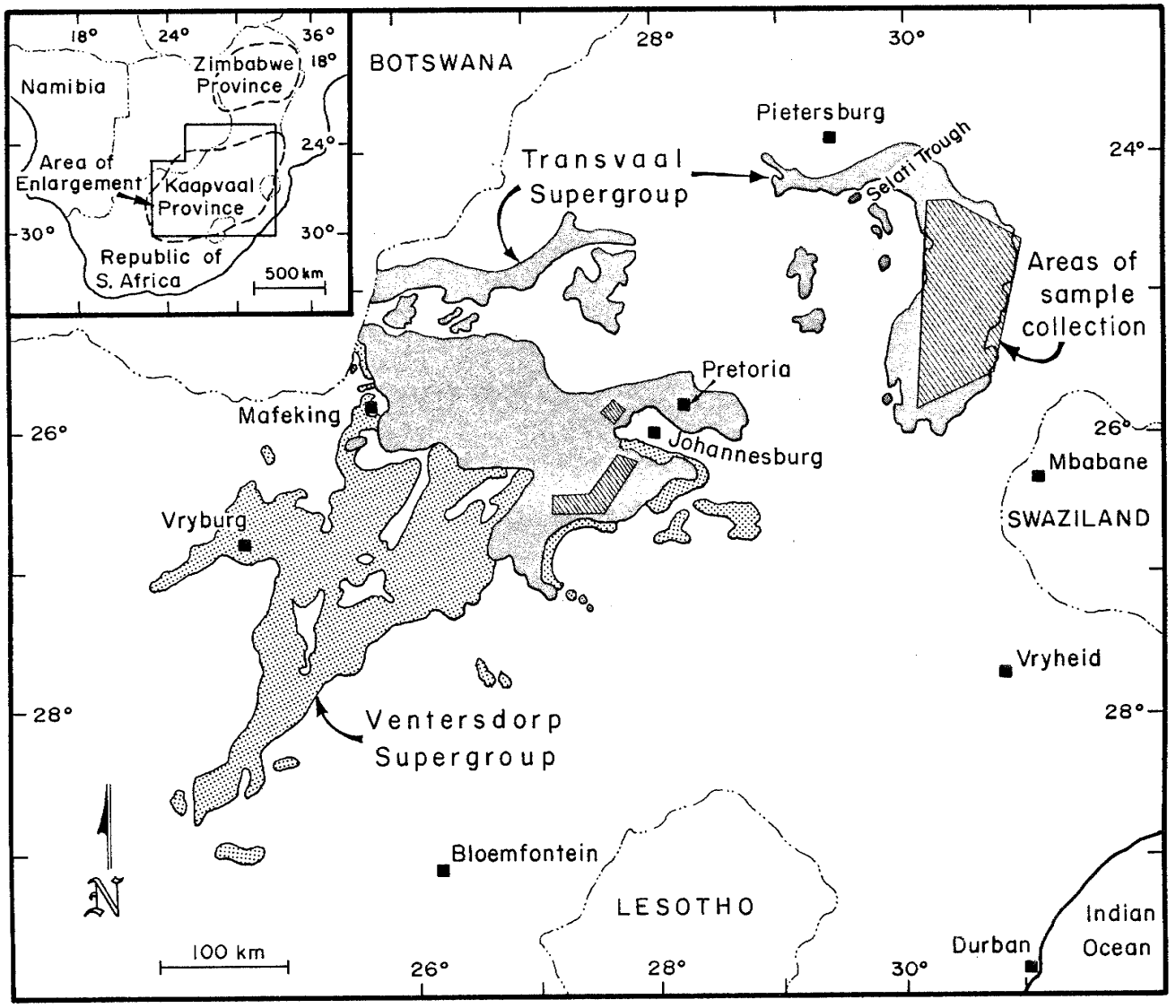
18°
24°
36°
18°
Zimbabwe
Province
Namibia
24°
Area of
Enlargement
Kaapvaal
Province
30°
30°
Republic of
S. Africa
500 km
BOTSWANA
28°
30°
Pietersburg
Transvaal
Supergroup
Selati Trough
24°
Areas of
sample
collection
Pretoria
Mafeking
26°
Johannesburg
26°
Mbabane
SWAZILAND
Vryburg
Vryheid
28°
28°
Ventersdorp
Supergroup
N
Bloemfontein
LESOTHO
Indian
Ocean
Durban
100 km
26°
28°
30°

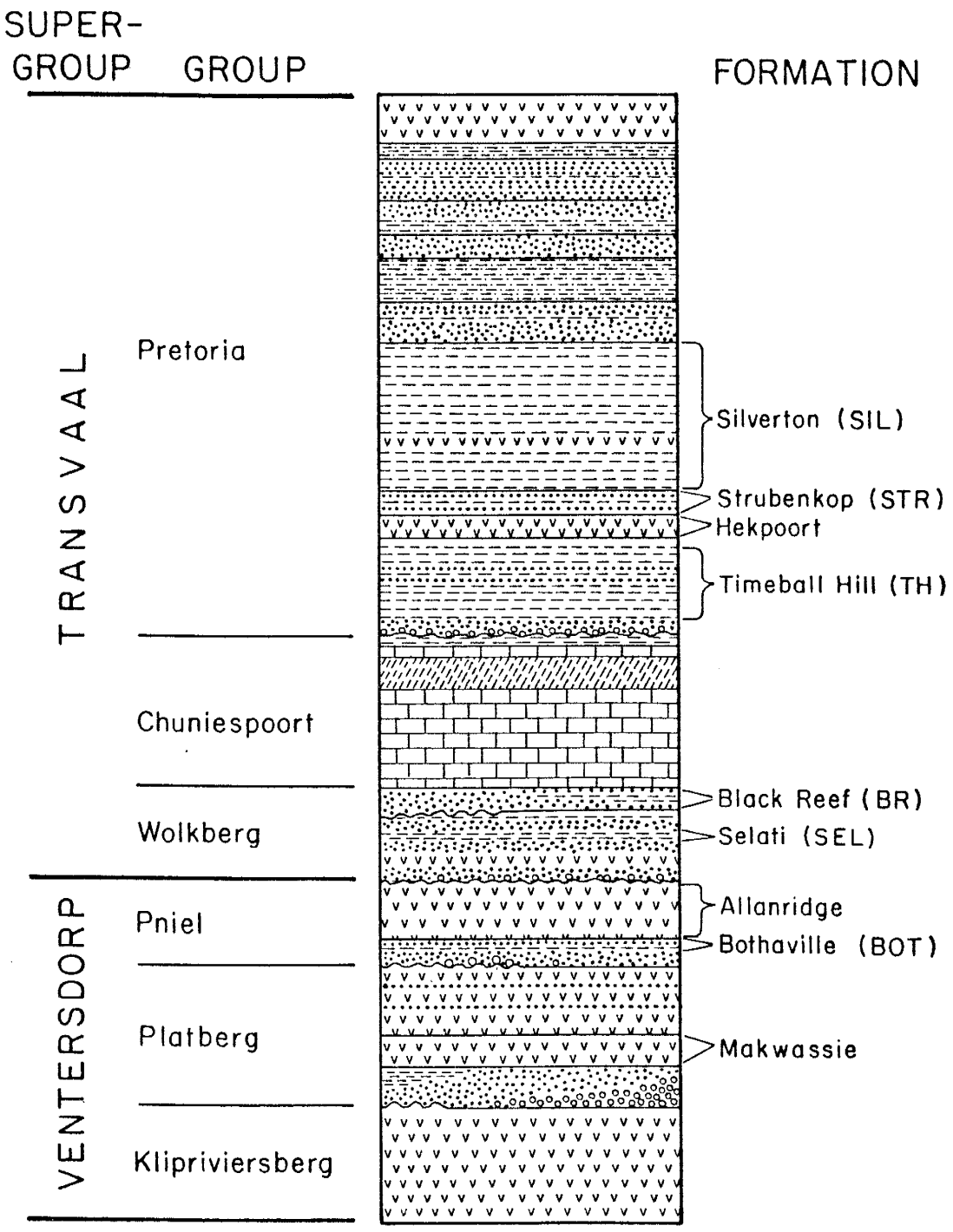
SUPER-GROUP
GROUP
GROUP
FORMATION
TRANSVAAL
Pretoria
Chuniespoort
Wolkberg
VENTERSDORP
Pniel
Platberg
Klipriviersberg
Silverton (SIL)
Strubenkop (STR)
Hekpoort
Timeball Hill (TH)
Black Reef (BR)
Selati (SEL)
Allanridge
Bothaville (BOT)
Makwassie

(Fig. 10). The 400m thick Bothaville Formation is characterized by cyclic, upward fining units of conglomerate, quartzite, pelite and carbonate (Button, 1981b). Tankard et al. (1982) favor an alluvial plain depositional setting for these sediments. The Ventersdorp basin is interpreted in terms of a continental rift setting, with rifting initiated during collision of the Kaapvaal and Zimbabwe cratons (Fig 2; Burke et al., 1985b). An abundance of marine quartzite, pelite and dolomite suggests that the Transvaal sequence represents a continental margin or platform setting.

The Transvaal Supergroup is best developed in the northeast portion of the basin where a 12 km thick section is exposed (Tankard et al., 1982). Deposition of the basal Wolkberg Group was strongly influenced by paleotopography, with maximum thicknesses of 2 km preserved in paleovalleys. Lower Wolkberg sediments represent the proto-basinal stage of Transvaal sedimentation and are composed of fluvial to shallow-marine feldspathic and subgreywacke quartzite, arkose, siltstone, pelite and conglomerate, as well as subaereal to subaqueously extruded basalt (Button, 1973a). Lobate distributions of arenaceous sediments suggest a fluvio-deltaic progradation into shallow water with sediment sources lying to the north and east (Button, 1973a). Distal sedimentation is dominated by thick accumulations of Selati Formation pelites which were deposited in the rapidly

subsiding Selati trough. Clendenin et al. (1987) suggest that the Selati trough formed in response to interarc spreading along zones of weakness aligned with the Murchison greenstone belt.

Black Reef quartzites show both conformable and locally unconformable relationships with lower Wolkberg sediments (Fig. 10), while they also transgress older units such as the Ventersdorp and Witwatersrand Supergroups (Button, 1973a, 1981b; Clendenin et al., 1987). Up to 500m of Black Reef mature fluvial and marine cross-bedded quartzite as well as 100m of basalt are preserved in the Selati trough. Elsewhere, this unit is usually <30m thick and is composed largely of mature cross-bedded quartzite, basal conglomerate and upper intertidal pelite and carbonate (Button, 1981b). Paleocurrents in the vicinity of the Selati trough indicate sources for the Black Reef sediments lying predominantly to the east, whereas in the Cape and northeast Transvaal regions sources appear to lie to the north, with a subordinate southern source noted during deposition of basal units (Button, 1973a).

A regional angular unconformity, marked by a chert-pelite breccia separates the Pretoria from the underlying Chuniespoort Group. The Pretoria Group is composed of marine tidal quartzite and pelite, with lesser carbonate and volcanics (Fig. 10). Glaciomarine and fluvio-glacial sediments are preserved in the Timeball Hill Formation in

the Cape region. Subaereal to submarine volcanic units typically show erosional contacts with underlying and/or overlying strata, indicating periodic exposure of these units to erosional forces. Pretoria Group sediments are interpreted to be derived from sources to the north and northeast (Button, 1975), with sedimentation controlled by uplift in the Limpopo area (Tankard et al., 1982). Preserved coarse, terrigenous-fluvial sediments are rare, possibly due to uplift and erosion of northern basin margins, while distal fine-grained and chemically precipitated sediments are abundant in southern regions.

WATERBERG AND SOUTPANSBERG GROUPS

The Waterberg and Soutpansberg Groups represent the earliest continental red-beds and youngest Precambrian sequences preserved in southern Africa. Northern Transvaal exposures of the Waterberg and Soutpansberg Groups are distributed over areas of 25,000 and 8000 km^2, respectively (Fig. 11). The central basin of the Waterberg is divided into two main units, the early Alma trough and the late Waterberg basin (Jansen, 1981). The Alma trough is further divided into the Swaershoek and overlying Alma Formations, whereas the late Waterberg basin is partitioned into the Skilpadkop, Aasvoelkop, Sandriviersberg, Cleremont and Vaalwater Formations (Fig. 12). A composite section up to 7 km thick is preserved in five sub-basins which

Figure 11. Generalized geologic map showing outcrop distributions of the Waterberg and Soutpansberg Groups, southern Africa. After Kent (1980d) and Kent and Jansen (1980).

Figure 12. (following page) Generalized stratigraphic section of the Waterberg Group. After Kent (1980d).

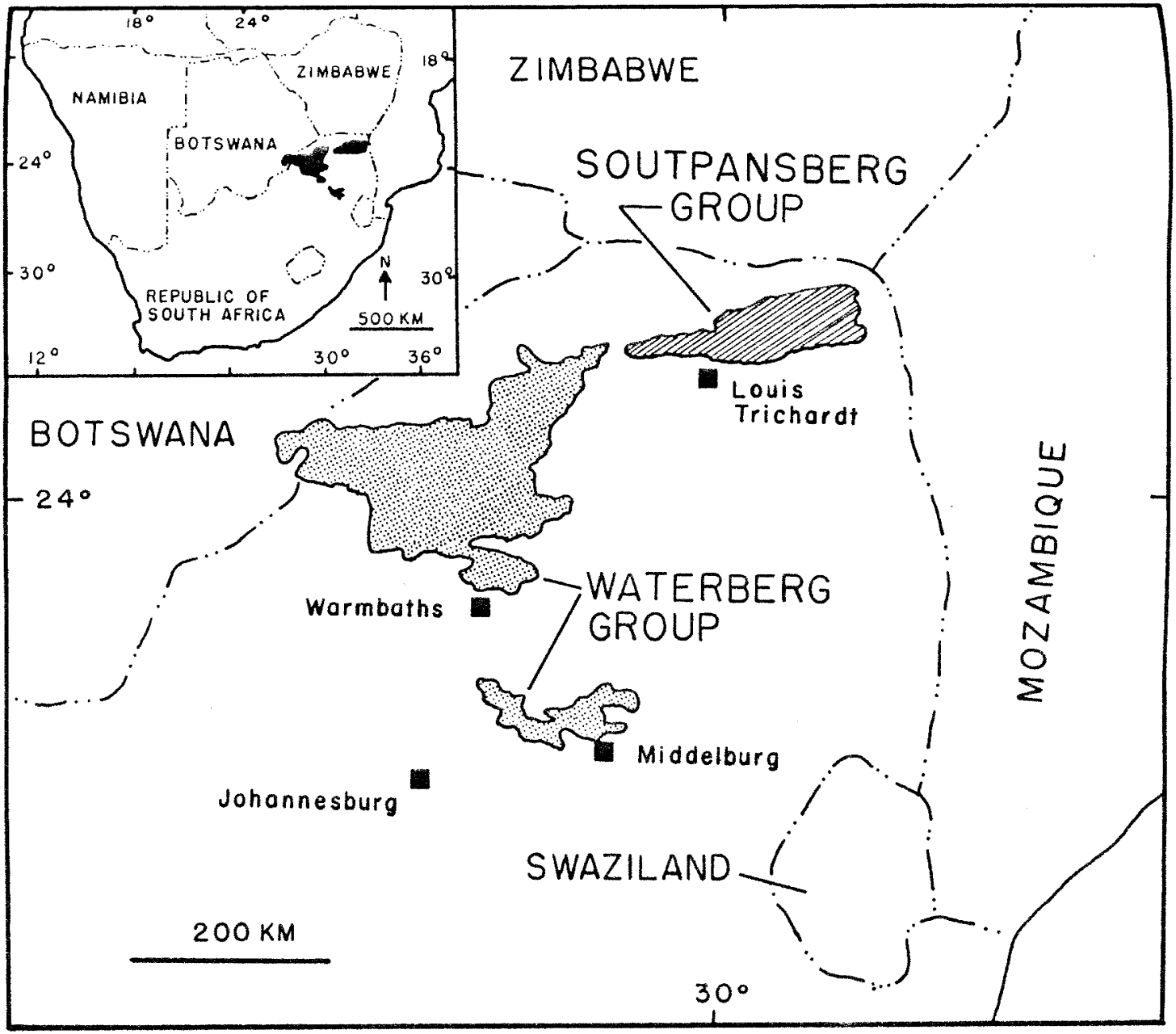
18°
24°
ZIMBABWE
18°
NAMIBIA
BOTSWANA
24°
30°
30°
REPUBLIC OF
SOUTH AFRICA
N
500 KM
12°
30°
36°
ZIMBABWE
SOUTPANSBERG
GROUP
Louis
Trichardt
BOTSWANA
24°
WATERBERG
GROUP
Warmbaths
MOZAMBIQUE
Middelburg
Johannesburg
SWAZILAND
200 KM
30°

FORMATION

Vaalwater

Cleremont

Sandriviersberg

Aasvoëlkop

Skilpadkop

Alma

Swaershoek

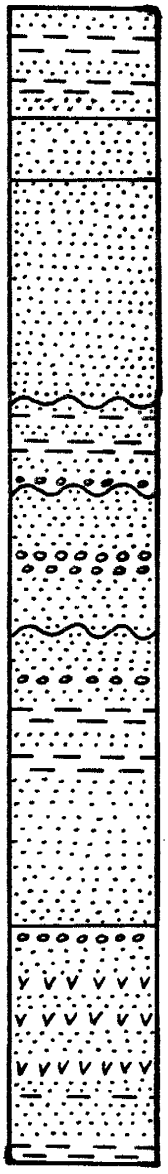

progressively and uncomformably overlap northward with time. Cheney and Twist (1986) suggest that the section probably never exceeded 5 km in thickness in any one locality due to the unconformable relationships of sub-basins. The Waterberg basin probably formed by subsidence of the underlying crust, with centers of deposition shifting to the north with time. The succession is composed mostly of intracratonic arenaceous and conglomeritic sediments with <10% finer-grained siltstone, shale and volcanic rock (De Vries, 1968; Vos and Eriksson, 1977). Conglomerate pebbles include rounded to subangular felsite, quartzite and jasper, with lesser chert, iron-formation, quartz and granophyre clasts (Tankard et al., 1982). Sandstones are mostly arkosic to lithic arenite and feldspathic to lithic greywacke compositions with monocrystalline quartz, felsite, quartzite, chert, siltstone, K-feldspar, pyroxene, sphene, and magnetite framework grains. Mature quartz arenite also occurs in the Waterberg sequence, but is not as abundant as other types of sandstones. These arenites may result from stabilization of alluvial fans and tidal reworking in shallow water. Cross-bedded sandstone formed in transverse aeolian dune environments also are reported from the eastern Waterberg basin (Meinster and Tickell, 1976). Planar and trough cross-bedded alluvial-fan sediments indicate transport predominantly from sources to the north, northeast and east (Eriksson and Vos, 1979; Jansen, 1981), with

deposition taking place primarily in fluvial, shallow water and aeolian conditions. Transport directions indicate sediment sources mainly in the southern and central portions of the Limpopo belt, and thus Waterberg sediments may have been derived from the same granitic and metamorphic terrains that provided detritus for Transvaal sediments.

Deposition of upper stratigraphic units of the Soutpansberg Group post-date those of the Waterberg as indicated by unconformable stratigraphic relationships in the western Soutpansberg basin (Tankard et al., 1982). The 5500m thick Soutpansberg Group is composed of subaereal amygdaloidal Sibasa Formation basalt and overlying Musekwa Formation subarkosic arenite, lithic arenite, conglomerate and volcanic rock (Fig. 13). These units are succeeded by Ngwanedzi Formation basaltic lava, ash flow tuff and epiclastic sediments, and Nzhelele Formation sandstone, siltstone, tuff and shale. Soutpansberg sediments occur as distal braided-alluvial and shallow water deposits which accumulated in a graben setting formed on basement rocks of the Limpopo Province (Fig. 2). Paleocurrents indicate sediment sources to the north of the basin (De Villiers, 1967; Barker, 1979). The Soutpansberg trough developed on a permanent zone of weakness marked by westward spreading rifting and downwarping (Jansen, 1981). This tectonic style contrasts that of the northward migrating Waterberg basin. Graben development and basin-margin faulting have led to proposals that the Soutpansberg basin represents an

Figure 13. Generalized stratigraphic section of the Soutpansberg Group. After Kent and Jansen (1980).

FORMATION

Nzhelele

Ngwanedzi

Musekwa

Sibasa

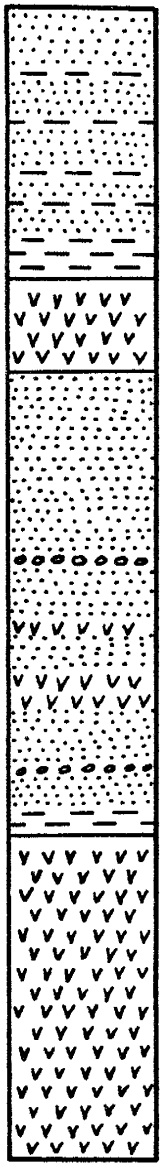

aulacogen (Jansen, 1975, 1976a, 1976b). Barker (1976, 1979) suggests that the Soutpansberg formed as a yoked basin during asymmetric faulting of the stabilized craton. He cites an absence of marine sedimentation and transport directions normal to the basin axis (sediment transport in an aulacogen is generally parallel to the graben axis) as evidence supporting a continental rift setting.

AGE RELATIONSHIPS

The Moodies Group represents the stratigraphically uppermost Swaziland Supergroup member of the Barberton Greenstone belt. A minimum age of 3210 +/- 3 Ma is provided for this unit by the intrusive Kaap Valley pluton (York, 1988). Felsic volcanics of the Nsuze Group yield a conventional U-Pb zircon age of 2940 +/- 22 Ma, which is consistent with a Nsuze Sm-Nd whole rock errorchron date of 2934 +/- 114 Ma (Hegner et al., 1984). A maximum age for the Pongola Supergroup is constrained by a Rb-Sr whole rock isochron of 3028 +/- 14 Ma for the underlying granitic Mpuluzi (Lochiel) batholith (Barton et al., 1983). A minimum age is provided by a 2871 +/- 30 Ma Sm-Nd mineral isochron and a 2876 +/- 45 Ma average Rb-Sr whole-rock isochron from the post-Pongola, Usushwana intrusive complex (Hegner et al., 1984; Layer et al., 1988). Thus, it appears that deposition of the Pongola succession occurred during a time interval of <150 Ma.

Conventional U-Pb zircon ages from felsic volcanics in the Dominion Group indicate deposition of this unit at ~2830 Ma (Van Niekerk and Burger, 1969). This age also effectively constrains the earliest deposition of the conformably overlying Witwatersrand Supergroup. A 3060 Ma ion microprobe age from Dominion zircons (Minter et al., 1988) contrasts the previously given age determined for Dominion lavas. The cause of this discrepancy is uncertain, but may result from the older age reflecting a relict basement provenance age for the lavas. Ion-microprobe zircon dates of 2750-2700 Ma from Ventersdorp-Klipriviersberg lavas provide a minimum age of Witwatersrand deposition (Armstrong et al., 1986; R. Armstrong, personal communication reported in Phillips, 1986a; R. Armstrong and W. Compston, personal communication reported in Minter et al., 1988). Combined Dominion and Klipriviersberg zircon ages suggest that deposition of the Witwatersrand Supergroup occurred over a time interval of <130 Ma.

Quartz porphyry rocks of the Ventersdorp-Makwassie Formation yield conventional U-Pb zircon ages of 2634 +/- 14 Ma and 2643 +/- 8 Ma (A. Kroner, personel communication, 1986; Van Niekerk and Burger, 1978), and a U-Pb ion microprobe zircon age of 2699 +/- 16 Ma (Armstrong et al., 1986). These ages suggest that Bothaville sediments, which unconformably overlie the Makwassie Formation, are probably late Archean in age. In combination with the previously

listed Klipriviersberg ages, these data suggest that Ventersdorp deposition took place between 2.75-$\lesssim$2.6 Ga.

Volcanic rocks of the Transvaal-Hekpoort Formation yield Rb-Sr whole-rock isochron ages of 2224 +/- 21 Ma (D. Crampton, quoted in Button, 1981b). Post-Transvaal Bushveld granites have a Rb-Sr whole-rock isochron age of 2095 +/- 24 (Hamilton, 1977) and post-Transvaal volcanics in the Griqualand West region have a Rb-Sr whole-rock isochron age of 2070 +/- 90 Ma (Crampton, 1974). Thus, Transvaal sedimentation probably took place from $\sim$2.3-2.1 Ga. An extensive erosional interval is recorded between deposition of the Ventersdorp and Transvaal Supergroups. Rb-Sr systems of Ventersdorp rocks were reset during this prolonged period of erosion, possibly indicating the occurrence of a major regional metamorphic event which ended between 2400-2300 Ma ago (Barton et al., 1986).

Deposition of the Waterberg Group post-dates intrusion of 1913 +/- 30 and 1920 +/- 40 Ma Bushveld granites and their subsequent exposure due to erosion (Rb-Sr whole-rock isochrons; Davies et al., 1969; Coertze et al., 1978), whereas upper Waterberg sediments also post-date emplacement of the Palala Granite (1770 +/- 60 Ma) and subsequent faulting of this pluton (Walraven et al., 1983; Barton and McCourt, 1983). Coeval porphyry lava flows in the southern Waterberg basin have a conventional U-Pb zircon age of 1790 +/- 70 Ma (Oosthuyzen and Burger, 1964; Hunter, 1974).

Intrusive alkaline rocks dated at 1420 +/- 70 Ma provide a minimum age of Waterberg deposition (Oosthuyzen and Burger, 1964; conventional U-Pb zircon). Sedimentary units of the upper Soutpansberg Group locally overlie Waterberg sediments with an unconformity, indicating that Soutpansberg deposition probably continued after Waterberg deposition had ceased (Jansen, 1976b). Deposition of the Soutpansberg Group also appears to have begun after an 1800 +/- 50 Ma thermal metamorphic event recorded in gneissic basement rocks (Rb-Sr whole-rock isochron; Barton, 1979). A Rb-Sr whole rock isochron from basal Soutpansberg-Sibasa lavas of 1769 +/- 34 suggests a similar age for the Waterberg and Soutpansberg Groups. It appears that Waterberg deposition probably began $\sim$ 1800 Ma ago and ceased prior to 1400 Ma as well as prior to the end of Soutpansberg sedimentation. Soutpansberg basin development began 1770 Ma ago with the extrusion of basal Sibasa lavas and is considered to be coeval with the middle to upper portions of of the Waterberg Group (Coertze et al., 1980).

PELITE RESULTS

MINERALOGY

X-ray diffraction analyses (Appendix B.4) of Pongola pelite samples indicate that the major mineral species present are muscovite (illite) and chlorite, with minor amounts (<10%) of pyrophyllite, K-feldspar, kaolinite (probably secondary), mixed-layer illite/smectite (probably secondary), calcite and hydromagnesite (Table 1). Quartz also is present in most samples. Pelites from the Nsuze Group have relatively constant mineral distributions, with mean and one standard deviation values of 70+/-20% muscovite and 30+/-20% chlorite. Mozaan mineral contents are more variable, with 40+/-40% muscovite and 60+/-40% chlorite. Both Fe- and Mg-rich chlorites are present, with Fe-rich varieties dominating in both Groups. These mineralogic results complement those of Hunter (1963) and Beukes (1973), who identified andalusite, pyrophyllite, sericite and quartz from Al-rich pelites and chlorite, magnetite, tremolite-actinolite, quartz and spessartite from Fe-rich pelites. Watchorn and Armstrong (1980) also report chloritoid in basal clastics of the Nsuze Group.

Pelites from the Witwatersrand Supergroup are composed principally of muscovite (illite) and chlorite. Chlorite is the most predominant mineral in Booysens, Roodepoort, Promise and Parktown Formation pelites (Table 1), whereas muscovite and pyrophyllite are most prevalent in K8 pelites.

Table 1. Semi-quantitative mineral analyses of Kaapvaal craton pelites.

Unit	Sample	Illite/ Muscovite	Chlorite	Pyroph- yllite	Mixed-Layer I/S	Other- Trace
TRANSVAAL						
-Silverton	D 70	80	10	nd	10	-
	D 72	20	80	nd	<10	a
	D 75	100	nd	nd	tr	e
	D 97	60	40	nd	nd	i
-Strubenkop	CDV1-4	90	nd	pr	10	-
-Timeball	C 19	60	40	nd	<10	a,i
	C 214	60	nd	nd	30	a,e,h
	D 27	80	10	nd	<10	i
	CDV1-17	70	20	nd	<10	i
	CDV1-25	80	10	pr	10	i
	MSF1-3	70	20	nd	<10	-
	MSF2-3	50	30	nd	20	a
	MSF2-7	50	20	nd	30	a
	WBK1-2	70	30	nd	<10	e,i
	WBK1-4	80	10	pr	<10	j
-Black Reef	MEE 4	70	30	nd	tr	b
	MEE 25	90	10	nd	nd	a,d
	MEE 31	80	20	nd	nd	-
	MEE 38	80	20	nd	nd	b
VENTERSDORP						
-Bothaville	JWS-8-9	60	40	nd	nd	b,f
WITWATERSRAND						
-K8	MEE 1	100	nd	pr	nd	-
	MEE 13	50	50	pr	nd	b
	MEE 23	90	<10	pr	nd	b,d
	MEE 39	100	nd	pr	nd	-
	MED 6	80	<10	pr	nd	b
	MED 9	90	nd	pr	nd	-
-Booysens	MEE 5	70	20	nd	<10	b,c
	MEE 24	40	60	nd	nd	b,c,d
	MEE 27	10	90	nd	<10	b,c
	SJ3-4	30	70	nd	nd	b,c
-Roodepoort	MED 17	nd	100	nd	nd	b
	MED 18	<10	100	nd	nd	-
-Promise	MED 13	30	70	nd	tr	-
-Parktown	C 71	40	60	nd	<10	-
PONGOLA						
-Mozaan	MW 170	<10	90	nd	<10	-
	MW 253	80	10	pr	nd	a,e
	P 31	nd	100	nd	nd	-
	P 34	100	nd	nd	nd	-
	P 50	nd	100	nd	nd	-
	P 51	20	80	pr	nd	a,g
-Nsuze	P 5	100	nd	nd	nd	-
	P 8	30	70	nd	nd	-
	P 58	80	20	nd	nd	e
	P 61	70	20	nd	<10	e,f
	P 62	80	20	nd	nd	e,f

Values in percent; Analyses in part-per-ten accuracy; tr, <1% detected; nd, none detected; pr, present but not quantitatively analyzed for; I/S, illite/smectite; a, kaolinite; b, quartz; c, paragonite; d, chloritoid; e, K-feldspar; f, calcite; g, hydromagnesite; h, chromite; i,heulandite; j, spodumene; k, apatite.

Additionally, mixed-layer illite/smectite, paragonite and chloritoid are detected in trace quantities and quartz is present in most samples. Both Mg- and Fe-rich chlorites are detectable in Witwatersrand pelites in approximately equal amounts, however, Fe-rich chlorites dominate slightly in Booysens pelites.

The single Ventersdorp pelite sample analyzed is composed of muscovite (illite), Fe-rich chlorite and quartz (Table 1). Pelites from the Transvaal Supergroup are dominated by muscovite and chlorite, with both Fe- and Mg-rich chlorites are present in approximately equal amounts. Pelites from the Black Reef Formation also contain trace quantities of chloritoid, while those from the Pretoria Group contain variable amounts of pyrophyllite, mixed-layer illite/smectite, kaolinite, vermiculite and K-feldspar. Relatively abundant mixed-layer clays in the Pretoria Group suggest that these sediments may be classified as shales rather than pelites.

GEOCHEMISTRY

Major Elements

Both stratigraphic and geographic variations are evident in the major element contents of Pongola pelites. Mozaan Wit-Mfolozi (MWM) samples show the greatest range in K_2O/Na_2O ratios (0.3 to 160, Fig. 14a), while Mozaan Piet Retief (MPR) pelites are less variable and exhibit the

Figure 14. SiO2/Al2O3--K2O/Na2O log distributions in pelites from the Kaapvaal craton. Oxides in weight percent. Regions for shales from Gromet et al. (1984). NASC, North American Shale Composite. a) Pongola Supergroup, b) Witwatersrand Supergroup, c) Ventersdorp-Transvaal Supergroups.

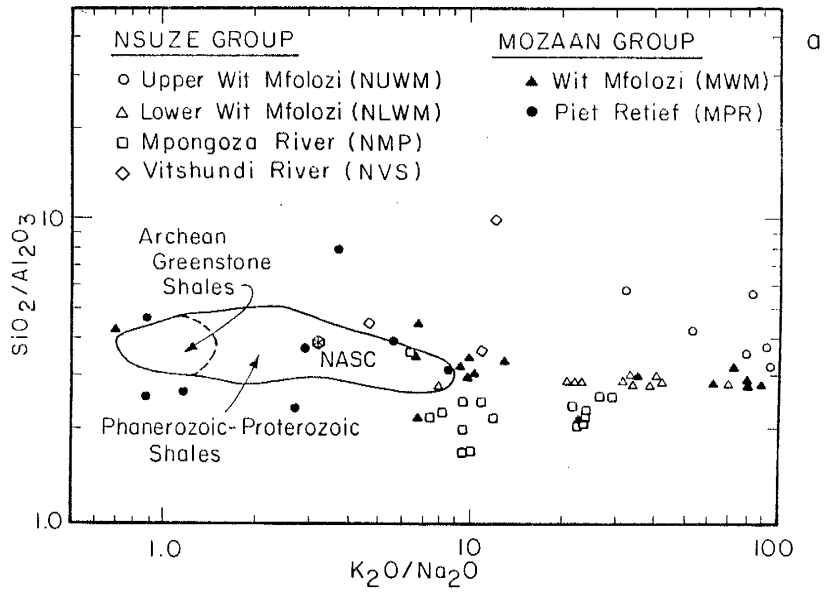
NSUZE GROUP
Upper Wit Mfolozi (NUWM)
Lower Wit Mfolozi (NLWM)
Mpongoza River (NMP)
Vitshundi River (NVS)
MOZAAN GROUP
Wit Mfolozi (MWM)
Piet Retief (MPR)
Archean Greenstone Shales
NASC
Phanerozoic-Proterozoic Shales
SiO2/Al2O3
K2O/Na2O
1.0
10
100
a

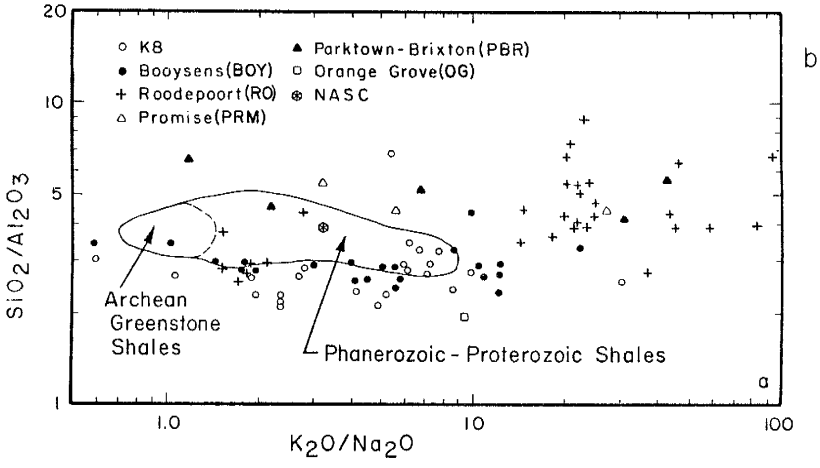
K8
Boysens(BOY)
Roodepoort(RO)
Promise(PRM)
Parktown-Brixton(PBR)
Orange Grove(OG)
NASC
Archean Greenstone Shales
Phanerozoic - Proterozoic Shales
SiO2/Al2O3
K2O/Na2O
20
10
5
1
1.0
10
100
b

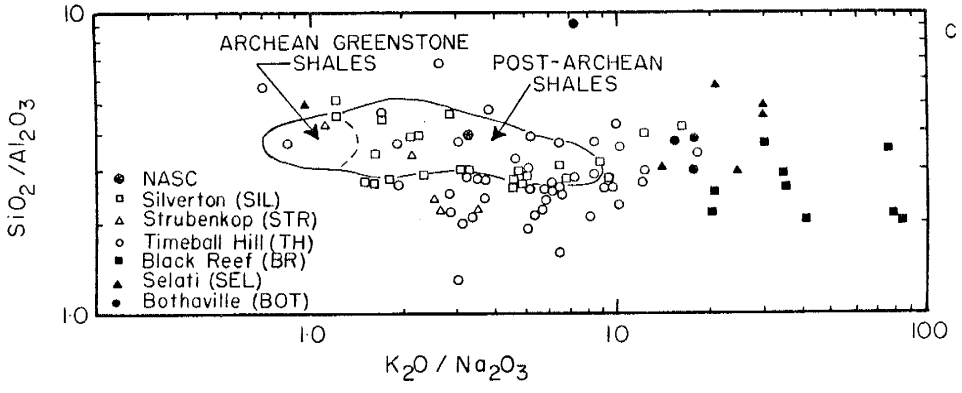
ARCHEAN GREENSTONE SHALES
POST-ARCHEAN SHALES
NASC
Silverton (SIL)
Strubenkop (STR)
Timeball Hill (TH)
Black Reef (BR)
Selati (SEL)
Bothaville (BOT)
SiO2/Al2O3
K2O / Na2O3
10
1.0
10
100
c

lowest K_2O/Na_2O ratios (0.9-8.4). All Nsuze pelites show moderate variations in K_2O/Na_2O and SiO_2/Al_2O_3 ratios. Most Pongola pelites have higher K_2O/Na_2O ratios and absolute K_2O contents relative to Moodies pelites from the Swaziland sequence (Taylor et al., 1986).

Relative to NASC, most Pongola pelites are depleted in MgO (except NUWM and NLWM samples), CaO and Na_2O (Table 2). Mozaan pelites are enriched in MnO and Fe_2O_3T, and with the exception of MPR and Nsuze Vitshundi River (NVS) pelites, Pongola pelites show K_2O enrichment relative to Phanerozoic shales. Upward stratigraphic increases of K_2O and MnO and decreases of MgO are apparent in pelites from the Wit-Mfolozi inlier, where from oldest to youngest the NLWM, NUWM and the MWM sections are exposed (Fig. 4; Table 2).

Major element concentrations in Witwatersrand pelites are variable, even within some of the individual pelite units (Table 3). The Hospital Hill Subgroup exhibits the greatest compositional range with 41-65% SiO_2 and 7-28% Al_2O_3. This variation is due primarily to differences between the lowermost Orange Grove (OG) pelite (1 analyses) and overlying Parktown-Brixton (PBR) pelites. In terms of SiO_2/Al_2O_3 and K_2O/Na_2O ratios, Booysens (BOY) and K8 pelites are similar to most Phanerozoic shales (Fig. 14b). OG, PBR, Promise (PRM), and Roodepoort pelites have higher and more variable K_2O/Na_2O ratios, exhibiting an overall similarity to the Pongola pelites. It is notworthy that

Table 1. Average chemical composition and ratios of pelites from the Pongola Supergroup and NASC.

	Mozaan Group				Nsuze Group								
	Piet Retief Area (MPR)		Wit-Mfolozi Inlier (MWM)		Upper Wit-Mfolozi (NUWM)		Lower Wit-Mfolozi (NLWM)		Mpongoza Inlier (NMP)		Vutshini Inlier (NVS)		NASC
	AVG	STD	AVG	STD	AVG	STD	AVG	STD	AVG	STD	AVG	STD	AVG
SiO2	59.53	7.75	57.43	4.52	64.27	3.00	58.75	0.88	56.23	3.83	70.71	8.82	64.80
TiO2	0.75	0.28	0.08	0.14	0.57	0.10	0.76	0.03	1.19	0.15	0.46	0.18	0.78
Al2O3	16.47	4.83	19.32	3.81	15.61	2.53	20.62	0.33	24.45	2.38	13.56	4.46	16.90
Fe2O3-T	13.19	7.10	9.87	7.57	6.06	0.68	6.57	0.63	6.22	0.79	5.59	5.35	6.33
MgO	1.86	0.75	1.79	1.23	2.97	0.40	3.26	0.83	1.11	0.85	1.58	0.64	2.85
CaO	0.09	0.07	0.07	0.04	0.96	0.85	0.04	0.03	0.03	0.02	0.01	0.00	3.56
Na2O	0.58	0.51	0.32	0.23	0.07	0.02	0.19	0.14	0.36	0.14	0.35	0.17	1.15
K2O	1.51	0.94	5.33	2.49	4.83	1.03	4.70	0.29	5.98	0.65	3.24	2.20	3.99
MnO	0.07	0.05	0.25	0.19	0.11	0.03	0.06	0.03	0.04	0.02	0.04	0.02	0.06
P2O5	0.10	0.11	0.08	0.15	0.15	0.05	0.09	0.02	0.04	0.02	0.02	0.02	0.11
LOI	5.52	1.63	4.48	0.88	3.62	0.73	4.64	0.30	4.47	0.71	2.47	0.97	-
TOTAL	99.65	0.72	99.55	0.91	99.19	0.94	99.67	0.40	100.11	0.56	98.03	0.88	100.53
Rb	71	50	226	112	193	39	162	11	200	23	118	83	125
Ba	369	231	461	200	639	165	446	49	260	65	460	139	636
Cs	3.6	4.1	8.5	4.6	5.2	1.1	6.4	0.8	2.7	0.4	1.9	0.4	5.2
Sr	54	51	29	13	21	11	50	11	25	5	14	1	142
Pb	20	8	12	4	10	1	29	14	13	6	13	5	-
Th	11	8	8.6	2.6	7.2	1.7	13	1	10	2	5.2	0.9	12
U	3.3	2.1	2.2	1.0	2.5	0.6	4.7	0.3	3.2	0.9	1.4	0.3	2.7
Sc	19	10	19	5	13	4	24	2	27	5	8.0	4.5	15
V	146	54	159	41	134	28	190	8	223	19	68	38	130
Cr	350	155	426	178	189	51	709	89	455	78	386	256	125
Co	29	25	21	12	17	4	19	4	19	8	10	6	26
Ni	264	261	100	42	88	6	144	16	149	20	74	42	58
Y	39	21	35	24	28	6	33	2	43	6	19	3	35
Zr	208	101	256	123	145	20	144	8	229	37	186	25	200
Nb	14	7	17	5	15	2	17	1	19	3	6.8	1.7	13
Hf	6.2	3.1	7.9	4.5	3.9	0.7	4.3	0.4	6.3	1.3	6.8	1.6	6.3
Ta	1.1	0.5	1.3	0.5	1.1	0.2	1.4	0.1	1.4	0.2	0.68	0.13	1.1
La	64	48	38	17	20	9	47	10	43	18	27	13	31
Ce	97	37	80	41	42	16	87	24	83	36	51	25	67
Sm	9.2	5.4	6.3	4.3	3.4	1.1	6.2	1.2	7.4	3.1	3.6	1.1	5.6
Eu	1.8	1.0	1.4	1.1	0.76	0.26	1.4	0.3	1.7	0.6	0.80	0.14	1.2
Tb	1.2	0.6	0.85	0.75	0.63	0.21	0.97	0.11	1.2	0.3	0.44	0.03	0.85
Yb	3.5	1.5	3.3	2.7	2.1	0.5	3.0	0.3	3.6	0.7	2.1	0.2	3.1
Lu	0.52	0.22	0.52	0.49	0.30	0.08	0.46	0.05	0.56	0.10	0.31	0.03	0.46

Table 2. continued

	(MPR)		(MWM)		(NUWM)		(NLWM)		(NMP)		(NVS)		NASC
	AVG	STD	AVG	STD	AVG	STD	AVG	STD	AVG	STD	AVG	STD	AVG
K2O/Na2O	4.6	4.9	38	42	73	23	33	15	19	7	9.2	3.2	3.5
SiO2/Al2O3	4.0	1.6	3.1	0.6	4.3	0.9	2.8	0.1	2.3	0.4	6.1	2.9	3.8
Th/U	3.2	0.5	4.3	1.0	3.0	0.5	2.7	0.1	3.2	0.5	3.7	0.7	4.4
K/Rb	165	64	181	56	208	9	241	3	248	6	231	6	265
Rb/Sr	5.8	6	9.0	8.0	11	4	3.4	0.8	8.1	1.6	8.7	6.7	0.88
Ba/Rb	11	11	2.5	1.1	3.3	0.4	2.7	0.2	1.3	0.3	5.0	1.6	5.1
Ba/Sr	22	15	19	12	38	17	9.3	1.9	11	4.0	33	12	4.5
Th/Sc	0.66	0.50	0.46	0.08	0.57	0.05	0.55	0.02	0.37	0.06	0.95	0.63	0.80
La/Sc	3.3	1.8	2.0	0.4	1.6	0.5	2.0	0.3	1.6	0.6	5.9	5.8	2.1
La/Th	7.2	5.6	4.4	0.7	2.8	0.7	3.6	0.6	4.2	1.5	5.0	2.0	2.6
Zr/Y	7.3	6.3	7.9	1.8	5.3	0.9	4.4	0.3	5.4	1.2	10	3	5.7
Ti/Zr	24	8	22	6	24	2	32	1	31	3	15	5	23
Zr/Nb	16	7	15	3	9.6	0.7	8.3	0.5	12	2	29	7	15
Ni/Co	11	7	5.8	2.7	5.7	2.3	8.0	1.8	11	11	7.8	1.2	2.2
Cr/V	2.8	1.8	2.8	1.2	1.4	0.3	3.8	0.5	2.0	0.3	5.4	2.9	0.96
V/Ni	1.1	1.0	2.1	1.8	1.5	0.3	1.3	0.2	1.5	0.3	0.60	0.42	2.2
Cr/Ni	1.9	0.8	4.5	1.8	2.1	0.5	5.0	0.7	3.1	0.6	4.9	2.2	2.2
Cr/Zr	2.2	1.4	2.0	0.9	1.3	0.3	5.0	0.7	2.0	0.3	1.9	1.2	0.63
Sc/Th	2.4	1.2	2.3	0.5	1.8	0.1	1.8	0.1	2.8	0.4	1.5	0.7	1.3
Co/Th	4.1	3.5	2.5	1.3	2.5	0.7	1.4	0.2	2.0	1.0	1.8	1.0	2.2
La/Yb	16	10	13	3	9.7	2.9	15	2	11	4	12	5	10
Eu/Eu*	0.68	0.13	0.67	0.18	0.64	0.04	0.69	0.03	0.70	0.06	0.74	0.06	0.66
CIA	87	5	77	7	75	2	79	1	78	1	77	7	69
n	9		18		6		11		16		3		

Major elements are reported in oxide weight percent; trace elements reported in ppm; Fe2O3T, total Fe reported as Fe2O3; Eu/Eu*, europium anomaly value calculated as Eu/Eu*=(Eu/.087)/(Abs.((Sm/..231)-(Abs.((Sm/.231)-(Tb/.058))/3))), where Abs. is "the absolute value of"; AVG, Mean anlytical value; STD, one standard deviation of the mean; n, number of samples; CIA,Chemical Index of Alteration (CIA=[Al2O3/(Al2O3+CaO+Na2O+K2O)]x100 using molecular values). Note: value corrected for carbonates and apatite as in Appendix C. NASC, North American Shale Composite (Gromet et al., 1984). Individual analyses in Appendix C.

Table 3. Average chemical composition and ratios of pelites from the Witwatersrand Supergroup and NASC

	West Rand Group						Central Rand Group				
	Parktown-Brixton Formations (PBR)		Promise Formation (PRM)		Roodepoort Formation (RO)		Booysens Formation (BOY)		K8 Pelites (K8)		NASC
	AVG	STD	AVG	STD	AVG	STD	AVG	STD	AVG	STD	AVG
SiO2	53.30	8.36	44.87	2.66	61.16	6.27	54.31	2.65	63.26	4.30	64.80
TiO2	0.40	0.12	0.32	0.04	0.73	0.24	0.67	0.12	0.83	0.17	0.78
Al2O3	10.58	2.60	9.73	1.08	15.13	4.00	18.61	2.27	23.61	4.24	16.90
Fe2O3-T	25.64	10.60	30.08	3.53	10.99	5.93	8.43	2.04	4.14	2.98	6.33
MgO	3.74	1.11	4.68	0.36	4.56	1.50	8.08	2.48	1.82	2.26	2.85
CaO	0.04	0.04	0.81	0.16	0.43	0.90	0.61	0.48	0.13	0.18	3.56
Na2O	0.12	0.07	0.24	0.14	0.52	1.24	0.71	0.60	0.59	0.61	1.15
K2O	0.86	0.52	1.48	0.14	1.70	1.22	2.09	1.05	1.87	1.11	3.99
MnO	0.28	0.26	2.42	1.44	0.13	0.27	0.08	0.05	0.04	0.06	0.06
P2O5	0.04	0.02	0.10	0.01	0.19	0.67	0.10	0.04	0.12	0.18	0.11
LOI	4.22	1.10	1.89	0.56	4.36	1.09	5.94	0.98	4.14	0.81	nd
TOTAL	99.20	0.84	97.76	0.73	99.91	0.74	99.58	0.53	100.34	0.37	100.53
Rb	43	26	116	4	70	49	83	40	69	39	125
Ba	140	61	440	137	337	149	444	184	338	182	636
Cs	2.6	2.5	10	4	7.7	4.8	5.0	2.4	4.0	2.6	5.2
Sr	8.4	4.5	27	5	34	38	73	39	100	91	142
Pb	5.8	3.9	5.2	2.3	14	5	14	4	20	6	nd
Th	3.9	1.7	3.5	0.5	5.5	0.8	4.7	0.9	9.8	2.9	12
U	1.7	1.5	0.66	0.06	1.7	0.6	1.6	0.4	4.3	1.9	2.7
Sc	13	3	13	2	25	4	27	5	24	5	15
V	106	22	98	8	174	20	183	27	189	45	130
Cr	484	116	431	56	959	607	1195	262	740	154	125
Co	25	4	29	5	45	14	59	13	52	27	26
Ni	280	126	265	19	330	35	529	108	418	211	58
Y	18	3	20	1	23	10	25	6	37	12	35
Zr	94	34	73	13	151	45	120	19	201	49	200
Nb	7.0	2.8	5.3	0.2	9.3	3.2	7.6	1.9	14	4	13
Hf	2.7	1.1	1.9	0.2	4.5	0.6	3.6	0.6	6.1	2.1	6.3
Ta	0.50	0.21	0.45	0.04	0.75	0.13	0.65	0.14	1.2	0.3	1.1
La	16	3	15	1	32	6	24	5	50	13	31
Ce	30	5	30	3	66	13	50	11	99	28	67
Sm	2.7	0.5	2.9	0.3	5.5	0.6	4.8	1.1	7.8	1.9	5.6
Eu	0.65	0.11	0.70	0.08	1.3	0.1	1.2	0.3	1.7	0.5	1.2
Tb	0.33	0.13	0.37	0.04	0.86	0.26	0.65	0.23	1.1	0.3	0.85
Yb	1.5	0.4	1.5	0.2	2.8	0.6	2.3	0.5	3.8	1.2	3.1
Lu	0.25	0.07	0.24	0.04	0.41	0.06	0.36	0.08	0.61	0.19	0.46

Table 3. continued

	(PBR)		(PRM)		(RO)		(BOY)		(K8)		NASC
	AVG	STD	AVG	STD	AVG	STD	AVG	STD	AVG	STD	AVG
K2O/Na2O	17	17	12	13	25	23	6.3	5.2	5.8	5.8	3.5
SiO2/Al2O3	5.2	0.9	4.7	0.4	4.4	1.5	3.0	0.5	2.9	1.2	3.8
Th/U	3.2	1.1	5.4	0.6	3.7	1.9	3.1	0.7	2.5	0.6	4.4
K/Rb	167	89	106	8	210	57	209	23	238	139	265
Rb/Sr	6.6	5.5	4.5	1.0	1.7	2.3	1.5	0.8	0.93	0.49	0.88
Ba/Rb	3.6	1.5	3.8	1.0	4.0	1.0	5.9	1.7	5.6	3.6	5.1
Ba/Sr	21	13	18	9	6.2	6.3	8.1	4.6	4.9	3.4	4.5
Th/Sc	0.29	0.06	0.28	0.04	0.22	0.04	0.19	0.07	0.43	0.13	0.80
La/Sc	1.2	0.1	1.2	0.1	1.3	0.2	0.94	0.36	2.1	0.5	2.1
La/Th	4.4	0.9	4.2	0.2	5.8	0.6	5.1	0.8	5.2	0.8	2.6
Zr/Y	5.1	1.5	3.6	0.4	7.1	2.6	5.2	2.0	5.8	2.1	5.7
Ti/Zr	26	2	27	1	30	11	34	6	26	6	23
Zr/Nb	10	4	6.4	0.8	18	7	18	5	18	5	15
Ni/Co	11	4	9.4	2.1	7.8	1.3	11	2	12	9	2.2
Cr/V	4.6	1.0	4.4	0.5	4.7	0.7	6.6	1.5	4.2	1.5	0.96
V/Ni	0.46	0.27	0.37	0.50	0.49	0.09	0.30	0.06	0.51	0.44	2.2
Cr/Ni	2.0	0.7	1.7	0.3	2.5	0.4	2.3	0.4	2.4	1.5	2.2
Cr/Zr	5.5	1.3	6.1	1.6	6.6	4.9	10	3	3.9	1.3	0.63
Sc/Th	3.6	0.6	3.6	0.4	4.6	0.9	5.8	1.4	2.6	0.9	1.3
Co/Th	6.3	2.9	8.4	1.1	8.2	1.9	13	4	6.0	3.3	2.2
La/Yb	11	2	9.8	0.3	12	3	10	3	14	4	10
Eu/Eu*	0.78	0.04	0.77	0.06	0.71	0.04	0.80	0.09	0.67	0.09	0.66
CIA	90	5	81	3	86	7	83	7	89	6	69
n	5		3		25		23		23		

Major elements are reported in oxide weight percent; trace elements reported in ppm; Fe2O3T, total Fe reported as Fe2O3; nd, none detected; Eu/Eu*, europium anomaly value calculated as Eu/Eu*=(Eu/.087)/(Abs.((Sm/.231)-(Abs.((Sm/.231)-(Tb/.058))/3))), where Abs. is the "absolute value of"; AVG, Mean analytical value; STD, one standard deviation of the mean; n, number of samples; CIA, Chemical Index of Alteration (CIA=[Al2O3/(Al2O3+CaO+Na2O+K2O)]x100 using molecular values). Note: value corrected for carbonates and apatite as in Appendix C. NASC, North American Shale Composite (Gromet et al., 1984). Individual analyses in Appendix C.

Witwatersrand pelites, unlike some published averages for Archean pelites (Ronov and Migdisov, 1971; Cameron and Garrels, 1980, Taylor and McLennan, 1985) do not exhibit K_2O/Na_2O ratios ≤ 1. This may reflect the fact that Archean pelite averages include chiefly pelites from greenstones rather than pelites from cratonic successions such as the Witwatersrand pelites.

Relative to NASC, most Witwatersrand pelites are depleted in CaO, Na_2O and K_2O and with the exception of the K8 pelites, also are depleted in TiO_2 and SiO_2. In addition, pelites from the PBR, RO and BOY Formations are enriched in MgO, Fe_2O_3T and MnO compared to NASC. BOY pelites and especially the K8 and OG pelites are strikingly enriched in Al_2O_3 compared to NASC and most Phanerozoic shales. Compositional changes of Witwatersrand pelites as a function of stratigraphic height indicate that the upper pelites (BOY, RO and K8) and the lowermost OG pelite are enriched in Na_2O, K_2O and Al_2O_3 and depleted in Fe_2O_3T, MgO (K8 pelites only) and MnO compared to the PBR and PRM pelites (Table 3).

In the Ventersdorp and Transvaal pelites, mean Bothaville (BOT), Selati (SEL) and Black Reef (BR) K_2O/Na_2O ratios and MgO and K_2O (except BOT) contents are greater, whereas concentrations of Na_2O and Al_2O_3 are lower than those of overlying Timeball Hill (TH), Strubenkop (STR), Silverton (SIL) formations and NASC (Fig. 14c; Table 4).

Table 4. Average chemical composition and ratios of pelites from the Ventersdorp and Transvaal Supergroups.

	Bothanville Formation (BOT)		Selati Formation (SEL)		Black Reef Formation (BR)		Timeball Hill Formaation (TH)		Strubenkop Formation (STR)		Silverton Formation (SIL)		NASC
	AVG	STD	AVG	STD	AVG	STD	AVG	STD	AVG	STD	AVG	STD	AVG
SiO2	63.64	7.30	59.86	10.54	53.84	13.85	59.36	7.15	57.89	4.49	61.18	4.43	64.80
TiO2	0.44	0.15	0.89	0.64	0.89	0.31	0.70	0.12	0.85	0.19	0.75	0.12	0.78
Al2O3	15.54	4.24	14.93	1.96	18.44	5.69	20.75	3.68	21.17	4.46	18.51	2.78	16.90
Fe2O3-T	6.29	2.08	10.88	9.48	7.45	6.35	8.52	4.48	12.18	5.71	7.48	2.18	6.33
MgO	4.98	1.04	3.71	1.91	4.44	2.87	1.78	0.54	1.35	0.21	2.74	1.43	2.85
CaO	1.25	1.36	0.60	0.95	2.02	5.16	0.70	0.72	0.20	0.08	0.66	1.24	3.56
Na2O	0.23	0.00	0.28	0.10	0.09	0.08	0.84	0.56	0.60	0.17	1.35	1.01	1.15
K2O	3.27	0.99	4.89	3.10	4.54	2.19	3.52	1.29	1.43	0.62	2.91	0.92	3.99
MnO	0.01	0.00	0.02	0.02	0.19	0.43	0.05	0.03	0.06	0.01	0.06	0.02	0.06
P2O5	0.12	0.03	0.19	0.15	0.14	0.06	0.19	0.22	0.14	0.06	0.08	0.06	0.11
LOI	4.57	0.25	3.81	2.09	7.49	7.01	4.23	1.01	4.12	0.73	4.15	1.58	-
TOTAL	100.31	0.24	100.06	1.27	99.53	0.71	100.63	0.89	99.99	0.87	99.88	0.59	100.53
Rb	127	41	125	83	126	59	177	47	71	29	154	50	125
Ba	476	118	699	370	293	131	674	244	588	443	544	303	636
Cs	5.5	2.0	5.9	5.7	5.5	3.8	14	8	7.3	2.7	8.9	3.7	5.2
Sr	61	61	24	9	27	18	127	68	86	21	83	35	142
Pb	27	11	9.0	1.7	15	5	34	19	20	2	21	7	-
Th	6.2	2.5	5.7	1.3	5.6	1.8	22	6	20	3	16	5	12
U	1.7	0.7	2.1	0.7	2.1	0.7	7.2	5.4	6.0	1.1	3.9	1.5	2.7
Sc	18	6	18	8	24	8	18	5	24	5	23	6	15
V	117	31	169	105	205	69	151	36	189	40	154	46	130
Cr	579	180	447	533	421	147	140	40	174	37	141	55	125
Co	41	15	17	12	39	32	21	17	29	3	18	11	26
Ni	266	81	142	151	327	223	57	20	90	22	66	27	58
Y	27	11	32	11	30	9	32	13	36	6	29	8	35
Zr	124	49	178	92	157	36	170	48	234	69	150	64	200
Nb	6.0	3.6	10	6	7.8	1.9	15	5	18	4	13	4	13
Hf	3.8	1.7	5.1	2.1	4.4	1.0	4.9	1.6	7.1	2.1	4.5	1.9	6.3
Ta	0.72	0.33	0.86	0.29	0.72	0.19	1.6	0.3	1.3	0.4	1.2	0.4	1.1
La	38	23	19	9	29	11	56	25	49	14	36	18	31
Ce	76	45	40	23	57	22	101	42	106	30	56	37	67
Sm	4.6	2.2	3.8	2.1	5.2	1.7	7.5	3.5	7.6	1.9	5.4	2.2	5.6
Eu	0.81	0.38	0.97	0.54	1.2	0.4	1.5	0.6	1.6	0.3	1.1	0.3	1.2
Tb	0.51	0.25	0.57	0.44	0.67	0.23	1.1	0.5	1.0	0.2	0.79	0.28	0.85
Yb	2.0	0.9	2.5	1.1	2.4	0.7	3.1	0.9	3.5	0.2	2.5	0.7	3.1
Lu	0.31	0.13	0.40	0.17	0.38	0.12	0.47	0.14	0.53	0.04	0.39	0.12	0.46

Table 4. continued

	(BOT)		(SEL)		(BR)		(TH)		(STR)		(SIL)		NASC
	AVG	STD	AVG	STD	AVG	STD	AVG	STD	AVG	STD	AVG	STD	AVG
K20/Na20	14	4	17	11	143	206	5.6	3.4	2.4	0.7	4.3	3.9	3.5
Si02/Al203	4.8	2.5	4.1	1.1	3.7	3.6	3.0	1.0	2.9	0.8	3.4	0.7	3.8
Th/U	3.6	0.2	3.0	0.9	2.7	0.5	3.8	1.3	3.4	0.4	4.4	0.9	4.4
K/Rb	214	200	276	141	297	46	165	35	164	15	166	36	265
Rb/Sr	4.4	2.4	4.5	2.8	6.3	3.6	1.7	0.8	0.80	0.18	2.4	1.7	0.88
Ba/Sr	16	9	27	11	14	7	6.5	4.3	7.9	7.9	7.9	6.8	4.5
Ba/Rb	3.9	0.5	9.2	10.4	2.7	1.4	4.2	3.6	11	12	4.5	3.7	5.1
La/Sc	2.0	1.2	1.1	0.4	1.3	0.4	3.1	1.2	2.1	0.5	1.7	1.0	2.1
La/Th	5.9	3.5	3.5	1.2	5.2	0.9	2.5	1.0	2.4	0.5	2.2	0.7	2.6
Zr/Y	4.7	0.5	5.5	1.5	5.5	1.6	6.2	2.8	6.6	1.9	5.1	1.6	5.7
Ti/Zr	22	3	29	8	33	10	26	6	23	5	33	9	23
Zr/Nb	37	30	18	5	21	6	12	6	13	3	11	3	15
Ni/Co	6.7	1.1	9.4	7.3	11	9	4.1	3.6	3.1	0.7	4.8	3.7	2.2
Cr/V	5.0	0.7	2.7	2.0	2.4	1.5	0.94	0.22	0.93	0.13	0.94	0.26	0.96
V/Ni	0.45	0.05	2.0	1.7	0.82	0.43	2.9	1.0	2.2	0.6	3.0	2.3	2.2
Cr/Ni	2.2	2.2	3.0	0.7	1.3	0.7	2.5	2.0	1.9	1.7	2.1	2.0	2.2
Cr/Zr	5.3	1.7	4.2	6.4	2.7	0.8	0.87	0.30	0.86	0.42	1.1	0.7	0.63
Sc/Th	2.9	2.4	3.1	1.3	4.6	1.9	0.82	0.83	1.2	1.7	1.4	1.2	1.3
Co/Th	6.9	0.6	2.9	2.0	9.0	13.5	1.0	0.8	1.5	0.2	1.5	1.7	2.2
La/Yb	20	15	7.7	2.7	12	3	18	7	14	4	14	4	10
Eu/Eu*	0.61	0.10	0.82	0.20	0.72	0.11	0.66	0.16	0.65	0.03	0.62	0.09	0.66
CIA	79	1	75	15	79	6	78	6	89	3	75	8	69
n	4		7		16		46		5		24		

Major elements are reported in oxide weight percent; trace elements reported in ppm; Fe203T, total Fe reported as Fe203; Eu/Eu*, europium anomaly value calculated as Eu/Eu*=(Eu/.087)/(Abs.((Sm/.231)-(Abs.((Sm/.231)-(Tb/.058))/3))), where Abs. is "the absolute value of"; AVG, Mean anlytical value; STD, one standard deviation of the mean; n, number of samples; CIA,Chemical Index of Alteration (CIA=[Al203/(Al203+CaO+Na20+K20)]x100 using molecular values). Note: value corrected for carbonates and apatite as in Appendix C. NASC, North American Shale Composite (Gromet et al., 1984). Individual analyses in Appendix C.

BOT-SEL-BR K_2O/Na_2O distributions are similar to those of Pongola and West Rand Group pelites (RO-PRM-PBR formations; Figs. 14a, 14b). Relative to NASC, TH-STR-SIL pelites generally show an enrichment of Fe_2O_3T and Al_2O_3, and a depletion of CaO, MgO, K_2O and SiO_2. These pelites have mean Na_2O and CaO concentrations that are greater than or equal to those of pelites from the Pongola Supergroup (Table 2), and lower than pelites from the Moodies and Beit Bridge Groups (Taylor and McLennan, 1985; Taylor et al., 1986; Condie and Boryta, 1989).

Major element contents of the single Waterberg shale sample analyzed are similar to NASC except for greater K_2O and lower MgO, CaO and Na_2O concentrations (Table 5). Shales from the Soutpansberg Group have major element contents which are quite variable, with mean concentrations showing enrichments of TiO_2 and Al_2O_3 and depletions of SiO_2, MgO, CaO, Na_2O_3, and K_2O relative to NASC. Low mean concentrations of K_2O in some Soutpansberg shales are surprising considering the arkosic nature of Waterberg sandstones. However, both K_2O contents of shales and K-feldspar concentrations of sandstones are noted to increase stratigraphically upsection within the Soutpansberg Group.

The single Waterberg shale sample is enriched in K_2O and depleted in MgO and CaO relative to most Pongola-Witwatersrand-Ventersdorp-Transvaal pelites. Soutpansberg

Table 5. Average chemical composition and ratios of pelites from the Waterberg and Soutpansberg Groups.

	Soutpansberg Group		Waterberg Group
Sample	AVG	STD	C 90
SiO2	55.75	14.62	62.76
TiO2	1.23	0.25	0.75
Al2O3	25.24	12.80	18.55
Fe2O3-T	5.59	5.32	7.33
MgO	1.14	1.40	1.24
CaO	0.31	0.45	0.02
Na2O	0.50	0.54	0.44
K2O	1.85	1.98	6.08
MnO	0.04	0.03	0.03
P2O5	0.20	0.09	0.05
LOI	8.44	5.99	2.96
TOTAL	100.27	0.28	100.21
Rb	71	75	415
Ba	613	337	904
Cs	2.0	0.8	14
Sr	196	166	30
Pb	34	25	19
Th	18	7	18
U	5.2	1.8	4.3
Sc	21	10	18
V	190	73	110
Cr	106	40	176
Co	10	11	6.8
Ni	48	32	31
Y	38	15	36
Zr	279	37	201
Nb	21	11	18
Hf	7.5	0.9	5.5
Ta	1.6	0.8	1.4
La	48	20	66
Ce	107	72	125
Sm	11	7	7.9
Eu	2.3	1.1	1.8
Tb	1.5	0.7	1.3
Yb	3.5	1.1	3.4
Lu	0.50	0.12	0.49

Table 5. Continued

	Soutpansberg Group		Waterberg Group
Sample	AVG	STD	C 90
K2O/Na2O	3.5	2.5	14
SiO2/Al2O3	4.1	4.2	3.4
Th/U	3.6	0.8	4.2
K/Rb	188	43	122
Rb/Sr	6.7	9.8	14
Ba/Rb	25	21	2.2
Ba/Sr	34	47	30
Th/Sc	1.1	0.4	1.0
La/Sc	2.5	1.0	3.7
La/Th	2.8	1.3	3.7
Zr/Y	9.5	5.8	5.6
Ti/Zr	27	7	22
Zr/Nb	22	18	11
Ni/Co	7.2	3.9	4.6
Cr/V	0.67	0.31	1.6
V/Ni	6.7	6.2	3.5
Cr/Ni	2.6	0.7	5.7
Cr/Zr	0.40	0.20	0.88
Sc/Th	1.3	1.0	1.0
Co/Th	0.80	0.99	0.38
La/Yb	13	4	19
Eu/Eu*	0.66	0.06	0.68
CIA	85	17	72
n	4		1

Major elements are reported in oxide weight percent; trace elements reported in ppm; Fe2O3T, total Fe reported as Fe2O3; Eu/Eu*, europium anomaly value calculated as Eu/Eu*= (Eu/.087)/(Abs.((Sm/.231)-(Abs.((Sm/.231)-(Tb/.058))/3))), where Abs. is "the absolute value of"; AVG, Mean analytical value; STD, one standard deviation of the mean; n, number of samples; CIA, Chemical Index of Alteration (CIA=[Al2O3/(Al2O3+CaO+Na2O+K2O)]x100 using molecular values). Note: value corrected for carbonates and apatite as in appendix C. NASC, North American Shale Composite (Gromet et al., 1984).

shales have higher mean TiO2, Al2O3 and P2O5 contents and lower Fe2O3T and MgO contents relative to older Kaapvaal craton sediments (Table 5).

Large-Ion Lithophile Elements (LILE)

Compared to NASC, Pongola pelites have similar or greater concentrations of K, U and Rb (Table 2). Ba and Th contents are equivalent to or slightly less than those of NASC, whereas Sr is strongly depleted in Pongola samples. With the exception of MWM and NLWM pelites, Cs contents are similar to, or lower than NASC concentrations, and Th/U, Th/Sc, and K/Rb ratios in Pongola pelites are generally greater than those of NASC.

LILE in most Pongola pelites are enriched relative to pelites from the Witwatersrand (~2.8 Ga) and the Beit Bridge (~3.3 Ga) successions in South Africa (Table 3; Taylor et al., 1986; Condie and Boryta, 1989). Relative to pelites from the Moodies Group (~3.2 Ga; McLennan et al., 1983), Pongola pelites have greater concentrations of Th and U; however, most other LILE concentrations are similar in the two successions.

A great deal of variability exists in the contents of LILE from Witwatersrand pelites (Table 3), due perhaps to the mobility of these elements during weathering, diagenesis and low-grade metamorphism. Compared to NASC and most Phanerozoic shales, Witwatersrand pelites are depleted in K,

Rb, Ba, and Sr and, with the exception of the OG and K8 pelites (and BOY pelites for Pb only), also in Th, U and Pb. It is noteworthy that the relative enrichment of K, Th, U and Pb in the upper three pelites parallels an enrichment in U and Au in stratigraphically equivalent quartzites and conglomerates (Feather and Koen, 1975). K8 pelites also exhibit a dramatic increase in both Th and U relative to underlying Witwatersrand units. Compared to NASC, Witwatersrand pelites exhibit lower K/Rb and Th/Sc ratios and higher Ba/Sr and Rb/Sr ratios (Table 3). Th/U ratios are also low in the PBR, BOY, and K8 pelites. The OG, BOY and K8 pelites are enriched in K, Sr and Pb and have lower Rb/Sr and higher Ba/Rb ratios than other Witwatersrand pelites. OG and K8 pelites also are strongly enriched in Th and U relative to other Witwatersrand pelites. Relative to Pongola sediments, Witwatersrand pelites are slightly enriched in Cs, whereas BOY and K8 pelites are enriched in Sr. Most Witwatersrand pelites are depleted in K, Rb, Th and U (except K8-Th and U) relative to the Pongola sequence.

With few exceptions, mean LILE (Rb, Ba, Cs, Sr, Pb, Th, U) contents of TH-STR-SIL pelites are greater and K/Rb, Rb/Sr and Ba/Sr ratios are lower than those of BOT-SEL-BR pelites. Relative to NASC, TH-STR-SIL pelites are enriched, and BOT-SEL-BR pelites are depleted in Th and U, whereas all Ventersdorp-Transvaal pelites have similar or lower mean Sr and Ba contents as well as Th/U and K/Rb ratios. Except

for K and Rb, most TH-STR-SIL pelites are enriched in LILE relative to the Beit Bridge, Moodies, Pongola and Witwatersrand sequences (Tables 2-4; Taylor and McLennan, 1985; Taylor et al., 1986; Condie and Boryta, 1989). Th, U, Pb and Ba contents of TH-STR-SIL pelites are notably enriched relative to older Kaapvaal craton pelites. Compared to the Witwatersrand, TH-STR-SIL pelites are enriched in Ba and Th, and have U contents which are similar to those of Witwatersrand-K8 pelites. Th and U contents of BOT-SEL-BR pelites are similar or lower than those of the Beit Bridge, Moodies, Pongola and Witwatersrand pelites. BOT-SEL-BR pelites have K and Rb contents which are similar to those of the Pongola and enriched relative to the Witwatersrand pelites.

Rb, Ba and Cs contents of Waterberg shales are greater than those of NASC, whereas NASC concentrations of these elements are typically greater than those of the Soutpansberg Group (Table 5). Th and U contents of both Waterberg and Soutpansberg shales are enriched relative to NASC, and similar to those characterizing the Transvaal-Pretoria Group (TH-STR-SIL) and Witwatersrand-K8 pelites (Tables 3 and 4). Similarly, LILE contents from the Waterberg Group are generally greater than previously deposited Kaapvaal craton pelites. Soutpansberg shales are enriched in Ba, Sr and Pb relative to older Kaapvaal pelites. Waterberg and Soutpansberg Th/U ratios are

similar, whereas K/Rb ratios are typically lower than those characteristic of NASC.

Rare Earth Elements (REE)

Although REE distributions in Pongola pelites are somewhat variable, overall features are similar to those of NASC (Table 2, Fig. 15). Light-REE range from 50-170 x chondrite and heavy-REE from 8-15 x chondrite. Except for NVS pelites, negative Eu anomalies (Eu/Eu* = 0.64-0.70) have similar mean values as NASC (Eu/Eu* = 0.66), while light-REE enrichments (La/Yb = 9.7-16) are similar to, or greater than NASC (La/Yb = 10). Prominent negative Eu anomalies, light-REE enrichment, and high REE contents of the Pongola pelites are similar to the K8 (Eu/Eu* = 0.67) and Roodepoort pelites (Eu/Eu* = 0.71) of the upper Witwatersrand Supergroup, and pelites from the Beit Bridge Group (Eu/Eu* = 0.69), while they contrast sharply with REE distributions in the Moodies (Eu/Eu* = 0.92) and lower Witwatersrand successions (Eu/Eu* = 0.78; Table 3; McLennan et al., 1983; Condie and Boryta, 1989).

REE distributions in Witwatersrand pelites are also variable, although chondrite-normalized patterns are parallel for the various pelite units (Fig. 16). Light-REE range from 40-200 x chondrite and heavy-REE from 6-20 x chondrite. All of the pelites have small to moderate negative Eu anomalies (Eu/Eu* = 0.67-0.80). Pelites of the

Figure 15. Chondrite-normalized REE distributions in pelites and quartzites from the Pongola Supergroup. Lines represent mean values for sediments from the Mozaan (upper diagram) and Nsuze Groups (lower diagram). MPR, Mozaan Piet Retief pelites; MWM, Mozaan Wit-Mfolozi pelites; MQ, Mozaan quartzites; NMP, Nsuze Mpongoza River pelites; NLWM, Nsuze Lower Wit-Mfolozi pelites; NUWM, Nsuze Upper Wit-Mfolozi pelites; NVS, Nsuze Vitshundi pelites; NQ, Nsuze quartzites. Ce value for MPR pelites calculated assuming no Ce depletion (see weathering discussion p. 101). Shown for comparison is the REE distribution of NASC, North American Shale Composite (from Gromet et al., 1984).

Figure 16. (following page) Chondrite-normalized REE distributions in pelites from the Witwatersrand Supergroup arranged in ascending stratigraphic order. Lines represent mean values and stippled areas represent ranges of one sigma variation. Eu/Eu*, europium anomaly; n, number of samples used to calculate mean. Shown for comparison is the REE distribution of NASC, North American Shale Composite (Gromet et al., 1984).

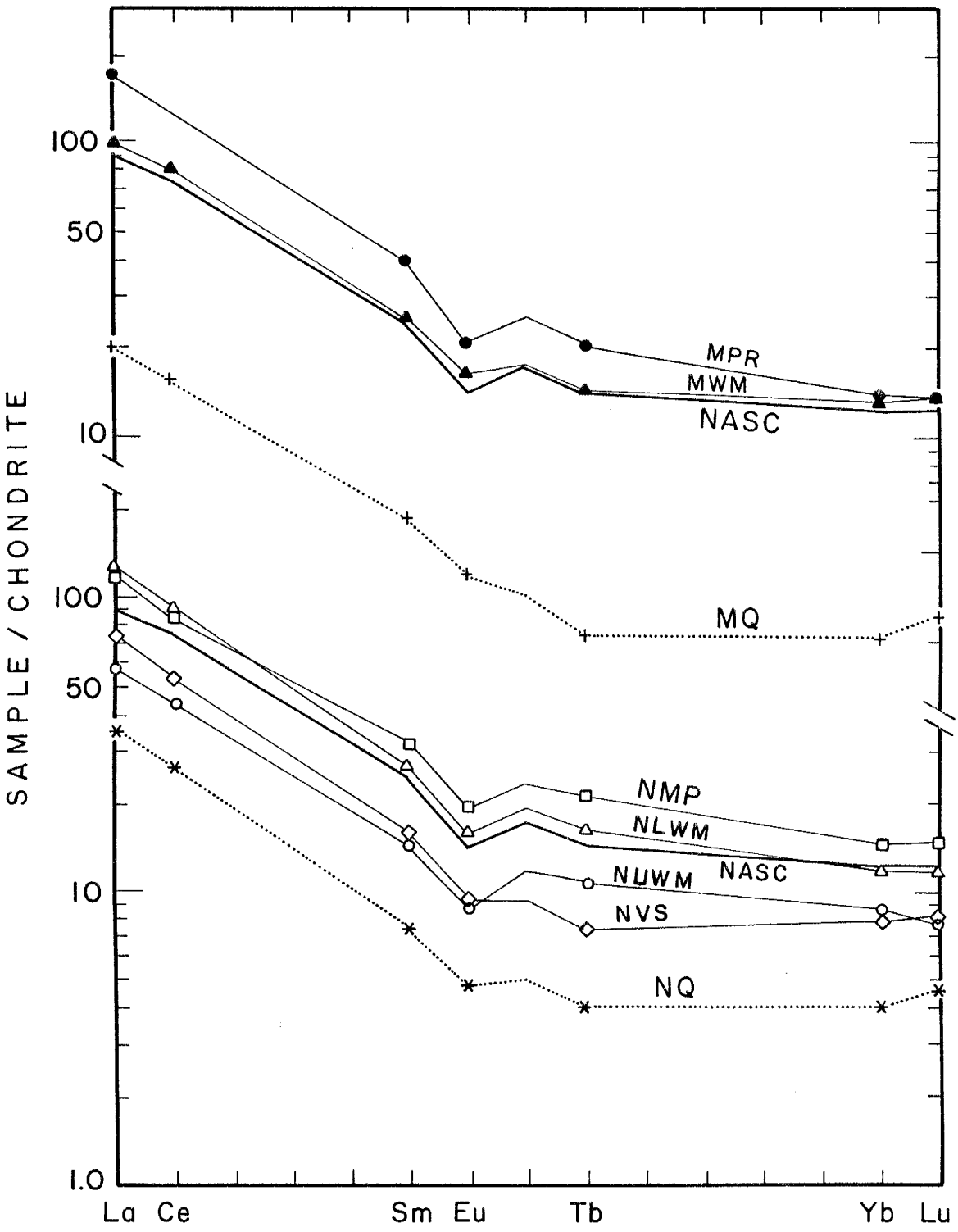
100
50
10
100
50
10
1.0
SAMPLE / CHONDRITE
MPR
MWM
NASC
MQ
NMP
NLWM
NUWM
NASC
NVS
NQ
La
Ce
Sm
Eu
Tb
Yb
Lu

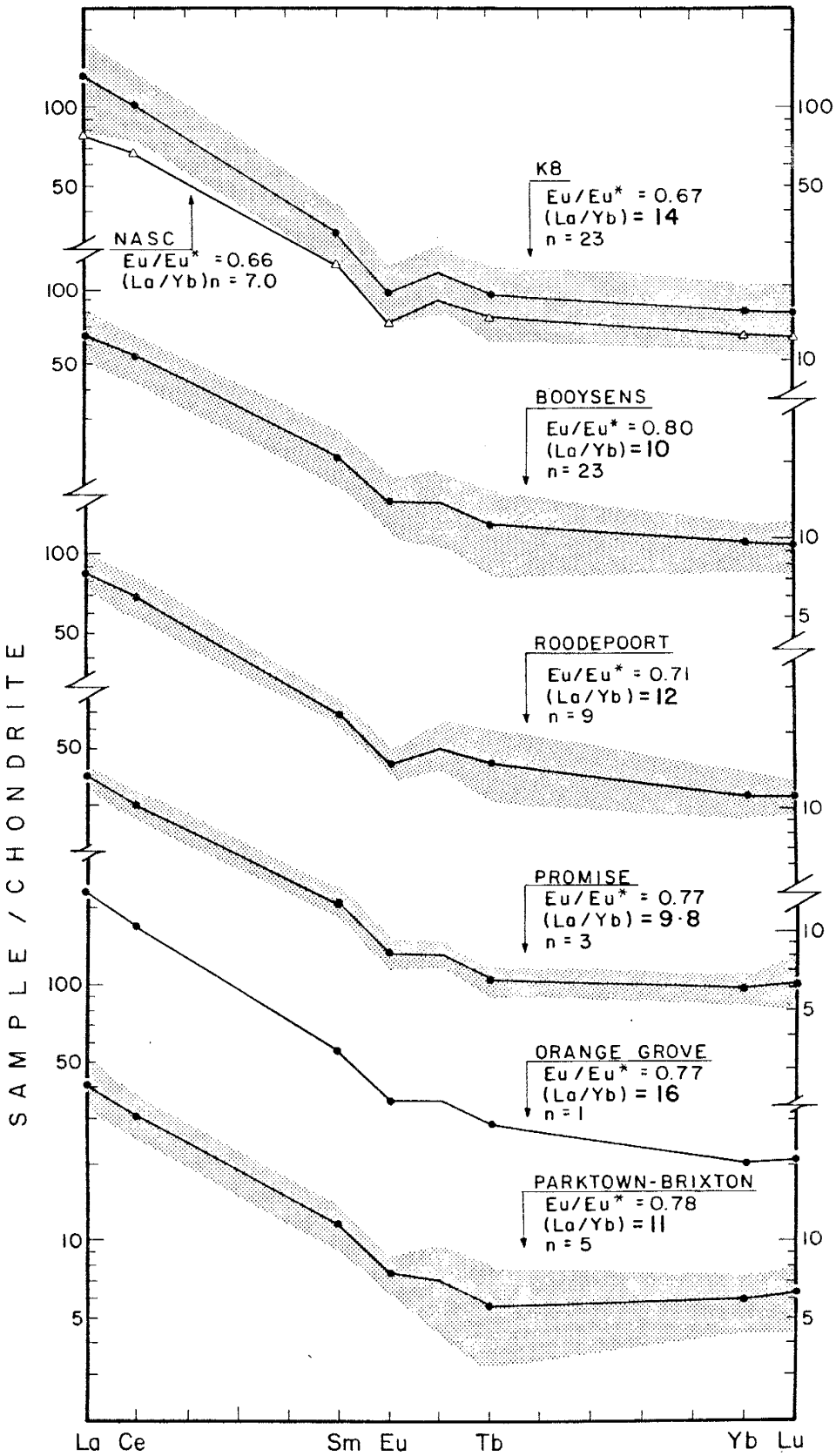
SAMPLE / CHONDRITE
100
50
10
5
K8
Eu/Eu* = 0.67
(La/Yb) = 14
n = 23
NASC
Eu/Eu* = 0.66
(La/Yb)n = 7.0
BOOYSENS
Eu/Eu* = 0.80
(La/Yb) = 10
n = 23
ROODEPOORT
Eu/Eu* = 0.71
(La/Yb) = 12
n = 9
PROMISE
Eu/Eu* = 0.77
(La/Yb) = 9·8
n = 3
ORANGE GROVE
Eu/Eu* = 0.77
(La/Yb) = 16
n = 1
PARKTOWN-BRIXTON
Eu/Eu* = 0.78
(La/Yb) = 11
n = 5
La Ce Sm Eu Tb Yb Lu

PBR, PRM and BOY units are depleted in all REE relative to NASC. Only the OG, RO and K8 pelites have both absolute and relative REE distributions (including a significant negative Eu anomaly) similar to NASC and other Phanerozoic shales (Fig. 16, Table 3). On the whole, Witwatersrand pelites show an increase in total REE content with stratigraphic height. The PBR and PRM pelites have mean light-REE contents of 40 x, RO and BOY pelites 70 x, and K8 pelites 150 x chondrite. The only exception to this systematic increase in REE is the one sample from the OG pelite at the base of the West Rand Group, which has a light-REE content of 200 x chondrite (Fig. 16).

With the exception of the OG and K8 units, Witwatersrand pelites exhibit total REE distributions which are similar to the Fig Tree and Moodies Groups ($\gtrsim$3.2 Ga) of southern Africa. Witwatersrand pelites differ from these older units by possessing relatively large negative Eu anomalies. Pelites from the Witwatersrand-RO and K8 units have negative Eu anomalies which are similar to those of the Pongola Supergroup (Tables 2 and 3), while La/Yb ratios of all Witwatersrand pelites are similar to those of the Pongola sequence.

Eu/Eu* ratios (0.61) from the Ventersdorp-BOT pelites are similar to those of NASC (0.66), while within the Transvaal Supergroup, mean Eu/Eu* ratios progressively decrease upsection in the SEL (0.85), BR (0.73), and

Figure 17. Chondrite-normalized REE distributions in pelites from the Ventersdorp and Transvaal Supergroups arranged in ascending stratigraphic order. Lines represent mean values and stippled areas represent ranges of one sigma variation. Eu/Eu*, europium anomaly; n, number of samples used to calculate mean. Shown for comparison is the REE distribution of NASC, North American Shale Composite (Gromet et al., 1984).

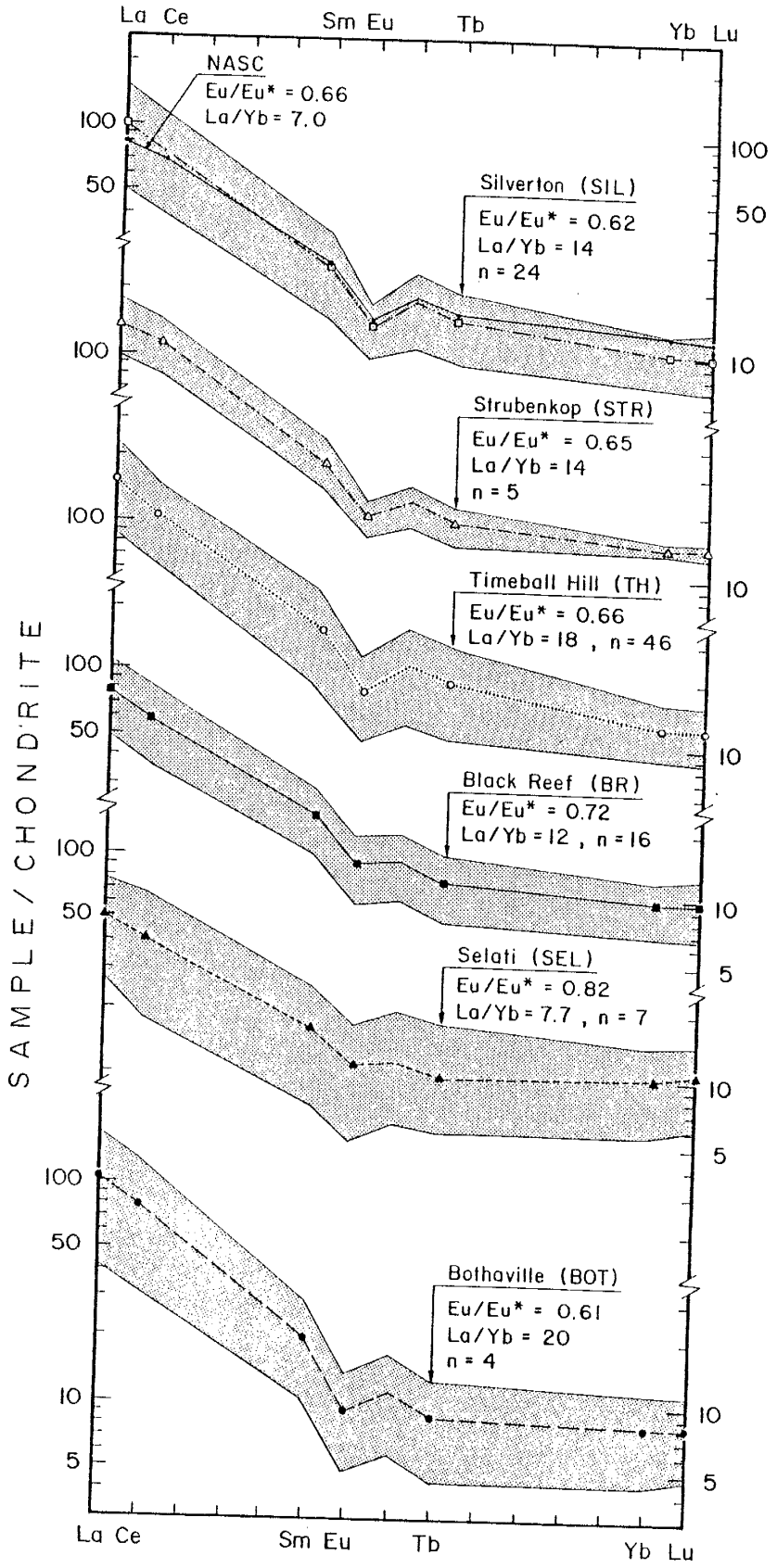
La Ce
Sm Eu
Tb
Yb Lu
NASC
Eu/Eu* = 0.66
La/Yb = 7.0
Silverton (SIL)
Eu/Eu* = 0.62
La/Yb = 14
n = 24
Strubenkop (STR)
Eu/Eu* = 0.65
La/Yb = 14
n = 5
Timeball Hill (TH)
Eu/Eu* = 0.66
La/Yb = 18 , n = 46
Black Reef (BR)
Eu/Eu* = 0.72
La/Yb = 12 , n = 16
Selati (SEL)
Eu/Eu* = 0.82
La/Yb = 7.7 , n = 7
Bothaville (BOT)
Eu/Eu* = 0.61
La/Yb = 20
n = 4
SAMPLE / CHONDRITE

pretoria Group (average for 3 formations $\approx$0.65; Fig. 17). Light-REE contents of BOT-TH-STR-SIL pelites are greater than those of NASC and SEL-BR pelites, whereas heavy-REE contents of TH-STR-SIL pelites are similar to NASC and greater than BOT-SEL-BR pelites (Table 4). Ventersdorp-Transvaal light-REE contents range from 45-150 x chondrite and heavy-REE from 8-14 x chondrite (Fig. 17). SEL-BR pelites have mean La/Yb ratios of 7.1 and 12, respectively, whereas TH-STR-SIL pelites have mean La/Yb ratios ranging from 14 to 18. La/Yb ratios of all Ventersdorp- Transvaal pelites (except SEL) are greater than those of NASC.

BOT-TH-STR-SIL mean light-REE contents and La/Yb ratios are greater than or equal to, and Eu/Eu* ratios less than or equal to those of most southern African Archean platform pelites (Tables 2 and 3; Taylor and McLennan, 1985; Taylor et al., 1986; Condie and Boryta, 1989). Light-REE contents and La/Yb ratios of SEL-BR pelites are similar to or less than, and Eu/Eu* ratios are similar or greater than those of Archean platform pelites from southern Africa. Heavy-REE contents of TH-STR-SIL pelites are similar to or greater than those of the Beit Bridge, Moodies, Pongola and Witwatersrand pelites, whereas BOT-SEL-BR heavy-REE contents are less than those of the Beit Bridge, Pongola and upper Witwatersrand, and greater than than those of the Moodies and lower Witwatersrand pelites.

Light-REE contents of both the Waterberg and

Soutpansberg shales exceed those of NASC and most Archean southern Africa pelite assemblages, whereas heavy-REE tend to be similar to NASC. Light-REE contents range from 50-200 x chondrite and heavy-REE range from 7-19 x chondrite (Fig. 18). Both the Waterberg and Soutpansberg shales have Eu/Eu* ratios which are similar to NASC, Pongola, Witwatersrand-K8, Ventersdorp-BOT and Transvaal-Pretoria Group ratios (Table 5). Mean La/Yb ratios of Soutpansberg shales are similar to NASC, whereas the La/Yb ratio of the single Waterberg shale sample is similar to that of Ventersdorp-BOT pelites and greater than that of NASC and most other southern African pelite assemblages examined in this study.

High Field Strength Elements (HFSE)

Pongola pelites show local geographic variations in the distribution of HFSE (Y, Zr, Ti, Nb, Hf and Ta). MWM, MPR and NMP pelites have HFSE contents that are equivalent to or greater then those of NASC, whereas NVS pelites have HFSE contents that are consistently lower than NASC (Table 2). NUWM and NLWM pelites have variable HFSE contents that are slightly depleted in Y, Zr, Ti and Hf and slightly enriched in Ta and Nb relative to NASC. Compared to average Archean upper-continental crust (Taylor and McLennan, 1985) and most Archean pelites from quartzite-pelite associations, Pongola pelites are strongly enriched in Y, Zr, Nb, Ta and Hf. Mozaan pelites have Ti/Zr and Zr/Nb ratios similar to,

Figure 18. Chondrite-normalized REE distributions in shales from the Waterberg and Soutpansberg Groups. Lines represent mean values for sediments. Eu/Eu*, europium anomaly; n, number of samples. Shown for comparison is the REE distribution of NASC, North American Shale Composite (from Gromet et al., 1984).

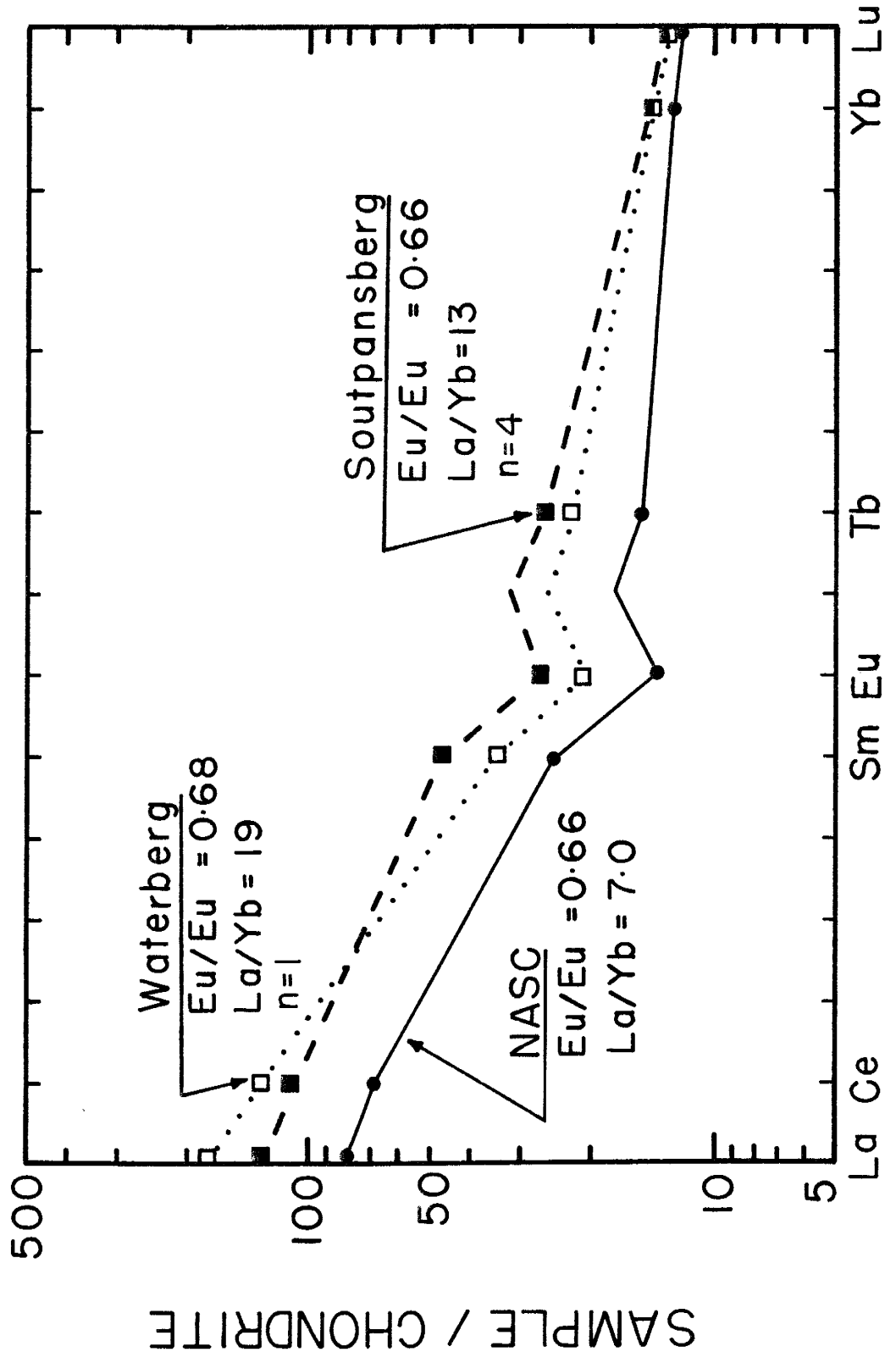
Waterberg
Eu/Eu =0·68
La/Yb = 19
n=1
Soutpansberg
Eu/Eu =0·66
La/Yb=13
n=4
NASC
Eu/Eu =0·66
La/Yb = 7·0
500
100
50
10
5
La Ce
Sm Eu
Tb
Yb Lu
SAMPLE / CHONDRITE

and Zr/Y ratios greater than NASC. Except for the NVS section, Nsuze pelites have Zr/Y and Zr/Nb ratios that are less than or equal to, and Ti/Zr ratios that are greater than or equal to NASC.

With the exception of the OG and K8 units, pelites from the Witwatersrand sequence have concentrations of HFSE (Y, Zr, Ti, Nb, Hf, Ta) that are lower than NASC and most other Phanerozoic pelites (Table 3). OG and K8 pelite HFSE contents are similar to NASC. Ti/Zr, Zr/Y and Zr/Nb ratios of Witwatersrand pelites are comparable those of Phanerozoic shales. With the exception of the single OG pelite sample, there is a tendency for contents of HFSE to increase with stratigraphic height with the greatest concentrations occurring in the K8 pelites. Zr/Nb ratios also show an overall increase in the upper three subgroups. Witwaters-rand pelites are typically depleted in most HFSE relative to Pongola pelites, although the HFSE concentrations of K8 pelites are often similar to those of Pongola pelites (Tables 2 and 3).

Concentrations of Zr, Hf, Nb and Ta are greater in TH-STR-SIL pelites, relative to BOT-SEL-BR pelites (except SIL Zr-Hf contents; Table 4). Contents of Y are similar between most Ventersdorp-Transvaal pelites and NASC, whereas Zr and Hf contents of Ventersdorp-Transvaal pelites (except STR) are less than those of NASC. NASC Nb and Ta contents are less than those of TH-STR-SIL and greater than those of

BOT-SEL-BR pelites. TH-STR-BR Ti contents are similar to, and BOT contents are depleted relative to NASC.

HFSE contents of TH-STR-SIL pelites are similar or enriched relative to pelites from the Beit Bridge, Moodies, Pongola and Witwatersrand pelites (except for Y and Nb in K8 pelites; Tables 2-4; Taylor and McLennan, 1985; Taylor et al., 1986; Condie and Boryta, 1989), whereas BOT-SEL-BR pelites have similar or depleted HFSE contents relative to the above listed southern Africa Archean platform pelites.

HFSE contents of Waterberg shales are similar to, whereas Soutpansberg concentrations slightly exceed those of NASC (Table 5). An exception to this trend is the Ta and Nb contents of Waterberg and Soutpansberg shales which are enriched 30-60% relative to NASC. These shales have overall HFSE contents which are similar to Witwatersrand-K8 and Pongola pelites. Waterberg Zr/Y and Ti/Zr ratios are similar to those of NASC, whereas Soutpansberg Zr/Y, Ti/Zr and Zr/Nb ratios exceed those of NASC.

Transition Metals

High Ni and Cr concentrations in Archean pelites were first documented by Danchin (1967) and McLennan et al. (1983). Pongola pelites show a 250-350% enrichment in Ni and Cr, relative to post-Archean shales (Fig. 19), while these elements are depleted 35-50% relative to pelites from the Witwatersrand, Fig Tree and Moodies Groups (Tables 2 and

Figure 19. Distribution of Ni and Cr in pelites and quartzites from the Pongola Supergroup. Early Archean, late Archean and post-Archean pelite fields after Taylor and McLennan (1985).

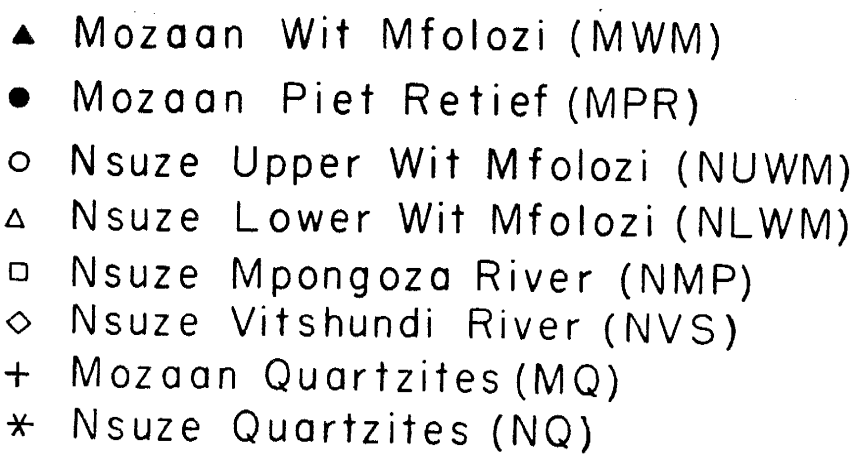

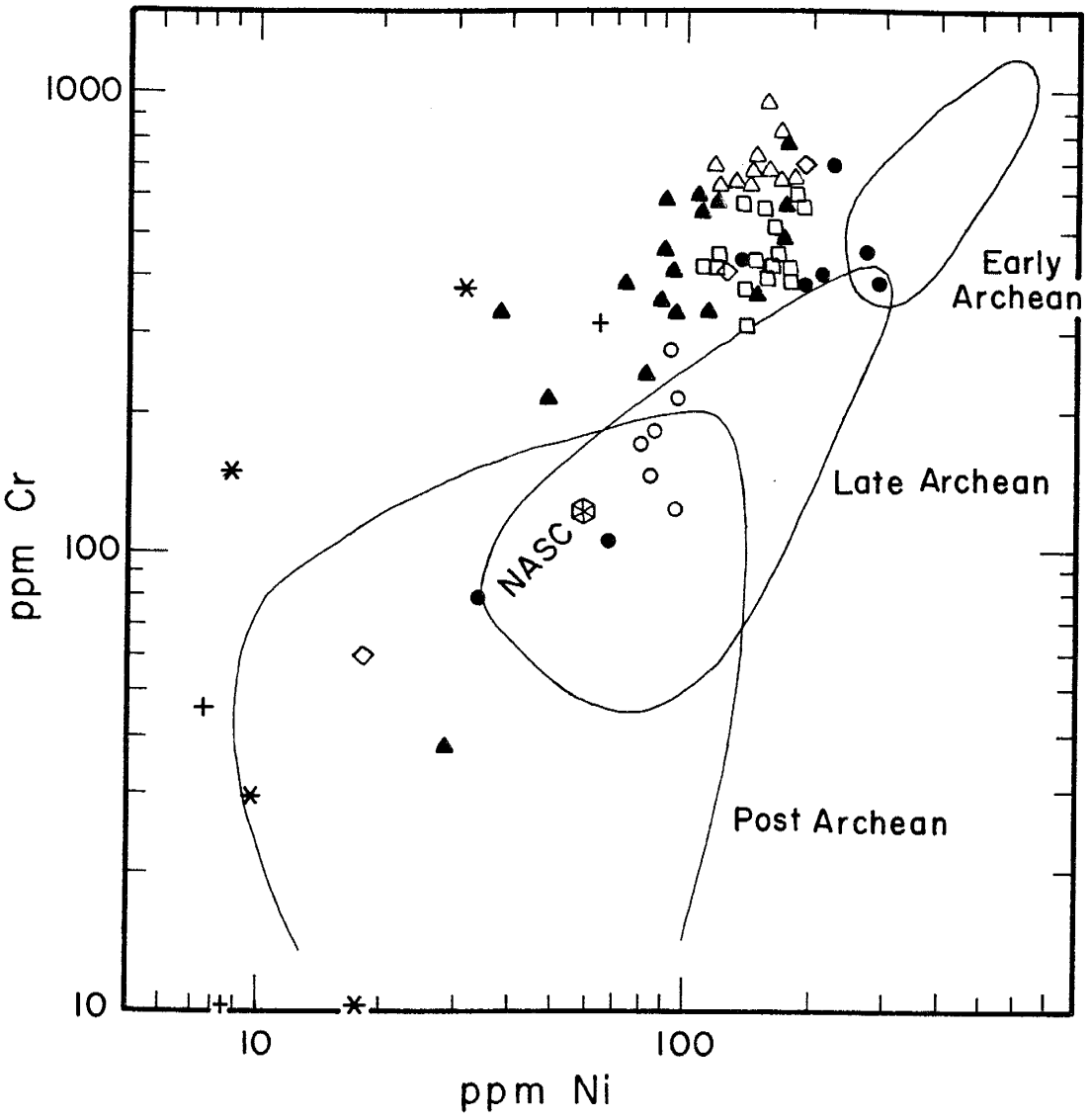
1000
100
10
ppm Cr
10
100
ppm Ni
Early
Archean
Late Archean
Post Archean
NASC

3; McLennan et al., 1983). Assertions that Nsuze pelites have higher Mg, Cr, Ni and V contents relative to the Mozaan pelites (McLennan et al., 1983) are not substantiated when a sufficiently large sample population is examined, as is the case with the present study. Ni and Cr contents in Pongola pelites are similar to those reported for Archean pelites from southwest Montana, USA and from the Beit Bridge Group in South Africa (Gibbs et al., 1986; Condie and Boryta, 1989). Most Pongola samples differ from other Archean pelites in having high Cr/Ni ratios (Table 2; Fig. 19) and positive Cr anomalies on NASC-normalized diagrams (Fig. 28).

In contrast to Ni and Cr, Sc and V contents of Pongola pelites are generally equivalent to or slightly greater than those of NASC, whereas Co and Mg are generally depleted relative to Phanerozoic shales (Table 2). Ni/Co, Cr/V and Cr/Zr ratios are greater than NASC ratios and lower than corresponding ratios in Witwatersrand, Fig Tree and Moodies pelites (Table 3; McLennan et al., 1983). V/Ni ratios are less than those of NASC, but greater than those of southern African pelite sequences mentioned above. Co/Th ratios are highest in MPR, MWM and NUWU pelites, while NLWM, NMP and NVS pelites have lower Co/Th ratios, which are also less than NASC ratios.

Witwatersrand pelites are also greatly enriched in Ni and Cr relative to Phanerozoic shales (Table 3, Fig. 20).

Figure 20. Distribution of Ni and Cr in pelites from the Witwatersrand Supergroup. Early Archean, late Archean and post-Archean pelite fields after data from Taylor and McLennan (1985).

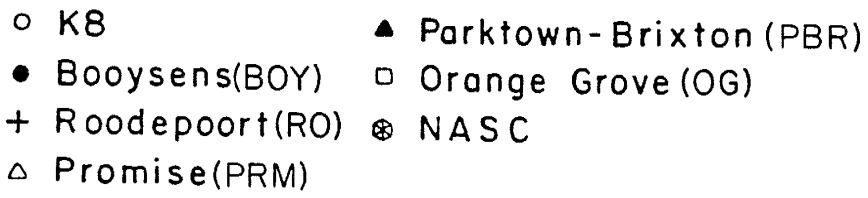

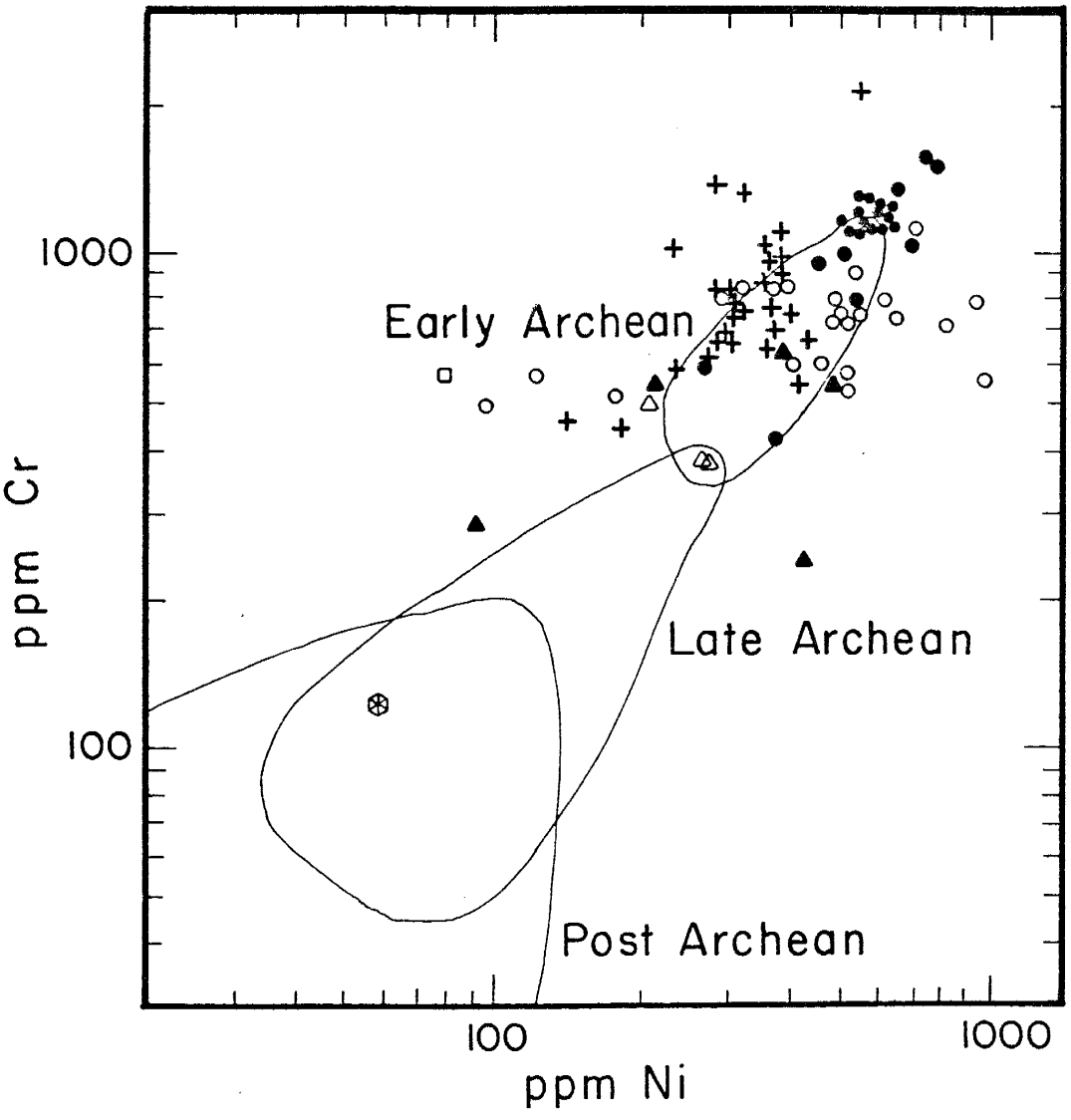
1000
100
ppm Cr
Early Archean
Late Archean
Post Archean
100
1000
ppm Ni

In addition, Witwatersrand pelites exhibit much higher Ni/Co and Cr/V ratios and lower V/Ni ratios than Phanerozoic shales. V contents are comparable to those of Phanerozoic shales, while compared to NASC, Sc and Co are enriched only in RO, BOY and K8 pelites. RO-BOY-K8 pelites are also enriched in all transition metals relative to PBR-PRM pelites (Table 3). Cr, Ni, Sc and Co contents reach maximum values in the BOY pelites, paralleling similar changes in MgO contents of these pelites. Witwatersrand pelites have Sc and V concentrations which are similar to those of the Pongola pelites. Cr concentrations of Central Rand Group pelites, as well as Co and Ni contents of all Witwatersrand pelites are enriched relative to Pongola pelites. Cr/Ni ratios of Witwatersrand pelites (1.7-2.5) are generally lower than those of the Pongola sequence (1.9-5.0).

BOT-BR pelites have Ni and Cr contents which are greater than those of TH-STR-SIL pelites and NASC, and similar to most other early Archean pelites. TH-STR-SIL Ni-Cr contents are similar to typical post-Archean pelites and shales, whereas SEL pelites are intermediate between Archean and post-Archean pelites (Fig. 21). Co contents are greatest for the BOT-BR-STR pelites, while Sc and V contents are similar in most Transvaal and Ventersdorp pelites. All Ventersdorp-Transvaal pelites (except BOT) have higher concentrations of Sc and V relative to NASC, while Co contents are enriched relative to NASC for only the

Figure 21. Distribution of Ni and Cr in pelites from the Ventersdorp and Transvaal Supergroups. Early Archean, late Archean and post-Archean pelite fields after data from Taylor and McLennan (1985).

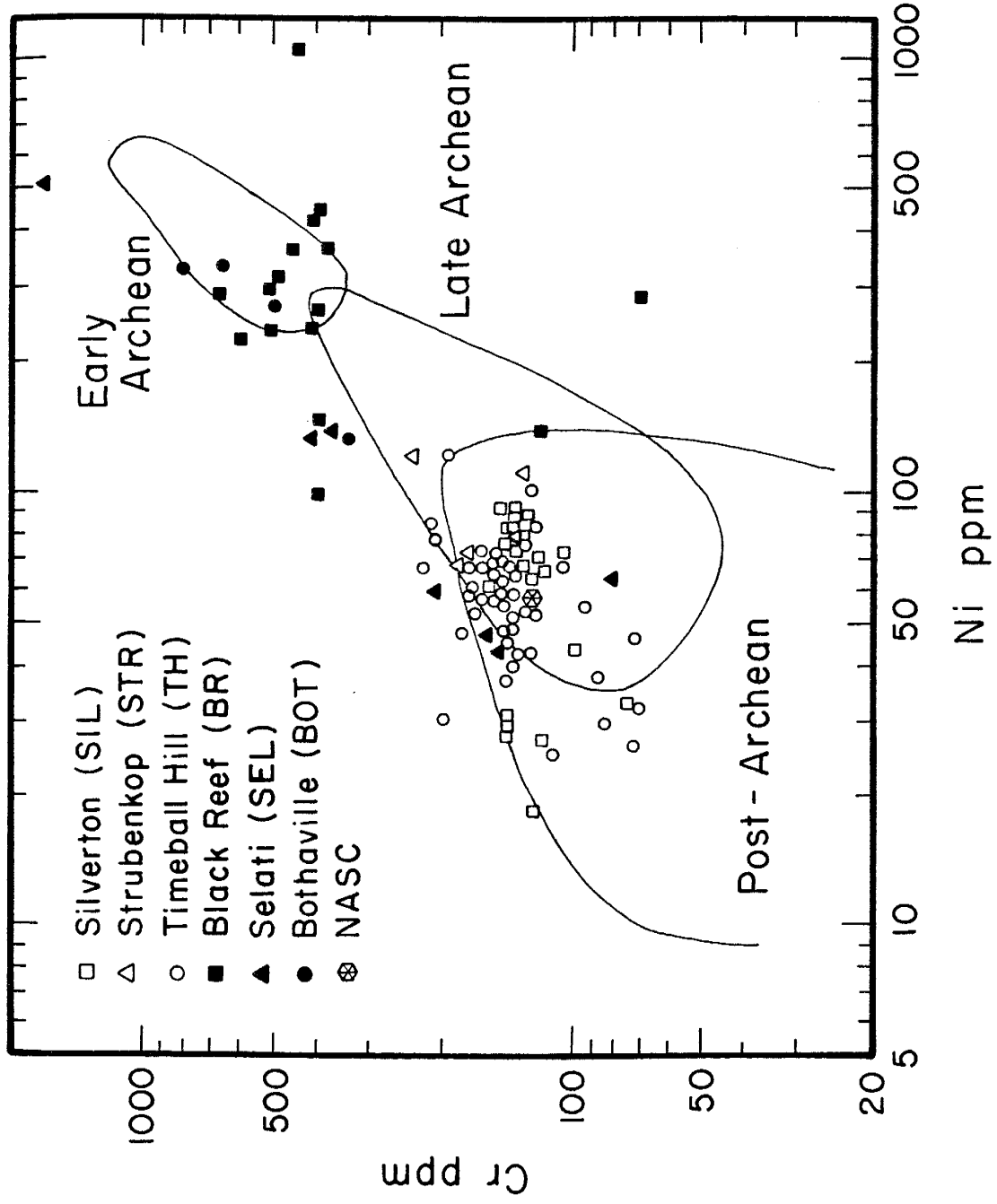
Silverton (SIL)
Strubenkop (STR)
Timeball Hill (TH)
Black Reef (BR)
Selati (SEL)
Bothaville (BOT)
NASC
Early Archean
Late Archean
Post-Archean
Cr ppm
Ni ppm
1000
500
100
50
20
5
10
50
100
500
1000

BOT-BR-STR pelites. Cr and Ni contents of TH-STR-SIL pelites are lower than those of the Pongola and Witwatersrand pelites (Tables 2-4).

Transition metal contents of most Waterberg and Soutpansberg shales are similar to or slightly less than those of NASC. Exceptions to this trend are elevated Sc and V contents of Soutpansberg and elevated Cr contents of Waterberg shales. Soutpansberg Cr and Ni contents are similar to those of NASC and the Transvaal-Pretoria Group pelites and less than those which typify most southern Africa Archean platform assemblage pelites (Fig. 22).

Figure 22. Distribution of Ni and Cr in pelites from the Waterberg and Soutpansberg Groups. Early Archean, late Archean and post-Archean pelite fields after data from Taylor and McLennan (1985).

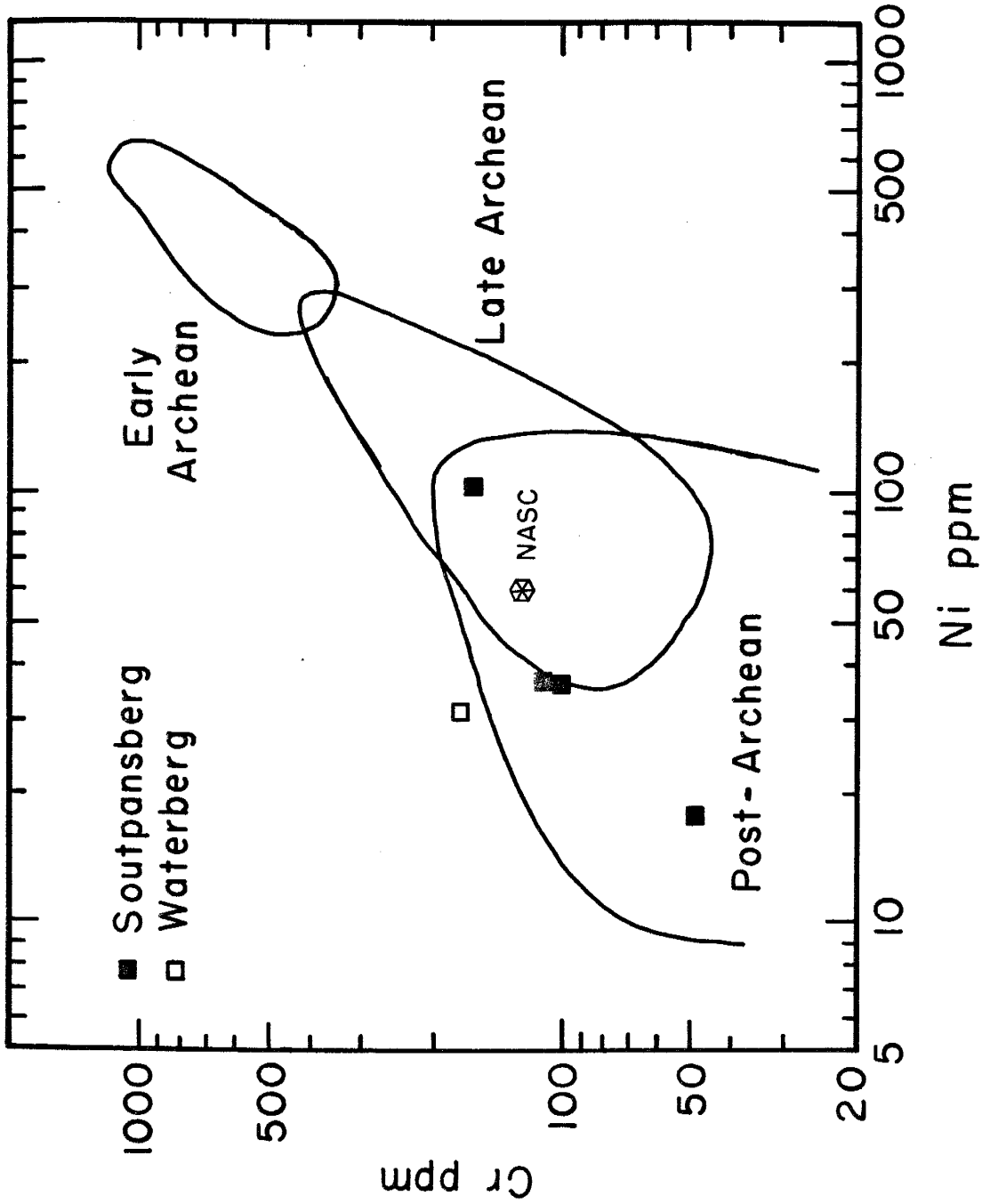
Soutpansberg
Waterberg
Early Archean
Late Archean
Post-Archean
NASC
Cr ppm
Ni ppm
1000
500
100
50
20
5
10
50
100
500
1000

QUARTZITE RESULTS

PETROGRAPHY AND DETRITAL MODES

Quartzites from the Pongola Supergroup are metamorphosed equivalents of quartz arenites, quartzwackes and subarkosic to arkosic wackes using the classification system and nomenclature of Pettijohn et al. (1973).* Although metamorphism has recrystallized the clay matrix of most quartzites examined, most detrital framework grains are still identifiable in thin section. Nsuze and Mozaan quartzites exhibit similar mineralogies, being dominated by monocrystalline quartz, with lesser polycrystalline quartz, K-feldspar, and trace amounts of muscovite, zircon, plagioclase, chlorite, magnetite, sedimentary-lithic and volcanic-lithic fragments (Table 6, Appendix E.1-2). Mozaan quartzites are typically enriched in detrital K-feldspar (including sericitic epimatrix) relative to Nsuze quartzites. Orthomatrix, composed principally of sericite and chlorite, comprises 8% of Nsuze and 2-30% of Mozaan quartzite matrices. Petrographic identification of up to 15% K-feldspar in Mozaan quartzites from the Wit-Mfolozi and Piet Retief areas is significant, in that this is the first reported occurrence of detrital feldspar in the Mozaan sequence (Table 6).

* The term ''quartzite'' is used as a field description which defines arenaceous sediments that fracture through, rather than around constituent grains. Quartzite is not intended to imply any specific mineralogic composition other than a sedimentary rock dominated by quartz.

Table 6. Framework grain mineralogies of Kaapvaal craton quartzites

Unit	Sample	Qt	Ft	L	Qm
Soutpansberg					
Nzhelele	C 188	67.9	20.8	10.6	45.9
Nzhelele	C 177	90.2	9.8	0	77.3
Ngwandzi	C 184	65.3	32.5	2.2	52.1
Musekwa	C 160	100	0	0	98.2
Mutshindi	C 124	99.3	0	0.7	88.3
Waterberg					
Vaalwater	C 100	81.6	17.9	0.5	72.7
Cleremont	C 99	99.3	0.7	0	99.1
Sandrvsbg.	C 98	100	0	0	100
Skilpadkop	C 96	99.6	0.2	0.2	68.2
Swaershoek	C 89	100	0	0	75.6
Transvaal					
Rayton	C 56	100	0	0	97.7
Silverton	C 207	92.9	6.5	0	92.7
Daspoort	MSF-2-10	99.5	0	0.5	95.1
Timeball	C 15	99.8	0	0	97.8
Rooihgoote	C 76	100	0	0	100
Black Reef	C 201	100	0	0	100
Black Reef	D 34	100	0	0	96.6
Selati	D 35	74.0	25.8	0	63.7
Sekororo	D 46	88.9	0.5	10.6	72.3
Godwan	D 53	100	0	0	99.3
Ventersdorp					
Bothaville	C 6	88.6	0	11.5	62.2
Witwatersrand					
VCR	JWS-8-40	97.4	0	2.6	79.9
Mondoer	C 73	99.4	0	0.6	89.0
Elsburg	D 8	99.2	0	0.8	59.8
Marisberg	C 74	99.1	0	0.9	80.8
Government	D 21	99.3	0	0.7	82.1
Brixton	C 70	99.3	0	0.7	91.8
Orange Grv.	D 15	100	0	0	100
Orange Grv.	C 67	100	0	0	98.8
Dominion	BSF-1-18	67.7	32.3	0	57.3
	BBS-3-19	80.3	19.7	0	53.0
Pongola					
Mozaan	P 33	84.0	15.2	0.7	82.1
Mozaan	P 45	97.4	2.6	0	92.2
Mozaan	P 63	100	0	0	98.5
Nsuze	P 4	99.9	0.2	0	92.5
Nsuze	P 7	100	0	0	100
Nsuze	P 12	86.7	13.3	0	83.6
Nsuze	P 26	99.5	0	0.5	94.5

Abbreviated column headings given in Table E.1-1; individual point count results in Table E.1-2; petrographic descriptions of individual samples given in Appendix E.2; All values in percent

Lt	K	P	Qp	Ls	Lv	Orthomatrix
33.3	19.4	1.4	22.0	10.6	0.7	15.2
12.9	9.0	0.8	12.9	0	0	7.5
15.5	31.9	0.6	13.2	0.3	1.9	39.2
1.8	0	0	1.8	0	0	8.2
11.7	0	0	11.1	0.2	0.4	15.4
9.4	14.0	3.9	8.9	0.5	0	36.4
28.6	0.7	0	28.6	0	0	22.0
25.8	0	0	25.8	0	0	29.8
31.6	0.2	0	31.4	0	0.2	14.7
24.4	0	0	24.4	0	0	29.0
2.3	0	0	2.3	0	0	2.5
0.2	6.5	0	0.2	0	0	0.4
4.9	0	0	4.4	0	0.5	14.9
2.0	0	0	2.0	0	0	8.0
0	0	0	0	0	0	0
0	0	0	0	0	0	17.2
3.4	0	0	3.4	0	0	6.3
10.3	25.8	0	10.3	0	0	34.6
27.2	0.5	0	16.6	0.2	10.4	40.7
0.7	0	0	0.7	0	0	9.2
37.9	0	0	26.4	5.2	6.3	50.5
20.1	0	0	17.6	1.2	1.4	55.2
10.8	0	0	10.2	0.6	0	1.7
40.2	0	0	39.5	0.8	0	30.2
19.2	0	0	18.3	0.6	0.2	10.4
17.9	0	0	17.2	0.7	0	39.7
7.6	0	0	6.9	0	0.7	7.1
0	0	0	0	0	0	2.9
1.0	0	0	1.0	0	0	1.7
10.4	30.8	1.4	10.4	0	0	29.8
27.3	19.7	0	27.3	0	0	8.2
2.6	14.7	0.5	1.9	0.7	0	42.3
5.2	2.4	0.2	5.2	0	0	2.2
1.5	0	0	1.5	0	0	5.8
7.2	0	0.2	7.2	0	0	18.4
0	0	0	0	0	0	7.5
3.1	13.3	0	3.1	0	0	2.6
5.5	0	0	5.0	0	0.5	7.3

Quartzites from the Dominion Group are predominantly composed of monocrystalline quartz, K-feldspar and polycrystalline quartz with an average of 16% orthomatrix material (Table 6). These metaquartzites may be classified as arkosic wackes and subarkoses. Trace amounts of plagioclase, zircon, muscovite, chlorite, authigenic calcite and tremolite, as well as granitic clasts containing quartz, biotite, muscovite and K-feldspar also occur in these sediments. Quartzites from the Witwatersrand Supergroup vary from mature quartz arenite to quartzwacke with detrital feldspars conspicuously absent (Table 6). Framework grains of West Rand Group quartzites are dominated by monocrystalline quartz, with lesser polycrystalline quartz and traces of volcanic-lithic, sedimentary-lithic, muscovite and zircon grains. Quartzites from the Central Rand Group are dominated by monocrystalline and polycrystalline quartz, with minor sedimentary-lithics and trace amounts of muscovite, volcanic-lithics, sphene and hornblende (Ventersdorp Contact Reef only). In the West Rand Group samples examined, orthomatrix contents increase stratigraphically upwards from 2.7% in the Orange Grove, to 6.6% for Brixton, and 28% for Government Reef quartzites. Overlying Central Rand Group quartzite orthomatrix contents also are highly variable, but unlike their West Rand Group counterparts, do not show any systematic variation with

stratigraphic height (Appendix F). Mondeor and Maraisburg quartzites are the most texturally mature, with 1.6 and 10% orthomatrix content respectively. Elsburg and VCR quartzites are more immature, with 23 and 36% orthomatrix, respectively.

Detrital minerals indicate that quartzites from the Ventersdorp-Bothaville and Wolkberg (Selati and Sekororo Formations) are metamorphic equivalents of lithic greywackes, while Black Reef, Gondwan and Pretoria Group samples are quartzwackes and quartz arenites. Framework grain detrital modes for Bothaville quartzites are dominated by subangular monocrystalline and polycrystalline quartz with lesser porphyritic mafic-volcanic and sedimentary- lithics and minor magnetite (Table 6, Appendix F). Quartzites from the Selati Formation contain an abundance of monocrystalline quartz, lesser K-feldspar, polycrystalline quartz and volcanic-lithic clasts, as well as trace amounts of muscovite, chlorite, sedimentary-lithics and zircon. Quartzites from the Black Reef Formation and Pretoria Group are composed mostly of well-rounded monocrystalline quartz, with minor polycrystalline quartz, and trace amounts of zircon, K-feldspar and muscovite. Overall patterns suggest that Bothaville and Selati quartzites are enriched in polycrystalline quartz and lithic fragments relative to overlying Pretoria quartzites. Granitic detritus in

Silverton Formation quartzites contains quartz encapsulated muscovite, biotite and K-feldspar crystals. Sericite and chlorite matrix contents of Ventersdorp-Transvaal quartzites examined in this study show progressive stratigraphic decreases upsection (Bothaville, 36%; Selati, 22%; Black Reef, 10%; and Pretoria Group quartzites, 5%). Matrix for the Bothaville quartzites is enriched in silt-sized quartz grains relative to Transvaal quartzite samples. These grains show evidence of sedimentary layering and are interpreted to be detrital in origin.

Arenaceous Waterberg Group sediments are quartzwackes and arkosic wackes whereas arenites from the Soutpansburg Group exhibit varied compositions ranging from arkosic wacke, quartzwacke, subarkose and quartz arenite. Both the Waterberg and Soutpansberg samples are dominated by well-rounded monocrystalline and polycrystalline quartz grains (Table 6, Appendix F). Soutpansberg samples also contain abundant detrital K-feldspar (12%), whereas Waterberg samples are characterized by minor K-feldspar concentrations (3%). Both sequences also contain minor plagioclase, sedimentary-lithic, volcanic-lithic, muscovite, chlorite and zircon framework grains. Orthomatrix contents for the Waterberg and Soutpansberg units average 21 and 17% respectively.

GEOCHEMISTRY

Major and trace element contents of individual Pongola quartzites are highly variable (Table 7), yet, mean values for the Nsuze and Mozaan Groups are similar. In comparison to Phanerozoic passive-margin sandstones (Hirst, 1962; Cullers et al., 1979; Bhatia, 1983; Bhatia and Crook, 1986), Pongola quartzites are enriched in Ni and Cr, and depleted in TiO2, Sr, Th, V, Nb, Ta, Zr and Hf. SiO2/Al2O3, K2O/Na2O, La/Yb (13-19) and Eu/Eu* ratios ($\sim$0.78) are also generally greater than those of Phanerozoic sandstones (La/Yb=8-12; Eu/Eu*$\approx$0.63). Pongola quartzites have low Sc, V, Ni, Y, Nb, Ta, Hf and REE contents relative to associated Pongola pelites. Individual quartzite samples with the greatest matrix proportions are generally also enriched in U, Sc, Co, Zr, Hf and light-REE, whereas samples with high proportions of K-feldspar tend to be enriched in K2O, Rb, Sr, Ba and Cs.

Quartzites from the Dominion and Witwatersrand sequences also exhibit a great deal of compositional variability (Table 8). Relative to Phanerozoic passive-margin sandstones, Dominion samples are enriched in Al2O3, Rb, Ba, Ni and light-REE, and depleted in TiO2, V, Zr, Nb and Ta. Witwatersrand quartzites are enriched in TiO2, Cr, Ni and Co, and depleted in Rb, Ba, Sr, Zr, Hf, Nb and Ta relative to Phanerozoic sandstones. Dominion quartzites

Table 7. Individual analyses of quartzites from the Pongola Supergroup.

	Nsuze Group				Nsuze Group			
Sample	P 4	P 7	P 12	P 26	P 33	P 40	P 45	P 63
SiO2	91.54	95.80	86.82	94.98	78.61	93.69	92.75	95.55
TiO2	0.12	0.05	0.01	0.05	0.20	0.03	0.10	0.01
Al2O3	4.08	2.35	6.70	2.96	10.74	4.68	2.71	2.06
Fe2O3-T	1.30	0.70	2.05	0.60	1.82	0.68	1.23	0.59
MgO	0.79	0.84	1.15	0.37	1.89	0.24	0.56	0.47
CaO	0.03	0.04	0.12	0.04	0.40	0.03	0.02	0.01
Na2O	0.13	0.21	0.00	0.00	0.99	0.00	0.37	0.18
K2O	0.94	0.24	2.54	0.35	3.42	0.00	0.37	0.11
MnO	0.00	0.00	0.00	0.00	0.07	0.00	0.01	0.00
P2O5	0.01	0.00	0.03	0.00	0.01	0.00	0.01	0.00
LOI	0.45	0.15	0.93	0.26	2.03	0.50	0.59	0.21
TOTAL	99.39	100.38	100.35	99.61	100.18	99.83	98.72	99.19
Rb	30	4.7	73	7.5	102	0.0	6.1	0.0
Ba	84	62	470	54	328	27	105	31
Cs	1.2	0.31	2.6	0.37	3.7	0.15	0.29	0.09
Sr	7.9	6.2	19	7.9	46	11	9.3	8.0
Pb	15	11	13	10	13	10	12	135
Th	6.8	1.1	1.9	4.4	3.7	3.3	1.5	0.92
U	3.7	0.46	0.96	0.95	0.98	0.88	0.49	0.46
Sc	2.4	0.69	1.0	0.73	2.5	0.92	1.5	0.32
V	9.4	5.0	2.5	0.00	16	0.00	10.0	0.00
Cr	378	149	9.5	29	96	46	319	10
Co	14	0.35	4.1	1.2	10	0.71	9.0	0.33
Ni	30	8.6	17	9.7	32	7.6	61	8.6
Y	13	3.5	12	8.1	10	5.4	4.8	3.4
Zr	278	58	45	73	199	72	62	34
Nb	4.8	3.7	4.1	4.2	5.1	4.3	3.8	3.5
Hf	10	2.1	1.3	2.5	5.5	2.4	1.9	0.96
Ta	0.58	0.09	0.22	0.35	0.43	0.36	0.16	0.60
La	23	5.7	13	11	24	9.4	8.5	5.2
Ce	45	12	22	22	40	19	17	10
Sm	2.6	0.86	1.9	1.6	2.0	1.5	1.3	0.90
Eu	0.64	0.24	0.44	0.32	0.50	0.37	0.32	0.19
Tb	0.36	0.09	0.25	0.24	0.16	0.15	0.12	0.10
Yb	1.7	0.38	0.97	1.1	0.83	0.64	0.55	0.35
Lu	0.30	0.07	0.16	0.19	0.14	0.10	0.10	0.08

Major elements are reported in oxide weight percent; trace elements reported in ppm; Fe2O3T, total Fe reported as Fe2O3; nd, none detected.

Table 8. Individual analyses of quartzites from the Dominion Group and Witwatersrand Supergroup.

	Dominion Group		Orange Grove Formation		Brixton Formation		Govt. Fm.	Marsbg. Fm.	Elsburg Fm.	VCR
Sample	BBS-3-19	BSF-1-18	C 67	D 15	C 70	C 73	D 21	C 74	D 8	JWS-8-40
SiO2	88.17	81.43	95.54	96.26	95.42	96.31	80.42	93.58	87.75	84.64
TiO2	0.05	0.07	0.02	0.00	0.01	0.01	9.03	0.05	0.15	0.21
Al2O3	5.40	9.28	1.83	1.93	2.25	1.75	6.49	3.15	7.16	3.83
Fe2O3-T	0.98	1.48	0.55	0.61	0.63	0.77	0.48	0.62	1.24	0.91
MgO	0.54	0.77	0.51	0.20	0.62	0.05	0.50	0.27	0.60	0.11
CaO	0.10	0.07	0.00	0.02	0.01	0.02	0.03	0.00	0.03	0.03
Na2O	0.25	1.01	0.24	0.00	0.24	0.00	0.00	0.15	0.38	0.40
K2O	3.21	4.33	0.11	0.12	0.28	0.09	1.02	0.29	1.54	0.88
MnO	0.00	0.01	0.00	0.00	0.00	0.00	0.14	0.00	0.00	0.00
P2O5	0.00	0.01	0.00	0.00	0.00	0.00	0.03	0.00	0.01	0.01
LOI	0.48	0.84	0.11	0.10	0.25	0.19	2.77	0.37	1.20	1.78
TOTAL	99.17	99.29	98.90	99.24	99.72	99.19	100.91	98.48	100.04	98.80
Rb	121	308	5.1	2.6	7.5	0.05	41	5.6	48	31
Ba	866	557	15	30	48	31	320	57	316	185
Cs	1.6	6.5	0.16	0.20	0.20	0.18	2.7	0.30	1.5	2.9
Sr	40	45	4.6	5.5	5.6	5.9	25	12	9.8	60
Pb	27	20	10	13	10	12	14	12	13	19
Th	5.8	6.1	1.0	1.0	1.5	0.73	2.0	1.1	3.4	5.1
U	1.6	3.1	0.41	0.30	0.45	0.34	0.91	0.47	2.3	1.5
Sc	0.75	1.6	0.53	0.72	0.31	0.50	6.8	0.84	3.0	4.7
V	3.6	5.6	2.7	1.7	0.74	3.2	55	5.4	13	34
Cr	19	16	41	17	30	26	126	156	88	165
Co	1.9	5.1	0.31	2.8	1.1	0.09	91	0.30	0.33	14
Ni	17	32	7.1	7.8	13	6.9	183	8.6	17	22
Y	9.5	14	2.8	2.1	4.4	4.2	6.7	4.3	5.2	6.8
Zr	118	59	32	30	40	33	90	57	77	91
Nb	3.8	5.2	3.4	3.3	3.3	3.5	4.7	3.7	4.5	4.9
Hf	4.4	1.8	0.88	0.92	1.0	0.99	2.6	1.8	2.9	3.1
Ta	0.23	0.42	0.07	0.06	0.05	0.09	0.38	0.06	0.33	0.52
La	60	16	5.4	4.3	7.7	6.9	6.9	7.7	7.2	22
Ce	103	32	10	7.8	13	13	14	15	12	42
Sm	5.5	1.6	0.80	0.50	1.5	1.5	1.3	0.95	0.95	2.3
Eu	0.67	0.30	0.16	0.12	0.30	0.32	0.44	0.25	0.34	0.64
Tb	0.37	0.15	0.07	0.08	0.11	0.16	0.21	0.10	0.13	0.12
Yb	0.82	0.58	0.28	0.27	0.34	0.41	0.81	0.47	0.55	0.76
Lu	0.13	0.08	0.05	0.05	0.06	0.05	0.14	0.08	0.09	0.08

Major elements are reported in oxide weight percent; trace elements reported in ppm; Fe2O3T, total Fe reported as Fe2O3; nd, none detected; Govt., Governmet Formation; Marsbg., Mariesberg Formation; VCR, Ventersdorp Contact Reef.

also are enriched in LILE, REE and Al2O3 relative to Pongola and Witwatersrand samples. Th and U concentrations in Dominion and Witwatersrand-Central Rand Group quartzites are similar to those of the Pongola sequence and enriched relative to West Rand Group quartzites.

Major and trace element contents of Ventersdorp and Transvaal quartzites also are highly variable (Table 9). Most of the variations correlate with K2O and Al2O3 contents, and thus may be related to detrital feldspar and clay mineral contents, respectively. As with samples from the Pongola sequence, quartzites with high proportions of K-feldspar also are enriched in K2O, Al2O3, Rb, Sr, Ba and Cs. In comparison to Phanerozoic passive-margin sandstones (Hirst, 1962; Cullers et al., 1979; Bhatia, 1983; Bhatia and Crook, 1986), quartzites from the Ventersdorp-Transvaal sequence are depleted in HFSE, Rb, Ba and Sr. Samples from the Pretoria Group are enriched in Th and U relative to other Ventersdorp and Transvaal quartzites, whereas Black Reef samples are enriched in Rb, V, and Co, and Bothaville quartzites are enriched in MnO, U and Ni.

Arenites from the Waterberg Group have overall compositions which are similar to Phanerozoic passive-margin sandstones. These sandstones differ from their Phanerozoic analogs by having enriched Al2O3, Fe2O3T and Th, and depleted Ta, Nb and Zr contents (Table 10a). Arenites from the Soutpansberg Group are enriched in Fe2O3T and depleted

Table 9. Individual analyses of quartzites from the Ventersdorp and Transvaal Supergroups.

	Bothaville Formation	Sekororo Formation			Selati Formation	Black Reef Quartzite		Rooihoogte Formation	Daspoort Formation		Magaliesberg Formation		Rayton Formation
Sample	C 6	D 53	D 36	D 47	D 35	D 34	C 201	C 76	C 81	MSF-2-10	C 207	D 77	C 56
SiO2	90.44	95.06	79.61	82.83	77.90	96.07	94.19	94.93	95.61	90.38	94.23	66.46	96.02
TiO2	0.07	0.01	0.03	0.06	0.15	0.02	0.01	0.01	0.06	0.05	0.03	0.47	0.02
Al2O3	3.18	2.28	8.27	8.19	12.15	2.05	4.11	2.31	2.05	3.38	2.58	13.19	1.82
Fe2O3-T	3.06	0.60	2.19	1.92	1.69	0.62	0.60	0.82	0.66	4.24	0.70	3.24	0.59
MgO	0.59	0.41	1.51	1.36	2.04	0.27	0.22	0.23	0.32	0.73	0.44	4.30	0.17
CaO	0.03	0.02	2.46	0.52	0.09	0.03	0.03	0.01	0.03	0.05	0.02	4.22	0.01
Na2O	0.29	0.08	nd	0.10	nd	0.52	nd	nd	0.34	0.56	0.33	1.79	0.16
K2O	0.24	0.29	2.82	2.32	6.26	0.12	0.04	nd	0.14	0.01	0.52	5.92	0.11
MnO	3.06	nd	0.02	0.01	nd	nd	nd	nd	nd	0.01	nd	0.06	nd
P2O5	0.08	0.01	0.02	0.02	0.03	0.01	nd	nd	nd	0.02	0.01	0.04	nd
LOI	1.28	0.36	3.36	1.77	0.36	0.36	0.44	0.47	0.32	0.78	0.63	0.89	0.07
TOTAL	102.32	99.11	100.29	99.10	100.67	100.07	99.62	98.77	99.52	100.20	99.49	100.58	98.95
Rb	12	3.4	55	56	142	nd	nd	nd	1.4	nd	12	178	0.79
Ba	113	34	440	365	1150	15	24	18	86	21	115	1530	41
Cs	0.47	0.13	1.8	1.7	5.8	0.05	0.04	0.07	0.17	0.09	0.39	2.5	0.13
Sr	15	3.1	19	11	39	9.0	9.5	3.2	5.6	5.5	13	255	3.7
Pb	18	9.9	12	8.5	22	176	11	14	8.0	34	8.0	34	11
Th	2.8	0.84	1.2	1.6	3.9	1.0	1.3	3.4	2.0	9.3	2.7	15	2.0
U	2.3	0.43	0.15	0.44	1.4	0.63	0.41	1.5	0.92	3.9	1.1	3.2	0.77
Sc	1.3	0.38	1.1	0.89	2.4	0.43	0.33	0.90	0.74	1.9	0.60	7.0	0.24
V	3.2	1.8	6.6	6.7	15	0.10	0.84	14	5.5	32	1.5	49	0.54
Cr	25	10	11	16	59	22	14	25	9.9	30	7.6	97	4.0
Co	5.2	0.29	3.8	3.8	2.0	0.07	0.18	0.80	0.13	4.0	0.31	8.0	0.11
Ni	35	8.1	11	14	13	5.8	5.6	12	7.4	9.6	7.9	35	5.4
Y	5.1	2.0	6.9	6.6	16	4.5	1.1	2.4	3.5	4.3	3.6	31	1.3
Zr	59	41	50	71	116	47	39	34	61	54	56	302	50
Nb	5.1	3.2	4.0	4.1	4.6	3.4	3.7	4.8	3.7	3.6	3.2	11	3.3
Hf	2.1	1.1	1.8	2.0	5.7	1.3	1.2	0.88	1.9	1.5	1.6	8.9	1.7
Ta	0.23	0.03	0.36	0.21	0.44	0.08	0.03	0.06	0.18	0.15	0.07	1.0	0.08
La	11	5.1	12	7.5	8.8	4.6	7.5	2.7	7.6	9.2	8.9	30	2.9
Ce	15	9.5	24	15	20	9.5	14	5.3	12	18	17	45	5.3
Sm	1.4	1.0	2.4	1.5	1.8	0.92	0.96	0.40	0.66	1.0	1.2	5.4	0.43
Eu	0.36	0.18	0.44	0.31	0.62	0.18	0.21	0.10	0.14	0.24	0.26	1.2	0.09
Tb	0.16	0.08	0.21	0.19	0.36	0.05	0.06	0.03	0.07	0.14	0.13	0.83	0.06
Yb	0.56	0.23	0.89	0.54	1.6	0.36	0.26	0.34	0.45	0.56	0.33	2.4	0.21
Lu	0.10	0.05	0.16	0.08	0.30	0.06	0.03	0.06	0.06	0.11	0.06	0.38	0.03

Major elements are reported in oxide weight percent; trace elements reported in ppm; Fe2O3T, total Fe reported as Fe2O3; nd, none detected.

Table 10a. Individual analyses of quartzites from the Waterberg Group.

	Swaershoek Formation		Schilpadk Formation	Sandriversberg Formation		Cleremont Formation	Vaalwater Formation
Sample	C 89	C 94	C 96	C 97	C 98	C 99	C 100
SiO2	87.07	91.66	91.57	91.10	86.98	82.67	77.86
TiO2	0.18	0.24	0.08	0.09	0.52	0.66	0.22
Al2O3	5.36	4.42	4.93	4.86	5.68	11.69	11.70
Fe2O3-T	3.77	2.44	1.12	1.21	4.30	2.92	1.71
MgO	0.16	0.15	0.08	0.14	0.33	0.30	0.38
CaO	0.02	0.00	0.00	0.00	0.00	0.11	0.16
Na2O	0.01	0.19	0.28	0.34	0.40	0.37	3.93
K2O	1.07	1.00	0.99	0.94	1.55	0.70	2.27
MnO	0.05	0.03	0.02	0.02	0.03	0.02	0.04
P2O5	0.01	0.02	0.03	0.03	0.02	0.07	0.05
LOI	0.94	0.64	0.76	0.77	0.87	0.83	0.94
TOTAL	98.64	100.79	99.86	99.50	100.68	100.34	99.26
Rb	44	41	27	24	53	22	84
Ba	404	882	265	209	419	252	750
Cs	0.66	0.87	0.27	2.8	0.68	0.23	1.4
Sr	17	6.1	9.7	15	10	276	98
Pb	4.6	5.7	2.4	2.7	13	1.3	30
Th	5.7	5.6	3.9	4.1	15	7.4	9.8
U	1.3	0.78	0.67	0.81	1.5	1.8	2.7
Sc	4.4	2.4	1.6	1.4	3.3	2.3	4.1
V	33	16	6.8	11	57	34	30
Cr	40	26	5.3	7.3	33	40	28
Co	7.8	2.0	5.5	4.8	3.8	0.60	6.9
Ni	19	12	14	14	22	11	21
Y	7.8	15	6.5	9.7	8.9	6.7	23
Zr	80	130	67	77	190	184	143
Nb	2.4	2.8	0.1	1.0	5.0	2.7	3.2
Hf	2.5	3.9	1.9	2.3	6.3	6.5	5.1
Ta	0.23	0.21	0.08	0.11	0.51	0.23	0.40
La	11	23	14	13	33	16	40
Ce	30	33	27	28	71	42	79
Sm	1.6	2.9	1.4	1.5	4.5	2.5	6.3
Eu	0.30	0.44	0.32	0.35	0.75	0.79	1.3
Tb	0.32	0.34	0.17	0.22	0.46	0.46	0.69
Yb	0.83	1.4	0.66	0.69	0.99	0.63	2.1
Lu	0.08	0.09	0.10	0.12	0.11	0.19	0.36

Major elements are reported in oxide weight percent; trace elements reported in ppm; Fe2O3T, Total Fe reported as Fe2O3; nd, none detected.

in Rb, Ba, Zr, Nb and Ta relative to Phanerozoic platform sandstones (Table 10b). Compared to the Soutpansberg, Waterberg sandstones are enriched in Al_2O_3, K_2O, Ba, Cs, Th, REE and Rb, and depleted in MgO, CaO, Sc, V and Nb. Waterberg samples also have higher mean La/Yb ratios (21) and larger negative Eu anomalies ($Eu/Eu^*=0.66$) than Soutpansberg sandstones ($La/Yb=14$; $Eu/Eu^*=0.73$).

Table 10b. Individual analyses of quartzites from the Soutpansberg Group.

	Mutshindudi Member-Sibasa Fm.		Musekwa Formation		Ngwanedzi Formation		Nzhelele Formation	
Sample	C 107	C 124	C 128	C 160	C 131	C 184	C 177	C 188
SiO2	92.99	92.39	94.58	93.03	94.99	67.19	85.85	83.74
TiO2	0.53	0.15	0.05	0.13	0.10	1.42	0.14	0.64
Al2O3	2.76	2.85	2.25	2.60	2.34	9.12	5.29	7.76
Fe2O3-T	3.05	2.29	0.88	1.80	1.38	7.55	1.50	3.40
MgO	0.13	0.58	0.55	0.73	0.40	3.24	0.63	0.94
CaO	0.00	0.02	0.01	0.02	0.03	4.43	2.68	0.98
Na2O	0.60	0.23	0.33	0.27	0.00	0.82	1.37	2.34
K2O	0.06	0.41	0.01	0.27	0.19	1.51	0.36	0.89
MnO	0.02	0.00	0.00	0.00	0.00	0.07	0.03	0.05
P2O5	0.03	0.01	0.01	0.01	0.00	0.07	0.03	0.07
LOI	0.72	0.28	0.52	0.24	0.26	4.61	1.58	0.75
TOTAL	100.89	99.21	99.18	99.10	99.70	100.02	99.45	101.55
Rb	2.1	7.5	0.00	3.6	4.0	47	9.2	31
Ba	36	69	24	47	46	375	145	210
Cs	0.05	0.15	0.09	0.04	0.08	0.66	0.15	0.54
Sr	19	7.0	7.6	7.8	7.3	44	212	118
Pb	2.7	11	15	18	14	17	15	19
Th	6.7	6.7	3.2	5.1	3.5	5.3	1.8	5.9
U	2.0	0.91	0.60	0.34	1.1	1.6	0.38	1.6
Sc	2.1	1.0	0.57	1.1	0.98	22	2.4	5.6
V	40	17	1.8	7.5	20	260	38	107
Cr	15	12	13	18	13	124	15	26
Co	0.80	0.75	0.82	0.74	0.35	25	2.5	5.1
Ni	4.4	7.8	8.7	8.0	6.5	55	22	21
Y	13	8.1	4.7	4.1	4.1	17	8.0	15
Zr	206	75	57	63	61	151	49	160
Nb	3.8	4.5	3.7	4.0	3.7	8.7	3.6	5.2
Hf	6.8	2.4	2.1	2.8	2.3	5.5	1.5	4.4
Ta	0.28	0.40	0.13	0.21	0.17	0.45	0.09	0.40
La	12	12	10	10	12	16	7.4	14
Ce	34	29	21	20	22	32	12	26
Sm	2.3	2.4	1.6	1.6	1.7	3.3	1.4	2.5
Eu	0.51	0.42	0.30	0.28	0.31	1.0	0.42	0.62
Tb	0.37	0.24	0.15	0.11	0.15	0.40	0.24	0.36
Yb	1.4	0.96	0.55	0.58	0.54	1.8	0.73	1.3
Lu	0.22	0.16	0.08	0.09	0.08	0.29	0.12	0.19

Same as Table 10a.

DISCUSSION

FACTORS CONTROLLING THE COMPOSITION OF PELITES

Although the chemical composition of pelites may be used to constrain source-area composition, several important and often overlooked factors contribute to the distribution of elements in pelites and other terrigenous sediments. The effects of each of the following factors must be taken into consideration when evaluating the provenance of terrigenous-clastic sediments:

1) Hydraulic sorting effect. The hydraulic sorting of grains during weathering, erosion, transport and deposition separates them by size, shape, mineralogy and density and may influence the chemical composition of terrigenous sediments.

2) Adsorption of ions by clays and other fine-grained particulate matter. Adsorption of ions may occur during weathering and erosion, as particles settle in seawater, or during the early stages of diagenesis.

3) Mobilization of elements during diagenesis and metamorphism.

4) Degree of chemical weathering of the source rock, which in turn is dependent on climate and rates of tectonic uplift.

5) Bulk composition of the source terrane.

6) Tectonic setting and its influence on composition of the source terrane and sedimentary processes.

These factors interact with each other and it is not an easy task to separate their cumulative effects when interpreting the geochemistry of pelites. Fortunately, some elements are affected by one factor more than another, allowing groups of elements to be useful in evaluating individual geologic processes. Pelites often have been used as provenance indicators with little discussion of the other factors listed above. Since we are not yet at a point where we can rigorously distinguish the effects of each of these factors, it is important to use caution in interpreting the composition of terrigenous sediments in terms of source-area composition or any other individual factor. The following discussion reviews each of these six factors as they relate to the geochemistry of Kaapvaal craton sediments.

HYDRAULIC SORTING EFFECT

Several studies have shown that hydraulic sorting of sediments by grain size and density can significantly influence their chemical composition (Reimer, 1985; Cullers et al., 1987, Cullers, 1988b; Nesbitt and Young, 1987). For example, variable flocculation rates of clays may cause fractionation of elements in sedimentary systems (Gibbs, 1977; Stanley and Liyanage, 1986). Although resistate phases such as zircon, magnetite and garnet are concentrated chiefly within silt and sand-sized fractions, some may end up in shales and be responsible for minor variations in the

concentrations of REE and HFSE in these sediments (Gromet et al., 1984). One way of minimizing the influence of these processes on sedimentary provenance studies is to compare sediments of approximately the same grain size and tectonic-sedimentary environment. Fine-grained pelites and shales tend to be more homogenous than coarser sediments such as quartzites and may be the most representative sediments for source-area studies. Element ratios such as La/Th, La/Sc and Th/Sc also can minimize the effects of mineral fractionation (Taylor and McLennan, 1985).

Some variations in Pongola pelite compositions may be related to mineral fractionation in the sedimentary environment. In the Wit-Mfolozi section of the Pongola Supergroup, absolute REE contents decrease from the NLWM to the overlying NUWM section, and then increase again in the MWM section (Fig. 15). REE contents of these pelites are paralleled by Al_2O_3 concentrations, suggesting that the amount of clay minerals originally contained in these sediments may have controlled their REE distributions. La/Yb and Eu/Eu* ratios show only modest corresponding changes, and may be more representative of their sources. Minor irregularities in the distribution of LILE in pelites may also reflect element fractionation during sedimentary transport. For example, elevated concentrations of K, Rb and V in most Kaapvaal pelites and lower concentrations in associated quartzites (Tables 2-10) suggest that K, V and Rb are strongly fractionated into clay minerals such as

illite. Compositions of some Kaapvaal arenites also appear to be controlled by mineral fractionation in the sedimentary cycle. For example, higher matrix (and Al2O3) contents of Waterberg arenites relative to Soutpansberg arenites, are paralleled by enriched K2O, Ba, Cs, Rb, Th and REE concentrations (Tables 6, 10a and 10b). Thus, higher LILE contents of Waterberg samples may reflect the accumulation of clay minerals in these sediments.

Relatively high contents of Zr in Witwatersrand-OG and K8 pelites (Table 3) are paralleled by high concentrations of Hf and Y and may reflect detrital zircon enrichment in these pelites relative to other Witwatersrand pelites. Elevated REE contents of the OG and K8 pelites may also be due to resistate phases such as zircon and monazite. Positive linear correlations between the contents of Al2O3 and both light- and heavy-REE in Witwatersrand pelites (with correlation coefficients of 0.82 and 0.72, respectively) also suggest that transport of REE and especially light-REE are dominated by clay minerals.

ADSORPTION EFFECT

Clay minerals and other particulate matter can adsorb REE and metals from seawater and weathering solutions (Roaldset, 1973; Nesbitt, 1979; Balistrieri and Murray, 1984). The importance of such adsorption in controlling trace element distributions in pelites and shales has not

been fully evaluated. Element adsorption and desorption onto particulate matter may be related to the pH of the fluid medium (Roaldset, 1973). Balashov et al. (1964) suggest that heavy-REE are preferentially transported in solution compared to light-REE because they form more soluble bicarbonate and organic complexes. Studies of Fleet (1984) support those of Balashov et al., by indicating that light-REE are more readily adsorbed onto particulate matter than the heavy-REE.

Mineral adsorption effects can be evaluated by comparing bi-element Pearson correlation coefficients from pelite assemblages (using statistical computer programs; Appendix F.1). An ideal suite of samples for correlation study should have a constant source-area composition and depositional setting so as not to mask any transport features with provenance effects. Pongola pelites are ideal in this regard because of their relatively constant source-area composition and the large number of samples analyzed. A comparison of major and trace element correlations can be used to identify the mineral species responsible for trace element transport. Correlation coefficient tables also can be compared to coefficient tables from weathering profiles and coarse-clastic sediments (Ogura et al., 1987; Dissanayake, 1987; Bhatia and Crook, 1986). These comparisons may offer important insights into the roles of weathering and transport on the distribution of

Table 11. Geochemical correlation coefficients for pelites from the Pongola Supergroup.

	SiO2	TiO2	Al2O3	Fe2O3	MgO	CaO	Na2O	K2O	MnO	Ba	Cs	Rb	Sr	Th	U	Sc	V	Cr	Co	Ni	Y	Zr	Nb	Hf	Ta	La	Ce	Sm	Eu	Yb
SiO2	1.0																													
TiO2	-.45	1.0																												
Al2O3	-.52	.84	1.0																											
Fe2O3	-.48	-.31	-.44	1.0																										
MgO			-.36	.38	1.0																									
CaO						1.0																								
Na2O							1.0																							
K2O		.48	.66	-.72				1.0																						
MnO									1.0																					
Ba				-.47				.36		1.0																				
Cs				-.30				.46	.47	.64	1.0																			
Rb		.37	.53	-.63				.94		.49	.62	1.0																		
Sr							.55						1.0																	
Th		.33	.51	-.37			.42				.32		.55	1.0																
U		.31	.49	-.39					-.38				.43	.90	1.0															
Sc	-.54	.34	.72										.34	.47	.39	1.0														
V	-.47		.69					.37					.43	.30	.34	.79	1.0													
Cr						-.34									.30	.39	.30	1.0												
Co	-.31			.32				-.36								.34			1.0											
Ni				.46				-.41		-.39	-.30	-.42							.55	1.0										
Y		.44	.51	-.32				.44				.55		.52	.41	.47	.41				1.0									
Zr		.43		-.36				.41			.30	.57		.34							.75	1.0								
Nb	-.32	.71	.80	-.51				.63			.34	.63		.66	.60	.59	.60				.58	.58	1.0							
Hf		.32		-.32				.34			.36	.52									.79	.95	.53	1.0						
Ta	-.30	.63	.76	-.49				.60		.32	.40	.63		.70	.65	.63	.64				.74	.65	.91	.63	1.0					
La		.37	.44				.46						.63	.58	.44		.33				.56	.32	.42	.37	.53	1.0				
Ce		.45	.55				.39						.51	.59	.54	.61	.36				.58	.57	.65	.55	.71	.84	1.0			
Sm		.38	.46										.38	.54	.40	.52	.35				.73	.52	.57	.55	.64	.87	.82	1.0		
Eu	-.30	.48	.48									.33	.30	.49	.36	.62	.40				.76	.55	.58	.59	.66	.82	.46	.98	1.0	
Yb		.42	.56					.33				.48		.52	.40	.51	.40				.86	.73	.70	.76	.76	.59	.70	.82	.86	1.0

Correlations not given for values $-0.3 > r < 0.3$; slight correlation $0.3 < r < 0.55$; moderate correlation $0.55 < r < 0.80$; strong correlation $0.80 < r < 1.0$. Number of samples, n=63. Significance of correlation coefficients given in Table F.1.

elements within the sedimentary cycle.

Correlation coefficients for Pongola pelites indicate a moderate to strong positive linear correlation between Al and Ti, K, Sc, V, Y, Nb, Ta and the REE (Table 11). Correlations between Al and Ti may be evidence for the adsorption of anatase onto clay surfaces and subsequent co-deposition of these mineral phases (Weaver and Pollard, 1973). V, Ta and Nb also may be incorporated in anatase, and hence, deposited with the clay-mineral fraction. Strong Al-Ti correlations in laterites (Dissanayake, 1987) suggest that these element associations may have developed in weathering profiles of the source rocks. A moderately strong correlation between Al and K, Ta and Nb further suggests that illite (with adsorbed anatase) may be the primary clay mineral responsible for this relationship. Strong to moderate correlations between K and Rb, as well as Na and Sr, suggest that illite and smectite, respectively, may have dominated the transport of Rb and Sr in the Pongola sedimentary cycle. V and Sc also show moderate correlations with each other and Al suggesting other possible clay mineral transport mechanisms for these elements. Strong Al-V correlations in laterites (Dissanayake, 1987) suggest that these relationships also may have developed in weathering profiles of source rocks. Comparisons of HFSE and REE indicate a strong linear correlation between the REE and Y, Ta, Nb and Hf. Associations of Y and the REE are not surprising considering the similar chemical properties

of Y and the lanthanide elements. Ta-Nb and REE correlations may result from adsorption of Ta-Nb enriched anatase and REE onto clay mineral surfaces. The association of Hf with the REE (especially heavy-REE) is unexpected unless detrital zircon is called upon to control the distributions of these elements. This speculation, however, is not supported by weak correlations between Zr and many of the REE in Pongola sediments. Th and U also show moderate correlations with Al2O3, Ta, Nb and some REE. These associations suggest that Th and U may be transported, at least in part, by clay mineral species.

Kaolinite flocculation is noted to cause clay mineral segregation in the Amazon River delta (Gibbs, 1977); however, Kronberg et al. (1986) conclude that Pleistocene muds from the Amazon do not show significant major or trace element variations as a function of distance from the river mouth towards the sea. Witwatersrand and Transvaal pelites were sampled along 20-30 km traverses normal to basin margins, yet systematic variations of trace or major element abundances are not observed in the data. Similar REE distributions in Witwatersrand and Transvaal pelites (Figs. 16 and 17) suggest that if clay mineral adsorption is important in producing these distributions, it acted in a similar manner for all of the pelites. Furthermore, the overall similarity of REE patterns in lower Witwatersrand pelites to those estimated for average upper Archean crust (Taylor and McLennan, 1985) suggests that fractionation of

REE by adsorption does not mask provenance input. Thus, clay mineral segregation by flocculation processes does not appear to have had a significant influence on the composition of Kaapvaal pelites.

Enrichment of transition metals in Kaapvaal pelites relative to associated quartzites and conglomerates (by factors of 5-25; Pretorius, 1976; Tables 2-10) probably reflects selective adsorption of these metals on clay minerals or other particulate matter. Positive linear correlations also exist between the contents of Al and both light- and heavy-REE (with correlation coefficients of 0.82 and 0.72, respectively) in Witwatersrand and Pongola pelites. This correlation suggests that REE and especially light-REE are dominantly contained in clay minerals. Parallel distributions of REE, LILE, Ni and Cr in pelites and quartzites (Tables 2-10) also suggest that transport of these elements in the sedimentary cycle is controlled principally by clay minerals.

DIAGENESIS AND METAMORPHISM

Diagenesis and low-grade metamorphism may cause mobility and redistribution of LILE and some major elements (Frey et al., 1968; Cullers et al., 1975; Fleet, 1984; Merriman et al., 1986). REE and HFSE are generally least susceptible to remobilization during secondary processes (Chaudhuri and Cullers, 1979; Ludden et al., 1982; Taylor and McLennan, 1985). Mobility of elements during diagenesis

and metamorphism also is dependent upon a number of physio-chemical conditions, including pH, Eh, temperature, pressure, sediment permeability and carbonate mineral contents. Comparisons of NASC and metamorphosed NASC (Appendix E; Wildman and Haskin, 1973; Gromet et al., 1984) show that variation between the two composites is <15% for REE, Co, Rb, U, SiO2, TiO2 and Al2O3, and 15-25% for Zr, Cs, Ba, Hf, Ta and Th. The similarities of both composites suggest that element mobility resulting from metamorphism and diagenesis has had a minimal effect on these pelites. Other studies of metamorphosed pelites ranging up to amphibolite grade indicate that major and trace element changes are minimal (Shaw, 1954, 1956; Cullers et al., 1974; Hower et al., 1976; Condie and Martell, 1983). These studies suggest that diagenesis and low-grade metamorphism do not greatly affect the composition of shales and pelites. However, element mobility of even generally immobile REE may be recorded under low pH weathering conditions or in sequences with interbedded carbonates and pelites (Nesbitt, 1979; Schieber, 1988).

Mineral assemblages in volcanic and sedimentary rocks from all successions in this study are characterized by zeolite to greenschist facies metamorphic conditions. Pongola pelite mineral compositions are consistent with the exposure of these sediments to a maximum of mid-greenschist facies metamorphism. The presence of pyrophyllite in Mozaan sediments (Table 1) limits maximum regional metamorphic

temperatures to 410-430 °C at pressures of 2-4 kb (Hemley, 1967; Kerrick, 1968). Mafic and felsic volcanic rocks from the Nsuze Group have metamorphic mineral assemblages that are typical of volcanic rocks exposed to a maximum of lower-greenschist facies conditions (Table 12; Watchorn and Armstrong, 1980). Higher grades of metamorphism are locally developed in the Pongola sequence along the Namaqua thrust belt to the south and with intrusive rocks along the basin margins (Fig. 4; Hunter, 1963; Matthews, 1967; Beukes, 1973). Vermiculite in pre-Pongola paleosols (Matthews and Scharrer, 1968) also indicates that some parts of the Pongola basin were metamorphosed to a maximum of upper-zeolite to lower-greenschist facies conditions.

Witwatersrand regional metamorphic grades are characterized by greenschist-facies conditions (Pretorius, 1981b). The presence of pyrophyllite in K8 pelites also limits maximum metamorphic conditions to mid-greenschist (Phillips, 1986a, 1986b). Results from this study confirm the presence of pyrophyllite in the K8 pelite unit (Table 1). The coexistance of chlorite and muscovite in all Witwatersrand pelites and the presence of chloritoid in BOY pelites furthermore suggest that upper-greenschist facies regional conditions were not exceeded for any portion of the Witwatersrand sequence. Locally higher metamorphic grades occur adjacent to granitic intrusions and the Bushveld Complex. Mineral assemblages from volcanic and sedimentary

Table 12. Metamorphic mineral assemblages from Precambrian sediments on the Kaapvaal craton, southern Africa.

Unit	Rock Type	Mineral Assemblage
Soutpansberg	vugs in quartzite	prehnite + calcite
Soutpansberg Sibasa Formation	mafic lava	pumpellyite + chlorite + quartz + epidote + sericite
Transvaal Pretoria Group	shale	mixed layer I/S clay
Transvaal Pretoria Group	mafic volcanic	tremolite/actinolite + chlorite + epidote + plagioclase + calcite
Transvaal Black Reef Formation	pelite	muscovite + chlorite + chloritoid
Ventersdorp Allanridge Formation	mafic lava	actinolite + chlorite + epidote
Ventersdorp Bothaville Formation	pelite	muscovite + chlorite
Ventersdorp Klipriversberg Group	mafic lava	pumpellyite
Ventersdorp Klipriversberg Group	mafic lava	tremolite/actinolite zoisite/clinozoisite + chlorite + epidote + albite + calcite
Witwatersrand K8 unit	pelite	pyrophyllite
Witwatersrand Booysens Formation	pelite	chloritoid
Witwatersrand West Rand Group	pelite	muscovite + chlorite
Dominion Group Rhenosterhoek Formation	mafic lava	tremolite/actinolite + chlorite + epidote + albite + carbonate
Dominion Group Rhenosterspruit Formation	vugs in quartzite	tremolite + calcite + quartz
Pongola Mozaan Group	pelite	pyrophyllite
Pongola Nsuze Group	mafic lava	zoisite/clinozoisite tremolite/actinolite + chlorite + albite + quartz
Pongola Nsuze Group	felsic lava	zoisite/clinozoisite + sericite + albite + quartz + biotite
Pre-Pongola	paleosol	vermiculite

Maximum Metamorphic Grade	Reference
low-pressure zeolite	This study
low-pressure zeolite	Barker (1979)
upper zeolite	This study
upper greenschist	Button (1973b)
mid- to upper greenschist	This study
mid-greenschist	Crow (1988)
mid- to upper greenschist	This study
low-pressure zeolite	Tyler (1979)
lower greenschist	McIver et al. (1981)
mid-greenschist	This study Phillips (1986a)
upper greenschist	This study
mid- to upper greenschist	This study
lower greenschist	Crow and Condie (1987)
upper greenschist	This study
mid-greenschist	This study
lower greenschist	Watchorn and Armstrong (1980)
lower greenschist	Watchorn and Armstrong (1980)
upper zeolite	Matthews and Scharrer (1968)

rocks of the underlying Dominion Group also have mineral assemblages which are suggestive of mid- to lower-greenschist facies metamorphism (Table 12; Crow et al., 1988). Layer et al. (1988) describe paleomagnetic and clay mineralogic temperature constraints which confirm that the Witwatersrand and Dominion basins were subjected to mid- to upper-greenschist facies temperatures approximately 2050-1950 Ma ago. The authors suggest that this metamorphic event occurred in response to heating during the intrusion of the Bushveld Intrusive Complex or doming of the Vredefort area.

Ventersdorp-BOT metamorphic conditions are constrained to a maximum of upper-greenschist facies by coexisting chlorite and muscovite in pelites. Mineral assemblages in Klipriviersberg and Allanridge lavas suggestive a maximum of lower-greenschist facies metamorphism, although pumpellyite in upper Klipriviersberg lavas also suggests that higher pressure (>3 kb) zeolite facies metamorphic conditions may have been locally prevalent (Table 12; Tyler, 1979; McIver et al., 1981; Crow et al., 1988). Oxygen isotope geothermometric studies indicate temperatures of 200-400 ^{o}C and pressures of 1.5 kb (Cornell, 1978), supporting the temperature-pressure interpretations from mineralogic investigations.

Mixed-layer illite/smectite clays in the Pretoria Group suggest that these sediments may be classified as shales

rather than pelites (Table 6). Pressure-temperature conditions characteristic of zeolite facies were probably not exceeded for these sediments (Frey, 1970, 1978; Thompson, 1970). Chloritoid and coexisting muscovite-chlorite suggest a maximum of upper-greenschist facies metamorphic conditions for BR pelites, while mineral assemblages in Transvaal volcanics indicate a lower-greenschist grade (Table 12). Locally higher grade contact metamorphic zones are noted in the Bushveld area (Button, 1973b).

Prehnite in Soutpansburg quartzites limits metamorphic conditions for these sediments to upper-zeolite facies. These findings support those of Barker (1979) who suggests zeolite to lower-greenschist metamorphism based on mineral assemblages in lower Soutpansberg Sibasa lavas (Table 12).

SOURCE-AREA WEATHERING

Weathering Past and Present

The weathering horizon acts as an interface between terrestrial rocks and the atmosphere and is a chemically active zone with weathering rates dependent upon a complex interplay between mechanical erosion, physio-chemical conditions of chemical weathering, source-rock composition and rock mineralogy (Nesbitt, 1979; Basu, 1981; Holland, 1984; Taylor and McLennan, 1985; Fritz, 1988; Cullers, 1988a). Easily weathered minerals are readily broken down

and elements liberated are converted into clay minerals or leached from the weathering profile. Readily leachable elements include Ca, Sr, Na, Cl and Mg, while immobile elements include Al, Ti, Ga, Zr, Hf, Y, Sc, Th, Nb, Ta and most REE (Goldich, 1938; Taylor and McLennan, 1985). REE may become fractionated in highly weathered modern bauxitic soils characterized by extensive acid leaching (Ronov et al., 1967; Nesbitt, 1979; Topp et al., 1984; Reimer, 1985; Kronberg et al., 1987). Light-REE/heavy-REE ratios are noted to decrease with depth in these soil profiles apparently because heavy-REE form more stable (and thus more soluble) aqueous carbonate complexes (Wheelwright et al., 1953; Balashov and Khirov, 1967; Nesbitt, 1979). Thus, the overall trend is one where heavy-REE are preferentially concentrated in lower soil horizons during the weathering process. First row transition metals tend to be immobile, although some Ni and V mobility is apparent under extreme weathering conditions (Kronberg et al., 1979). Elements which characteristically exhibit multivalent states under surficial conditions (Fe, Mn, U) either tend to be concentrated as residual weathering products, or are leached from weathering horizons and deposited along redox front boundaries.

Weathering during the Archean may have differed significantly from modern weathering due to different atmospheric, biologic or tectonic conditions. Since the Earth's early atmosphere probably contained a greater amount

of CO2 relative to the present-day atmosphere (Holland, 1984), associated rain water would contain greater concentrations of carbonic acid, and hence would be more acidic then modern rain water. Highly acidic water, in turn, leads to greater rates of chemical leaching in surface rocks. An absence of REE fractionation in four intensely weathered late Archean paleosols is documented by Kimberley and Grandstaff (1986). The authors attribute the lack of fractionation to erosion of upper soil layers prior to their ultimate burial by overlying sediments. A more plausible explanation for these soil trends may be the paucity of soil biota and associated acidic ground waters during the Archean. Dissolved CO2 in present-day soil water is one to two orders of magnitude greater than that in associated rain water, largely because the decay of vegetation in modern soils effectively increases the pCO2 relative to atmospheric levels (Holland, 1978). These secular variations in elemental mobility in soils attest to the importance of organic activity in the weathering process.

Kimberley and Grandstaff (1986) note strong depletions of Na in Archean soils, a pattern which is similar to that of modern weathering horizons, yet Archean profiles do not show any mobilization of other alkali-alkaline earth elements. Holland (1984) notes that significant losses of Fe occurred in Precambrian weathering profiles, while the rate of Fe depletion is proportional to the total Fe concentration of source-rocks. Paleosols developed on

Fe-poor rocks such as granite, show no detectable losses of Fe during the Precambrian. These authors also note that Mg, Sc, Ti, Hf, Th, Ni and Sc are stable in ancient weathering profiles, while Mn, U, Co and Cr are mobile.

Depletions of Ce, relative to La and Sm are noted in some Pongola-Piet Retief and Transvaal-Silverton samples (Appendix B; Pongola samples P41, P 47, P50, and Transvaal samples C 58, D 82, D 83, D 84, D 86, D 88, D 97 and D 99). Pongola and Transvaal Ce depletions may represent a modern-day weathering effect, since only samples collected from surface outcrops exhibit this pattern. Subsequently, Ce analyses from these samples were not included in chondrite normalize REE plots (Figs. 15 and 17). This depletion pattern may be related to the redox chemistry of Ce (Middelburg et al., 1988). Upon weathering, Ce^{+3} is oxidized to Ce^{+4} and becomes immobilized and fractionated from other REE in the weathering profile. The exact mechanism of fractionation is uncertain, but may be related to mobilization of other light-REE relative to Ce.

Chemical Index of Alteration (CIA)

A method of quantifying the degree of source-area weathering is to use the chemical index of alteration (CIA) proposed by Nesbitt and Young (1982). The CIA value is calculated by the general formula:

$$CIA = \frac{Al2O3}{(Al2O3+CaO+Na2O+K2O)} \times 100$$

Where CaO is the amount of Ca incorporated into silicate minerals only. Non-silicate CaO contributions from apatite and carbonates are calculating and subtracted from the totals by using appropriate amounts of CaO required to balance pelite P_2O_5 and Na_2O contents, respectively (Appendix C). Resultant values are a measure of the proportion of relatively immobile Al_2O_3 vs. the labile oxides in the sample. Typical CIA values range from 50 for unweathered rocks and glacial sediments, to 100 for kaolinite and laterite weathering horizons (Nesbitt and Young, 1982).

Although uncertainties exist in interpreting CIA values because of possible diagenetic or metamorphic mobility of alkali and alkaline earth elements, the CIA data appear to record moderate to intense chemical weathering of source-rocks during deposition of the Pongola sequence (Eriksson and Soegaard, 1985). CIA data for most Pongola pelites (except MPR) generally range from 71-81 (Fig. 23a; Table 2). These values are greater than those of most Moodies pelites (CIA=60-62). Relative to modern samples, most Pongola pelites have CIA values which are similar to or slightly higher than average Phanerozoic shales. An exception to this trend is the MPR and some MWM pelites which have scattered CIA distributions (CIA=79-99) which are higher than most other Pongola pelites. These pelites have CIA values similar to Amazon cone muds and residual clays,

Figure 23. Frequency histogram indicating Chemical Index of Alteration (CIA) of Kaapvaal pelites compared to various sediments and average Archean shield. Scale bars to left indicate number of samples in respective histograms. CIA index calculated as [Al2O3/(Al2O3+CaO+Na2O3+K2O)]x100, oxides as molecular values. This index is calculated using CaO in silicate minerals only (Appendix C).

a) CIA distributions of Pongola pelites, various sediments and average Archean shield. All Pongola samples are collected from surface exposures. Data sources: Pongola pelites-Table 2; Moodies pelites, McLennan et al. (1983); crustal sources and modern-day sediments in lower portion of diagram, Nesbitt and Young (1982).

b) CIA distributions of Witwatersrand, Ventersdorp, Transvaal, Soutpansberg and Waterberg pelites. Samples arranged in ascending stratigraphic order. Shaded rectangles represent drill-core samples, open rectangles indicate surface samples. Data sources: Witwatersrand pelites-Table 3; Ventersdorp and Transvaal pelites-Table 4; Waterberg and Soutpansberg shales-Table 5. After Nesbitt and Young (1982).

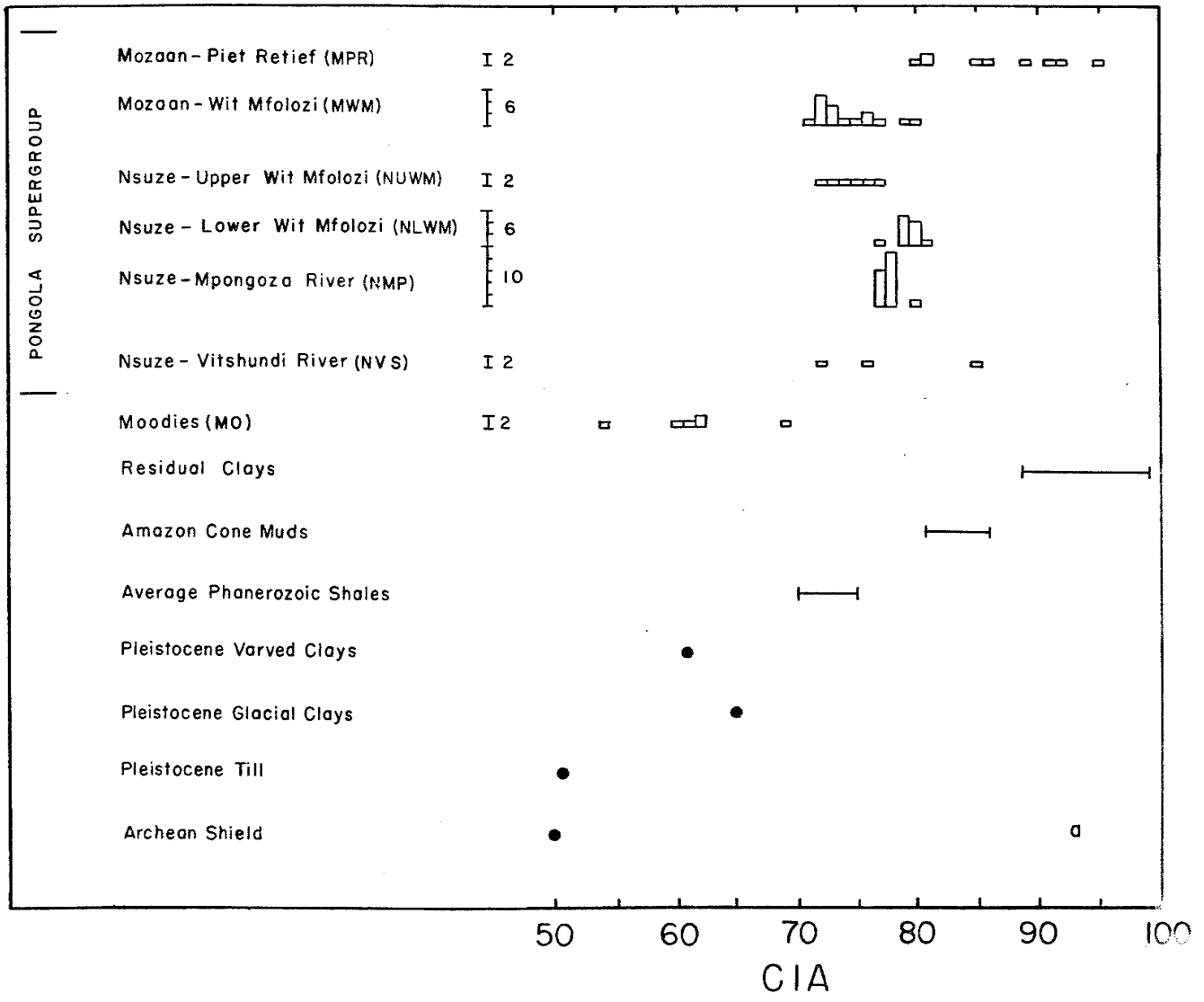
PONGOLA SUPERGROUP
Mozaan - Piet Retief (MPR)
Mozaan - Wit Mfolozi (MWM)
Nsuze - Upper Wit Mfolozi (NUWM)
Nsuze - Lower Wit Mfolozi (NLWM)
Nsuze - Mpongoza River (NMP)
Nsuze - Vitshundi River (NVS)
Moodies (MO)
Residual Clays
Amazon Cone Muds
Average Phanerozoic Shales
Pleistocene Varved Clays
Pleistocene Glacial Clays
Pleistocene Till
Archean Shield
1 2
6
1 2
6
10
1 2
1 2
50
60
70
80
90
100
CIA

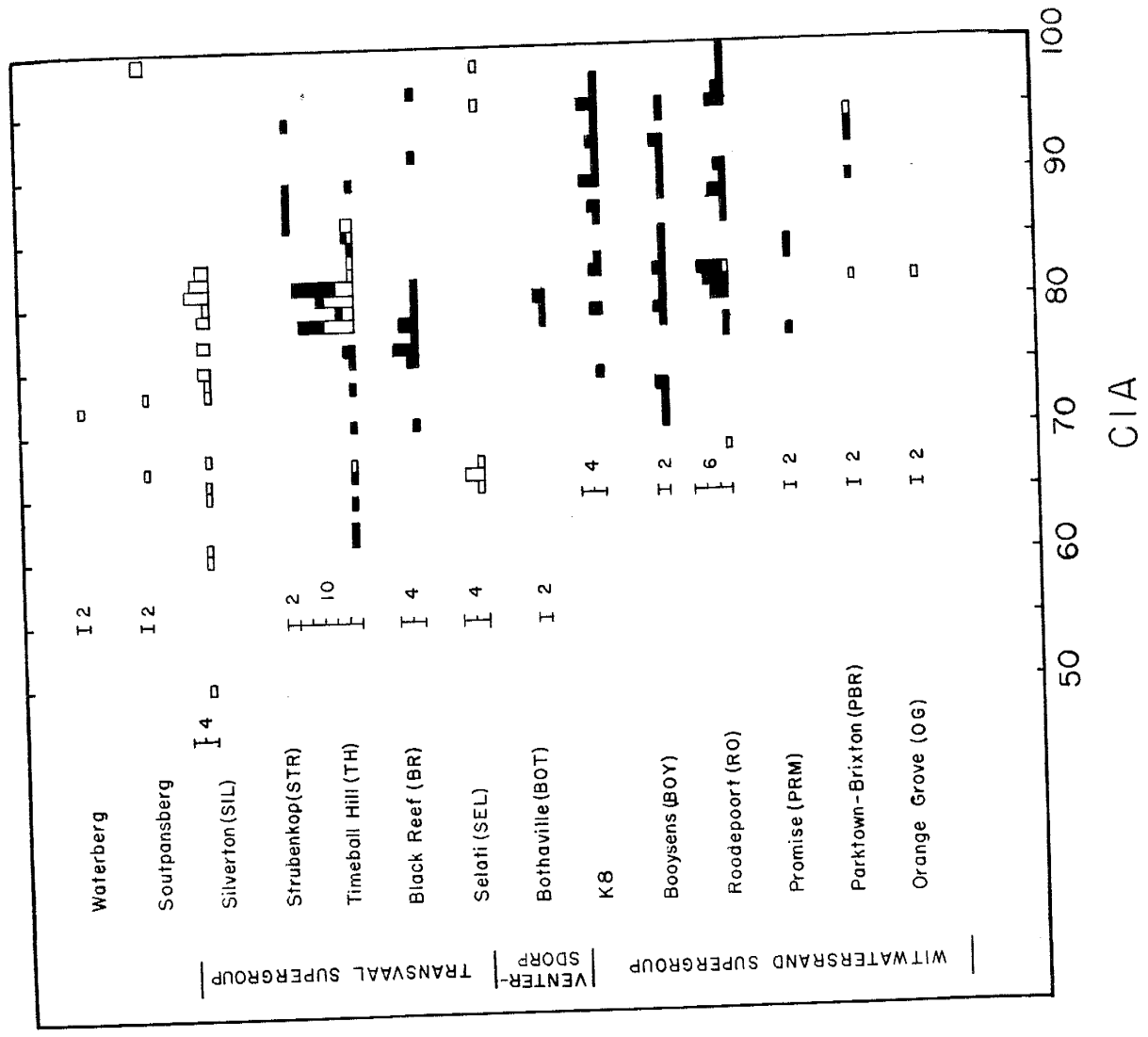
Waterberg
Soutpansberg
Silverton (SIL)
Strubenkop (STR)
Timeball Hill (TH)
Black Reef (BR)
Selati (SEL)
Bothaville (BOT)
K8
Booysens (BOY)
Roodepoort (RO)
Promise (PRM)
Parktown-Brixton (PBR)
Orange Grove (OG)
TRANSVAAL SUPERGROUP
VENTER-SDORP
WITWATERSRAND SUPERGROUP
50
60
70
80
90
100
CIA

possibly indicating more intense chemical weathering in northern Pongola source-regions relative to southern sources.

Nsuze Wit-Mfolozi pelites have CIA values that decrease stratigraphically upwards. Initially high values from the NLWM sequence (CIA=77-81; Fig. 23a) may reflect erosion of a deeply weathered source terrane during deposition of basal Pongola sediments. With increasing tectonic activity, relatively unweathered source material may have entered the Pongola basin, resulting in a decrease of CIA values in the NUWM section (CIA=72-77). Supporting this interpretation are deeply weathered paleosols underlying basal Pongola sediments in northern sections (Matthews and Scharrer, 1968; Armstrong et al., 1982; Grandstaff et al., 1986), and penecontemporaneous faulting in the Wit-Mfolozi area during deposition of upper Nsuze sediments (Matthews, 1967; Dix, 1984). The relatively unweathered source-material patterns in NUWM pelites also may be augmented by deposition of tuffaceous or carbonate sediments (Matthews, 1967).

Compositions of Witwatersrand pelites appear to reflect moderate to intense source weathering with CIA values chiefly in the range of 70-100 and most means from 80-90 (Fig. 23b). Witwatersrand pelites have CIA values which are more variable than those exhibited by Pongola pelites and appear to have the highest overall values from the Kaapvaal craton. Witwatersrand CIA values overlap those of Phanerozoic shales, Amazon river muds and residual laterite clays. The high Al_2O_3 contents and CIA values of some

Witwatersrand pelites (Fig. 23b; Table 3) may record intense weathering in the source-areas of these sediments (Reimer, 1985). Although average K8 and BOY pelites don't show a striking depletion of alkali elements (Table 3), samples with high CIA values (>90) also have the lowest K2O and Na2O contents (Table C.1-2). Thus, only some K8 and BOY pelites appear to be derived from intensely weathered sources. The range of CIA values exhibited by samples from the K8 and other Witwatersrand pelite horizons may reflect variations in climatic zones, rates of tectonism, flocculation- induced seggregation of clay minerals, or hydrothermally altered source regions. Variable Witwatersrand CIA values relative to Pongola pelites also may result from larger sampling region, and hence a potential for a more varied climatic regime. Provenance-composition effects and remobilization of elements during metamorphism are probably of less importance in contributing to this variation (Section V.4). Relatively small CIA ranges within the PRM and OG-PBR pelites probably reflect a small sample population.

CIA values of Ventersdorp pelites have a limited distribution (CIA=77-80), with values intermediate between those of Phanerozoic shales and Amazon cone muds (Fig. 23b). By contrast, pelites from the Transvaal sequence have CIA values which are quite variable. SIL-TH pelites exhibit the greatest range of variation, with CIA values between 60 and 85 and means from 75-80 (Table 4). This range correlates

with modern CIA values from a diverse suite of sediments including glacial clays, Phanerozoic shales and Amazon cone muds (Fig. 23b). CIA values for most Wolkberg pelites are generally low to moderate (SEL=65-67 and BR=75-81), with a small group from each population having CIA values >90. Mean CIA values for most Ventersdorp-Transvaal pelites (CIA=75-80) are similar to those of the Pongola (except MPR) and less than those of the Witwatersrand sequence (mean CIA=80-90). An exception is the STR and some BR-SEL pelites, which have high CIA values more characteristic of sediments derived from chemically weathered sources (>85).

Large standard deviations in CIA values for most Transvaal pelites (Table 4; Fig. 23b), may indicate that variable climatic conditions existed during deposition of these sediments. The larger sampling region of the Transvaal, relative to the Witwatersrand and Pongola units also may have caused the sampling of a varied climatic regime. Some of this variability also may result from element mobility during present-day weathering. For example, modern weathering may influence the CIA values of TH pelites, where samples collected from surface outcrops have higher values (CIA = 78-86) than drill-core samples (CIA = 61-85). This variability, however, is relatively minor compared to the overall range of values expressed by these sediments. As with the Pongola and Witwatersrand pelites, diagenesis and low-grade metamorphic conditions are

believed to have relatively minor effects on the major element compositions of these sediments.

Alkali and Alkaline Earth Element Distributions

The effect of variable degrees of weathering may be important in influencing the vertical distribution of alkali and alkaline earth elements in soil profiles (Nesbitt et al., 1980; Reimer, 1985; Schau and Henderson, 1983; and Grandstaff et al., 1986). Element fractionation trends developed in soils may be transferred into the sedimentary record, with little modification, during erosion of upper soil profiles. Thus, distributions of alkali-alkaline earth elements in sediments may record the weathering and tectonic histories of their source-rocks. Cations with relatively large ionic radii, such as Cs, Rb and Ba, are often fixed in weathering profiles by preferential exchange and adsorption on clays, while smaller cations such as Na, Ca and Sr are selectively leached from weathering profiles (Nesbitt et al., 1980). A graphical representation of this trend is portrayed in Figure 24 and compared to modern and ancient shales. Element concentrations are normalized to average upper-continental crust (Taylor and McLennan, 1985) on the vertical axis in order to express chemical variations in weathering profiles in reference to an average source-rock. Elements are grouped by valence and ionic radius on the horizontal axis in order to test their

Figure 24. Normalized element distributions in average Witwatersrand pelites compared to various weathering products (Modified after McLennan et al., 1983). Concentrations normalized to average upper-continental crust (Taylor and McClennan, 1985). Elements grouped by valence and arranged in order of increasing ionic radius from left to right within each valence group.

a)Progressively weathered samples of the Toorrongo granodiorite (data from Nesbitt et al., 1980).

b)Particulate matter from rivers in different climatic zones and tectonic environments (data from Martin and Meybeck, 1979).

c) NASC and PAAS shale compositions (data from Gromet et al., 1984; Taylor and McClennan, 1985). NASC, North American Shale Composite. PAAS, Post-Archean Average Shale.

d)Average pelites from the Witwatersrand Supergroup. PBR, Parktown-Brixton; PRM, Promise; RO, Roodepoort; BOY, Booysens; K8, K8 pelites. To eliminate the effects of modern weathering, only drill-core and underground mine samples are used in averages.

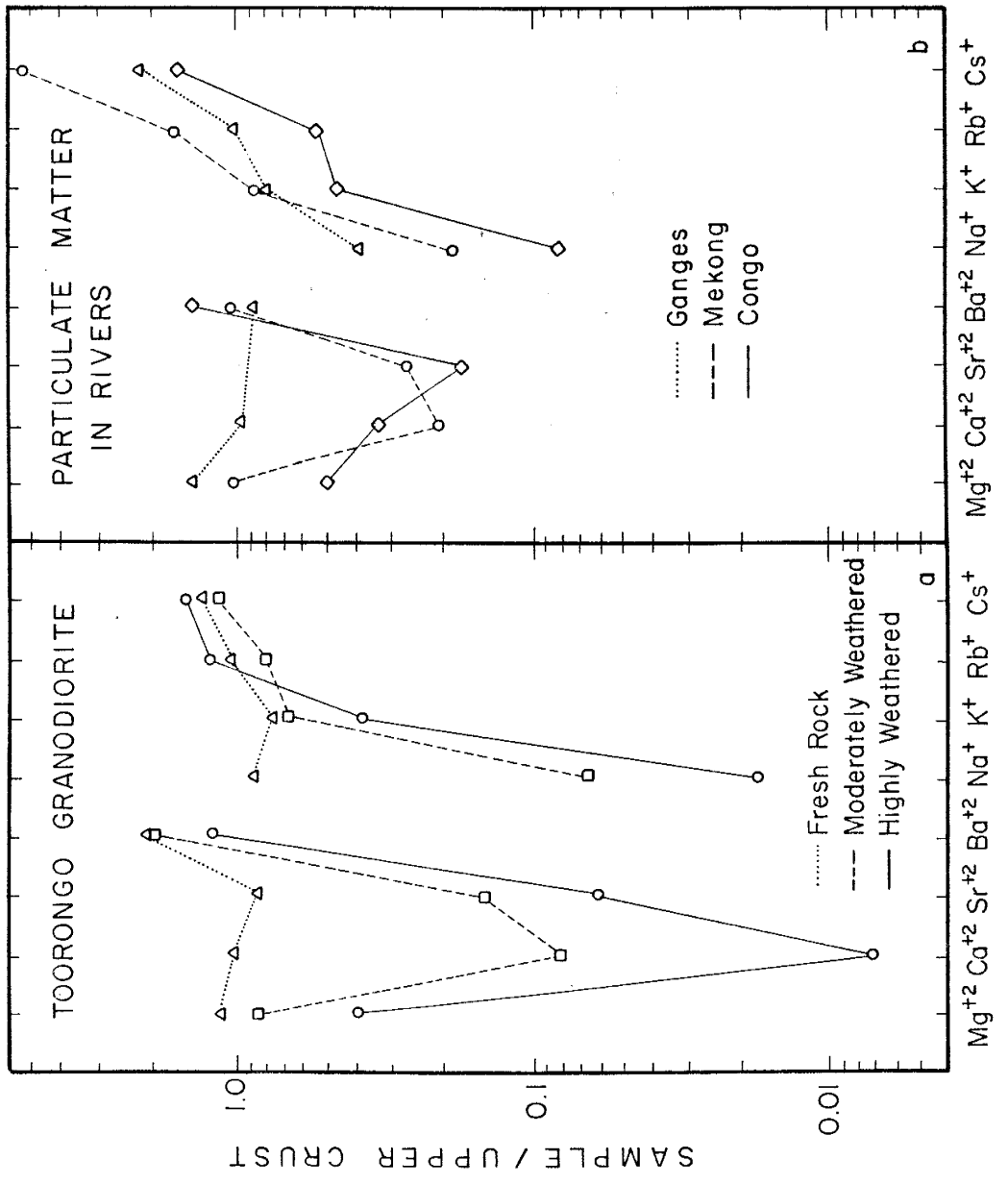
TOORONGO GRANODIORITE
PARTICULATE MATTER
IN RIVERS
SAMPLE / UPPER CRUST
1.0
0.1
0.01
Fresh Rock
Moderately Weathered
Highly Weathered
Ganges
Mekong
Congo
a
b
Mg+2 Ca+2 Sr+2 Ba+2 Na+ K+ Rb+ Cs+
Mg+2 Ca+2 Sr+2 Ba+2 Na+ K+ Rb+ Cs+

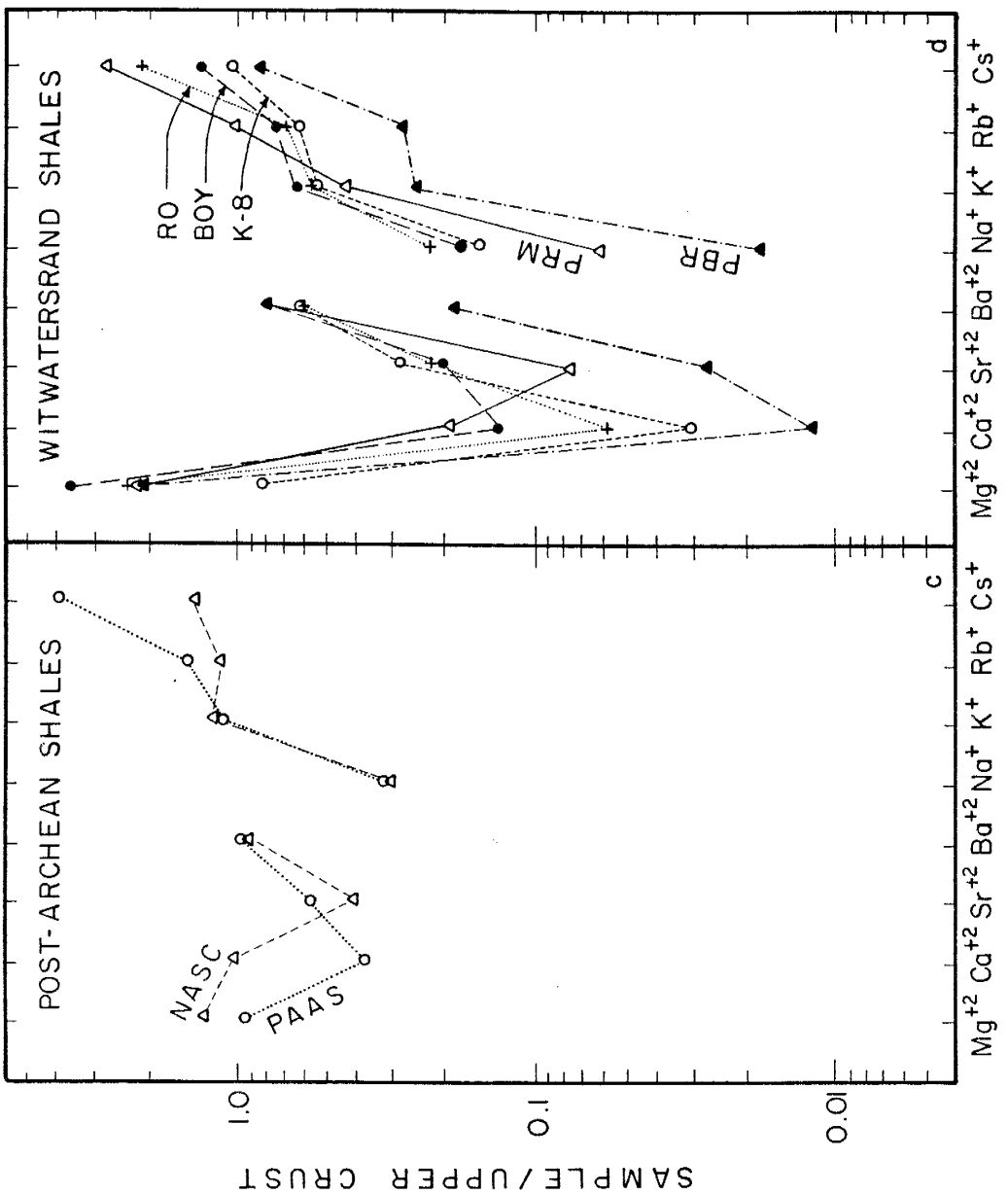
POST-ARCHEAN SHALES
WITWATERSRAND SHALES
NASC
PAAS
RO
BOY
K-8
PRM
PBR
c
d
SAMPLE/UPPER CRUST
1.0
0.1
0.01
Mg+2 Ca+2 Sr+2 Ba+2 Na+ K+ Rb+ Cs+

relative mobilities in relation to atomic size. In a study of progressive weathering of the Toorongo granodiorite of east-central Victoria, Australia, Nesbitt et al. (1980) noted that univalent and divalent cations show progressive depletion with decreasing ionic size, and as a function of depth in the weathering profile (Fig. 24a). This pattern may reflect selective adsorption and retention of large radii alkali and alkaline earth elements in preference to smaller radii elements on clays in the weathering horizons. Mg is an exception to the divalent cation trend, a feature which probably reflects the common substitution of Mg^{+2} for Al^{+3} in relatively stable octahedral sites of clays (Bailey, 1984).

The degree of chemical weathering is chiefly a function of climate and erosion rate, the latter of which varies with the rate of tectonic uplift. The influence of tectonism on alkali-alkaline earth element distributions in particulate matter from three modern rivers is shown in Figure 24b (data from Martin and Maybeck, 1979). The patterns for the Mekong and Congo Rivers, which lie in tropical climatic regions with little tectonic uplift, exhibit extreme depletions in Na, Ca and Sr. The pattern for the Ganges River (India) exhibits less depletion and reflects limited chemical weathering in a region of active tectonic uplift in the Himalayas.

Weathering patterns shown in Figures 24a and b may be

quantitatively transferred into sedimentary rocks. The patterns, for instance, from Phanerozoic composite shales, as represented by NASC (Fig. 24c; Gromet et al., 1984) and the Post Archean Average Shale (PAAS; Appendix D; Taylor and McLennan, 1985) exhibit only moderate degrees of alkali-alkaline earth element depletion, yet preserve the relative shapes of weathering patterns seen in Figures 24a and b. Because these composites reflect a variety of climatic conditions, and perhaps also different tectonic regimes, these patterns represent those of an ''average'' weathered source of Phanerozoic shales. Apparent differences in Ca concentration between NASC and PAAS are due to PAAS values being calculated on a carbonate free basis. Carbonate corrections have not been applied to Ca concentrations of NASC and Witwatersrand pelites (Fig. 24d).

Patterns exhibited by the Witwatersrand pelites (Fig. 24d) show strongly depleted alkali-alkaline earth patterns for the PBR, PRM and RO pelites, and thus appear to reflect the most intense chemically weathered sources. The BOY and K8 pelites, which occur in the upper portion of the Witwatersrand succession, show only moderate depletion of smaller cations, and thus may represent moderate chemical leaching of their source-areas. The single OG sample (not shown) is strongly depleted in Ca and Mg, yet shows only moderate depletion of Ba, Sr and the univalent cations. Although diagenisis and metamorphism may be responsible for the redistribution of some of these generally mobile

elements (Hower et al., 1976; Merriman et al., 1986), it is interesting to note that this transformation from strongly to moderately depleted alkali-alkaline earth patterns can be correlated with the transformation from argillite-arenite dominated sequences in the lower Witwatersrand successions, to conglomerate-arenite dominated sequences (Robb and Meyer, 1985) in the upper two units. Thus, the change in element distribution patterns of Witwatersrand pelites is interpreted to reflect the transformation from a low-lying source with a well-developed soil profile, to one which is characterized by active tectonism and rapid erosion. This interpretation is supported by the existence of well-developed paleosols on an Archean terrane characterized by a peneplaned surface (Pretorius, 1981b; Eriksson and Soegaard, 1985) which directly underlies lower Witwatersrand strata and by penecontemporaneous faulting during deposition of Central Rand sediments. Pelites from the Pongola, Ventersdorp and Transvaal sequences exhibit relatively limited inter-formational variability on alkali-alkaline earth element plots (not shown). Lack of element variability from these sequences suggests that alkali-alkaline earth element changes are sensitive to only dramatic changes in tectonic or climatic conditions. Cation trends for the Pongola, Ventersdorp and Transvaal sequences do not show any systematic stratigraphic variations. Thus these element patterns may only be useful in distinguishing dramatic tectonic or climatic variations.

Weathering interpretations based on alkali-alkaline earth element distributions contrast with CIA based interpretations. For example, high CIA values for K8 pelites suggest intense weathering of source-regions, yet relatively flat alkali-alkaline earth element distributions suggest more rapid erosion of sources for these sediments. As previously discussed, coarse grain sediments and active basin margin faulting during Central Rand sedimentation suggest that intense weathering of K8 pelite sources is unlikely. Therefor weathering interpretations based on alkali-alkaline earth element distributions are favored for K8 pelites. High CIA values for these sediments may result from hydrothermally altered sources which have undergone Al enrichment and only minor cation depletion. Hydrothermally altered granites located along the north to northwestern perimeter of the Witwatersrand basin are characterized by sericitic, propylitic, albitic and carbonate alteration (Robb and Meyer, 1987; Klemd and Hallbauer, 1987). These alteration processes could conceivably raise the CIA values of these granites without seriously diminishing their alkali-alkaline earth element contents.

K2O-Fe2O3T-Al2O3 Distributions

Paleoweathering conditions also may be examined with K2O-Fe2O3-Al2O3 ternary diagrams where two subparallel linear trends are apparent in the distribution of Pongola pelites (Fig. 25a). Trend-A pelites include the NMP and

Figure 25. K_2O-Fe_2O_3-Al_2O_3 distributions in pelites from the Kaapvaal craton. Regions for shales and residual clays from Reimer (1985). NASC, North American Shale Composite (Gromet et al., 1984); GR, granite; TON, tonalite; TH, Archean tholeiite; KOM, komatiite. Idealized compositions for magnetite, chlorite, illite, muscovite and K-feldspar indicated on diagram. a) Pongola pelites, trends a and b discussed in text, b) Witwatersrand pelites, Pongola trends a and b are shown for reference, c) Ventersdorp-Transvaal pelites, Pongola trends a and b are shown for reference.

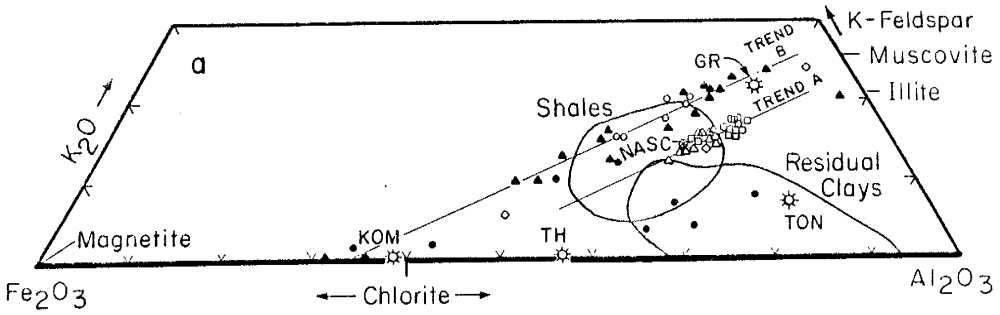

NSUZE GROUP

- ○ Upper Wit Mfolozi (NUWM)
- △ Lower Wit Mfolozi (NLWM)
- □ Mpongoza River (NMP)
- ◇ Vitshundi River (NVS)

MOZAAN GROUP

- ▲ Wit Mfolozi (MWM)
- ● Piet Retief (MPR)

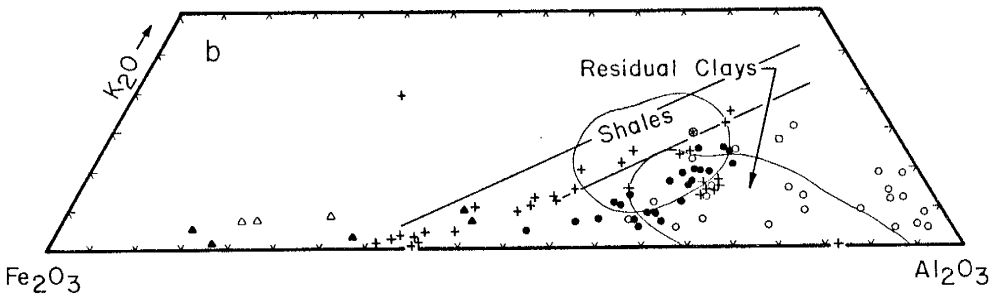

- ○ K8
- ● Booysens (BOY)
- \+ Roodepoort (RO)
- △ Promise (PRM)
- ▲ Parktown-Brixton (PBR)
- □ Orange Grove (OG)
- ⊕ NASC

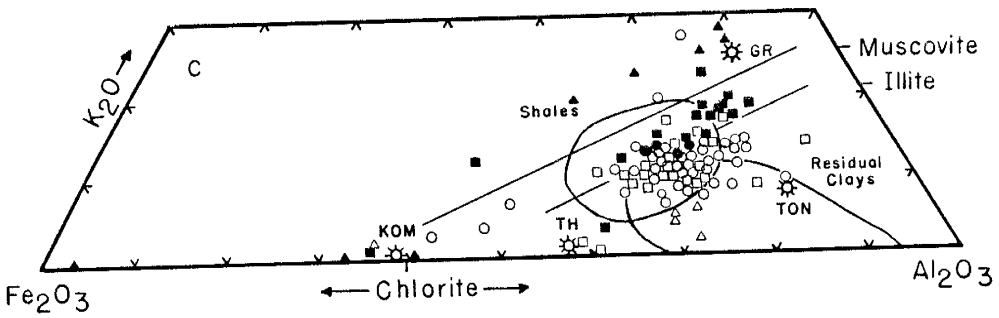

- □—□ Silverton (SIL)
- △—△ Strubenkop (STR)
- ○—○ Timeball Hill (TH)
- ■—■ Black Reef (BR)
- ▲—▲ Selati (SEL)
- ●—● Bothaville (BOT)

NLWM sections, which define a tight compositional cluster centered near NASC (Gromet et al., 1984; Appendix D). These samples also fall along a mixing line defined by chlorite and illite-muscovite end members. Enriched Al_2O_3 contents of trend-A pelites suggests that they are derived from more intensely weathered sources relative to trend-B pelites. Pelites of trend-B are composed of NUWM, MWM and some MPR samples. These pelites are depleted in Al_2O_3 relative to pelites of trend-A while some Mozaan trend-B samples also are enriched in Fe_2O_3T (Table 2). Trend-B pelites lie along a mixing line defined by chlorite and muscovite (perhaps mixed with minor K-feldspar) end members. Relatively enriched K_2O concentrations suggest that trend-B pelites are derived from a tectonically or volcanically active source, where a large proportion of rapidly eroded rock is deposited in the basin. CIA values of NUWM and MWM (CIA=70-77) are generally the lowest overall for Pongola pelites and support weathering interpretations based on K_2O-Fe_2O_3T-Al_2O_3 distributions. Thus, detritus may have changed from kaolinite and illite-rich (trend-A weathered rock) to K-feldspar and muscovite-rich (relatively unweathered trend-B granite and metamorphic rocks) with time.

Pelites from the Mozaan trend-B sequence with the highest Fe contents are collected from areas stratigraphically adjacent to banded iron formation. This relationship suggests that co-deposition of terrigenous-clastic sediments and Fe-rich chemical precipitates may have

caused this Fe-enrichment trend (Watchorn, 1980a). Four MPR pelites that plot in the residual clay field are interpreted to reflect K depletion during modern weathering.

Distributions of Witwatersrand pelites on K_2O-Fe_2O_3T-Al_2O_3 diagrams are more variable than most Phanerozoic shales and Pongola pelites (Figs. 25a and b). Most pelites from the West Rand Group (RO and especially PBR-PRM) are enriched in Fe_2O_3T, while K8 and OG pelites are enriched in Al_2O_3, having compositions similar to modern residual clays. K8 pelites have the highest overall K_2O/Al_2O_3 ratios of pelites from the Kaapvaal craton, suggesting that these sediments are derived from highly weathered or leached sources. Most Witwatersrand pelites are depleted in K_2O relative to pelites from the Pongola Supergroup.

Distributions of BOT-BR-TH-SIL pelites on K_2O-Fe_2O_3T-Al_2O_3 diagrams are similar to those of Phanerozoic shales and Pongola trend-A pelites (Fig. 25c). Unlike the Pongola sequence, these pelites do not exhibit linear distributions, suggesting that Ventersdorp-Transvaal samples have a more homogenous source, were exposed to constant climatic conditions, and/or are more thoroughly mixed than the Pongola pelites. K_2O/Al_2O_3 distributions of most TH-SIL pelites are slightly lower than those of Pongola trend-A pelites, whereas BOT-BR pelites have K_2O/Al_2O_3 distributions intermediate between those of Pongola trend-A and trend-B pelites. SEL pelites have the greatest relative K_2O or

Fe2O3T contents and STR pelites have the highest Al2O3 contents relative to most other Ventersdorp-Transvaal pelites. K2O/Al2O3 ratios of these pelites correlate well with CIA values. SEL pelites with the highest K2O/Al2O3 ratios also have the lowest CIA values (CIA=65-67) suggesting rapid erosion of their source-rocks. SEL pelites with high-Fe contents also have high CIA values (>95), suggesting a possible correlation between the concentration of Fe and depletion of alkali-alkaline earth earth elements in these sediments or their sources. Pelites from the STR sequence have the highest overall CIA values (86-94) and the lowest K2O/Al2O3 ratios of all Transvaal pelites. These patterns suggest that STR pelites are derived from highly weathered sources.

Ventersdorp-Transvaal sediment distributions on log-K verses log-Rb plots (Fig. 26) indicate that BOT-TH-STR-SIL pelites are depleted in K, and have lower overall K/Rb ratios relative to SEL-BR pelites. Sediments characterized by large contributions from late-stage granites may have low K/Rb ratios, but decreased ratios in these granites usually result from addition of Rb rather than decreased K concentrations (Taylor, 1965; Fig. 26). Decreasing K concentrations of BOT-TH-STR-SIL pelites are unusual considering the increased concentration of source granites suggested for these sediments by REE, Th and U concentrations (Table 4). A mechanism which can decrease sedimentary K and hold Rb contents constant during a period

Figure 26. K-Rb plot for pelites from the Ventersdorp and Transvaal Supergroups (After Taylor, 1965). K/Rb=230 line represents an average crustal ratio. Weathering trend calculated from data in Nesbitt et al. (1980), late-stage granite field from Taylor (1965). Pelite data from Table 4.

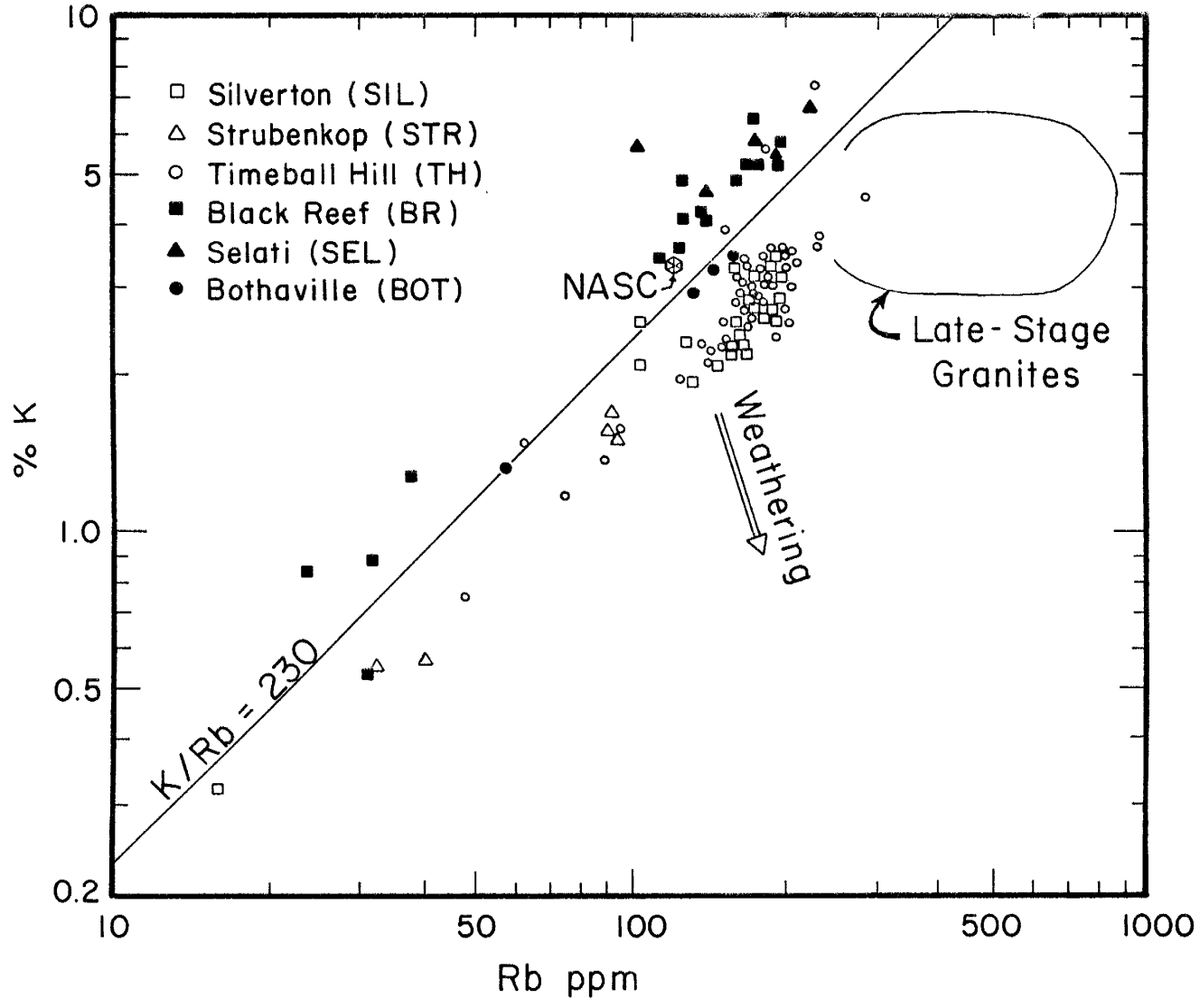
10
5
1.0
0.5
0.2
% K
10
50
100
500
1000
Rb ppm
Silverton (SIL)
Strubenkop (STR)
Timeball Hill (TH)
Black Reef (BR)
Selati (SEL)
Bothaville (BOT)
NASC
Late-Stage Granites
Weathering
K/Rb = 230

of increased granite exposure is an increase in weathering intensity. Decreased K and slightly increased Rb concentrations are apparent in weathering horizons and sediments derived from highly weathered sources (Nesbitt et al., 1980; Wronkiewicz and Condie, 1987). The weathering trend shown in Figure 26 can produce K-depleted sediments from the same sources which produced SEL-BR pelites or modify the composition of more granite-rich sources. Some SEL pelites exhibit high Cr/Ni ratios and depleted NASC-normalized Co anomalies, features suggestive of a weathered source terrane, yet do not show any K depletion. Thus, some variations also may result from mobility of K and/or Rb during metamorphism and diagenesis (Weaver and Beck, 1971; Ludden et al., 1982; Merriman et al., 1986).

The Ni-Cr Problem

Most Kaapvaal pelites deposited prior to 2.2 Ga exhibit an enrichment of Cr and Ni relative to NASC (Figs. 27-29). High Ni and Cr concentrations in Pongola pelites has led to the suggestion that these sediments are derived from sources with substantial mafic or komatiitic components (Laskowski and Kroner, 1985). This interpretation, however, is not supported by Pongola pelite REE, HFSE and LILE contents. Concentrations of these elements are similar to those of NASC, suggesting a Pongola source-area which is similar in overall composition to average Phanerozoic upper-continental crust (Table 2). Pongola pelites also are

depleted in Co and Mg relative to NASC, a pattern opposite to that expected if these sediments were derived from ultramafic-rich sources.

Hydraulic sorting of grains may be important in influencing the composition of some sediments, however, similar mean Cr/Ni ratios in both Pongola quartzites and pelites (Fig. 28; Tables 2 and 7) suggests that separation by grain size or density is not responsible for Ni-Cr patterns in these pelites.

Archean oceans may have been enriched in Cr and Ni, relative to modern oceans, due to ocean-ridge or back-arc hydrothermal leaching of komatiite oceanic crust (Condie and Wronkiewicz, 1988). Clay-particle scavenging of Ni and Cr in enriched Archean seawater could thus explain the high Ni and Cr concentrations in some Kaapvaal pelites. Rapid mixing of open ocean waters with cratonic basin waters is required for this model in order to maintain high Ni-Cr seawater concentrations. Problems with this model include, 1) relatively low Co concentrations in Pongola, Witwatersrand-RO and Transvaal-SEL pelites (Tables 2-4), since modern oceanic crust acts as a source for Co (Honnorez, 1983); 2) high Pongola, Witwatersrand-RO, Transvaal-SEL Cr/Ni ratios (Figs. 19-21), since Cr-Ni fractionation is not observed in modern ocean-ridge hydrothermal systems; and 3) an absence of hydrothermal fluid leaching of Ni and Cr from modern oceanic crust (Humphris and Thompson, 1978; Mottl et al., 1979; Seyfried and Mottl, 1982; Trocine and Trefry,

(1988).

An alternate, and preferred model that can explain the enriched Cr and Ni contents of Pongola, Witwatersrand-RO and Transvaal-SEL pelites is intense chemical weathering of komatiitic source rocks (Wronkiewicz and Condie, 1989a). Studies of modern terrestrial weathering profiles indicate that Cr and Ni can be enriched and fractionated from each other in tropical weathering environments. For example, enrichments up to ten-fold for Cr and three-fold for Ni have been documented in modern laterite profiles developed on mafic rocks in Australia and India (Ball and Gilkes, 1987; Narayanaswamy and Ghosh, 1987). Deeply weathered Precambrian soil profiles could have provided detritus for some Kaapvaal pelites, in the way that weathered rocks from the Andes Mountains and Brazilian Platform presently provide detritus for the Amazon River system (Kronberg et al., 1986). Thick paleoregoliths on pre-Pongola basement (Matthews and Scharrer, 1968; Armstrong et al., 1982) also support this interpretation. Modern upper-laterite profiles developed on ultramafic rocks in Australia, South America and Indonesia also are depleted in Mg and Co, slightly enriched in Ni, and strongly enriched in Cr. These compositional trends are similar to those exhibited by Pongola, Witwatersrand-RO, and Transvaal-SEL pelites (Tables 2-4; Zeissink, 1971; Webber, 1972; Golightly, 1981). Intense chemical weathering also may account for increased Cr/Ni ratios of these pelites, in that studies of Cenozoic

laterites indicate that Cr is retained in upper soil layers in Cr-rich chlorite (penninite), chromite and magnetite, whereas Ni is liberated during the breakdown of olivine and pyroxene, or is leached from secondary clay minerals (Zeissink, 1971; Webber, 1972). Progressive downward migration of Ni in these laterites causes increased Cr/Ni ratios in the upper layers. Erosion of upper portions of Precambrian laterite horizons developed on komatiites could thus account for the high Cr/Ni ratios observed in some Kaapvaal pelites.

Parallel changes in Cr/Ni ratios and the CIA values in Wit-Mfolozi area pelites also support models suggesting enrichment of Cr and Ni during weathering. NLWM and MWM pelites, which have the highest CIA indices, also have the highest Cr/Ni ratios ($\sim$4.5; Figs. 19 and 23a). NUWM pelites, which have lower CIA indices and appear to be derived from a tectonically active source region, have Cr-Ni distributions which are more typical of Precambrian pelites. If correct, this model also predicts that residual nickeliferous paleolaterites may exist in ultramafic portions of the Kaapvaal craton basement, and offer an exploration guide to nickel deposits in the region.

PELITE PROVENANCE

Pelites as Source-Area Composites

Because of their homogeneity and post-depositional impermeability, shales and pelites are considered to be

representative samples for geochemical provenance studies. Quartzites are less desirable due to their low trace element contents, pre-lithified permeability, and hydraulic segregation introduced heterogeneity. In order to evaluate the overall effects of element fractionation in the sedimentary cycle, quartzites however, must be considered together with pelites.

Sedimentary Recycling Constraints

The role of recycling in the evolution of sediments is difficult to evaluate. One way of approaching this problem is to consider ratios of elements in pelites with strikingly different incompatibilities such as the Th/Sc and La/Sc ratios (Taylor and McLennan, 1985). In the absence of sedimentary recycling, these ratios should reflect the proportion of felsic components relative to mafic-ultramafic components. If recycling is important, then changes in these ratios should be buffered by the incorporation of previously deposited sediments. Isotopic data from sediments also may provide information on the likelihood of sediment recycling. Sediments with crustal residence ages approximately equal to their depositional ages are derived from juvenile crustal sources with the inclusion of little or no recycled sediments. By contrast, sediments with crustal residence ages that are significantly older than their depositional ages may have incorporated large amounts of recycled sediments or may be derived from older first-cycle igneous or metamorphic sources. A final method

may be important.

Th/Sc and La/Sc ratios in pelites from the Pongola Supergroup show considerable overlap without consistent stratigraphic variations (Table 2). These trends suggest that ratios were either buffered during recycling of sediments or that a compositionally constant Pongola source-area remained exposed during deposition of the entire sequence. Nd isotopic data indicate that Pongola sediments are derived from sources with crustal residence ages that are virtually indistinguishable from Pongola depositional ages (Miller and O'Nions, 1985). This observation suggests that sediment recycling did not significantly influence the composition of the Pongola sequence. The limited occurrence of polycrystalline quartz (~3%) and the near absence of lithic-sedimentary clasts in Pongola quartzites also support this interpretation (Table 6).

The lower three subgroups of the Witwatersrand Supergroup have relatively invariant Th/Sc and La/Sc ratios (Table 3; except for the high La/Sc ratio in OG), suggesting that these ratios either are buffered by recycling or source-area compositions remained relatively constant. Minor Th/Sc changes in BOY pelites and large increases in both ratios for K8 pelites suggest exposure of new sources for these sediments. Stratigraphic upsection increases of polycrystalline quartz and lithic-sedimentary clasts (Table 6) suggest that recycling became increasingly important for upper-Witwatersrand strata, an interpretation which is

opposite to that based on element ratios. Isotopic data from pelites of the Witwatersrand sequence may be needed to resolve this dilemma.

Th/Sc and La/Sc ratios show marked changes between deposition of the BOT-SEL-BR and TH-STR-SIL pelites (Table 4). Rapid changes in these ratios thus argue against significant sediment recycling and suggest that new sediment sources were exposed during deposition of the Pretoria Group. Pelites from the BR unit have La, Sc and Th concentrations, as well as Th/Sc, La/Sc and La/Th ratios that are similar to those of the Witwatersrand pelites. These similarities suggest that BR pelites may be partially derived from the erosion of older Witwatersrand strata and/or the same crustal sources which gave rise to the Witwatersrand sediments. A temporary change in sediment transport direction, from northern to southern sources (Button, 1973a), during deposition of basal BR sediments and the occurrence of reworked Witwatersrand gold in lower Transvaal sediments (Pretorius, 1976) supports this speculation. An abundance of polycrystalline quartz and lithic-sediment clasts in Ventersdorp-Bothaville, Transvaal-Wolkberg, Waterberg and Soutpansberg quartzites indicates that sedimentary recycling may have influenced the compositions of these units. An absence of recycled clasts in Pretoria Group quartzites indicates that these sediments are mostly from first-cycle sources (Table 6).

NASC-Normalized Distributions

Element distributions of sediments normalized to potential sources can be used to monitor the combined effects of weathering, diagenesis, metamorphism and transport on sediment composition. Secondary effects influencing the composition of both Phanerozoic shales and Archean pelites can be identified and compared by normalizing NASC to present-day average upper-continental crust (PUC) and average Witwatersrand pelites to Archean upper-continental crust (AUC; Fig. 27a). Both sediment patterns have similar distributions suggesting that the cumulative effects of weathering, diagenesis, metamorphism and transport are similar for both Archean pelites and Phanerozoic shales. Most elements generally are enriched relative to their crustal sources by factors of 1.1 to 1.5. A depletion in Ta (also Nb, not shown), is exhibited by both Witwatersrand pelites and Phanerozoic shales. The cause of this relative depletion is uncertain but may reflect hydraulic fractionation of minor phases enriched in Nb and Ta into coarser sediments or errors in the estimated concentration of these elements in AUC and PUC. A possible example of a minor phase that can fractionate Nb and Ta is rutile, which may be concentrated as needle-like crystals in the sand-sized grain fraction of sediments.

Because of the similar element distributions in Witwatersrand pelites and NASC (Fig. 27a), we can compare

Figure 27. NASC-normalized distributions of various elements in average Witwatersrand pelites. Elements are ordered from left to right to represent contributions of felsic and mafic end member sources, respectively. Data from Table 3. After Wronkiewicz and Condie (1987).

a) Comparison of Witwatersrand pelites (WS) to the North American Shale Composite (NASC; Gromet et al., 1984; Appendix D), with each composite sample normalized to corresponding average upper-continental crust composition of a similar age. PUC, present-day upper-continental crust and AUC, Archean upper-continental crust (Appendix D). Upper-crust data chiefly from Weaver and Tarney (1984), and Taylor and McLennan (1985). Other values for AUC Nb=13 ppm, Ta=Nb/12=1.1 ppm, V=100 ppm.

b) NASC-normalized element distributions in Witwatersrand pelites. Data from Table 3. K8, K8 pelites; BOY, Booysens pelites; RO, Roodepoort pelites; PRM, Promise pelites; PBR, Parktown-Brixton pelites.

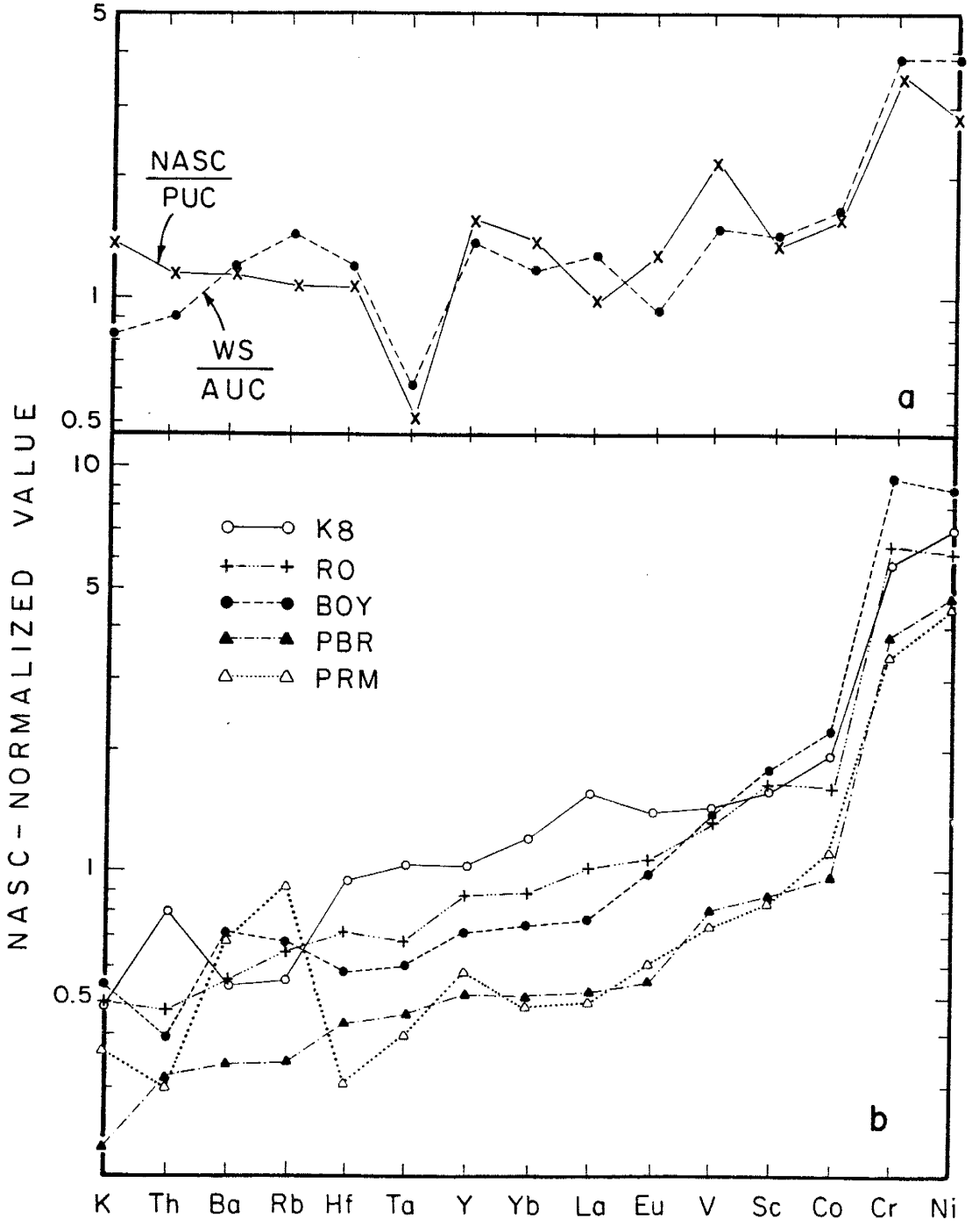
5
1
0.5
NASC
PUC
WS
AUC
a
10
5
1
0.5
K8
RO
BOY
PBR
PRM
b
NASC-NORMALIZED VALUE
K
Th
Ba
Rb
Hf
Ta
Y
Yb
La
Eu
V
Sc
Co
Cr
Ni

the source area of Kaapvaal craton pelites to present-day average upper-continental crust by normalizing element contents in these pelites to NASC. Distributions of Pongola pelites on NASC-normalized plots indicate similarities in distributions of LILE, HFSE, REE, V and Sc (Fig. 28). These similar patterns suggest that the Pongola source is remarkably similar in composition to average Phanerozoic upper-continental crust, whereas it differs significantly from published estimates of Archean upper-continental crust (Condie, 1981; Taylor and McLennan, 1985). A significant proportion of high-K2O granites (and/or felsic volcanics) were probably present in the source-area at the onset of Pongola sedimentation. Moderately large negative Eu anomalies and La/Yb ratios (Fig. 15) suggest that these granites were derived by intra-crustal melting involving fractionation of feldspars (Taylor and McLennan, 1985). Based on paleocurrent measurements, Von Brunn and Hobday (1976) and Von Brunn and Mason (1977) suggest that these granitic sources may lie to the north for Pongola sediments in the Wit-Mfolozi area, whereas Watchorn and Armstrong (1980) indicate a western source for sediments in the Piet Retief area. Dix (1984) proposes that Mozaan sediments in the Wit-Mfolozi area were derived from sources to the south-southwest, and suggests that differences between his and previous paleocurrent studies may result from irregular basin margins.

pelites from the Witwatersrand Supergroup are depleted

Figure 28. NASC-normalized distributions of various elements in average Pongola pelites and quartzites. Elements are ordered from left to right to represent increasing contributions of felsic and mafic end member sources, respectively. Data from Table 2. After Wronkiewicz and Condie (1987). a) pelites and quartzites of the Mozaan Group: MPR, Mozaan Piet Retief; MWM, Mozaan Wit-Mfolozi; MQ, Mozaan quartzites undifferentiated. b) pelites and quartzites from the Nsuze Group. NMP, Nsuze Mpongoza River; NUWM, Nsuze Upper Wit-Mfolozi River; NLWM, Nsuze Lower Wit-Mfolozi River; NVS, Nsuze Vitshundi River.

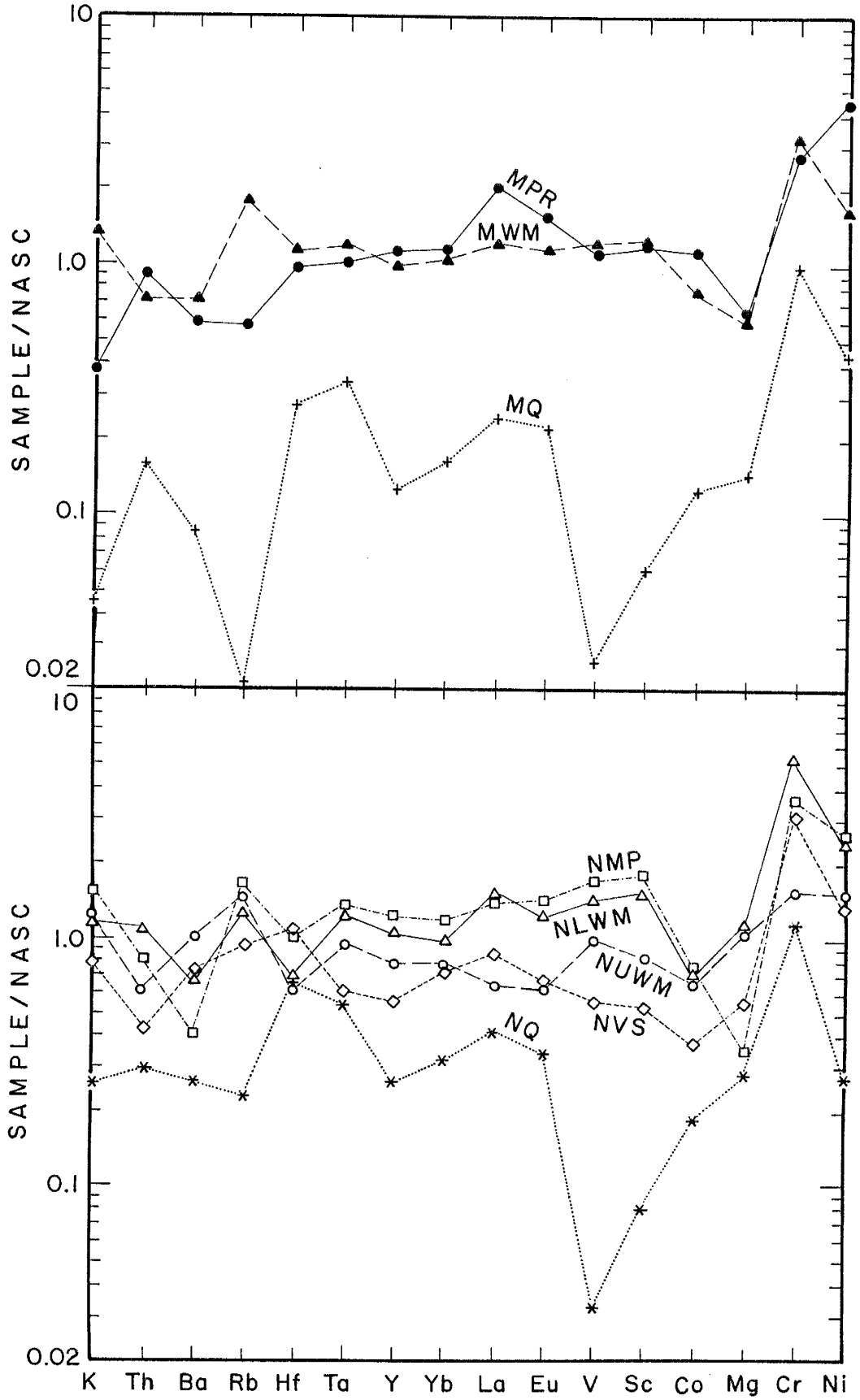
10
1.0
0.1
0.02
SAMPLE/NASC
MPR
MWM
MQ
10
1.0
0.1
0.02
SAMPLE/NASC
NMP
NLWM
NUWM
NVS
NQ
K
Th
Ba
Rb
Hf
Ta
Y
Yb
La
Eu
V
Sc
Co
Mg
Cr
Ni

in LILE relative to NASC, and with the exception of K8 (and OG, not shown) also are depleted in REE and HFSE (Fig. 27b). Irregularities in the distrbution of some LILE probably reflect mobilization of these elements during weathering or other secondary processes. Witwatersrand pelites are enriched in Cr and Ni and the RO, BOY an K8 pelites also are enriched in V, Sc, and Co. These compositional differences imply that the Witwatersrand sources are enriched in mafic and ultramafic components relative to Phanerozoic upper-continental NASC and Pongola sources. High MgO contents of BOY pelites (Table 3) also are consistent with significant ultramafic input into these rocks. Data in Figure 27b and Table 3 indicate that REE, HFSE and transition metals tend to increase in abundance with stratigraphic height. The basal OG pelite (not shown) is an exception to this trend having higher REE and HFSE contents relative to overlying pelites. This stratigraphic geochemical trend is unusual in that it suggests that both granitic and komatiite-basalt sources increased with time during deposition of Witwatersrand sediments. Contributions from komatiitic and basaltic components appear to have peaked during deposition of BOY pelites. Increasing La/Yb ratios and well-developed negative Eu anomalies indicate that a significant increase in the proportion of granite must have occurred during deposition of the RO and BOY pelites, peaking perhaps during deposition of the K8 pelites (Fig. 18). Granites characterized by large negative Eu anomalies must have been

present, at least locally, during deposition of the OG pelite. Robb and Meyer (1985) suggest that hydrothermally altered granites (HAGS) may be an important source for Au and U in the Central Rand Group. Such HAGS commonly show large enrichments in most alkali elements and depletion in Na2O and CaO. The K8 and BOY pelites from the Central Rand Group do not show unusual enrichment in alkalies (Table 3) and their low Na2O and CaO can be interpreted in terms of weathering as previously discussed. Thus, HAG sources for these pelites are compatible but not demanded by the geochemical data.

NASC-normalized element distributions of Ventersdorp-Transvaal pelites also indicate a progression from primitive to evolved crustal sources. BOT-SEL-BR pelites have LILE contents which generally are depleted relative to TH-STR-SIL pelites and NASC (Fig. 29). REE, HFSE and Th contents also are generally low for BOT-SEL-BR pelites, ranging from 40-85% of the NASC concentration. Exceptions to this trend are La in BOT pelites, which is similar to concentrations in NASC, and La and Eu in BR pelites which are only slightly depleted relative to NASC. These features suggest that although overall sources for the BOT-SEL-BR sediments were largely of a primitive composition, evolved source-rocks were periodically exposed during deposition of BOT and BR sediments. Transition metal and Mg contents of these pelites also are generally enriched relative to NASC (except

Figure 29. NASC-normalized distributions of various elements in average Ventersdorp and Transvaal pelites. Elements are ordered from left to right to represent increasing contributions from felsic to mafic end member sources, respectively. Data from Table 4. After Wronkiewicz and Condie (1987).

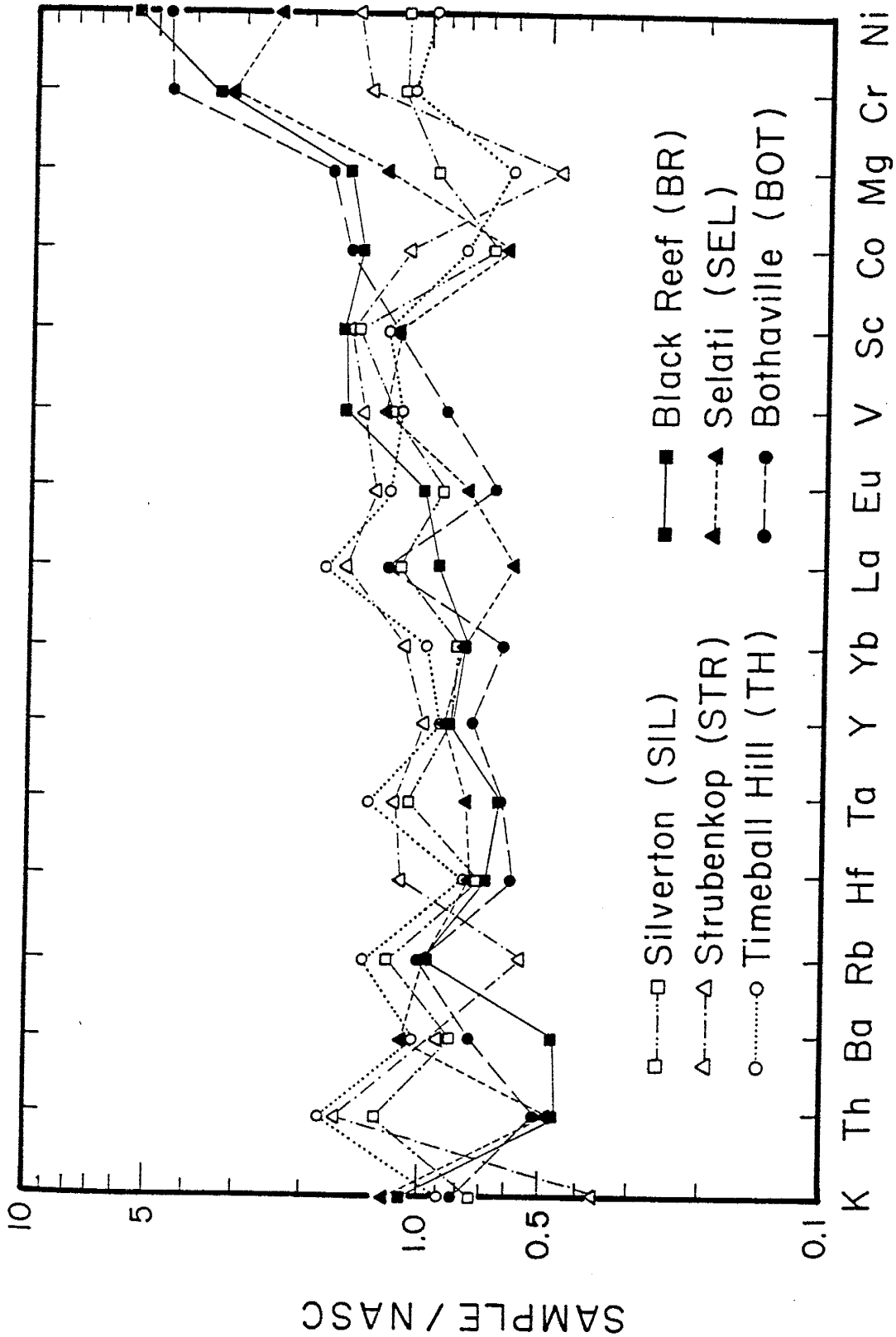
SAMPLE / NASC
10
5
1.0
0.5
0.1
K Th Ba Rb Hf Ta Y Yb La Eu V Sc Co Mg Cr Ni
Silverton (SIL)
Strubenkop (STR)
Timeball Hill (TH)
Black Reef (BR)
Selati (SEL)
Bothaville (BOT)

SEL Mg and Co, which may reflect chemical weathering of sources). TH-STR-SIL pelites exhibit LILE, HFSE, REE and transition metal distributions that are similar to NASC, indicating that the source of these sediments is similar in average composition to Phanerozoic upper-continental crust and to the K8-Pongola pelite sources. These pelites differ from NASC by having slightly higher Th and La, and lower K and Mg contents. Although negative Eu anomalies and La/Yb ratios are variable, mean ratios increase stratigraphically upsection within the Transvaal sequence (Fig. 17, Table 4). These trends also suggest increasing exposure of evolved granite sources upsection within the Transvaal sequence.

Since exposures of Waterberg and Soutpansberg rocks are characterized by extensive present-day weathering, caution should be exercised in making provenance interpretations due to possible mobilization of major and LILE. NASC-normalized distributions of Waterberg and Soutpansberg shales (Fig. 30) indicate that sources for these sediments are similar in composition to average Phanerozoic upper-continental crust and the Transvaal-Pretoria Group source (Fig. 29). HFSE and REE distributions are particularly diagnostic due to their overall stability in weathering profiles (Taylor and McLennan, 1985). Granites must have been an important source for these sediments as indicated by well-developed negative Eu anomalies and large La/Yb ratios for both the Waterberg ($Eu/Eu^*=0.68$; La/Yb=21)

Figure 30. NASC-normalized distributions of various elements in Waterberg and average Soutpansberg shales. Elements are ordered from left to right to represent increasing contributions from felsic to mafic end member sources, respectively. Data from Table 5. After Wronkiewicz and Condie (1987).

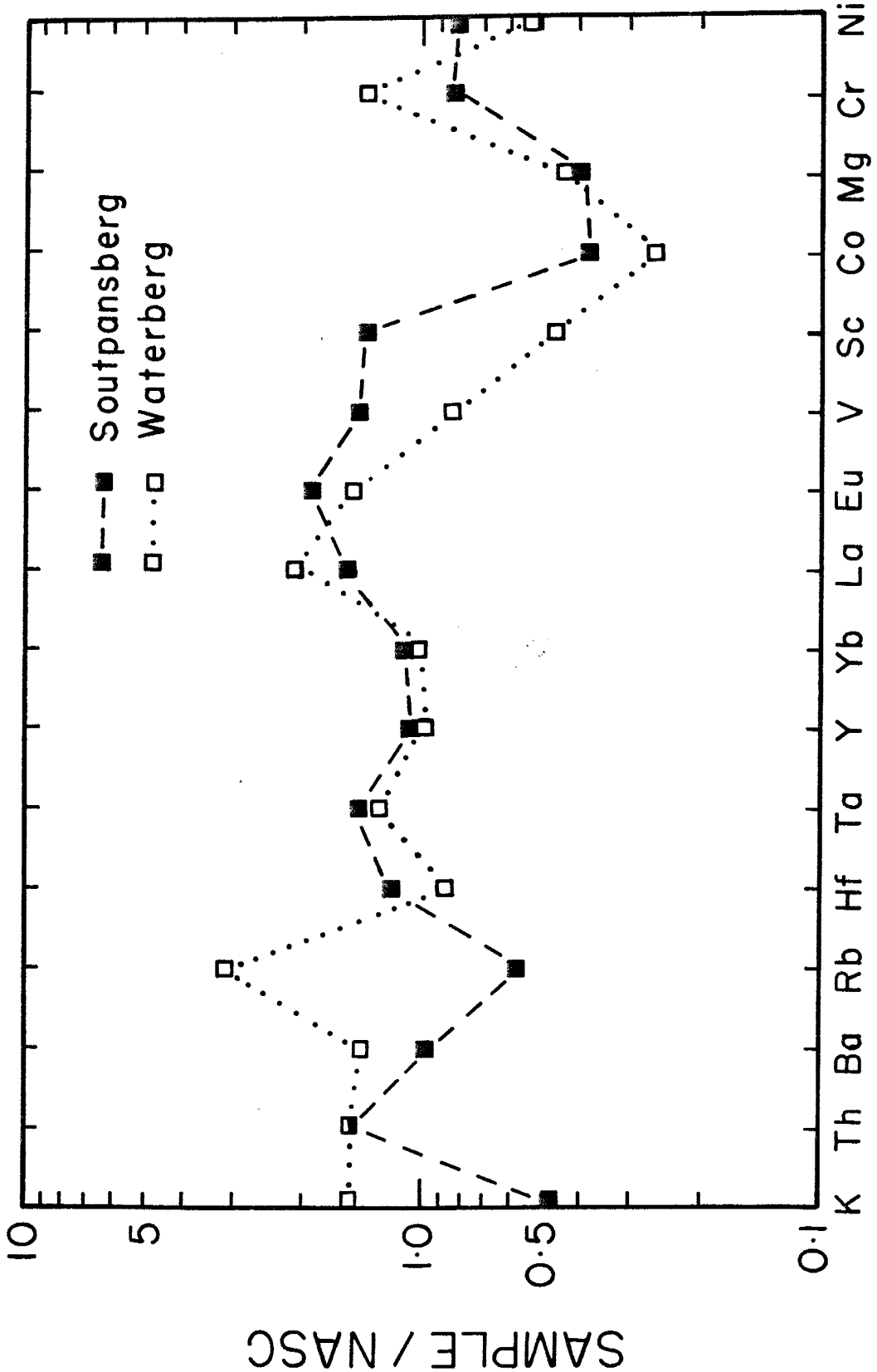
Soutpansberg
Waterberg
10
5
1·0
0·5
0·1
SAMPLE / NASC
K Th Ba Rb Hf Ta Y Yb La Eu V Sc Co Mg Cr Ni

and Soutpansberg shales (Eu/Eu*=0.66; La/Yb=13; Table 5). Concentrations of Co and Mg are depleted relative to NASC, but these features may be modified by modern weathering. Cr contents are similar to those of NASC, indicating that relative proportions of mafic and ultramafic source-regions for Waterberg and Soutpansberg sediments may be similar to proportions in exposed Phanerozoic crust. This speculation is supported by Ni-Cr distributions of Waterberg and Soutpansberg shales which approximate those of NASC (Fig. 22).

Cr/Zr and Sc/Th Ratios

Relative contributions of komatiite/granite sources should be reflected in the distribution of Cr/Zr, since these two elements monitor pyroxene-chromite and zircon contents, respectively. Pongola pelites have Cr/Zr ratios (1.3-5.0; Table 2) that are equal to or less than those exhibited by pelites from the Moodies succession ($\sim$5.5; McLennan et al., 1983) implying a more evolved (felsic) crustal source for Pongola pelites relative to that of the Moodies. Similarly, Sc/Th ratios may reflect relative contributions from (basalt + komatiite)/granite. Pongola pelite Sc/Th ratios (1.7-2.7) are generally less than those of the Moodies pelites ($\sim$ 2.6), supporting previous interpretations based on Cr/Zr ratios.

The three upper Witwatersrand pelite units are enriched in both Cr and Zr (Table 3), a feature suggestive of

increased input into the Witwatersrand basin of both granite and komatiite. It is noteworthy that Cr/Zr ratios reach a maximum value (9.9) in the BOY pelites as do bulk Cr, MgO and Ni contents. Decreased Cr/Zr ratios in K8 pelites probably reflect rapid increases in the proportion of granite relative to komatiite in the Witwatersrand sources (Fig. 8). The low Cr/Zr ratio (2.4) of the OG pelite also indicates the importance of granite sources during initial Witwatersrand basin development. Sc/Th ratios in Witwatersrand pelites also record the same stratigraphic evolution recorded by Cr/Zr ratios. Mean Sc/Th ratios increase from deposition of basal PBR-PRM units to the BOY sequence (3.6 to 5.8), then decrease again in the K8 pelites (2.6).

Pelites from the lower portion of the Ventersdorp-Transvaal sequence (BOT-SEL-BR) have mean Cr/Zr ratios (2.5-5.3) that are similar to those of the Moodies, Pongola and Witwatersrand pelites (Tables 2-4; McLennan et al., 1983). TH-STR-SIL mean Cr/Zr ratios (0.9-1.1) are similar to those of NASC (0.6) and significantly lower than those of all previously deposited Kaapvaal pelites. These decreased Cr/Zr ratios imply greater proportions of evolved (felsic) sources for TH-STR-SIL pelites relative to BOT-SEL-BR, Witwatersrand, Pongola and Moodies pelites. BOT-SEL-BR pelites have mean Sc/Th ratios (2.9-4.6) which are similar to those of Moodies and Witwatersrand pelites, whereas TH-STR-SIL mean Sc/Th ratios (0.8-1.4) are less than those

of the Moodies, Pongola and Witwatersrand, and similar to NASC (1.3). This again suggests that the TH-STR-SIL pelites were derived from a source enriched in felsic components relative to the BOT-SEL-BR pelites and Archean pelites of southern Africa.

Cr/Zr ratios of Waterberg and Soutpansberg shales (0.9 and 0.4, respectively) are significantly lower than those of Kaapvaal pelites deposited prior to the Transvaal-Pretoria Group. This pattern indicates that evolved crustal sources exposed during deposition of the Pretoria Group probably remained exposed during deposition of the Waterberg and Soutpansberg sediments. Sc/Th ratios of Waterberg (1.0) and Soutpansberg pelites (1.2) also are similar to NASC and Pretoria Group ratios (Table 4) and significantly lower than ratios of other southern Africa pelites.

Ni and Cr Distributions

Despite possible secondary modification due to weathering, Cr and Ni distributions can still be used to constrain the provenance of sediments. Pongola NUWM pelites exhibit Cr/Ni ratios similar to most Precambrian pelites (Fig. 19), have relatively low CIA indices (CIA=71), and were eroded during a tectonically active period of Pongola basin development (Matthews, 1967; Dix, 1984). These pelites may be more representative of the overall Pongola source-area than pelites exhibiting elevated Cr/Ni ratios. Ni and Cr concentrations of NUWM pelites are only moderately

enriched relative to NASC and post-Archean pelites in general (Fig. 19), suggesting that the Pongola source is enriched in mafic/ultramafic components by ~50% relative to average Phanerozoic upper-continental crust.

Large enrichments (300-1000%) of Cr and Ni in Witwatersrand pelites relative to Phanerozoic shales may partially reflect adsorption or substitution of these metals onto clay-sized particles during weathering or deposition in seawater (Li, 1981; Balistieri and Murrey, 1984; Manceau and Calas, 1986; Wronkiewicz and Condie, 1989a; Condie and Wronkiewicz, 1989). However, overall Ni-Cr distributions (Fig. 20) suggest a source-area enriched in mafic/ultramafic components relative to NASC and Pongola sediment sources. Ni and Cr contents are highest for BOY pelites, indicating that mafic/ultramafic source contributions peaked during deposition of this unit. High Ni/Co, Cr/V and low V/Ni ratios in Witwatersrand pelites are comparable to averages given for Archean pelites by Taylor and McLennan (1985), reflecting significantly greater contributions from mafic-ultramafic components than are present in the sources of most Phanerozoic shales. The low Ni and Co concentrations in the OG pelite are anomalous with respect to other Witwatersrand pelites.

BOT-BR pelites have Ni-Cr distributions that are characteristic of early Archean pelites from greenstone successions (Fig. 21). Ni-Cr contents in these pelites are also similar to those of Moodies and lower Witwatersrand,

and greater than those of TH-STR-SIL pelites. SEL pelites exhibit a wide range of Ni-Cr concentrations, however, slightly elevated Cr/Ni ratios suggests that these elements have been enriched during intense chemical weathering of komatiitic lava sources (Wronkiewicz and Condie, 1989a). TH-STR-SIL, Soutpansberg and Waterberg pelites (Figs. 21 and 22) have Ni-Cr concentrations similar to those of NASC and post-Archean pelites. TH-STR-TH pelites are the first fine grained sediments from the Kaapvaal craton to exhibit such a pattern, possibly signifying the first emergence of fully evolved upper-continental crust on the Kaapvaal craton at 2.2 Ga ago.

Th/U and La/Th Ratios

Th/U ratios of Pongola pelites are variable, with the range of mean values (2.7-4.3; Table 2) being similar to, but more varied than those of average Archean fine-grained sedimentary rocks (3.5-4.1; Taylor and McLennan, 1985), and similar to or less than the NASC ratio (Th/U=4.4). Low Th/U ratios for Archean sediments may reflect a provenance effect, an absence of significant sedimentary recycling, and/or an Archean atmosphere which was less oxygenating than the present one (Taylor and McLennan, 1985). Pelites from the Pongola sequence have La/Th ratios that are highly variable, with mean ratios ranging from 2.8 to 7.2 (Fig. 31a; Table 2). Based on other trace element patterns, NUWM pelites appear to be the least effected by paleoweathering,

Figure 31. Log La vs. log Th plot for Kaapvaal craton pelites. La/Th=3.5 and La/Th=2.8 lines represent ratios which typify Archean and post-Archean pelites, respectively. After Taylor and McLennan (1985).

a) Pelites from the Pongola Supergroup. Data from Table 2.

b) Pelites from the Witwatersrand Supergroup. Data from Table 3.

c) Pelites from the Ventersdorp and Transvaal Supergroups. Data from Table 4.

d) Shales from the Waterberg and Soutpansberg Groups. Data from Table 5.

Figure Key:

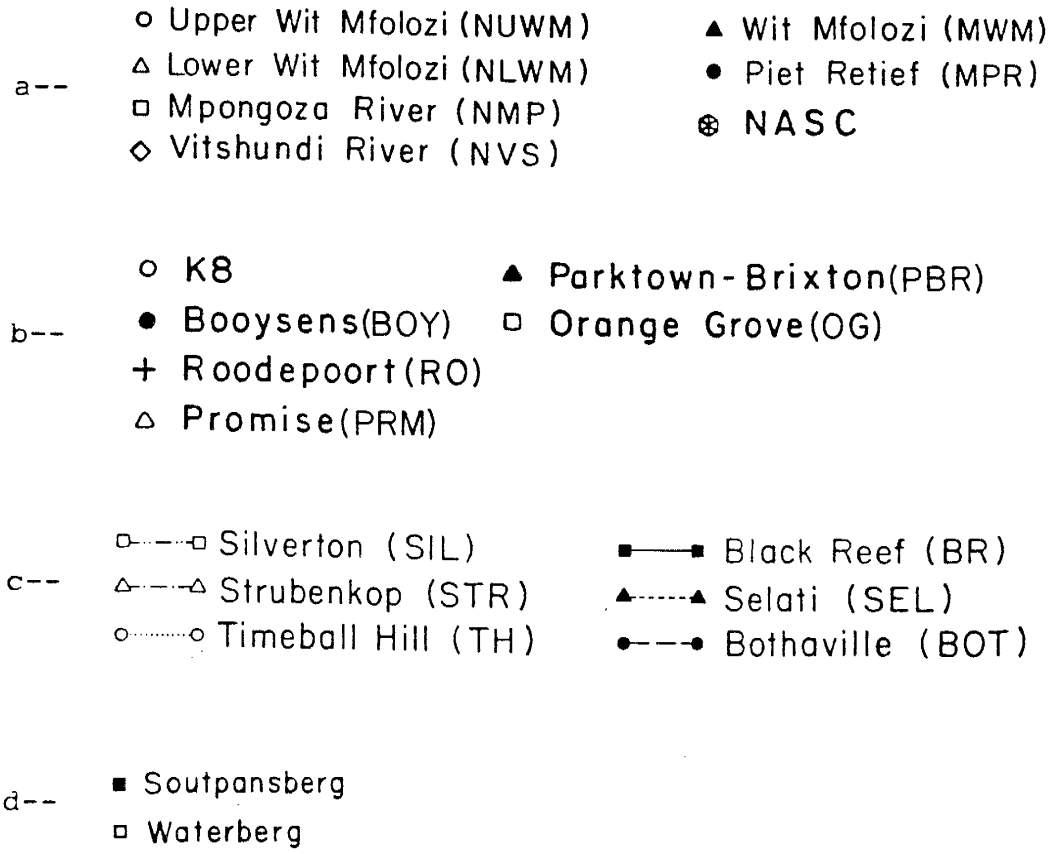

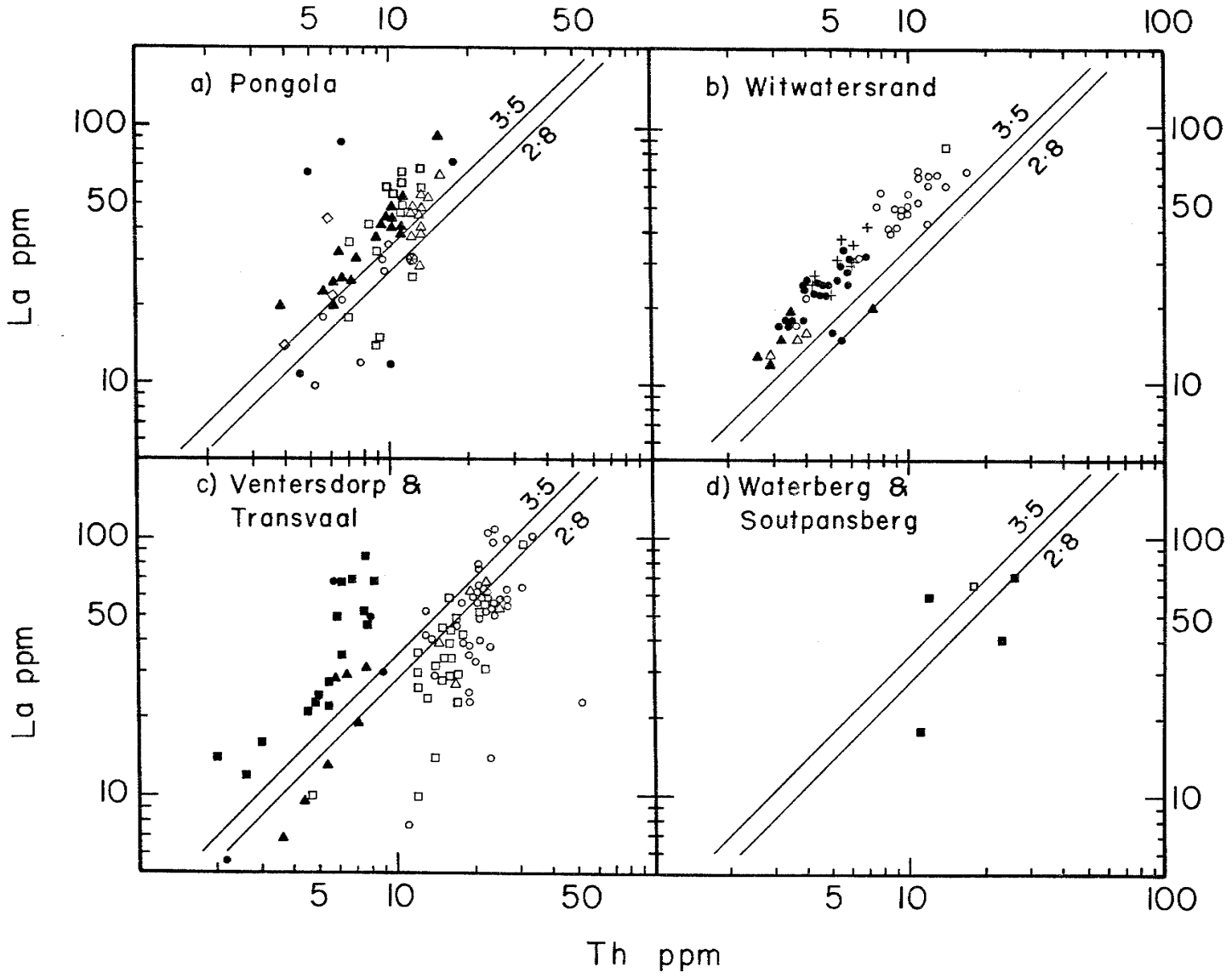
a) Pongola
b) Witwatersrand
c) Ventersdorp & Transvaal
d) Waterberg & Soutpansberg
3·5
2·8
La ppm
Th ppm
5
10
50
100

and thus may be the most representative samples of Pongola La/Th source concentrations. NUWM pelites have La/Th ratios (2.8 +/- 0.7) which are identical to those which characterize Phanerozoic shales (McLennan et al., 1980). Other Pongola pelites have higher La/Th ratios which are more characteristic of estimates of Archean pelite compositions (Taylor and McLennan, 1985).

Th/U ratios in Witwatersrand pelites do not vary systematically with stratigraphic height and the range of mean values (2.5-5.5; Table 3) extends both above and below the range of means and 95% confidence levels for Archean pelites given by Taylor and McLennan (1985). Overall, Witwatersrand Th/U ratios are similar to, but more variable than Pongola ratios. This range in variability also overlaps the means and confidence levels of Precambrian pelites used by McLennan and Taylor to suggest a secular increase in the Th/U ratios of shales and pelites with time. Witwatersrand K8 pelites have very low Th/U ratios (2.5 +/- 0.6), possibly reflecting the emergence of U enriched source granites for these sediments, metasomatic enrichment of U in these sediments, and/or relative retention of U in these sediments resulting from rapid erosion and deposition. La/Th ratios for all Witwatersrand pelites (4.4-5.8; Fig. 31b; Table 3) exceed those which characterize Archean (3.5) and post-Archean pelites (2.8; McLennan et al., 1980). While these La/Th ratios remain relatively constant, concentrations of both La and Th increase upsection,

indicating that the percentage of detritus derived from granite sources also increased upsection within Witwatersrand strata.

Mean Th/U ratios of Transvaal pelites tend to increase upsection, with BOT-TH-STR-SIL pelites possessing ratios (3.4-4.4) which approach those of NASC (4.4), and are higher than those of SEL-BR pelites (2.7-3.0; Table 4). Th enrichment in Pretoria Group pelites (16-22 ppm), relative to NASC (12 ppm), Witwatersrand (4-10) and Pongola pelites (5-13 ppm), indicates a Th-enriched granite source for these sediments. The implied high-Th granites for Pretoria Group sediments contrasts the high-U granite sources suggested for the Witwatersrand-K8 pelites. Possible source candidates are the 2.7-2.5 Ga Randian granites which are located along the northern and northeastern margins of the Transvaal basin (Kent et al., 1980). Although Th analyses for these granites are not available, they are of the same general age as those of high-Th, third magmatic cycle granites from the Barberton region (Meyer et al., 1986). The location and age of these granites suggests that they may be related to subduction or collisional events related to accretion of the Kaapvaal and Zimbabwe cratons. Paleocurrent measurements also suggest that Limpopo sources may have contributed detritus to the Transvaal basin (Fig. 2; Button, 1973a; Tankard et al., 1982).

Ventersdorp-Transvaal pelites clearly fall into two distinct populations based on La and Th distributions (Fig.

31c), although most of the variability is related to the elevated Th concentrations of Pretoria Group pelites. La/Th ratios of BOT-SEL-BR pelites (3.5-5.9) are similar or greater than those characteristic of Archean pelites (3.5), whereas TH-STR-SIL pelites have mean La/Th ratios (2.3-2.5) which are less than post-Archean ratios (2.8; McLennan et al., 1980).

Th/U ratios of Waterberg and Soutpansberg pelites (3.6-4.2) are similar to those of NASC, Transvaal-Pretoria Group and Ventersdorp sequences. Th/U ratios of all Kaapvaal craton pelites tend to increase with decreasing age, suggesting a provenance effect for these changes, or increasing fractionation of these elements as the Earth's atmosphere became more oxygenated. Increased solubility of U relative to Th in oxidizing surficial environments should lead to increased Th/U ratios in sandstones and decreased ratios in the reducing environments of shales. This pattern is opposite to that observed in the Pretoria, Waterberg and Soutpansberg Group sediments. Despite the progressive secular changes observed in pelite Th/U ratios, most sequences show considerable overlap in their values, indicating that this ratio is not very diagnostic in Kaapvaal provenance determinations.

Both La and Th are enriched in Waterberg and Soutpansberg shales (Fig. 31d) a feature suggestive of their derivation from granite-rich sources. The single Waterberg sample analyzed has a La/Th ratio characteristic of Archean

pelites (3.5). Soutpansberg La/Th ratios also are variable, but the mean value (La/Th=2.8) is identical to that characteristic of post-Archean pelites (McLennan et al., 1980).

Th-Hf-Co and La-Th-Sc Distributions

Ternary diagrams can be used to constrain source-area composition and source mixing of sediments (Taylor and McLennan, 1985). Distributions of pelites from the Pongola Supergroup are scattered on Th-Hf-Co and La-Th-Sc diagrams and many samples show a depletion in Th relative to Phanerozoic shales (Fig. 32). Mozaan pelites are enriched in Hf and Co relative to Nsuze pelites. Enrichment of Hf (and Zr) in Mozaan pelites may reflect greater concentrations of detrital zircon. Relatively small enrichments of Co and Sc relative to Phanerozoic shales suggests a source slightly enriched in basalt (and/or komatiite) relative to Phanerozoic upper-continental crust. Variable enrichment of Co and Sc for certain geographic groups of pelites suggests a decoupling of these elements, possibly during weathering, erosion or sedimentation. Pongola pelites have higher La/Sc and Th/Co ratios relative to Archean upper-continental crust and Moodies pelites, whereas they have higher La/Sc ratios relative to the $\leq$ 3.3 Ga Beit Bridge Group pelites. Thus, the Pongola and Beit Bridge pelites reflect derivation from fractionated and evolved

Figure 32. Distribution of pelites from the Pongola Supergroup on Th-Hf-Co and La-Th-Sc diagrams. NASC, North American Shale Composite (Gromet et al., 1984); PAAS, Post-Archean Average Australian Shale (Taylor and McLennan, 1985); fields of Phanerozoic shales after data from Taylor and McLennan (1985); GR, homogenous hood granite (Hunter, 1973; Meyer et al., 1986); TON, tonalite; TH, Archean tholeiite; KOM, komatiite. Lines connect four end members used in mixing calculations (Table 13a). After Taylor and McLennan (1985), pelite data from Table 2.

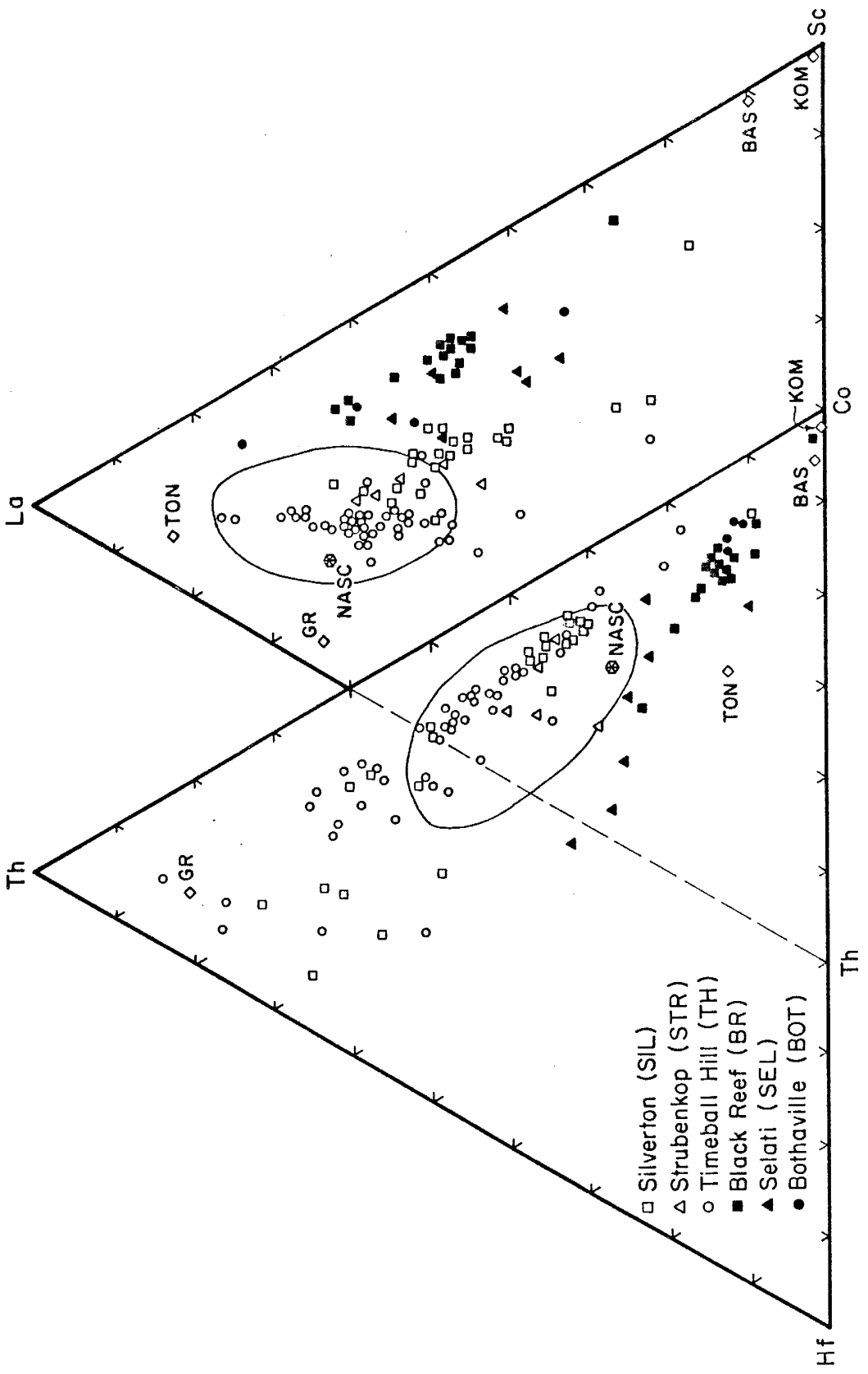
La
Th
Hf
Sc
Co
Th
TON
GR
NASC
KOM
BAS
□ Silverton (SIL)
△ Strubenkop (STR)
○ Timeball Hill (TH)
■ Black Reef (BR)
▲ Selati (SEL)
● Bothaville (BOT)

crustal sources, while Moodies pelites reflect derivation from sources with greater proportions of mafic-komatiitic components.

Distributions of Witwatersrand pelites on Th-Hf-Co and La-Th-Sc diagrams clearly show a large contribution of mafic or ultramafic sources compared to Phanerozoic shales and Pongola pelites as shown by their relatively high Co and Sc contents (Fig. 33). Most samples fall within mixing lines defined by granite, tonalite and tholeiite-komatiite end members. Stratigraphic evolution of the Witwatersrand sequence also is evident on these diagrams with BOY pelites showing increasing concentrations of Co and Sc relative to basal PBR-PRM-RO pelites. K8 pelites are characterized by increased concentrations of Th and La relative to underlying BOY pelites. K8 pelite compositions most closely approximate those of Pongola pelites and Phanerozoic shales. Most Witwatersrand pelites (except for OG and K8 pelites) have higher Sc/Th and lower La/Sc ratios than corresponding ratios in Phanerozoic shales (Table 3). This appears to reflect a higher mafic-ultramafic component in the Witwatersrand pelites.

Pelites from the Ventersdorp-Transvaal successions show two distinct but scattered populations on La-Th-Sc and Th-Hf-Co diagrams (Fig. 34). Relatively high concentrations of Co and Sc in BOT-SEL-BR pelites are suggestive of abundant mafic or komatiitic sources. These pelites have compositional distributions which are similar to those of

Figure 33. Distribution of pelites from the Witwatersrand Supergroup on Th-Hf-Co and La-Th-Sc diagrams. NASC, North American Shale Composite (Gromet et al., 1984); PAAS, Post-Archean Average Australian Shale (Taylor and McLennan, (1985); fields of Phanerozoic shales after data from Taylor and McLennan (1985); GR, granite; TON, tonalite; TH, Archean tholeiite; KOM, komatiite. Lines connect four end members used in mixing calculations (Table 13a). After Taylor and McLennan (1985), pelite data from Table 3.

Figure 34. Distribution of pelites from the Ventersdorp and Transvaal Supergroups on Th-Hf-Co and La-Th-Sc diagrams. NASC, North American Shale Composite (Gromet et al., 1984); circled regions represent fields of Phanerozoic shales after data from Taylor and McLennan (1985); GR, granite; QM, quartz monzonite; TON, tonalite; TH, Archean tholeiite; KOM, komatiite. End member compositions given in Table 13a. After Taylor and McLennan (1985), data from Table 4.

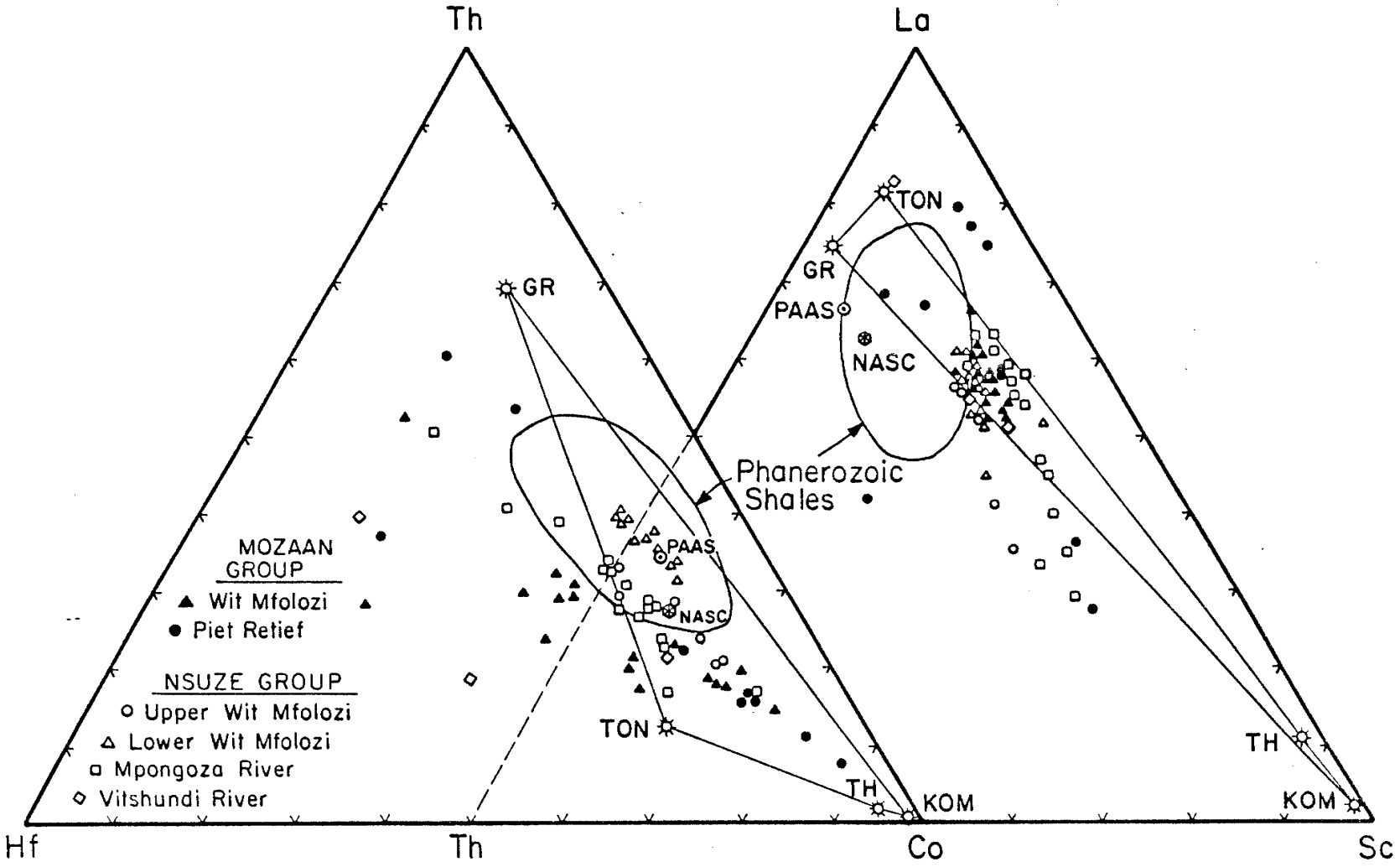
Th
La
GR
TON
PAAS
NASC
Phanerozoic
Shales
MOZAAN
GROUP
Wit Mfolozi
Piet Retief
NSUZE GROUP
Upper Wit Mfolozi
Lower Wit Mfolozi
Mpongoza River
Vitshundi River
TON
TH
KOM
Hf
Th
Co
Sc

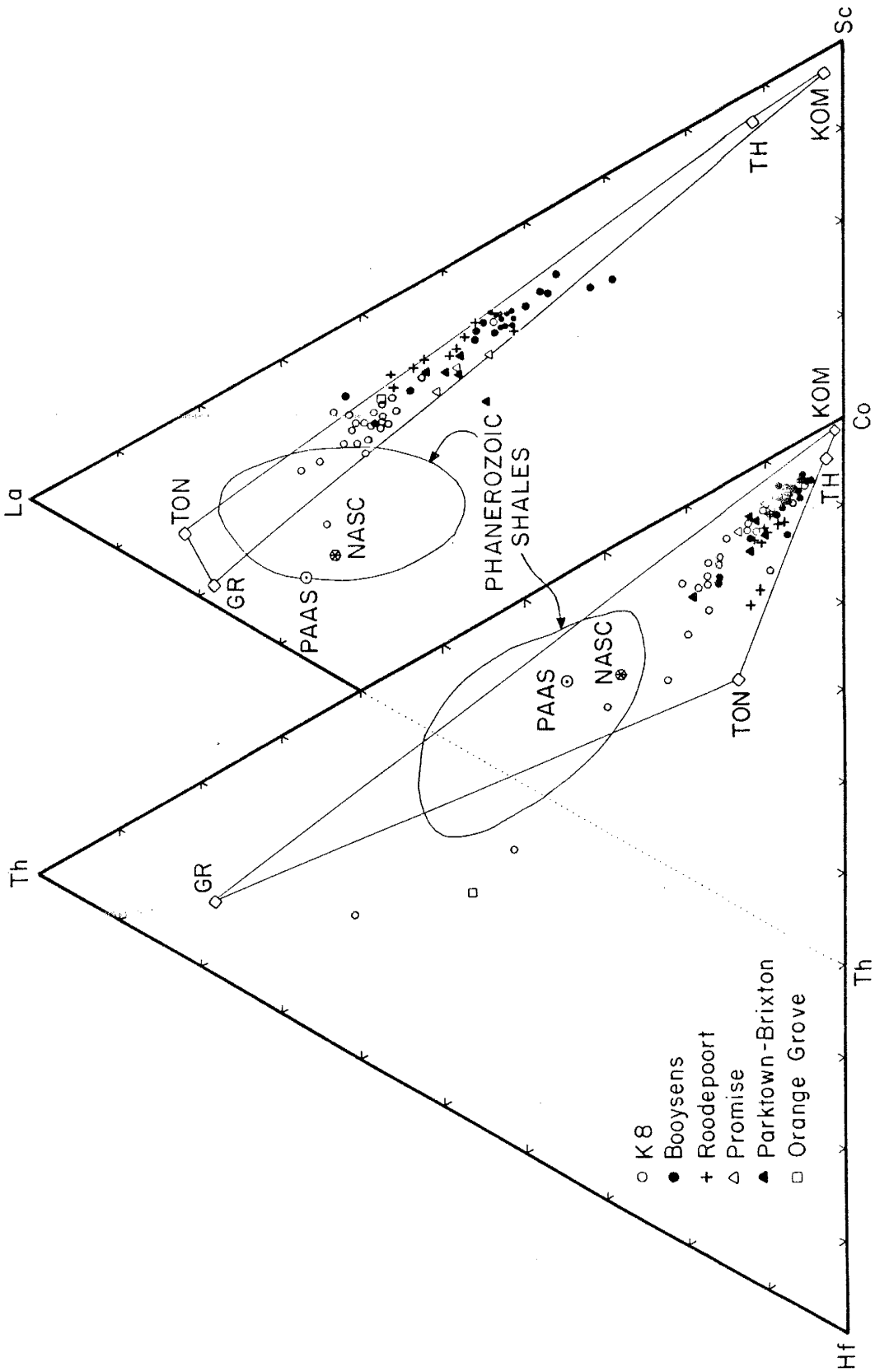
La
Th
Hf
Sc
Co
Th
TON
GR
PAAS
NASC
KOM
TH
PHANEROZOIC
SHALES
K8
Booysens
Roodepoort
Promise
Parktown-Brixton
Orange Grove

the Witwatersrand succession, with most pelites falling along a mixing line defined by komatiite-basalt and tonalite end members. By contrast, TH-STR-SIL pelites have greater Th and La contents, suggesting derivation from sources with large proportions of granitic rocks. These pelites fall along a mixing line dominated by high-K granite or quartz monzonite sources, with lesser contributions from komatiite and basalt. The two mixing trends of Ventersdorp-Transvaal pelites contrast the single progressive trends of Pongola and Witwatersrand pelites. These patterns mirror variations seen in La/Th ratios of these pelites (Fig. 31a-31c), suggesting exposure of entirely new sources for Pretoria Group sediments rather than the progressive exhumation of granitic sources suggested for the Witwatersrand sequence. Most TH-STR-SIL pelites are enriched in Th relative to Phanerozoic shales and NASC. This feature, which also is evident on NASC-normalized distributions (Fig. 29), may reflect a Th-enriched (35-40 ppm) granitic source for these sediments.

Th-Hf-Co and La-Th-Sc distributions of pelites from the Waterberg and Soutpansberg Groups indicate that source-rock compositions of these sediments are dominated by felsic sources, whereas mafic and ultramafic sources appear to be limited (Fig. 35). Distributions of Waterberg-Soutpansberg pelites on these diagrams are similar to those exhibited by Pretoria Group pelites. Th/Co ratios of Waterberg and

Figure 35. Distribution of shales from the Waterberg and Soutpansberg Groups on Th-Hf-Co and La-Th-Sc diagrams. NASC, North American Shale Composite (Gromet et al., 1984); PAAS, Post-Archean Average Australian Shale (Taylor and McLennan, 1985); circled regions represent fields of Phanerozoic shales after data from Taylor and McLennan (1985); GR, granite; TON, tonalite; TH, Archean tholeiite; KOM, komatiite. End members compositions given in Table 13a. After Taylor and McLennan (1985), Waterberg-Soutpansberg shale data from Table 5.

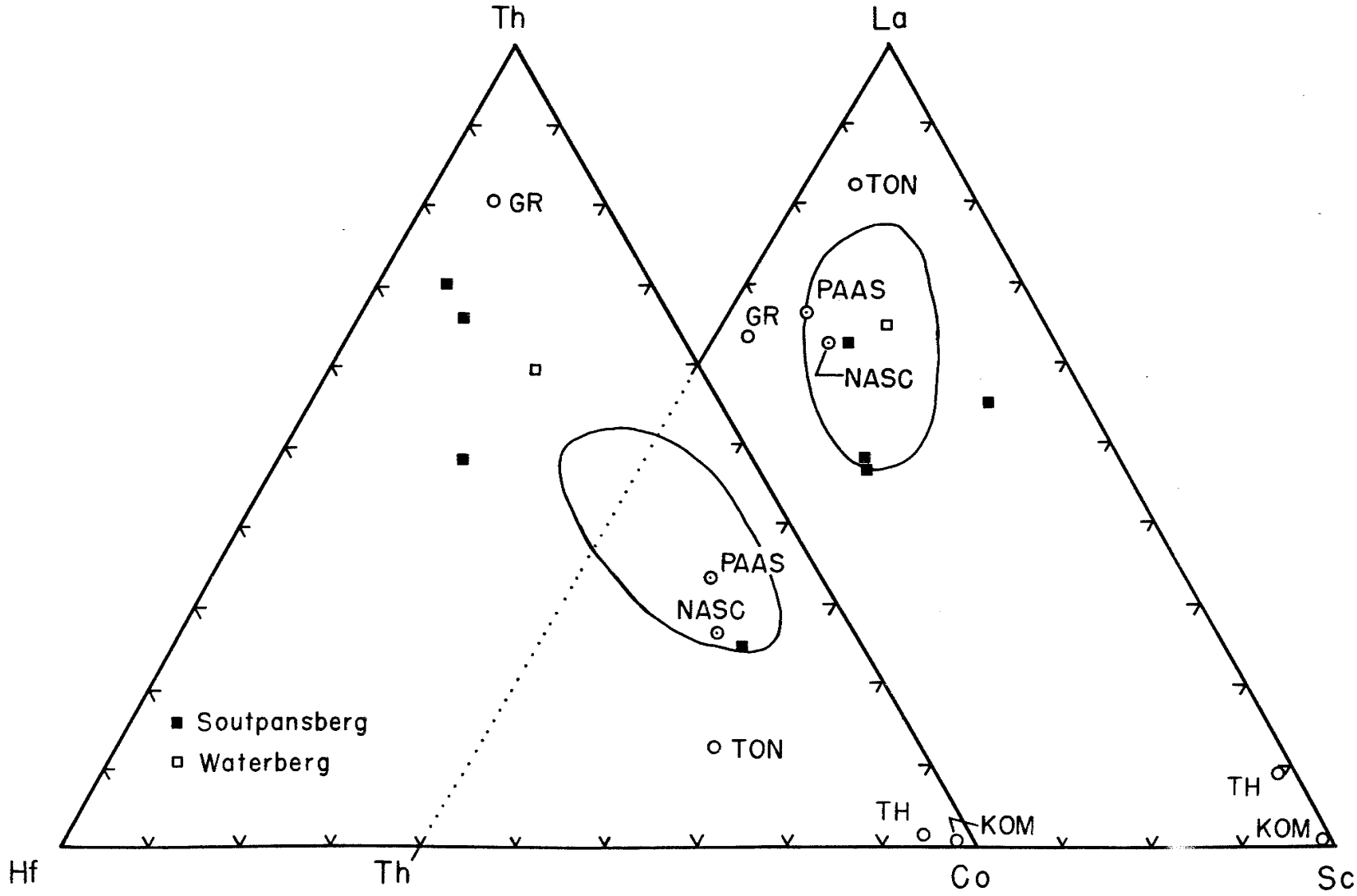
Th
La
GR
TON
PAAS
GR
NASC
PAAS
NASC
Soutpansberg
Waterberg
TON
TH
KOM
TH
KOM
Hf
Th
Co
Sc

Soutpansberg pelites are generally greater than those of Phanerozoic shales.

Computer Modelling

Contributions of source end members can be further evaluated with computer models using mass balance equations (Table F.2). The models use five relatively immobile trace elements (Th, La, Yb, Sc and Co) and assume four hypothetical mixing end members (granite, tonalite, tholeiite and komatiite; Table 13a). Potential contributions from recycled sediments are assumed to be representative of their original source lithologies. Average end member compositions are estimated from a variety of published and unpublished data for Archean rocks from South Africa and are plotted on Th-Hf-Co and La-Th-Sc diagrams (Figs. 32-35). Because quantitative provenance estimates should also include weighted compositions of coarse clastic sediments, the results generated here should only be compared to provenance determinations for other sources based on pelite or shale compositions. Thus, lithologic percentages summarized in Table 13b should not be equated with absolute rock abundances of sources for the respective basins. For example, Sc may be preferentially concentrated in pelites relative to La and Th, causing estimates of basaltic contributions to these sediments to be overestimated.

Pelites from the Moodies succession appear to be derived from sources composed mostly of tonalite, komatiite

Table 13a. End member compositions used in mixing calculations. Values in ppm.

	Th	Sc	Co	La	Yb
Granite	30(35)	3	3	120	5
Tonalite	6	5	10	30	0.5
Basalt	0.7	40	52	4.5	1.9
Komatiite	0.1	28	110	0.5	0.9

Values calculated from multiple sources.
35ppm Th value used in mixing calculations for Waterberg, Soutpansberg, Silverton, Strubenkop and Timeball pelites.

Table 13b. Summary of provenance computer mixing models for pelites from the Kaapvaal craton. Values in percent.

Unit	Granite	Tonalite	Basalt	Komatiite
SOUTPANSBERG	35-40	20	45	<5
WATERSBERG	45-50	20-30	25-35	<5
TRANSVAAL				
-Silverton	25-45	20-25	45-50	<5
-Strubenkop	45-60	<10	45-55	5
-Timeball	50-70	10	35-40	<5
-Black Reef	10-15	30	45-50	10-15
-Selati	<10	50-70	25-35	<5
VENTERSDORP				
-Bothanville	10-20	35-45	25-30	15-20
WITWATERSRAND				
-K8	30-50	<10	40	20-30
-Booysens	15-20	<10	40-45	30-35
-Roodepoort	15-25	10-20	40-45	20
-Promise	<10	40-60	15-25	10-15
-Parktown	<10	40-60	15-25	10-15
-Orange Grove	50-70	<10	40-50	<5
PONGOLA				
-Mozaan	40-50	10-15	30-40	<10
-Nsuze	45-55	10-15	30-40	<10
MOODIES	10-15	30-40	15-25	20-25

Note: Mixing percentages calculated indicate relative differences in source-area contributions and are not intended to be representative of absolute contributions from source lithologies.

and basalt, with relatively minor contributions from granite (Table 13b). Mixing results from the Pongola Supergroup suggest that pelites are derived from a source enriched in granite by a factor of 2-4 relative to Moodies and most other Archean pelites in southern Africa (except K8 pelites). Relatively minor contributions from tonalite and komatiite sources are allowed. Homogenous hood granites are favored for the granitic source component because their trace element and K2O contents (Hunter, 1973) match the granite composition required by Pongola sediment compositions. A similar conclusion also is favored by Laskowski and Kroner (1985). In order to be consistent, compositions of hood granites are used to model both Moodies and Pongola pelite sources, even though these granites post-date Moodies sedimentation. These granites, the most extensive of which is the Mpuluzi (Lochiel) batholith, occur adjacent to and may underlie much of the Pongola basin (Fig. 4). Mixing models also indicate that a significant proportion of the Pongola pelites may be derived from erosion of older basaltic greenstone belts or from penecontemporaneous Nsuze volcanics. An angular unconformity between the Nsuze and Mozaan Groups in the southern Pongola basin, and volcaniclastic sediments in both the Nsuze and Mozaan Groups (Matthews, 1967; Watchorn and Armstrong, 1980) also suggest that Nsuze volcanic rocks may be a sediment source.

Mixing results from the Witwatersrand succession indicate that contributions from both komatiite and granite

sources tend to increased upsection (Table 13b). Pelites from the PRM and PBR Formations had relatively minor contributions from granite, basalt and komatiite and large contributions from tonalite. The basal OG, however, requires a large contribution from granitic sources if the one sample analyzed is representative. RO and BOY pelites require moderate contributions of granite, basalt and komatiite with relatively small contributions from tonalite. The K8 pelites require large amounts of granite, moderate amounts of basalt and komatiite, and small tonalite contributions. The overall picture is one in which granite and greenstone contributions increase with stratigraphic height, whereas tonalite contributions decrease. Granite also must be locally available to erosion in the source-area at the onset of Witwatersrand deposition as dictated by the composition of the single OG sample. The occurrence of detrital uraninite, cassiterite, monazite, zircon and K-feldspar in underlying Dominion quartzites (Viljoen et al., 1970) indicates that these granite sources were probably exposed to erosion prior to Witwatersrand deposition.

Results from the Ventersdorp and Transvaal Supergroups suggest that BOT-SEL-BR pelites had relatively minor contributions from granite and large contributions from tonalite (Table 13b). Moderate basalt and komatiite contributions are recorded for these sediments with basalt peaking during deposition of BR pelites and komatiite

contributions appearing greatest for BOT-BR pelites. TH-STR-SIL pelites require large contributions from granite and basalt with only minor contributions from tonalite and komatiite. Granitic sources for these pelites are probably enriched in Th (35-40 ppm) as evidenced by high Th contents of Pretoria Group pelites and quartzites (Tables 4 and 9). TH-STR-SIL pelites have greater contributions from granite sources relative to Moodies and Witwatersrand pelites (except K8 and OG successions), and contributions of granite which are similar to those of Pongola pelites. Mixing models suggest that BOT-SEL-BR sources are similar in overall composition to those of the Moodies pelites.

Waterberg and Soutpansberg pelites appear to be derived from the erosion of crustal sources with a similar proportion of exposed crustal granites and basalts as the Pongola, Witwatersrand-K8 and Transvaal-Pretoria Group successions (Table 13b). Tonalite contributions to Waterberg and Soutpansberg sediments are limited while komatiite contributions are too minor to be detected.

QUARTZITE PROVENANCE

Source-Area Composition Estimates

Parallel chondrite-normalized REE distributions for Kaapvaal quartzites and pelites (Fig. 17; Tables 7-10) suggest that REE in the quartzites are contained chiefly in micas and clay minerals which now comprise their matrix. REE distributions in the quartzites are typically depleted by a factor of 50-100% relative to associated pelites. This

observation is important in that quartzite REE patterns do not appear to be controlled by minor detrital phases such as zircon or monazite. Mass balance considerations using total Zr contents in Pongola, Ventersdorp and Transvaal quartzites and measured Yb concentrations in zircons (Taylor and McLennan, 1985) indicate that <25% of the Yb in these quartzites is contributed by detrital zircon. Positive anomalies of Hf and Ta in Pongola quartzites (also for Zr and Nb, not plotted) on NASC-normalized diagrams (Fig. 28) probably result from detrital accumulations of minerals such as zircon, rutile or magnetite. Similar enrichments are evident in the compositions of Dominion, Witwatersrand, Ventersdorp and Transvaal quartzites (Tables 8-10). Depletions of Rb, V and Sc in Kaapvaal quartzites relative to associated pelites (Tables 7-10) may result from segregation of these elements into the clay-sized mineral fraction, although corresponding enrichments of these elements in pelites are not readily apparent (Fig. 28). Strong correlations between the distribution of Al-V and Al-Sc in Pongola pelites (Table 11) suggests that sedimentary transport of V and Sc is dominated by aluminous clay minerals. The near absence of detrital magnetite in Pongola quartzites, which commonly includes partial substitution of V for Fe^{+3}, also may contribute to V depletion. V also may be incorporated in anatase, which in turn is commonly adsorbed onto kaolinite (Weaver and Pollard, 1973). Strong correlations between Al and Ti

supports a mineralogic link between these three elements (Table 11).

Pongola quartzites are enriched in Ni and Cr and have higher La/Yb ratios relative to Phanerozoic passive-margin sandstones (Table 7). Distributions of most Pongola pelites and quartzites on K2O/Na2O vs. %SiO2 plots (Fig. 36) indicate a compositional similarity to Phanerozoic quartzites and pelites deposited in passive margin settings. A portion of the Pongola pelites plotting in the oceanic island arc field are spatially associated with banded iron formation, and are not believed to be representative samples for tectonic setting determinations. Both major and trace element distributions of most Kaapvaal quartzites (Figs. 37 and 38, respectively) show similarities to Phanerozoic sandstones deposited in passive margin, and to a lesser degree, in active continental margin settings. Granite-rich sources for most Pongola, Dominion, Central Rand, Pretoria, Soutpansberg and Waterberg sequence quartzites are reflected in their elevated La and Th contents. High-Th granite sources for Pretoria Group pelites also are readily apparent in the Th concentrations of associated quartzites (Fig. 38). Quartzites from the Central Rand Group are generally enriched in mafic (Ni, Cr) and felsic components (Th, U, K2O) relative to the West Rand Group (Table 8). This pattern is consistent with upsection increases in both felsic and mafic components exhibited by the Witwatersrand pelites.

Figure 36. K_2O/Na_2O vs. SiO_2 tectonic discrimination diagram for pelites and quartzites from the Pongola Supergroup. PM, passive continental margin (stable cratonic margins and intracratonic basins); ACM, active continental margin (continental margin magmatic arc including trench, forearc, intraarc, backarc and strike-slip basins); OIA, oceanic island arc setting (forearc, intraarc and backarc basins and trenches). After Roser and Korsch (1986).

▲ Mozaan Wit Mfolozi (MWM)
● Mozaan Piet Retief (MPR)
o Nsuze Upper Wit Mfolozi (NUWM)
△ Nsuze Lower Wit Mfolozi (NLWM)
□ Nsuze Mpongoza River (NMP)
◇ Nsuze Vitshundi River (NVS)
+ Mozaan Quartzites (MQ)
* Nsuze Quartzites (NQ)

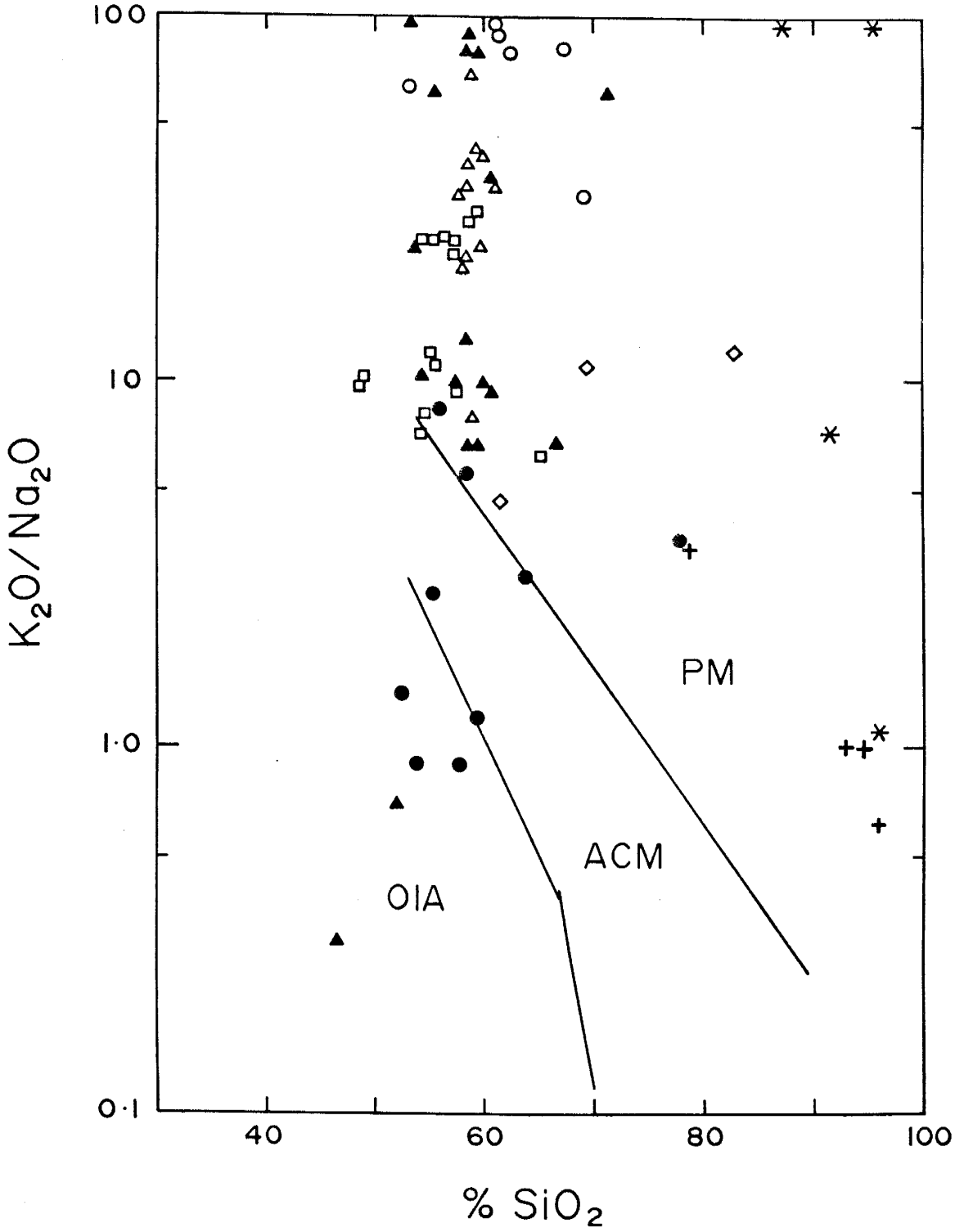
100
10
1·0
0·1
40
60
80
100
K_2O/Na_2O
% SiO_2
PM
ACM
OIA

Figure 37. (Next Page) Kaapvaal quartzite distributions on log SiO_2/Al_2O_3 vs. Fe_2O_3T+MgO tectonic discrimination diagram. Fe_2O_3T represents total iron as Fe_2O_3. Quartzite data from Tables 7-10. Passive margins include stable continental margin, intracratonic and continental-rift basins; active continental margins include Andean type continental arc and convergent strike-slip basins; continental island arcs include fore-, inter- and back-arc settings; oceanic island arcs includes oceanic fore- and back-arc settings. After Bhatia (1983).

◇ Soutpansberg
◆ Waterberg
○ Pretoria
● Wolkberg
⊕ Bothaville
□ Central Rand
■ West Rand
⊞ Dominion
△ Mozaan
▲ Nsuze

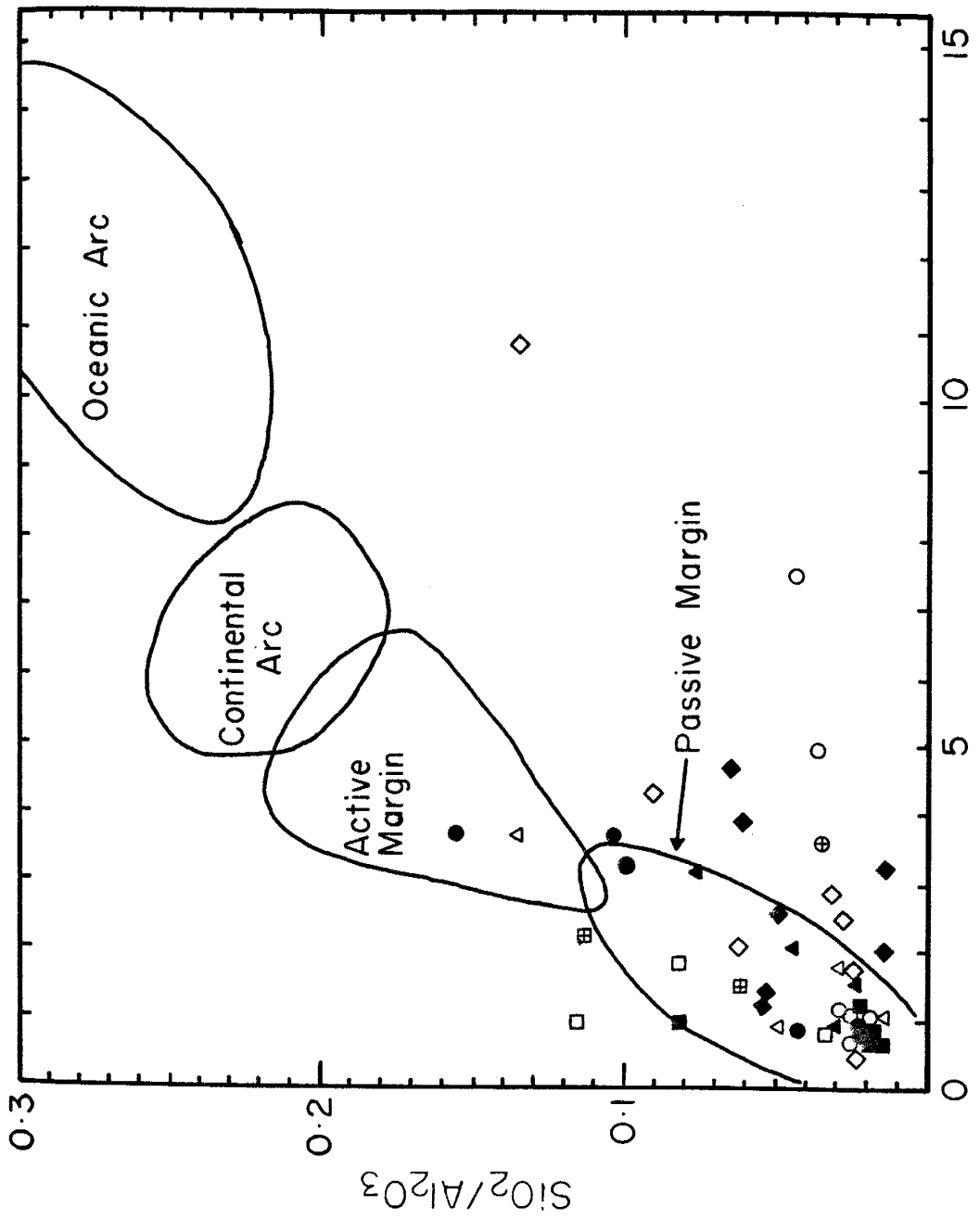
Oceanic Arc
Continental Arc
Active Margin
Passive Margin
0·3
0·2
0·1
0
5
10
15
SiO2/Al2O3
Fe2O3 + MgO

Figure 38. La-Th-Sc tectonic discrimination plot showing the distribution of Kaapvaal quartzites. Data from Tables 7-10. Tectonic-sedimentary fields same as in Figure 37. After Bhatia and Crook (1986).

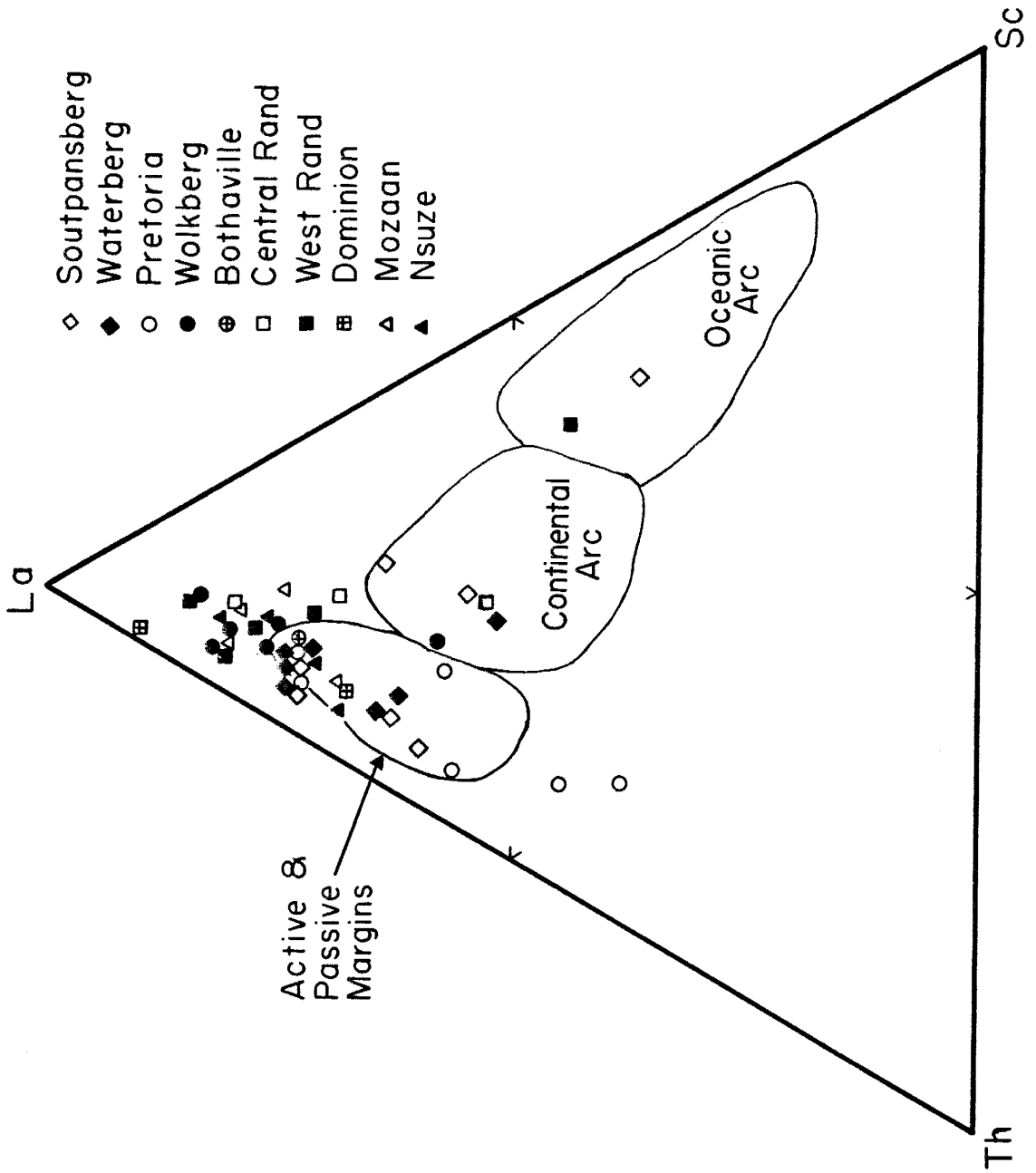
Soutpansberg
Waterberg
Pretoria
Wolkberg
Bothaville
Central Rand
West Rand
Dominion
Mozaan
Nsuze
La
Sc
Th
Oceanic Arc
Continental Arc
Active & Passive Margins

Tectonic Setting

Quartzite point-count results, when plotted on QtFtL and QmFtLt provenance diagrams (Dickinson and Suczek, 1979; Dickinson et al., 1983), indicate a similarity between Pongola quartzites and Phanerozoic sandstones from cratonic interior or transitional basement uplift terranes (Fig. 39). These distributions are consistent with tectonic interpretations based on chemical compositions of Pongola quartzites (Figs. 36-38). K-feldspar alteration to clay and/or micas is visible in many Pongola quartzite samples. This K-feldspar derived epimatrix is point-count classified along with framework K-feldspar grains. Calculated maximum K-feldspar contents, based on the major element compositions of quartzites (Reed and Condie, 1987), is indicated by the shaded regions on QtFtL and QmFtLt diagrams (Figs. 39-42). Similar Nsuze and Mozaan mean framework grain mineralogies suggest that source-area and transport processes have affected quartzites from both units to a similar degree (Table 6).

An abundance of detrital feldspar in quartzites from the Dominion Group suggest that these sediments were derived from rapidly eroded granitic sources (Table 6). The presence of polycrystalline quartz also indicates significant contributions from recrystallized chert and/or recycled arenaceous sedimentary sources. Plots of Dominion quartzites on QtFtL and QmFtLt discrimination diagrams

Figure 39. QtFtL and QmFtLt tectonic discrimination diagram for Pongola quartzites. Qm, monocrystalline quartz; Qt, total quartz; Ft, total feldspar; L, framework lithic fragments; Lt, total lithic fragments (Lt=L + polycrystalline quartz; Table E.1-1). Shaded regions represent maximum allowable detrital K-feldspar originally contained in these sediments, calculated using K_2O analyses of quartzites (Reed and Condie, 1987). Framework grain categories, determinations and data in Appendix E and Table 6. After Dickinson et al. (1983).

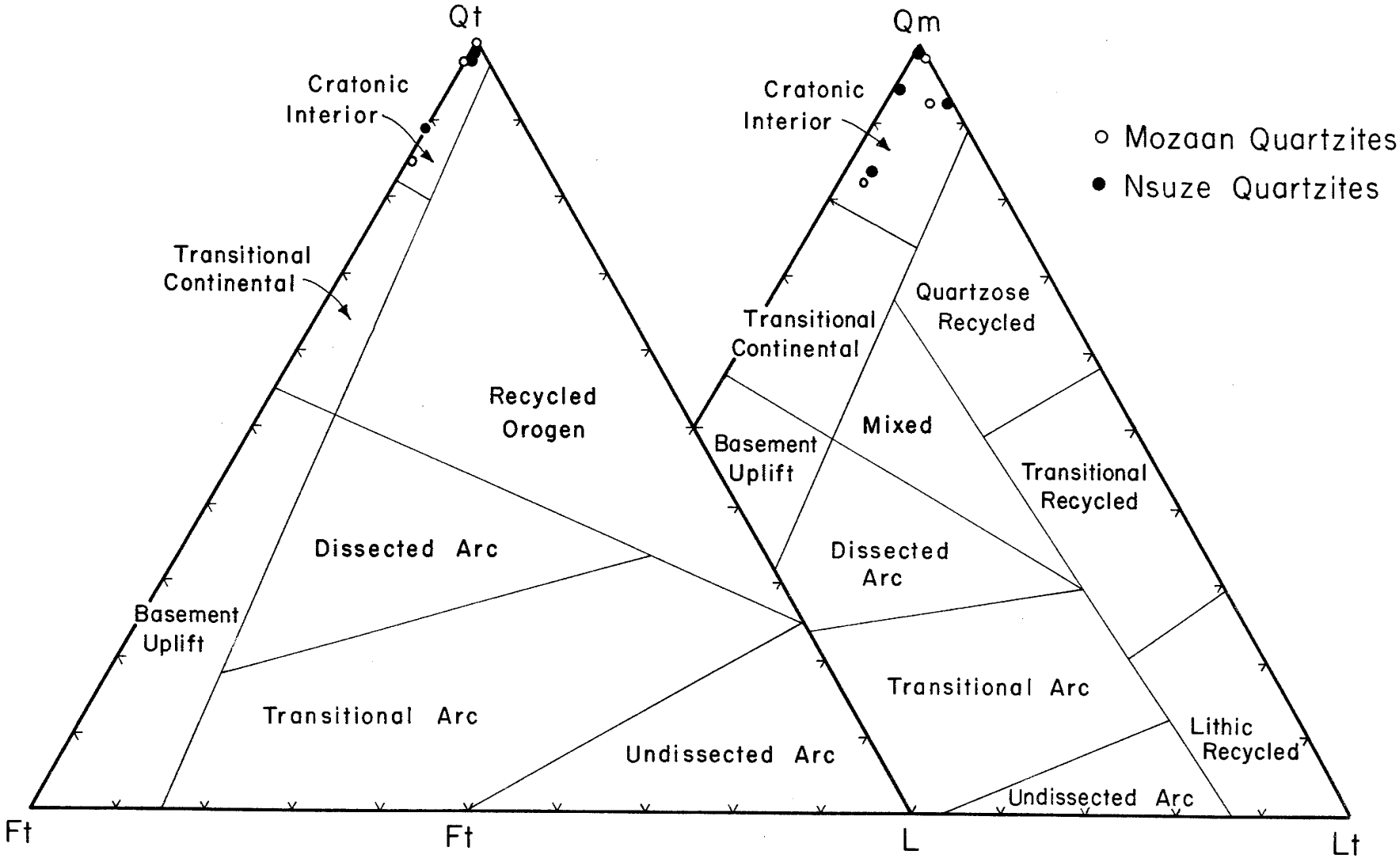
Qt
Cratonic Interior
Transitional Continental
Recycled Orogen
Dissected Arc
Basement Uplift
Transitional Arc
Undissected Arc
Ft
Ft
Qm
Cratonic Interior
Transitional Continental
Quartzose Recycled
Basement Uplift
Mixed
Transitional Recycled
Dissected Arc
Transitional Arc
Lithic Recycled
Undissected Arc
L
Lt
Mozaan Quartzites
Nsuze Quartzites

(164)

(Dickinson et al., 1983) indicate a resemblance to Phanerozoic sandstones deposited in basement uplift and recycled orogenic zones (Fig. 40). Quartzites from the basal Witwatersrand-Orange Grove Formation are composed almost entirely of monocrystalline quartz grains indicating extensive reworking during deposition. Large scale symmetrical ripples and tidal features are suggestive of their reworking in intertidal environments (P. Camden-Smith, personal communication 1985). Increasing concentrations of both matrix and lithic fragments stratigraphically up-section within the West and Central Rand Groups indicate decreasing maturity of these sediments with age. Although framework grain distributions of these quartzites overlap, most West Rand sediments plot within cratonic interior fields while Central Rand quartzites mostly plot within recycled orogenic fields (Fig. 40). Geochemical modelling of pelite compositions suggest that granitic sources are an important component in the Witwatersrand hinterland, especially during deposition of the Central Rand Group. However, high CIA values and the presence of pyrophyllite in associated Witwatersrand pelites suggests extensive chemical leaching of Witwatersrand source-rocks, either due to weathering or hydrothermal alteration. It is suspected that leaching may be responsible for destruction of feldspars in the Witwatersrand source-region, thus tectonic interpretations based solely on framework grain distributions may underestimate contributions from proximal granitic sources.

Figure 40. QtFtL and QmFtLt tectonic discrimination diagram for Dominion and Witwatersrand quartzites. Framework grain abbreviations given in Figure 39 and Table E.1-1, categories and determinations given in Table 6 and Appendix E. Shaded regions represent maximum allowable original detrital K-feldspar based on K2O analyses of quartzites (Reed and Condie, 1987). After Dickinson et al. (1983).

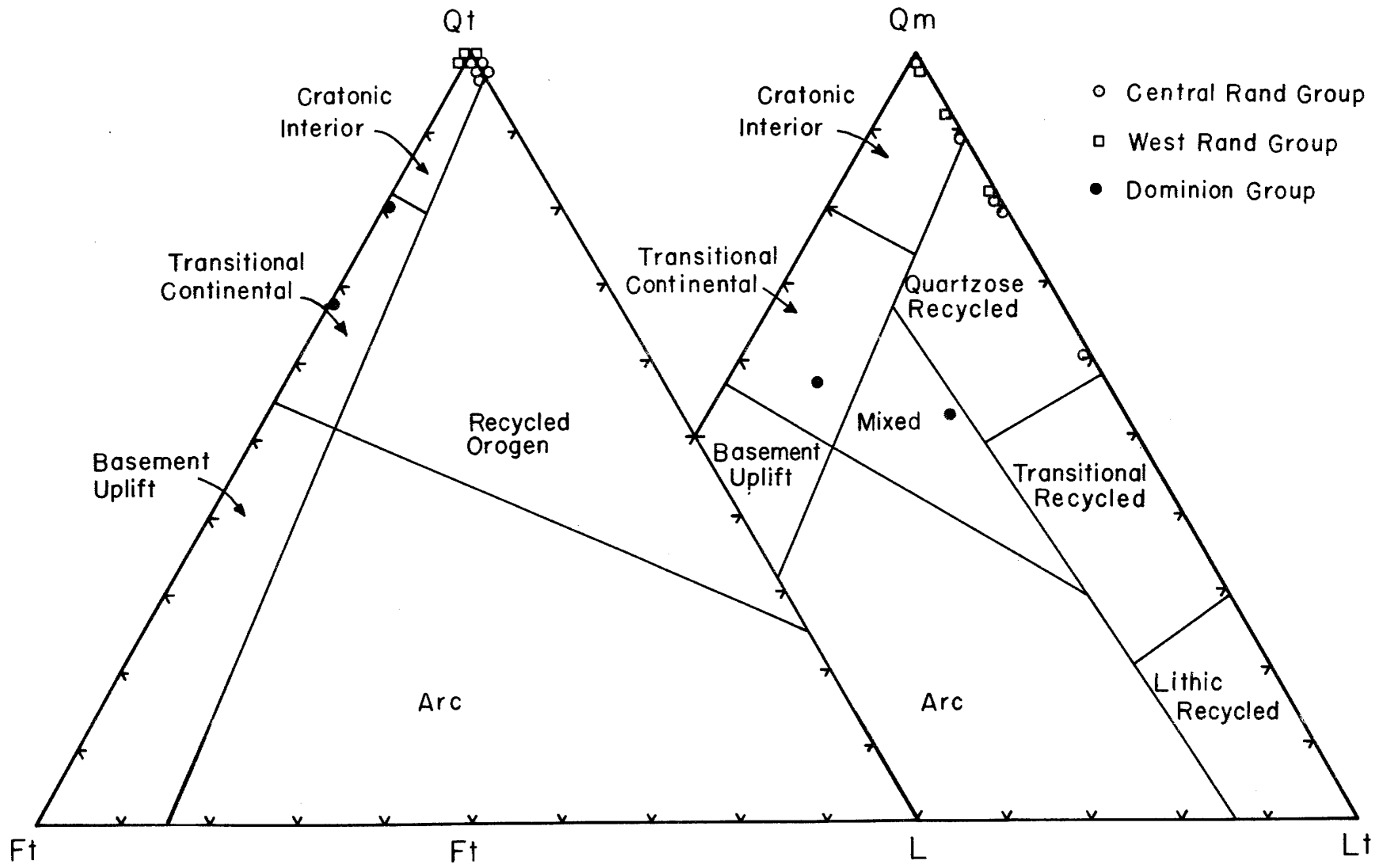
Qt
Cratonic Interior
Transitional Continental
Recycled Orogen
Basement Uplift
Arc
Ft
Ft
Qm
Cratonic Interior
Transitional Continental
Quartzose Recycled
Mixed
Basement Uplift
Transitional Recycled
Lithic Recycled
Arc
L
Lt
Central Rand Group
West Rand Group
Dominion Group

(1966)

Similarly, unstable volcanic- and sedimentary-lithic grain contributions also may be underestimated. Recalculated maximum K-feldspar contributions to Witwatersrand quartzites (Reed and Condie, 1987), however, do not allow significant increases in the proportion of detrital K-feldspar originally contained in these sediments (Fig. 40).

QtFtL and QmFtLt distributions (Dickinson et al., 1983) of Ventersdorp-Transvaal quartzites indicate that Black Reef and Pretoria Group sediments have framework grain distributions similar to Phanerozoic sandstones deposited in cratonic interiors (Fig. 41). Selati quartzites have varied distributions with affinities to cratonic interior, transitional continental and recycled orogenic zones. The single Bothaville quartzite sample plots in the recycled orogenic and quartzose recycled fields. Pretoria Group quartzites contain granitic clasts (quartz encapsulated muscovite, biotite and potassium feldspar) which suggest the exposure of plutonic or hypabyssal granitic sources to erosion during deposition of the upper-Transvaal sequence. Recalculated maximum K-feldspar contributions for these sediments do not allow significant increases in the detrital K-feldspar component (Fig. 41, shaded regions). Some polycrystalline quartz grains in Bothaville and Selati quartzites resemble recrystallized chert clasts and may be derived in part from eroded greenstone remnants.

Quartzites from the Waterberg Group have varied framework grain mineralogies, with 18% total-feldspar in

Figure 41. QtFtL and QmFtLt tectonic discrimination diagram for Ventersdorp and Transvaal quartzites. Framework grain abbreviations given in Figure 39 and Table E.1-1, categories and determinations given in Table 6 and Appendix E. Shaded regions represent maximum allowable original detrital K-feldspar based on K_2O analyses of quartzites (Reed and Condie, 1987). After Dickinson et al. (1983).

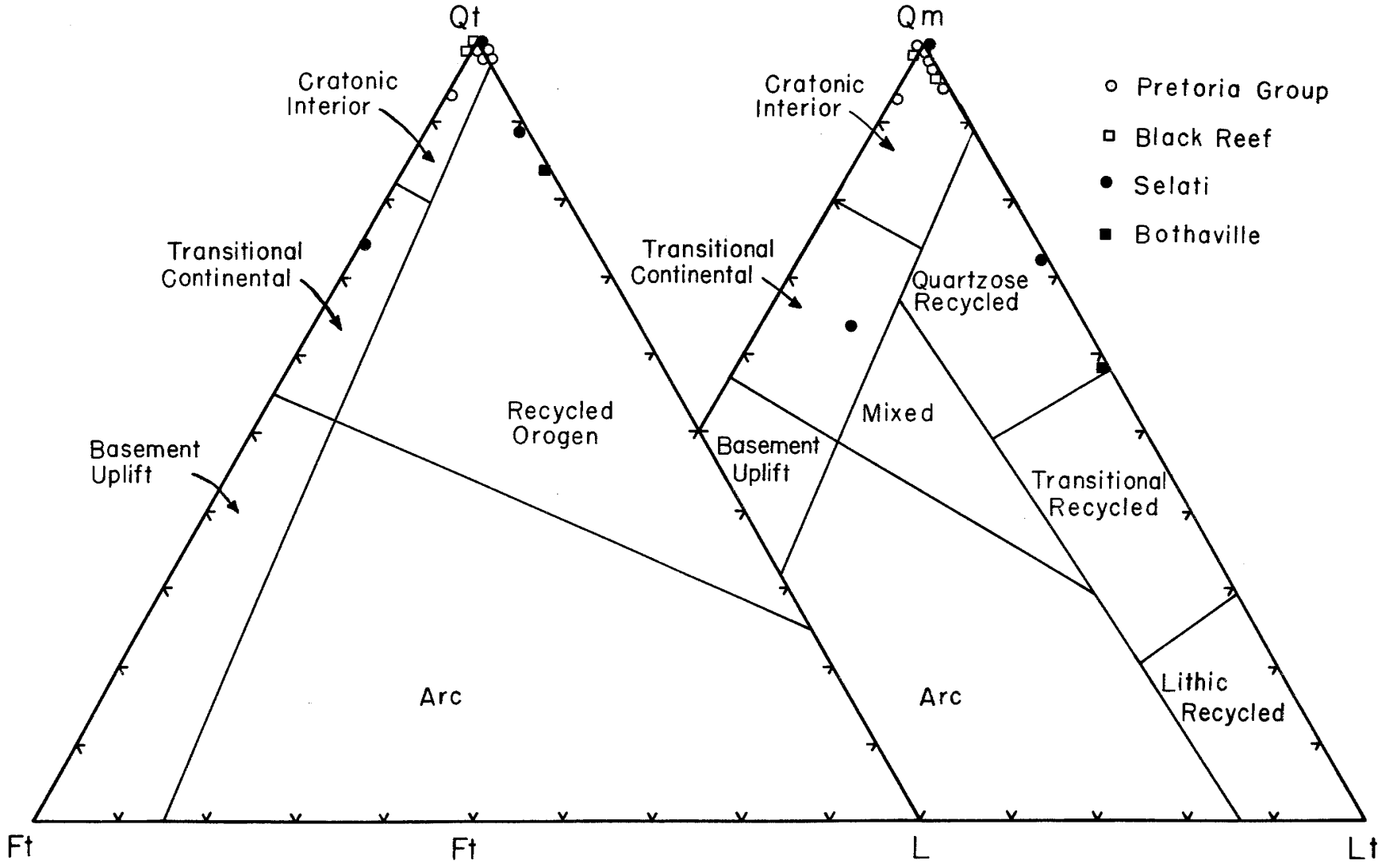
Qt
Cratonic Interior
Transitional Continental
Basement Uplift
Recycled Orogen
Arc
Ft
Ft
Qm
Cratonic Interior
Transitional Continental
Quartzose Recycled
Mixed
Basement Uplift
Transitional Recycled
Lithic Recycled
Arc
L
Lt
Pretoria Group
Black Reef
Selati
Bothaville

(168)

Vaalwater Formation quartzites and total-lithic fragment contents of underlying quartzites ranging from 25 to 32%. Distributions of these quartzites on QtFtL and QmFtLt plots (Dickinson et al., 1983) indicate similarities with cratonic interior, transitional basement uplift, and transitional recycled zones (Fig. 42). Calculated maximum K-feldspar contributions to these sediments (shaded region in Fig. 42; Reed and Condie, 1987) also do not allow any significant increase in amounts of K-feldspar originally contained in these sediments. QtFtL-QmFtLt distributions of quartzites from the Soutpansburg Group are similar to transitional basement uplift and recycled zones for Nzhelele and Ngwandzi Formations, whereas Musekwa and Mutshindi quartzites plot within cratonic interior fields (Fig. 42). These findings suggest that the lower portion of this sequence was deposited during a period of relative tectonic quiescence, whereas upper Soutpansberg sediments record an increase in tectonic activity of the basin margins. Concentrations of lithic-volcanic and lithic-sedimentary clasts also are noted to increase upsection, possibly recording cannibalistic erosion of underlying Soutpansberg volcanic and sedimentary sequences, respectively, along basin margins.

Figure 42. QtFtL and QmFtLt tectonic discrimination diagram for Waterberg and Soutpansberg quartzites. Framework grain abbreviations given in Figure 39 and Table E.1-1, categories and determinations given in Appendix E and Table 6. Shaded regions represent maximum allowable original detrital K-feldspar for Waterberg samples based on K_2O analyses of quartzites (Reed and Condie, 1987). No increase in the concentration of detrital K-feldspar in Soutpansberg quartzites is allowed based on K_2O analyses. After Dickinson et al. (1983).

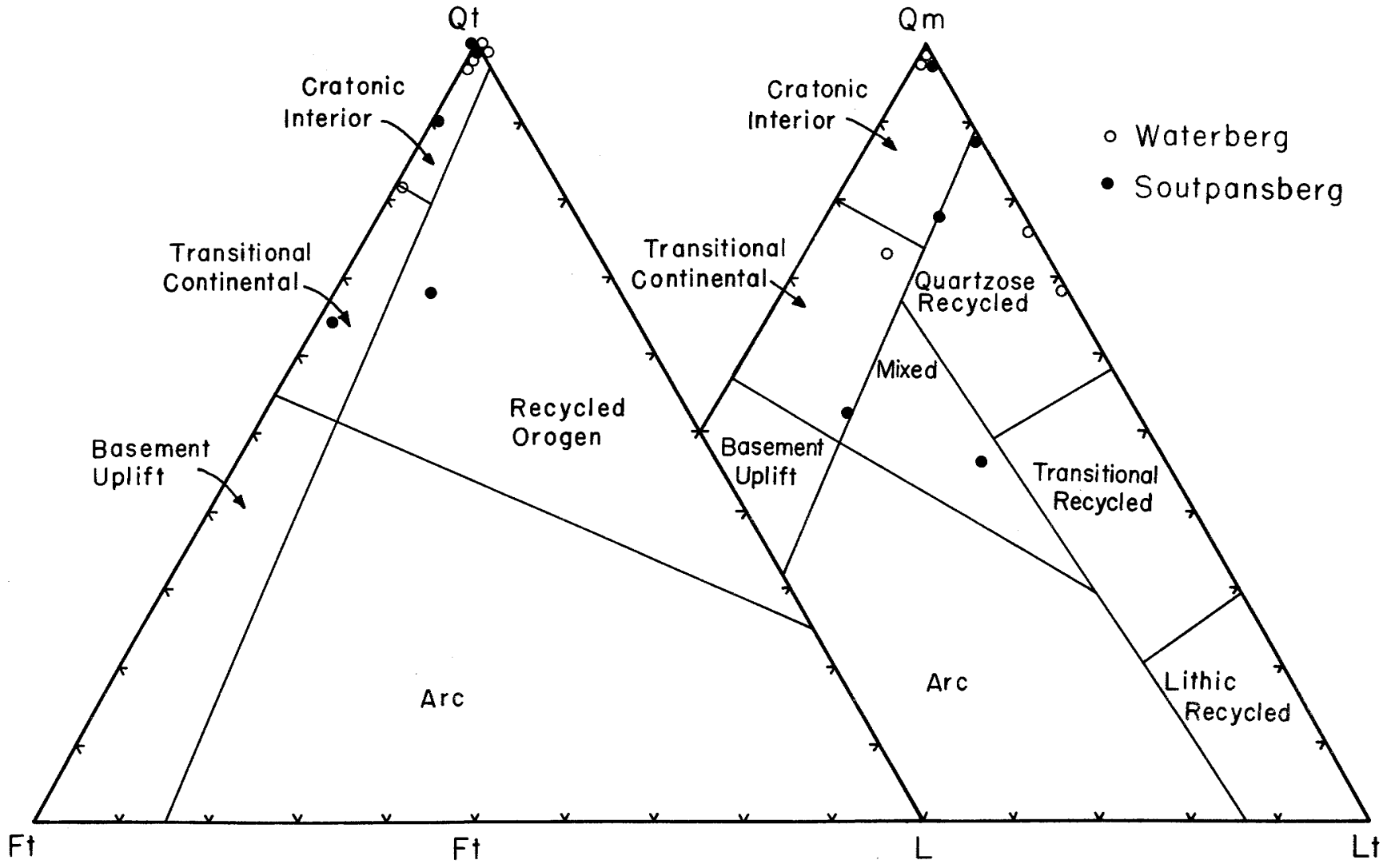
Qt
Cratonic Interior
Transitional Continental
Basement Uplift
Recycled Orogen
Arc
Ft
Ft
Qm
Cratonic Interior
Transitional Continental
Basement Uplift
Quartzose Recycled
Mixed
Transitional Recycled
Lithic Recycled
Arc
L
Lt
Waterberg
Soutpansberg

IMPLICATIONS FOR CRUSTAL DEVELOPMENT

PONGOLA SUPERGROUP

Sediments from the Pongola Supergroup have geochemical and mineralogical characteristics suggesting their derivation from a source-terrane similar in overall composition to average Phanerozoic upper-continental crust. Granite clasts in conglomerates of the Moodies Group indicate that K-rich granites were emplaced into the Kaapvaal crust by 3.3 Ga (Reimer et al., 1985; Tegtmeyer and Kroner, 1987). However, Nd isotopic data (Miller and O'Nions, 1985) indicate that few, if any, of these older granites served as sources for the Pongola sediments. Instead, crustal residence ages of Pongola pelites (tDM= 3.1-2.9) are similar to the ages of homogenous hood granites (3.2-3.0 Ga) supporting a hood granite provenance model for Pongola sediments (Laskowski and Kroner, 1985). Contributions from the Ancient Gneiss Complex ($\sim$3.5 Ga), Swaziland Supergroup ($\sim$ 3.4 Ga) or other greenstone belts are similarly restricted by these isotopic data.

The short time interval ($\approx$90 Ma) between emplacement of the hood granites (Mpuluzi batholith) and deposition of Nsuze volcanics indicates that rapid uplift and exposure followed granite intrusion (Section II.7). The fact that Nsuze sediments rest unconformably on fresh granites in the southern Pongola basin confirms that uplift continued until sedimentation began in this area. Although rates of

tectonic activity probably varied during Pongola deposition, the composition of sediments appears to have remained relatively constant. This suggests that Pongola sources retained their Phanerozoic-like composition during deposition of the entire sequence. High Ni and Cr contents of most Pongola pelites probably reflect enrichment of these elements during intense chemical weathering of komatiitic source-rocks rather than a large komatiite source component. If the rapidly eroded NUWM pelites are representative of relatively unweathered Pongola sources, then their Ni-Cr contents suggest a provenance which is enriched in komatiite by approximately 50% relative to Phanerozoic upper-continental NASC sources.

Geologic, geochemical and petrographic evidence are consistent with deposition of Nsuze and Mozaan sediments in a cratonic basin or intracratonic rift. The presence of arkose, feldspathic sandstone and granite clasts in Pongola sediments favors the latter interpretation (Matthews, 1967; Matthews and Scharrer, 1968; Watchorn and Armstrong, 1980). In either case, a craton must have existed in South Africa by 3.0 Ga ago. Although the dimensions of this early craton are unknown, the preserved areal distribution of Pongola sediments and pre-Pongola granites-greenstone remnants suggest a minimum size of 70,000 km^2.

WITWATERSRAND SUPERGROUP

Based on overall lithologic distributions in the Witwatersrand Supergroup, Viljoen et al. (1970) and Pretorius (1976) suggest that the sources of these sediments reflect progressive unroofing of early Archean granite-greenstone terranes. An increase in the proportion of ultramafic (komatiitic) component with increasing stratigraphic level reflects deeper erosion into the greenstone successions. Although this model may be partly acceptable in terms of geochemical data from this study in that it explains the increasing amount of ultramafic component at high stratigraphic levels, it cannot explain the parallel increases in granitic components. The large volume of quartzites and conglomerates in the Witwatersrand Supergroup demands that quartz-rich plutonic sources be important throughout deposition of the succession, and especially during deposition of the Central Rand Group.

The Witwatersrand sediments record a slightly different primitive to evolved crustal transformation than that exhibited by the Moodies-Pongola succession. Uplift of older granite-greenstone terranes ($\sim$3.4 Ga) exposed large regions of tonalitic gneiss in the Witwatersrand source-area beginning at about 2.8 Ga. It is from such sources that the PBR and PRM pelites were derived. Granite must also be locally exposed during initial Witwatersrand basin

development as indicated by the composition of OG pelites and mineralogy of Dominion quartzites. Deepening erosion of greenstone sources exposed more basalt and komatiite which contributed significantly to the RO and BOY pelites. Unroofing of granites, some of which may have been emplaced about 2.8 Ga (Robb and Meyer, 1985) led to significantly larger influxes of granite detritus into the Witwatersrand basin as the upper pelites were deposited. The overall pattern is one where both komatiite-basalt and granite sources increased upsection at the expense of tonalite. Komatiite contributions peaked during deposition of BOY pelites, whereas granite sources increased through deposition of K8 pelites. The increasing granite and basalt-komatiite component for the RO, BOY and K8 pelites also is coincident with increased amounts of Au and U entering the basin at this time (Robb and Meyer, 1985).

Burke et al. (1986) summarized geologic evidence for a foreland basin model for the Witwatersrand basin. If this model is correct, then lithologic changes between the West Rand (chiefly pelites and subgreywackes) and Central Rand Groups (mostly quartzites and conglomerates) may represent a transition from a foreland basin associated with a convergent plate margin to one associated with collision in the Limpopo belt (Burke et al., 1986; Fig. 2). Lithic-sedimentary framework grains may record the onset of thin-skinned thrusting events during deposition of the upper

Witwatersrand succession. Wrench-faulting, also may be important in the formation of the Witwatersrand basin and in exposure of source-rocks to erosion (Stannistreet et al., 1986). Large proportions of granitic material entering the Witwatersrand Basin, as implied by the geochemistry of RO, BOY and K8 pelites, may be derived from syntectonic collisional granites in the Limpopo belt ~500 km to the north. Alternatively, such granites may be located in domal or faulted uplifts along the northern boundary of the Witwatersrand basin, a model more consistent with source-area studies of Witwatersrand sediments (Pretorius, 1974, 1976, 1981b; Robb and Meyer, 1985). Granitic intrusions may have produced the domal uplifts and the granitic magmas may have originated by thickening and partial melting of the lower crust in response to a Limpopo collision. Most of the dated granites north of the Witwatersrand basin were emplaced approximately 2.8-2.6 Ga ago (Robb and Meyer, 1985) thus bracketing the timing of a possible collision. Geochemical studies from the Limpopo belt support such a model (Condie and Boryta, 1989).

VENTERSDORP AND TRANSVAAL SUPERGROUPS

Sediments from the Transvaal and Ventersdorp Supergroups record a significant change in provenance from 2.6 to 2.1 Ga ago. BOT-SEL-BR sediments appear to be derived from the erosion of sources enriched in tonalite and basalt,

with minor contributions from granite and komatiite. Archean greenstone and/or lower Ventersdorp basaltic and komatiitic volcanics may serve as the mafic-ultramafic sources for these sediments. Reworked Witwatersrand sediments also may be important for basal Black Reef sediments as indicated by paleocurrent data, similar Black Reef and Witwatersrand pelite compositions, and reworked Witwatersrand gold in Black Reef quartzites.

TH-STR-SIL sediment sources are dominated by high-K and Th granites with significant contributions from basalt and limited contributions from tonalite and komatiite. 2.7-2.5 Ga Randian aged intrusives located to the north of the Transvaal basin may represent the granitic source for these sediments. Pelites from these units have geochemical characteristics suggestive of a source-terrane similar in composition to average Phanerozoic upper-continental crust. A Rb/Sr whole-rock isotopic date for TH pelite (2263 +/- 85 Ma; Button, 1981b) suggests a significant contribution to these sediments from relatively young sources; however, it is not clear whether this date represents a mean provenance or depositional-diagenetic age (Gebauer and Grunenfelder, 1974; Perry and Turekian, 1974; Goldstein and Jacobson, 1988). The overall Ventersdorp-Transvaal mafic to felsic transition is similar to that exhibited by the Moodies-Pongola successions. The large areal extent of the Transvaal sequence, as well as the chemical and

mineralogical composition of quartzites are consistent with the deposition of these sediments in a passive margin or cratonic interior setting.

WATERBERG AND SOUTPANSBERG GROUPS

The relatively small number of pelite samples analyzed from the Waterberg and Soutpansberg Groups does not allow a thorough evaluation of basin development. The similarities of these sediments to the composition of NASC suggests that a Phanerozoic-like upper crustal source, similar to that which supplied detritus to the upper Transvaal sediments may have remained exposed throughout deposition of the Waterberg and Soutpansberg Groups. The chemical and mineralogical composition of Waterberg quartzites suggests deposition in passive margin or cratonic interior setting, whereas the abundance of detrital K-feldspar, volcanism and basin margin faulting suggest a continental-rift setting for Soutpansberg sediments.

KAAPVAAL CRATON EVOLUTION

Engel et al. (1975), Veizer and Jansen (1979) and Veizer (1979) indicate that sediments display a marked evolution from mafic-rich to felsic rich compositions, with a clear transition occurring at or near the Archean-Proterozoic boundary. These changes are thought to reflect a change in the composition of the upper-continental crust where primitive (ultramafic-mafic) material is volumetrically reduced in importance by the addition of evolved

(felsic) material. This proposed upper-crustal transition reflects two distinct, but related events. The first is an increase in the volume of material added to the crust from the mantle, and the second includes intracrustal melting and production of granitic magmas which are emplaced in the upper-continental crust (Taylor and McLennan, 1983). These changes in upper-crustal composition are diachronous on a worldwide scale, occurring over a protracted period of events lasting from about 3.2 to 2.5 Ga (Taylor and McLennan, 1983). Primitive to evolved transitions probably occurred earlier in the Kaapvaal relative to other cratons (Taylor and McLennan, 1981; McLennan et al., 1983). In southern Africa, the change in sedimentary REE patterns reflecting this transition is proposed to occur during the late Archean, at about 3.0-2.8 Ga (McLennan and Taylor, 1988). Gibbs et al. (1986) dispute the evidence used to support these crustal transitions, noting that most pelites representing the primitive Archean crust are from greenstone successions whereas post-Archean samples are from cratonic platform successions. Compositions of Kaapvaaal craton sediments offer a unique opportunity to resolve this conflict. Cratonic sediments are preserved here in a nearly continuous time-span from 3.2 to 2.1 Ga. Thus, the composition of these sediments should record the secular evolution of the Kaapvaal craton across the Archean-Proterozoic boundary.

Data from this study record several primitive to evolved cyclical changes in upper crust composition during the Archean and early Proterozoic (Wronkiewicz and Condie, 1989c). An early cycle is recorded in the eastern portion of the Kaapvaal craton with the transition from the mafic-rich Moodies to the felsic-rich Pongola successions (3.2-2.9 Ga). The felsic-rich portion of this cycle also may include Dominion Group quartzites ($\sim$2.8 Ga) and Witwatersrand-OG pelites in the western portion of the craton, both units which have features suggestive of their derivation from granite-rich sources (Viljoen et al., 1970; Wronkiewicz and Condie, 1987). An erosional interval of approximately 200 Ma between the Moodies and Pongola sequences also may mask portions of this or additional cycles. A second cycle is recorded during deposition of the Witwatersrand Supergroup (2.8-2.7 Ga; excluding the OG pelites). This sequence exhibits a mafic to felsic transition which differs from that of the Moodies-Pongola cycle. Initial Witwatersrand sediment compositions are dominated by tonalite and basalt-rich sources, while both granite and komatiite sources increase upsection at the expense of tonalite. Komatiitic contributions peak during deposition of BOY pelites while granite contributions continue to increase upsection through deposition of the K8 pelites. Results from Ventersdorp and Transvaal pelites (2.6-2.1 Ga) record a third mafic to felsic cycle during the

Figure 43. Cr/Zr secular variations of mid-Archean to early Proterozoic pelites from the Kaapvaal craton. Dots indicate mean values, vertical rectangles represent one sigma ranges of variation, rectangle width represents approximate stratigraphic age of sequence. MO, Moodies; NSZ, Nsuze; MZN, Mozaan; OG, Orange Grove; PRM-PBR, Promise-Parktown-Brixton; RO, Roodepoort; BOY, Booysens; K8, K8 pelites; BOT, Bothaville; SEL, Selati; BR, Black Reef; TH, Timeball Hill; STR, Strubenkop; SIL, Silverton; WAT, Waterberg; and SOT, Soutpansberg pelites. Moodies-Pongola cycle discussed in text is indicated in pink, Witwatersrand in yellow, and Ventersdorp-Transvaal (including Waterberg and Soutpansberg shales) is in orange. Data from Tables 2-5 and McLennan et al. (1983).

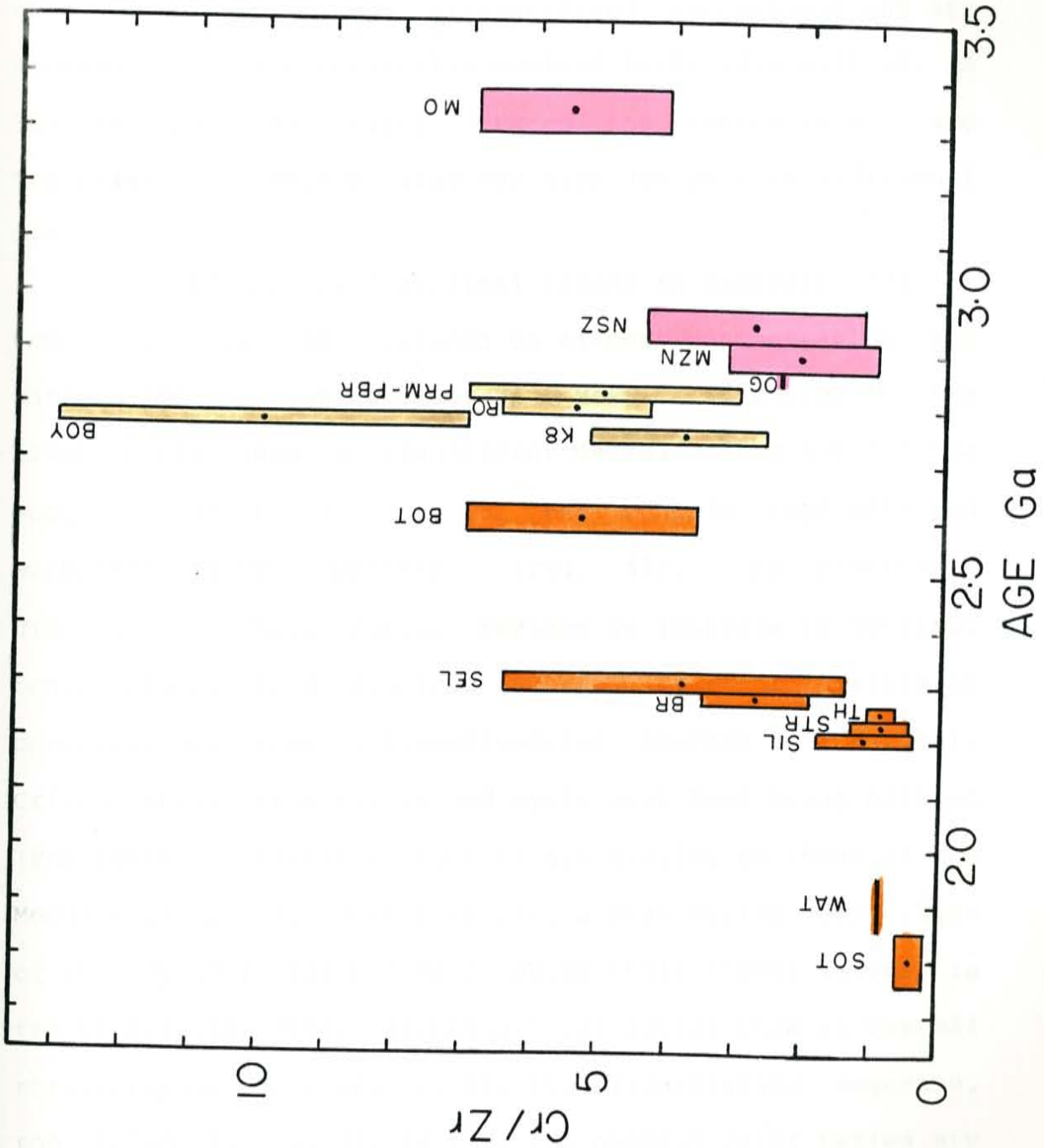
MO
NSZ
MZN
OG
PRM-PBR
RO
K8
BOY
BOT
SEL
BR
TH
STR
SIL
WAT
SOT
0
5
10
Cr / Zr
2.0
2.5
3.0
3.5
AGE Ga

early Proterozoic (Wronkiewicz and Condie, 1989b, 1989c). BOT and especially SEL-BR pelites possess primitive ''Archean-type'' geochemical signatures similar to those of the Moodies and lower Witwatersrand successions and are succeeded by the chemically evolved TH-STR-SIL pelites. A 300 Ma erosional hiatus between the Ventersdorp and Transvaal successions also may mask one or more additional cycles.

The three proposed cyclical trends in Kaapvaal sediment composition can be examined on element concentration and ratio secular variation diagrams. Mean Cr/Zr ratios in the first cycle show a significant decrease from 5.5 for the Moodies (MO) to 2.1-2.8 for the Pongola (MZN-NSZ) and Witwatersrand-OG pelites (Fig. 43). As previously discussed, these ratios reflect an increase in detritus contributions from granitic sources (Zr-rich) relative to contributions from ultramafic-mafic sources (Cr-rich). Cr/Zr ratios from the second cycle West Rand Group pelites (PRM-PBR-RO; Cr/Zr=5.5 to 6.6) are similar to those of the Moodies Group. Witwatersrand ratios peak during deposition of the BOY unit (10) before reaching their lowest values in the K8 pelites (3.9). Although Cr/Zr ratios show an overall stratigraphic decrease within the Witwatersrand sequence, the trend is unusual in that the highest Cr/Zr ratios are recorded for BOY pelites located stratigraphically near the center of the succession. Cr/Zr ratios of BOY pelites are

the highest recorded from the Kaapvaal craton and may record the exposure of an anomalously Cr-rich crustal source. Within the third sedimentary cycle, Cr/Zr ratios are highest for the Ventersdorp-BOT and Transvaal-SEL pelites (5.3-4.2), before decreasing for BR pelites (2.7) and decreasing again in the overlying Pretoria Group pelites (TH-STR-SIL; 0.9-1.1). Pretoria Group sediments (2.2 Ga) record the first exposure of fully-evolved crust in southern Africa. Waterberg (WAT) and Soutpansberg (SOT) pelites continue to exhibit the low Cr/Zr ratios first observed in the Pretoria Group sediments.

Sc/Th ratios also can be used to examine the three-cycle evolution of Kaapvaal craton sediments, with Sc recording komatiitic-mafic sources and Th indicating contributions from granitic source-rocks (Fig. 44). In contrast to Cr/Zr ratios, the Moodies-Pongola cycle does not show any significant variation in Sc/Th distributions, although mean values decrease slightly during the transition from the Moodies (MO) to Pongola units (MZN-NSZ). Witwatersrand pelites show an overall stratigraphic decrease in Sc/Th ratios with maximum values are recorded for the BOY pelites near the center of the sequence. Relatively high Sc/Th ratios of mafic-rich BOT-SEL-BR pelites contrast the felsic-rich sources recorded by TH-STR-SIL pelites. This compositional break at 2.2 Ga is identical to the transition

Figure 44. Sc/Th secular variations of mid-Archean to early Proterozoic pelites from the Kaapvaal craton. Symbols, abbreviations, color scheme, and data sources same as in Figure 43.

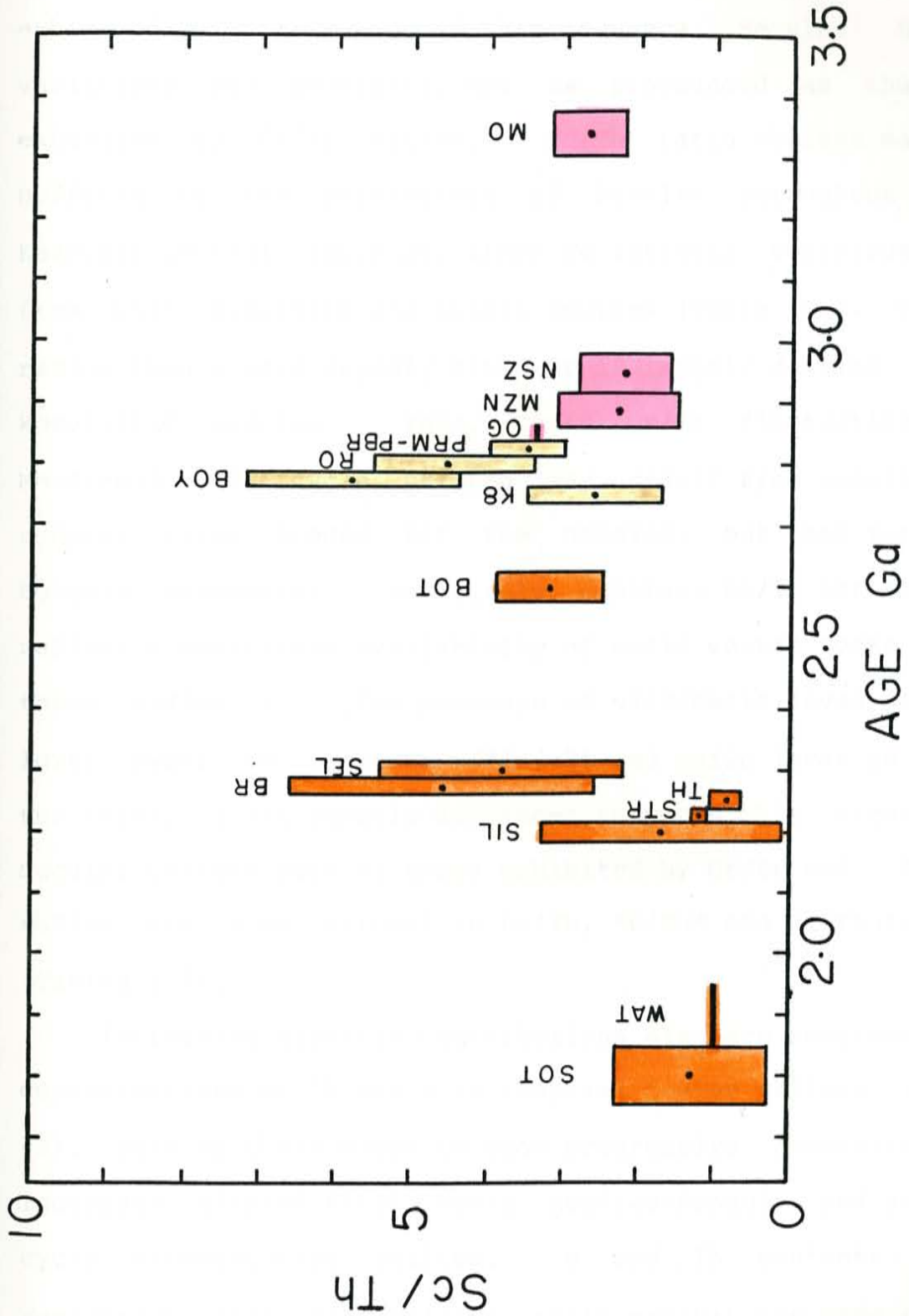
MO
NSZ
MZN
OG
PRM-PBR
RO
BOY
K8
BOT
SEL
BR
TH
STR
SIL
WAT
SOT
3.5
3.0
2.5
2.0
AGE Ga
10
5
0
Sc/Th

exhibited by Cr/Zr ratios of this sequence. Secular Sc/Th variations are generally not as pronounced as changes exhibited by Cr/Zr ratios. Sc/Th ratio changes may be buffered by the persistence of basalts throughout the Kaapvaal geologic sequence, since Sc reflects contributions from both komatiite and basalt sources (Table 13a). Cr/Zr ratios change more rapidly since Cr is largely derived from komatiitic sources. Thus, rapid Cr/Zr fluctuations of Moodies-Pongola cycle pelites may result from komatiitic sources being eroded for the Moodies, but not for the Pongola sediments. Relatively constant Sc/Th ratios may reflect a consistent availability of mafic source rocks for these sediments. The presence of ultramafic lavas in the lower Swaziland sequence (Fig. 3) and mafic lavas in both the Swaziland and Pongola sequences supports this argument. Secular changes such as those exhibited by Cr/Zr and Sc/Th ratios are also evident in La/Yb, Eu/Eu* and Cr/Th ratios (Tables 2-5).

Increasing granitic contributions also are recorded in concentrations of Th and U in Kaapvaal craton pelites (Fig. 45). Both of these elements show progressive concentration increases within first cycle Moodies-Pongola and second cycle Witwatersrand pelites. U and Th contents of Ventersdorp-Transvaal pelites again exhibit the same sharp composition change at 2.2 Ga indicating the exposure of fully evolved continental crust at this time.

Figure 45. Secular variation of Th and U concentrations from mid-Archean to early Proterozoic pelites from sedimentary basins of the Kaapvaal craton. Height of vertical rectangles represent mean concentrations of U (lower rectangle height-colored in blue) and Th (total rectangle height-colored in green). All concentrations in ppm. Abbreviations and data sources same as in Figure 43. 1st, 2nd and 3rd cycles discussed in text and in Figure 43.

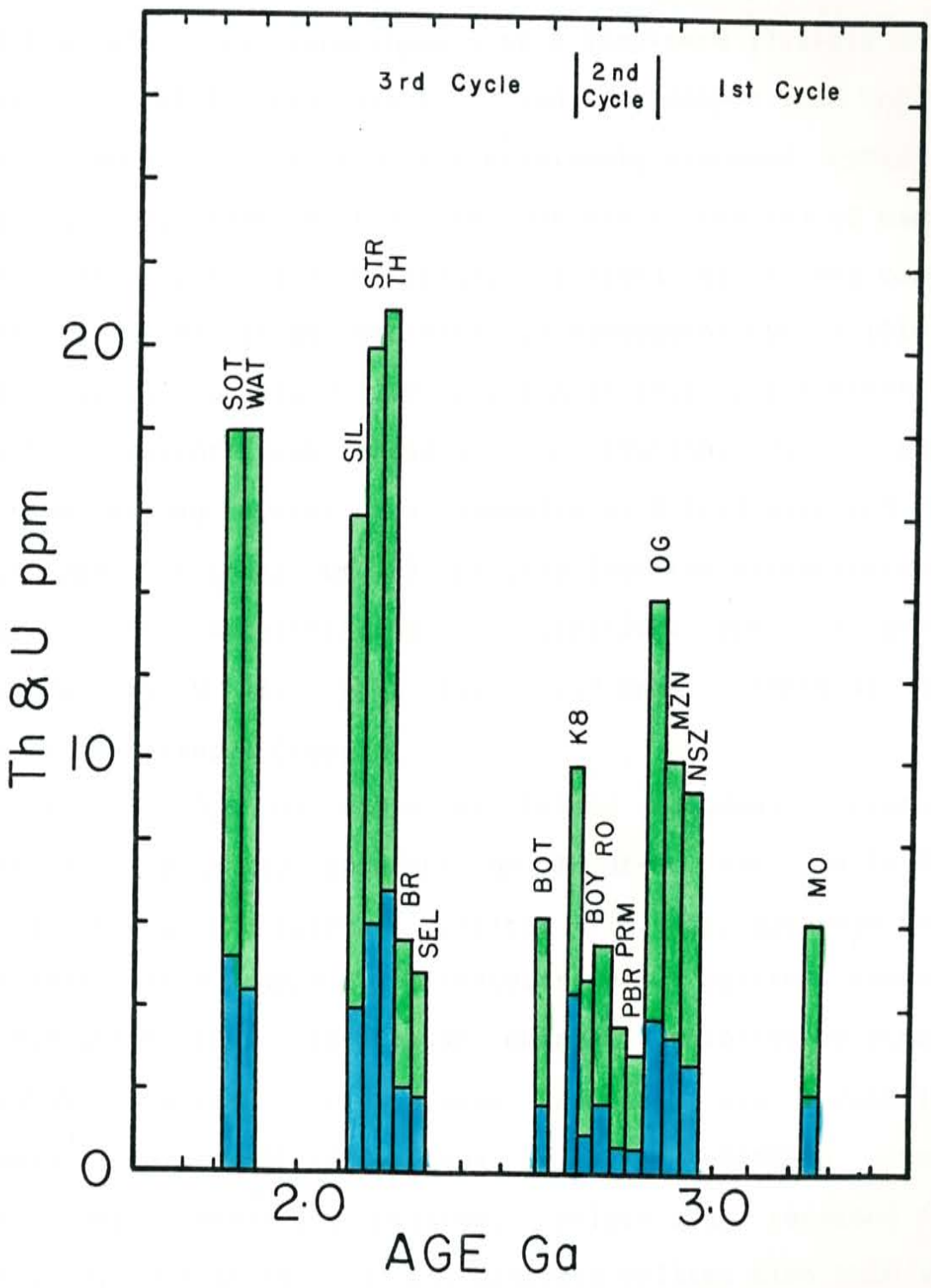
3rd Cycle
2nd Cycle
1st Cycle
Th & U ppm
0
10
20
2·0
3·0
AGE Ga
SOT
WAT
SIL
STR
TH
BR
SEL
BOT
K8
BOY
RO
PRM
PBR
OG
NSZ
MZN
MO

Mafic to felsic cycles exhibited by Kaapvaal craton pelites also are superimposed on a long-term (3.2-2.1 Ga) mafic to felsic transition in sediment composition which incorporates all three of the previously proposed cycles. For example, maximum U and Th contents at the end of each short-term cycle are generally exceeded by maximum concentrations of these elements in subsequent cycles (Fig. 45). Average Pongola U (2.9 ppm) and Th (9.1 ppm) contents, which represent peak granitic contributions during the Moodies-Pongola cycle, are exceeded by U (4.3 ppm) and Th (9.8 ppm) contents of K8 pelites from the Witwatersrand cycle. The Witwatersrand concentrations are, in turn, exceeded by U (5.7 ppm) and Th (19 ppm) contents of the Transvaal-Pretoria Group.

The 3.2-2.1 Ga mafic to felsic Kaapvaal craton transition also is apparent on Th-Hf-Co and La-Th-Sc distributions of Kaapvaal pelites (Fig. 46), although the ultramafic-rich source for Witwatersrand-BOY pelites causes a deviation from progressive changes exhibited by other secular diagrams. Significant increases are readily apparent in (Th+Hf)/Co ratios of Moodies-Pongola and Ventersdorp- Transvaal pelites. Felsic peaks recorded in Pretoria, Waterberg and Soutpansberg pelites also show an increase in Th relative to all previously deposited Kaapvaal craton pelites. Witwatersrand samples show a progressive

Figure 46. Secular variation plots showing distributions of Kaapvaal craton pelites on Th-Hf-Co and La-Th-Sc diagrams. Progressive evolution of the Moodies-Pongola, Witwatersrand and Ventersdorp-Transvaal (includes Waterberg and Soutpansberg Groups) pelites are recorded by the indicated symbols and lines. Symbols with dots indicate the basal sediment succession of each cycle, whereas arrows indicate increasing stratigraphic height. Red colored symbols designate the felsic-rich upper portion of each cycle, whereas yellow colored symbols indicate the mafic- and/or komatiitic-rich lower portions of each cycle.

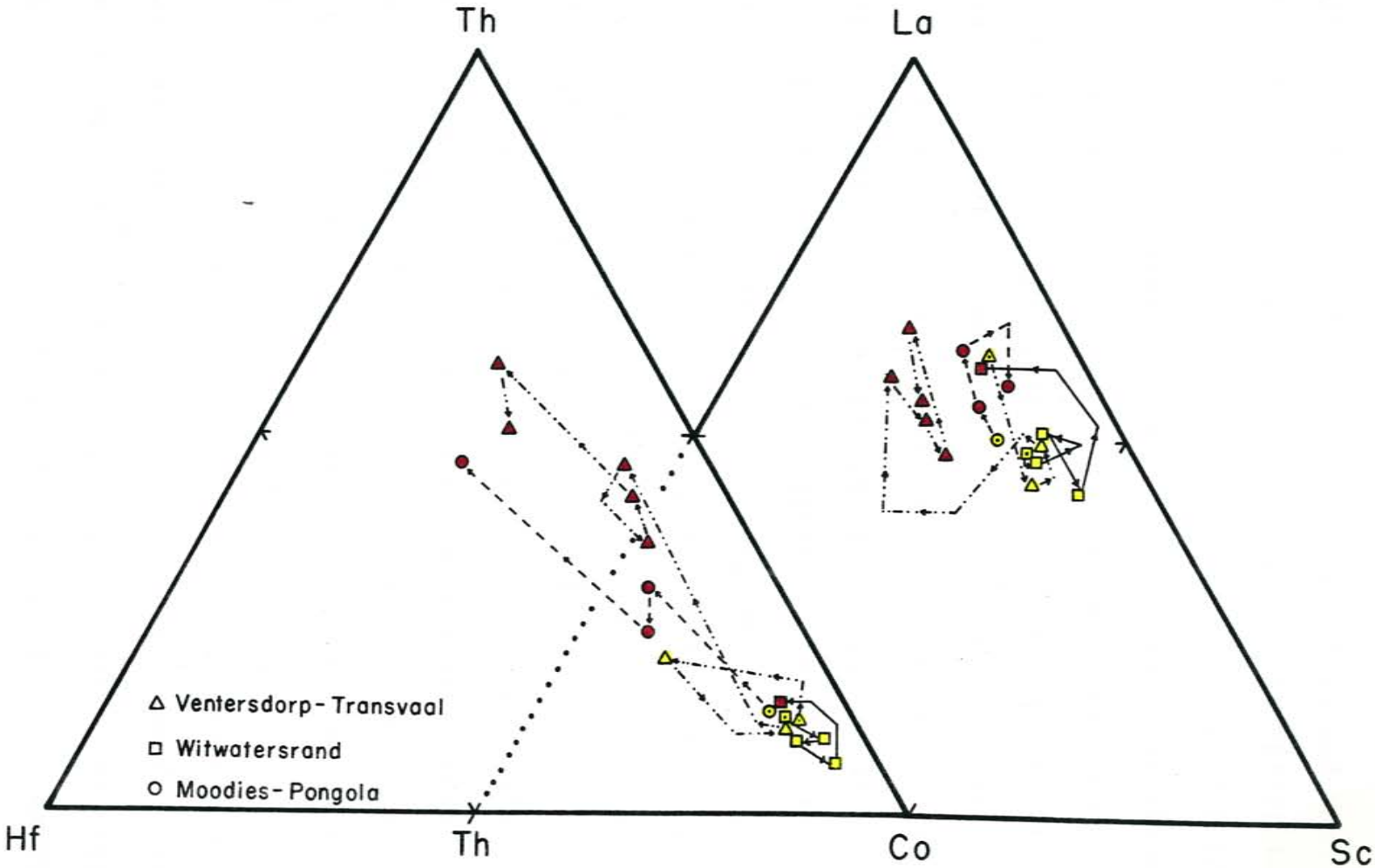
Th
La
Hf
Th
Co
Sc
△ Ventersdorp - Transvaal
□ Witwatersrand
○ Moodies - Pongola

increase in komatiitic components (higher Co) during deposition of the PBR through the BOY pelites, and then show a significant increase in felsic components (Th+Hf) in K8 pelites. Although the progression from the basal PBR to BOY pelites is a gradual change, the overall variation is significant within one standard deviation of the mean.

Mafic to felsic cycles are not as readily apparent on La-Th-Sc diagrams, however, mafic to felsic stratigraphic changes are still apparent. The Moodies-Pongola cycle shows small progressive increases in La, before deviating with the composition of OG pelites. Changes along the Moodies-Pongola trend are, however, not statistically significant, largely due to variable La contents of Pongola pelites (Table 2). Witwatersrand-BOY pelites show a significant increase in komatiitic-mafic components (higher Sc) relative to underlying West Rand Group pelites (PBR-PRM-RO), while the felsic-rich K8 pelites record a significant increase in granite contributions relative to BOY pelites. The Ventersdorp-Transvaal sequence again shows a sharp compositional change at 2.2 Ga. This sequence can be divided into two groups on La-Th-Sc diagrams, the relatively mafic-rich BOT-SEL-BR pelites, and felsic-rich Pretoria-Waterberg-Soutpansberg Groups. Partial exposure of granite during deposition of BOT pelites also is expressed in high La/Sc ratios of these sediments relative to the SEL-BR pelites. La and Th contents also increase relative

to Sc during deposition of the entire Kaapvaal sequence.

Rapid changes in incompatible-compatible element ratios, such as Th/Sc and La/Sc, attest to minimal sediment recycling during deposition of most of the Witwatersrand and Ventersdorp-Transvaal sequences. This observation is important in that it documents that secular changes in Kaapvaal sediment compositions are related to changes in the exposed crust and not to recycling of older sedimentary rocks (Taylor and McLennan, 1985). Isotopic constraints also indicate that Pongola sediments are derived largely from primary sources (Miller and O'Nions, 1985). Sedimentary Nd-isotopic patterns from the North Atlantic region have led Allegre and Rousseau (1984) to propose that sedimentary stratigraphic ages are indistinguishable from crustal residence ages for most sediments deposited prior to 2.5 Ga ago. Northward migration of successive Kaapvaal craton basins (Fig. 2) and a consistent northerly source for most of these sediments also precludes significant recycling between successive basins. These data all suggest that recycling is probably not a dominant force in Kaapvaal sediment evolution, however, elevated concentrations of lithic-sedimentary framework grains in some Kaapvaal quartzites (Table 6) imply that sedimentary recycling occasionally may have been important.

Results imply that the upper crust of the Kaapvaal craton has undergone a minimum of three primitive to evolved

transitions during the time interval from 3.2 to 2.1 Ga. Although the exact cause of these cycles is unknown, they may be related to orogenic pulses associated with growth of the Kaapvaal and Zimbabwe cratons. These orogenic pulses, may in turn, be related to collisional events along along destructive plate boundaries and/or pulses of granitic magmatism associated with evolution of the Kaapvaal craton. Evidence supporting collisional episodes between the Kaapvaal and Zimbabwe cratons is cited in Table 14. Evolution of each sedimentary cycle coincides with major collisional episodes proposed to have occurred along the northern Kaapvaal craton margin (Barton and Key, 1981; Light, 1982). The timing of these proposed collision events are poorly constrained (mostly Rb-Sr whole-rock dates) and future age determinations may require modification or abandonment of the collision induced sedimentary cycle model. Despite this caveat, two episodes of granulite facies metamorphism in the Limpopo region support at least two major collision episodes along the northern Kaapvaal craton margin.

The first proposed collisional episode may have been initiated during accretion of 3.5-3.4 Ga greenstones such as the Barberton and Murchison belts and continued with a 3.4-3.1 Ga collision event with the Zimbabwe craton or an island arc system to the north. The Moodies-Pongola cycle was initiated after these deformation events began and the

Table 14. Evidence suggesting craton collision events in the Kaapvaal-Limpopo-Zimbabwe provinces

MOODIES-PONGOLA CYCLE EVENTS

1) F1 recumbent folding of Beit Bridge metasediments from 3270-3150, Rb/Sr [2-4].
2) F2 isoclinal folding of Beit Bridge metasediments on NE-SE axes at 3150 Ma, Rb/Sr [2,3].
3) ''Collisional style'' thrust and fold nappes within the Central Limpopo Zone [14].
4) Granulite facies metasediments in the Central Limpopo Zone characterized by ~35 km burial depth at ~3150 Ma, Rb/Sr followed by ~25 km of rapid isothermal uplift; and 30 km total burial depth in the Limpopo Southern Marginal Zone [5,9,14,18].
5) Formation of Pongola depository as a (collision induced?) rift structure at 3.0-2.9 Ga [7].

WITWATERSRAND CYCLE EVENTS

1) Deposition of lower Witwatersrand sediments in a foreland basin associated with a convergent plate margin to the north [8].
2) F3 tight folding of Beit Bridge metasediments on NE-NNE axes at 2700-2600 Ma, Rb/Sr, Pb/Pb [5].
3) Formation of anatectic granites in response to crustal thickening and regional isothermal uplift at 2700 Ma, Rb/Sr [2,3,15,17].
4) Granulite facies metavolcanics and metasediments in Limpopo Central and Southern Marginal Zones characterized by ~27 km burial depths followed by rapid isothermal decompression at 2700-2650 Ma [15-16]
5) Thrusting along northern Witwatersrand basin margins and development of foreland basin during collision episode (~2750-2700 Ma, [8]).
6) Extensive resetting of Rb-Sr isotopic systems at ~2650 Ma during a widespread metamorphic event [3,4].
7) Intrusion of 2650 Ma, Rb/Sr mantle derived dikes during a period of extensional tectonics [19].
8) Formation of Ventersdorp rift due to Limpopo collision episode 2.7-2.6 Ga [7].

VENTERSDORP-TRANSVAAL CYCLE EVENTS

1) F4 dextral shearing of Beitbridge metasediments in the Northern Limpopo Zone at 2600 Ma, Rb/Sr [2,4,5].
2) 100 x 700 km NE-SW belt of calc-alkaline volcanics and associated plutonics (~2700-2600 Ma, Rb/Sr) formed in the Upper Sebakwian greenstone along the NW margin of the Zimbabwe craton [20].
3) Cessation of all movement and deformation in the Limpopo Province at 2500 Ma [11].
4) Formation of Great Dyke (~2500 Ma, Rb/Sr) in release fractures formed at right angles to compression in the Limpopo belt [10,11].
5) Paleomagnetic evidence suggesting that the Kaapvaal and Zimbabwe cratons have behaved as a single unit since 2300 Ma [12,13].
6) Gradual uplift and erosion of the Limpopo region from 2600-1950 Ma, Rb/Sr [1,3].

References:

1] Barton and Ryan, 1977
2] Barton et al., 1979
3] Barton and Key, 1981
4] Barton et al., 1981
5] Barton, 1983
6] Barton et al., 1983
7] Burke et al., 1985a
8] Burke et al., 1986
9] Du Toit et al., 1983
10] Hamilton, 1977
11] Light, 1982
12] McElhinny and McWilliams, 1977
13] Piper, 1976
14] Shackleton, 1986
15] Van Reenen et al., 1987
16] Van Reenen et al., 1988
17] Watkeys, 1981
18] Watkeys et al., 1981
19] Watkeys and Armstrong, 1985
20] Wilson et al., 1978

Pongola felsic peak followed cessation of collision and Limpopo uplift at ~3.0 Ga. The Witwatersrand sedimentary cycle was initiated during renewed collisional movement between the Kaapvaal and Zimbabwe cratons after 2.9 Ga. The felsic peak of the Witwatersrand cycle also coincides with cessation of collisional movement and Limpopo uplift at 2.7 Ga. Development of the Ventersdorp-Transvaal cycle (2.6-2.1) coincides with initiation of a third deformational event along the northern Kaapvaal craton margin at ~2.6 Ga, whereas the Pretoria Group felsic peak (~2.2 Ga) follows cessation of Kaapvaal-Zimbabwe collisional movements at 2.5-2.3 Ga (Piper, 1976; McElhinny and McWilliams, 1977; Light, 1982). Deformation of the Limpopo region at 2.6 Ga also may result from reactivation of zones of weakness in the Limpopo crust due to compressive forces generated elsewhere, possibly along the northern perimeter of the Zimbabwe craton. Transmission of tectonic stresses across continental basement is proposed for western North America during the Larimide Orogeny (Sales, 1968; Dickinson and Snyder, 1978) and thus may be possible during the evolution of southern Africa.

More recent analogs for multi-collisional growth of craton boundaries include: 1) the 1800-1600 Ma accretion of a 1200-km-wide band of material along the southwestern part of the North American craton (Silver et al., 1977; Condie, 1982; Duebendorfer and Houston, 1987); 2) a succession of

collisions recorded by the Penokean Orogeny (1.8), Grenville Orogeny (1.2-1.0 Ga) and the Ouachita-Marithon and Ancestral Rocky Mountains deformation events (late-Paleozoic) resulting from collision events along the southern-southeastern margin of the North American craton (Baer, 1981; Van Schmus and Bickford, 1981; Kluth and Coney, 1981); and 3) suspect terrane collision along the western edge of the North American craton during the late Mesozoic and Cenozoic (Coney et al., 1980).

Cyclical variations in Kaapvaal sediment compositions also may be related to cycles of granitic magmatism involved in the evolution of the Kaapvaal craton. Granitic cycles of the eastern Kaapvaal craton are proposed to occur at 3.5, 3.2-3.0, and 3.2-2.5 Ga (Anheausser and Robb, 1981). Granites intruded during the 3.2-3.0 Ga cycles are coincident with the development of the Moodies-Pongola cycle. Five periods of granitic intrusion, at 3.0 Ga, 2.7 Ga, 2.3 Ga, 2.0 Ga and 1.8 Ga also are proposed to occur across the entire Kaapvaal province (Hunter, 1974). The first three granitic cycles correspond to the felsic-rich portions of the Moodies-Pongola, Witwatersrand, and Ventersdorp-Transvaal sedimentary cycles. The 2.0 Ga granitic cycle is related to crustal melting during intrusion of the Bushveld complex, whereas the final granite cycle coincides with deposition of the felsic-rich Waterberg and Soutpansberg sediments.

Regardless of their ultimate cause, cyclic geochemical trends in sediment composition suggest a multi-episodic evolution of the Kaapvaal upper crust, with each cycle recording increasing exposure of felsic-rich sources during orogenic episodes. The cycles also are superimposed on a long-term mafic to felsic transition which records an overall increase in the exposure of felsic material on the Kaapvaal craton from 3.2 to 2.1 Ga. Although the early Kaapvaal crust appears to be enriched in mafic sources relative to the post-2.2 Ga crust, the changes in crustal composition over this transition period are not as pronounced as earlier studies have indicated (Taylor and McLennan, 1985). Evolutionary changes over this transition period also record a complex and long-lived transition period for the Kaapvaal craton upper-continental crust.

Witwatersrand Gold Genesis

Although the Witwatersrand deposit accounts for approximately 50% of the world's annual gold, 30% of historic gold, and 10% of annual uranium production, the genesis of this deposit still remains a matter of considerable controversy. Consensus from the majority of geologists working on the Witwatersrand is that this deposit represents detrital accumulation of gold and uranium derived from erosion and denudation of flanking Archean highlands (Whiteside et al., 1976). Post- depositional metamorphism and mobilization of some metals has led to the ''modified placer theory'', where the ultimate metal source is still detrital in origin, but gold, uranium and sulfides were mobilized and redeposited during metamorphism. Evidence for metamorphic mobility of metals includes secondary overgrowths on allochthonous pyrite and uraninite, as well as autochthonous gold, pyrite and uraninite. Alternative metalogenic theories for the Witwatersrand include: 1) hydrothermal introduction of gold and uranium after conglomerate lithification (Davidson, 1957, 1964; Giusti, 1988); 2) reworking of submarine hydrothermal exhalitive gold-pyrite deposits associated with Dominion Group volcanism (Hirdes and Saager, 1983; Hutchinson and Viljoen, 1986; Hutchinson, 1987); and 3) post-burial metamorphic fluid introduction of gold and uranium

(Phillips, 1986a, 1986b, 1987; Phillips et al., 1987). If the modified placer theory is accepted, and if pelites are derived from the same source as auriferous and uraniferous conglomerates, then the composition of these pelites becomes an important tool for constraining the origin of the Witwatersrand deposit.

The conglomerates, or 'reefs' as is concurrent with local usage, are the dominant gold and uranium bearing strata of the basin. Heavy mineral assemblages of the reefs include >90% pyrite, with lesser arsenopyrite, cobaltite, sphalerite, uraninite, chromite, zircon and gold (Feather and Koen, 1975). Additional detrital grains include rare occurrences of platinum group metals, thoraninite, garnet, diamond, molybdenite, kyanite, cassiterite, tourmaline, monazite, cobaltite, Fe-Ti oxides and thucholite (biogenic origin). These heavy-mineral associations suggest a diverse source lithology, including felsic to ultramafic, and plutonic to metamorphic sources. Gold occurs both as autochthonous and allochthonous particles averaging 0.005-0.5 mm in diameter (Hallbauer and Joughin, 1972, 1973). Gold grains are generally of a high purity, containing approximately 10% Ag, 2% Hg, 0.3% Cu and lesser Fe, Ni, Mo, Co, Bi, Pb, Sn and As (Schidlowski, 1968; Saager, 1969; Viljoen, 1971; Feather and Koen, 1973; Reid et al., 1988). Detrital ''buck-shot'' pyrite indicates proximal sources for at least a portion of these sulfides (Hutchinson and

Viljoen, 1986). By contrast, pebble roundness determinations for Central Rand Group conglomerates indicate 160 km of downstream travel (Els, 1988). Thus, Witwatersrand sediments may have had both distal and proximital sources.

Placer models for the Witwatersrand deposit suggest that source-rocks for the gold could be represented by eroded greenstones such as the Barberton and Letaba districts, located to the north and northeast of the basin (Viljoen et al., 1970; Minter, 1978). Gold occurs in these greenstone as veined deposits hosted in megashears located within mafic or komatiite-rich lower portions of the sequences (Anhaeusser, 1971, 1981; Roberts, 1987; Fig. 3). Lead isotopic compositions of some detrital Witwatersrand pyrites are similar to those observed in sulfides from primary gold deposits in the Barberton, evidence which supports the greenstone origin for Witwatersrand gold (Koppel and Saager, 1974). The enormous volume of gold and uranium deposited in the Witwatersrand basin is, however, problematic as the total concentration of gold contained in Archean greenstone deposits is deficient as a provenance for the conglomeratic ores (Reimer, 1984; Robb and Meyer, 1985). For example, the 35,100 tons ($\sim$1.3 billion ounces; Hutchinson and Viljoen, 1986) of historic gold production from the Witwatersrand basin would require the erosion of 20 to 35 world-class Archean greenstone deposits the size of

Timmons, Canada, Homestake, USA, or Kalgoorlie, Australia (1000-1700 tons Au each; Phillips, 1986c).

Clearly additional and/or entirely different sources are required to account for the sheer volume of gold contained in the Witwatersrand. Auriferous banded iron formation clasts in the Evander gold fields have led Hirdes and Saager (1983) to suggest that these chemical precipitates also may be an important source for gold. Although banded iron formation sources are important in the Evander goldfield, other reefs have relatively minor occurrences of these clasts types, yet are still enriched in gold. Thus, auriferous banded irons may be of only local importance for Witwatersrand gold genesis. Uranium occurrences in the Witwatersrand deposit also necessitate the presence of felsic sources. Robb and Meyer (1985, 1987) and Klemd and Hallbauer (1987) have identified extensive zones of hydrothermally altered granites (HAGS) with anomalous gold concentrations, occurring along the periphery of the Witwatersrand basin. These HAGS represent another potential source for Witwatersrand gold and uranium. Pelite provenance data resulting from this study indicate that contributions from granite must have peaked during and subsequent to the main gold depositional stages. Rb/Sr ratios show progressive stratigraphic decreases upsection within the Witwatersrand sequence (5.1-0.7; Table 3). Rb/Sr

ratios also show marked depletions from fresh granites (7.6-2.2) to HAGS (2.0-0.2; Govett, 1983), suggesting that increased contributions of hydrothermally altered material may have occurred concurrent with gold deposition. K/Rb ratios also typically increase in HAGS associated with gold mineralization. The highest Witwatersrand K/Rb ratios are those of K8 pelites associated with the paleoplacer ores, adding further evidence for a HAG source for Witwatersrand gold. Unfortunately, both Rb/Sr and K/Rb ratios may be modified during weathering of surface rocks (Fig. 24a). Thus, Rb/Sr and K/Rb ratio trends observed in Witwatersrand pelites may reflect chemical changes during weathering or hydrothermal alteration. High Co concentrations and elevated Co/Ni ratios of detrital Witwatersrand pyrite also provides evidence for HAG sources (Von Rahden and Hiemstra, 1967). Lower Co concentrations and Co/Ni ratios in pyrites from the Kimberley placer, near the top of the Witwatersrand succession, may indicate the exhaustion of HAG sources due to erosion.

Pyrophyllite occurs as a major mineral constituent of Central Rand Group pelites, while it is conspicuously absent in the underlying West Rand Group (Table 1). This mineral commonly occurs as an alteration product in hydrothermal systems, and thus may 'fingerprint' the first exposure of HAG sources to Witwatersrand erosion. Alternatively,

pyrophyllite may originate during metamorphism of sediments rich in detrital kaolinite. Laterite sources providing kaolinite for Central Rand Group sediments are unlikely, however, considering the active tectonism implied by the coarse nature and minimal cation depletion trends of Central Rand Group sediments (Figs. 8 and 24d). Secondary fluid inclusions, located along healed fractures in Central Rand Group quartz clasts, suggest rapid metastable cooling of source-rocks. Rapid cooling rates are common in hydrothermal systems, and thus, these fluid inclusions provide additional evidence supporting the HAG source theory for Witwatersrand gold.

Increased granite and gold contributions to West Rand Group sediments correspond to the change from pelite-quartzite to quartzite-conglomerate dominated lithologies, and are thought to reflect increased tectonic activity along the basin margins (Pretorius, 1981b). Thus, exposure of auriferous granites and accumulation of gold in conglomerates may result from tectonic exposure of new source-rock lithologies in the Witwatersrand hinterland. Increasing granitic and mafic-ultramafic sources for Central Rand Group pelites show a secular association with gold deposition, suggesting that mineralization resulted from the progressive unroofing and erosion of both low-grade gold and uranium hosted in HAG sources and high-grade gold hosted

in greenstone megashears. Gold contained in banded iron formations also may be locally important. Komatiitic sources culminated during deposition of BOY pelites, representing the exhumation of lower portions of the greenstones. Decreases in komatiitic contributions recorded in overlying K8 pelites indicate the final stripping and erosion of lower portions of these greenstones. Continued erosion of HAG sources, and exposure of unaltered and unmineralized interior portions of granitic plutons is recorded in the trailing off of gold concentrations in uppermost Witwatersrand sediments. Post-depositional mobilization of gold, uranium and sulfides may have occurred during diagenesis or during regional metamorphic events recorded at 2400-2300 Ma (Barton et al., 1986), 2050 Ma (Bushveld intrusive event) and/or 2000 Ma (Vredefort dome formation).

CONCLUSIONS

Precambrian sediments from the Kaapvaal craton provide a semi-continuous geochemical record of crustal evolution for $\sim$ 1.5 Ga in southern Africa. Major events recorded in Kaapvaal craton sediments are as follows:

1) Mineral assemblages in Kaapvaal craton sediments and volcanics indicate that Pretoria, Dominion, Witwatersrand, Ventersdorp and lower Transvaal sequences were exposed to maximum regional pressure-temperature conditions characterized by greenschist facies metamorphism. Transvaal-Pretoria, Soutpansberg and Waterberg Group sediments and volcanics exhibit a maximum of zeolite facies metamorphic conditions.

2) Intense chemical weathering of komatiitic source-rocks may have caused increased Cr-Ni contents and elevated Cr/Ni ratios in most Pongola and some Witwatersrand and Transvaal pelites. Relative mafic and ultramafic contributions to these sediments have previously been overestimated when pelite Ni and Cr concentrations were assumed to be representative of their sources.

3) Elevated Cr/Ni ratios may provide a method of identifying intensely weathered komatiitic sources for sediments. Elevated Cr/Ni ratios in Pongola pelites also indicate a potential for the discovery of nickeliferous paleolaterites in Pongola basement rocks.

4) Depletion of Ca, Na and Sr in Witwatersrand pelites suggest that West Rand Group sediments were eroded from deeply weathered, flat lying source-regions. Central Rand Group element depletion patterns suggest a source undergoing more rapid erosion, and hence, more active tectonism relative to the West Rand Group source. This conclusion is supported by an increase in mean detrital grain size and the onset of basin margin faulting during deposition of the Central Rand Group.

5) Mineralogical and chemical compositions of most Kaapvaal craton quartzites are indistinguishable from those of Phanerozoic sandstones deposited in cratonic interiors and passive margin settings. Exceptions include the: a) Witwatersrand-Central Rand Group and Ventersdorp-Bothaville quartzites which have affinities to recycled orogenic sandstones; b) Quartzites from the Dominion Group which are similar to Phanerozoic sandstones deposited in transitional basement uplift zones; and c) Transvaal-Wolkberg, Soutpansberg and Waterberg sandstones which have scattered distributions with similarities to cratonic interior, recycled orogenic and transitional basement uplift zones.

6) A minimum of three primitive to evolved crustal cycles are recorded in chemical compositions of Moodies-Pongola (>3.2-3.0 Ga), Witwatersrand (2.8-2.7 Ga), and Ventersdorp-Transvaal sediments ($\sim$2.6-2.1 Ga). Each cycle represents a

change in composition of sediment sources, from those enriched in mafic-komatiitic components to those enriched in felsic components (chiefly granite).

7) Sedimentary cycles coincide with deformational events recorded in the Limpopo Mobile Belt to the north, although the timing of these events are poorly constrained. The earliest recorded cycle (Moodies-Pongola) begins after accretion of 3.4-3.5 Ga greenstone belts (i.e. Barberton-type) and continued through Limpopo deformation at 3.1 Ga. The latter two cycles (Witwatersrand and Ventersdorp-Transvaal cycles) begin after Limpopo belt deformations at 2.9-2.7 and 2.6-2.5 Ga (Light, 1982).

8) Such a correspondence of sediment cycles and deformation events along the perimeter of the craton suggests a cause and effect relationship between arc and/or microcontinent accretion and Kaapvaal sedimentary geochemical cycles. These cycles may result from collisional events between the Kaapvaal and Zimbabwe cratons and/or associated subduction related island arc systems. Alternatively, these sedimentary cycles may be related to pulses of granitic magmatism into the Kaapvaal craton. These granite pulses are may be related to crustal collision events, arc magmatism and/or mantle plumes.

9) Following each deformational event, new mafic-komatiitic sources may have become available to weathering and erosion in the accreted terranes, leading to the initiation of a

new sedimentary cycle. Continued uplift of these sources progressively exhumed granitic rocks leading to a more felsic input into derivative sediments. Felsic peaks in sediment composition follow cessation of deformational events along the Kaapvaal craton perimeter.

10) Each of the short-term cycles appear to be superimposed on a long-term (3.2-2.1) mafic to felsic compositional transition for the Kaapvaal craton. This long-term transition records a gradual, but complex change from an upper-continental crust which was initially more mafic in composition than average Phanerozoic upper-continental crust. This long-term transition certainly does not record a clear transition at or near the Archean-Proterozoic boundary, nor does the Archean crust appear to be as mafic as previous studies have indicated (Veizer and Jansen, 1979; Taylor and McLennan, 1985).

11) The first exposure of fully-evolved upper continental crust is recorded during deposition of the Transvaal-Pretoria Group (~2.2 Ga).

12) Witwatersrand-Booysens pelites record the exposure of the most primitive sources exposed during Kaapvaal craton evolution. These sources may play a key role in the genesis of the Witwatersrand paleoplacer deposit as discussed in conclusion #14.

13) Mineralogic and chemical constraints from sediments suggest that granites exposed during Witwatersrand

deposition may have undergone pre-erosional hydrothermal alteration and gold enrichment. Erosion of these granites may have provided a portion of the gold and most of the uranium deposited in the Witwatersrand paleoplacer ores.

14) A secular correspondence between the peak contributions from mafic-ultramafic (Booysens pelites) and felsic source-rocks (K3 pelites) with gold deposition in the Witwatersrand basin suggests a dual source for these precious metal deposits. Gold may be derived from the erosion of both megashear deposits hosted in lower portions of Archean greenstones and hydrothermally altered granites (HAGS), whereas uranium may be from the HAGS.

15) Whether cyclical evolutionary trends observed in Kaapvaal sediments provide a model for early craton evolution, or whether these patterns are anomalous with respect to craton growth awaits further testing in other regions.

Appendix A. Sample Locations

A.1 Sample Collection

A total of 27 Mozaan and 36 Nsuze pelites from the Pongola Supergroup were selected for chemical analysis. In addition, four Mozaan and four Nsuze quartzites were analyzed. All samples are from surface outcrops. Nsuze pelites are from four strato-geographic horizons; the upper Wit-Mfolozi (NUWM), lower Wit-Mfolozi (NLWM), Mpongoza (NMP) and Vutshini River (NVS) sections (Fig. 4). NUWM and NLWM samples come from the quartzite-dolomite and banded shale zones, respectively (Matthews, 1967). Mozaan pelites are from two localities: the Wit-Mfolozi (MWM) and Piet Retief (MPR) areas. MWM samples include both the quartzite-ironstone and shale-quartzite zones of Matthews (1967). All quartzites are from the Wit-Mfolozi, Piet Retief and Vutshini River areas. Most samples appear fresh in hand specimen; however, some MPR pelites visibly show effects of modern weathering.

Two quartzites from the Dominion-Rhenosterspruit Formation are from diamond-drill core cuttings from the western Witwatersrand basin (Fig. 5). A total of 46 Central Rand and 40 West Rand Group pelite samples were selected for analysis. Most of these samples are from diamond-drill core cuttings donated by various mining companies in the region. General locations are given for these samples in Figure 7. Partial chemical analyses from the Booysens and Roodepoort pelites published by Fuller et al. (1981) are

used to supplement data from this study. Witwatersrand pelites include 23 samples from the K8, 23 samples from the Booysens (BOY), 31 samples from the Roodepoort (RO), 3 samples from the Promise (PRM), 5 samples from the Parktown-Brixton (PBR), and 1 sample from the Orange Grove (OG) Formations (Fig. 8). In addition, eight quartzites from the Orange Grove, Brixton, Government, Marisberg, Elsberg and Ventersdorp Contact Reef units were chemically and mineralogically analyzed.

Four Bothaville pelite samples were analyzed from the dominantly volcanogenic Ventersdorp Supergroup. One additional quartzite sample from the Bothaville Formation has been analyzed, both geochemically and petrographically. Transvaal pelites include 24 samples from the Silverton (SIL), 5 samples from the Strubenkop (STR), 46 samples from the Timeball Hill (TH), 16 samples from the Black Reef (BR), and 7 samples from the Selati (SEL) Formations (Fig. 10). Additionally, three Wolkberg, two Black Reef, and six Pretoria Group quartzites were analyzed. Pelite samples are equally divided between surface and diamond-drill core samples, whereas most quartzites are from surface exposures.

One Waterberg shale and seven arenite samples were selected for analysis. Most samples have been oxidized by modern weathering processes. Four shale and seven arenite samples have also been analyzed from the Soutpansberg Group. All Waterberg and Soutpansberg samples are from surface exposures (Fig. 11).

A.2 Sample Localities

Locations for pelite-shale and quartzite-sandstone (Table A.2) samples analyzed in this study are given in this appendix. Locations are referenced by latitude and longitude (in degrees, minutes and seconds), and by distance and bearing from the nearest urban center. Location maps (Figs. A.2-1 through A.2-7) also are given. Most surface samples are from exposed roadcuts or river beds. Exact locations for some drill-core samples are confidential at the request of donating mining companies. Locations of these samples are presented as approximate distances and general directions from the nearest urban center. Sample locations are stratigraphically ordered from oldest to youngest.

Table A.2-1 Pongola pelite sample locations

Sample	Latitude - Longitude	Map Location	Fig.#
-P 41	27 12'47''S-31 10'00''E	41.3 km N17W of Louwsburg	A.2-5
-P 47	27 22'32''S-31 12'48''E	23.0 km N16W of Louwsburg	A.2-5
-P 49	27 23'16''S-31 14'21''E	21.2 km N12W of Louwsburg	A.2-5
-P 50	27 24'09''S-31 14'37''E	19.6 km N12W of Louwsburg	A.2-5
-P 51	27 25'38''S-31 16'04''E	16.8 km N06W of Louwsburg	A.2-5
-MW 100	D.Hunter samples located N	Pongola River, S Swaziland	A.2-5
-MW 147		''	''
-MW 170		''	''
-MW 253		''	''
-Po 53	28 16'18''S-31 12'49''E	7.3 km N61W of Denny Dalton	A.2-1
-Po 54	'' ''	''	''
-Po 55	'' ''	''	''
-Po 56	'' ''	''	''
-Po 57	'' ''	''	''
-Po 58	'' ''	''	''
-Po 59	'' ''	''	''
-Po 60	'' ''	''	''
-Po 61	'' ''	''	''
-Po 62	'' ''	''	''
-Po 63	'' ''	''	''
-Po 64	'' ''	''	''
-Po 65	'' ''	''	''
-Po 66	'' ''	''	''
-Po 67	28 16'21''S-31 12'30''E	7.6 km N64W of Denny Dalton	A.2-1
-P 28	28 16'18''S-31 12'49''E	7.3 km N61W of Denny Dalton	A.2-1
-P 31	28 16'21''S-31 12'30''E	7.6 km N64W of Denny Dalton	A.2-1
-P 34	28 16'18''S-31 12'49''E	7.3 km N61W of Denny Dalton	A.2-1
-Po 32	28 15'53''S-31 11'07''E	8.2 km N70W of Denny Dalton	A.2-1
-Po 33	'' ''	''	''
-Po 34	'' ''	''	''
-Po 35	'' ''	''	''
-Po 36	28 16'06''S-31 11'18''E	8.2 km N67W of Denny Dalton	A.2-1
-Po 37	'' ''	''	''
-Po 83	28 15'00''S-31 10'38''E	8.2 km N75W of Denny Dalton	A.2-1
-Po 84	'' ''	''	''
-Po 85	'' ''	''	''
-Po 86	'' ''	''	''
-Po 87	'' ''	''	''
-Po 88	'' ''	''	''
-Po 89	'' ''	''	''
-Po 90	'' ''	''	''
-Po 91	'' ''	''	''
-Po 92	'' ''	''	''
-Po 93	'' ''	''	''

Table A.2-1 (Continued)

Sample	Latitude - Longitude	Map Location	Fig.#
-Po 101	27 56'09''S-31 14'44''E	38.3 km S06W of Louwsburg	A.2-5
-Po 102	'' ''	''	''
-Po 103	'' ''	''	''
-Po 104	'' ''	''	''
-Po 105	'' ''	''	''
-Po 106	'' ''	''	''
-Po 107	'' ''	''	''
-P 54	'' ''	''	''
-P 55	'' ''	''	''
-P 56	'' ''	''	''
-P 57	'' ''	''	''
-P 58	'' ''	''	''
-P 59	'' ''	''	''
-P 60	'' ''	''	''
-P 61	'' ''	''	''
-P 62	'' ''	''	''
-P 5	28 35'46''S-31 01'51''E	34.8 km S87W of Melmoth	A.2-1
-P 8	28 36'37''S-31 01'44''E	35.0 km S90W of Melmoth	A.2-1
-P 10	28 36'37''S-31 01'44''E	35.0 km S90W of Melmoth	A.2-1

Table A.2-2 Witwatersrand pelite sample locations

Sample	Latitude - Longitude	Map Location	Fig.#
-MEE 1	Location confidential	4 km east of Westonaria	A.2-3
-MEE 3	''	10 km west of Soweto	A.2-3
-MEE 11	''	4 km east of Westonaria	A.2-3
-MEE 13	''	6 km southeast of Westonaria	A.2-3
-MEE 14	''	4 km east of Westonaria	A.2-3
-MEE 16	''	4 km east of Westonaria	A.2-3
-MEE 19	''	4 km east of Westonaria	A.2-3
-MEE 21	''	4 km east of Westonaria	A.2-3
-MEE 23	''	7 km southeast of Westonaria	A.2-3
-MEE 26	''	8 km northwest of Soweto	A.2-3
-MEE 28	''	6 km northwest of Soweto	A.2-3
-MEE 30	''	10 km south of Westonaria	A.2-3
-MEE 34	''	11 km west of Soweto	A.2-3
-MEE 36	''	11 km west of Soweto	A.2-3
-MEE 39	''	8 km west of Soweto	A.2-3
-MED 1	''	6 km southeast of Westonaria	A.2-3
-MED 2	''	4 km northeast of Westonaria	A.2-3
-MED 3	''	''	A.2-3
-MED 4	''	''	''
-MED 6	''	''	''
-MED 7	''	''	''
-MED 8	''	''	''
-MED 9	''	''	''
-MEE 5	Location confidential	11 km west of Soweto	A.2-3
-MEE 24	''	7 km southeast of Westonaria	A.2-3
-MEE 27	''	6 km northwest of Soweto	A.2-3
-MEE 32	''	10 km south of Westonaria	A.2-3
-MEE 33	''	10 km south of Westonaria	A.2-3
-SJ3-1	26 14'41''S-28 08'57''E	0.8 km S34W of Germiston	A.2-3
-SJ3-2	'' ''	''	A.2-3
-SJ3-3	'' ''	''	''
-SJ3-4	'' ''	''	''
-SJ3-5	'' ''	''	''
-SJ3-6	'' ''	''	''
-SJ3-7	'' ''	''	''
-UR-1140	26 20'14''S-28 31'44''E	10.3 km N36E of Nigel	A.2-3
-439-3	26 30'21''S-29 01'23''E	8.3 km S69W of Evander	A.2-3
-615-7	26 33'49''S-29 08'30''E	10.6 km S18E of Evander	A.2-3
-615-8	'' ''	''	''
-615-9	'' ''	''	''
-730-4	26 25'36''S-29 04'14''E	6.3 km N38W of Evander	A.2-3
-730-5	'' ''	''	''
-730-6	'' ''	''	''
-V56-58	26 15'56''S-28 18'37''E	6.5 km S60W of Brakpan	A.2-3
-GV2-28	28 28'51''S-26 14'14''E	11.7 km S88E of Brakpan	A.2-3
-UC-760	26 20'14''S-28 31'44''E	10.3 km N36E of Nigel	A.2-3

Table A.2-2 (Continued)

Sample	Latitude - Longitude	Map Location	Fig.#
-MED 17	Location confidential	3 km southwest of Westonaria	A.2-3
-MED 18	''	3 km southwest of Westonaria	A.2-3
-C 75	26 30'00''S-28 26'58''E	8.2 km S89E of Heidelberg	A.2-3
-AA0096	26 24'54''S-28 28'39''E	0.3 km N45E of Nigel	A.2-3
-AA0097	'' ''	''	''
-AA0098	'' ''	''	''
-AA0099	'' ''	''	''
-AA0100	'' ''	''	''
-AA0101	'' ''	''	''
-MED 13	Location confidential	9 km west of Carletonville	A.2-3
-MED 14	''	9 km west of Carletonville	''
-MED 15	''	9 km west of Carletonville	''
-MED 10	Location confidential	13 km west of Krugersdorp	A.2-3
-MED 11	''	14 km west of Krugersdorp	''
-MED 12	''	9 km west of Krugersdorp	''
-C 71	26 31'32''S-28 30'02''E	13.4 km S79E of Heidelberg	''
-C 72	26 31'32''S-28 30'02''E	13.4 km S79E of Heidelberg	''
-D 14	26 10'25''S-28 01'55''E	w/in Johannesburg city limits	A.2-3

Table A.2-3 Ventersdorp pelite sample locations

Sample	Latitude - Longitude	Map Location	Fig.#
-JWS8-9	Location confidential	7 km southwest of Orkney	A.2-3
-JWS8-10	''	''	''
-JWS8-11	''	''	''
-JWS8-12	''	''	''

Table A.2-4. Transvaal pelite sample locations.

Sample	Latitude - Longitude	Map Location	Fig.#
-C 58	25 39'00''S-30 15'56''E	5.9 km S81W of Waterval Boven	A.2-5
-C 86	25 47'47''S-27 21'08''E	23.3 km S27E of Rustenburg	A.2-3
-C 87	25 47'47''S-27 21'08''E	23.3 km S27E of Rustenburg	A.2-3
-C 213	24 23'16''S-30 12'40''E	7.1 km S78W of Penge	A.2-6
-D 70	24 29'33''S-30 29'46''E	26.9 km S70W of Pilgrim's Rest	A.2-7
-D 71	25 00'34''S-30 30'00''E	9.7 km N25E of Lydenburg	A.2-7
-D 72	25 00'34''S-30 30'00''E	9.7 km N25E of Lydenburg	A.2-7
-D 73	25 06'50''S-30 26'48''E	0.7 km S24W of Lydenburg	A.2-7
-D 75	25 13'06''S-30 19'23''E	17.2 km S46W of Lydenburg	A.2-5
-D 79	25 42'40''S-30 10'29''E	16.6 km S64W of Waterval Boven	A.2-5
-D 80	25 42'40''S-30 10'29''E	16.6 km S64W of Waterval Boven	A.2-5
-D 81	25 41'23''S-30 12'23''E	12.8 km S67W of Waterval Boven	A.2-5
-D 82	25 41'23''S-30 12'23''E	12.8 km S67W of Waterval Boven	A.2-5
-D 83	25 40'00''S-30 14'09''E	9.7 km S74W of Waterval Boven	A.2-5
-D 84	25 38'55''S-30 14'40''E	7.8 km S88W of Waterval Boven	A.2-5
-D 85	25 38'55''S-30 14'40''E	7.8 km S88W of Waterval Boven	A.2-5
-D 86	25 36'20''S-30 16'55''E	6.2 km N52W of Waterval Boven	A.2-5
-D 87	25 34'34''S-30 17'41''E	7.2 km N32W of Waterval Boven	A.2-5
-D 88	25 32'52''S-30 18'52''E	10.0 km N07W of Waterval Boven	A.2-5
-D 95	25 29'16''S-30 19'20''E	16.1 km N13E of Waterval Boven	A.2-5
-D 97	25 28'51''S-30 21'30''E	16.5 km N09E of Waterval Boven	A.2-5
-D 99	25 37'32''S-30 19'59''E	0.6 km N01W of Waterval Boven	A.2-5
-D 113	25 46'39''S-30 14'13''E	16.9 km S32W of Waterval Boven	A.2-5
-D 114	25 52'47''S-30 12'24''E	28.1 km S26W of Waterval Boven	A.2-5
-CDV1-1	Location confidential	17 km south of Westonaria	A.2-3
-CDV1-2	''	''	''
-CDV1-3	''	''	''
-CDV1-4	''	''	''
-CDV1-5	''	''	''
-C 16	25 08'22''S-30 45'41''E	3.5 km S22W of Sabie	A.2-7
-C 18	25 08'53''S-30 42'10''E	5.1 km S29W of Sabie	A.2-7
-C 19	25 10'56''S-30 44'51''E	10.9 km S39W of Sabie	A.2-7
-C 21	25 10'06''S-30 38'31''E	14.9 km S60W of Sabie	A.2-7
-C 77	26 00'35''S-27 34'07''E	19.2 km N65W of Krugersdorp	A.2-3
-C 78	25 00'35''S-27 34'07''E	19.2 km N65W of Krugersdorp	A.2-3
-C 214	24 23'51''S-30 12'58''E	6.5 km S78W of Penge	A.2-6
-D 23	24 42'47''S-30 35'14''E	5.4 km N29E of Ohrigstad	A.2-7
-D 26	24 40'55''S-30 35'00''E	8.2 km N18E of Ohrigstad	A.2-7
-D 27	24 40'41''S-30 34'55''E	9.5 km N16E of Ohrigstad	A.2-7
-D 29	24 40'32''S-30 34'33''E	9.8 km N15E of Ohrigstad	A.2-7
-D 30	24 40'33''S-30 35'45''E	9.2 km N23E of Ohrigstad	A.2-7
-D 31	24 39'43''S-30 36'31''E	11.3 km N27E of Ohrigstad	A.2-7
-D 32	24 38'03''S-30 37'14''E	19.2 km N26E of Ohrigstad	A.2-7
-D 59	24 53'02''S-30 43'18''E	3.4 km N56W of Pilgrim's Rest	A.2-7
-D 61	24 52'54''S-30 43'02''E	4.0 km N56W of Pilgrim's Rest	A.2-7
-D 63	24 52'52''S-30 42'34''E	4.7 km N58W of Pilgrim's Rest	A.2-7
-D 66	24 53'36''S-30 40'16''E	7.7 km N54W of Pilgrim's Rest	A.2-7
-D 67	24 54'25''S-30 37'38''E	12.0 km N89W of Pilgrim's Rest	A.2-7
-D 106	25 37'13''S-30 29'58''E	15.9 km N84E of Waterval Boven	A.2-5
-D 107	25 36'40''S-30 33'57''E	22.5 km NS2E of Waterval Boven	A.2-5

Table A.2-4. (Continued)

Sample	Latitude - Longitude	Map Location	Fig.#
-MSF1-1	26 33'17''S-27 11'21''E	16.0 km N28E of Potchefstroom	A.2-5
-MSF1-2	'' ''	''	''
-MSF1-3	'' ''	''	''
-MSF1-4	'' ''	''	''
-MSF2-1	26 31'35''S-27 12'15''E	18.7 km N28E of Potchefstroom	A.2-3
-MSF2-2	'' ''	''	''
-MSF2-3	'' ''	''	''
-MSF2-5	'' ''	''	''
-MSF2-7	'' ''	''	''
-MSF2-8	'' ''	''	''
-MSF2-9	'' ''	''	''
-WBK1-1	Location confidential	15 km south of Westonaria	A.2-3
-WBK1-2	''	''	''
-WBK1-3	''	''	''
-WBK1-4	''	''	''
-WBK1-5	''	''	''
-CDV1-14	Location confidential	17 km south of Westonaria	A.2-3
-CDV1-16	''	''	''
-CDV1-17	''	''	''
-CDV1-19	''	''	''
-CDV1-21	''	''	''
-CDV1-22	''	''	''
-CDV1-24	''	''	''
-CDV1-25	''	''	''
-CDV1-27	''	''	''
-CDV1-28	26 29'30''S-27 38'09''E	16.6 km S01W of Westonaria	A.2-3
-MEE 4	Location confidential	10 km west of Soweto	A.2-3
-MEE 6	''	11 km west of Soweto	A.2-3
-MEE 8	''	11 km west of Soweto	A.2-3
-MEE 9	''	10 km west of Soweto	A.2-3
-MEE 17	''	4 km east of Westonaria	A.2-3
-MEE 18	''	4 km east of Westonaria	A.2-3
-MEE 20	''	4 km east of Westonaria	A.2-3
-MEE 22	''	7 km southeast of Westonaria	A.2-3
-MEE 25	''	8 km northwest of Soweto	A.2-3
-MEE 29	''	6 km northwest of Soweto	A.2-3
-MEE 31	''	10 km south of Westonaria	A.2-3
-MEE 35	''	11 km west of Soweto	A.2-3
-MEE 37	''	11 km west of Soweto	A.2-3
-MEE 38	''	8 km west of Soweto	A.2-3
-MEE 40	''	11 km west of Soweto	A.2-3
-C 196	24 12'50''S-29 28'38''E	32.9 km S03E of Pietersburg	A.2-6
-C 197	24 12'50''S-29 28'38''E	32.9 km S03E of Pietersburg	A.2-6
-C 198	24 12'50''S-29 28'38''E	32.9 km S03E of Pietersburg	A.2-6
-D 50	24 27'11''S-30 36'34''E	33.5 km S79E of Penge	A.2-6
-D 53	25 00'35''S-30 49'35''E	12.2 km N16E of Sabie	A.2-7
-D 56	24 57'33''S-30 50'29''E	3.2 km S24E of Graskop	A.2-7
-D 111	25 32'52''S-30 41'02''E	28.5 km S77W of Nelspruit	A.2-5

Table A.2-5. Waterberg and Soutpansberg shale sample locations.

Sample	Latitude - Longitude	Map Location	Fig.#
-C 90	24 33'27''S-28 18'40''E	19.1 km N31W of Nylstroom	A.2-6
-C 130	22 58'53''S-30 09'51''E	27.4 km N74E of Louis Trichardt	A.2-6
-C 168	22 53'12''S-29 49'14''E	19.1 km N25W of Louis Trichardt	A.2-6
-C 169	22 53'12''S-29 49'14''E	19.1 km N25W of Louis Trichardt	A.2-6
-C 181	22 30'01''S-30 52'12''E	67.4 km N40E of Sibasa	A.2-6

Appendex A.2-6 Kaapvaal craton quartzite sample locations.

Sample	Latitude - Longitude	Map Location	Fig.#
-P 4	28 33'37''S-30 58'57''E	39.9 km S83W of Melmoth	A.2-1
-P 7	28 36'37''S-31 01'44''E	35.0 km S90W of Melmoth	A.2-1
-P 12	28 16'06''S-31 11'18''E	8.2 km N67W of Denny Dalton	A.2-1
-P 26	28 16'06''S-31 11'18''E	8.2 km N67W of Denny Dalton	A.2-1
-P 33	28 16'18''S-31 12'49''E	7.3 km N61W of Denny Dalton	A.2-1
-P 40	27 11'50''S-31 08'05''E	41.9 km N21W of Louwsburg	A.2-3
-P 45	27 14'25''S-31 13'39''E	36.8 km N09W of Louwsburg	A.2-3
-P 63	27 22'53''S-31 33'26''E	5.2 km S89W of Pongola	A.2-5
-BBS3-19	26 43'37''S-26 36'01''E	11.9 km N22W of Klerksdorp	A.2-3
-BSF1-18	26 43'57''S-26 34'40''E	12.3 km N30W of Klerksdorp	A.2-3
-C 67	26 29'45''S-28 33'09''E	10.4 km S46E of Nigel	A.2-3
-C 70	26 31'32''S-28 30'02''E	13.4 km S79E of Heidelberg	A.2-3
-C 73	26 27'26''S-28 32'14''E	6.4 km S58E of Nigel	A.2-3
-C 74	26 30'00''S-28 26'58''E	8.2 km S89E of Heidelberg	A.2-3
-D 8	26 14'35''S-28 02'58''E	w/in Johannesburg city limits	A.2-3
-D 15	26 11'39''S-28 04'44''E	w/in Johannesburg city limits	A.2-3
-D 21	26 11'30''S-28 05'60''E	w/in Johannesburg city limits	A.2-3
-JWS8-40	Location confidential	7 km southwest of Orkney	
-C 6	26 46'25''S-26 20'44''E	7.3 km S81W of Hartbeesfontein	A.2-2
-C 56	25 24'08''S-30 01'49''E	6.8 km N83W of Dullstrom	A.2-4
-C 76	26 01'38''S-27 35'55''E	15.2 km N66W of Krugersdorp	A.2-3
-C 81	25 57'34''S-27 31'45''E	3.7 km N17W of Magaliesburg	A.2-3
-C 201	24 13'39''S-29 29'25''E	34.2 km S05E of Pietersburg	A.2-6
-C 207	24 21'32''S-30 05'40''E	18.7 km N82W of Penge	A.2-6
-D 34	24 27'38''S-30 36'29''E	33.3 km S75E of Penge	A.2-6
-D 35	24 26'57''S-30 36'38''E	32.8 km S77E of Penge	A.2-6
-D 36	24 26'27''S-30 37'19''E	34.1 km S79E of Penge	A.2-6
-D 47	24 26'27''S-30 37'19''E	34.1 km S79E of Penge	A.2-6
-D 53	24 36'19''S-30 48'05''E	32.8 km N09E of Pilgrim's Rest	A.3-7
-D 77	25 15'00''S-30 15'41''E	24.8 km S50W of Lydenburg	A.3-5
-MSF2-10	26 31'35''S-27 12'15''E	18.7 km N28E of Potchefstroom	A.3-3
-C 89	24 39'44''S-28 22'16''E	4.0 km N45W of Nylstroom	A.2-6
-C 94	24 31'06''S-28 15'39''E	24.4 km N37W of Nylstroom	A.2-6
-C 96	24 27'02''S-28 09'27''E	37.2 km N43W of Nylstroom	A.2-6
-C 97	24 25'10''S-28 07'55''E	41.5 km N43W of Nylstroom	A.2-6
-C 98	24 23'02''S-28 08'04''E	44.0 km N38W of Nylstroom	A.2-6
-C 99	24 18'10''S-28 06'53''E	52.8 km N35W of Nylstroom	A.2-6
-C 100	24 12'15''S-28 07'16''E	61.7 km N28W of Nylstroom	A.2-6
-C 124	23 01'34''S-29 45'23''E	13.2 km N86W of Louis Trichardt	A.2-6
-C 128	22 59'16''S-30 02'04''E	14.5 km N64E of Louis Trichardt	A.2-6
-C 131	22 57'25''S-30 11'38''E	30.9 km N72E of Louis Trichardt	A.2-6
-C 160	22 55'11''S-29 45'39''E	12.3 km N11E of Louis Trichardt	A.2-6
-C 177	22 29'27''S-30 52'26''E	65.5 km N37E of Sibasa	A.2-6
-C 184	22 30'29''S-30 52'08''E	63.6 km N38E of Sibasa	A.2-6
-C 188	22 32'46''S-30 52'26''E	60.7 km N42E of Sibasa	A.2-6

Figure A.2-1. Location map for Pongola samples collected in Zululand and Natal Provinces. Urban centers referred to in sample Appendix Table A.2 are indicated.

Figure A.2-2. Location map for southwestern Transvaal and northern Orange Free State Provinces. Urban centers referred to in sample Appendix Table A.2 are indicated. Map scale same as in Figure A.2-1.

Figure A.2-3. Location map for southern Transvaal and northern Orange Free State Provinces. Urban centers referred to in sample Appendix Table A.2 are indicated. Map scale same as in Figure A.2-1.

Figure A.2-4. Location map for southern Transvaal and northern Orange Free State Provinces. Urban centers referred to in sample Appendix Table A.2 are indicated. Map scale same as in Figure A.2-1.

Figure A.2-5. Location map for the Kingdom of Swaziland and southeast Transvaal Province. Urban centers referred to in sample Appendix Table A.2 are indicated. Map scale same as in Figure A.2-1.

Figure A.2-6. Location map for northern Transvaal Province. Urban centers referred to in sample Appendix Table A.2 are indicated. Map scale same as in Figure A.2-1.

Figure A.2-7. Location map for eastern Transvaal Province. Urban centers referred to in sample Appendix Table A.2 are indicated. Map scale same as in Figure A.2-1.

Figure A.2-1

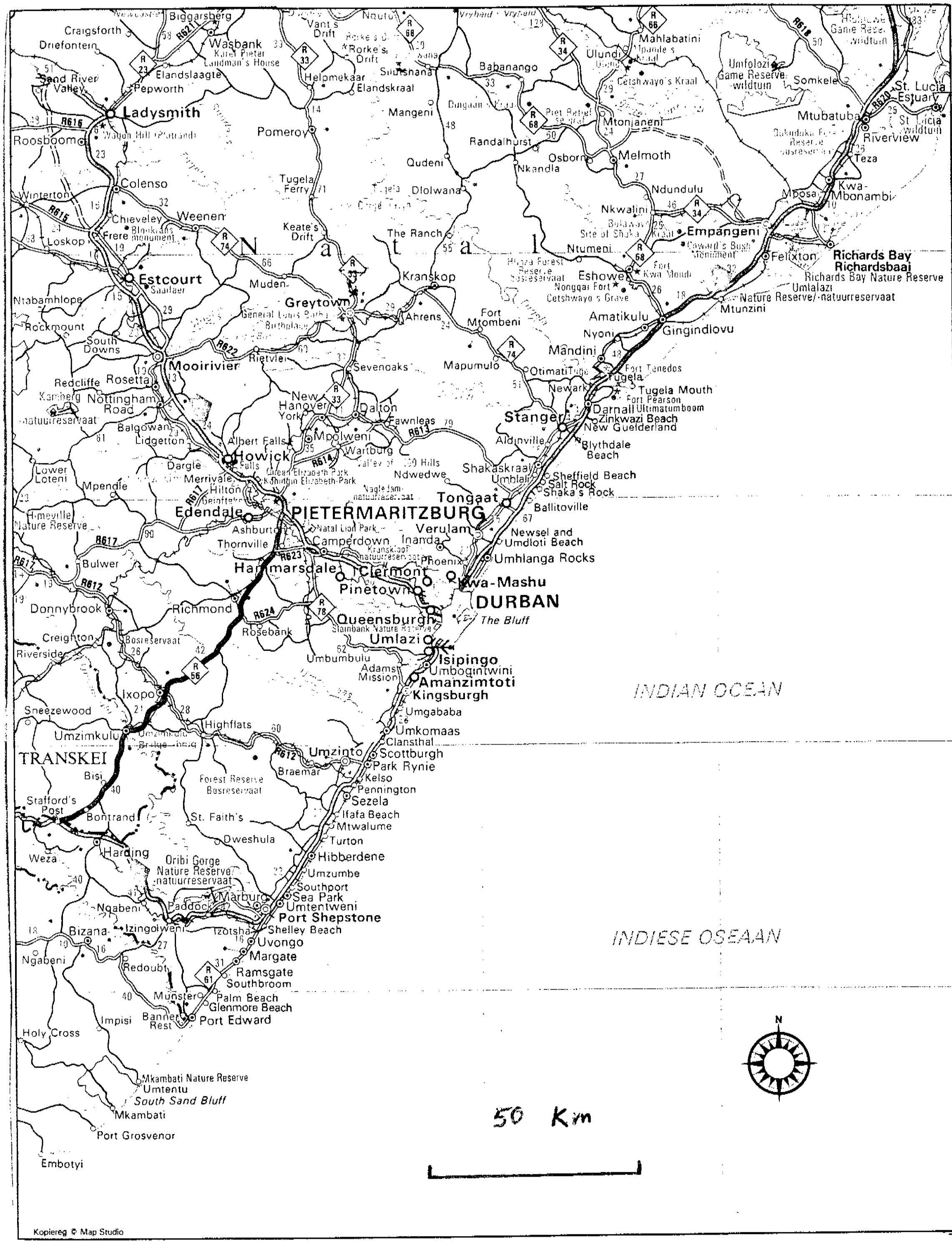

Natal
Ladysmith
Estcourt
Mooirivier
Howick
PIETERMARITZBURG
DURBAN
Greytown
Kranskop
Stanger
Tongaat
Verulam
Umhlanga Rocks
Kwa-Mashu
Pinetown
Queensburgh
Umlazi
Isipingo
Amanzimtoti
Kingsburgh
Umkomaas
Scottburgh
Park Rynie
Hibberdene
Port Shepstone
Margate
Ramsgate
Port Edward
Ixopo
Richmond
Harding
Umzinto
Empangeni
Richards Bay
Richardsbaai
Eshowe
Melmoth
Ulundi
Gingindlovu
Mtunzini
St. Lucia Estuary
Mtubatuba
Riverview
TRANSKEI
Bizana
Mkambati
Port Grosvenor
Embotyi
INDIAN OCEAN
INDIESE OSEAAN
50 Km
N
Kopiereg © Map Studio

Figure A.2-2

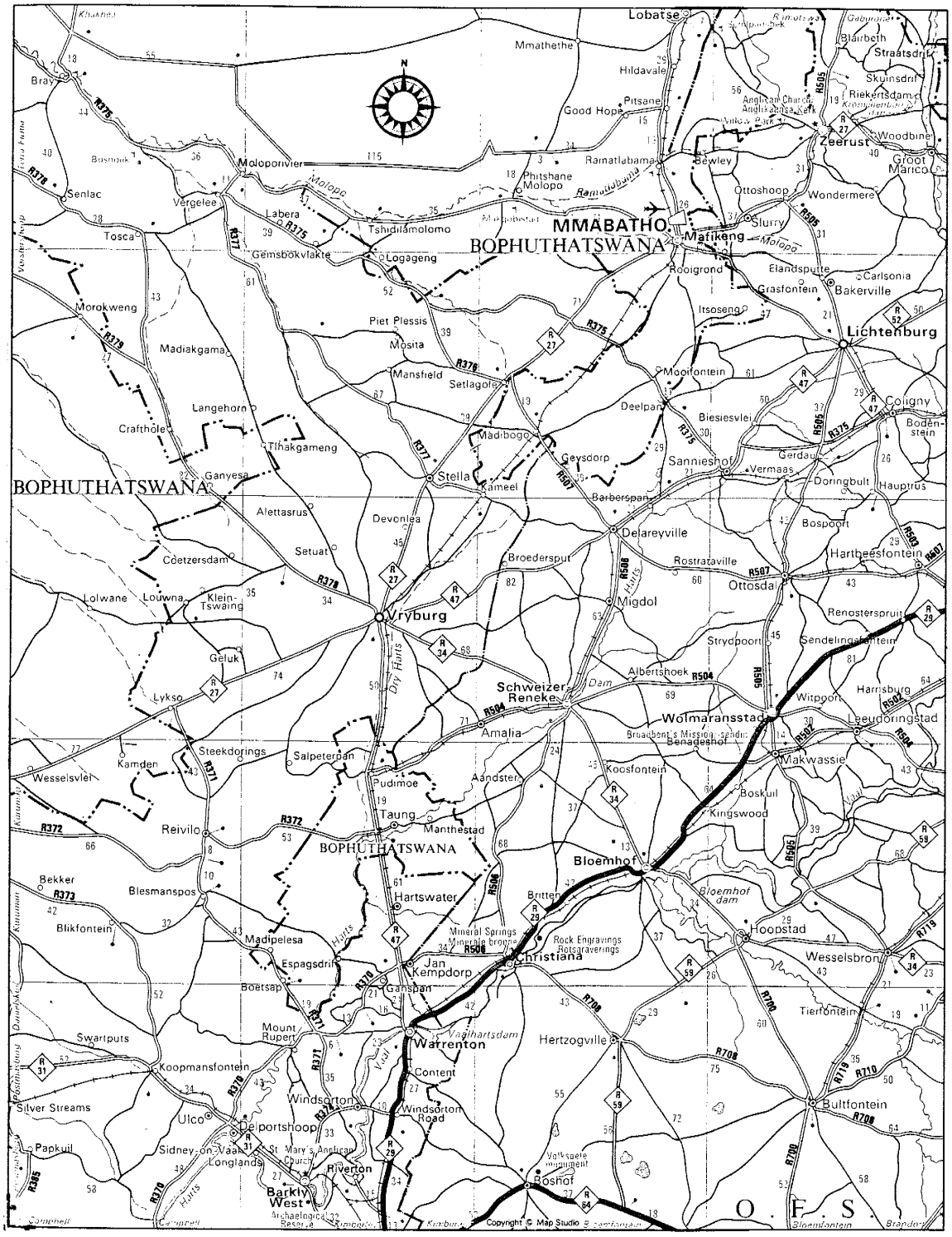
Lobatse
Mmathethe
Hildavale
Pitsane
Good Hope
Bray
Moloporivier
Molopo
Phitshane Molopo
Ramatlabama
Bewley
Zeerust
Woodbine
Groot Marico
Senlac
Vergelee
Labera
Tshidilamolomo
MMABATHO
BOPHUTHATSWANA
Mafikeng
Slurry
Ottoshoop
Wondermere
Tosca
Gemsbokvlakte
Logageng
Rooigrond
Elandsputte
Carlsonia
Grasfontein
Bakerville
Morokweng
Piet Plessis
Mosita
Itsoseng
Lichtenburg
Madiakgama
Mansfield
Setlagole
Mooifontein
Langehorn
Craftholle
Tlhakgameng
Madibogo
Deelpan
Biesiesvlei
Coligny
Geysdorp
Sannieshof
Gerdau
Vermaas
Ganyesa
Stella
Kameel
Doringbult
Hauptrus
Alettasrus
Devonlea
Barberspan
Delareyville
Bospoort
Setuat
Broedersput
Rostrataville
Hartbeesfontein
Coetzersdam
Ottosdal
Lolwane
Louwna
Klein-Tswaing
Migdol
Renostersput
Vryburg
Strydpoort
Sendelingsfontein
Geluk
Albertshoek
Schweizer-Reneke
Witpoort
Harrisburg
Lykso
Amalia
Wolmaransstad
Leeudoringstad
Steekdorings
Salpeterpan
Broadbent's Mission
Benadeshof
Makwassie
Kamden
Wesselsvlei
Pudimoe
Aandster
Koosfontein
Taung
Manthestad
Boskuil
Kingswood
Reivilo
BOPHUTHATSWANA
Bloemhof
Bekker
Hartswater
Britten
Bloemhof dam
Blesmanspos
Hoopstad
Blikfontein
Madipelesa
Mineral Springs
Rock Engravings
Christiana
Wesselsbron
Espagsdrift
Jan Kempdorp
Boetsap
Ganspan
Tierfontein
Mount Rupert
Vaalhartsdam
Hertzogville
Swartputs
Warrenton
Koopmansfontein
Content
Silver Streams
Windsorton
Bultfontein
Ulco
Delportshoop
Windsorton Road
Papkuil
Sidney-on-Vaal
St Mary's Anglican Church
Longlands
Riverton
Valksgele monument
Barkly West
Boshof
O. F. S
Copyright © Map Studio

Figure A.2-3

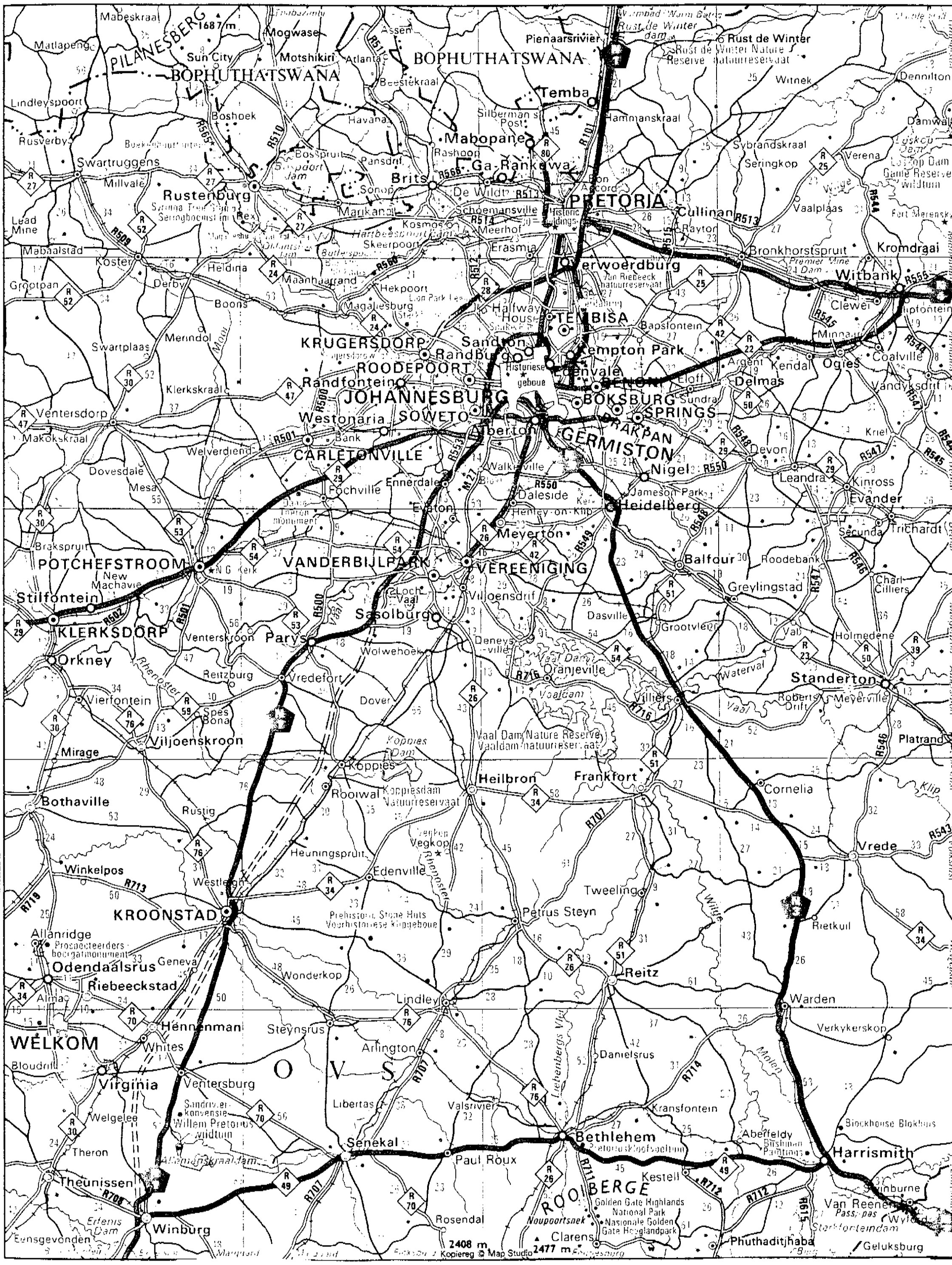
PILANESBERG
BOPHUTHATSWANA
Mabeskraal
Matlapeng
Sun City
Mogwase
Motshikiri
Atlanta
Assen
Pienaarsrivier
Rust de Winter
Witnek
Dennilton
Lindleyspoort
Rusverby
Boshoek
Havana
Temba
Hammanskraal
Mabopane
Ga-Rankuwa
Swartruggens
Millvale
Rustenburg
Brits
Sonop
Bosspruit
Pansdrif
Rashoop
De Wildt
Sybrandskraal
Seringkop
Verena
PRETORIA
Cullinan
Rayton
Vaalplaas
Lead Mine
Mabaalstad
Koster
Derby
Heldina
Maanhaarrand
Hekpoort
Skeerpoort
Kosmos
Meerhof
Marikana
Erasmia
Verwoerdburg
Bronkhorstspruit
Kromdraai
Witbank
Clewer
Grootpan
Boons
Magaliesburg
Halfway House
TEMBISA
Bapsfontein
Swartplaas
Merindol
KRUGERSDORP
Randburg
Sandton
Kempton Park
Minnaar
Coalville
Ogies
Kendal
ROODEPOORT
Randfontein
JOHANNESBURG
Edenvale
BENONI
Argent
Delmas
Eloff
Vandyksdrif
Klerkskraal
Westonaria
SOWETO
BOKSBURG
SPRINGS
BRAKPAN
Ventersdorp
Makokskraal
Bank
Alberton
GERMISTON
Kriel
Welverdiend
CARLETONVILLE
Walkerville
Nigel
Devon
Leandra
Kinross
Dovesdale
Mesa
Fochville
Ennerdale
Daleside
Jameson Park
Heidelberg
Evander
Secunda
Trichardt
Evaton
Henley-on-Klip
Meyerton
Brakspruit
POTCHEFSTROOM
VANDERBIJLPARK
VEREENIGING
Balfour
Roodebank
Charl Cilliers
Greylingstad
Stilfontein
KLERKSDORP
Viljoensdrif
Sasolburg
Dasville
Grootvlei
Holmedene
Orkney
Venterskroon
Parys
Wolwehoek
Deneysville
Vaal Dam
Oranjeville
Waterval
Standerton
Meyerville
Reitzburg
Vredefort
Dover
Villiers
Vierfontein
Spes Bona
Viljoenskroon
Vaal Dam Nature Reserve
Platrand
Mirage
Koppies
Heilbron
Frankfort
Cornelia
Bothaville
Rooiwal
Rustig
Vrede
Winkelpos
Heuningspruit
Edenville
Vegkop
Tweeling
Westleigh
KROONSTAD
Petrus Steyn
Rietkuil
Allanridge
Odendaalsrus
Riebeeckstad
Geneva
Wonderkop
Reitz
Warden
Hennenman
Whites
Steynsrus
Lindley
Arlington
Verkykerskop
WELKOM
Bloudrif
Virginia
Ventersburg
O V S
Danielsrus
Kransfontein
Welgelee
Theron
Libertas
Valsrivier
Bethlehem
Aberfeldy
Harrismith
Senekal
Paul Roux
Theunissen
ROOIBERGE
Kestell
Swinburne
Van Reenen
Winburg
Rosendal
Golden Gate Highlands National Park
Clarens
Phuthaditjhaba
Eensgevonden
Geluksburg
2408 m
2477 m
Kopiereg © Map Studio

Figure A.2-4

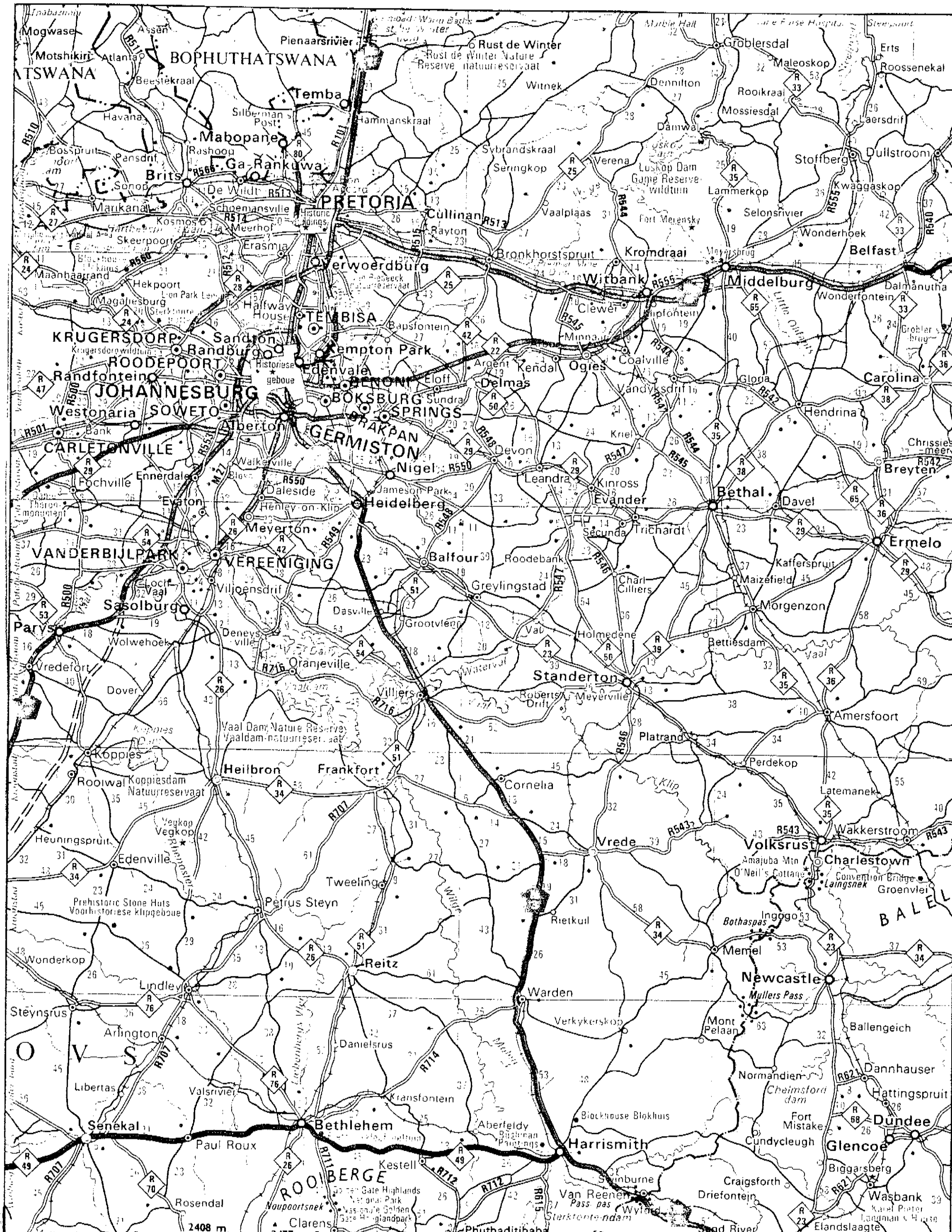
Mogwase
Motshikiri
BOPHUTHATSWANA
Pienaarsrivier
Rust de Winter
Groblersdal
Erts
Roossenekal
Temba
Mabopane
Ga-Rankuwa
Brits
PRETORIA
Cullinan
Witnek
Dennilton
Maleoskop
Rooikraal
Mossiesdal
Laersdrif
Stoffberg
Dullstroom
Kwaggaskop
Verena
Loskop Dam
Game Reserve
Lammerkop
Selonsrivier
Wonderhoek
Belfast
Marikana
Skeerpoort
Erasmia
Verwoerdburg
Bronkhorstspruit
Kromdraai
Witbank
Middelburg
Dalmanutha
Hekpoort
Magaliesburg
KRUGERSDORP
Randburg
Sandton
TEMBISA
Kempton Park
Edenvale
BENONI
ROODEPOORT
Randfontein
JOHANNESBURG
SOWETO
Westonaria
BOKSBURG
SPRINGS
GERMISTON
Alberton
Delmas
Kendal
Ogies
Coalville
Clewer
Vandyksdrif
Carolina
Hendrina
Chrissiesmeer
Breyten
CARLETONVILLE
Fochville
Ennerdale
Walkerville
Nigel
Devon
Leandra
Kinross
Evander
Trichardt
Secunda
Bethal
Davel
Ermelo
Evaton
Heidelberg
Meyerton
Daleside
Henley-on-Klip
VANDERBIJLPARK
VEREENIGING
Balfour
Roodebank
Greylingstad
Charl Cilliers
Kaffirspruit
Maizefield
Morgenzon
Sasolburg
Parys
Viljoensdrif
Deneysville
Dasville
Grootvlei
Holmedene
Bettiesdam
Vredefort
Wolwehoek
Oranjeville
Standerton
Meyerville
Amersfoort
Dover
Villiers
Vaal Dam Nature Reserve
Vaaldam-natuurreservaat
Platrand
Perdekop
Koppies
Heilbron
Frankfort
Cornelia
Latemanek
Rooiwal
Koppiesdam Natuurreservaat
Vrede
Volksrust
Wakkerstroom
Charlestown
Heuningspruit
Vegkop
Edenville
Tweeling
Laingsnek
Groenvlei
Prehistoric Stone Huts
Voorhistoriese klipgeboue
Petrus Steyn
Rietkuil
Ingogo
Bothaspas
Memel
Wonderkop
Reitz
Newcastle
Lindley
Warden
Mullers Pass
Steynsrus
Arlington
Verkykerskop
Mont Pelaan
Ballengeich
O V S
Danielsrus
Normandien
Dannhauser
Libertas
Valsrivier
Kransfontein
Chelmsford dam
Hattingspruit
Fort Mistake
Dundee
Senekal
Bethlehem
Aberfeldy
Harrismith
Cundycleugh
Glencoe
Paul Roux
Kestell
Biggarsberg
ROOIBERGE
Swinburne
Craigsforth
Wasbank
Rosendal
Golden Gate Highlands National Park
Van Reenen
Driefontein
Elandslaagte
Clarens
Phuthaditjhaba
Geluksburg
Sand River Valley
Pepworth
2408 m
2477 m
Copyright © Map Studio

Figure A.2-5

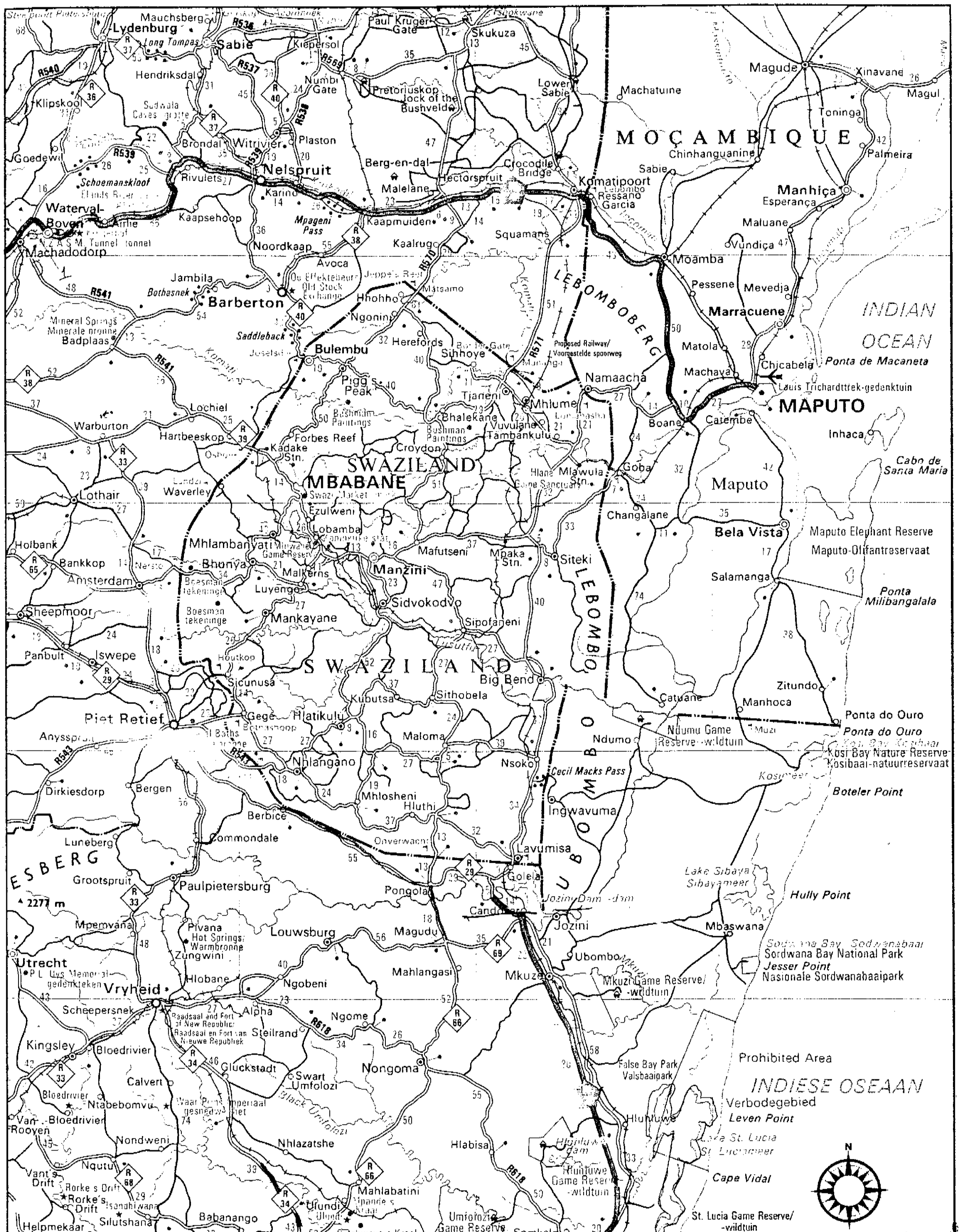
Lydenburg
Mauchsberg
Sabie
Paul Kruger Gate
Skukuza
Hendriksdal
Kiepersol
Numbi Gate
Pretoriuskop
Jock of the Bushveld
Lower Sabie
Machatuine
Magude
Xinavane
Magul
Toninga
Klipskool
Plaston
Witrivier
Brondal
MOÇAMBIQUE
Chinhanguanine
Palmeira
Goedewil
Nelspruit
Berg-en-dal
Hectorspruit
Crocodile Bridge
Komatipoort
Ressano Garcia
Sabie
Manhiça
Esperança
Schoemanskloof
Rivulets
Karino
Malelane
Kaapmuiden
Waterval-Boven
Kaapsehoop
Mpageni Pass
Noordkaap
Kaalrug
Squamans
Maluane
Vundiça
Machadodorp
Avoca
Moamba
LEBOMBOBERG
Jambila
Bothasnek
Barberton
Hhohho
Matsamo
Pessene
Mevedja
Marracuene
INDIAN OCEAN
Ngonini
Mineral Springs
Badplaas
Saddleback
Bulembu
Herefords
Sihhoye
Matola
Machava
Chicabela
Ponta de Macaneta
Proposed Railway/ Voorgestelde spoorweg
Namaacha
Luis Trichardttrek-gedenktuin
MAPUTO
Piggs Peak
Tjaneni
Mhlume
Lochiel
Warburton
Bhalekane
Vuvulane
Tambankulu
Boane
Catembe
Inhaca
Hartbeeskop
Forbes Reef
Kadake Stn.
Croydon
SWAZILAND
MBABANE
Hlane
Mlawula Stn.
Goba
Cabo de Santa Maria
Lothair
Waverley
Maputo
Ezulweni
Lobamba
Changalane
Bela Vista
Maputo Elephant Reserve
Maputo-Olifantreservaat
Holbank
Bankkop
Amsterdam
Mhlambanyati
Bhunya
Malkerns
Mafutseni
Mpaka Stn.
Manzini
Siteki
LEBOMBO
Salamanga
Ponta Milibangalala
Luyengo
Sidvokodvo
Sheepmoor
Mankayane
Sipofaneni
Panbult
Iswepe
Houtkop
Sicunusa
SWAZILAND
Big Bend
Catuane
Zitundo
Manhoca
Ponta do Ouro
Piet Retief
Anyspruit
Gege
Hlatikulu
Kubutsa
Sithobela
Maloma
Ndumo
Ndumu Game Reserve-wildtuin
Kosi Bay Nature Reserve
Kosibaai-natuurreservaat
Nhlangano
Nsoko
Cecil Macks Pass
Dirkiesdorp
Bergen
Mhlosheni
Hluthi
Ingwavuma
Boteler Point
Berbice
Commondale
Luneberg
Lavumisa
UBOMBO
Golela
Lake Sibaya
Sibayameer
Grootspruit
Paulpietersburg
Pongola
Candover
Jozini Dam
Hully Point
2277 m
Mpemvana
Pivana Hot Springs Warmbronne
Louwsburg
Magudu
Jozini
Mbaswana
Zungwini
Utrecht
Vryheid
Hlobane
Ngobeni
Mahlangasi
Mkuzi
Ubombo
Sordwana Bay National Park
Jesser Point
Nasionale Sordwanabaaipark
Mkuzi Game Reserve/ -wildtuin
Scheepersnek
Alpha
Ngome
Steilrand
Kingsley
Bloedrivier
Calvert
Gluckstadt
Swart Umfolozi
Nongoma
False Bay Park
Valsbaaipark
Prohibited Area
INDIESE OSEAAN
Verbodegebied
Leven Point
Ntabebomvu
Van Rooyen
Nondweni
Nhlazatshe
Hlabisa
Hluhluwe
Nqutu
Vant's Drift
Rorke's Drift
Mahlabatini
Ulundi
Cape Vidal
Babanango
Silutshana
Helpmekaar
Elandskraal
Umfolozi Game Reserve -wildtuin
Somkele
St. Lucia Game Reserve/ -wildtuin
Kopiereg © Map Studio

Figure A.2-6

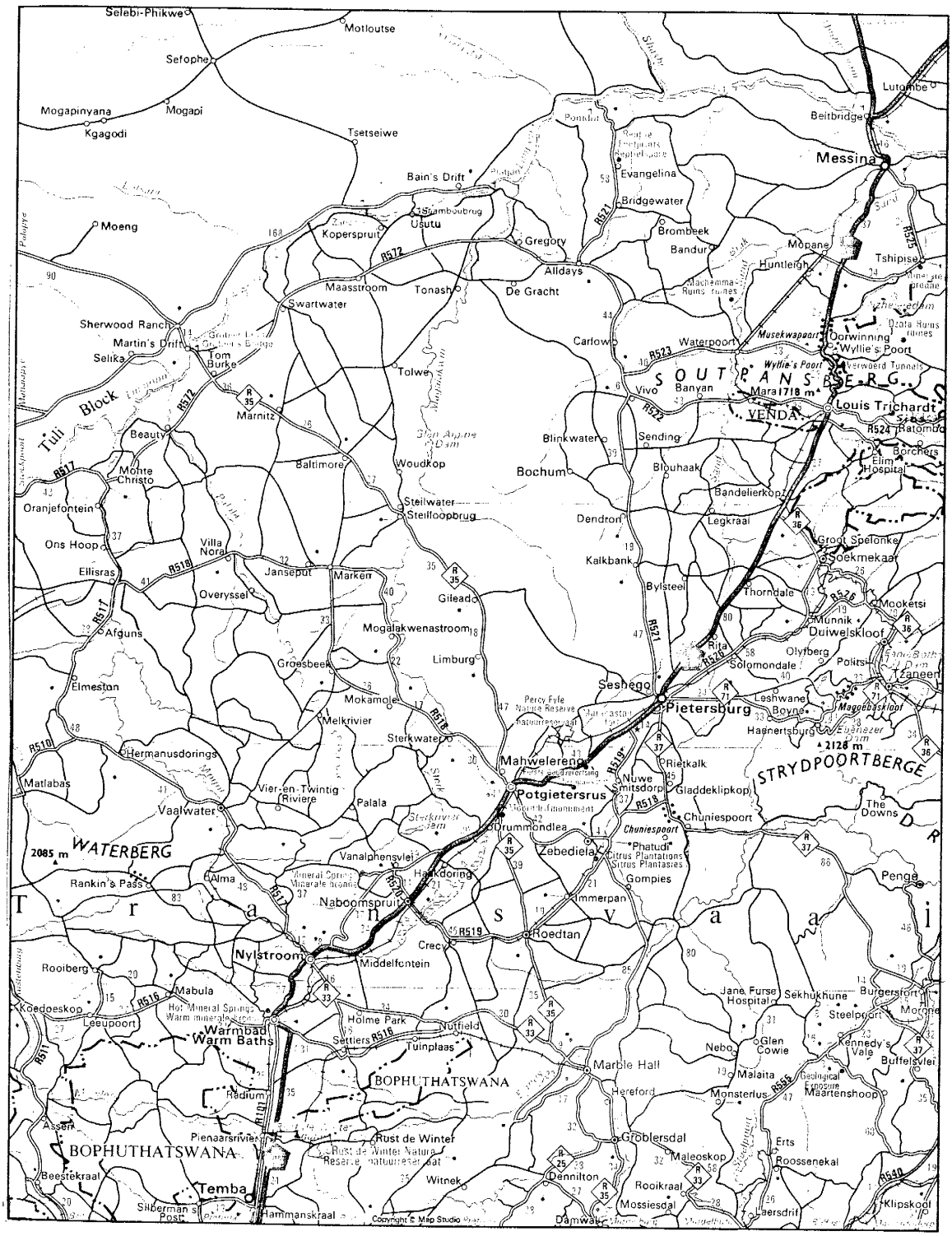
Selebi-Phikwe
Motloutse
Sefophe
Mogapinyana
Mogapi
Kgagodi
Tsetseiwe
Bain's Drift
Moeng
Koperspruit
Ususu
Gregory
Evangelina
Bridgewater
Brombeek
Bandur
Messina
Beitbridge
Lutombe
Mopane
Huntleigh
Tshipise
Alldays
De Gracht
Tonash
Maasstroom
Swartwater
Sherwood Ranch
Martin's Drift
Selika
Tom Burke
Marnitz
Tolwe
Carlow
Waterpoort
Musekwapoort
Ooorwinning
Wyllie's Poort
Vivo
Banyan
Mara 1718 m
SOUTPANSBERG
VENDA
Louis Trichardt
Blinkwater
Sending
Bochum
Woudkop
Baltimore
Blouhaak
Bandelierkop
Legkraal
Groot Spelonke
Soekmekaar
Elim Hospital
Tuli Block
Beauty
Monte Christo
Oranjefontein
Ons Hoop
Villa Nora
Ellisras
Overyssel
Janseput
Marken
Steilwater
Steilloopbrug
Dendron
Kalkbank
Bysteel
Thorndale
Munnik
Duiwelskloof
Mooketsi
Gileado
Mogalakwenastroom
Limburg
Afguns
Groesbeek
Olifberg
Solomondale
Polfontein
Zaneen
Elmeston
Mokamole
Melkrivier
Sterkwater
Seshego
Pietersburg
Leshwane
Boyne
Moggebaskloof
Hagnertsburg
Ebenezer Dam
2128 m
Hermanusdorings
Matlabas
Vaalwater
Vier-en-Twintig Riviere
Palala
Mahwelereng
Potgietersrus
Nuwe Smitsdorp
Rietkalk
Gladdeklipkop
Chuniespoort
The Downs
STRYDPOORTBERGE
Drummondlea
Zebediela
Phatudi
Citrus Plantations
Citrus Plantasies
Gompies
2085 m
WATERBERG
Rankin's Pass
Vanalphensvlei
Alma
Hakkdoring
Naboomspruit
Immerpan
Penge
Roedtan
Nylstroom
Crecy
Middelfontein
Rooiberg
Mabula
Koedoeskop
Leeupoort
Hot Mineral Springs
Warm mineral water
Warmbad
Warm Baths
Hölme Park
Settlers
Nutfield
Tuinplaas
Marble Hall
Jane Furse Hospital
Sekhukhune
Burgersfort
Steelpoort
Morone
Nebo
Glen Cowie
Kennedy's Vale
Buffelsvlei
Malaita
Geological Exposure
Monsterlus
Maartenshoop
Hereford
BOPHUTHATSWANA
Radium
Assen
Pienaarsrivier
Rust de Winter
Rust de Winter Nature Reserve
Beestekraal
Temba
Silberman's Post
Hammanskraal
Witnek
Gröblersdal
Maleoskop
Roossenekal
Erts
Dennilton
Rooikraal
Mossiesdal
Laersdrif
Klipskool
Damwal
Copyright © Map Studio

Figure A.2-7

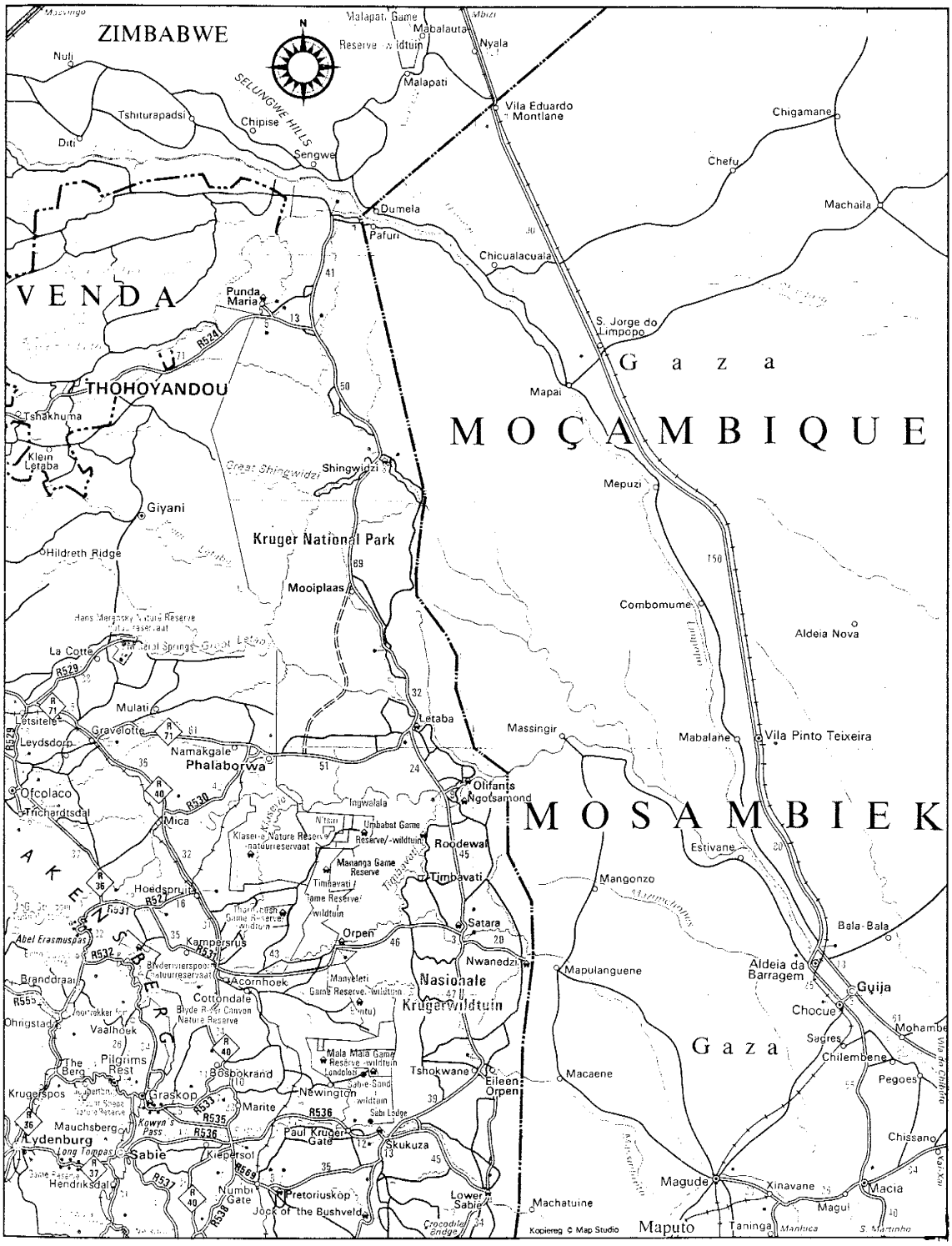
ZIMBABWE
VENDA
THOHOYANDOU
MOÇAMBIQUE
Gaza
MOSAMBIEK
Gaza
Kruger National Park
Krugerwildtuin
Nasionale
Malapati
Vila Eduardo Montlane
Nyala
Chigamane
Chefu
Machaila
Dumela
Pafuri
Chicualacuala
Punda Maria
S. Jorge do Limpopo
Mapai
Tshakhuma
Shingwidzi
Mepuzi
Giyani
Hildreth Ridge
Mooiplaas
Combomune
Aldeia Nova
Letaba
Massingir
Mabalane
Vila Pinto Teixeira
Mulati
Gravelotte
Namakgale
Phalaborwa
Olifants
Ngotsamond
Ofcolaco
Trichardtsdal
Mica
Roodewal
Timbavati
Mangonzo
Estivane
Hoedspruit
Orpen
Satara
Kampersrus
Nwanedzi
Mapulanguene
Aldeia da Barragem
Bala-Bala
Gwija
Chocue
Acornhoek
Cottondale
Brandraai
Ohrigstad
Vaalhoek
Sagres
Chilembene
Mohambe
Pegoes
The Berg
Pilgrims Rest
Bosbokrand
Tshokwane
Eileen Orpen
Macaene
Graskop
Newington
Marite
Sabi Lodge
Paul Kruger Gate
Skukuza
Mauchsberg
Sabie
Kiepersol
Hendriksdal
Numbi Gate
Pretoriuskop
Jock of the Bushveld
Lower Sabie
Machatuine
Magude
Xinavane
Macia
Magul
Maputo
Taninga
Chissano
Kopiereg © Map Studio

APPENDIX B. Analytical Methods

B.1 Initial Sample Processing

Surface samples collected are hand-trimmed in the field to remove weathering rinds, whereas weathered fractures, if present, are handpicked and discarded during preliminary crushing stages. Samples are pulverized (-200 mesh; <0.004 mm) in porcelain grinding disks. This grinding technique is preferred to eliminate possibilities of trace element contamination from steel or tungsten carbide grinding equipment. A sufficient quantity of each sample ($\sim$0.5 kg) is processed to insure against effects of rock heterogeneities, to provide specimens for petrologic and collaborative stable and radiogenic isotopic investigations, and to accumulate a sample library for future research.

B.2 X-Ray Fluorescence (XRF)

a) Sample Preparation and Analytical Technique

Major element concentrations are determined by X-ray fluorescence (XRF) on fused glass disks using an automated Rigaku 3064 XRF spectrometer, following the methods of Norrish and Chappel (1977). Element abundances are determined using a linear regression line normalized to a variety of standards (Table B.2-1). Data reduction is performed using an on-line DEC computer. Fused disks are prepared by mixing a 0.5 g split of pulverized sample with 2.68 g of lanthanum oxide (spectroflux 105) and a few grains of ammonium nitrate, and then fusing the mixture in a platinum crucible at ~1000 °C. Loss on ignition (H2O-) is determined by measuring the weight loss of powdered samples heated between 110 and 1110 °C. Zr, Y, Sr, Rb, V, Nb, Ni and Pb are determined by the XRF technique using (~ 8 g) pressed powder pellets mixed with a polyvinyl alcohol binder, and pressed to a pressure of 20 tons per square inch.

b) Detection Limits

A list of excited electron shells, measured energies, detection limits and lower limits of determination are presented in this section in tabular form (Table B.2-2). Detection limits describe the minimum concentration of an element needed for qualitative analytical detection. Lower limit of determination describes the minimum concentration

Table B.2-1

International rock standards used for XRF calibration

Major Element Analysis	Trace Element Analysis
NBS-1413	AN-G
NBS-88B	BCR-1
NBS-70A	BE-N
NBS-99A	BIR-1
QCO-1	BR
STM-1	BX-N
	DNC-1
	DR-N
	DT-N
	FK-N
	G-2
	GA
	GC-O
	GH
	GS-N
	IF-G
	MAG-1
	MA-N
	MICA-FE
	MICA-MG
	NIM-D
	NIM-G
	NIM-L
	NIM-N
	NIM-P
	NIM-S
	PCC-1
	RGM-1
	SCo-1
	SDC-1
	SY-2
	SY-3
	UB-N
	US-N
	W-2

Values from Abbey (1983)

Table B.2-2 Information for X-Ray fluorescence analyses

Element	Electron Shell	* KeV Measured	Lower Limit Detection (ppm)	Lower Limit Determination (ppm)
Si	Ka 1,2	1.739	-	100
Ti	Ka 1,2	4.508	-	100
Al	Ka 1,2	1.486	-	100
Fe	Ka 1,2	6.398	-	20
Mg	Ka 1,2	1.253	-	100
Ca	Ka 1,2	3.690	-	100
Na	Ka 1,2	1.041	-	100
K	Ka 1,2	3.312	-	100
Mn	Ka 1,2	5.874	7.0	22
P	Ka 1,2	2.013	-	100
Rb	Ka 1,2	13.373	1.02	3.0
Sr	Ka 1,2	14.140	0.94	3.0
Pb	La 1	10.550	3.28	9.8
V	Ka 1,2	4.949	-	-
Ni	Ka 1,2	7.471	0.68	2.0
Y	Ka 1,2	14.931	1.08	3.2
Zr	Ka 1,2	15.744	0.78	2.5
Nb	Ka 1,2	16.581	2.0	3.0

* = After White and Johnson (1970)
- = Not determined

of an element needed for quantitative analytical determination.

c) Accuracy and Precision

Tables in this section present mean and standard deviation values for standards run as unknown samples, as well as individual analytical dates. Accepted element abundances for standards also are given. Calculated accuracy (closeness of the analytical value to an accepted value, calculated as % deviation from the accepted value), and precision (ability to repeat measurements, calculated as coefficient of variation = [standard deviation/mean] x 100) have been determined from multiple analyses of standards BCR-1, G-2, GS-N, NIM-D and W-2 (Tables B.2-3 to B.2-9). Precision, as determined by these standards, is generally <5% for most major elements, Rb, Sr, V, Ni, Y and Zr; and <10% for Na2O, MnO and Nb. Large coefficients of variation for triplicate analyses of standard G-2 may be due to sample heterogeneity.

TABLE B.2-3

XRF Accuracy and Precision
G-2 (Granite)
n=8

Element	Mean	SD	Accepted*	CV(%)	Accuracy(%)**
Rb	166	2	170	1.20	2.35
Sr	468	6	478	1.28	2.09
V	39	0	36	0.0	8.33
Ni	-	-	5	-	-
Y	16	0	11	0.0	45.0
Zr	298	5	300	1.68	0.66
Nb	8.9	0.9	13	10.1	31.5

All analytical values in ppm
n = Number of samples analyzed
- = Not determined
* = Accepted value from Gladney and Burns (1983)
**= Accuracy = [(Mean-Accepted)/Accepted]x100
SD= Standard deviation of the mean value at 1 sigma confidence interval
CV= Coefficient of variation = (SD/Mean)x100
Analyses dates: 10/85 (1 analysis)
11/85 (2 analyses)
4/86 (2 analyses)
6/86 (1 analysis)
3/87 (2 analyses)

TABLE B.2-4

XRF Accuracy and Precision
NIM-D (Dunite)
n=8

Element	Mean	SD	Accepted*	CV(%)	Accuracy(%)**
Rb	-	-	-	-	-
Sr	-	-	3	-	-
V	33	1	40	3.03	17.5
Ni	2234	12	2050	0.54	8.98
Y	-	-	-	-	-
Zr	-	-	20	-	-
Nb	-	-	-	-	-

All analytical values in ppm
n = Number of samples analyzed
- = Not determined
* = Accepted value from Abbey (1983)
**= Accuracy = [(Mean-Accepted)/Accepted]x100
SD= Standard deviation of the mean value at 1 sigma confidence interval
CV= Coefficient of variation = (SD/Mean)x100
Analyses dates: 2/86 (4 analyses)
10/86 (1 analysis)
10/87 (3 analyses)

TABLE B.2-5

XRF Accuracy and Precision
W-2 (Diabase)
n=8

Element	Mean	SD	Accepted*	CV(%)	Accuracy(%)**
Rb	21	0	20	0.0	5.00
Sr	198	1	194	0.51	2.06
V	-	-	262	-	-
Ni	69	2	70	2.90	1.43
Y	24	0	24	0.0	0.0
Zr	96	1	94	1.04	2.13
Nb	7.0	0.4	7.9	5.71	11.4

All analytical values in ppm
n = Number of samples analyzed
- = Not determined
* = Accepted value from Gladney and Roelandts (1988)
**= Accuracy = [(Mean-Accepted)/Accepted]x100
SD= Standard deviation of the mean value at 1 sigma confidence interval
CV= Coefficient of variation = (SD/Mean)x100
Analyses dates: 4/87 (2 analyses)
5/87 (1 analysis)
8/87 (1 analysis)
10/87 (3 analyses)
11/87 (1 analysis)

TABLE B.2-6

XRF Precision-Triplicate Analyses of
BCR-1 (Basalt)

Element	BCR-1(1)	BCR-1(2)	BCR-1(3)	Mean	SD	CV(%)
Rb	51	50	51	51	1	1.96
Sr	331	340	339	337	5	1.48
V	426	420	418	421	4	0.95
Ni	16	9.4	11	12	3	25.0
Y	39	41	40	40	1	2.50
Zr	189	193	192	191	2	1.05
Nb	13	11	11	12	1	8.33

Triplicate analyses performed on a single split of standard BCR-1 (V, Ni-2/10/86; Rb, Sr, Y, Zr, Nb-4/4/86).
All analytical values in ppm
SD= Standard deviation of the mean value at 1 sigma confidence interval
CV= Coefficient of variation = (SD/Mean)x100

TABLE B.2-7

XRF Precision-Triplicate Analyses of
GS-N (Granite)

Element	GS-N(1)	GS-N(2)	GS-N(3)	Mean	SD	CV(%)
Rb	187	187	187	187	0	0.0
Sr	578	578	580	579	1	0.17
V	-	-	-	-	-	-
Ni	-	-	-	-	-	-
Y	17	16	17	17	1	3.45
Zr	214	213	214	214	1	0.27
Nb	24	24	24	24	0	0.84

Triplicate analyses performed on a single split of standard GS-N (10/10/87).
All analytical values in ppm
- = Not determined
SD= Standard deviation of the mean value at 1 sigma confidence interval
CV= Coefficient of variation = (SD/Mean)x100

TABLE B.2-8

XRF Precision-Triplicate Analyses of
NIM-D (Dunite)

Element	NIM-D(1)	NIM-D(2)	NIM-D(3)	Mean	SD	CV(%)
Rb	-	-	-	-	-	-
Sr	-	-	-	-	-	-
V	33	34	32	33	1	3.03
Ni	2232	2224	2247	2234	12	0.54
Y	-	-	-	-	-	-
Zr	-	-	-	-	-	-
Nb	-	-	-	-	-	-

Triplicate analyses performed on a single split of standard NIM-D (2/11/86).
All analytical values in ppm
- = Not determined
SD= Standard deviation of the mean value at 1 sigma confidence interval
CV= Coefficient of variation = (SD/Mean)x100

TABLE B.2-9

XRF Precision-Triplicate Analyses of
W-2 (Diabase)

Element	W-2(1)	W-2(2)	W-2(3)	Mean	SD	CV(%)
Rb	22	21	21	21	1	4.76
Sr	198	197	198	198	1	0.51
V	-	-	-	-	-	-
Ni	66	72	69	69	3	4.35
Y	24	24	23	24	1	4.17
Zr	96	96	96	96	0	0.0
Nb	7.5	7.2	6.8	7.2	0.4	5.56

Triplicate analyses performed on a single split of standard W-2 (Ni-4/25/87; Rb, Sr, Y, Zr, Nb-10/10/87).
All analytical values in ppm
- = Not determined
SD= Standard deviation of the mean value at 1 sigma confidence interval
CV= Coefficient of variation = (SD/Mean)x100

B.3 Instrumental Neutron Activation Analysis (INAA)

a) Sample Preparation and Analytical Technique

Hf, Ta, Sc, Cr, Co, Ba, Cs, Th, U and seven REE are analyzed by instrumental neutron activation analyses (INAA) using a Nuclear Data 6600 gamma-ray spectrometer connected to twin high-purity Ge detectors. Approximately 300 milligram sample splits are sealed in polyvinal containers, neutron irradiated at Sandia National Laboratories test reactor, and then counted both seven and forty days after irradiation for an average time of three hours per sample. Analytical procedures follow those described by Gibson and Jagam (1980). INAA data reduction is performed by the TEABAGS spectral processing program (Lindstrom and Korotev, 1982) with element abundances calibrated to the standard NBS 1633a (coal fly ash; Table B.3-1).

b) Detection Limits

A list of parent nuclides, daughter nuclides, decay energies, detection limits and lower limits of determination are presented in this section (Table B.3-2). Lower limit of detection describes the minimum concentration of an element needed for qualitative analytical detection. Lower limit of determination describes minimum concentration of an element needed for quantitative analytical determination. Data pertinent to the reactor facility at Sandia National Laboratory also is presented in this section.

Table B.3-1. Elemental abundances of NBS 1633A (Coal Fly Ash) used for Instrumental Neutron Activation Analysis.

SAMPLE	NBS 1633A
Ba	1320
Cs	10.42
Th	24.0
U	10.3
Sc	38.6
Cr	193
Co	44.1
Hf	7.29
Ta	1.93
La	76.7
Ce	168.8
Sm	16.61
Eu	3.5
Tb	2.69
Yb	7.68
Lu	1.146

Table B.3-2 Information for instrumental neutron activation

Parent Nuclide	Daughter Nuclide	KeV Measured	Count Time in days	Detection Limit-ppm	Determination Limit-ppm
Ba-130	Ba-131	373	7	2.0	25
		496*			
Ce-140	Ce-141	145*	40	0.12	1.5
Co-59	Co-60	1173*	40	0.05	1.0
		1332			
Cr-50	Cr-51	320*	40	0.3	1.0
Cs-133	Cs-134	605	40	0.04	0.5
		796*			
Eu-151	Eu-152	245	40	0.02	0.15
		344*			
		779			
		1408*			
Hf-180	Hf-181	482*	7,40	0.02	0.1
La-139	La-140	329*	7	-	0.9
		487*			
		816			
		1596			
Lu-176	Lu-177	208*	7	-	0.04
Sc-45	Sc-46	889*	7	0.20	0.5
		1121*			
Sm-152	Sm-153	103*	7	-	0.5
Ta-181	Ta-182	1189*	7,40	0.002	0.04
		1221*			
		1231			
Tb-159	Tb-160	299*	7	0.01	0.05
		879			
		966*			
		1178			
Th-232	Pa-232	312*	7	0.04	0.1
U-238	Np-239	228	7	0.017	0.020
		278*			
Yb-174	Yb-175	177*	40	0.017	0.020
		198			

* = preferred KeV

Irradiations at Sandia National Labs, Albuquerque, New Mexico

-Irradiation time - 10,000 seconds

-Flux - 0.6200×10^{13} neutrons/cm^2.second

-Cadmium ratio - 0.31

c) Accuracy And Precision

This section presents mean and standard deviation values for standards run as unknown samples, as well as individual analytical counting dates. Accepted element abundances for standards also are given. Calculated accuracy and precision are determined from multiple analyses of standards BCR-1, G-2, MAG-1 and SCo-1 (Tables B.3-3 to B.3-6). Precision of multiple analyses also are presented as triplicate runs of standards and Witwatersrand Supergroup sample 615-9 (Table B.3-7). Triplicate analyses are preformed with both triplicate sample splits and multiple analyses of the same sample split, in order to measure the effects of sample heterogeneities, variable reactor neutron flux, and analytical drift. Precision for standards and samples as determined by the above methods, are generally <5% for Ba, Hf and Ce; <10% for Cs, Th, U, Cr, Co, Ta, Sm, Eu, Tb and Yb; and <15% for Sc, La and Lu. Precision determined for Witwatersrand pelite sample 615-9 (Table B.3-7) is generally less than that determined for standards, indicating that analytical variation caused by sample heterogeneity is less than that inherent in the analytical technique.

TABLE B.3-3

INNA Accuracy and Precision
BCR-1 (Basalt)
n=5

Element	Mean	SD	Accepted*	CV(%)	Accuracy(%)**
Ba	682	28	678	4.11	0.59
Cs	1.0	0.0	1.0	0.0	0.0
Th	5.9	0.3	6.0	5.08	1.67
U	1.7	0.1	1.7	5.88	0.0
Sc	32	0	33	0.0	3.03
Cr	14	1	16	7.14	12.5
Co	38	1	36	2.63	5.56
Hf	5.3	0.1	4.9	1.89	8.16
Ta	0.79	0.04	0.79	5.06	0.0
La	25	1	25	4.00	0.0
Ce	54	1	54	1.85	0.0
Sm	6.9	0.2	6.6	2.90	4.55
Eu	1.9	0.0	2.0	0.0	5.00
Tb	1.1	0.1	1.1	9.09	0.0
Yb	3.5	0.2	3.4	5.71	2.94
Lu	0.52	0.02	0.51	3.85	1.96

All analytical values in ppm
n = Number of samples analyzed
* = Accepted value from Gladney and Burns (1983)
**= Accuracy = [(Mean-Accepted)/Accepted]x100
SD= Standard deviation of the mean value at 1 sigma confidence interval
CV= Coefficient of variation = (SD/Mean)x100
Analyses dates: 6/87 (2 analyses)
8/87 (2 analyses)
10/87 (1 analysis)

TABLE B.3-4

INNA Accuracy and Precision
G-2 (Granite)
n=9

Element	Mean	SD	Accepted*	CV(%)	Accuracy(%)**
Ba	1906	133	1880	6.98	1.38
Cs	1.4	0.1	1.3	7.14	7.69
Th	24	2	25	8.33	4.00
U	2.0	0.1	2.0	5.00	0.0
Sc	3.4	0.3	3.5	8.82	2.86
Cr	9	1	9	11.1	0.00
Co	4.4	0.5	4.6	11.4	4.35
Hf	9.0	0.9	7.9	10.0	13.9
Ta	0.80	0.05	0.88	6.25	9.09
La	87	7	90	8.05	3.33
Ce	168	19	160	11.3	5.00
Sm	7.7	0.7	7.2	9.09	6.94
Eu	1.4	0.2	1.4	14.3	0.00
Tb	0.51	0.04	0.48	7.84	6.25
Yb	0.9	0.1	0.8	11.1	12.5
Lu	0.11	0.01	0.11	9.09	0.00

All analytical values in ppm
n = Number of samples analyzed
* = Accepted value from Gladney and Burns (1983)
**= Accuracy = [(Mean-Accepted)/Accepted]x100
SD= Standard deviation of the mean value at 1 sigma confidence interval
CV= Coefficient of variation = (SD/Mean)x100
Analyses dates: 2/85 (2 analyses)
3/86 (1 analysis)
11/86 (1 analysis)
12/86 (1 analysis)
6/87 (3 analyses)
12/87 (1 analysis)

TABLE B.3-5

INNA Accuracy and Precision
MAG-1 (Marine Mud)
n=5

Element	Mean	SD	Accepted*	CV(%)	Accuracy(%)**
Ba	476	13	480	2.73	0.83
Cs	8.5	0.2	8.6	2.35	1.16
Th	12	1	13	8.33	7.69
U	2.7	0.1	2.8	3.70	3.57
Sc	16	0	17	0.0	5.88
Cr	96	5	105	5.21	8.57
Co	21	1	20	4.76	5.00
Hf	3.6	0.1	3.6	2.78	0.0
Ta	1.1	0.1	1.1	9.09	0.0
La	41	2	41	4.88	0.0
Ce	84	2	86	2.38	2.33
Sm	7.4	0.1	8.1	1.35	8.64
Eu	1.3	0.1	1.5	7.69	13.3
Tb	1.0	0	1.0	0.00	0.00
Yb	2.6	0.2	2.6	7.69	0.00
Lu	0.40	0.02	-	5.00	-

All analytical values in ppm
n = Number of samples analyzed
- = Not determined
* = Accepted value from Abbey (1983)
**= Accuracy = [(Mean-Accepted)/Accepted]x100
SD= Standard deviation of the mean value at 1 sigma confidence interval
CV= Coefficient of variation = (SD/Mean)x100
Analyses dates: 11/86 (1 analysis)
12/86 (1 analysis)
10/87 (2 analyses)
12/87 (1 analysis)

TABLE B.3-6

INNA Accuracy and Precision
SCo-1 (Cody Shale)
n=5

Element	Mean	SD	Accepted*	CV(%)	Accuracy(%)**
Ba	587	33	590	5.62	0.51
Cs	8.0	0.8	7.8	10.0	2.56
Th	9.6	0.9	9.6	9.38	0.00
U	3.1	0.2	2.9	6.45	6.90
Sc	12	2	11	16.7	9.09
Cr	70	4	71	5.71	1.41
Co	11	1	11	9.09	0.00
Hf	4.9	0.1	4.3	2.04	14.0
Ta	0.8	0.0	0.9	0.00	11.1
La	31	4	29	12.9	6.90
Ce	57	1	63	1.75	9.52
Sm	5.3	0.5	5.1	9.43	3.92
Eu	1.1	0.1	1.2	9.09	8.33
Tb	0.7	0.0	0.8	0.00	12.5
Yb	2.3	0.1	2.2	4.35	4.55
Lu	0.39	0.05	-	12.8	-

All analytical values in ppm
n = Number of samples analyzed
- = Not determined
* = Accepted value from Abbey (1983)
**= Accuracy = [(Mean-Accepted)/Accepted]x100
SD= Standard deviation of the mean value at 1 sigma confidence interval
CV= Coefficient of variation = (SD/Mean)x100
Analyses dates: 2/85 (1 analysis)
7/86 (1 analysis)
11/86 (1 analysis)
10/87 (1 analysis)
12/87 (1 analysis)

APPENDIX B.3-7

INNA Precision-Triplicate Analyses of
615-9 (Witwatersrand Pelite)

Element	615-9(A)	615-9(B)	615-9(C)	Mean	SD	CV(%)
Ba	428	449	444	440	11	2.50
Cs	7.8	7.8	7.8	7.8	0.0	0.0
Th	6.2	5.6	5.6	5.8	0.4	6.90
U	2.0	2.1	1.9	2.0	0.1	5.00
Sc	31	32	31	31	1	3.23
Cr	1289	1286	1283	1286	3	0.23
Co	66	67	66	66	1	1.52
Hf	4.3	4.1	4.2	4.2	0.1	2.38
Ta	0.73	0.75	0.77	0.75	0.02	2.67
La	28	30	29	29	1	3.45
Ce	63	62	62	62	1	1.61
Sm	6.1	6.1	6.0	6.1	0.1	1.64
Eu	1.6	1.7	1.7	1.7	0.1	5.88
Tb	0.96	0.81	0.88	0.88	0.08	9.09
Yb	2.83	2.9	2.9	2.9	0.1	3.45
Lu	0.43	0.47	0.45	0.47	0.02	4.26

Analyses performed on triplicate split of sample 11/21/86.
All analytical values in ppm
SD= Standard deviation of the mean value at 1 sigma
confidence interval
CV= Coefficient of variation = (SD/Mean)x100

B.4 X-Ray Diffraction (XRD)

XRD analyses are used in a semi-quantitative determination of the mineralogy of fine-grained sediments. Disaggregation of samples is accomplished in an agate mortar and pestle by hand-crushing samples into a wet-slurry while immersed in deionized water. This crushing technique is preferred over mechanical grinding to avoid damaging delicate crystal structures of clay or mica minerals. Sedimented sample mounts are prepared following the general procedures outlined by Gibbs (1968). Analytical techniques for semi-quantitative mineral determination follow a four-step procedure described by Austin (1987). Samples are run (1) untreated from 2-39 degrees 2θ at 2 degrees 2θ/minute, (2) untreated from 24-26 degrees 2θ at 0.5 degrees 2θ/minute, (3) after 24 hours in an ethylene glycol atmosphere, 2-15 degrees 2θ at 2 degrees 2θ/minute, and (4) after 30 minutes at 375 ^{o}C, 2-15 degrees 2θ at 2 degrees 2θ/minute. Peak heights over background are used to calculate parts in 10 analyses, following procedures outlined by Austin (1987; Table B.4). Additional heated slides are run at 500 and 600^{o}C to determine the presence of Fe- and Mg-rich chlorite respectively. Mineralogical results are presented in Table 1.

Table B.4
X-Ray diffraction information

I. Semiquantitative mineral calculations (Abbreviations given below in part II):

Illite = [I(1G)/T] x 10

Montmorillinite = [[M(1)/4] x 10]/T

Chlorite = [C(3)/I(2)] x [I(1G)/T] x 10

Mixed Layer Clays = [[I(1H)-[I(1G)+[M(1)/4]]/T] x 10

Kaolinite (with chlorite absent) = [K(1)/T] x 10

Kaolinite (with chlorite present) =
[K(2)/2C(4)] x [C(3)/I(2)] x [I(1G)/T] x 10

Total (with chlorite absent) = I(1H) + K(1)

Total (chlorite present) = I(1H)+[[C(3)][I(1G)]/[I(2)]]
+ [[K(2)][C(3)][I(1G)]]/[[2C(4)][I(2)]]

II. Mineralogic Peak Identification:

K(1) Kaolinite at 12.4° 2θ, untreated run
K(2) Kaolinite at 24.9° 2θ, slow untreated run
I(1G) Illite-Muscovite at 8.8° 2θ, glycol run
I(1H) Illite-Muscovite at 8.8° 2θ, 375°C run
I(2) Illite-Muscovite at 17.8° 2θ, untreated run
C(3) Chlorite at 18.4-18.9° 2θ, untreated run
C(4) Chlorite at 25.1° 2θ, slow untreated run
M(1) Montmorillinite at 5.2° 2θ, glycol run
T Total counts (see part I)

APPENDIX C. Geochemical Results

Major and trace element analyses of individual pelite samples are presented in stratigraphic order along with important element ratios (Tables C.1-1 through C.1-6). Moodies pelite data from McLennan et al. (1983). Individual quartzite analyses presented in Tables 7-10 will not be repeated here. Major elements, Zr, Y, Sr, Nb, V, Pb, Ni and Rb are determined by XRF, whereas Hf, Ta, Sc, Cr, Co, Ba, Cs, Th, U and seven REE are determined by INAA. Major elements are reported in oxide weight percent determined on a volatile free basis and trace elements in parts-per-million (ppm). Total Fe reported as Fe2O3T; nd, below detection limit; -, not determined; LOI, loss on ignition; AVG, mean analytical value; STD, one standard deviation of the mean. CIA, Chemical Index of Alteration. CIA calculated as:

$$CIA = \frac{Al2O3}{(Al2O3+CaO+Na2O+K2O)} \times 100 \qquad (C.1)$$

, with oxides as molecular values. This index is calculated using CaO in silicate minerals only. CaO contributions from apatite [Ca5(F,Cl)(PO4)3] are corrected for by using the P2O5 content of pelites and adjusting the appropriate amount of CaO required to make the mineral phase. Carbonate phases are corrected for by assuming a maximum CaO/Na2O ratio of 0.8 for the silicate fraction in these sediments (Kronberg et al., 1986). CaO in excess of the value

calculated from this ratio is considered to be included in the carbonate fraction and is not included in CIA calculations. Most Kaapvaal pelites are characterized by an absence or insignificant concentrations of CaO. Therefor, corrections based on CaO/Na2O ratios result in a <1% change in CIA values for most Ponola and <2% change for most Witwatersrand and Transvaal pelites. Between 25-50% of all Pongola-NUWM and NVS, Witwatersrand-PRM and Ventersdorp-BOT pelites show significant (>3%) changes in CIA values calculated using the CaO/Na2O ratio correction. Europium anomaly calculated as:

$$Eu/Eu^* = \frac{Eu/.087}{Sm/.231 - [((Sm/.231)-(Tb/.058))/3]} \qquad (C.2)$$

Note: differences in europium anomalies may result from calculations using Tb-Sm-Eu (Eqn. C.2) and those calculated using Gd-Sm-Eu (Taylor and Mclennan, 1985). All Eu anomaly results discussed in this study are recalculated using equation C.2.

Table C.1-1

Moodies Pelite Analyses

SAMPLE	MOODIES PELITES AVG	STD
SiO2	59.32	2.36
TiO2	0.44	0.07
Al2O3	14.53	2.26
Fe2O3-T	7.36	1.12
MgO	5.09	0.22
CaO	1.35	0.77
Na2O	1.76	0.46
K2O	4.87	0.80
MnO	0.13	0.02
P2O5	-	-
LOI	5.76	2.15
TOTAL	100.60	1.20
Rb	-	-
Ba	535	127
Cs	7.3	6.5
Sr	-	-
Pb	7.6	2.0
Th	6.2	0.9
U	1.9	0.4
Sc	15	1
V	98	20
Cr	715	106
Co	35	3
Ni	331	43
Y	21	4
Zr	148	38
Nb	11	2
Hf	4.3	0.9
Ta	-	-
La	22	8
Ce	46	15
Sm	3.6	1.1
Eu	0.96	0.28
Tb	0.46	0.10
Yb	1.7	0.3
Lu	-	-

SAMPLE	MOODIES PELITES AVG	STD
K2O/Na2O	2.9	0.6
SiO2/Al2O3	4.2	0.8
Th/U	3.2	0.2
K/Rb	-	-
Rb/Sr	-	-
Ba/Rb	-	-
Ba/Sr	-	-
Th/Sc	0.40	0.04
La/Sc	1.4	0.4
La/Th	3.5	0.8
Zr/Y	6.9	1.1
Ti/Zr	19	4
Zr/Nb	13	2
Ni/Co	9.4	0.8
Cr/V	7.5	1.3
V/Ni	0.29	0.03
Cr/Ni	2.2	0.1
Cr/Zr	5.0	0.8
Sc/Th	2.5	0.3
Co/Th	5.7	0.6
La/Yb	13	2
Eu/Eu*	0.85	0.03
CIA	58	4

MOODIES PELITES

SAMPLE	79NC123	79NC124	79NC129	79NC130	79NC131
SiO2	61.93	59.44	58.12	61.59	55.53
TiO2	0.36	0.38	0.55	0.47	0.43
Al2O3	11.07	13.30	15.37	17.86	15.04
Fe2O3-T	7.79	6.01	9.21	6.46	7.34
MgO	5.19	4.97	5.45	4.78	5.07
CaO	2.59	1.92	0.58	0.87	0.80
Na2O	0.96	2.07	2.03	2.21	1.52
K2O	3.59	4.62	4.71	5.92	5.49
MnO	0.14	0.14	0.11	0.09	0.15
P2O5	-	-	-	-	-
LOI	6.36	7.18	3.89	2.74	8.61
TOTAL	99.98	100.03	100.02	102.99	99.98
Rb	-	-	-	-	-
Ba	345	547	606	718	458
Cs	2.2	4.0	3.8	20	6.6
Sr	-	-	-	-	-
Pb	4.8	9.7	9.6	8.1	5.9
Th	5.3	5.2	7.1	6.2	7.2
U	1.6	1.5	2.4	1.9	2.3
Sc	14	15	18	15	15
V	65	91	124	100	109
Cr	643	577	822	679	855
Co	30	36	39	35	36
Ni	287	287	394	323	366
Y	15	21	26	22	23
Zr	115	131	209	109	175
Nb	9.8	10	14	11	11
Hf	3.4	3.1	4.4	5.1	5.5
Ta	-	-	-	-	-
La	15	17	35	18	27
Ce	29	36	70	38	55
Sm	2.4	2.7	5.3	3.0	4.6
Eu	0.68	0.73	1.3	0.80	1.3
Tb	0.36	0.37	0.56	0.42	0.61
Yb	1.3	1.4	2.0	1.6	2.1
Lu	-	-	-	-	-

MOODIES PELITES

SAMPLE	79NC123	79NC124	79NC129	79NC130	79NC131
K2O/Na2O	3.7	2.2	2.3	2.7	3.6
SiO2/Al2O3	5.6	4.5	3.8	3.4	3.7
Th/U	3.3	3.5	3.0	3.3	3.1
K/Rb	-	-	-	-	-
Rb/Sr	-	-	-	-	-
Ba/Rb	-	-	-	-	-
Ba/Sr	-	-	-	-	-
Th/Sc	0.38	0.35	0.39	0.41	0.48
La/Sc	1.1	1.1	1.9	1.2	1.8
La/Th	2.8	3.3	4.9	2.9	3.8
Zr/Y	7.7	6.2	8.0	5.0	7.6
Ti/Zr	19	17	16	26	15
Zr/Nb	12	13	15	9.9	16
Ni/Co	9.6	8.0	10	9.2	10
Cr/V	9.9	6.3	6.6	6.8	7.8
V/Ni	0.23	0.32	0.31	0.31	0.30
Cr/Ni	2.2	2.0	2.1	2.1	2.3
Cr/Zr	5.6	4.4	3.9	6.2	4.9
Sc/Th	2.6	2.9	2.5	2.4	2.1
Co/Th	5.7	6.9	5.5	5.6	5.0
La/Yb	12	12	18	11	13
Eu/Eu*	0.87	0.85	0.81	0.83	0.89
CIA	52	53	62	61	60

MOZAAN PELITES-PIET RETIEF (MPR)

	AVG	STD
SiO2	59.53	7.75
TiO2	0.75	0.28
Al2O3	16.47	4.83
Fe2O3-T	13.19	7.10
MgO	1.86	0.75
CaO	0.09	0.07
Na2O	0.58	0.51
K2O	1.51	0.94
MnO	0.07	0.05
P2O5	0.10	0.11
LOI	5.52	1.63
TOTAL	99.65	0.72
Rb	71	50
Ba	369	231
Cs	3.6	4.1
Sr	54	51
Pb	20	8
Th	11	8
U	3.3	2.1
Sc	19	10
V	146	54
Cr	350	155
Co	29	25
Ni	264	261
Y	39	21
Zr	208	101
Nb	14	7
Hf	6.2	3.1
Ta	1.1	0.5
La	64	48
Ce	87	79
Sm	9.2	5.4
Eu	1.8	1.0
Tb	1.2	0.6
Yb	3.5	1.5
Lu	0.52	0.22

MOZAAN PELITES-PIET RETIEF (MPR)

	AVG	STD
K2O/Na2O	4.6	4.9
SiO2/Al2O3	4.0	1.6
Th/U	3.2	0.5
K/Rb	165	64
Rb/Sr	3.8	5.0
Ba/Rb	8.6	8.6
Ba/Sr	14	14
Th/Sc	0.66	0.50
La/Sc	3.1	1.9
La/Th	6.7	5.4
Zr/Y	7.3	6.3
Ti/Zr	24	8
Zr/Nb	16	7
Ni/Co	11	7
Cr/V	2.8	1.8
V/Ni	1.1	1.0
Cr/Ni	1.9	0.8
Cr/Zr	2.2	1.4
Sc/Th	2.4	1.2
Co/Th	4.1	3.5
La/Yb	16	10
Eu/Eu*	0.68	0.13
CIA	87	5

Table C.1-2
Pongola Pelite Analyses

MOZAAN PELITES-PIET RETIEF AREA (MPR)

	P 41	P 47	P 49	P 50	P 51
SiO2	59.18	79.36	62.89	53.10	52.20
TiO2	0.60	0.62	0.71	0.49	0.53
Al2O3	14.99	9.75	17.32	12.40	14.37
Fe2O3-T	12.92	3.71	9.31	23.77	21.76
MgO	3.28	1.71	1.31	2.20	2.80
CaO	0.02	0.02	0.06	0.01	0.13
Na2O	0.27	0.14	0.36	0.38	0.35
K2O	3.08	2.07	1.93	<0.01	0.68
MnO	0.07	0.03	0.06	0.09	0.05
P2O5	0.02	0.02	0.06	0.38	0.05
LOI	5.65	2.82	5.85	7.20	7.51
TOTAL	100.08	100.25	99.86	100.02	100.43
Rb	171	82	119	<3.0	28
Ba	474	304	613	81	287
Cs	7.4	1.7	13	<0.5	1.0
Sr	10	13	33	82	16
Pb	13	15	38	21	14
Th	6.4	9.9	17	4.8	4.4
U	2.1	3.7	5.3	1.8	1.4
Sc	16	6.7	19	15	15
V	151	63	151	110	130
Cr	597	427	106	318	382
Co	18	5.8	9.0	56	19
Ni	219	138	67	967	289
Y	69	16	60	38	14
Zr	160	388	174	122	108
Nb	9.1	11	19	7.5	6.2
Hf	4.4	11	5.7	3.2	2.8
Ta	1.0	0.92	1.2	0.70	0.59
La	88	12	73	68	11
Ce	10	16	136	62	19
Sm	14	2.5	13	12	1.9
Eu	2.8	0.79	2.3	2.6	0.44
Tb	1.7	0.41	1.8	1.4	0.48
Yb	4.2	1.8	5.1	3.0	1.4
Lu	0.64	0.29	0.82	0.49	0.21

MOZAAN PELITES-PIET RETIEF AREA (MPR)

	P 41	P 47	P 49	P 50	P 51
K2O/Na2O	11	15	5.4	<0.03	1.9
SiO2/Al2O3	3.9	8.1	3.6	4.3	3.6
Th/U	3.0	2.7	3.2	2.7	3.1
K/Rb	149	210	135	-	202
Rb/Sr	17	6.3	3.6	<0.04	1.8
Ba/Rb	2.8	3.7	5.2	>27	10
Ba/Sr	47	23	19	0.99	18
Th/Sc	0.40	1.5	0.89	0.32	0.29
La/Sc	5.5	1.8	3.8	4.5	0.73
La/Th	14	1.2	4.3	14	2.5
Zr/Y	2.3	24	2.9	3.2	7.7
Ti/Zr	22	9.6	24	24.1	29
Zr/Nb	18	35	9	16	17
Ni/Co	12	24	7.4	17	15
Cr/V	4.0	6.8	0.70	2.9	2.9
V/Ni	0.69	0.46	2.3	0.11	0.45
Cr/Ni	2.7	3.1	1.6	0.3	1.3
Cr/Zr	3.7	1.1	0.61	2.6	3.5
Sc/Th	2.5	0.7	1.1	3.1	3.4
Co/Th	2.8	0.59	0.53	12	4.3
La/Yb	21	6.7	14	23	7.9
Eu/Eu*	0.62	0.91	0.58	0.70	0.60
CIA	80	80	87	95	91

MOZAAN PELITES-PIET RETIEF AREA (MPR)

	MW 100	MW 147	MW 170	MW 253
SiO2	57.70	54.54	60.58	56.18
TiO2	1.28	0.51	0.79	1.20
Al2O3	22.12	11.43	22.49	23.35
Fe2O3-T	8.25	21.89	5.36	11.72
MgO	0.70	1.51	1.81	1.38
CaO	0.24	0.04	0.13	0.15
Na2O	1.09	0.45	1.84	0.33
K2O	1.36	0.56	2.54	1.34
MnO	0.03	0.05	0.05	0.19
P2O5	0.12	0.04	0.04	0.19
LOI	6.46	6.86	4.07	3.27
TOTAL	99.35	97.88	99.70	99.30
Rb	51	27	106	56
Ba	580	75	745	160
Cs	0.74	0.71	6.0	1.9
Sr	143	8.4	136	43
Pb	25	15	26	17
Th	11	4.0	30	11
U	2.6	1.2	8.2	3.6
Sc	43	13	19	28
V	255	124	114	212
Cr	448	403	80	390
Co	50	18	8.7	80
Ni	261	207	34	190
Y	38	12	63	42
Zr	236	90	362	236
Nb	18	6.3	26	21
Hf	8.2	2.5	11	6.9
Ta	1.4	0.56	1.9	1.7
La	160	6.4	108	54
Ce	212	10	212	104
Sm	15	1.3	14	8.8
Eu	3.1	0.44	2.3	1.9
Tb	1.6	0.32	2.1	1.3
Yb	4.3	1.5	5.5	4.4
Lu	0.65	0.23	0.79	0.58

MOZAAN PELITES-PIET RETIEF AREA (MPR)

	MW 100	MW 147	MW 170	MW 253
K2O/Na2O	1.2	1.2	1.4	4.1
SiO2/Al2O3	2.6	4.8	2.7	2.4
Th/U	4.2	3.3	3.7	3.1
K/Rb	221	172	199	199
Rb/Sr	0.36	3.2	0.78	1.3
Ba/Rb	11	2.8	7.0	2.9
Ba/Sr	4.1	8.9	5.5	3.7
Th/Sc	0.26	0.31	1.6	0.4
La/Sc	3.7	0.49	5.7	1.9
La/Th	15	1.6	3.6	4.9
Zr/Y	6.2	7.5	5.7	5.6
Ti/Zr	33	34	13	30
Zr/Nb	13	14	14	11
Ni/Co	5.2	12	3.9	2.4
Cr/V	1.8	3.3	0.7	1.8
V/Ni	0.98	0.60	3.4	1.1
Cr/Ni	1.7	1.9	2.4	2.1
Cr/Zr	1.9	4.5	0.2	1.7
Sc/Th	3.9	3.3	0.6	2.5
Co/Th	4.5	4.5	0.29	7.3
La/Yb	37	4.3	20	12
Eu/Eu*	0.68	0.90	0.50	0.66
CIA	86	89	79	92

MOZAAN PELITES-WIT MFOLOZI RIVER (MWM)

	AVG	STD
SiO2	57.43	4.52
TiO2	0.83	0.14
Al2O3	19.32	3.81
Fe2O3-T	9.87	7.57
MgO	1.79	1.23
CaO	0.07	0.04
Na2O	0.32	0.23
K2O	5.33	2.49
MnO	0.25	0.19
P2O5	0.08	0.15
LOI	4.48	0.88
TOTAL	99.55	0.91
Rb	226	112
Ba	461	200
Cs	8.5	4.6
Sr	29	13
Pb	12	4
Th	8.6	2.6
U	2.2	1.0
Sc	19	5
V	159	41
Cr	426	178
Co	21	12
Ni	100	42
Y	35	24
Zr	256	123
Nb	17	5
Hf	7.9	4.5
Ta	1.3	0.5
La	38	17
Ce	80	41
Sm	6.3	4.3
Eu	1.4	1.1
Tb	0.85	0.75
Yb	3.3	2.7
Lu	0.52	0.49

MOZAAN PELITES-WIT MFOLOZI RIVER (MWM)

	AVG	STD
K2O/Na2O	38	42
SiO2/Al2O3	3.1	0.6
Th/U	4.3	1.0
K/Rb	181	56
Rb/Sr	9.0	8.0
Ba/Rb	2.4	1.1
Ba/Sr	19	12
Th/Sc	0.46	0.08
La/Sc	2.0	0.4
La/Th	4.4	0.7
Zr/Y	7.9	1.8
Ti/Zr	22	6
Zr/Nb	15	3
Ni/Co	5.8	2.7
Cr/V	2.8	1.2
V/Ni	2.1	1.8
Cr/Ni	4.5	1.8
Cr/Zr	2.0	0.9
Sc/Th	2.3	0.5
Co/Th	2.5	1.3
La/Yb	13	3
Eu/Eu*	0.71	0.08
CIA	77	7

MOZAAN PELITES-WIT MFOLOZI RIVER (MWM)

	Po 53	Po 54	Po 55	Po 56	Po 57
SiO2	58.24	55.10	59.85	60.59	59.32
TiO2	0.71	0.83	0.92	0.93	0.77
Al2O3	17.01	19.77	19.79	18.53	17.01
Fe2O3-T	12.11	11.28	6.03	6.96	9.42
MgO	1.94	1.78	1.87	2.05	3.22
CaO	0.07	0.07	0.06	0.06	0.06
Na2O	0.34	0.09	0.59	0.55	0.57
K2O	4.32	5.60	5.84	5.14	3.84
MnO	0.32	0.24	0.08	0.09	0.12
P2O5	0.03	0.04	0.03	0.03	0.03
LOI	3.81	6.75	3.69	3.91	6.41
TOTAL	98.90	100.68	98.75	98.84	99.51
Rb	190	264	257	225	173
Ba	568	780	464	407	372
Cs	8.5	12	9.5	8.3	7.3
Sr	29	22	33	31	28
Pb	<9.8	10	11	12	21
Th	7.1	9.7	11	11	10
U	1.6	2.6	3.8	3.8	2.7
Sc	14	22	19	17	25
V	102	149	181	162	162
Cr	336	448	651	576	782
Co	19	19	15	42	37
Ni	92	86	106	172	172
Y	25	29	34	37	30
Zr	241	229	287	327	211
Nb	16	17	18	18	16
Hf	7.0	7.2	8.4	8.7	8.1
Ta	1.2	1.4	1.5	1.5	1.3
La	25	45	39	40	41
Ce	54	91	81	81	86
Sm	3.9	5.8	5.5	6.3	6.3
Eu	0.79	1.2	1.2	1.2	1.6
Tb	0.59	0.69	0.80	0.94	0.97
Yb	2.2	2.6	2.9	3.1	3.2
Lu	0.33	0.41	0.44	0.48	0.52

MOZAAN PELITES-WIT MFOLOZI RIVER (MWM)

	Po 53	Po 54	Po 55	Po 56	Po 57
K2O/Na2O	13	62	9.9	9.3	6.7
SiO2/Al2O3	3.4	2.8	3.0	3.3	3.5
Th/U	4.4	3.7	2.9	2.9	3.7
K/Rb	189	176	189	190	184
Rb/Sr	6.6	12	7.8	7.3	6.2
Ba/Rb	3.0	3.0	1.8	1.8	2.2
Ba/Sr	20	35	14	13	13
Th/Sc	0.51	0.44	0.58	0.65	0.40
La/Sc	1.8	2.0	2.1	2.4	1.6
La/Th	3.5	4.6	3.5	3.6	4.1
Zr/Y	9.6	7.9	8.4	8.8	7.0
Ti/Zr	18	22	19	17	22
Zr/Nb	15	13	16	18	13
Ni/Co	4.8	4.5	7.1	4.1	4.6
Cr/V	3.3	3.0	3.6	3.6	4.8
V/Ni	1.1	1.7	1.7	0.94	0.94
Cr/Ni	3.7	5.2	6.1	3.3	4.5
Cr/Zr	1.4	2.0	2.3	1.8	3.7
Sc/Th	2.0	2.3	1.7	1.5	2.5
Co/Th	2.7	2.0	1.4	3.8	3.7
La/Yb	11	17	13	13	13
Eu/Eu*	0.62	0.67	0.87	0.58	0.77
CIA	76	76	73	74	77

MOZAAN PELITES-WIT MFOLOZI RIVER (MWM)

	Po 58	Po 59	Po 60	Po 61	Po 62
SiO2	52.97	61.64	66.50	54.18	57.35
TiO2	1.08	0.82	0.64	0.75	0.76
Al2O3	26.80	19.25	14.90	17.57	16.40
Fe2O3-T	3.43	4.58	8.22	16.04	13.31
MgO	1.37	1.26	0.84	2.46	3.39
CaO	0.06	0.03	0.06	0.09	0.05
Na2O	0.06	0.09	0.65	0.36	0.32
K2O	9.46	6.37	4.43	3.70	3.26
MnO	0.10	0.14	0.20	0.32	0.31
P2O5	0.06	0.02	0.03	0.04	0.02
LOI	4.33	4.88	4.71	5.22	4.34
TOTAL	99.72	99.08	100.54	99.53	99.51
Rb	501	313	184	158	137
Ba	683	556	616	495	317
Cs	13	8.5	8.1	7.8	6.0
Sr	14	13	42	31	22
Pb	<9.8	13	17	11	13
Th	15	9.1	6.1	6.5	6.0
U	4.1	2.7	1.5	1.6	1.3
Sc	32	18	12	16	15
V	207	255	251	130	117
Cr	38	225	395	359	369
Co	13	13	12	19	21
Ni	28	46	70	85	146
Y	125	54	23	23	20
Zr	700	357	269	205	220
Nb	34	22	13	17	15
Hf	25	9.2	7.7	7.4	8.0
Ta	2.8	1.7	1.0	1.2	1.1
La	93	42	20	26	25
Ce	227	85	39	53	49
Sm	23	6.8	3.1	4.3	3.5
Eu	5.3	1.7	0.62	0.85	0.73
Tb	3.7	1.1	0.47	0.54	0.39
Yb	14	5.6	2.0	2.3	1.9
Lu	2.5	0.82	0.29	0.32	0.29

MOZAAN PELITES-WIT MFOLOZI RIVER (MWM)

	Po 58	Po 59	Po 60	Po 61	Po 62
K2O/Na2O	158	71	6.8	10	10
SiO2/Al2O3	2.0	3.2	4.5	3.1	3.5
Th/U	3.7	3.4	4.1	4.1	4.6
K/Rb	157	169	200	194	198
Rb/Sr	36	24	4.4	5.1	6.2
Ba/Rb	1.4	1.8	3.3	3.1	2.3
Ba/Sr	49	43	15	16	14
Th/Sc	0.47	0.51	0.51	0.41	0.40
La/Sc	2.9	2.3	1.7	1.6	1.7
La/Th	6.2	4.6	3.3	4.0	4.2
Zr/Y	5.6	6.6	12	8.9	11
Ti/Zr	9.2	14	14	22	21
Zr/Nb	21	16	21	12	15
Ni/Co	2.2	3.5	5.8	4.5	7.0
Cr/V	0.18	0.88	1.6	2.8	3.2
V/Ni	7.4	5.5	3.6	1.5	0.80
Cr/Ni	1.4	4.9	5.6	4.2	2.5
Cr/Zr	0.05	0.63	1.5	1.8	1.7
Sc/Th	2.1	2.0	2.0	2.5	2.5
Co/Th	0.87	1.4	2.0	2.9	3.5
La/Yb	6.6	7.5	10	11	13
Eu/Eu*	0.70	0.75	0.61	0.63	0.68
CIA	72	73	72	79	80

MOZAAN PELITES-WIT MFOLOZI RIVER (MWM)

	Po 63	Po 64	Po 65	Po 66	Po 67
SiO2	60.50	58.11	59.24	58.63	51.80
TiO2	0.90	0.87	0.88	0.91	0.53
Al2O3	20.17	20.91	20.78	20.67	12.18
Fe2O3-T	5.35	5.63	5.54	6.61	26.71
MgO	0.76	0.59	0.35	0.27	3.03
CaO	0.07	0.08	0.16	0.09	0.16
Na2O	0.18	0.09	0.09	0.08	0.07
K2O	6.49	7.31	7.20	7.18	0.05
MnO	0.13	0.62	0.42	0.60	0.31
P2O5	0.04	0.69	0.02	0.04	0.16
LOI	3.78	4.09	3.94	3.55	4.39
TOTAL	98.37	98.99	98.54	98.63	99.39
Rb	270	283	282	283	4.7
Ba	552	586	457	288	<25
Cs	15	15	3.2	8.3	ND
Sr	32	41	36	38	11
Pb	10	15	15	<9.8	<9.8
Th	10	11	7.4	5.5	3.8
U	2.3	2.2	1.8	1.2	0.51
Sc	23	24	17	11	10
V	142	139	132	139	118
Cr	591	598	411	244	239
Co	16	45	12	8.2	14
Ni	89	104	91	89	110
Y	28	34	30	32	17
Zr	261	227	211	237	98
Nb	16	16	17	17	7.2
Hf	8.9	8.4	6.1	4.1	2.1
Ta	1.4	1.4	1.3	0.77	0.48
La	45	54	31	23	20
Ce	93	107	63	48	40
Sm	5.0	7.8	5.0	3.7	3.3
Eu	1.4	1.9	1.2	0.80	0.76
Tb	0.79	0.97	0.60	0.44	0.54
Yb	2.8	2.9	2.3	1.6	1.5
Lu	0.45	0.46	0.36	0.24	0.20

MOZAAN PELITES-WIT MFOLOZI RIVER (MWM)

	Po 63	Po 64	Po 65	Po 66	Po 67
K2O/Na2O	36	81	80	90	0.71
SiO2/Al2O3	3.0	2.8	2.9	2.8	4.3
Th/U	4.3	5.0	4.1	4.6	7.5
K/Rb	200	214	212	211	88
Rb/Sr	8.4	6.9	7.8	7.4	0.43
Ba/Rb	2.0	2.1	1.6	1.0	<5.3
Ba/Sr	17	14	13	7.6	<2.3
Th/Sc	0.43	0.46	0.44	0.50	0.38
La/Sc	2.0	2.3	1.8	2.1	2.0
La/Th	4.5	4.9	4.2	4.2	5.3
Zr/Y	9.3	6.7	7.0	7.4	5.8
Ti/Zr	21	23	25	23	32
Zr/Nb	16	14	12	14	14
Ni/Co	5.6	2.3	7.6	11	7.9
Cr/V	4.2	4.3	3.1	1.8	2.0
V/Ni	1.6	1.3	1.5	1.6	1.1
Cr/Ni	6.6	5.8	4.5	2.7	2.2
Cr/Zr	2.3	2.6	1.9	1.0	2.4
Sc/Th	2.3	2.2	2.3	2.0	2.6
Co/Th	1.6	4.1	1.6	1.5	3.7
La/Yb	16	19	13	14	13
Eu/Eu*	0.85	0.78	0.77	0.70	0.69
CIA	73	72	72	72	99

MOZAAN PELITES-WIT MFOLOZI RIVER (MWM)

	P 28	P 31	P 34
SiO2	59.88	45.10	54.67
TiO2	0.86	0.63	1.06
Al2O3	26.99	14.77	24.26
Fe2O3-T	1.00	30.50	4.90
MgO	0.35	4.98	1.65
CaO	0.11	<0.01	0.05
Na2O	0.71	0.56	0.27
K2O	7.15	0.01	8.58
MnO	0.03	0.31	0.70
P2O5	0.10	<0.002	0.04
LOI	3.61	4.85	4.30
TOTAL	100.79	101.71	100.48
Rb	212	<3.0	332
Ba	519	<25	611
Cs	5.2	<0.5	17
Sr	55	<3.0	46
Pb	12	17	12
Th	8.7	6.3	10
U	2.0	1.2	2.2
Sc	19	24	21
V	138	159	170
Cr	334	496	582
Co	2.8	34	27
Ni	36	164	122
Y	38	14	36
Zr	174	123	225
Nb	20	9.8	19
Hf	5.1	4.1	7.0
Ta	1.6	0.81	1.5
La	38	33	50
Ce	80	68	100
Sm	7.7	4.5	7.0
Eu	1.5	1.1	1.6
Tb	1.2	0.53	0.81
Yb	3.1	2.4	2.5
Lu	0.44	0.41	0.45

MOZAAN PELITES-WIT MFOLOZI RIVER (MWM)

	P 28	P 31	P 34
K2O/Na2O	10	<0.02	32
SiO2/Al2O3	2.2	3.1	2.3
Th/U	4.4	5.3	4.5
K/Rb	280	-	215
Rb/Sr	3.9	-	7.2
Ba/Rb	2.4	-	1.8
Ba/Sr	9.4	-	13
Th/Sc	0.46	0.26	0.48
La/Sc	2.0	1.4	2.4
La/Th	4.4	5.2	5.0
Zr/Y	4.6	8.8	6.3
Ti/Zr	30	31	28
Zr/Nb	8.7	13	12
Ni/Co	13	4.8	4.5
Cr/V	2.4	3.1	3.4
V/Ni	3.8	0.97	1.4
Cr/Ni	9.3	3.0	4.8
Cr/Zr	1.9	4.0	2.6
Sc/Th	2.2	3.8	2.1
Co/Th	0.32	5.4	2.7
La/Yb	12	14	20
Eu/Eu*	0.59	0.79	0.74
CIA	75	94	71

NSUZE PELITES-UPPER WIT MFOLOZI (NUWM)

SAMPLE	AVG	STD
SiO2	64.24	3.00
TiO2	0.57	0.10
Al2O3	15.61	2.53
Fe2O3-T	6.06	0.68
MgO	2.97	0.40
CaO	0.96	0.85
Na2O	0.07	0.02
K2O	4.83	1.03
MnO	0.11	0.03
P2O5	0.15	0.05
LOI	3.62	0.73
TOTAL	99.19	0.94
Rb	193	39
Ba	639	165
Cs	5.2	1.1
Sr	21	11
Pb	9.9	1.3
Th	7.2	1.7
U	2.5	0.6
Sc	13	4
V	134	28
Cr	189	51
Co	17	4
Ni	88	6
Y	28	6
Zr	145	20
Nb	15	2
Hf	3.9	0.7
Ta	1.1	0.2
La	20	9
Ce	42	16
Sm	3.4	1.1
Eu	0.76	0.26
Tb	0.63	0.21
Yb	2.1	0.5
Lu	0.30	0.08

NSUZE PELITES-UPPER WIT MFOLOZI (NUWM)

SAMPLE	AVG	STD
K2O/Na2O	73	23
SiO2/Al2O3	4.3	0.9
Th/U	3.0	0.5
K/Rb	208	9
Rb/Sr	11	4
Ba/Rb	3.3	0.4
Ba/Sr	38	17
Th/Sc	0.57	0.05
La/Sc	1.6	0.5
La/Th	5.7	2.3
Zr/Y	5.3	0.9
Ti/Zr	24	2
Zr/Nb	9.6	0.7
Ni/Co	5.7	2.3
Cr/V	1.4	0.3
V/Ni	1.5	0.3
Cr/Ni	2.1	0.5
Cr/Zr	1.3	0.3
Sc/Th	1.8	0.1
Co/Th	2.5	0.7
La/Yb	9.7	3
Eu/Eu*	0.64	0.04
CIA	75	2

NSUZE PELITES-UPPER WIT MFOLOZI (NUWM)

SAMPLE	Po 32	Po 33	Po 34	Po 35	Po 36
SiO2	62.37	68.98	67.14	61.03	64.67
TiO2	0.69	0.45	0.44	0.69	0.55
Al2O3	17.59	12.74	12.02	19.15	15.58
Fe2O3-T	5.65	6.48	6.22	7.24	5.59
MgO	2.49	3.08	2.38	3.51	3.17
CaO	0.19	0.37	2.53	0.35	0.67
Na2O	0.07	0.11	0.04	0.06	0.10
K2O	5.60	3.48	3.28	5.75	5.33
MnO	0.07	0.11	0.15	0.08	0.12
P2O5	0.13	0.12	0.12	0.26	0.11
LOI	3.94	3.33	3.32	2.73	3.36
TOTAL	98.79	99.25	97.64	100.85	99.25
Rb	231	144	136	232	196
Ba	776	469	466	920	560
Cs	6.6	3.8	4.1	6.3	4.4
Sr	13	11	16	16	25
Pb	11	<9.8	10	<9.8	<9.8
Th	9.7	5.5	6.4	9.1	5.1
U	3.6	1.9	2.0	2.6	2.4
Sc	18	8.7	10	16	9.1
V	169	103	97	162	127
Cr	276	147	173	229	122
Co	15	18	21	19	9.1
Ni	91	84	80	94	95
Y	29	25	24	40	24
Zr	178	121	119	151	149
Nb	16	13	13	17	15
Hf	5.1	3.1	3.7	4.2	3.2
Ta	1.4	0.84	1.0	1.2	0.89
La	35	18	21	27	9.9
Ce	71	38	46	49	23
Sm	5.0	3.2	3.5	4.6	2.0
Eu	1.1	0.64	0.74	1.1	0.42
Tb	0.81	0.59	0.52	0.99	0.37
Yb	2.3	1.8	2.0	3.0	1.4
Lu	0.39	0.24	0.28	0.43	0.22

NSUZE PELITES-UPPER WIT MFOLOZI (NUWM)

SAMPLE	Po 32	Po 33	Po 34	Po 35	Po 36
K2O/Na2O	80	32	82	96	53
SiO2/Al2O3	3.5	5.4	5.6	3.2	4.2
Th/U	2.7	2.9	3.2	3.5	2.1
K/Rb	201	201	200	206	226
Rb/Sr	18	13	8.5	15	7.8
Ba/Rb	3.4	3.3	3.4	4.0	2.9
Ba/Sr	60	43	29	58	22
Th/Sc	0.54	0.64	0.64	0.57	0.56
La/Sc	1.9	2.1	2.1	1.7	1.1
La/Th	3.6	3.3	3.3	3.0	1.9
Zr/Y	6.1	4.8	5.0	3.8	6.2
Ti/Zr	23	22	22	27	22
Zr/Nb	11	9.3	9.2	8.9	9.9
Ni/Co	6.1	4.7	3.8	4.9	10
Cr/V	1.6	1.4	1.8	1.4	1.0
V/Ni	1.9	1.2	1.2	1.7	1.3
Cr/Ni	3.0	1.8	2.2	2.4	1.3
Cr/Zr	1.6	1.2	1.5	1.5	0.82
Sc/Th	1.9	1.6	1.6	1.8	1.8
Co/Th	1.5	3.3	3.3	2.1	1.8
La/Yb	15	10	11	9.0	7.1
Eu/Eu*	0.66	0.58	0.65	0.67	0.61
CIA	74	76	77	75	72

NSUZE PELITES-UPPER WIT MFOLOZI (NUWM)

SAMPLE	Po 37
SiO2	61.23
TiO2	0.62
Al2O3	16.56
Fe2O3-T	5.16
MgO	3.17
CaO	1.65
Na2O	0.06
K2O	5.54
MnO	0.13
P2O5	0.16
LOI	5.05
TOTAL	99.33
Rb	217
Ba	640
Cs	5.9
Sr	43
Pb	12
Th	7.6
U	2.3
Sc	15
V	148
Cr	184
Co	21
Ni	84
Y	26
Zr	151
Nb	16
Hf	4.2
Ta	1.1
La	12
Ce	26
Sm	2.3
Eu	0.57
Tb	0.51
Yb	1.9
Lu	0.27

NSUZE PELITES-UPPER WIT MFOLOZI (NUWM)

SAMPLE	Po 37
K2O/Na2O	92
SiO2/Al2O3	3.7
Th/U	3.3
K/Rb	212
Rb/Sr	5.0
Ba/Rb	2.9
Ba/Sr	15
Th/Sc	0.51
La/Sc	0.80
La/Th	1.6
Zr/Y	5.8
Ti/Zr	25
Zr/Nb	9.4
Ni/Co	4.0
Cr/V	1.2
V/Ni	1.8
Cr/Ni	2.2
Cr/Zr	1.2
Sc/Th	2.0
Co/Th	2.8
La/Yb	6.3
Eu/Eu*	0.68
CIA	73

NSUZE PELITES-LOWER WIT MFOLOZI (NLWM)

SAMPLE	AVG	STD
SiO2	58.75	0.88
TiO2	0.76	0.03
Al2O3	20.62	0.33
Fe2O3-T	6.57	0.63
MgO	3.26	0.83
CaO	0.04	0.03
Na2O	0.19	0.14
K2O	4.70	0.29
MnO	0.06	0.03
P2O5	0.09	0.02
LOI	4.64	0.30
TOTAL	99.67	0.40
Rb	162	11
Ba	446	49
Cs	6.4	0.8
Sr	50	11
Pb	29	14
Th	13	1
U	4.7	0.3
Sc	24	2
V	190	8
Cr	709	89
Co	19	4
Ni	144	16
Y	33	2
Zr	144	8
Nb	17	1
Hf	4.3	0.4
Ta	1.4	0.1
La	47	10
Ce	87	24
Sm	6.2	1.2
Eu	1.4	0.3
Tb	0.97	0.11
Yb	3.0	0.3
Lu	0.46	0.05

NSUZE PELITES-LOWER WIT MFOLOZI (NLWM)

SAMPLE	AVG	STD
K2O/Na2O	33	15
SiO2/Al2O3	2.8	0.1
Th/U	2.7	0.1
K/Rb	241	3
Rb/Sr	3.4	0.8
Ba/Rb	2.7	0.2
Ba/Sr	9.3	1.9
Th/Sc	0.55	0.02
La/Sc	2.0	0.3
La/Th	3.6	0.6
Zr/Y	4.4	0.3
Ti/Zr	32	1
Zr/Nb	8.3	0.5
Ni/Co	8.0	1.8
Cr/V	3.8	0.5
V/Ni	1.3	0.2
Cr/Ni	5.0	0.7
Cr/Zr	5.0	0.7
Sc/Th	1.8	0.1
Co/Th	1.4	0.2
La/Yb	15	2
Eu/Eu*	0.69	0.03
CIA	79	1

NSUZE PELITES-LOWER WIT MFOLOZI (NLWM)

SAMPLE	Po 83	Po 84	Po 85	Po 86	Po 87
SiO2	59.51	58.74	58.81	58.00	57.74
TiO2	0.79	0.72	0.75	0.74	0.74
Al2O3	20.83	21.03	20.95	20.23	20.18
Fe2O3-T	6.01	6.21	6.12	7.14	7.43
MgO	2.67	3.49	3.75	4.21	3.67
CaO	0.04	0.02	0.02	0.03	0.04
Na2O	0.12	0.07	0.62	0.21	0.19
K2O	4.99	4.87	4.95	4.40	4.24
MnO	0.09	0.04	0.04	0.09	0.10
P2O5	0.11	0.07	0.08	0.09	0.11
LOI	4.90	4.40	4.46	4.59	5.03
TOTAL	100.06	99.66	100.55	99.73	99.47
Rb	172	167	172	153	148
Ba	505	464	510	463	394
Cs	7.5	6.3	7.2	6.5	5.5
Sr	58	41	50	52	65
Pb	51	24	15	30	45
Th	13	13	15	14	12
U	5.0	5.0	5.1	4.8	4.1
Sc	23	22	27	28	22
V	187	178	187	184	186
Cr	652	647	726	951	807
Co	15	18	23	26	17
Ni	162	127	144	151	165
Y	32	28	33	35	34
Zr	146	136	139	150	134
Nb	19	18	18	18	16
Hf	4.4	3.8	4.8	5.1	3.8
Ta	1.5	1.4	1.5	1.5	1.3
La	47	29	67	54	46
Ce	75	58	140	110	76
Sm	5.7	3.8	9.0	7.2	6.3
Eu	1.3	0.94	2.1	1.7	1.4
Tb	1.0	0.77	1.2	1.0	0.92
Yb	3.0	2.6	3.5	3.3	2.7
Lu	0.46	0.39	0.52	0.55	0.42

NSUZE PELITES-LOWER WIT MFOLOZI (NLWM)

SAMPLE	Po 83	Po 84	Po 85	Po 86	Po 87
K2O/Na2O	42	70	8.0	21	22
SiO2/Al2O3	2.9	2.8	2.8	2.9	2.9
Th/U	2.5	2.6	2.9	2.9	2.9
K/Rb	241	242	239	239	238
Rb/Sr	3.0	4.1	3.4	2.9	2.3
Ba/Rb	2.9	2.8	3.0	3.0	2.7
Ba/Sr	8.7	11	10	8.9	6.1
Th/Sc	0.55	0.59	0.56	0.50	0.55
La/Sc	2.0	1.3	2.5	1.9	2.1
La/Th	3.7	2.2	4.5	3.9	3.8
Zr/Y	4.6	4.9	4.2	4.3	4.0
Ti/Zr	32	32	32	30	33
Zr/Nb	7.7	7.6	7.7	8.3	8.4
Ni/Co	11	7.1	6.3	5.8	9.7
Cr/V	3.5	3.6	3.9	5.2	4.3
V/Ni	1.2	1.4	1.3	1.2	1.1
Cr/Ni	4.0	5.1	5.0	6.3	4.9
Cr/Zr	4.5	4.8	5.2	6.3	6.0
Sc/Th	1.8	1.7	1.8	2.0	1.8
Co/Th	1.2	1.4	1.5	1.9	1.4
La/Yb	16	11	19	16	17
Eu/Eu*	0.67	0.70	0.73	0.74	0.69
CIA	79	80	77	80	80

NSUZE PELITES-LOWER WIT MFOLOZI (NLWM)

SAMPLE	Po 88	Po 89	Po 90	Po 91	Po 92
SiO2	58.31	60.71	59.06	59.57	58.26
TiO2	0.79	0.79	0.79	0.75	0.75
Al2O3	20.88	20.41	20.51	20.77	20.92
Fe2O3-T	5.94	5.94	6.68	6.42	6.48
MgO	3.42	1.39	3.06	2.45	3.24
CaO	0.11	0.04	0.01	0.04	0.02
Na2O	0.13	0.14	0.11	0.21	0.14
K2O	5.06	4.81	4.60	4.77	4.81
MnO	0.11	0.02	0.03	0.03	0.04
P2O5	0.10	0.10	0.09	0.13	0.08
LOI	4.31	5.25	4.30	4.74	4.44
TOTAL	99.17	99.60	99.24	99.88	99.18
Rb	178	166	156	167	162
Ba	475	483	376	453	425
Cs	7.0	6.9	5.6	6.7	6.0
Sr	39	68	39	64	36
Pb	42	35	18	37	11
Th	13	13	13	12	13
U	4.8	4.8	5.1	4.2	4.9
Sc	23	24	24	22	23
V	196	182	204	185	191
Cr	687	659	627	664	694
Co	22	18	16	14	16
Ni	151	138	118	162	117
Y	34	30	35	33	33
Zr	143	157	157	139	145
Nb	17	18	17	17	17
Hf	4.3	4.8	4.5	3.9	4.1
Ta	1.4	1.5	1.4	1.4	1.4
La	39	41	54	49	49
Ce	81	63	110	68	99
Sm	5.8	5.4	7.1	5.8	6.7
Eu	1.4	1.3	1.5	1.3	1.4
Tb	0.99	0.93	1.1	0.98	0.91
Yb	2.9	3.0	3.3	2.9	3.1
Lu	0.44	0.46	0.49	0.41	0.46

NSUZE PELITES-LOWER WIT MFOLOZI (NLWM)

SAMPLE	Po 88	Po 89	Po 90	Po 91	Po 92
K2O/Na2O	39	34	42	23	34
SiO2/Al2O3	2.8	3.0	2.9	2.9	2.8
Th/U	2.7	2.7	2.5	2.9	2.7
K/Rb	236	241	245	237	246
Rb/Sr	4.6	2.4	4.0	2.6	4.5
Ba/Rb	2.7	2.9	2.4	2.7	2.6
Ba/Sr	12	7.1	9.6	7.1	12
Th/Sc	0.57	0.54	0.54	0.55	0.57
La/Sc	1.7	1.7	2.3	2.2	2.1
La/Th	3.0	3.2	4.2	4.1	3.8
Zr/Y	4.2	5.2	4.5	4.2	4.4
Ti/Zr	33	30	30	32	31
Zr/Nb	8.4	8.7	9.2	8.2	8.5
Ni/Co	6.9	7.7	7.4	12	7.3
Cr/V	3.5	3.6	3.1	3.6	3.6
V/Ni	1.3	1.3	1.7	1.1	1.6
Cr/Ni	4.5	4.8	5.3	4.1	5.9
Cr/Zr	4.8	4.2	4.0	4.8	4.8
Sc/Th	1.8	1.8	1.8	1.8	1.8
Co/Th	1.7	1.4	1.2	1.2	1.2
La/Yb	13	14	16	17	16
Eu/Eu*	0.72	0.71	0.64	0.67	0.66
CIA	79	79	80	79	79

NSUZE PELITES-LOWER WIT MFOLOZI (NLWM)

SAMPLE	Po 93
SiO2	57.57
TiO2	0.73
Al2O3	20.10
Fe2O3-T	7.90
MgO	4.54
CaO	0.02
Na2O	0.13
K2O	4.15
MnO	0.05
P2O5	0.08
LOI	4.57
TOTAL	99.84
Rb	141
Ba	356
Cs	4.8
Sr	40
Pb	9.9
Th	12
U	4.3
Sc	22
V	206
Cr	690
Co	20
Ni	146
Y	33
Zr	135
Nb	16
Hf	3.8
Ta	1.2
La	38
Ce	76
Sm	5.9
Eu	1.3
Tb	0.87
Yb	2.8
Lu	0.44

NSUZE PELITES-LOWER WIT MFOLOZI (NLWM)

SAMPLE	Po 93
K2O/Na2O	32
SiO2/Al2O3	2.9
Th/U	2.8
K/Rb	244
Rb/Sr	3.5
Ba/Rb	2.5
Ba/Sr	8.9
Th/Sc	0.55
La/Sc	1.7
La/Th	3.2
Zr/Y	4.1
Ti/Zr	32
Zr/Nb	8.4
Ni/Co	7.3
Cr/V	3.3
V/Ni	1.4
Cr/Ni	4.7
Cr/Zr	5.1
Sc/Th	1.8
Co/Th	1.7
La/Yb	14
Eu/Eu*	0.68
CIA	81

NSUZE PELITES-MPONGOZA RIVER (NMP)

SAMPLE	AVG	STD
SiO2	56.23	3.83
TiO2	1.19	0.15
Al2O3	24.45	2.38
Fe2O3-T	6.22	0.79
MgO	1.11	0.85
CaO	0.03	0.02
Na2O	0.36	0.14
K2O	5.98	0.65
MnO	0.04	0.02
P2O5	0.04	0.02
LOI	4.47	0.71
TOTAL	100.11	0.56
Rb	200	23
Ba	260	65
Cs	2.7	0.4
Sr	25	5
Pb	13	6
Th	10.0	1.8
U	3.2	0.9
Sc	27	5
V	223	19
Cr	455	78
Co	19	8
Ni	149	20
Y	43	6
Zr	229	37
Nb	19	3
Hf	6.3	1.3
Ta	1.4	0.2
La	43	18
Ce	83	36
Sm	7.4	3.1
Eu	1.7	0.6
Tb	1.2	0.3
Yb	3.6	0.7
Lu	0.56	0.10

NSUZE PELITES-MPONGOZA RIVER (NMP)

SAMPLE	AVG	STD
K2O/Na2O	19	7
SiO2/Al2O3	2.3	0.4
Th/U	3.2	0.5
K/Rb	248	6
Ba/Sr	8.1	1.6
Ba/Rb	1.3	0.3
Ba/Sr	11	4
Th/Sc	0.37	0.06
La/Sc	1.6	0.6
La/Th	4.2	1.5
Zr/Y	5.4	1.2
Ti/Zr	31	3
Zr/Nb	12	2
Ni/Co	11	11
Cr/V	2.0	0.3
V/Ni	1.5	0.3
Cr/Ni	3.1	0.6
Cr/Zr	2.0	0.3
Sc/Th	2.8	0.4
Co/Th	2.0	1.0
La/Yb	11	4
Eu/Eu*	0.70	0.06
CIA	78	1

NSUZE PELITES-MPONGOZA RIVER (NMP)

SAMPLE	Po 101	Po 102	Po 103	Po 104	Po 105
SiO2	56.88	54.19	57.76	55.80	54.68
TiO2	1.15	1.19	1.14	1.13	1.25
Al2O3	24.73	25.26	23.88	25.01	25.57
Fe2O3-T	5.57	6.91	5.73	5.88	5.63
MgO	<0.01	0.54	<0.01	<0.01	0.94
CaO	0.01	0.02	0.05	0.01	0.02
Na2O	0.26	0.25	0.27	0.26	0.27
K2O	6.12	6.05	5.85	6.20	6.48
MnO	<0.002	0.03	0.01	0.01	0.04
P2O5	0.03	0.07	0.04	0.04	0.02
LOI	4.62	5.91	4.78	4.63	5.38
TOTAL	99.37	100.42	99.51	98.97	100.28
Rb	208	199	197	206	218
Ba	172	240	247	310	301
Cs	2.0	2.9	2.4	3.3	2.7
Sr	27	39	28	28	24
Pb	11	<9.8	<9.8	<9.8	<9.8
Th	6.8	11	9.2	12	9.7
U	2.2	3.1	2.7	3.2	3.3
Sc	20	31	28	37	25
V	229	247	233	234	213
Cr	308	446	377	568	434
Co	2.8	19	9.7	10	20
Ni	142	122	137	137	143
Y	46	46	46	40	53
Zr	198	223	194	211	228
Nb	20	19	19	20	24
Hf	3.8	6.3	4.8	7.5	5.6
Ta	1.0	1.4	1.2	1.5	1.6
La	18	51	31	26	60
Ce	33	102	61	58	120
Sm	3.3	7.4	6.6	5.1	11
Eu	0.89	1.8	1.4	1.5	2.5
Tb	0.96	1.4	1.3	1.3	1.6
Yb	2.7	3.8	3.6	4.3	4.0
Lu	0.42	0.58	0.57	0.70	0.60

NSUZE PELITES-MPONGOZA RIVER (NMP)

SAMPLE	Po 101	Po 102	Po 103	Po 104	Po 105
K2O/Na2O	24	24	22	24	24
SiO2/Al2O3	2.3	2.1	2.4	2.2	2.1
Th/U	3.1	3.5	3.4	3.8	2.9
K/Rb	244	252	246	250	247
Ba/Sr	7.7	5.1	7.0	7.4	9.1
Ba/Rb	0.83	1.2	1.3	1.5	1.4
Ba/Sr	6.4	6.2	8.8	11	13
Th/Sc	0.34	0.35	0.33	0.32	0.39
La/Sc	0.90	1.6	1.1	0.70	2.4
La/Th	2.6	4.6	3.4	2.2	6.2
Zr/Y	4.3	4.8	4.2	5.3	4.3
Ti/Zr	35	32	35	32	33
Zr/Nb	10	12	10	11	10
Ni/Co	51	6.4	14	14	7.2
Cr/V	1.3	1.8	1.6	2.4	2.0
V/Ni	1.6	2.0	1.7	1.7	1.5
Cr/Ni	2.2	3.7	2.8	4.1	3.0
Cr/Zr	1.6	2.0	1.9	2.7	1.9
Sc/Th	2.9	2.8	3.0	3.1	2.6
Co/Th	0.41	1.7	1.1	0.83	2.1
La/Yb	6.7	13	8.6	6.0	15
Eu/Eu*	0.76	0.70	0.61	0.78	0.70
CIA	78	78	78	78	77

NSUZE PELITES-MPONGOZA RIVER (NMP)

SAMPLE	Po 106	Po 107	P 54	P 55	P 56
SiO2	58.69	59.20	56.68	56.46	55.78
TiO2	1.13	1.04	1.01	1.11	1.19
Al2O3	23.00	22.60	22.33	24.76	25.21
Fe2O3-T	5.70	5.92	8.39	5.61	6.04
MgO	0.29	<0.01	2.46	1.10	1.38
CaO	0.06	0.04	0.03	0.01	0.02
Na2O	0.21	0.19	0.38	0.42	0.63
K2O	5.65	5.48	5.73	6.29	5.85
MnO	0.03	0.01	0.08	0.03	0.05
P2O5	0.06	0.05	0.04	0.04	0.03
LOI	5.17	4.53	3.67	4.36	4.25
TOTAL	99.99	99.06	100.80	100.19	100.43
Rb	188	185	203	206	206
Ba	192	240	421	242	267
Cs	2.8	2.9	1.8	2.6	2.8
Sr	30	28	18	22	21
Pb	<9.8	28	15	16	15
Th	10	8.2	8.7	8.8	9.0
U	2.9	2.5	2.8	2.3	4.3
Sc	26	27	26	28	21
V	237	218	209	227	199
Cr	419	406	389	448	410
Co	15	22	38	18	23
Ni	108	152	175	164	172
Y	45	42	31	43	40
Zr	226	215	188	198	246
Nb	19	16	16	19	20
Hf	5.8	6.1	5.1	5.0	6.4
Ta	1.3	1.2	1.3	1.3	1.5
La	56	42	14	33	15
Ce	132	62	22	66	30
Sm	14	6.7	2.3	6.5	3.4
Eu	3.0	1.6	0.67	1.4	0.70
Tb	1.4	1.2	0.68	1.1	0.94
Yb	3.5	3.3	2.6	3.4	3.5
Lu	0.50	0.50	0.44	0.51	0.50

NSUZE PELITES-MPONGOZA RIVER (NMP)

SAMPLE	Po 106	Po 107	P 54	P 55	P 56
K2O/Na2O	27	29	15	15	9.3
SiO2/Al2O3	2.6	2.6	2.5	2.3	2.2
Th/U	3.4	3.3	3.1	3.8	2.1
K/Rb	249	246	234	253	236
Ba/Sr	6.3	6.6	11	9.4	9.8
Ba/Rb	1.0	1.3	2.1	1.2	1.3
Ba/Sr	6.4	8.6	23	11	13
Th/Sc	0.38	0.30	0.33	0.31	0.43
La/Sc	2.2	1.6	0.54	1.2	0.71
La/Th	5.6	5.1	1.6	3.8	1.7
Zr/Y	5.0	5.1	6.1	4.6	6.2
Ti/Zr	30	29	32	34	29
Zr/Nb	12	13	12	10	12
Ni/Co	7.2	6.9	4.6	9.1	7.5
Cr/V	1.8	1.9	1.9	2.0	2.1
V/Ni	2.2	1.4	1.2	1.4	1.2
Cr/Ni	3.9	2.7	2.2	2.7	2.4
Cr/Zr	1.9	1.9	2.1	2.3	1.7
Sc/Th	2.6	3.3	3.0	3.2	2.3
Co/Th	1.5	2.7	4.4	2.0	2.6
La/Yb	16	13	5.4	9.7	4.3
Eu/Eu*	0.71	0.70	0.82	0.64	0.57
CIA	78	78	77	77	77

NSUZE PELITES-MPONGOZA RIVER (NMP)

SAMPLE	P 57	P 58	P 59	P 60	P 61
SiO2	49.96	58.92	49.10	53.50	55.61
TiO2	1.50	1.21	1.58	1.18	1.17
Al2O3	28.42	23.19	28.98	25.81	24.07
Fe2O3-T	6.94	5.24	6.15	6.74	7.23
MgO	1.61	1.76	2.21	2.02	1.92
CaO	0.01	0.02	0.01	0.01	0.08
Na2O	0.58	0.20	0.42	0.34	0.45
K2O	6.87	5.78	7.28	6.20	5.64
MnO	0.05	0.05	0.08	0.05	0.06
P2O5	0.04	0.03	0.03	0.04	0.10
LOI	4.63	3.68	4.61	4.48	4.03
TOTAL	100.61	100.08	100.45	100.37	100.36
Rb	228	192	244	207	186
Ba	278	213	363	254	263
Cs	2.9	2.8	3.3	2.8	3.0
Sr	25	21	25	26	27
Pb	17	11	<9.8	15	17
Th	13	11	13	11	11
U	4.0	3.2	6.3	3.0	3.0
Sc	26	25	27	32	38
V	227	208	245	245	229
Cr	569	426	589	509	560
Co	19	22	25	17	23
Ni	169	118	178	161	153
Y	51	37	46	43	48
Zr	259	225	340	217	222
Nb	23	21	24	17	18
Hf	6.9	6.2	9.3	6.2	7.5
Ta	1.7	1.7	2.0	1.4	1.5
La	55	47	68	61	67
Ce	108	93	128	104	134
Sm	9.8	8.0	11	7.9	9.6
Eu	2.2	1.7	2.1	1.8	2.4
Tb	1.5	1.0	1.2	1.3	1.6
Yb	4.9	3.0	4.1	4.0	4.7
Lu	0.68	0.47	0.66	0.59	0.74

NSUZE PELITES-MPONGOZA RIVER (NMP)

SAMPLE	P 57	P 58	P 59	P 60	P 61
K2O/Na2O	12	28.9	17.3	18.2	12.5
SiO2/Al2O3	1.8	2.5	1.7	2.1	2.3
Th/U	3.3	3.4	2.1	3.7	3.7
K/Rb	250	250	248	249	252
Ba/Sr	9.1	9.1	9.8	8.0	6.9
Ba/Rb	1.2	1.1	1.5	1.2	1.4
Ba/Sr	11	10	15	9.8	9.7
Th/Sc	0.50	0.44	0.48	0.34	0.29
La/Sc	2.1	1.9	2.5	1.9	1.8
La/Th	4.2	4.3	5.2	5.5	6.1
Zr/Y	5.1	6.1	7.4	5.0	4.6
Ti/Zr	35	32	28	33	32
Zr/Nb	11	11	14	13	12
Ni/Co	8.9	5.4	7.1	9.5	6.7
Cr/V	2.5	2.0	2.4	2.1	2.4
V/Ni	1.3	1.8	1.4	1.5	1.5
Cr/Ni	3.4	3.6	3.3	3.2	3.7
Cr/Zr	2.2	1.9	1.7	2.3	2.5
Sc/Th	2.0	2.3	2.1	2.9	3.5
Co/Th	1.5	2.0	1.9	1.5	2.1
La/Yb	11	16	17	15	14
Eu/Eu*	0.69	0.68	0.62	0.68	0.75
CIA	80	78	77	78	78

NSUZE PELITES-MPONGOZA RIVER (NMP)

SAMPLE	P 62
SiO2	66.44
TiO2	1.00
Al2O3	18.31
Fe2O3-T	5.87
MgO	1.59
CaO	0.01
Na2O	0.58
K2O	4.19
MnO	0.05
P2O5	0.04
LOI	2.73
TOTAL	100.81
Rb	133
Ba	159
Cs	2.2
Sr	18
Pb	20
Th	6.9
U	2.9
Sc	20
V	173
Cr	414
Co	26
Ni	153
Y	31
Zr	277
Nb	16
Hf	8.1
Ta	1.3
La	36
Ce	71
Sm	5.7
Eu	1.4
Tb	0.94
Yb	2.8
Lu	0.46

NSUZE PELITES-MPONGOZA RIVER (NMP)

SAMPLE	P 62
K2O/Na2O	7.2
SiO2/Al2O3	3.6
Th/U	2.4
K/Rb	261
Ba/Sr	7.4
Ba/Rb	1.2
Ba/Sr	8.8
Th/Sc	0.35
La/Sc	1.8
La/Th	5.2
Zr/Y	8.9
Ti/Zr	22
Zr/Nb	17
Ni/Co	5.9
Cr/V	2.4
V/Ni	1.1
Cr/Ni	2.7
Cr/Zr	1.5
Sc/Th	2.9
Co/Th	3.8
La/Yb	13
Eu/Eu*	0.74
CIA	77

NSUZE PELITES VUTSHINI RIVER (NVS)

SAMPLE	AVG	STD
SiO2	70.71	8.82
TiO2	0.46	0.18
Al2O3	13.56	4.46
Fe2O3-T	5.59	5.35
MgO	1.58	0.64
CaO	0.01	0.00
Na2O	0.35	0.17
K2O	3.24	2.20
MnO	0.04	0.02
P2O5	0.02	0.02
LOI	2.47	0.97
TOTAL	98.03	0.88
Rb	118	83
Ba	460	139
Cs	1.9	0.4
Sr	14	1
Pb	13	5
Th	5.2	0.9
U	1.4	0.3
Sc	8.0	4.5
V	68	38
Cr	386	256
Co	9.5	5.9
Ni	74	42
Y	19	3
Zr	186	25
Nb	6.8	1.7
Hf	6.8	1.6
Ta	0.68	0.13
La	27	13
Ce	51	25
Sm	3.6	1.1
Eu	0.80	0.14
Tb	0.44	0.03
Yb	2.1	0.2
Lu	0.31	0.03

NSUZE PELITES VUTSHINI RIVER (NVS)

SAMPLE	AVG	STD
K2O/Na2O	9.2	3.2
SiO2/Al2O3	6.1	2.9
Th/U	3.7	0.7
K/Rb	231	6
Ba/Sr	8.7	6.7
Ba/Rb	5.0	1.6
Ba/Sr	33	12
Th/Sc	0.95	0.63
La/Sc	5.9	5.8
La/Th	7.8	1.2
Zr/Y	10	3
Ti/Zr	15	5
Zr/Nb	29	7
Ni/Co	7.8	1.2
Cr/V	5.4	2.9
V/Ni	0.60	0.42
Cr/Ni	4.9	2.2
Cr/Zr	1.9	1.2
Sc/Th	1.5	0.7
Co/Th	1.8	1.0
La/Yb	12	5
Eu/Eu*	0.74	0.06
CIA	77	7

NSUZE PELITES VUTSHINI RIVER (NVS)

SAMPLE	P 5	P 8	P 10
SiO2	68.17	61.40	82.56
TiO2	0.21	0.61	0.55
Al2O3	19.02	13.58	8.09
Fe2O3-T	1.19	13.12	2.46
MgO	1.15	2.48	1.10
CaO	0.01	0.01	0.01
Na2O	0.56	0.35	0.15
K2O	6.36	1.63	1.74
MnO	0.01	0.07	0.03
P2O5	0.01	0.05	<0.01
LOI	2.44	3.67	1.30
TOTAL	99.13	96.97	97.99
Rb	236	58	61
Ba	657	358	366
Cs	2.3	1.4	2.0
Sr	13	14	16
Pb	20	12	<9.8
Th	5.7	6.0	4.0
U	1.2	1.9	1.2
Sc	3.1	14	6.9
V	20	112	72
Cr	59	413	685
Co	2.6	17	9.0
Ni	18	119	85
Y	23	18	15
Zr	163	174	221
Nb	5.3	9.1	6.0
Hf	6.1	5.3	9.1
Ta	0.81	0.72	0.51
La	44	22	14
Ce	86	39	29
Sm	5.1	3.0	2.6
Eu	1.0	0.73	0.68
Tb	0.48	0.43	0.40
Yb	2.3	2.0	1.9
Lu	0.35	0.27	0.30

NSUZE PELITES VUTSHINI RIVER (NVS)

SAMPLE	P 5	P 8	P 10
K2O/Na2O	11	4.7	12
SiO2/Al2O3	3.6	4.5	10
Th/U	4.8	3.2	3.3
K/Rb	224	233	237
Ba/Sr	18	4.1	3.8
Ba/Rb	2.8	6.2	6.0
Ba/Sr	51	26	23
Th/Sc	1.8	0.43	0.58
La/Sc	14	1.6	2.0
La/Th	7.7	3.7	3.5
Zr/Y	7	9.7	15
Ti/Zr	7.7	21	15
Zr/Nb	31	19	37
Ni/Co	6.9	7.0	9.4
Cr/V	3.0	3.7	9.5
V/Ni	1.1	0.94	0.85
Cr/Ni	3.3	3.5	8.1
Cr/Zr	0.36	2.4	3.1
Sc/Th	0.5	2.3	1.7
Co/Th	0.46	2.8	2.3
La/Yb	19	11	7.4
Eu/Eu*	0.66	0.75	0.80
CIA	72	85	75

Table C.1-3

Witwatersrand Pelite Analyses

	K8 PELITES	
SAMPLE	AVG	STD
SiO2	63.26	4.30
TiO2	0.83	0.17
Al2O3	23.61	4.24
Fe2O3-T	4.14	2.98
MgO	1.82	2.26
CaO	0.13	0.18
Na2O	0.59	0.61
K2O	1.87	1.11
MnO	0.04	0.06
P2O5	0.12	0.18
LOI	4.14	0.81
TOTAL	100.34	0.37
Rb	69	39
Ba	338	182
Cs	4.0	2.6
Sr	100	91
Pb	20	6
Th	9.8	2.9
U	4.3	1.9
Sc	24	5
V	189	45
Cr	740	154
Co	52	27
Ni	418	211
Y	37	12
Zr	201	49
Nb	13	4
Hf	6.1	2.1
Ta	1.2	0.3
La	50	13
Ce	99	28
Sm	7.8	1.9
Eu	1.7	0.5
Tb	1.1	0.3
Yb	3.8	1.2
Lu	0.61	0.19

	K8 PELITES	
SAMPLE	AVG	STD
K2O/Na2O	5.8	5.8
SiO2/Al2O3	2.8	1.0
Th/U	2.5	0.6
K/Rb	238	139
Rb/Sr	0.93	0.49
Ba/Rb	5.6	3.6
Ba/Sr	4.9	3.4
Th/Sc	0.42	0.13
La/Sc	2.1	0.5
La/Th	5.2	0.8
Zr/Y	5.8	2.1
Ti/Zr	26	6
Zr/Nb	17	5
Ni/Co	11	9
Cr/V	4.2	1.5
V/Ni	0.67	0.57
Cr/Ni	2.4	1.5
Cr/Zr	3.9	1.3
Sc/Th	2.6	0.9
Co/Th	6.0	3.3
La/Yb	14	4
Eu/Eu*	0.67	0.09
CIA	89	6

K8 PELITES

SAMPLE	MEE-1	MEE-3	MEE-11	MEE-13	MEE-14
SiO2	70.80	62.47	65.98	61.00	64.26
TiO2	0.61	0.84	1.00	0.76	0.74
Al2O3	22.04	21.67	26.25	20.93	19.58
Fe2O3-T	1.44	9.73	1.29	6.99	6.98
MgO	0.28	1.55	0.30	3.42	2.80
CaO	0.02	0.03	0.04	0.15	0.07
Na2O	0.07	0.14	0.09	0.33	0.27
K2O	0.51	0.84	2.85	2.40	1.77
MnO	<0.002	0.07	<0.002	0.05	0.06
P2O5	0.05	0.06	0.07	0.80	0.06
LOI	4.50	3.06	4.87	3.92	3.52
TOTAL	100.31	100.08	100.63	100.00	100.09
Rb	40	32	27	104	68
Ba	115	671	141	482	443
Cs	1.2	1.7	1.9	5.3	5.8
Sr	224	47	44	64	38
Pb	14	16	21	24	15
Th	7.8	7.5	10	9.4	8.9
U	3.6	2.9	3.9	3.1	4.0
Sc	25	27	27	26	22
V	144	203	253	177	165
Cr	860	805	749	729	770
Co	65	52	111	54	25
Ni	763	881	335	514	517
Y	30	44	36	34	36
Zr	171	176	196	182	212
Nb	13	16	17	15	11
Hf	4.1	5.8	6.2	4.5	7.5
Ta	1.2	1.1	1.2	1.1	1.1
La	57	51	51	49	49
Ce	111	98	107	94	89
Sm	8.8	8.1	7.9	6.9	6.8
Eu	1.8	1.9	1.8	1.7	1.3
Tb	1.0	1.1	0.98	0.84	0.96
Yb	3.8	4.6	3.7	2.9	4.0
Lu	0.71	0.70	0.59	0.53	0.60

K8 PELITES

SAMPLE	MEE-1	MEE-3	MEE-11	MEE-13	MEE-14
K2O/Na2O	7.7	5.9	30.3	7.2	6.6
SiO2/Al2O3	3.2	2.9	2.5	2.9	3.3
Th/U	2.2	2.6	2.6	3.0	2.2
K/Rb	106	218	875	191	216
Rb/Sr	0.18	0.68	0.61	1.6	1.8
Ba/Rb	2.9	21	5.2	4.6	6.5
Ba/Sr	0.51	14	3.2	7.5	12
Th/Sc	0.31	0.28	0.37	0.36	0.40
La/Sc	2.3	1.9	1.9	1.9	2.2
La/Th	7.3	6.8	5.1	5.2	5.5
Zr/Y	5.7	4.0	5.4	5.3	5.9
Ti/Zr	21	29	31	25	21
Zr/Nb	13	11	12	12	20
Ni/Co	12	17	3.0	10	21
Cr/V	6.0	4.0	3.0	4.1	4.7
V/Ni	0.19	0.23	0.76	0.34	0.32
Cr/Ni	1.1	0.91	2.2	1.4	1.5
Cr/Zr	5.0	4.6	3.8	4.0	3.6
Sc/Th	3.2	3.6	2.7	2.8	2.5
Co/Th	8.3	6.9	11	5.7	2.8
La/Yb	15	11	14	17	12
Eu/Eu*	0.67	0.72	0.73	0.80	0.60
CIA	97	95	89	87	89

K8 PELITES

SAMPLE	MEE-16	MEE-19	MEE-21	MEE-23	MEE-26
SiO2	60.63	62.17	58.50	62.31	55.62
TiO2	0.83	1.11	0.92	0.92	0.59
Al2O3	22.09	29.69	24.48	27.15	19.77
Fe2O3-T	8.35	0.67	6.54	0.51	7.20
MgO	2.52	0.41	1.02	0.43	6.74
CaO	0.04	0.08	0.05	0.10	0.71
Na2O	0.11	0.56	0.50	1.42	1.22
K2O	1.12	1.32	4.32	2.76	3.39
MnO	0.07	<0.002	0.30	<0.002	0.05
P2O5	0.06	0.06	0.06	0.06	0.09
LOI	3.81	5.00	3.51	4.18	4.74
TOTAL	99.60	101.06	99.92	99.83	100.11
Rb	45	52	141	120	132
Ba	272	303	261	626	853
Cs	2.2	3.5	3.9	13	7.7
Sr	42	94	105	133	87
Pb	16	22	20	31	10
Th	8.4	12	10	11	6.4
U	3.5	6.1	3.9	4.3	2.4
Sc	21	25	31	30	24
V	197	249	222	141	166
Cr	583	838	816	750	927
Co	34	55	46	123	50
Ni	411	136	347	386	388
Y	41	46	63	24	26
Zr	179	233	193	158	127
Nb	12	18	16	7.5	7.9
Hf	4.8	7.1	6.3	5.0	4.7
Ta	1.1	1.4	1.2	1.2	0.88
La	43	61	56	65	34
Ce	81	131	111	124	68
Sm	7.2	9.5	9.7	11	5.9
Eu	1.4	1.9	2.0	2.8	1.5
Tb	1.0	1.3	1.5	1.6	0.68
Yb	3.3	4.2	6.5	4.3	2.1
Lu	0.57	0.65	1.08	0.70	0.38

K8 PELITES

SAMPLE	MEE-16	MEE-19	MEE-21	MEE-23	MEE-26
K2O/Na2O	9.9	2.3	8.6	1.9	2.8
SiO2/Al2O3	2.7	2.1	2.4	2.3	2.8
Th/U	2.4	2.0	2.6	2.6	2.7
K/Rb	206	210	254	191	213
Rb/Sr	1.1	0.55	1.3	0.90	1.5
Ba/Rb	6.0	5.8	1.9	5.2	6.5
Ba/Sr	6.5	3.2	2.5	4.7	9.8
Th/Sc	0.40	0.48	0.32	0.37	0.27
La/Sc	2.0	2.4	1.8	2.2	1.4
La/Th	5.1	5.1	5.6	5.9	5.3
Zr/Y	4.4	5.1	3.1	6.6	4.8
Ti/Zr	28	29	29	35	28
Zr/Nb	15	13	12	21	16
Ni/Co	12	2.5	7.6	3.1	7.7
Cr/V	3.0	3.4	3.7	5.3	5.6
V/Ni	0.48	1.8	0.64	0.37	0.43
Cr/Ni	1.4	6.2	2.4	1.9	2.4
Cr/Zr	3.2	3.6	4.2	4.8	7.3
Sc/Th	2.5	2.1	3.1	2.7	3.8
Co/Th	4.0	4.6	4.6	11	7.9
La/Yb	13	15	8.6	15	16
Eu/Eu*	0.58	0.63	0.63	0.78	0.81
CIA	94	93	82	83	74

K8 PELITES

SAMPLE	MEE-28	MEE-30	MEE-34	MEE-36	MEE-39
SiO2	68.54	57.22	59.36	67.34	62.41
TiO2	0.90	0.56	0.97	0.92	0.99
Al2O3	22.64	16.52	26.10	24.37	29.44
Fe2O3-T	0.83	9.12	6.58	1.18	1.02
MgO	0.53	9.69	1.55	0.37	0.34
CaO	0.19	0.16	0.03	0.03	0.07
Na2O	2.54	0.16	0.18	0.31	0.39
K2O	1.50	0.99	0.94	1.91	0.90
MnO	0.01	0.11	0.03	<0.002	<0.002
P2O5	0.05	0.11	0.60	0.04	0.07
LOI	2.88	5.49	4.35	4.04	5.40
TOTAL	100.60	100.12	100.14	100.44	101.00
Rb	48	40	36	63	35
Ba	248	283	156	187	245
Cs	3.2	2.5	2.1	2.4	2.3
Sr	457	40	51	66	80
Pb	30	14	17	16	27
Th	12	4.0	11	9.0	10
U	4.4	1.0	3.8	4.1	2.6
Sc	24	24	27	19	25
V	186	160	235	205	252
Cr	826	1162	765	608	581
Co	52	55	52	63	36
Ni	422	667	419	345	99
Y	47	19	52	24	31
Zr	324	163	181	196	173
Nb	17	5.5	12	16	12
Hf	9.8	3.9	5.6	5.2	4.2
Ta	1.5	0.55	1.1	1.1	1.1
La	47	22	53	42	47
Ce	95	40	110	72	86
Sm	8.0	3.9	9.2	5.6	8.0
Eu	1.9	0.72	2.0	1.2	1.5
Tb	1.3	0.42	1.5	0.65	0.83
Yb	4.6	3.3	4.8	2.3	2.8
Lu	0.73	0.33	0.70	0.35	0.45

K8 PELITES

SAMPLE	MEE-28	MEE-30	MEE-34	MEE-36	MEE-39
K2O/Na2O	0.59	6.1	5.1	6.2	2.3
SiO2/Al2O3	3.0	3.5	2.3	2.8	2.1
Th/U	2.7	4.0	2.9	2.2	3.8
K/Rb	260	205	216	252	213
Rb/Sr	0.11	1.0	0.71	0.95	0.44
Ba/Rb	5.2	7.1	4.3	3.0	7.0
Ba/Sr	0.54	7.1	3.1	2.8	3.1
Th/Sc	0.50	0.17	0.41	0.47	0.40
La/Sc	2.0	0.90	2.0	2.2	1.9
La/Th	3.9	5.4	4.8	4.6	4.7
Zr/Y	6.9	8.7	3.5	8.1	5.6
Ti/Zr	17	21	32	28	34
Zr/Nb	19	30	15	12	14
Ni/Co	8.1	12	8.1	5.5	2.7
Cr/V	4.4	7.3	3.3	3.0	2.3
V/Ni	0.44	0.24	0.56	0.59	2.5
Cr/Ni	2.0	1.7	1.8	1.8	5.9
Cr/Zr	2.6	7.1	4.2	3.1	3.4
Sc/Th	2.0	6.0	2.5	2.1	2.5
Co/Th	4.3	14	4.7	7.0	3.6
La/Yb	10	6.6	11	18	17
Eu/Eu*	0.71	0.60	0.65	0.70	0.63
CIA	79	92	95	90	95

K8 PELITES

SAMPLE	MED-1	MED-2	MED-3	MED-4	MED-6
SiO2	63.13	75.75	63.07	60.85	61.61
TiO2	0.90	0.36	0.83	1.00	0.78
Al2O3	23.64	10.90	23.93	25.95	28.97
Fe2O3-T	3.36	5.20	4.64	4.72	1.51
MgO	0.61	3.82	1.39	1.60	0.64
CaO	0.06	0.03	0.09	0.04	0.03
Na2O	0.68	0.17	0.85	0.37	0.39
K2O	4.82	0.95	2.30	1.54	1.93
MnO	<0.002	0.01	0.04	0.03	<0.002
P2O5	0.06	0.04	0.07	0.06	0.06
LOI	3.27	2.76	3.37	4.33	4.62
TOTAL	100.52	100.00	100.57	100.49	100.54
Rb	165	41	101	66	84
Ba	450	178	407	290	354
Cs	6.9	1.5	4.4	3.6	3.9
Sr	110	26	113	57	56
Pb	24	14	24	19	19
Th	9.4	3.7	14	11	13
U	4.1	2.2	10	4.7	4.5
Sc	25	7.4	19	34	22
V	204	63	151	243	159
Cr	724	563	614	875	513
Co	85	34	11	57	3.2
Ni	547	846	361	323	102
Y	40	18	38	55	31
Zr	203	168	288	196	173
Nb	12	4.9	18	13	13
Hf	5.8	5.4	9.1	6.2	5.1
Ta	1.3	0.60	1.6	1.3	1.4
La	47	17	60	67	67
Ce	98	37	124	127	143
Sm	7.3	2.9	7.5	11	9.9
Eu	1.6	0.77	1.6	2.5	1.9
Tb	1.1	0.33	1.1	1.6	1.1
Yb	3.7	1.5	3.6	6.3	3.0
Lu	0.60	0.24	0.56	1.02	0.44

K8 PELITES

SAMPLE	MED-1	MED-2	MED-3	MED-4	MED-6
K2O/Na2O	7.1	5.5	2.7	4.2	4.9
SiO2/Al2O3	2.7	7.0	2.6	2.3	2.1
Th/U	2.3	1.7	1.4	2.3	2.9
K/Rb	242	192	189	194	191
Rb/Sr	1.5	1.6	0.89	1.2	1.5
Ba/Rb	2.7	4.3	4.0	4.4	4.2
Ba/Sr	4.1	6.8	3.6	5.1	6.3
Th/Sc	0.38	0.50	0.74	0.32	0.59
La/Sc	1.9	2.3	3.2	2.0	3.0
La/Th	5.0	4.6	4.3	6.1	5.2
Zr/Y	5.1	9.1	7.5	3.6	5.6
Ti/Zr	26	13	17	31	27
Zr/Nb	17	34	16	15	13
Ni/Co	6.4	25	33	5.6	32
Cr/V	3.5	8.9	4.1	3.6	3.2
V/Ni	0.37	0.07	0.42	0.75	1.6
Cr/Ni	1.3	0.67	1.7	2.7	5.0
Cr/Zr	3.6	3.3	2.1	4.5	3.0
Sc/Th	2.7	2.0	1.4	3.1	1.7
Co/Th	9.0	9.2	0.79	5.2	0.25
La/Yb	13	11	17	11	22
Eu/Eu*	0.67	0.86	0.66	0.69	0.62
CIA	79	89	86	92	91

K8 PELITES

SAMPLE	MED-7	MED-8	MED-9
SiO2	64.22	64.85	63.00
TiO2	0.78	0.90	0.93
Al2O3	28.09	24.89	24.01
Fe2O3-T	0.76	2.46	4.21
MgO	0.46	0.44	0.95
CaO	0.18	0.70	0.10
Na2O	0.26	0.71	1.84
K2O	0.61	1.34	1.96
MnO	<0.002	<0.002	0.04
P2O5	0.06	0.05	0.05
LOI	5.17	5.14	3.30
TOTAL	100.57	100.85	100.38
Rb	23	55	74
Ba	162	237	405
Cs	3.0	4.8	5.2
Sr	72	82	220
Pb	21	21	34
Th	12	17	8.5
U	7.1	7.6	4.2
Sc	19	29	23
V	152	181	229
Cr	532	884	543
Co	23	60	61
Ni	141	277	384
Y	43	28	55
Zr	211	334	188
Nb	12	18	11
Hf	7.3	13	4.5
Ta	1.3	1.8	1.0
La	66	68	40
Ce	125	141	75
Sm	8.7	8.1	8.1
Eu	1.5	1.5	1.3
Tb	1.2	0.94	1.4
Yb	4.7	3.2	4.9
Lu	0.72	0.63	0.70

K8 PELITES

SAMPLE	MED-7	MED-8	MED-9
K2O/Na2O	2.3	1.9	1.1
SiO2/Al2O3	2.3	2.6	2.6
Th/U	1.7	2.2	2.0
K/Rb	221	203	220
Rb/Sr	0.32	0.67	0.34
Ba/Rb	7.0	4.3	5.5
Ba/Sr	2.3	2.9	1.8
Th/Sc	0.63	0.59	0.37
La/Sc	3.4	2.3	1.7
La/Th	5.5	4.0	4.6
Zr/Y	5.0	12	3.4
Ti/Zr	22	16	29
Zr/Nb	18	19	17
Ni/Co	6.1	4.6	6.3
Cr/V	3.5	4.9	2.4
V/Ni	1.1	0.65	0.60
Cr/Ni	3.8	3.2	1.4
Cr/Zr	2.5	2.6	2.9
Sc/Th	1.6	1.7	2.7
Co/Th	1.9	3.5	7.2
La/Yb	14	21	8.1
Eu/Eu*	0.54	0.59	0.48
CIA	96	87	82

BOOYSENS PELITE (BOY)

SAMPLE	AVG	STD
SiO2	54.31	2.65
TiO2	0.67	0.12
Al2O3	18.61	2.27
Fe2O3-T	8.43	2.04
MgO	8.08	2.48
CaO	0.61	0.48
Na2O	0.71	0.60
K2O	2.09	1.05
MnO	0.08	0.05
P2O5	0.10	0.04
LOI	5.94	0.98
TOTAL	99.58	0.53
Rb	83	40
Ba	444	184
Cs	5.0	2.4
Sr	73	39
Pb	14	4
Th	4.7	0.9
U	1.6	0.4
Sc	27	5
V	183	27
Cr	1195	262
Co	59	13
Ni	529	108
Y	25	6
Zr	120	19
Nb	7.6	1.9
Hf	3.6	0.6
Ta	0.65	0.14
La	24	5
Ce	50	11
Sm	4.8	1.1
Eu	1.2	0.3
Tb	0.65	0.23
Yb	2.3	0.5
Lu	0.36	0.08

BOOYSENS PELITE (BOY)

SAMPLE	AVG	STD
K2O/Na2O	6.3	5.2
SiO2/Al2O3	3.0	0.5
Th/U	3.1	0.7
K/Rb	209	23
Rb/Sr	1.5	0.8
Ba/Rb	5.9	1.7
Ba/Sr	8.1	4.6
Th/Sc	0.19	0.07
La/Sc	0.94	0.36
La/Th	5.1	0.8
Zr/Y	5.2	2.0
Ti/Zr	34	6
Zr/Nb	16	4
Ni/Co	9.3	2.4
Cr/V	6.6	1.5
V/Ni	0.36	0.08
Cr/Ni	2.3	0.4
Cr/Zr	10	3
Sc/Th	5.8	1.4
Co/Th	13	4
La/Yb	10	3
Eu/Eu*	0.80	0.09
CIA	83	7

BOOYSENS PELITE (BOY)

SAMPLE	MEE-5	MEE-24	MEE-27	MEE-32	MEE-33
SiO2	55.75	58.79	54.01	52.45	54.35
TiO2	0.62	0.55	0.50	0.64	0.57
Al2O3	19.44	19.95	15.67	18.39	16.59
Fe2O3-T	6.73	7.07	7.80	8.80	8.95
MgO	6.14	5.12	11.20	11.49	11.16
CaO	0.97	0.50	1.70	0.23	0.68
Na2O	1.21	0.72	1.04	0.13	0.10
K2O	3.62	2.87	1.05	1.35	0.87
MnO	0.05	0.07	0.08	0.15	0.12
P2O5	0.09	0.10	0.09	0.13	0.24
LOI	4.50	4.41	6.25	6.36	6.35
TOTAL	98.94	100.16	99.39	99.39	99.39
Rb	144	121	42	54	36
Ba	776	630	275	499	301
Cs	7.4	4.8	3.1	3.1	3.0
Sr	95	133	78	35	42
Pb	17	12	14	19	24
Th	6.0	4.7	3.9	4.2	4.2
U	1.8	1.9	0.92	0.77	1.8
Sc	21	12	27	25	28
V	166	145	167	216	189
Cr	806	425	1528	1060	1561
Co	44	23	77	56	67
Ni	441	393	582	620	681
Y	28	23	19	27	27
Zr	132	156	94	103	110
Nb	8.8	7.7	4.9	6.0	5.5
Hf	4.1	3.3	3.6	2.8	4.0
Ta	0.84	0.62	0.50	0.54	0.53
La	32	23	18	24	26
Ce	63	41	37	50	51
Sm	5.5	3.2	3.9	5.3	4.9
Eu	1.4	0.85	1.2	1.2	1.5
Tb	0.68	0.39	0.48	0.66	0.71
Yb	2.2	1.3	2.0	2.0	2.9
Lu	0.36	0.19	0.34	0.30	0.42

BOOYSENS PELITE (BOY)

SAMPLE	MEE-5	MEE-24	MEE-27	MEE-32	MEE-33
K2O/Na2O	3.0	4.0	1.0	10	8.7
SiO2/Al2O3	2.9	2.9	3.4	2.9	3.3
Th/U	3.3	2.5	4.2	5.5	2.3
K/Rb	209	197	208	208	201
Rb/Sr	1.5	0.91	0.54	1.5	0.86
Ba/Rb	5.4	5.2	6.5	9.2	8.4
Ba/Sr	8.2	4.7	3.5	14	7.2
Th/Sc	0.29	0.39	0.14	0.17	0.15
La/Sc	1.5	1.9	0.67	0.96	0.93
La/Th	5.3	4.9	4.6	5.7	6.2
Zr/Y	4.7	6.8	4.9	3.8	4.1
Ti/Zr	28	21	32	37	31
Zr/Nb	15	20	19	17	20
Ni/Co	10	17	7.6	11	10
Cr/V	4.9	2.9	9.1	4.9	8.3
V/Ni	0.38	0.37	0.29	0.35	0.28
Cr/Ni	1.8	1.1	2.6	1.7	2.3
Cr/Zr	6.1	2.7	16	10	14
Sc/Th	3.5	2.6	6.9	6.0	6.7
Co/Th	7.3	4.9	20	13	16
La/Yb	15	18	9.0	12	9.0
Eu/Eu*	0.81	0.85	0.98	0.72	0.95
CIA	72	80	79	92	94

BOOYSENS PELITE (BOY)

SAMPLE	SJ-3-1	SJ-3-2	SJ-3-3	SJ-3-4	SJ-3-5
SiO2	58.35	53.64	58.37	52.40	53.65
TiO2	0.57	0.61	0.56	0.60	0.64
Al2O3	20.08	15.84	14.99	18.82	19.38
Fe2O3-T	5.83	8.52	7.07	7.93	7.63
MgO	4.75	12.21	10.61	9.94	8.41
CaO	0.89	1.37	1.10	0.91	1.02
Na2O	2.02	1.27	2.02	1.41	1.41
K2O	3.61	0.74	0.72	2.48	2.73
MnO	0.03	0.06	0.04	0.05	0.04
P2O5	0.12	0.09	0.07	0.09	0.11
LOI	3.79	5.78	4.85	5.36	4.93
TOTAL	100.05	100.11	100.40	99.99	99.95
Rb	145	32	32	118	121
Ba	832	299	268	771	643
Cs	8.3	2.5	2.5	7.7	7.0
Sr	118	108	140	100	105
Pb	13	<9.8	13	13	<9.8
Th	6.7	3.1	3.4	4.6	4.9
U	2.7	0.97	1.3	1.3	1.7
Sc	17	27	22	26	26
V	130	185	154	191	190
Cr	603	1384	1283	1209	1017
Co	34	62	57	68	51
Ni	211	547	455	457	370
Y	31	23	20	30	34
Zr	145	97	106	101	125
Nb	13	5.7	6.2	6.3	8.0
Hf	4.5	2.9	3.3	3.3	3.8
Ta	0.95	0.46	0.49	0.56	0.64
La	32	17	17	23	25
Ce	69	38	38	50	56
Sm	5.5	3.8	3.4	4.7	5.4
Eu	1.0	0.91	0.90	1.2	1.4
Tb	0.66	0.40	0.37	0.52	0.77
Yb	2.0	1.8	1.7	2.1	2.5
Lu	0.29	0.31	0.24	0.31	0.37

BOOYSENS PELITE (BOY)

SAMPLE	SJ-3-1	SJ-3-2	SJ-3-3	SJ-3-4	SJ-3-5
K2O/Na2O	1.8	0.58	0.36	1.8	1.9
SiO2/Al2O3	2.9	3.4	3.9	2.8	2.8
Th/U	2.5	3.2	2.6	3.5	2.9
K/Rb	207	192	187	174	187
Rb/Sr	1.2	0.30	0.23	1.2	1.2
Ba/Rb	5.7	9.3	8.4	6.5	5.3
Ba/Sr	7.1	2.8	1.9	7.7	6.1
Th/Sc	0.39	0.11	0.15	0.18	0.19
La/Sc	1.9	0.63	0.77	0.88	0.96
La/Th	4.8	5.5	5.0	5.0	5.1
Zr/Y	4.7	4.2	5.3	3.4	3.7
Ti/Zr	23	38	32	36	31
Zr/Nb	11	17	17	16	16
Ni/Co	6.2	8.8	8.0	6.7	7.3
Cr/V	4.6	7.5	8.3	6.3	5.4
V/Ni	0.62	0.34	0.34	0.42	0.51
Cr/Ni	2.9	2.5	2.8	2.6	2.7
Cr/Zr	4.2	14	12	12	8.1
Sc/Th	2.5	8.7	6.5	5.7	5.3
Co/Th	5.1	20	17	15	10
La/Yb	16	9.4	10	11	10
Eu/Eu*	0.58	0.79	0.87	0.83	0.80
CIA	70	78	71	74	74

BOOYSENS PELITE (BOY)

SAMPLE	SJ-3-6	SJ-3-7	UR-1140	439-3	615-7
SiO2	53.76	51.13	59.89	54.18	57.00
TiO2	0.62	0.80	0.55	0.60	0.81
Al2O3	17.90	19.92	13.67	18.52	19.86
Fe2O3-T	7.41	7.67	9.77	9.86	7.54
MgO	11.20	10.48	7.05	6.58	5.45
CaO	1.17	0.94	0.84	0.09	0.14
Na2O	1.04	0.57	0.09	0.17	0.49
K2O	1.52	2.37	0.88	2.08	2.51
MnO	0.04	0.04	0.16	0.12	0.04
P2O5	0.12	0.10	0.06	0.10	0.09
LOI	5.58	5.91	5.84	6.65	5.99
TOTAL	100.37	99.93	98.80	98.95	99.92
Rb	69	102	33	78	99
Ba	362	522	238	389	366
Cs	4.1	5.4	1.1	4.0	6.3
Sr	122	95	17	33	76
Pb	12	<9.8	-	-	-
Th	4.3	5.3	3.4	4.2	5.8
U	1.4	1.6	1.4	1.5	1.8
Sc	28	31	18	28	30
V	190	218	121	179	191
Cr	1306	1237	1171	1277	1348
Co	59	62	70	51	67
Ni	558	474	507	572	558
Y	29	35	12	21	25
Zr	101	115	134	95	153
Nb	6.9	7.8	4.5	7.2	9.2
Hf	3.1	3.5	4.1	2.9	4.4
Ta	0.55	0.80	0.43	0.60	0.70
La	23	26	18	25	25
Ce	50	56	37	56	53
Sm	4.9	5.5	3.2	5.3	5.4
Eu	1.4	1.4	0.80	1.2	1.5
Tb	0.56	0.80	0.40	0.78	0.92
Yb	2.4	2.7	1.3	2.5	3.0
Lu	0.35	0.38	0.24	0.34	0.46

BOOYSENS PELITE (BOY)

SAMPLE	SJ-3-6	SJ-3-7	UR-1140	439-3	615-7
K2O/Na2O	1.5	4.2	9.8	12	5.1
SiO2/Al2O3	3.0	2.6	4.4	2.9	2.9
Th/U	3.1	3.3	2.4	2.8	3.2
K/Rb	183	193	221	221	210
Rb/Sr	0.57	1.1	1.9	2.4	1.3
Ba/Rb	5.2	5.1	7.2	5.0	3.7
Ba/Sr	3.0	5.5	14	12	4.8
Th/Sc	0.15	0.17	0.19	0.15	0.19
La/Sc	0.82	0.84	1.0	0.89	0.83
La/Th	5.3	4.9	5.3	6.0	4.3
Zr/Y	3.5	3.3	11	4.5	6.1
Ti/Zr	37	42	25	38	32
Zr/Nb	15	15	30	13	17
Ni/Co	9.5	7.6	7.2	11	8.3
Cr/V	6.9	5.7	9.7	7.1	7.1
V/Ni	0.34	0.46	0.24	0.31	0.34
Cr/Ni	2.3	2.6	2.3	2.2	2.4
Cr/Zr	13	11	8.7	13	8.8
Sc/Th	6.5	5.8	5.3	6.7	5.2
Co/Th	14	12	21	12	12
La/Yb	9.6	9.6	14	10	8.3
Eu/Eu*	0.93	0.79	0.80	0.70	0.83
CIA	79	83	92	88	85

BOOYSENS PELITE (BOY)

SAMPLE	615-8	615-9	730-4	730-5	730-6
SiO2	54.24	55.13	50.87	51.09	54.09
TiO2	0.92	0.85	0.72	0.75	0.95
Al2O3	22.67	21.37	19.22	18.94	22.99
Fe2O3-T	6.41	7.13	11.37	10.87	6.39
MgO	4.62	4.97	7.43	7.75	4.83
CaO	0.21	0.13	0.11	0.12	0.09
Na2O	0.63	0.53	0.17	0.14	0.33
K2O	3.46	3.01	1.87	1.70	4.11
MnO	0.03	0.03	0.06	0.08	0.03
P2O5	0.14	0.09	0.08	0.08	0.07
LOI	5.86	6.10	7.48	7.33	5.89
TOTAL	99.19	99.34	99.38	98.85	99.77
Rb	98	116	68	64	145
Ba	485	440	281	286	549
Cs	9.7	7.8	4.0	4.1	6.3
Sr	95	84	28	26	45
Pb	-	-	-	-	-
Th	5.4	5.8	4.5	5.1	5.6
U	1.8	2.0	1.7	1.6	2.0
Sc	35	31	29	30	35
V	228	201	192	193	223
Cr	1301	1283	1255	1202	1451
Co	73	66	79	43	65
Ni	610	561	629	563	570
Y	30	25	22	23	30
Zr	139	143	114	121	145
Nb	9.8	7.7	6.7	9.2	11
Hf	4.1	4.2	3.5	3.6	4.2
Ta	0.78	0.77	0.62	0.69	0.86
La	30	28	25	16	34
Ce	66	62	50	34	69
Sm	6.7	6.1	4.9	3.6	7.0
Eu	1.8	1.7	1.0	0.88	1.7
Tb	1.1	0.88	0.53	0.76	1.1
Yb	3.2	2.9	2.4	2.7	3.2
Lu	0.51	0.47	0.38	0.43	0.49

BOOYSENS PELITE (BOY)

SAMPLE	615-8	615-9	730-4	730-5	730-6
K2O/Na2O	5.5	5.7	11	12	12
SiO2/Al2O3	2.4	2.6	2.6	2.7	2.4
Th/U	3.0	2.9	2.6	3.2	2.8
K/Rb	293	215	228	220	235
Rb/Sr	1.0	1.4	2.4	2.5	3.2
Ba/Rb	4.9	3.8	4.1	4.5	3.8
Ba/Sr	5.1	5.2	10	11	12
Th/Sc	0.15	0.19	0.16	0.17	0.16
La/Sc	0.86	0.90	0.86	0.53	0.97
La/Th	5.6	4.8	5.6	3.1	6.1
Zr/Y	4.6	5.7	5.2	5.3	4.8
Ti/Zr	40	36	38	37	39
Zr/Nb	14	19	17	13	13
Ni/Co	8.4	8.5	8.0	13	8.8
Cr/V	5.7	6.4	6.5	6.2	6.5
V/Ni	0.37	0.36	0.31	0.34	0.39
Cr/Ni	2.1	2.3	2.0	2.1	2.5
Cr/Zr	9.4	9.0	11	9.9	10
Sc/Th	6.5	5.3	6.4	5.9	6.3
Co/Th	14	11	18	8.4	12
La/Yb	9.4	9.7	10	5.9	11
Eu/Eu*	0.81	0.86	0.67	0.69	0.74
CIA	82	84	89	90	82

BOOYSENS PELITE (BOY)

SAMPLE	V56-58	GV2-28	UC-760
SiO2	53.98	52.54	49.47
TiO2	0.71	0.59	0.79
Al2O3	19.00	15.84	19.03
Fe2O3-T	6.81	14.18	12.19
MgO	9.08	7.27	8.08
CaO	0.56	0.12	0.15
Na2O	0.50	0.03	0.25
K2O	2.83	0.67	1.12
MnO	0.08	0.23	0.12
P2O5	0.07	0.09	0.07
LOI	6.58	7.31	7.62
TOTAL	100.20	98.87	98.89
Rb	112	25	48
Ba	548	183	280
Cs	7.8	1.3	3.0
Sr	37	9.1	66
Pb	-	-	-
Th	5.5	3.5	4.6
U	1.8	1.3	1.6
Sc	32	26	30
V	168	170	196
Cr	1306	1271	1195
Co	63	58	56
Ni	466	654	681
Y	12	20	23
Zr	129	105	108
Nb	8.4	7.2	7.2
Hf	4.6	2.9	3.1
Ta	0.77	0.48	0.76
La	15	18	25
Ce	37	40	55
Sm	2.9	3.8	6.0
Eu	0.59	0.95	1.5
Tb	0.27	0.38	0.80
Yb	2.1	2.3	2.7
Lu	0.36	0.32	0.39

BOOYSENS PELITE (BOY)

SAMPLE	V56-58	GV2-28	UC-760
K2O/Na2O	5.7	22	4.5
SiO2/Al2O3	2.8	3.3	2.6
Th/U	3.1	2.7	2.9
K/Rb	210	222	194
Rb/Sr	3.0	2.7	0.73
Ba/Rb	4.9	7.3	5.8
Ba/Sr	15	20	4.2
Th/Sc	0.17	0.13	0.15
La/Sc	0.47	0.69	0.83
La/Th	2.7	5.1	5.4
Zr/Y	11	5.3	4.7
Ti/Zr	33	34	44
Zr/Nb	15	15	15
Ni/Co	7.4	11	12
Cr/V	7.8	7.5	6.1
V/Ni	0.36	0.26	0.29
Cr/Ni	2.8	1.9	1.8
Cr/Zr	10	12	11
Sc/Th	5.8	7.4	6.5
Co/Th	11	17	12
La/Yb	7.1	7.8	9.3
Eu/Eu*	0.68	0.83	0.79
CIA	81	95	91

ROODEPOORT PELITES (RO)

SAMPLE	AVG	STD
SiO2	58.23	2.84
TiO2	0.84	0.17
Al2O3	18.35	3.08
Fe2O3-T	9.86	4.66
MgO	5.16	0.92
CaO	0.25	0.15
Na2O	0.90	0.59
K2O	1.92	0.91
MnO	0.07	0.01
P2O5	0.07	0.03
LOI	4.79	0.42
TOTAL	100.44	0.73
Rb	80	35
Ba	337	149
Cs	7.7	4.8
Sr	76	45
Pb	14	5
Th	5.5	0.8
U	1.7	0.6
Sc	25	4
V	194	26
Cr	817	138
Co	43	8
Ni	330	35
Y	31	14
Zr	153	19
Nb	11	2
Hf	4.5	0.6
Ta	0.75	0.13
La	32	6
Ce	66	13
Sm	5.5	0.6
Eu	1.3	0.1
Tb	0.86	0.26
Yb	2.8	0.6
Lu	0.41	0.06

ROODEPOORT PELITES (RO)

SAMPLE	AVG	STD
K2O/Na2O	5.5	7.3
SiO2/Al2O3	3.3	0.6
Th/U	3.7	1.9
K/Rb	180	48
Rb/Sr	1.7	2.3
Ba/Rb	4.0	1.0
Ba/Sr	6.2	6.3
Th/Sc	0.22	0.04
La/Sc	1.3	0.2
La/Th	5.8	0.6
Zr/Y	5.6	1.7
Ti/Zr	33	4
Zr/Nb	15	1
Ni/Co	7.8	1.3
Cr/V	4.2	0.6
V/Ni	0.60	0.10
Cr/Ni	2.5	0.4
Cr/Zr	5.4	1.1
Sc/Th	4.6	0.9
Co/Th	8.2	1.9
La/Yb	12	3
Eu/Eu*	0.71	0.04
CIA	84	7

ROODEPOORT PELITES (RO)

SAMPLE	MED-17	MED-18	C 75	AA0096	AA0097
SiO2	55.32	53.92	59.33	56.83	64.65
TiO2	0.53	0.60	0.78	1.01	0.78
Al2O3	12.77	13.98	17.51	21.75	16.84
Fe2O3-T	19.13	17.20	11.04	7.03	6.14
MgO	6.49	7.02	3.99	4.80	4.44
CaO	0.17	0.68	0.14	0.19	0.23
Na2O	0.01	0.03	0.22	1.47	1.18
K2O	0.02	0.67	3.09	2.48	1.76
MnO	0.07	0.09	0.05	0.07	0.06
P2O5	0.11	0.09	0.12	0.06	0.04
LOI	4.76	5.34	3.82	5.24	4.46
TOTAL	99.38	99.62	100.09	100.93	100.58
Rb	3.3	34	121	102	74
Ba	5.5	150	349	422	327
Cs	<0.5	1.3	2.2	14	8.6
Sr	6.7	19	15	110	87
Pb	<9.8	<9.8	<9.8	15	15
Th	4.2	4.8	4.3	6.0	5.3
U	1.0	0.55	1.2	2.2	2.2
Sc	24	19	28	27	19
V	154	161	210	230	164
Cr	794	686	1112	867	644
Co	43	43	48	46	38
Ni	322	403	365	319	286
Y	23	25	42	24	66
Zr	115	146	141	168	144
Nb	7.0	8.4	9.2	12	11
Hf	3.9	4.4	4.2	5.1	3.9
Ta	0.51	0.64	0.72	0.89	0.70
La	25	23	27	31	31
Ce	49	47	57	66	66
Sm	4.6	4.5	5.3	5.4	5.6
Eu	1.2	1.0	1.2	1.2	1.4
Tb	0.62	0.62	0.90	0.83	1.5
Yb	2.9	2.7	3.0	2.4	4.5
Lu	0.47	0.41	0.43	0.38	0.53

ROODEPOORT PELITES (RO)

SAMPLE	MED-17	MED-18	C 75	AA0096	AA0097
K2O/Na2O	2.0	23	14	1.7	1.5
SiO2/Al2O3	4.3	3.9	3.4	2.6	3.8
Th/U	4.2	8.7	3.6	2.7	2.4
K/Rb	50	164	212	202	197
Rb/Sr	0.49	1.8	8.1	0.93	0.85
Ba/Rb	1.7	4.4	2.9	4.1	4.4
Ba/Sr	0.82	7.9	23	3.8	3.8
Th/Sc	0.18	0.25	0.15	0.22	0.28
La/Sc	1.0	1.2	0.96	1.1	1.6
La/Th	6.0	4.8	6.3	5.2	5.8
Zr/Y	5.0	5.8	3.4	7.0	2.2
Ti/Zr	28	25	33	36	32
Zr/Nb	16	17	15	14	13
Ni/Co	7.5	9.4	7.6	6.9	7.5
Cr/V	5.2	4.3	5.3	3.8	3.9
V/Ni	0.48	0.40	0.58	0.72	0.57
Cr/Ni	2.5	1.7	3.0	2.7	2.3
Cr/Zr	6.9	4.7	7.9	5.2	4.5
Sc/Th	5.7	4.0	6.5	4.5	3.6
Co/Th	10	9.0	11	7.7	7.2
La/Yb	8.6	8.5	9.0	13	6.9
Eu/Eu*	0.82	0.69	0.67	0.68	0.68
CIA	100	95	82	80	80

ROODEPOORT PELITES (RO)

SAMPLE	AA0098	AA0099	AA0100	AA0101
SiO2	58.82	58.88	58.54	57.79
TiO2	0.90	0.94	1.02	0.97
Al2O3	19.97	20.51	21.06	20.78
Fe2O3-T	7.02	6.68	7.45	7.02
MgO	5.00	4.69	5.00	5.03
CaO	0.22	0.24	0.22	0.20
Na2O	1.12	1.29	1.30	1.48
K2O	2.33	2.35	2.31	2.28
MnO	0.06	0.06	0.07	0.06
P2O5	0.06	0.08	0.04	0.05
LOI	4.82	4.81	5.04	4.81
TOTAL	100.32	100.53	102.05	100.47
Rb	98	98	95	96
Ba	423	443	473	439
Cs	9.9	9.7	12	11
Sr	103	117	113	117
Pb	20	16	19	16
Th	5.5	6.0	6.9	6.1
U	2.3	2.1	2.1	2.0
Sc	24	25	30	27
V	210	199	208	214
Cr	690	776	944	840
Co	51	30	58	34
Ni	338	281	335	325
Y	23	23	28	24
Zr	143	171	179	169
Nb	11	12	13	12
Hf	3.9	4.9	5.7	4.8
Ta	0.71	0.82	0.93	0.85
La	38	30	43	36
Ce	79	65	87	75
Sm	6.0	5.7	6.7	5.9
Eu	1.3	1.3	1.5	1.4
Tb	0.74	0.73	1.0	0.77
Yb	2.3	2.3	2.7	2.5
Lu	0.30	0.36	0.44	0.38

ROODEPOORT PELITES (RO)

SAMPLE	AA0098	AA0099	AA0100	AA0101
K2O/Na2O	2.1	1.8	1.8	1.5
SiO2/Al2O3	2.9	2.9	2.8	2.8
Th/U	2.4	2.9	3.3	3.1
K/Rb	197	199	202	197
Rb/Sr	0.95	0.84	0.84	0.82
Ba/Rb	4.3	4.5	5.0	4.6
Ba/Sr	4.1	3.8	4.2	3.8
Th/Sc	0.23	0.24	0.23	0.23
La/Sc	1.6	1.2	1.4	1.3
La/Th	6.9	5.0	6.2	5.9
Zr/Y	6.2	7.4	6.4	7.0
Ti/Zr	38	33	34	34
Zr/Nb	13	14	14	14
Ni/Co	6.6	9.4	5.8	9.6
Cr/V	3.3	3.9	4.5	3.9
V/Ni	0.62	0.71	0.62	0.66
Cr/Ni	2.0	2.8	2.8	2.6
Cr/Zr	4.8	4.5	5.3	5.0
Sc/Th	4.4	4.2	4.3	4.4
Co/Th	9.3	5.0	8.4	5.6
La/Yb	17	13	16	14
Eu/Eu*	0.69	0.72	0.69	0.75
CIA	81	81	81	80

PROMISE PELITES (PRM)

SAMPLE	AVG	STD
SiO2	44.87	2.66
TiO2	0.32	0.04
Al2O3	9.73	1.08
Fe2O3-T	30.08	3.53
MgO	4.68	0.36
CaO	0.81	0.16
Na2O	0.24	0.14
K2O	1.48	0.14
MnO	2.42	1.44
P2O5	0.10	0.01
LOI	1.89	0.56
TOTAL	97.76	0.73
Rb	116	4
Ba	440	137
Cs	10	4
Sr	27	5
Pb	<9.8	-
Th	3.5	0.5
U	0.66	0.06
Sc	13	2
V	98	8
Cr	431	56
Co	29	5
Ni	265	19
Y	20	1
Zr	73	13
Nb	5.3	0.2
Hf	1.9	0.2
Ta	0.45	0.04
La	15	1
Ce	30	3
Sm	2.9	0.3
Eu	0.70	0.08
Tb	0.37	0.04
Yb	1.5	0.2
Lu	0.24	0.04

PROMISE PELITES (PRM)

SAMPLE	AVG	STD
K2O/Na2O	12	11
SiO2/Al2O3	4.6	0.4
Th/U	5.4	0.6
K/Rb	106	8
Rb/Sr	4.5	1.0
Ba/Rb	3.8	1.0
Ba/Sr	18	9
Th/Sc	0.28	0.04
La/Sc	1.2	0.1
La/Th	4.2	0.2
Zr/Y	3.6	0.4
Ti/Zr	27	1
Zr/Nb	14	2
Ni/Co	9.3	2.0
Cr/V	4.4	0.5
V/Ni	0.37	0.04
Cr/Ni	1.7	0.3
Cr/Zr	6.1	1.5
Sc/Th	3.6	0.4
Co/Th	8.4	1.1
La/Yb	9.8	0.3
Eu/Eu*	0.77	0.06
CIA	81	3

PROMISE PELITES (PRM)

SAMPLE	MED-13	MED-14	MED-15
SiO2	48.45	44.06	42.09
TiO2	0.38	0.28	0.31
Al2O3	11.11	8.48	9.61
Fe2O3-T	25.15	31.84	33.24
MgO	4.69	5.12	4.23
CaO	0.94	0.91	0.57
Na2O	0.27	0.40	0.06
K2O	1.50	1.30	1.65
MnO	3.44	0.38	3.44
P2O5	0.10	0.08	0.11
LOI	2.66	1.40	1.59
TOTAL	98.69	97.70	96.90
Rb	112	113	122
Ba	403	293	623
Cs	5.1	16	9.3
Sr	33	27	21
Pb	<9.8	<9.8	nd
Th	3.7	2.9	4.0
U	0.61	0.62	0.75
Sc	11	11	16
V	105	87	101
Cr	395	388	510
Co	25	27	36
Ni	282	274	238
Y	22	19	19
Zr	91	64	64
Nb	5.5	5.0	5.4
Hf	2.1	1.7	2.0
Ta	0.47	0.39	0.48
La	15	13	16
Ce	31	26	34
Sm	3.1	2.5	3.2
Eu	0.66	0.64	0.81
Tb	0.40	0.32	0.40
Yb	1.5	1.3	1.7
Lu	0.27	0.19	0.27

PROMISE PELITES (PRM)

SAMPLE	MED-13	MED-14	MED-15
K2O/Na2O	5.5	3.2	27
SiO2/Al2O3	4.4	5.2	4.4
Th/U	6.1	4.7	5.3
K/Rb	111	95	112
Rb/Sr	3.4	4.2	5.8
Ba/Rb	3.6	2.6	5.1
Ba/Sr	12	11	30
Th/Sc	0.34	0.26	0.25
La/Sc	1.4	1.2	1.0
La/Th	4.1	4.5	4.0
Zr/Y	4.1	3.4	3.4
Ti/Zr	25	26	29
Zr/Nb	17	13	12
Ni/Co	11	10	6.6
Cr/V	3.8	4.5	5.0
V/Ni	0.37	0.32	0.42
Cr/Ni	1.4	1.4	2.1
Cr/Zr	4.3	6.1	8.0
Sc/Th	3.0	3.8	4.0
Co/Th	6.8	9.3	9.0
La/Yb	10	10	9.4
Eu/Eu*	0.68	0.81	0.81
CIA	83	77	84

PARKTOWN-BRIXTON (PBR)

SAMPLE	AVG	STD
SiO2	53.30	8.36
TiO2	0.40	0.12
Al2O3	10.58	2.60
Fe2O3-T	25.64	10.60
MgO	3.74	1.11
CaO	0.04	0.04
Na2O	0.12	0.07
K2O	0.86	0.52
MnO	0.28	0.26
P2O5	0.04	0.02
LOI	4.22	1.10
TOTAL	99.20	0.84
Rb	43	26
Ba	140	61
Cs	2.6	2.5
Sr	8.4	4.5
Pb	<9.8	-
Th	3.9	1.7
U	1.7	1.5
Sc	13	3
V	106	22
Cr	484	116
Co	25	3.6
Ni	280	126
Y	18	3
Zr	94	34
Nb	6.4	1.9
Hf	2.7	1.1
Ta	0.50	0.21
La	16	3
Ce	30	5
Sm	2.7	0.5
Eu	0.65	0.11
Tb	0.33	0.13
Yb	1.5	0.4
Lu	0.25	0.07

PARKTOWN-BRIXTON (PBR)

SAMPLE	AVG	STD
K2O/Na2O	17	17
SiO2/Al2O3	5.2	0.9
Th/U	3.2	1.1
K/Rb	167	89
Rb/Sr	6.6	5.5
Ba/Rb	3.6	1.5
Ba/Sr	21	13
Th/Sc	0.29	0.06
La/Sc	1.2	0.1
La/Th	4.4	0.9
Zr/Y	5.1	1.5
Ti/Zr	26	2
Zr/Nb	14	2
Ni/Co	11	4
Cr/V	4.6	1.0
V/Ni	0.50	0.32
Cr/Ni	2.0	0.7
Cr/Zr	5.5	1.3
Sc/Th	3.6	0.6
Co/Th	7.2	1.7
La/Yb	11	2
Eu/Eu*	0.78	0.04
CIA	90	5

PARKTOWN-BRIXTON PELITES (PBR)

SAMPLE	MED-10	MED-11	MED-12	C 71	C 72
SiO2	57.84	47.72	65.32	40.98	54.62
TiO2	0.53	0.24	0.47	0.27	0.49
Al2O3	14.02	7.25	11.71	7.85	12.04
Fe2O3-T	16.51	31.70	13.40	42.64	23.96
MgO	5.33	4.02	4.36	2.64	2.33
CaO	0.02	0.12	0.02	0.03	0.02
Na2O	0.05	0.13	0.02	0.20	0.19
K2O	1.49	0.16	0.86	1.36	0.42
MnO	0.03	0.47	0.10	0.70	0.11
P2O5	0.02	0.03	0.02	0.08	0.04
LOI	4.18	5.79	3.52	2.64	4.96
TOTAL	100.01	97.63	99.79	99.40	99.18
Rb	40	22	32	93	29
Ba	99	50	155	226	172
Cs	1.1	7.5	0.73	2.4	1.1
Sr	17	4.5	6.8	5.3	8.2
Pb	<9.8	nd	10	nd	<9.8
Th	7.2	2.6	3.2	2.9	3.5
U	4.7	0.60	1.3	0.68	1.1
Sc	18	11	12	10	14
V	130	70	122	94	115
Cr	619	436	543	284	538
Co	29	21	29	21	26
Ni	360	243	459	84	252
Y	23	15	17	18	17
Zr	141	55	106	54	114
Nb	9.7	4.7	6.1	4.3	7.2
Hf	4.4	1.6	2.9	1.4	3.1
Ta	0.87	0.30	0.46	0.32	0.56
La	20	13	15	12	19
Ce	38	26	32	22	30
Sm	3.6	2.3	2.5	2.3	2.8
Eu	0.83	0.60	0.62	0.51	0.68
Tb	0.55	0.31	0.35	0.17	0.26
Yb	2.2	1.4	1.2	1.3	1.4
Lu	0.37	0.23	0.24	0.18	0.21

PARKTOWN-BRIXTON PELITES (PBR)

SAMPLE	MED-10	MED-11	MED-12	C 71	C 72
K2O/Na2O	31	1.2	43	6.8	2.2
SiO2/Al2O3	4.1	6.6	5.6	5.2	4.5
Th/U	1.5	4.3	2.5	4.3	3.2
K/Rb	309	59	223	121	120
Rb/Sr	2.4	4.9	4.7	18	3.5
Ba/Rb	2.5	2.3	4.8	2.4	5.9
Ba/Sr	5.8	11	23	43	21
Th/Sc	0.40	0.24	0.27	0.29	0.25
La/Sc	1.1	1.2	1.3	1.2	1.4
La/Th	2.8	5.0	4.7	4.1	5.4
Zr/Y	6.1	3.7	6.2	3.0	6.7
Ti/Zr	22	26	27	30	26
Zr/Nb	15	12	17	13	16
Ni/Co	12	12	16	4.0	9.7
Cr/V	4.8	6.2	4.5	3.0	4.7
V/Ni	0.36	0.29	0.27	1.1	0.46
Cr/Ni	1.7	1.8	1.2	3.4	2.1
Cr/Zr	4.4	7.9	5.1	5.3	4.7
Sc/Th	2.5	4.2	3.8	3.4	4.0
Co/Th	4.0	8.1	9.1	7.2	7.4
La/Yb	9.1	9.3	13	9.2	14
Eu/Eu*	0.71	0.82	0.77	0.77	0.82
CIA	89	93	92	81	94

	ORANGE GROVE (OG)
SAMPLE	D 14
SiO2	53.52
TiO2	1.19
Al2O3	27.68
Fe2O3-T	4.84
MgO	0.20
CaO	0.01
Na2O	0.55
K2O	5.07
MnO	ND
P2O5	0.14
LOI	6.01
TOTAL	99.20
Rb	240
Ba	313
Cs	6.6
Sr	92
Pb	12
Th	14
U	3.7
Sc	48
V	278
Cr	572
Co	7.6
Ni	77
Y	61
Zr	239
Nb	18
Hf	8.8
Ta	1.5
La	84
Ce	159
Sm	13
Eu	3.1
Tb	1.7
Yb	5.2
Lu	0.82

	ORANGE GROVE (OG)
SAMPLE	D 14
K2O/Na2O	9.2
SiO2/Al2O3	1.9
Th/U	3.8
K/Rb	175
Rb/Sr	2.6
Ba/Rb	1.3
Ba/Sr	3.4
Th/Sc	0.29
La/Sc	1.7
La/Th	6.0
Zr/Y	3.9
Ti/Zr	30
Zr/Nb	13
Ni/Co	10
Cr/V	2.1
V/Ni	3.6
Cr/Ni	7.4
Cr/Zr	2.4
Sc/Th	3.4
Co/Th	0.54
La/Yb	16
Eu/Eu*	0.77
CIA	94

BOTHAVILLE PELITES (BOT)

SAMPLE	AVG	STD	AVG*	STD*
SiO2	63.64	7.30	59.65	2.75
TiO2	0.44	0.15	0.52	0.05
Al2O3	15.54	4.24	17.94	0.93
Fe2O3-T	6.29	2.08	7.34	1.16
MgO	4.98	1.04	5.56	0.27
CaO	1.25	1.36	0.49	0.40
Na2O	0.23	0.00	0.23	.00
K2O	3.27	0.99	3.83	0.25
MnO	0.01	0.00	0.01	.00
P2O5	0.12	0.03	0.14	.00
LOI	4.57	0.25	4.54	0.28
TOTAL	100.31	0.24	100.24	0.23
Rb	127	41	150	11
Ba	476	118	543	4
Cs	5.5	2.0	6.6	0.7
Sr	61	61	26	4
Pb	27	11	33	8
Th	6.2	2.5	7.5	1.2
U	1.7	0.7	2.1	0.3
Sc	18	6	21	3
V	117	31	134	9
Cr	579	180	660	131
Co	41	15	49	5
Ni	266	81	311	23
Y	27	11	32	6
Zr	124	49	150	18
Nb	6.0	3.5	7.9	1.6
Hf	3.8	1.7	4.6	0.9
Ta	0.72	0.33	0.88	0.21
La	38	23	49	16
Ce	76	45	98	28
Sm	4.6	2.2	5.8	0.8
Eu	0.81	0.38	1.0	0.2
Tb	0.51	0.25	0.64	0.13
Yb	2.0	0.9	2.4	0.6
Lu	0.31	0.13	0.37	0.09

BOTHAVILLE PELITES (BOT)

SAMPLE	AVG	STD	AVG*	STD*
K2O/Na2O	14	4	17	1
SiO2/Al2O3	4.8	2.5	3.3	0.3
Th/U	3.6	0.2	3.6	0.1
K/Rb	215	7	212	4
Rb/Sr	4.4	2.4	5.8	0.6
Ba/Rb	3.9	0.5	3.6	0.3
Ba/Sr	16	9	21	3
Th/Sc	0.34	0.08	0.37	0.07
La/Sc	2.0	1.2	2.4	1.0
La/Th	5.9	3.5	7.0	3.4
Zr/Y	4.7	0.5	4.8	0.5
Ti/Zr	22	3	21	2
Zr/Nb	37	30	19	2
Ni/Co	6.7	1.1	6.4	1.1
Cr/V	5.0	0.7	4.9	0.8
V/Ni	0.45	0.05	0.43	0.05
Cr/Ni	2.2	0.3	2.1	0.3
Cr/Zr	5.3	1.7	4.5	1.2
Sc/Th	3.2	0.7	2.8	0.4
Co/Th	6.9	0.6	6.6	0.5
La/Yb	20	15	24	15
Eu/Eu*	0.61	0.10	0.56	0.06
CIA	79	1	80	0

* excluding sample JWS-8-12

Table C.1-4 Ventersdorp Pelite Analyses

BOTHAVILLE PELITES (BOT)

SAMPLE	JWS-8-9	JWS-8-10	JWS-8-11	JWS-8-12
SiO2	58.63	56.91	63.41	75.59
TiO2	0.57	0.55	0.45	0.19
Al2O3	18.45	18.74	16.63	8.32
Fe2O3-T	8.33	7.98	5.72	3.14
MgO	5.34	5.40	5.94	3.23
CaO	0.20	1.05	0.21	3.52
Na2O	0.22	0.23	0.23	0.22
K2O	3.92	4.08	3.48	1.60
MnO	0.01	0.01	<0.002	0.01
P2O5	0.14	0.14	0.13	0.07
LOI	4.32	4.94	4.36	4.64
TOTAL	100.13	100.03	100.56	100.53
Rb	150	164	136	59
Ba	543	539	548	272
Cs	7.5	6.6	5.7	2.2
Sr	23	32	24	166
Pb	30	43	25	11
Th	7.9	8.8	5.9	2.2
U	2.1	2.4	1.7	0.66
Sc	25	19	18	9.3
V	145	134	123	64
Cr	821	500	659	337
Co	49	56	43	17
Ni	323	279	330	130
Y	35	37	24	10
Zr	144	175	131	44
Nb	7.6	10	6.0	0.5
Hf	5.4	5.2	3.3	1.3
Ta	0.93	1.1	0.60	0.23
La	48	30	68	5.6
Ce	100	62	131	11
Sm	6.6	4.8	6.1	0.91
Eu	1.3	0.84	0.87	0.22
Tb	0.81	0.61	0.49	0.13
Yb	2.9	2.7	1.5	0.72
Lu	0.45	0.41	0.24	0.13

BOTHAVILLE PELITES (BOT)

SAMPLE	JWS-8-9	JWS-8-10	JWS-8-11	JWS-8-12
K2O/Na2O	18	18	15	7.3
SiO2/Al2O3	3.2	3.0	3.8	9.1
Th/U	3.8	3.7	3.5	3.3
K/Rb	217	206	212	225
Rb/Sr	6.5	5.1	5.7	0.36
Ba/Rb	3.6	3.3	4.0	4.6
Ba/Sr	24	17	23	1.6
Th/Sc	0.32	0.46	0.33	0.24
La/Sc	1.9	1.6	3.8	0.60
La/Th	6.1	3.4	12	2.5
Zr/Y	4.1	4.7	5.5	4.4
Ti/Zr	24	19	21	26
Zr/Nb	19	18	22	88
Ni/Co	6.6	5.0	7.7	7.6
Cr/V	5.7	3.7	5.4	5.3
V/Ni	0.45	0.48	0.37	0.49
Cr/Ni	2.5	1.8	2.0	2.6
Cr/Zr	5.7	2.9	5.0	7.7
Sc/Th	3.2	2.2	3.1	4.2
Co/Th	6.2	6.4	7.3	7.7
La/Yb	17	11	45	7.8
Eu/Eu*	0.63	0.56	0.49	0.75
CIA	80	79	80	78

Table C.1-5
Transvaal Pelite Analyses

SILVERTON SHALE (SIL)

SAMPLE	AVG	STD
SiO2	61.18	4.43
TiO2	0.75	0.12
Al2O3	18.51	2.78
Fe2O3-T	7.48	2.18
MgO	2.74	1.43
CaO	0.66	1.24
Na2O	1.35	1.01
K2O	2.91	0.92
MnO	0.06	0.02
P2O5	0.08	0.06
LOI	4.15	1.58
TOTAL	99.88	0.59
Rb	154	50
Ba	544	303
Cs	8.9	3.7
Sr	83	35
Pb	21	7
Th	16	5
U	3.9	1.5
Sc	23	6
V	154	46
Cr	141	55
Co	18	11
Ni	66	27
Y	29	8
Zr	150	64
Nb	13	4
Hf	4.5	1.9
Ta	1.2	0.4
La	36	18
Ce	56	37
Sm	5.4	2.2
Eu	1.1	0.3
Tb	0.79	0.28
Yb	2.5	0.7
Lu	0.39	0.12

SILVERTON SHALE (SIL)

SAMPLE	AVG	STD
K2O/Na2O	4.3	3.9
SiO2/Al2O3	3.4	0.7
Th/U	4.4	0.9
K/Rb	166	36
Rb/Sr	2.4	1.7
Ba/Rb	4.5	3.7
Ba/Sr	7.9	6.8
Th/Sc	0.77	0.35
La/Sc	1.7	1.0
La/Th	2.2	0.7
Zr/Y	5.1	1.6
Ti/Zr	33	9
Zr/Nb	11	3
Ni/Co	4.8	3.7
Cr/V	0.94	0.26
V/Ni	3.0	2.3
Cr/Ni	2.6	1.5
Cr/Zr	1.1	0.7
Sc/Th	1.7	1.6
Co/Th	1.5	1.7
La/Yb	14	4
Eu/Eu*	0.62	0.09
CIA	75	8

SILVERTON SHALE (SIL)

SAMPLE	C 58	C 86	C 87	C 213	D 70
SiO2	58.13	67.77	70.48	54.91	67.11
TiO2	0.73	1.13	0.95	0.70	0.58
Al2O3	20.28	17.11	15.30	14.30	16.04
Fe2O3-T	8.23	2.10	3.77	9.87	5.07
MgO	3.15	0.68	0.36	8.13	2.38
CaO	0.12	0.07	0.38	6.30	0.26
Na2O	0.72	0.25	1.40	4.43	0.23
K2O	3.30	3.07	3.91	0.38	3.71
MnO	0.07	0.04	0.05	0.13	0.04
P2O5	0.04	0.08	0.08	0.07	0.04
LOI	4.86	7.90	3.91	1.20	3.78
TOTAL	99.63	100.20	100.59	100.42	99.24
Rb	179	107	164	16	178
Ba	420	384	705	205	849
Cs	7.6	5.5	8.5	1.9	6.8
Sr	55	97	152	76	23
Pb	14	42	26	11	14
Th	15	16	15	4.7	17
U	2.6	6.5	5.4	0.88	3.9
Sc	26	20	17	43	20
V	147	256	265	240	106
Cr	138	144	146	389	118
Co	28	1.5	4.1	43	11
Ni	91	31	30	128	67
Y	27	31	29	22	28
Zr	108	230	234	90	137
Nb	12	14	14	6.5	11
Hf	3.0	7.0	7.5	3.1	4.9
Ta	1.2	1.4	1.3	0.46	1.1
La	34	59	45	10	23
Ce	40	79	61	20	51
Sm	5.1	6.6	5.2	3.1	4.0
Eu	0.89	0.96	1.2	0.95	0.85
Tb	0.65	0.96	0.77	0.69	0.77
Yb	2.2	3.0	2.9	2.2	3.0
Lu	0.35	0.49	0.41	0.37	0.52

SILVERTON SHALE (SIL)

SAMPLE	C 58	C 86	C 87	C 213	D 70
K2O/Na2O	4.6	12	2.8	0.09	16
SiO2/Al2O3	2.9	4.0	4.6	3.8	4.2
Th/U	5.8	2.5	2.8	5.3	4.4
K/Rb	153	238	198	197	173
Rb/Sr	3.3	1.1	1.1	0.21	7.7
Ba/Rb	2.3	3.6	4.3	13	4.8
Ba/Sr	7.6	4.0	4.6	2.7	37
Th/Sc	0.58	0.80	0.88	0.11	0.85
La/Sc	1.3	3.0	2.6	0.23	1.2
La/Th	2.3	3.7	3.0	2.1	1.4
Zr/Y	4.0	7.4	8.1	4.1	4.9
Ti/Zr	41	29	24	47	25
Zr/Nb	9.0	16	17	14	12
Ni/Co	3.3	21	7.3	3.0	6.1
Cr/V	0.94	0.56	0.55	1.6	1.1
V/Ni	1.6	8.3	8.8	1.9	1.6
Cr/Ni	1.5	4.6	4.9	3.0	1.8
Cr/Zr	1.3	0.63	0.62	4.3	0.86
Sc/Th	1.7	1.3	1.1	9.1	1.2
Co/Th	1.9	0.09	0.27	9.1	0.65
La/Yb	15	20	16	4.5	7.7
Eu/Eu*	0.55	0.45	0.71	0.85	0.61
CIA	81	82	68	50	77

SILVERTON SHALE (SIL)

SAMPLE	D 71	D 72	D 73	D 75	D 79
SiO2	60.42	59.95	58.16	67.10	69.44
TiO2	0.78	0.85	0.76	0.67	0.62
Al2O3	22.52	21.71	20.55	14.80	13.45
Fe2O3-T	5.39	7.22	8.12	5.64	5.48
MgO	2.06	2.20	2.68	2.51	2.92
CaO	0.13	0.17	0.07	1.08	0.60
Na2O	1.72	1.57	0.41	2.45	2.10
K2O	2.56	2.84	3.78	4.08	2.53
MnO	0.04	0.05	0.06	0.07	0.07
P2O5	0.04	0.07	0.04	0.32	0.15
LOI	4.08	4.17	4.95	1.47	3.10
TOTAL	99.74	100.80	99.58	100.19	100.46
Rb	108	132	203	195	151
Ba	702	800	570	1675	482
Cs	5.9	8.5	7.2	9.5	12
Sr	136	101	42	142	104
Pb	25	24	15	15	25
Th	31	22	12	22	12
U	7.7	5.2	2.5	6.4	3.3
Sc	18	26	24	13	13
V	116	161	150	91	87
Cr	74	126	140	95	119
Co	8.2	6.2	22	12	6.3
Ni	33	18	83	44	27
Y	62	39	27	23	23
Zr	361	239	107	167	200
Nb	26	18	11	12	10
Hf	9.7	7.8	3.2	4.8	6.3
Ta	1.8	1.4	1.1	1.0	0.47
La	96	57	36	31	26
Ce	182	126	65	71	58
Sm	13	8.4	5.6	5.1	4.5
Eu	2.0	1.6	0.96	1.1	0.97
Tb	1.9	1.0	0.67	0.67	0.61
Yb	5.0	3.5	2.3	1.8	1.9
Lu	0.75	0.61	0.33	0.25	0.29

SILVERTON SHALE (SIL)

SAMPLE	D 71	D 72	D 73	D 75	D 79
K2O/Na2O	1.5	1.8	9.2	1.7	1.2
SiO2/Al2O3	2.7	2.8	2.8	4.5	5.2
Th/U	4.0	4.2	4.8	3.4	3.6
K/Rb	197	179	155	174	139
Rb/Sr	0.79	1.3	4.8	1.4	1.5
Ba/Rb	6.5	6.1	2.8	8.6	3.2
Ba/Sr	5.2	7.9	14	12	4.6
Th/Sc	1.7	0.85	0.50	1.7	0.92
La/Sc	5.3	2.2	1.5	2.4	2.0
La/Th	3.1	2.6	3.0	1.4	2.2
Zr/Y	5.8	6.1	4.0	7.3	8.7
Ti/Zr	13	21	43	24	19
Zr/Nb	14	13	9.7	14	20
Ni/Co	4.0	2.9	3.8	3.7	4.3
Cr/V	0.64	0.78	0.93	1.0	1.4
V/Ni	3.5	8.9	1.8	2.1	3.2
Cr/Ni	2.2	7.0	1.7	2.2	4.4
Cr/Zr	0.20	0.53	1.3	0.57	0.60
Sc/Th	0.58	1.2	2.0	0.59	1.1
Co/Th	0.26	0.28	1.8	0.55	0.53
La/Yb	19	16	16	17	14
Eu/Eu*	0.48	0.61	0.55	0.69	0.68
CIA	80	79	81	60	66

SILVERTON SHALE (SIL)

SAMPLE	D 80	D 81	D 82	D 83	D 84
SiO2	66.08	62.63	58.34	58.17	57.84
TiO2	0.64	0.77	0.80	0.71	0.77
Al2O3	14.33	18.39	18.43	20.33	21.54
Fe2O3-T	5.46	8.61	9.70	7.65	7.55
MgO	2.62	3.39	2.75	2.47	1.75
CaO	0.93	0.56	0.16	0.24	0.25
Na2O	2.65	1.73	0.34	0.84	0.72
K2O	3.08	2.69	2.92	2.72	3.26
MnO	0.06	0.10	0.09	0.06	0.05
P2O5	0.21	0.08	0.07	0.07	0.05
LOI	3.75	1.88	5.90	5.67	5.51
TOTAL	99.81	100.83	99.50	98.93	99.29
Rb	165	163	169	162	193
Ba	790	365	466	424	416
Cs	10	14	6.8	8.3	10
Sr	147	88	37	78	63
Pb	25	23	20	25	30
Th	16	14	13	16	17
U	4.4	3.6	2.3	3.5	4.2
Sc	14	21	23	25	27
V	93	149	148	148	170
Cr	148	124	121	131	156
Co	24	29	20	13	8.2
Ni	91	63	70	68	61
Y	23	30	32	29	32
Zr	194	120	121	105	113
Nb	11	15	15	13	13
Hf	5.9	3.7	3.2	3.0	3.0
Ta	0.73	1.7	0.98	1.3	1.4
La	29	32	24	34	48
Ce	61	69	16	26	32
Sm	4.7	5.5	4.0	5.3	7.3
Eu	1.0	1.1	0.92	0.96	1.3
Tb	0.60	0.69	0.71	0.83	0.87
Yb	1.8	2.3	2.4	2.4	2.7
Lu	0.29	0.22	0.36	0.36	0.41

SILVERTON SHALE (SIL)

SAMPLE	D 80	D 81	D 82	D 83	D 84
K2O/Na2O	1.2	1.6	8.6	3.2	4.5
SiO2/Al2O3	4.6	3.4	3.2	2.9	2.7
Th/U	3.6	3.9	5.7	4.6	4.0
K/Rb	155	137	143	139	140
Rb/Sr	1.1	1.9	4.6	2.1	3.1
Ba/Rb	4.8	2.2	2.8	2.6	2.2
Ba/Sr	5.4	4.1	13	5.4	6.6
Th/Sc	1.1	0.67	0.57	0.64	0.63
La/Sc	2.1	1.5	1.0	1.4	1.8
La/Th	1.8	2.3	1.8	2.1	2.8
Zr/Y	8.4	4.0	3.8	3.6	3.5
Ti/Zr	20	38	40	41	41
Zr/Nb	18	8.0	8.1	8.1	8.7
Ni/Co	3.8	2.2	3.5	5.2	7.4
Cr/V	1.6	0.83	0.82	0.89	0.92
V/Ni	1.0	2.4	2.1	2.2	2.8
Cr/Ni	1.6	2.0	1.7	1.9	2.6
Cr/Zr	0.76	1.0	1.0	1.2	1.4
Sc/Th	0.88	1.5	1.8	1.6	1.6
Co/Th	1.5	2.1	1.5	0.81	0.48
La/Yb	16	14	10	14	18
Eu/Eu*	0.68	0.64	0.68	0.55	0.57
CIA	61	73	83	81	81

SILVERTON SHALE (SIL)

SAMPLE	D 85	D 86	D 87	D 88	D 95
SiO2	57.78	57.19	59.10	57.88	58.65
TiO2	0.70	0.66	0.81	0.70	0.60
Al2O3	20.76	20.24	20.11	21.72	15.41
Fe2O3-T	8.80	9.35	9.19	8.99	9.88
MgO	3.31	3.24	3.56	3.23	4.09
CaO	0.20	0.25	0.49	0.12	1.83
Na2O	0.47	0.59	1.50	0.63	3.03
K2O	3.13	2.77	3.41	3.09	0.16
MnO	0.06	0.05	0.08	0.05	0.05
P2O5	0.06	0.04	0.08	0.02	0.05
LOI	4.59	5.26	2.08	4.29	5.25
TOTAL	99.86	99.64	100.41	100.72	99.00
Rb	186	168	200	195	4.6
Ba	445	340	802	387	81
Cs	9.5	8.3	18	11	<0.5
Sr	74	65	87	80	80
Pb	23	22	18	20	16
Th	14	15	18	16	12
U	4.0	2.7	4.0	3.5	2.9
Sc	25	25	25	26	22
V	164	147	177	167	131
Cr	135	135	144	134	128
Co	28	22	29	26	24
Ni	79	81	87	81	88
Y	25	28	32	28	21
Zr	108	102	132	114	108
Nb	12	12	16	13	10
Hf	3.3	3.0	3.8	3.0	3.0
Ta	1.2	1.2	1.7	1.3	0.86
La	14	28	42	29	10
Ce	39	32	83	18	21
Sm	2.7	4.3	5.6	4.6	3.8
Eu	0.66	1.0	1.1	0.95	0.58
Tb	0.46	0.76	0.83	0.69	0.62
Yb	2.1	2.1	2.7	2.2	2.1
Lu	0.33	0.34	0.40	0.37	0.35

SILVERTON SHALE (SIL)

SAMPLE	D 85	D 86	D 87	D 88	D 95
K2O/Na2O	6.7	4.7	2.3	4.9	0.05
SiO2/Al2O3	2.8	2.8	2.9	2.7	3.8
Th/U	3.5	5.6	4.5	4.6	4.1
K/Rb	140	137	142	132	289
Rb/Sr	2.5	2.6	2.3	2.4	0.06
Ba/Rb	2.4	2.0	4.0	2.0	18
Ba/Sr	6.0	5.2	9.2	4.8	1.0
Th/Sc	0.56	0.60	0.72	0.62	0.55
La/Sc	0.56	1.1	1.7	1.1	0.44
La/Th	1.0	1.9	2.3	1.8	0.81
Zr/Y	4.3	3.6	4.1	4.1	5.1
Ti/Zr	39	39	37	37	33
Zr/Nb	9.0	8.5	8.3	8.8	11
Ni/Co	2.8	3.7	3.0	3.1	3.7
Cr/V	0.82	0.92	0.81	0.80	0.98
V/Ni	2.1	1.8	2.0	2.1	1.5
Cr/Ni	1.7	1.7	1.7	1.7	1.5
Cr/Zr	1.3	1.3	1.1	1.2	1.2
Sc/Th	1.8	1.7	1.4	1.6	1.8
Co/Th	2.0	1.5	1.6	1.6	2.0
La/Yb	6.7	13	16	13	4.6
Eu/Eu*	0.73	0.69	0.60	0.63	0.46
CIA	82	82	74	83	65

SILVERTON SHALE (SIL)

SAMPLE	D 97	D 99	D 113	D 114
SiO2	56.76	61.56	58.32	64.44
TiO2	0.75	0.89	0.75	0.65
Al2O3	18.78	19.79	21.67	16.59
Fe2O3-T	11.51	5.92	7.49	8.64
MgO	2.02	0.89	2.68	2.77
CaO	0.58	0.06	0.73	0.37
Na2O	1.07	0.62	1.79	1.15
K2O	3.39	3.96	2.78	2.37
MnO	0.06	0.03	0.07	0.06
P2O5	0.06	0.02	0.07	0.03
LOI	5.22	5.35	3.54	1.93
TOTAL	100.20	99.09	99.89	99.00
Rb	174	190	169	134
Ba	473	510	459	313
Cs	10	9.6	16	8.5
Sr	42	60	109	49
Pb	15	22	22	13
Th	17	22	16	11
U	3.4	4.4	3.5	2.0
Sc	26	21	25	21
V	147	152	172	116
Cr	142	144	137	107
Co	25	3.3	30	20
Ni	84	28	80	71
Y	32	38	27	18
Zr	113	184	112	93
Nb	11	19	14	9.8
Hf	3.8	5.4	2.8	2.6
Ta	1.8	1.7	1.5	0.81
La	47	52	39	30
Ce	9.3	62	78	56
Sm	6.2	8.4	5.0	2.7
Eu	1.2	1.5	0.89	0.67
Tb	0.99	1.1	0.65	0.38
Yb	3.0	3.3	2.3	1.7
Lu	0.46	0.49	0.35	0.26

SILVERTON SHALE (SIL)

SAMPLE	D 97	D 99	D 113	D 114
K2O/Na2O	3.2	6.4	1.6	2.1
SiO2/Al2O3	3.0	3.1	2.7	3.9
Th/U	5.0	5.0	4.6	5.5
K/Rb	162	173	137	147
Rb/Sr	4.1	3.2	1.6	2.7
Ba/Rb	2.7	2.7	2.7	2.3
Ba/Sr	11	8.5	4.2	6.4
Th/Sc	0.65	1.0	0.64	0.52
La/Sc	1.8	2.5	1.6	1.4
La/Th	2.8	2.4	2.4	2.7
Zr/Y	3.5	4.8	4.1	5.2
Ti/Zr	40	29	40	42
Zr/Nb	10	9.7	8.0	9.5
Ni/Co	3.4	8.5	2.7	3.6
Cr/V	0.97	0.95	0.80	0.92
V/Ni	1.8	5.4	2.2	1.6
Cr/Ni	1.7	5.1	1.7	1.5
Cr/Zr	1.3	0.78	1.2	1.2
Sc/Th	1.5	0.95	1.6	1.9
Co/Th	1.5	0.15	1.9	1.8
La/Yb	16	16	17	18
Eu/Eu*	0.58	0.56	0.56	0.77
CIA	75	79	75	77

STRUBENKOP (STR)

SAMPLE	AVG	STD
SiO2	57.89	4.49
TiO2	0.85	0.19
Al2O3	21.17	4.46
Fe2O3-T	12.18	5.71
MgO	1.35	0.21
CaO	0.20	0.08
Na2O	0.60	0.17
K2O	1.43	0.62
MnO	0.06	0.01
P2O5	0.14	0.06
LOI	4.12	0.73
TOTAL	99.99	0.87
Rb	71	29
Ba	588	443
Cs	7.3	2.7
Sr	86	21
Pb	20	2
Th	20	3
U	6.0	1.1
Sc	24	5
V	189	40
Cr	174	37
Co	29	3
Ni	90	22
Y	36	6
Zr	234	69
Nb	18	4
Hf	7.1	2.1
Ta	1.3	0.4
La	49	14
Ce	106	30
Sm	7.6	1.9
Eu	1.6	0.3
Tb	1.0	0.2
Yb	3.5	0.2
Lu	0.53	0.04

STRUBENKOP (STR)

SAMPLE	AVG	STD
K2O/Na2O	2.4	0.7
SiO2/Al2O3	2.9	0.8
Th/U	3.4	0.4
K/Rb	164	15
Rb/Sr	0.80	0.18
Ba/Rb	11	12
Ba/Sr	7.9	7.9
Th/Sc	0.84	0.09
La/Sc	2.1	0.5
La/Th	2.4	0.5
Zr/Y	6.6	1.9
Ti/Zr	23	5
Zr/Nb	13	3
Ni/Co	3.1	0.7
Cr/V	0.93	0.13
V/Ni	2.2	0.6
Cr/Ni	2.0	0.6
Cr/Zr	0.86	0.42
Sc/Th	1.2	0.1
Co/Th	1.5	0.2
La/Yb	14	4
Eu/Eu*	0.65	0.03
CIA	89	3

STRUBENKOP SHALE (STR)

SAMPLE	CDV1-1	CDV1-2	CDV1-3	CDV1-4	CDV1-5
SiO2	56.19	56.82	55.24	66.72	54.46
TiO2	0.51	1.00	0.96	0.80	1.00
Al2O3	12.99	24.04	24.70	19.81	24.33
Fe2O3-T	23.40	8.97	10.53	7.63	10.36
MgO	1.31	1.14	1.49	1.12	1.67
CaO	0.12	0.24	0.30	0.09	0.25
Na2O	0.61	0.83	0.56	0.31	0.69
K2O	0.69	2.09	1.90	0.66	1.82
MnO	0.06	0.05	0.07	0.05	0.08
P2O5	0.06	0.14	0.23	0.08	0.18
LOI	2.87	4.15	4.83	3.89	4.87
TOTAL	98.81	99.47	100.81	101.16	99.71
Rb	41	94	93	32	97
Ba	1450	525	375	197	395
Cs	4.3	10	8.6	3.8	9.7
Sr	61	100	112	62	95
Pb	20	23	22	16	21
Th	17	21	23	15	24
U	5.7	5.3	6.1	4.8	8.1
Sc	20	23	24	19	34
V	217	154	185	140	249
Cr	188	177	138	132	234
Co	29	28	27	27	36
Ni	67	71	80	114	120
Y	26	33	38	36	45
Zr	123	280	249	322	197
Nb	9.6	20	22	18	19
Hf	3.7	8.3	7.1	10	6.2
Ta	0.50	1.7	1.5	1.3	1.5
La	28	58	68	39	54
Ce	60	122	143	84	120
Sm	4.8	8.5	9.7	5.9	8.9
Eu	1.1	1.7	1.9	1.3	1.8
Tb	0.75	1.0	1.2	0.85	1.3
Yb	3.3	3.3	3.6	3.4	3.9
Lu	0.45	0.55	0.55	0.52	0.56

STRUBENKOP SHALE (STR)

SAMPLE	CDV1-1	CDV1-2	CDV1-3	CDV1-4	CDV1-5
K2O/Na2O	1.1	2.5	3.4	2.1	2.6
SiO2/Al2O3	4.3	2.4	2.2	3.4	2.2
Th/U	3.0	4.0	3.8	3.1	3.0
K/Rb	140	185	170	171	156
Rb/Sr	0.67	0.94	0.83	0.52	1.0
Ba/Rb	35	5.6	4.0	6.2	4.1
Ba/Sr	24	5.3	3.3	3.2	4.2
Th/Sc	0.85	0.91	0.96	0.79	0.71
La/Sc	1.4	2.5	2.8	2.1	1.6
La/Th	1.6	2.8	3.0	2.6	2.3
Zr/Y	4.7	8.5	6.6	8.9	4.4
Ti/Zr	25	21	23	15	30
Zr/Nb	13	14	11	18	10
Ni/Co	2.3	2.5	3.0	4.2	3.3
Cr/V	0.87	1.1	0.75	0.94	0.94
V/Ni	3.2	2.2	2.3	1.2	2.1
Cr/Ni	2.8	2.5	1.7	1.2	2.0
Cr/Zr	1.5	0.63	0.55	0.41	1.2
Sc/Th	1.2	1.1	1.0	1.3	1.4
Co/Th	1.7	1.3	1.2	1.8	1.5
La/Yb	8.5	18	19	11	14
Eu/Eu*	0.70	0.65	0.63	0.68	0.62
CIA	87	86	89	94	88

TIMEBALL HILL SHALE (TH)

SAMPLE	AVG	STD
SiO2	59.36	7.15
TiO2	0.70	0.12
Al2O3	20.75	3.68
Fe2O3-T	8.52	4.48
MgO	1.78	0.54
CaO	0.70	0.72
Na2O	0.84	0.56
K2O	3.52	1.29
MnO	0.05	0.03
P2O5	0.19	0.22
LOI	4.23	1.01
TOTAL	100.63	0.89
Rb	177	47
Ba	674	244
Cs	14	8
Sr	127	68
Pb	34	19
Th	22	6
U	7.2	5.4
Sc	18	5
V	151	36
Cr	140	40
Co	21	17
Ni	57	20
Y	32	13
Zr	170	48
Nb	15	5
Hf	4.9	1.6
Ta	1.6	0.3
La	56	25
Ce	101	42
Sm	7.5	3.5
Eu	1.5	0.6
Tb	1.1	0.5
Yb	3.1	0.9
Lu	0.47	0.14

TIMEBALL HILL SHALE (TH)

SAMPLE	AVG	STD
K2O/Na2O	5.6	3.4
SiO2/Al2O3	3.0	1.0
Th/U	3.8	1.3
K/Rb	165	35
Rb/Sr	1.7	0.8
Ba/Rb	4.2	3.6
Ba/Sr	6.5	4.3
Th/Sc	1.3	0.7
La/Sc	3.1	1.2
La/Th	2.5	1.0
Zr/Y	6.2	2.8
Ti/Zr	26	6
Zr/Nb	12	6
Ni/Co	4.1	3.6
Cr/V	0.94	0.22
V/Ni	2.9	1.0
Cr/Ni	2.6	0.9
Cr/Zr	0.87	0.30
Sc/Th	0.84	0.22
Co/Th	1.0	0.8
La/Yb	18	7
Eu/Eu*	0.66	0.16
CIA	78	6

TIMEBALL HILL SHALE (TH)

SAMPLE	C 16	C 18	C 19	C 21	C 77
SiO2	54.76	56.45	51.69	59.16	58.85
TiO2	0.74	0.62	0.76	0.74	0.68
Al2O3	26.68	24.00	26.14	20.82	23.05
Fe2O3-T	8.70	7.74	11.51	8.66	10.14
MgO	1.73	1.34	2.22	1.85	2.66
CaO	0.34	0.08	0.80	0.13	0.19
Na2O	1.00	0.78	0.85	0.94	0.43
K2O	3.25	4.53	2.67	3.32	2.74
MnO	0.05	0.01	0.04	0.04	0.16
P2O5	0.21	0.10	0.54	0.06	0.16
LOI	3.07	5.07	3.46	3.94	2.06
TOTAL	100.53	100.72	100.68	99.66	101.12
Rb	170	241	146	203	154
Ba	588	801	588	616	707
Cs	9.2	24	8.0	9.3	9.1
Sr	128	147	107	164	220
Pb	41	41	37	38	54
Th	27	27	34	23	23
U	7.2	4.7	9.7	6.2	8.3
Sc	20	25	27	17	18
V	193	198	205	154	142
Cr	176	197	224	148	127
Co	15	21	17	16	11
Ni	70	30	67	59	54
Y	37	41	51	23	57
Zr	135	132	137	233	185
Nb	19	13	20	18	20
Hf	4.0	4.5	4.7	7.1	5.2
Ta	1.8	1.4	1.8	1.7	1.8
La	63	58	104	38	121
Ce	126	84	213	53	168
Sm	8.1	9.7	17	5.0	19
Eu	1.6	2.1	3.1	1.2	3.1
Tb	1.1	1.3	2.4	0.80	2.1
Yb	3.3	4.2	4.4	2.5	4.2
Lu	0.50	0.65	0.70	0.42	0.67

TIMEBALL HILL SHALE (TH)

SAMPLE	C 16	C 18	C 19	C 21	C 77
K2O/Na2O	3.3	5.8	3.1	3.5	6.4
SiO2/Al2O3	2.1	2.4	2.0	2.8	2.6
Th/U	3.8	5.7	3.5	3.7	2.8
K/Rb	159	156	152	136	148
Rb/Sr	1.3	1.6	1.4	1.2	0.70
Ba/Rb	3.5	3.3	4.0	3.0	4.6
Ba/Sr	4.6	5.4	5.5	3.8	3.2
Th/Sc	1.4	1.1	1.3	1.4	1.3
La/Sc	3.2	2.3	3.9	2.2	6.7
La/Th	2.3	2.1	3.1	1.7	5.3
Zr/Y	3.6	3.2	2.7	10	3.2
Ti/Zr	33	28	33	19	22
Zr/Nb	7.1	10	6.9	13	9.3
Ni/Co	4.7	1.4	3.9	3.7	4.9
Cr/V	0.91	0.99	1.1	0.96	0.89
V/Ni	2.8	6.6	3.1	2.6	2.6
Cr/Ni	2.5	6.6	3.3	2.5	2.4
Cr/Zr	1.3	1.5	1.6	0.64	0.69
Sc/Th	0.74	0.93	0.79	0.74	0.78
Co/Th	0.56	0.78	0.50	0.70	0.48
La/Yb	19	14	24	15	29
Eu/Eu*	0.62	0.68	0.57	0.72	0.53
CIA	83	79	85	80	86

TIMEBALL HILL SHALE (TH)

SAMPLE	C 78	C 214	D 23	D 26	D 27
SiO2	62.61	68.37	59.85	67.99	59.62
TiO2	0.53	0.64	0.76	0.68	0.70
Al2O3	19.05	14.98	21.76	18.58	23.33
Fe2O3-T	7.38	4.27	7.85	4.45	5.49
MgO	2.57	2.74	1.06	0.84	1.02
CaO	0.05	0.83	0.63	0.38	0.40
Na2O	0.79	2.53	0.86	0.44	0.85
K2O	3.67	1.80	3.10	3.65	4.33
MnO	0.02	0.09	0.03	<0.002	0.01
P2O5	0.06	0.05	0.18	0.04	0.06
LOI	4.35	4.21	4.21	3.14	4.27
TOTAL	101.08	100.51	100.29	100.19	100.08
Rb	179	64	175	213	240
Ba	860	1755	435	628	803
Cs	11	6.0	12	13	15
Sr	114	60	153	113	158
Pb	39	27	43	28	41
Th	20	11	21	19	24
U	3.0	2.4	5.6	7.3	8.2
Sc	17	16	18	13	18
V	142	123	151	123	161
Cr	138	141	150	112	136
Co	19	8.1	8.2	3.5	8.7
Ni	52	46	70	25	43
Y	16	21	27	19	23
Zr	144	131	168	231	188
Nb	11	11	17	19	17
Hf	4.6	3.9	4.7	7.2	5.6
Ta	1.3	1.1	1.9	2.0	1.9
La	33	7.7	78	25	38
Ce	94	19	155	37	66
Sm	3.5	2.8	9.2	3.3	4.6
Eu	0.98	0.69	1.5	0.94	0.93
Tb	0.65	0.63	1.0	0.54	0.67
Yb	1.9	2.4	3.0	2.4	2.4
Lu	0.34	0.38	0.41	0.36	0.38

TIMEBALL HILL SHALE (TH)

SAMPLE	C 78	C 214	D 23	D 26	D 27
K2O/Na2O	4.6	0.71	3.6	8.3	5.1
SiO2/Al2O3	3.3	4.6	2.8	3.7	2.6
Th/U	6.7	4.6	3.8	2.6	2.9
K/Rb	170	233	147	142	150
Rb/Sr	1.6	1.1	1.1	1.9	1.5
Ba/Rb	4.8	27	2.5	2.9	3.3
Ba/Sr	7.5	29	2.8	5.6	5.1
Th/Sc	1.2	0.69	1.2	1.5	1.3
La/Sc	1.9	0.48	4.3	1.9	2.1
La/Th	1.7	0.70	3.7	1.3	1.6
Zr/Y	9.0	6.2	6.2	12	8.2
Ti/Zr	22	29	27	18	22
Zr/Nb	13	12	9.9	12	11
Ni/Co	2.7	5.7	8.5	7.1	4.9
Cr/V	0.97	1.1	0.99	0.91	0.84
V/Ni	2.7	2.7	2.2	4.9	3.7
Cr/Ni	2.7	3.1	2.1	4.5	3.2
Cr/Zr	0.96	1.1	0.89	0.48	0.72
Sc/Th	0.85	1.5	0.86	0.68	0.75
Co/Th	0.95	0.74	0.39	0.18	0.36
La/Yb	17	3.2	26	10	16
Eu/Eu*	0.81	0.68	0.53	0.86	0.62
CIA	78	67	80	78	78

TIMEBALL HILL SHALE (TH)

SAMPLE	D 29	D 30	D 31	D 32	D 59
SiO2	60.63	54.55	71.78	50.85	56.60
TiO2	0.34	0.91	0.53	1.11	0.79
Al2O3	23.78	21.22	10.56	23.92	25.65
Fe2O3-T	4.40	11.75	11.32	11.91	8.74
MgO	1.36	2.27	1.57	2.65	1.51
CaO	2.15	0.41	0.23	0.14	0.08
Na2O	1.02	0.68	0.34	0.76	0.73
K2O	2.88	3.88	0.89	4.05	4.06
MnO	0.01	0.07	0.06	0.04	0.06
P2O5	0.13	0.44	0.14	0.09	0.09
LOI	2.82	4.68	2.64	4.39	2.90
TOTAL	99.52	100.86	100.06	99.91	101.21
Rb	197	175	48	218	171
Ba	851	717	160	642	810
Cs	9.8	9.0	2.1	9.3	9.5
Sr	211	105	29	123	116
Pb	50	24	11	12	39
Th	51	18	23	26	26
U	25	9.7	3.5	4.9	7.0
Sc	9.4	23	8.6	31	21
V	73	234	139	247	185
Cr	8.1	169	85	210	169
Co	4.4	20	8.2	28	15
Ni	18	61	30	77	54
Y	36	34	25	32	34
Zr	141	173	449	166	148
Nb	6.5	17	11	13	19
Hf	5.3	4.8	14	4.5	4.7
Ta	1.6	1.4	1.3	1.2	2.0
La	23	56	14	58	66
Ce	52	118	31	123	113
Sm	2.2	8.7	2.8	9.5	7.4
Eu	1.0	1.7	1.0	1.5	1.2
Tb	0.78	1.3	0.61	1.2	1.1
Yb	3.0	3.3	2.7	3.4	3.3
Lu	0.50	0.47	0.46	0.53	0.55

TIMEBALL HILL SHALE (TH)

SAMPLE	D 29	D 30	D 31	D 32	D 59
K2O/Na2O	2.8	5.7	2.6	5.3	5.6
SiO2/Al2O3	2.5	2.6	6.8	2.1	2.2
Th/U	2.0	1.9	6.6	5.3	3.7
K/Rb	121	184	154	154	197
Rb/Sr	0.93	1.7	1.7	1.8	1.5
Ba/Rb	4.3	4.1	3.3	2.9	4.7
Ba/Sr	4.0	6.8	5.5	5.2	7.0
Th/Sc	5.4	0.78	2.7	0.84	1.2
La/Sc	2.4	2.4	1.6	1.9	3.1
La/Th	0.45	3.1	0.61	2.2	2.5
Zr/Y	3.9	5.1	18	5.2	4.4
Ti/Zr	14	32	7.1	40	32
Zr/Nb	22	10	41	13	7.8
Ni/Co	4.1	3.1	3.7	2.8	3.6
Cr/V	0.11	0.72	0.61	0.85	0.91
V/Ni	4.1	3.8	4.6	3.2	3.4
Cr/Ni	0.45	2.8	2.8	2.7	3.1
Cr/Zr	0.06	0.98	0.19	1.3	1.1
Sc/Th	0.18	1.3	0.37	1.2	0.81
Co/Th	0.09	1.1	0.36	1.1	0.58
La/Yb	7.7	17	5.2	17	20
Eu/Eu*	1.4	0.60	0.99	0.50	0.50
CIA	80	80	86	81	82

TIMEBALL HILL SHALE (TH)

SAMPLE	D 61	D 63	D 66	D 67	D 106
SiO2	55.39	68.25	59.66	54.72	59.73
TiO2	0.81	0.59	0.76	0.83	0.74
Al2O3	22.75	16.01	23.22	26.27	20.55
Fe2O3-T	10.56	7.69	6.99	6.02	8.66
MgO	1.94	2.04	0.71	0.87	0.84
CaO	0.27	0.05	0.05	1.15	0.04
Na2O	0.91	0.38	0.51	0.67	0.47
K2O	3.41	3.69	4.71	5.38	3.84
MnO	0.06	0.03	0.02	0.06	0.03
P2O5	0.23	0.09	0.19	1.06	0.09
LOI	4.24	2.26	4.01	3.95	4.88
TOTAL	100.57	101.08	100.83	100.98	99.87
Rb	182	171	258	294	169
Ba	909	475	778	982	912
Cs	8.0	5.6	11	14	4.8
Sr	144	42	120	242	99
Pb	<9.8	<9.8	56	37	14
Th	22	14	24	28	19
U	5.2	4.6	10	25	6.9
Sc	20	12	19	25	18
V	178	161	157	202	171
Cr	160	87	143	169	134
Co	51	20	1.8	3.2	13
Ni	68	37	36	60	80
Y	31	25	33	80	21
Zr	148	223	189	193	184
Nb	18	11	19	22	13
Hf	3.8	6.5	5.6	5.6	5.3
Ta	1.5	1.1	1.8	1.9	1.2
La	52	29	139	101	35
Ce	110	53	79	203	65
Sm	7.6	4.8	14	17	4.9
Eu	1.4	1.1	2.3	3.4	1.0
Tb	1.0	0.77	1.3	2.8	0.66
Yb	2.9	2.5	3.3	6.4	2.7
Lu	0.44	0.40	0.50	0.93	0.41

TIMEBALL HILL SHALE (TH)

SAMPLE	D 61	D 63	D 66	D 67	D 106
K2O/Na2O	3.7	9.7	9.2	8.0	8.2
SiO2/Al2O3	2.4	4.3	2.6	2.1	2.9
Th/U	4.2	3.0	2.4	1.1	2.8
K/Rb	156	179	152	152	189
Rb/Sr	1.3	4.1	2.2	1.2	1.7
Ba/Rb	5.0	2.8	3.0	3.3	5.4
Ba/Sr	6.3	11	6.5	4.1	9.2
Th/Sc	1.1	1.2	1.3	1.1	1.1
La/Sc	2.6	2.4	7.3	4.0	1.9
La/Th	2.4	2.1	5.8	3.6	1.8
Zr/Y	4.8	8.9	5.7	2.4	8.8
Ti/Zr	33	16	24	26	24
Zr/Nb	8.2	20	9.9	8.8	14
Ni/Co	1.3	1.9	20	19	6.2
Cr/V	0.90	0.54	0.91	0.84	0.78
V/Ni	2.6	4.4	4.4	3.4	2.1
Cr/Ni	2.4	2.4	4.0	2.8	1.7
Cr/Zr	1.1	0.39	0.76	0.88	0.73
Sc/Th	0.91	0.86	0.79	0.89	0.95
Co/Th	2.3	1.4	0.08	0.11	0.68
La/Yb	18	12	42	16	13
Eu/Eu*	0.58	0.69	0.55	0.60	0.64
CIA	81	78	80	79	81

TIMEBALL HILL SHALE (TH)

SAMPLE	D 107	MSF1-1	MSF1-2	MSF1-3	MSF1-4
SiO2	54.98	65.56	64.56	61.54	62.41
TiO2	0.79	0.51	0.53	0.69	0.66
Al2O3	25.46	13.98	15.43	19.83	18.46
Fe2O3-T	6.59	7.49	6.74	7.58	5.18
MgO	1.18	2.52	2.08	1.73	2.06
CaO	0.39	2.82	3.15	0.43	0.28
Na2O	1.43	1.12	0.63	0.55	0.50
K2O	3.99	1.85	2.39	6.70	8.85
MnO	0.03	0.06	0.05	0.05	0.03
P2O5	0.09	0.13	0.11	0.18	0.19
LOI	4.59	4.73	5.00	3.99	2.70
TOTAL	99.52	100.77	100.67	103.27	101.32
Rb	207	97	129	192	235
Ba	913	469	555	651	853
Cs	11	5.6	6.8	16	17
Sr	230	131	184	64	49
Pb	47	33	31	31	12
Th	27	13	14	21	19
U	5.3	2.2	2.9	6.9	4.5
Sc	20	10	12	17	18
V	182	88	116	142	141
Cr	180	73	76	147	213
Co	11	6.9	24	21	22
Ni	47	27	47	59	85
Y	27	16	18	35	24
Zr	142	137	138	175	155
Nb	19	8.2	7.4	17	12
Hf	3.7	4.0	3.8	4.8	4.5
Ta	1.7	0.82	0.71	1.7	1.4
La	55	42	40	54	23
Ce	35	76	77	104	45
Sm	7.6	5.4	5.1	7.3	3.5
Eu	1.7	1.1	1.3	1.4	0.77
Tb	0.99	0.62	0.58	1.1	0.67
Yb	2.8	1.5	1.7	3.2	2.2
Lu	0.39	0.25	0.26	0.46	0.36

TIMEBALL HILL SHALE (TH)

SAMPLE	D 107	MSF1-1	MSF1-2	MSF1-3	MSF1-4
K2O/Na2O	2.8	1.7	3.8	12	18
SiO2/Al2O3	2.2	4.7	4.2	3.1	3.4
Th/U	5.1	5.9	4.8	3.0	4.2
K/Rb	160	158	154	290	313
Rb/Sr	0.90	0.74	0.70	3.0	4.8
Ba/Rb	4.4	4.8	4.3	3.4	3.6
Ba/Sr	4.0	3.6	3.0	10	17
Th/Sc	1.4	1.3	1.2	1.2	1.1
La/Sc	2.8	4.2	3.3	3.2	1.3
La/Th	2.0	3.2	2.9	2.6	1.2
Zr/Y	5.3	8.6	7.7	5.0	6.5
Ti/Zr	33	22	23	24	26
Zr/Nb	7.5	17	19	10	13
Ni/Co	4.3	3.9	2.0	2.8	3.9
Cr/V	0.99	0.83	0.66	1.0	1.5
V/Ni	3.9	3.3	2.5	2.4	1.7
Cr/Ni	3.8	2.7	1.6	2.5	2.5
Cr/Zr	1.3	0.53	0.55	0.84	1.4
Sc/Th	0.74	0.77	0.86	0.81	0.95
Co/Th	0.41	0.53	1.7	1.0	1.2
La/Yb	20	28	24	17	10
Eu/Eu*	0.71	0.66	0.83	0.59	0.63
CIA	78	73	78	70	64

TIMEBALL HILL SHALE (TH)

SAMPLE	MSF2-1	MSF2-2	MSF2-3	MSF2-5	MSF2-7
SiO2	58.81	64.64	61.47	57.87	59.98
TiO2	0.70	0.53	0.70	0.72	0.62
Al2O3	20.75	16.61	20.08	21.53	20.78
Fe2O3-T	8.69	6.90	7.15	7.58	6.78
MgO	2.22	2.09	1.50	1.59	1.44
CaO	0.53	1.40	0.32	0.53	0.38
Na2O	0.56	0.55	0.61	1.16	0.95
K2O	3.99	2.78	3.05	2.24	3.07
MnO	0.05	0.04	0.04	0.05	0.06
P2O5	0.16	0.07	0.09	0.06	0.08
LOI	4.24	4.73	4.52	6.90	5.82
TOTAL	100.70	100.34	99.53	100.23	99.96
Rb	193	143	173	175	209
Ba	772	520	460	330	705
Cs	16	11	28	30	34
Sr	99	92	142	150	95
Pb	84	35	26	24	14
Th	21	17	21	21	22
U	5.8	3.3	4.2	6.0	8.2
Sc	19	14	19	17	16
V	144	131	144	108	138
Cr	144	95	140	134	126
Co	17	15	22	12	20
Ni	47	55	68	66	43
Y	35	17	32	52	29
Zr	155	159	147	145	172
Nb	14	9.2	13	14	20
Hf	4.6	3.8	4.2	4.4	4.5
Ta	1.8	0.85	1.6	1.6	2.2
La	76	46	55	59	53
Ce	184	81	100	104	116
Sm	9.4	4.3	7.9	5.8	6.6
Eu	1.6	1.1	1.7	0.92	1.5
Tb	1.3	0.59	0.92	0.93	0.88
Yb	3.8	1.9	3.7	3.3	4.5
Lu	0.47	0.27	0.58	0.52	0.43

TIMEBALL HILL SHALE (TH)

SAMPLE	MSF2-1	MSF2-2	MSF2-3	MSF2-5	MSF2-7
K2O/Na2O	7.1	5.1	5.0	1.9	3.2
SiO2/Al2O3	2.8	3.9	3.1	2.7	2.9
Th/U	3.6	5.2	5.0	3.5	2.7
K/Rb	172	161	146	106	122
Rb/Sr	1.9	1.6	1.2	1.2	2.2
Ba/Rb	4.0	3.6	2.7	1.9	3.4
Ba/Sr	7.8	5.7	3.2	2.2	7.4
Th/Sc	1.1	1.2	1.1	1.2	1.4
La/Sc	4.0	3.3	2.9	3.5	3.3
La/Th	3.6	2.7	2.6	2.8	2.4
Zr/Y	4.4	9.4	4.6	2.8	5.9
Ti/Zr	27	20	29	30	22
Zr/Nb	11	17	11	10	8.6
Ni/Co	2.8	3.7	3.1	5.5	2.2
Cr/V	1.0	0.73	0.97	1.2	0.91
V/Ni	3.1	2.4	2.1	1.6	3.2
Cr/Ni	3.1	1.7	2.1	2.0	2.9
Cr/Zr	0.93	0.60	0.95	0.92	0.73
Sc/Th	0.90	0.892	0.90	0.81	0.73
Co/Th	0.81	0.88	1.0	0.57	0.91
La/Yb	20	24	15	18	12
Eu/Eu*	0.53	0.80	0.70	0.48	0.72
CIA	78	78	81	81	79

TIMEBALL HILL SHALE (TH)

SAMPLE	MSF2-8	MSF2-9	WBK-1-1	WBK-1-2	WBK-1-3
SiO2	59.18	54.55	63.57	71.64	60.02
TiO2	0.72	0.81	0.74	0.48	0.73
Al2O3	23.93	23.95	17.30	12.67	22.35
Fe2O3-T	6.93	9.76	7.20	4.86	7.80
MgO	1.06	1.72	2.09	1.76	1.66
CaO	0.29	0.33	1.13	1.77	0.14
Na2O	0.72	0.41	1.94	2.06	0.35
K2O	4.25	4.11	3.63	1.42	4.10
MnO	0.06	0.07	0.05	0.06	0.05
P2O5	0.14	0.16	0.13	0.11	0.07
LOI	4.05	4.49	2.88	3.29	3.85
TOTAL	101.33	100.36	100.66	100.12	101.12
Rb	211	191	196	76	203
Ba	507	670	575	452	740
Cs	30	32	16	5.1	13
Sr	95	84	131	202	105
Pb	14	11	65	19	77
Th	22	21	18	13	22
U	7.0	7.9	6.1	4.4	4.6
Sc	17	19	16	12	17
V	147	158	130	71	136
Cr	137	150	192	72	160
Co	20	28	64	12	20
Ni	40	59	121	32	56
Y	27	29	23	14	28
Zr	172	168	190	146	162
Nb	20	20	11	5.7	18
Hf	3.7	4.8	5.5	4.7	4.5
Ta	1.8	1.8	1.1	0.85	1.8
La	64	60	39	52	57
Ce	103	117	80	94	108
Sm	7.3	7.7	4.8	4.9	7.5
Eu	1.4	1.4	1.2	1.2	1.4
Tb	1.4	0.97	0.67	0.55	0.90
Yb	3.1	2.8	2.0	1.7	2.8
Lu	0.66	0.40	0.30	0.30	0.41

TIMEBALL HILL SHALE (TH)

SAMPLE	MSF2-8	MSF2-9	WBK-1-1	WBK-1-2	WBK-1-3
K2O/Na2O	5.9	10	1.9	0.69	12
SiO2/Al2O3	2.5	2.3	3.7	5.7	2.7
Th/U	3.1	2.7	3.0	3.0	4.8
K/Rb	167	179	154	155	168
Rb/Sr	2.2	2.3	1.5	0.38	1.9
Ba/Rb	2.4	3.5	2.9	5.9	3.6
Ba/Sr	5.3	8.0	4.4	2.2	7.0
Th/Sc	1.3	1.1	1.1	1.1	1.3
La/Sc	3.8	3.2	2.4	4.3	3.4
La/Th	2.9	2.9	2.2	4.0	2.6
Zr/Y	6.4	5.8	8.3	10	5.8
Ti/Zr	25	29	23	20	27
Zr/Nb	8.6	8.4	17	26	9.0
Ni/Co	2.0	2.1	1.9	2.7	2.8
Cr/V	0.93	0.95	1.5	1.0	1.2
V/Ni	3.7	2.7	1.1	2.2	2.4
Cr/Ni	3.4	2.5	1.6	2.3	2.9
Cr/Zr	0.80	0.89	1.0	0.49	0.99
Sc/Th	0.77	0.90	0.89	0.92	0.77
Co/Th	0.91	1.3	3.6	0.92	0.91
La/Yb	21	21	20	31	20
Eu/Eu*	0.55	0.58	0.78	0.80	0.60
CIA	80	81	66	62	81

TIMEBALL HILL SHALE (TH)

SAMPLE	WBK-1-4	WBK-1-5	CDV-1-14	CDV-1-16	CDV-1-17
SiO2	59.13	66.81	63.47	58.63	64.22
TiO2	0.73	0.67	0.80	0.71	0.62
Al2O3	21.79	18.41	17.37	21.16	17.42
Fe2O3-T	7.84	4.37	6.74	9.31	7.83
MgO	1.86	1.36	2.41	1.97	1.81
CaO	0.70	0.57	2.00	1.30	0.70
Na2O	0.56	0.38	3.11	0.91	0.95
K2O	3.36	3.78	2.57	4.25	2.83
MnO	0.05	0.03	0.07	0.05	0.05
P2O5	0.24	0.05	0.15	0.50	0.09
LOI	5.00	5.95	3.85	3.85	4.03
TOTAL	101.26	102.38	102.54	102.64	100.55
Rb	165	191	144	203	157
Ba	557	728	1057	650	475
Cs	15	19	12	15	15
Sr	95	113	446	101	157
Pb	33	22	55	80	40
Th	25	21	24	21	24
U	6.6	4.0	5.2	6.5	4.5
Sc	17	17	23	18	16
V	147	107	162	156	120
Cr	149	126	142	128	107
Co	25	29	32	22	30
Ni	61	105	47	54	69
Y	33	51	22	26	29
Zr	155	165	162	148	173
Nb	19	12	10	14	12
Hf	4.3	4.9	5.0	3.8	5.0
Ta	1.8	1.4	1.3	1.7	1.4
La	58	49	56	40	56
Ce	115	99	101	90	113
Sm	8.7	7.5	6.2	8.3	8.7
Eu	1.7	1.5	1.5	1.3	1.5
Tb	1.2	1.4	0.82	0.99	1.1
Yb	3.0	4.5	2.9	2.9	3.6
Lu	0.43	0.70	0.43	0.39	0.56

TIMEBALL HILL SHALE (TH)

SAMPLE	WBK-1-4	WBK-1-5	CDV-1-14	CDV-1-16	CDV-1-17
K2O/Na2O	6.0	9.9	0.83	4.7	3.0
SiO2/Al2O3	2.7	3.6	3.7	2.8	3.7
Th/U	3.8	5.3	4.6	3.2	5.3
K/Rb	169	164	148	174	150
Rb/Sr	1.7	1.7	0.32	2.0	1.0
Ba/Rb	3.4	3.8	7.3	3.2	3.0
Ba/Sr	5.9	6.4	2.4	6.4	3.0
Th/Sc	1.5	1.2	1.0	1.2	1.5
La/Sc	3.4	2.9	2.4	2.2	3.5
La/Th	2.3	2.3	2.3	1.9	2.3
Zr/Y	4.7	3.2	7.4	5.7	6.0
Ti/Zr	28	24	30	29	21
Zr/Nb	8.2	14	16	11	14
Ni/Co	2.4	3.6	1.5	2.5	2.3
Cr/V	1.0	1.2	0.88	0.82	0.89
V/Ni	2.4	1.0	3.4	2.9	1.7
Cr/Ni	2.4	1.2	3.0	2.4	1.6
Cr/Zr	0.96	0.76	0.88	0.86	0.62
Sc/Th	0.68	0.81	0.96	0.86	0.67
Co/Th	1.0	1.4	1.3	1.0	1.3
La/Yb	19	11	19	14	16
Eu/Eu*	0.61	0.58	0.76	0.50	0.55
CIA	81	78	61	76	75

TIMEBALL HILL SHALE (TH)

SAMPLE	CDV-1-19	CDV-1-21	CDV-1-22	CDV-1-24	CDV-1-25
SiO2	31.16	38.42	56.12	56.81	57.56
TiO2	0.78	0.76	0.77	0.71	0.71
Al2O3	23.22	24.07	23.38	22.11	22.12
Fe2O3-T	31.36	22.71	8.64	8.62	8.21
MgO	2.90	1.90	1.91	2.06	1.80
CaO	0.24	1.50	0.19	1.19	0.50
Na2O	0.56	0.53	0.76	0.34	0.55
K2O	1.67	3.38	3.88	3.06	3.45
MnO	0.11	0.07	0.05	0.05	0.05
P2O5	0.08	1.07	0.12	0.40	0.21
LOI	5.94	5.08	4.45	5.26	5.67
TOTAL	98.02	99.49	100.27	100.61	100.83
Rb	91	177	187	156	170
Ba	273	515	729	529	599
Cs	9.6	24	23	12	15
Sr	34	63	103	97	88
Pb	24	39	12	13	39
Th	21	24	23	31	22
U	6.4	29	5.9	7.3	6.1
Sc	19	20	17	17	34
V	161	213	144	143	144
Cr	149	162	151	145	148
Co	46	102	20	11	28
Ni	68	73	69	56	62
Y	27	49	27	36	30
Zr	160	155	166	164	147
Nb	24	23	19	18	18
Hf	4.5	4.4	4.7	4.6	4.1
Ta	1.8	2.0	1.7	1.7	1.7
La	57	97	60	65	58
Ce	120	168	114	127	113
Sm	8.2	7.5	7.6	11	8.0
Eu	1.4	2.3	1.4	2.0	1.6
Tb	0.84	1.6	0.91	1.4	1.0
Yb	2.7	4.0	2.5	3.0	2.8
Lu	0.45	0.58	0.39	0.46	0.40

TIMEBALL HILL SHALE (TH)

SAMPLE	CDV-1-19	CDV-1-21	CDV-1-22	CDV-1-24	CDV-1-25
K2O/Na2O	3.0	6.4	5.1	9.0	6.3
SiO2/Al2O3	1.3	1.6	2.4	2.6	2.6
Th/U	3.3	0.83	3.9	4.2	3.6
K/Rb	152	158	172	163	168
Rb/Sr	2.7	2.8	1.8	1.6	1.9
Ba/Rb	3.0	2.9	3.9	3.4	3.5
Ba/Sr	8.0	8.2	7.1	5.5	6.8
Th/Sc	1.1	1.2	1.4	1.8	0.65
La/Sc	3.0	4.9	3.5	3.8	1.7
La/Th	2.7	4.0	2.6	2.1	2.6
Zr/Y	5.9	3.2	6.1	4.6	4.9
Ti/Zr	29	29	28	26	29
Zr/Nb	6.7	6.7	8.7	9.1	8.2
Ni/Co	1.5	0.72	3.5	5.1	2.2
Cr/V	0.93	0.76	1.0	1.0	1.0
V/Ni	2.4	2.9	2.1	2.6	2.3
Cr/Ni	2.2	2.2	2.2	2.6	2.4
Cr/Zr	0.93	1.0	0.91	0.88	1.0
Sc/Th	0.90	0.83	0.74	0.55	1.6
Co/Th	2.2	4.3	0.87	0.35	1.3
La/Yb	21	24	24	22	21
Eu/Eu*	0.56	0.86	0.59	0.58	0.64
CIA	88	84	81	85	81

TIMEBALL HILL SHALE (TH)	
SAMPLE	CDV-1-27
SiO2	65.85
TiO2	0.69
Al2O3	17.97
Fe2O3-T	4.79
MgO	1.23
CaO	0.80
Na2O	0.57
K2O	3.62
MnO	0.04
P2O5	0.05
LOI	5.07
TOTAL	100.68
Rb	189
Ba	712
Cs	20
Sr	102
Pb	19
Th	24
U	4.6
Sc	19
V	113
Cr	133
Co	27
Ni	86
Y	51
Zr	172
Nb	13
Hf	5.1
Ta	1.5
La	50
Ce	96
Sm	7.7
Eu	1.5
Tb	1.5
Yb	4.9
Lu	0.79

TIMEBALL HILL SHALE (TH)	
SAMPLE	CDV-1-27
K2O/Na2O	6.4
SiO2/Al2O3	3.7
Th/U	5.2
K/Rb	159
Rb/Sr	1.9
Ba/Rb	3.8
Ba/Sr	7.0
Th/Sc	1.3
La/Sc	2.6
La/Th	2.1
Zr/Y	3.4
Ti/Zr	24
Zr/Nb	13
Ni/Co	3.2
Cr/V	1.2
V/Ni	1.3
Cr/Ni	1.5
Cr/Zr	0.77
Sc/Th	0.79
Co/Th	1.1
La/Yb	10
Eu/Eu*	0.56
CIA	76

BLACK REEF PELITES (BR)

SAMPLE	AVG	STD	AVG*	STD*
SiO2	53.84	13.85	55.62	4.28
TiO2	0.89	0.31	0.99	0.11
Al2O3	18.44	5.69	20.59	2.78
Fe2O3-T	7.45	6.35	6.13	1.64
MgO	4.44	2.87	3.98	1.52
CaO	2.02	5.16	0.75	1.48
Na2O	0.09	0.08	0.11	0.09
K2O	4.54	2.19	5.34	1.56
MnO	0.19	0.43	0.08	0.10
P2O5	0.14	0.06	0.15	0.06
LOI	7.49	7.01	5.97	1.51
TOTAL	99.53	0.71	99.69	0.41
Rb	126	59	148	43
Ba	293	131	332	109
Cs	5.5	3.8	6.4	3.7
Sr	27	18	31	18
Pb	15	5	15	6
Th	5.6	1.8	6.2	1.2
U	2.1	0.7	2.4	0.6
Sc	24	8	26	5
V	205	69	224	39
Cr	421	147	469	89
Co	39	32	33	10
Ni	327	223	284	97
Y	30	9	33	6
Zr	157	36	171	14
Nb	7.8	1.9	8.4	1.0
Hf	4.4	1.0	4.8	0.5
Ta	0.72	0.19	0.79	0.11
La	29	11	32	9
Ce	57	22	63	19
Sm	5.2	1.7	5.7	1.4
Eu	1.2	0.4	1.3	0.3
Tb	0.67	0.23	0.74	0.19
Yb	2.4	0.7	2.7	0.5
Lu	0.38	0.12	0.42	0.08

BLACK REEF PELITES (BR)

SAMPLE	AVG	STD	AVG*	STD*
K2O/Na2O	143	206	164	223
SiO2/Al2O3	3.7	3.6	2.8	0.5
Th/U	2.7	0.5	2.7	0.5
K/Rb	297	46	300	29
Rb/Sr	6.3	3.6	6.7	3.7
Ba/Rb	2.7	1.4	2.4	0.7
Ba/Sr	14	7	14	7
Th/Sc	0.24	0.06	0.24	0.04
La/Sc	1.3	0.4	1.2	0.2
La/Th	5.2	0.9	5.1	0.8
Zr/Y	5.5	1.6	5.4	1.6
Ti/Zr	33	10	35	3
Zr/Nb	21	6	21	2
Ni/Co	11	9	8.9	3.4
Cr/V	2.4	1.5	2.1	0.5
V/Ni	0.82	0.43	0.91	0.39
Cr/Ni	1.6	1.0	1.9	0.9
Cr/Zr	2.7	0.8	2.8	0.6
Sc/Th	4.6	1.9	4.3	0.6
Co/Th	9.0	13.5	5.4	1.6
La/Yb	12	3	12	3
Eu/Eu*	0.72	0.11	0.73	0.12
CIA	79	6	78	4

* excluding samples MEE-8, MEE-9 and MEE-18

BLACK REEF PELITES (BR)

SAMPLE	MEE-4	MEE-6	MEE-8	MEE-9	MEE-17
SiO2	55.92	55.23	36.90	85.95	60.61
TiO2	0.95	1.00	1.16	0.03	0.98
Al2O3	21.42	18.53	17.20	4.87	19.14
Fe2O3-T	5.42	5.75	31.13	2.58	5.32
MgO	3.04	8.49	4.33	1.06	2.73
CaO	0.15	0.09	0.08	1.21	0.29
Na2O	0.17	0.01	0.03	0.01	0.01
K2O	5.88	4.17	0.65	1.02	5.04
MnO	0.04	0.04	0.18	0.04	0.05
P2O5	0.11	0.06	0.07	0.09	0.21
LOI	5.64	6.18	5.48	2.73	4.92
TOTAL	98.64	99.39	97.20	99.83	99.19
Rb	168	117	33	24	142
Ba	466	251	36	171	432
Cs	6.6	2.0	0.79	1.0	5.4
Sr	34	10	4.0	7.3	23
Pb	13	12	<9.8	14	15
Th	7.7	5.0	2.6	3.0	4.5
U	2.7	2.2	0.84	1.8	2.3
Sc	31	24	30	7.8	21
V	206	207	275	59	215
Cr	678	397	73	443	389
Co	41	30	158	26	22
Ni	285	264	287	1111	359
Y	35	16	18	18	34
Zr	167	172	128	113	173
Nb	9.2	8.0	9	2.7	7.4
Hf	5.5	4.6	3.7	3.5	4.1
Ta	0.95	0.74	0.53	0.39	0.70
La	46	24	12	16	21
Ce	88	47	25	32	39
Sm	7.1	3.0	3.0	3.5	4.7
Eu	1.7	0.56	0.66	0.78	1.1
Tb	0.82	0.21	0.33	0.58	0.73
Yb	3.2	1.8	1.7	1.6	2.5
Lu	0.55	0.33	0.27	0.23	0.38

BLACK REEF PELITES (BR)

SAMPLE	MEE-4	MEE-6	MEE-8	MEE-9	MEE-17
K2O/Na2O	35	417	20	102	840
SiO2/Al2O3	2.6	3.0	2.1	18	3.2
Th/U	2.9	2.3	3.1	1.7	2.0
K/Rb	291	296	163	353	295
Rb/Sr	4.9	12	8.3	3.3	6.2
Ba/Rb	2.8	2.1	1.1	7.1	3.0
Ba/Sr	14	25	9.0	23	19
Th/Sc	0.25	0.21	0.09	0.38	0.21
La/Sc	1.5	1.0	0.40	2.1	1.0
La/Th	6.0	4.8	4.6	5.3	4.7
Zr/Y	4.8	11	7.1	6.3	5.1
Ti/Zr	34	35	54	1.5	34
Zr/Nb	18	22	15	42	23
Ni/Co	7.0	8.8	1.8	43	16
Cr/V	3.3	1.9	0.27	7.5	1.8
V/Ni	0.72	0.78	0.96	0.05	0.60
Cr/Ni	2.4	1.5	0.25	0.40	1.1
Cr/Zr	4.1	2.3	0.57	3.9	2.2
Sc/Th	4.0	4.8	12	2.6	4.7
Co/Th	5.3	6.0	61	8.7	4.9
La/Yb	14	13	7.1	10	8.4
Eu/Eu*	0.78	0.65	0.72	0.66	0.71
CIA	76	80	96	81	78

BLACK REEF PELITES (BR)

SAMPLE	MEE-18	MEE-20	MEE-22	MEE-25	MEE-29
SiO2	15.50	48.46	55.57	55.37	55.76
TiO2	0.20	0.87	1.09	0.98	1.13
Al2O3	5.31	17.96	21.44	21.72	17.93
Fe2O3-T	5.89	5.50	6.12	7.51	11.04
MgO	13.82	5.26	3.13	3.47	4.92
CaO	21.33	5.78	0.27	0.21	1.01
Na2O	0.05	0.03	0.03	0.24	0.25
K2O	1.53	4.88	6.24	4.96	1.07
MnO	1.81	0.40	0.04	0.05	0.13
P2O5	0.13	0.13	0.19	0.16	0.11
LOI	33.94	10.60	5.86	5.10	6.10
TOTAL	99.50	99.87	99.96	99.76	99.44
Rb	38	145	173	131	32
Ba	161	292	325	453	117
Cs	2.7	12	7.5	6.3	1.2
Sr	24	53	13	45	74
Pb	12	26	19	14	20
Th	2.0	6.1	5.5	7.5	4.8
U	0.75	1.8	1.6	2.6	2.3
Sc	6.6	31	27	27	21
V	44	203	234	227	241
Cr	120	464	408	518	404
Co	10	40	33	44	46
Ni	139	362	235	294	452
Y	12	32	38	33	27
Zr	47	151	182	163	161
Nb	4.4	7.9	8.2	8.2	8.4
Hf	1.2	5.0	4.6	4.6	4.2
Ta	0.24	0.69	0.75	0.77	0.68
La	14	35	27	52	23
Ce	28	68	50	103	45
Sm	1.9	6.2	5.7	8.8	4.6
Eu	0.42	1.4	1.3	1.7	1.6
Tb	0.23	0.81	0.84	0.88	0.62
Yb	0.94	3.4	2.6	2.5	2.1
Lu	0.08	0.52	0.38	0.43	0.35

BLACK REEF PELITES (BR)

SAMPLE	MEE-18	MEE-20	MEE-22	MEE-25	MEE-29
K2O/Na2O	34	143	231	21	4.2
SiO2/Al2O3	2.9	2.7	2.6	2.5	3.1
Th/U	2.7	3.4	3.4	2.9	2.1
K/Rb	335	279	299	314	277
Rb/Sr	1.6	2.7	13	2.9	0.43
Ba/Rb	4.2	2.0	1.9	3.5	3.7
Ba/Sr	6.7	5.5	25	10	1.6
Th/Sc	0.30	0.20	0.20	0.28	0.23
La/Sc	2.1	1.1	1.0	1.9	1.1
La/Th	7.0	5.7	4.9	6.9	4.8
Zr/Y	3.9	4.7	4.8	4.9	6.0
Ti/Zr	25	34	36	36	42
Zr/Nb	11	19	22	20	19
Ni/Co	14	9.1	7.1	6.7	9.8
Cr/V	2.7	2.3	1.7	2.3	1.7
V/Ni	0.32	0.56	1.0	0.77	0.53
Cr/Ni	0.86	1.3	1.7	1.8	0.89
Cr/Zr	2.6	3.1	2.2	3.2	2.5
Sc/Th	3.3	5.1	4.9	3.6	4.4
Co/Th	5.0	6.6	6.0	5.9	9.6
La/Yb	15	10	10	21	11
Eu/Eu*	0.71	0.71	0.70	0.64	1.1
CIA	75	77	76	79	91

BLACK REEF PELITES (BR)

SAMPLE	MEE-31	MEE-35	MEE-37	MEE-38	MEE-40
SiO2	50.05	60.14	61.49	51.93	50.75
TiO2	1.21	1.00	0.83	1.06	1.00
Al2O3	25.24	20.55	17.46	25.10	24.19
Fe2O3-T	5.76	5.04	7.27	4.79	5.61
MgO	3.67	2.40	2.97	3.63	4.19
CaO	0.17	0.05	0.26	0.22	0.74
Na2O	0.09	0.05	0.06	0.17	0.08
K2O	7.56	5.88	4.35	6.90	6.23
MnO	0.04	0.02	0.07	0.05	0.12
P2O5	0.14	0.05	0.19	0.17	0.14
LOI	6.08	4.55	4.86	6.24	6.95
TOTAL	100.00	99.72	99.82	100.25	99.98
Rb	178	131	129	201	178
Ba	311	306	277	525	356
Cs	13	3.3	3.7	4.8	5.0
Sr	26	13	22	42	27
Pb	22	12	14	16	16
Th	6.2	8.2	5.9	6.8	7.6
U	1.9	3.9	2.3	2.1	3.0
Sc	33	27	20	29	33
V	254	217	188	324	242
Cr	397	500	409	518	615
Co	35	46	26	30	26
Ni	146	314	423	234	231
Y	43	33	32	37	35
Zr	202	192	159	179	172
Nb	9.1	9.6	9.6	9.5	9.0
Hf	5.3	5.8	4.3	4.8	5.3
Ta	0.80	0.98	0.72	0.85	0.99
La	35	31	25	36	38
Ce	68	68	49	69	85
Sm	6.1	5.0	4.9	6.7	6.8
Eu	1.4	1.2	1.2	1.2	1.7
Tb	0.98	0.76	0.70	0.80	0.92
Yb	3.6	3.0	2.3	2.6	3.3
Lu	0.54	0.48	0.37	0.36	0.46

BLACK REEF PELITES (BR)

SAMPLE	MEE-31	MEE-35	MEE-37	MEE-38	MEE-40
K2O/Na2O	84	131	76	41	77
SiO2/Al2O3	2.0	2.9	3.5	2.1	2.1
Th/U	3.3	2.1	2.6	3.2	2.5
K/Rb	352	372	280	285	290
Rb/Sr	6.8	10	5.9	4.8	6.6
Ba/Rb	1.7	2.3	2.1	2.6	2.0
Ba/Sr	12	24	13	13	13
Th/Sc	0.19	0.30	0.30	0.23	0.23
La/Sc	1.1	1.1	1.3	1.2	1.2
La/Th	5.6	3.8	4.2	5.3	5.0
Zr/Y	4.7	5.8	5.0	4.8	4.9
Ti/Zr	36	31	31	35	35
Zr/Nb	22	20	17	19	19
Ni/Co	4.2	6.8	16	7.8	8.9
Cr/V	1.6	2.3	2.2	1.6	2.5
V/Ni	1.7	0.69	0.44	1.4	1.0
Cr/Ni	2.7	1.6	0.97	2.2	2.7
Cr/Zr	2.0	2.6	2.6	2.9	3.6
Sc/Th	5.3	3.3	3.4	4.3	4.3
Co/Th	5.6	5.6	4.4	4.4	3.4
La/Yb	9.7	10	11	14	12
Eu/Eu*	0.69	0.73	0.76	0.58	0.78
CIA	75	76	78	76	78

	BLACK REEF (BR)
SAMPLE	CDV-1-28
SiO2	61.82
TiO2	0.82
Al2O3	16.99
Fe2O3-T	4.51
MgO	3.86
CaO	0.49
Na2O	0.21
K2O	6.32
MnO	0.01
P2O5	0.27
LOI	4.60
TOTAL	99.90
Rb	198
Ba	209
Cs	12
Sr	18
Pb	<9.8
Th	5.4
U	1.9
Sc	20
V	149
Cr	402
Co	13
Ni	99
Y	36
Zr	151
Nb	5.7
Hf	4.7
Ta	0.66
La	22
Ce	46
Sm	4.4
Eu	0.86
Tb	0.53
Yb	2.0
Lu	0.30

	BLACK REEF (BR)
SAMPLE	CDV-1-28
K2O/Na2O	30
SiO2/Al2O3	3.6
Th/U	2.8
K/Rb	265
Rb/Sr	11
Ba/Rb	1.1
Ba/Sr	12
Th/Sc	0.27
La/Sc	1.1
La/Th	4.1
Zr/Y	4.2
Ti/Zr	33
Zr/Nb	26
Ni/Co	7.6
Cr/V	2.7
V/Ni	1.5
Cr/Ni	4.1
Cr/Zr	2.7
Sc/Th	3.7
Co/Th	2.4
La/Yb	11
Eu/Eu*	0.63
CIA	70

SELATI PELITES (SEL)

SAMPLE	AVG	STD
SiO2	59.86	10.54
TiO2	0.89	0.64
Al2O3	14.93	1.96
Fe2O3-T	10.88	9.48
MgO	3.71	1.91
CaO	0.60	0.95
Na2O	0.28	0.10
K2O	4.89	3.10
MnO	0.02	0.02
P2O5	0.19	0.15
LOI	3.81	2.09
TOTAL	100.06	1.27
Rb	125	83
Ba	699	370
Cs	5.9	5.7
Sr	24	9
Pb	9.0	1.7
Th	5.7	1.3
U	2.1	0.7
Sc	18	8
V	169	105
Cr	447	533
Co	17	12
Ni	142	151
Y	32	11
Zr	178	92
Nb	10.2	5.7
Hf	5.1	2.1
Ta	0.86	0.29
La	19	9
Ce	40	23
Sm	3.8	2.1
Eu	0.97	0.54
Tb	0.57	0.44
Yb	2.5	1.1
Lu	0.40	0.17

SELATI PELITES (SEL)

SAMPLE	AVG	STD
K2O/Na2O	17	11
SiO2/Al2O3	4.1	1.1
Th/U	3.0	0.9
K/Rb	276	141
Rb/Sr	4.5	2.8
Ba/Rb	10.4	10.6
Ba/Sr	27	11
Th/Sc	0.36	0.11
La/Sc	1.1	0.4
La/Th	3.2	1.1
Zr/Y	5.5	1.5
Ti/Zr	29	8
Zr/Nb	18	5
Ni/Co	9.4	7.3
Cr/V	2.7	2.0
V/Ni	2.0	1.7
Cr/Ni	3.0	0.7
Cr/Zr	4.2	6.4
Sc/Th	3.1	1.3
Co/Th	2.9	2.0
La/Yb	7.7	2.7
Eu/Eu*	0.82	0.20
CIA	75	15

SELATI PELITES (SEL)

SAMPLE	D 50	D 53	D 56	D 111	C 196
SiO2	54.31	60.45	50.44	42.35	68.76
TiO2	0.87	0.47	2.42	0.66	0.53
Al2O3	18.44	12.23	16.54	14.91	15.13
Fe2O3-T	8.07	18.18	10.74	30.35	2.88
MgO	6.06	1.42	7.14	2.96	2.82
CaO	0.49	0.13	2.90	0.13	0.15
Na2O	0.33	0.18	0.49	0.20	0.23
K2O	8.04	0.17	6.83	0.02	6.67
MnO	0.02	<0.002	0.04	0.05	<0.002
P2O5	0.16	0.05	0.55	0.13	0.12
LOI	2.83	6.05	4.92	7.27	2.09
TOTAL	99.62	99.33	103.01	99.03	99.38
Rb	233	8.3	107	5.5	196
Ba	1145	300	607	54	963
Cs	19	0.58	2.7	1.6	5.8
Sr	36	15	31	9.0	24
Pb	<9.8	12	10	<9.8	<9.8
Th	7.6	5.4	5.7	6.4	4.4
U	1.7	1.7	1.7	1.7	2.9
Sc	18	15	35	23	11
V	162	112	391	246	92
Cr	373	419	82	1723	214
Co	17	15	43	19	7.0
Ni	139	132	65	502	60
Y	49	16	47	21	33
Zr	195	110	377	88	140
Nb	12	6.4	23	10	6.0
Hf	5.5	3.6	9.3	2.4	4.8
Ta	0.94	0.67	1.5	0.81	0.69
La	31	13	28	29	9.4
Ce	75	26	65	50	15
Sm	6.1	2.2	7.1	4.9	1.7
Eu	1.3	0.58	1.6	1.8	0.42
Tb	0.93	0.19	1.5	0.39	0.30
Yb	3.2	1.6	4.9	2.3	1.8
Lu	0.48	0.25	0.78	0.41	0.28

SELATI PELITES (SEL)

SAMPLE	D 50	D 53	D 56	D 111	C 196
K2O/Na2O	24	0.94	14	0.10	29
SiO2/Al2O3	2.9	4.9	3.0	2.8	4.5
Th/U	4.5	3.2	3.4	3.8	1.5
K/Rb	286	170	530	30	282
Rb/Sr	6.5	0.55	3.5	0.61	8.2
Ba/Rb	4.9	36	5.7	9.8	4.9
Ba/Sr	32	20	20	6.0	40
Th/Sc	0.42	0.36	0.16	0.28	0.40
La/Sc	1.7	0.87	0.80	1.3	0.85
La/Th	4.1	2.4	4.9	4.5	2.1
Zr/Y	4.0	6.9	8.0	4.2	4.2
Ti/Zr	27	26	38	45	23
Zr/Nb	16	17	16	8.8	23
Ni/Co	8.2	8.8	1.5	26	8.6
Cr/V	2.3	3.7	0.21	7.0	2.3
V/Ni	1.2	0.85	6.0	0.49	1.5
Cr/Ni	2.7	3.2	1.3	3.4	3.6
Cr/Zr	1.9	3.8	0.22	20	1.5
Sc/Th	2.4	2.8	6.1	3.6	2.5
Co/Th	2.2	2.8	7.5	3.0	1.6
La/Yb	9.7	8.1	5.7	13	5.2
Eu/Eu*	0.65	0.90	0.63	1.26	0.73
CIA	66	95	67	98	67

	SELATI (SEL)	
SAMPLE	C 197	C 198
SiO2	73.14	69.60
TiO2	0.46	0.85
Al2O3	12.82	14.43
Fe2O3-T	3.23	2.71
MgO	2.90	2.65
CaO	0.12	0.26
Na2O	0.27	0.24
K2O	5.60	6.91
MnO	<0.002	<0.002
P2O5	0.10	0.21
LOI	1.77	1.77
TOTAL	100.41	99.63
Rb	146	182
Ba	831	993
Cs	5.4	6.0
Sr	22	31
Pb	<9.8	<9.8
Th	3.6	7.1
U	1.5	3.4
Sc	10	13
V	83	94
Cr	165	152
Co	7.0	8.2
Ni	48	47
Y	27	32
Zr	119	214
Nb	5.0	9.2
Hf	3.6	6.7
Ta	0.53	0.91
La	6.8	19
Ce	12	38
Sm	1.3	3.2
Eu	0.36	0.76
Tb	0.23	0.48
Yb	1.6	2.3
Lu	0.27	0.37

	SELATI (SEL)	
SAMPLE	C 197	C 198
K2O/Na2O	21	29
SiO2/Al2O3	5.7	4.8
Th/U	2.4	2.1
K/Rb	318	315
Rb/Sr	6.6	5.9
Ba/Rb	5.7	5.5
Ba/Sr	38	32
Th/Sc	0.36	0.55
La/Sc	0.68	1.5
La/Th	1.9	2.7
Zr/Y	4.4	6.7
Ti/Zr	23	24
Zr/Nb	24	23
Ni/Co	6.9	5.7
Cr/V	2.0	1.6
V/Ni	1.7	2.0
Cr/Ni	3.4	3.2
Cr/Zr	1.4	0.71
Sc/Th	2.8	1.8
Co/Th	1.9	1.2
La/Yb	4.3	8.3
Eu/Eu*	0.82	0.73
CIA	66	65

SOUTPANSBURG SHALES

SAMPLE	AVG	STD	AVG*	STD*
SiO2	55.75	14.62	47.43	2.82
TiO2	1.23	0.25	1.32	0.21
Al2O3	25.24	12.80	31.28	8.51
Fe2O3-T	5.59	5.32	4.97	6.02
MgO	1.14	1.40	1.34	1.57
CaO	0.31	0.45	0.41	0.47
Na2O	0.50	0.54	0.58	0.60
K2O	1.85	1.98	1.80	2.28
MnO	0.04	0.03	0.04	0.03
P2O5	0.20	0.09	0.25	0.05
LOI	8.44	5.99	10.79	5.06
TOTAL	100.27	0.28	100.21	0.30
Rb	71	75	72	87
Ba	613	337	707	341
Cs	2.0	0.8	2.3	0.6
Sr	196	166	261	142
Pb	34	25	43	23
Th	18	7	21	6
U	5.2	1.8	5.4	2.1
Sc	21	10	24	8
V	190	73	150	25
Cr	106	40	125	26
Co	10	11	12	13
Ni	48	32	58	31
Y	38	15	46	7
Zr	279	37	282	42
Nb	21	11	26	7
Hf	7.5	0.9	7.6	1.0
Ta	1.6	0.8	1.9	0.7
La	48	20	57	13
Ce	107	72	134	63
Sm	11	7	14	5
Eu	2.3	1.1	2.8	0.7
Tb	1.5	0.7	1.9	0.4
Yb	3.5	1.1	4.1	0.4
Lu	0.50	0.12	0.57	0.04

SOUTPANSBURG SHALES

SAMPLE	AVG	STD	AVG*	STD*
K2O/Na2O	3.5	2.5	2.2	1.1
SiO2/Al2O3	4.1	4.2	1.7	0.7
Th/U	3.6	0.8	4.0	0.5
K/Rb	188	43	169	33
Rb/Sr	6.7	9.8	1.1	1.5
Ba/Rb	25	21	32	20
Ba/Sr	34	47	7.2	8.4
Th/Sc	1.1	0.4	1.0	0.5
La/Sc	2.5	1.0	2.6	1.1
La/Th	2.8	1.3	3.1	1.3
Zr/Y	9.5	5.8	6.3	1.2
Ti/Zr	27	7	29	7
Zr/Nb	22	18	11	2
Ni/Co	7.2	3.9	8.3	3.9
Cr/V	0.67	0.31	0.84	0.10
V/Ni	6.7	6.2	3.1	1.1
Cr/Ni	2.6	0.6	2.5	0.7
Cr/Zr	0.40	0.20	0.47	0.18
Sc/Th	1.3	1.0	1.5	1.1
Co/Th	0.80	0.99	0.93	1.11
La/Yb	13	4	15	4
Eu/Eu*	0.66	0.06	0.65	0.07
CIA	84	14	88	15

Table C.1-6 Waterberg-Soutpansberg Pelite Analyses

SOUTPANSBERG SHALES

SAMPLE	C 130	C 168	C 169	C 181
SiO2	80.72	45.66	45.22	51.40
TiO2	0.93	1.54	1.04	1.39
Al2O3	7.12	37.19	37.41	19.25
Fe2O3-T	7.44	0.68	0.74	13.48
MgO	0.52	0.38	0.09	3.55
CaO	<0.01	0.09	0.07	1.08
Na2O	0.27	0.09	0.22	1.43
K2O	1.99	0.20	0.17	5.03
MnO	0.03	0.02	0.01	0.08
P2O5	0.05	0.29	0.27	0.18
LOI	1.38	14.18	14.56	3.64
TOTAL	100.45	100.32	99.80	100.51
Rb	68	11	10	194
Ba	331	402	535	1183
Cs	1.0	1.8	1.9	3.1
Sr	<3.0	379	342	62
Pb	<9.8	75	29	25
Th	11	26	24	12
U	4.7	7.8	5.7	2.7
Sc	9.5	17	20	36
V	312	116	159	174
Cr	49	102	111	162
Co	4.6	2.8	4.1	30
Ni	18	36	36	102
Y	14	40	55	42
Zr	271	319	303	223
Nb	5.2	34	26	17
Hf	7.2	8.3	8.3	6.2
Ta	0.68	2.9	1.8	1.1
La	18	72	41	59
Ce	27	221	107	73
Sm	3.0	21	13	8.6
Eu	0.69	3.7	2.7	2.1
Tb	0.47	2.2	2.1	1.3
Yb	1.8	3.7	4.7	3.8
Lu	0.31	0.51	0.62	0.57

SOUTPANSBERG SHALES

SAMPLE	C 130	C 168	C 169	C 181
K2O/Na2O	7.4	2.2	0.77	3.5
SiO2/Al2O3	11	1.2	1.2	2.7
Th/U	2.3	3.3	4.2	4.4
K/Rb	243	151	141	215
Rb/Sr	23	0.03	0.03	3.1
Ba/Rb	4.9	37	54	6.1
Ba/Sr	114	1.1	1.6	19
Th/Sc	1.2	1.5	1.2	0.33
La/Sc	1.9	4.2	2.1	1.6
La/Th	1.6	2.8	1.7	4.9
Zr/Y	19	8.0	5.5	5.3
Ti/Zr	21	29	21	37
Zr/Nb	52	9.4	12	13
Ni/Co	3.9	13	8.8	3.4
Cr/V	0.16	0.88	0.70	0.93
V/Ni	17	3.2	4.4	1.7
Cr/Ni	2.7	2.8	3.1	1.6
Cr/Zr	0.18	0.32	0.37	0.73
Sc/Th	0.86	0.65	0.83	3.0
Co/Th	0.42	0.11	0.17	2.5
La/Yb	10	19	8.7	16
Eu/Eu*	0.70	0.58	0.63	0.75
CIA	73	99	99	67

	WATERBERG SHALE
SAMPLE	C 90
SiO2	62.76
TiO2	0.75
Al2O3	18.55
Fe2O3-T	7.33
MgO	1.24
CaO	0.02
Na2O	0.44
K2O	6.08
MnO	0.03
P2O5	0.05
LOI	2.96
TOTAL	100.21
Rb	415
Ba	904
Cs	14
Sr	30
Pb	19
Th	18
U	4.3
Sc	18
V	110
Cr	176
Co	6.8
Ni	31
Y	36
Zr	201
Nb	18
Hf	5.5
Ta	1.4
La	66
Ce	125
Sm	7.9
Eu	1.8
Tb	1.3
Yb	1.6
Lu	0.49

	WATERBERG SHALE
SAMPLE	C 90
K2O/Na2O	14
SiO2/Al2O3	3.4
Th/U	4.2
K/Rb	122
Rb/Sr	14
Ba/Rb	2.2
Ba/Sr	30
Th/Sc	1.0
La/Sc	3.7
La/Th	3.7
Zr/Y	5.6
Ti/Zr	22
Zr/Nb	11
Ni/Co	4.6
Cr/V	1.6
V/Ni	3.5
Cr/Ni	5.7
Cr/Zr	0.88
Sc/Th	1.0
Co/Th	0.38
La/Yb	41
Eu/Eu*	0.68
CIA	72

APPENDIX D. Normalizing Sample Composites

A number of the figures used in this study have sample values which are normalized to a variety of reference standards. Element contents for these standards are given in this section (Table D.1) along with a discussion of the advantages and problems in their use. The North American Shale Composite (NASC) provides an indication of the overall properties and compositions of shales (Gromet et al., 1984). NASC is composed of 40 Phanerozoic shale samples, approximately half of which are from North America. The remaining samples are from Antarctica and Zambia, with approximately 35% of the samples having unknown origins. The similar composition of NASC and to other Phanerozoic composites, especially for the REE, gives NASC credibility as a representative sample of the Earth's Phanerozoic upper-continental crust. Normalizing Kaapvaal pelite compositions to NASC allows for a comparison of the similarities and differences of Kaapvaal pelite sources and the composition of Phanerozoic upper-continental crust (Figs. 27-30). This comparison of ancient and modern sediments is advantageous in that it minimizes compositional variations caused by weathering and hydraulic sorting of grains during sediment transport. REE contents of NASC appear to be partly contained in detrital phases such as zircon and apatite, leading to some trace element heterogeneity in sample aliquants (Gromet et al., 1984).

While the effects of sample heterogenieties may be pronounced for individual samples, the use of composites such as NASC tends to eliminate these effects. An average of 23 post-Archean shales from Australia (PAAS) also is provided by Nance and Taylor (1976). The similarities between NASC and PAAS confirm that shale composites are representative of their upper-continental sources.

Estimated compositions of Phanerozoic (PUC) and Archean upper-continental crusts (AUC) are given in Table D.1. These compositional estimates are calculated from mass balance relationships with representative sedimentary rocks and direct sampling of the exposed cratons (Taylor and McLennan, 1985). PUC and AUC are used in this study to provide a reference standard which measures the effects of weathering (Fig. 24) and fractionation in the sedimentary cycle (Fig. 27a). The quality of these composites is dependent upon the representativeness of the samples used to calculate their values. Crustal estimates based on sediment compositions may also be influenced by fractionation effects in the sedimentary cycle and preferential preservation of certain tectonic environments.

Element concentrations for chondrites are provided in Table D.1 on a volatile-free basis. These values represent an estimate of the composition of the primitive solar nebula (Evensen et al., 1978). Sediment REE values normalized to chondrites thus represent the amount of REE fractionation in these sediments relative to primitive abundances (Figs. 15-18).

Table 0.1. Chemical compositions of various rock composites used to normalize geochemical data.

SAMPLE	NASC	PAAS	PUC	AUC	CHONDRITE
SiO2	64.8	62.8	66.0	60.1	
TiO2	0.7	1.0	0.5	0.8	
Al2O3	16.9	18.9	15.2	15.3	
Fe2O3-T	6.3	7.2	5.0	8.9	
MgO	2.86	2.2	2.2	4.7	
CaO	3.63	1.3	4.2	6.2	
Na2O	1.14	1.2	3.9	3.3	
K2O	3.97	3.7	3.4	1.8	
MnO	0.06	0.11	0.08	0.18	
P2O5	0.13	0.16	-	-	
Rb	125	160	112	50	
Ba	636	650	550	265	
Cs	5.2	15	3.7	-	
Sr	142	200	350	240	
Pb	-	20	20	-	
Th	12.3	14.6	10.7	5.7	
U	2.7	3.1	2.8	1.5	
Sc	15	16	11	14	
V	130	150	60	195	
Cr	125	110	35	180	
Co	26	-	10	25	
Ni	58	55	20	105	
Y	35	-	22	18	
Zr	200	210	190	125	
Nb	13	19	25	-	
Hf	6.3	5.0	5.8	3.0	
Ta	1.1	-	2.2	-	
La	31	38	30	20	0.37
Ce	67	80	64	42	0.96
Sm	5.6	5.6	4.5	4.0	0.23
Eu	1.2	1.1	0.88	1.2	0.09
Tb	0.85	0.77	0.64	0.57	0.06
Yb	3.1	2.8	2.2	2.0	0.25
Lu	0.46	0.43	0.32	0.31	0.038
Eu/Eu*	0.66	0.61	0.61	0.93	1.00
CIA	69	69	46	45	
Data source	1	2	2	2	3

Major elements in oxide weight percent, all others in ppm; NASC, North American Shale Composite; PAAS, Post-Archean Australian Shale; PUC, Phanerozoic Upper Crust; AUC, Archean Upper Crust. References, 1- Gromet et al., 1984, 2 - Taylor and McLennan, 1985 (PAAS-p.28, Table 2.9; PUC-p.46, Table 2.15; AUC-p.183, Table 7.10), 3 - Evensen et al.,1978; Fe2O3T, total Fe reported as Fe2O3 (Fe2O3T=1.111 x FeO); Eu/Eu*, europium anomaly, calculated as in appendix C; CIA, Chemical Index of Alteration, calculated as in Appendix C (Note CaO reported for PAAS is on a carbonate free basis); -, no value reported.

APPENDIX E. Quartzite Petrographic Descriptions

E.1 Point Count Classification and Summary

Thin sections discussed are those for which framework grain modes are reported in Table 6. Petrographic investigations aid in determining modal contents and primary textures of quartzites. K-stained thin sections have approximately 500 framework grains counted on a 4.5 X 2.5 cm grid of each sample. A total count of >400 points ensures a two sigma confidence range (>95% of the whole rock) for calculated modal percentage (Van der Plas and Tobi, 1965). Standard QtFtL and QmFtLt (Dickinson and Suczek, 1979; Dickinson et al., 1983) ternary diagrams are plotted to illustrate modal characteristics of quartzites (Figs. 39-42). Mineralogic and lithologic classification of framework grains follows procedures outlined by Ingersol et al. (1984) and Lawton (1986). These classification schemes are presented in Table E.1-1, whereas individual point count results are summarized in Table E.1-2. Orthomatrix is a term introduced by Dickinson (1970) for recrystallized detrital lutum or clayey matrix. Pseudomatrix is defined as discontinuous interstitial paste formed by mechanical deformation of weak detrital grains (e.g., soft sediment deformation of muscovite and chlorite). Epimatrix is a term for inhomogenous interstitial materials grown during diagenesis and includes diagenetic alteration of detrital

feldspars. Pseudomatrix and Epimatrix encountered during point counting is assigned to the original framework-grain precursor, when that source can be positively identified.

Table E.1-1 Quartzite framework grain categories used in calculating QtFtL and QmFtLt plots.

(1) Qt: Total framework quartz (Qt=Qm+Qp)
- (A) Qm: Monocrystalline quartz
- (B) Qp: Polycrystalline quartz
  - (a) Chert
  - (b) Polycrystalline quartz of sedimentary, igneous and metamorphic origin
  - (c) Aggregate quartz of indeterminate origin

(2) Ft: Total framework feldspar (Ft=K+P)
- (A) K: Potassium feldspar
- (B) P: Plagioclase

(3) L: Framework lithic fragments (L=Ls+Lv)
- (A) Ls: Sedimentary lithic fragments
  - (a) Pelite-shale
  - (b) Very fine grained feldspathic sandstone
  - (c) Very fine grained quartz wacke
- (B) Lv: Volcanic and hypabyssal lithic fragments

(4) Lt: Total framework lithic fragments (Lt=L+Qp)

Table E.1-2. Quartzite point count results

	Soutpansberg Group				
	C 124	C 160	C 177	C 184	C 188
Qm	406	432	394	165	260
Qp	51	8	66	42	125
Fk	0	0	46	95	110
Fp	0	0	4	2	9
Lv	2	0	0	6	4
Ls	1	0	0	1	60
Qt	457	440	460	207	385
Ft	0	0	50	97	118
L	3	0	0	7	64
Lt	54	8	66	49	189
Ft + Epimatrix	0	0	50	103	118
Mica	0	0	0	7	1
Quartz Cement	128	266	127	23	73
Calcite Cement	0	0	24	0	0
Iron Cement	6	4	0	80	6
Epimatrix	0	0	0	6	0
Orthomatrix	71	36	38	209	102
Pseudomatrix	0	0	0	0	0
% Matrix (Ortho)	15.4	8.2	7.5	39.2	15.2
% Cement (Total)	29.1	61.4	29.6	31.8	12.2

% Matrix calculated on a cement free basis; % cement calculated on an orthomatrix free basis; framework grain classification given in Table E.1-1.

Table E.1-2. (continued)

	Waterberg Group				
	C 89	C 96	C 98	C 99	C 100
Qm	368	328	316	314	301
Qp	117	151	110	127	37
Fk	0	1	0	3	59
Fp	0	0	0	0	16
Lv	0	1	0	0	0
Ls	0	0	0	0	2
Qt	480	479	426	441	338
Ft	0	1	0	3	74
L	0	1	0	0	2
Lt	117	152	110	127	39
Ft + Epimatrix	0	1	0	3	74
Mica	0	8	3	1	1
Quartz Cement	123	88	70	119	68
Calcite Cement	0	0	0	0	0
Iron Cement	10	4	11	18	1
Epimatrix	0	0	0	0	0
Orthomatrix	139	73	128	98	151
Pseudomatrix	0	7	0	0	0
% Matrix (Ortho)	29.0	14.7	29.8	22.0	36.4
% Cement (Total)	27.7	18.5	18.9	30.8	16.6

% Matrix calculated on a cement free basis; % cement calculated on an orthomatrix free basis; framework grain classification given in Table E.1-1.

Table E.1-2. (continued)

	Transvaal Supergroup				
	C 56	C 207	MSF-2-10	C 15	C 76
Qm	422	444	389	402	399
Qp	10	1	18	8	0
Fk	0	25	0	0	0
Fp	0	0	0	0	0
Lv	0	0	2	0	0
Ls	0	0	0	0	0
Qt	432	445	407	410	399
Ft	0	26	0	0	0
L	0	0	2	0	0
Lt	10	1	20	8	0
Ft + Epimatrix	0	31	0	0	0
Mica	0	3	0	1	0
Quartz Cement	159	163	149	113	216
Calcite Cement	0	0	0	0	0
Iron Cement	0	0	0	34	5
Epimatrix	0	5	0	0	0
Orthomatrix	11	2	61	33	0
Pseudomatrix	0	0	0	1	0
% Matrix (Ortho)	2.5	0.4	14.9	8.0	0.0
% Cement (Total)	36.8	34.0	36.4	35.7	55.4

% Matrix calculated on a cement free basis; % cement calculated on an orthomatrix free basis; framework grain classification given in Table E.1-1.

Table E.1-2. (continued)

	Transvaal Supergroup				
	D 34	C 201	D 35	D 47	D 58
Qm	431	401	309	397	412
Qp	15	0	50	91	3
Fk	0	0	100	3	0
Fp	0	0	0	0	0
Lv	0	0	0	57	0
Ls	0	0	0	1	0
Qt	446	401	359	488	415
Ft	0	0	100	3	0
L	0	0	0	58	0
Lt	15	0	50	149	3
Ft + Epimatrix	0	0	125	3	0
Mica	0	0	1	0	0
Quartz Cement	173	236	52	9	175
Calcite Cement	0	0	0	1	0
Iron Cement	0	0	0	1	2
Epimatrix	0	0	25	0	0
Orthomatrix	28	69	168	224	38
Pseudomatrix	0	0	0	1	0
% Matrix (Ortho)	6.3	17.2	34.6	40.7	9.2
% Cement (Total)	38.8	58.9	10.7	2.0	42.7

% Matrix calculated on a cement free basis; % cement calculated on an orthomatrix free basis; framework grain classification given in Table E.1-1.

Table E.1-2. (continued)

Ventersdorp Supergroup

	C 6
Qm	276
Qp	117
Fk	1
Fp	0
Lv	31
Ls	45
Qt	393
Ft	1
L	76
Lt	193
Ft + Epimatrix	5
Mica	0
Quartz Cement	0
Calcite Cement	0
Iron Cement	29
Epimatrix	4
Orthomatrix	241
Pseudomatrix	3
% Matrix (Ortho)	50.5
% Cement (Total)	6.1

% Matrix calculated on a cement free basis; % cement calculated on an orthomatrix free basis; framework grain classification given in Table E.1-1.

Table E.1-2. (continued)

	Witwatersrand Supergroup				
	JWS-8-40	D 8	C 73	C 74	D 21
Qm	468	312	481	379	238
Qp	103	206	55	86	50
Fk	0	0	0	0	0
Fp	0	0	0	0	0
Lv	8	0	0	1	0
Ls	7	4	3	3	2
Qt	571	518	536	465	288
Ft	0	0	0	0	0
L	15	4	3	4	2
Lt	118	210	58	90	52
Ft + Epimatrix	0	0	0	0	0
Micas	13	3	0	0	2
Quartz Cement	0	139	140	79	9
Calcite Cement	0	0	0	0	0
Iron Cement	2	7	2	0	120
Epimatrix	0	0	0	0	0
Orthomatrix	340	159	9	49	116
Pseudomatrix	17	1	0	0	0
% Matrix (Ortho)	55.2	30.2	1.7	10.4	39.7
% Cement (Total)	0.3	27.8	26.3	16.8	44.2

% Matrix calculated on a cement free basis; % cement calculated on an orthomatrix free basis; framework grain classification given in Table E.1-1.

Table E.1-2. (continued)

Witwatersrand Supergroup

	C 70	D 15	C 67
Qm	532	418	592
Qp	40	0	6
Fk	0	0	0
Fp	0	0	0
Lv	4	0	0
Ls	0	0	0
Qt	572	418	598
Ft	0	0	0
L	4	0	0
Lt	44	0	6
Ft + Epimatrix	0	0	0
Mica	0	139	0
Quartz Cement	80	0	45
Calcite Cement	0	0	0
Iron Cement	0	0	1
Epimatrix	0	0	0
Orthomatrix	41	16	10
Pseudomatrix	0	0	0
% Matrix (Ortho)	7.1	2.9	1.7
% Cement (Total)	13.9	0.0	7.7

% Matrix calculated on a cement free basis; % cement calculated on an orthomatrix free basis; framework grain classification given in Table E.1-1.

Table E.1-2. (continued)

Dominion Group

	BBS-3-19	BSF-1-18
Qm	277	277
Qp	143	50
Fk	88	120
Fp	0	7
Lv	0	0
Ls	0	0
Qt	420	327
Ft	88	127
L	0	0
Lt	143	50
Ft + Epimatrix	103	156
Mica	0	9
Quartz Cement	67	4
Calcite Cement	0	0
Iron Cement	0	0
Epimatrix	15	29
Orthomatrix	43	147
Pseudomatrix	0	1
% Matrix (Ortho)	8.2	29.8
% Cement (Total)	12.8	0.8

% Matrix calculated on a cement free basis; % cement calculated on an orthomatrix free basis; framework grain classification given in Table E.1-1.

Table E.1-2. (continued)

	Pongola Supergroup				
	P 33	P45	P 63	P 4	P 7
Qm	340	501	510	396	372
Qp	8	28	8	31	0
Fk	61	13	0	0	0
Fp	2	1	0	1	0
Lv	0	0	0	0	0
Ls	3	0	0	0	0
Qt	348	529	518	427	372
Ft	63	14	0	1	0
L	3	0	0	0	0
Lt	11	28	8	31	0
Ft + Epimatrix	109	21	0	1	0
Mica	3	0	0	1	0
Quartz Cement	43	43	76	51	?
Calcite Cement	13	0	0	0	0
Iron Cement	2	0	1	2	0
Epimatrix	46	7	0	0	0
Orthomatrix	199	12	30	79	28
Pseudomatrix	2	0	0	1	0
% Matrix (Ortho)	42.3	2.2	5.8	18.4	7.5
% Cement (Total)	12.3	7.8	14.9	12.3	0.0

% Matrix calculated on a cement free basis; % cement calculated on an orthomatrix free basis; framework grain classification given in Table E.1-1.

Table E.1-2. (continued)

Pongola Supergroup

	P 12	P 26
Qm	453	412
Qp	17	22
Fk	72	0
Fp	0	0
Lv	0	2
Ls	0	0
Qt	470	434
Ft	72	0
L	0	2
Lt	17	24
Ft + Epimatrix	112	0
Mica	0	0
Quartz Cement	20	55
Calcite Cement	0	0
Iron Cement	0	0
Epimatrix	40	0
Orthomatrix	15	32
Pseudomatrix	0	0
% Matrix (Ortho)	2.6	7.3
% Cement (Total)	3.4	12.6

% Matrix calculated on a cement free basis; % cement calculated on an orthomatrix free basis; framework grain classification given in Table E.1-1.

E.2 Petrographic Descriptions

Individual thin section descriptions of quartzites are arranged in stratigraphic order. Locations of quartzite stratigraphic sections are as follows: Pongola Supergroup, Figure 4; Dominion Group, Figure 6; Witwatersrand Supergroup, Figure E.2-2; Ventersdorp Supergroup, Figure 10; Transvaal Supergroup, Figure E.2-1; Waterberg Group, Figure 12; Soutpansberg Group, Figure 13. FeOx, iron oxides of undetermined mineralogy.

PONGOLA SUPERGROUP

P 33 Mozaan Group (Wit-Mfolozi)

Immature arkosic wacke, moderately sorted, angular quartz (mostly monocrystalline) and subrounded K-feldspar and plagioclase framework grains. Minor lithic-sedimentary, muscovite and chlorite, with trace (<1%) zircon grains. Fine grain sand averages 0.2mm in diameter. Clasts mostly grain supported with point and line contacts. Diagenetic-metamorphic effects are minor, with recrystallization of matrix, development of phyllosilicate rims around clasts, minor fracturing of quartz clasts, minor suturing along quartz grain boundaries, quartz cementation, and soft sediment deformation of micas. Thin shale partings and graded bedding evident in thin section.

P 45 Mozaan Group (Piet Retief)

Supermature (?) quartz arenite, subarkosic with well sorted grains, well rounded where original framework grains are visible. Dominated by monocrystalline and polycrystalline quartz, with lesser K-feldspar and trace plagioclase. Medium to coarse grain sand averages 0.35mm in diameter. Clasts mostly grain supported with sutured and line contacts. Diagenetic-metamorphic quartz cementation and suturing along framework grain boundaries, alteration of K-feldspar, silt infillings of original pore space, minor fracturing of quartz grains.

P 63 Mozaan Group (Piet Retief)

Supermature quartz arenite, well sorted, well rounded where original framework grains are visible. Composed of monocrystalline and polycrystalline quartz. Medium to coarse grain sand averages 0.4mm in diameter. Clasts mostly grain supported with sutured and line contacts. Diagenetic-metamorphic quartz cementation and suturing along framework grain boundaries, extensive microfracturing of quartz grains, recrystallization of matrix, phyllosilicate rims along some grain bounaries.

P 4 Nsuze Group (Vutshini Inlier)

Immature quartz arenite to quartzwacke, moderately sorted, original grain shapes generally not discernible. Dominated by monocrystalline quartz, with lesser polycrystalline quartz and trace plagioclase, muscovite and zircon. Very fine grain sand averages 0.1mm in diameter. Clasts mostly grain supported with line to sutured contacts. Diagenetic-metamorphic quartz cementation and suturing along framework grain boundaries, recrystallization of matrix.

P 7 Nsuze Group (Vutshini Inlier)

Immature quartzwacke (?), extensive shearing and deformation has destroyed most sedimentary features. Dominated by monocrystalline quartz, with lesser phyllosilicates. Suturing along quartz grain boundaries, recrystallization of matrix.

P 12 Nsuze Group (Upper Wit-Mfolozi)

Immature subarkosic wacke, poorly sorted, both subangular and subrounded grains. Dominated by monocrystalline quartz, with lesser polycrystalline quartz and K-feldspar. Medium grain sand averages 0.4mm in diameter. Clasts mostly grain supported with point and line contacts. Diagenetic-metamorphic alteration of feldspar, quartz cementation and suturing along framework grain boundaries, recrystallization of matrix.

P 26 Nsuze Group (Upper Wit-Mfolozi)

Submature quartz arenite, moderately sorted, well rounded where original framework grains are visible. Dominated by monocrystalline and polycrystalline quartz, with traces of porphyritic lithic-volcanics and zircon. Coarse grain sand averages 0.8mm in diameter. Clasts mostly grain supported with sutured and line contacts. Diagenetic-metamorphic quartz cementation and suturing along framework grain boundaries, extensive microfracturing of quartz grains indicated by trails of fluid inclusions, recrystallization of matrix.

DOMINION GROUP

BSF-1-18 Rhenosterspruit Formation

Immature arkosic wacke, very poorly sorted, subangular framework grains dominated by monocrystalline quartz, K-feldspar and polycrystalline quartz, with lesser plagioclase, muscovite, chlorite and grainte clasts (containing quartz, K-feldspar and biotite). Coarse silt to very coarse sand up to 1.8mm in diameter. Clasts mostly grain supported with point and line contacts. Diagenetic-metamorphic recrystallization of matrix and quartz grain fracturing, deformation of detrital micas.

BBS-3-19 Rhenosterspruit Formation

Immature arkosic wacke to subarkose, very poorly sorted, subrounded framework grains dominated by monocrystalline quartz, polycrystalline quartz and K-feldspar, with traces of zircon and granite? (quartz and muscovite). Coarse silt to very coarse sand up to 1.2mm in diameter. Clasts mostly grain supported with point contacts. Diagenetic-metamorphic quartz cementation, suturing along quartz grain boundaries, recrystallization of matrix, formation of tremolite. Graded bedding visible in thin section.

WITWATERSRAND SUPERGROUP

JWS-8-40 Ventersdorp Contact Reef (VCR)

Immature quartzwacke, poorly sorted, angular framework grains dominated by monocrystalline and polycrystalline quartz, with lesser porphyritic lithic-volcanic, lithic-sediment, muscovite, and trace detrital hornblende. Grain size varies from coarse sand to silt and clay matrix. Clasts mostly grain supported with point contacts and lesser matrix support. Diagenetic-metamorphic recrystallization of matrix and soft sediment deformation of muscovite grains.

C 73 Mondeor Conglomerate

Submature quartz arenite, moderately sorted, well rounded framework grains dominated by monocrystalline and polycrystalline quartz, with trace lithic-sedimentary grains. Coarse grain sand averages 0.7mm in diameter. Clasts mostly grain supported with line and suture contacts. Extensive diagenetic-metamorphic quartz cementation, minor suturing and phyllosilicate cement.

Figure E.2-1. Detailed stratigraphic column of the Witwatersrand Supergroup. After Kent, 1980b.

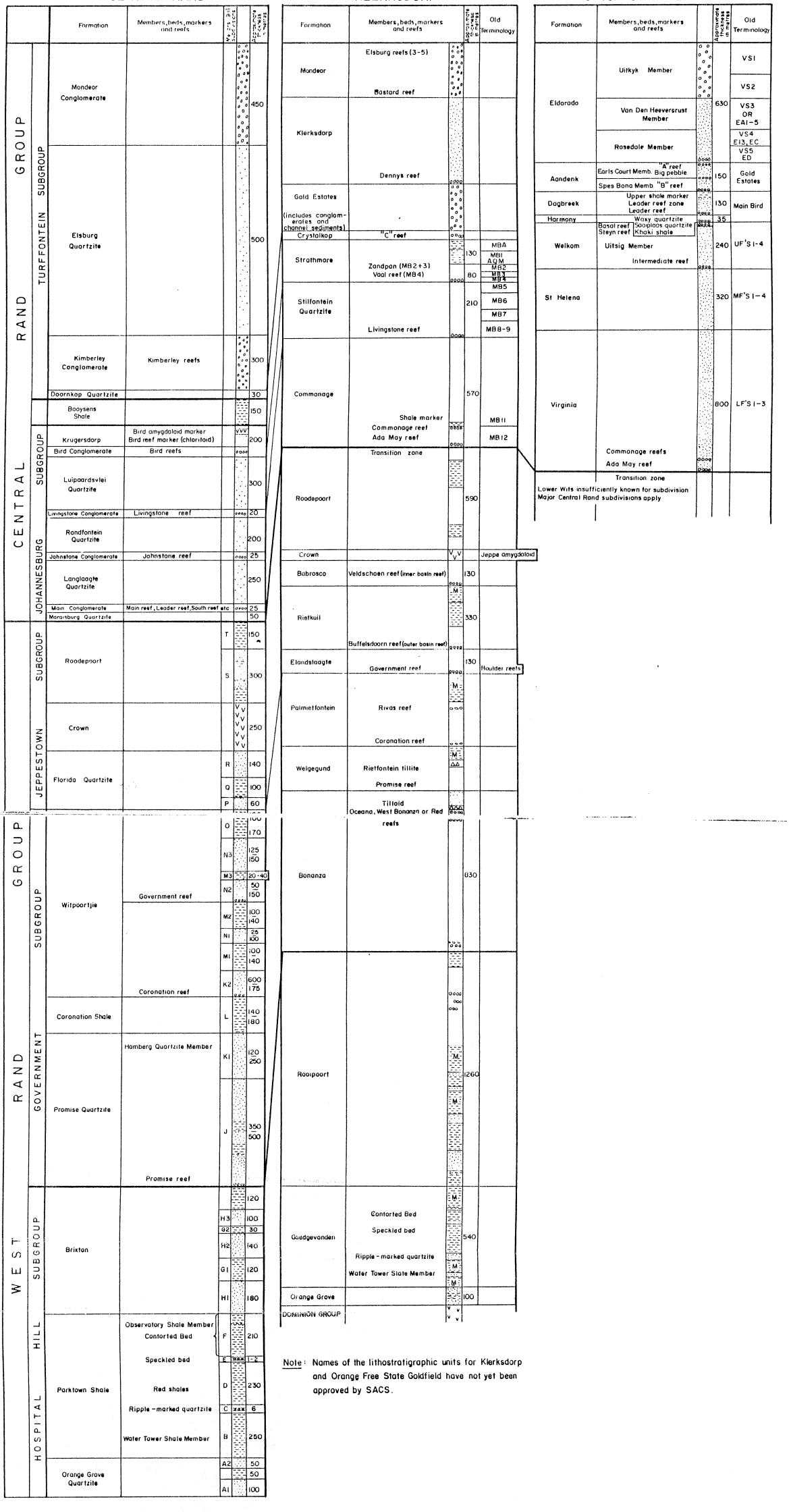

Note: Names of the lithostratigraphic units for Klerksdorp and Orange Free State Goldfield have not yet been approved by SACS.

Fig. 3.2.3.– Lithostratigraphic columns of the Witwatersrand Supergroup in the Central Rand, Klerksdorp area and in the Orange Free State Goldfield

D8 Elsburg Quartzite

Immature quartzwacke, poorly sorted, subangular framework grains dominated by monocrystalline and polycrystalline quartz, with trace lithic-sedimentary, muscovite, zircon and FeOx-rich clasts. Fine to medium grain sand averages 0.20-0.25mm in diameter. Clasts mostly grain supported with point and line contacts. Diagenetic-metamorphic recrystallization of matrix, quartz cementation, fracturing of quartz framework grains, and soft sediment deformation of muscovite.

C 74 Maraisberg Quartzite

Submature to immature quartzwacke, moderately sorted, subrounded framework grains dominated by monocrystalline and polycrystalline quartz, with trace lithic-sedimentary, porphyritic lithic-volcanic, sphene and granite? clasts (containing quartz and muscovite). Medium to coarse grain sand averages 0.4mm in diameter. Clasts mostly grain supported with line and minor suture contacts. Diagenetic-metamorphic recrystallization of matrix, quartz cementation, suturing of quartz grains boundaries.

C 70 Maraisberg Quartzite

Immature to submature quartz arenite to quartzwacke, moderately sorted, subrounded to rounded framework grains dominated by monocrystalline and polycrystalline quartz, with trace porphyritic lithic-volcanic grains and zircon. Medium grain sand averages 0.35mm in diameter. Clasts are grain supported with line and suture contacts. Diagenetic-metamorphic recrystallization of matrix, quartz cementation, minor suturing of quartz grains boundaries.

D 21 Government Subgroup

Immature quartzwacke, poorly sorted, angular framework grains dominated by monocrystalline and polycrystalline quartz, with trace lithic-sediment and muscovite grains. Fine grain sand averages 0.15mm in diameter. Grain and matrix supported clasts with point contacts. Diagenetic-metamorphic recrystallization of matrix, FeOx cementation, fracturing of quartz framework grains, and soft sediment deformation of muscovite.

D 15 Orange Grove Quartzite

Supermature quartz arenite, well sorted, subrounded framework grains composed of monocrystalline quartz. Medium to fine grain sand averages 0.3mm in diameter. Clasts mostly grain supported with line contacts. Extensive diagenetic-metamorphic quartz cementation and minor fracturing of quartz grains.

C 67 Orange Grove Quartzite

Supermature quartz arenite, well sorted, rounded framework grains dominated by monocrystalline quartz and minor polycrystalline quartz. Fine to medium sand averages 0.25mm in diameter. Clasts mostly grain supported with line and sutured contacts. Extensive diagenetic-metamorphic quartz cementation and minor suturing along quartz boundaries.

VENTERSDORP SUPERGROUP

C 6 Bothaville Formation

Immature lithic greywacke, very poorly sorted, angular grains. Dominated by monocrystalline quartz, polycrystalline quartz, and lithic-sedimentary and mafic porphyritic lithic-volcanics, with traces of FeOx rich clasts. Coarse silt to coarse grain sand ranges up to 0.8mm in diameter. Clasts mostly grain supported with point contacts. Diagenetic-metamorphic FeOx cement and rims over framework grains, fracturing of large quartz grains, minor recrystallization of matrix.

TRANSVAAL SUPERGROUP

C 56 Rayton Formation (Uppermost Pretoria Group-not shown on Figure E.2-1)

Supermature quartz arenite, well sorted grains, well rounded where original framework grains are visible. Dominated by monocrystalline quartz, with lesser polycrystalline quartz and trace zircon. Medium grain sand averages 0.35mm in diameter. Clasts mostly grain supported with line contacts. Diagenetic-metamorphic quartz cementation.

Figure E.2-2. Detailed stratigraphic column of the Transvaal Supergroup. After Coertze et al., 1980.

EASTERN TRANSVAAL

GROUP	FORMATION		LITHOLOGY and Mb	Thickness (m)
PRETORIA	Dullstroom Basalt		Mafic to intermediate lava, felsite, some pyroclastics, arenite and hornfels	Up to 1 400
	Houtenbek		Quartzite Hornfels Carbonate and chert	140–255
	Steenkampsberg Quartzite		Quartzite, minor shaly rocks	470–630
	Nederhorst		Argillaceous quartzite, arkose Hornfels	200–800
	Lakenvalei Quartzite		Quartzite, feldspathic quartzite, arkose	160–300
	Vermont Hornfels		Hornfels, minor quartzite, dolomite and chert	450–800
	Magaliesberg Quartzite		Quartzite, minor shale	500
	Silverton Shale		Lydenburg Shale Mb Chert and dolomite. Machadodorp Member (tuff, agglomerate, basalt) Boven Shale Mb	1 000–3 300
	Daspoort Quartzite		Quartzite, some shale	5–90
	Strubenkop Shale		Shale, minor quartzite	20–80
	Dwaalheuwel Quartzite		Quartzite Siltstone, some shale Conglomerate	40–110
	Hekpoort Andesite		Andesite with pyroclastics, some quartzite and shale	0–500
	Boshoek		Siltstone and shale Quartzite, subgraywacke Conglomerate	0–90
	Timeball Hill		Shale with diamictite Quartzite, siltstone, ironstone Shale and mudstone	900–1 600
	Rooihoogte		Quartzite Bevets Conglomerate Member / breccia	0–50
CHUNIESPOORT	Duitschland		Limestone with quartzite, conglomerate, diamictite Shale Dolomite	0–700
	Penge		Iron formation, carbonaceous shale, minor carbonate and breccia	0–600
Malmani Subgroup	Frisco		Chert-free dolomite, primary limestone; carbonaceous shale at base	350
	Eccles		Chert-rich dolomite	400
	Lyttelton		Chert-free dolomite	120
	Monte Christo		Chert-rich dolomite	400
	Oaktree		Dark dolomite-incorporates carbonaceous shale and quartzite	90
WOLKBERG	Black Reef Quartzite		Quartzite, minor shale Serala Basalt Member Quartzite, Conglomerate	0–500
	Sodowa Shale		Quartzite Shale, mudstone	0–150
	Mabin Quartzite		Feldspathic quartzite, some subgraywacke	0–100
	Selati Shale		Shale Argillaceous quartzite, subgraywacke and carbonate Shale	0–1 000
	Schelem		Sericitic quartzite, subgraywacke Shale Arkose Conglomerate	0–140
	Abel Erasmus Basalt		Basalt, pyroclastics Sericitic quartzite, arkose, subgraywacke Basalt Dolomitic shale, chert Basalt	0–500
	Sekororo		Arkose Shale Sericitic quartzite, subgraywacke Conglomerate	0–240

C 207 Silverton Formation (Pretoria Group)

Mature to supermature (?) sublithic arenite, origional grain shapes, contacts and sizes cannot be determined due to post-depositional alteration but framework grains in this sample appear to be composed of coarse sand. Dominated by monocrystalline quartz, with minor K-feldspar and trace amounts of muscovite, polycrystalline quartz, zircon and granite clasts (containing quartz, K-feldspar, biotite and muscovite). Clasts probably grain supported. Diagenetic-metamorphic quartz cementation and recrystallization of matrix.

MSF 2-10 Daspoort Quartzite (Pretoria Group)

Mature to supermature quartzwacke to quartz arenite, well sorted, rounded to well rounded grains. Dominated by monocrystalline quartz, with lesser polycrystalline quartz and porphyritic lithic-volcanics. Very fine to fine grained sand ranges from 0.08 to 0.25mm in diameter. Clasts mostly grain supported with point contacts. Metamorphic and diagenetic quartz cementation and minor recrystallization of matrix. Alternating matrix-rich and matrix-poor bedding layers observed in thin section.

C 15 Timeball Hill Formation (Pretoria Group)

Mature to immature quartzwacke to quartz arenite, poorly sorted, rounded to subrounded. Dominated by monocrystalline quartz, with lesser polycrystalline quartz and traces of muscovite and zircon. Very fine to coarse grain sand ranges from 0.1 to 0.8mm in diameter. Clasts mostly grain supported with point and line contacts. Metamorphic and diagenetic quartz cementation and recrystallization of matrix.

C 76 Rooihoogte Formation (Pretoria Group)

Supermature quartz arenite, very well sorted, rounded grains. Dominated by monocrystalline quartz with traces of zircon and muscovite. Medium grain sand averages 0.4mm in diameter. Clasts mostly grain supported with point, line and sutured contacts. Diagenetic-metamorphic quartz cementation and suturing, microfracturing of quartz grains.

C 201 Black Reef Quartzite (Wolkberg Group)

Immature quartzwacke, well rounded where original grain shapes are visible, well sorted. Composed entirely of monocrystalline quartz. Medium grain sand averages 0.3mm in diameter. Mostly grain supported with line and point contacts. Diagenetic-metamorphic quartz cementation and extensive suturing along quartz grain boundaries, recrystallization of matrix.

D 34 Black Reef Quartzite (Wolkberg Group)

Submature quartz arenite to quartzwacke, moderately sorted, rounded grains. Dominated by monocrystalline quartz, with lesser polycrystalline quartz. Medium grain sand averages 0.4mm in diameter. Clasts mostly grain supported with point contacts. Diagenetic-metamorphic quartz cementation, recrystallization of matrix, microfracturing of quartz grains and growth of phyllosilicate rims around clasts.

D 35 Selati Shale (Wolkberg Group)

Immature lithic greywacke, poorly sorted, subangular to subrounded grains. Dominated by monocrystalline quartz, polycrystalline quartz and K-feldspar, with trace muscovite and zircon. Very fine to coarse grain sand ranges from 0.1 to 0.6mm in diameter. Clasts mostly grain supported with point and line contacts. Diagenetic-metamorphic recrystallization of matrix.

D 47 Sekororo Formation (Wolkberg Group)

Immature lithic greywacke, moderately sorted, subangular grains. Embayed quartz grains noted. Framework grains dominated by monocrystalline quartz, polycrystalline quartz and porphyritic lithic-volcanics, with lesser K-feldspar and lithic-sediments and trace horblende and zircon. Fine to coarse grain sand ranges from 0.2 to 0.6mm in diameter. Clasts mostly grain supported with point and line contacts. Minor diagenetic-metamorphic recrystallization of matrix and calcite cement.

C 53 Godwan Formation (Lowermost Transvaal Supergroup-not shown on Figure E.2-1)

Supermature to mature quartz arenite to quartzwacke, well sorted, subrounded grains. Dominated by monocrystalline quartz, with lesser polycrystalline quartz. Fine grain sand averages 0.15 to 0.20mm in diameter. Clasts mostly grain supported with point and line contacts. Metamorphic and diagenetic quartz cementation, recrystallization of matrix and phyllosilicate overgrowths on grains.

WATERBERG GROUP

C 100 Vaalwater Formation

Immature arkosic wacke, well sorted, angular to subangular grains. Dominated by monocrystalline quartz, K-feldspar and polycrystalline quartz, with lesser plagioclase and trace lithic-sedimentary and muscovite grains. Very coarse silt to very fine grain sand averages 0.08mm in diameter. Clasts mostly grain supported with point and line contacts. Diagenetic-metamorphic recrystallization of matrix, phyllosilicate rims around feldspars, and phyllosilicate filled fractures.

C 99 Cleremont Formation

Immature quartzwacke, poorly sorted, subrounded to subangular grains. Dominated by monocrystalline and polycrystalline quartz, with lesser K-feldspar and muscovite. Fine to very coarse grain sand ranges from 0.2 to 2.0mm in diameter. Clasts mostly grain supported with line and point contacts. Diagenetic and metamorphic quartz and FeOx cementation, recrystallization of matrix and quartz grain fracturing, pore space filling of zoned phyllosilicate cement.

C 98 Sandriversberg Formation

Immature quartzwacke, very poorly sorted, subangular grains. Dominated by monocrystalline and polycrystalline quartz, with lesser muscovite. Fine sand to fine pebble grain sizes range in diameter from 0.2 to 3.2mm. Clasts mostly grain supported with point and line contacts. Metamorphic and diagenetic quartz cementation, recrystallization of matrix and quartz grains and deformation of micas. Graded bedding observable in thin section.

C 96 Skilpadkop Formation

Immature quartzwacke, poorly sorted, subangular grains. Dominated by monocrystalline and polycrystalline quartz, with lesser muscovite, K-feldspar and porphyritic lithic-volcancis. Fine to coarse grain sand ranges from 0.2 to 0.8mm in diameter. Clasts mostly grain supported with point and line contacts. Diagenetic-metamorphic quartz and FeOx cementation, recrystallization of matrix.

C 89 Swaershock Formation

Immature quartzwacke, moderately sorted, subangular grains. Composed of monocrystalline and polycrystalline quartz. Fine to coarse grain sand ranges from 0.15 to 0.80mm in diameter. Clasts mostly grain supported with point and line contacts. Diagenetic-metamorphic quartz cementation, recrys- tallization of matrix, and fracturing of quartz grains.

SOUTPANSBERG GROUP

C 177 Nzhelele Formation

Immature to submature subarkose to arkosic wacke, moderately sorted, subangular grains. Dominated by monocrystalline quartz, polycrystalline quartz and K-feldspar, with trace plagioclase. Fine to medium grain sand, mostly 0.2-0.3mm in diameter. Clasts mostly grain supported with line and point contacts. Diagenetic-metamorphic effects include carbonate and quartz cementation, recrystallization of matrix and formation of phrenite.

C 188 Nzhelele Formation

Immature arkosic wacke, poorly sorted, subangular framework grains. Dominated by monocrystalline quartz, polycrys- talline quartz, lithic-sediments and K-feldspar, with lesser plagioclase, and trace porphyritic lithic-volcanics, chlorite and zircon. Very fine to coarse grain sand diameters range mostly from 0.1 to 0.5mm. Clasts mostly grain supported with point contacts. Diagenetic-metamorphic quartz cementation, recrystallization of matrix, defor- mation of shale clasts and minor fracturing of quartz grains. Graded bedding observable in thin section.

C 184 Ngwanedzi Formation

Immature arkosic wacke, very poorly sorted, subangular framework grains. Dominated by monocrystalline quartz, K-feldspar and polycrystalline quartz with lesser muscovite, chlorite, porphyritic lithic-volcanics, plagioclase and lithic-sedimentary clasts. Coarse silt to very coarse grain sand ranging up to 1.8mm in diameter. Clasts mostly grain supported with point contacts. Diagenetic-metamorphic calcite and FeOx cementation, minor recrystallization of matrix, deformation of micas and minor fracturing of quartz grains.

C 160 Musekwa Formation

Immature to submature quartzwacke to quartz arenite, well sorted, subrounded grains. Dominated by monocrystalline quartz, with lesser polycrystalline quartz. Medium to coarse grain sand averages 0.45mm in diameter. Clasts mostly grain supported with point contacts. Metamorphic-diagenetic quartz cementation and recrystallization of matrix.

C 124 Mutshindidi Member-Sibasa Formation

Immature to submature quartzwacke, well sorted, subrounded grains. Dominated by monocrystalline and polycrystalline quartz, with lesser porphyritic lithic-volcanics and lithic-sedimentary clasts. Medium to coarse grain sand averages 0.5mm in diameter. Clasts mostly grain supported with line contacts. Diagenetic-metamorphic quartz and FeOx cementation and recrystallization of matrix.

Appendix F. Computer Modelling Programs

F.1 Pearson Correlation Coefficients

Pearson correlation coefficients provide a numerical assessment of bivariate data (Goldman and Weinberg, 1985). These coefficients are a quantitative measure of the tendency of bivariate data to lie along a straight line. Pearson correlation coefficients are calculated by the formula:

$$r = \frac{n\Sigma xiyi - (\Sigma xi)(\Sigma yi)}{\sqrt{[n\Sigma xi^2 - (\Sigma xi)^2][n\Sigma yi^2 - (\Sigma yi)^2]}} \qquad (F.1)$$

where r = correlation coefficient
n = number of data points
xi = individual x data points
yi = individual y data points
Σ = the sum of

The degree of correlation is numerically classified as follows:

Weak when	-0.3	< r >	0.3			
Slight when	-0.55	< r <	-0.3	and 0.3	> r >	0.55
Moderate when	-0.8	< r <	-0.55	and 0.55	> r >	0.8
Strong when	-1.0	< r <	-0.8	and 0.8	> r >	1.0

Correlation coefficients used in this study are calculated using the Statistical Programs for Social Scientists package (SPSS). This software program can be accessed on New Mexico Tech's SUN computer system. The tests of significance determine the probability that the observed correlation exists from random variation. The significance value is dependent on the sample population size and correlation coefficient values. A significance value of 0 indicates a high level of confidence in the observed relationship. Significance values for correlation coefficient calculations are given in Table F.1.

Table F.1 Tests of significance for correlation coefficient calculations (n=63).

Correlation coefficient (r)*	Significance
1.00-0.53	.00000
0.52-0.50	.00001
0.49	.00002
0.48	.00003
0.47	.00005
0.46	.00006
0.45	.00010
0.44	.00016
0.43	.00021
0.42	.00029
0.41	.00047
0.40	.00065
0.39	.00073
0.38	.00115
0.37	.00147
0.36	.00194
0.35	.00240
0.34	.00325
0.33	.00432
0.32	.00566
0.31	.00691
0.30	.00812

*, absolute value

F.2 Mass Balance Equations

Mass balance mixing equations are used to calculate the relative contributions of end member source-rocks (granite, tonalite, tholeiite and komatiite) to the various Kaapvaal craton sedimentary sequences. End member compositions and calculated mixing results are summarized in section V.6(H), Table 13a and Table 13b. The MASSBAL mixing program is given in Table F.2. This program calculates an elemental concentration in a mixing product (sediments) derived by mixing various proportions of end member source rocks. This calculation follows the general formula:

$$(Ag \times z1) + (At \times z2) + (Ab \times z3) + (Ak \times z4) = As \qquad (F.2)$$

where Ag = Concentration of element A in granite
At = Concentration of element A in tonalite
Ab = Concentration of element A in basalt
Ak = Concentration of element A in komatiite
As = Concentration of element A in sediment
$z1 + z2 + z3 + z4 = 1.0$

Calculations of this equation are repeated until a best fit is obtained for each of the five elements given in Table 13a.

Table F.2 Mass balance mixing program (in MBASIC) used for calculating source-area abundances.

```
10 LPRINT TAB(25) "MASS BALANCE EQUATION":LPRINT:LPRINT
20 LPRINT "R = A1X1 + A2X2 + A3X3 + . . . . .ANXN"
30 INPUT "NUMBER OF ENTRIES";N
35 DIM A(N)
40 INPUT "SOLVE FOR R,A,OR X--TYPE R,A,OR X <RET>";H$
50 IF H$="R" THEN 60 ELSE 120
60 LPRINT "ENTER DATA:"
70 FOR I = 1 TO N
80 LPRINT "A";I;"=";:INPUT A(I):NEXT I
85 FOR I = 1 TO N:LPRINT "X";I;"=";:INPUT X(I):NEXT I
90 R=0:FOR I = 1 TO N
100 R = R + A(I)*X(I):NEXT I
110 LPRINT "R = ";R
115 INPUT "RETURN TO BEGINNING? Y/N";D$
117 IF D$="Y" THEN 40 ELSE 220
120 LPRINT:LPRINT "M = R/L - A1X1/L - A2X2/L - ..... ANXN/L"
130 LPRINT "ENTER DATA:"
150 INPUT "R=";R:INPUT "L=";L
155 FOR I= 1 TO N
160 LPRINT "A";I;"=";:INPUT A(I):NEXT I
165 FOR I = 1 TO N:LPRINT "X";I;"=";:INPUT X(I):NEXT I
170 Y=0:FOR I = 1 TO N
180 Y = Y - A(I)*X(I):NEXT I
182 M =(Y/L) + (R/L)
190 LPRINT "M = ";M
200 INPUT "RETURN TO BEGINNING? Y/N";B$
210 IF B$="Y" THEN 40 ELSE 220
220 END
```

REFERENCES

Abbey, S. (1983) Studies in ''standard samples'' of silicate rocks and minerals 1969-1982. Geol. Surv. Can., paper 83-15, 114 p.

Allegre, C.J. and Rousseau, D. (1984) The growth of the continent through geological time studied by Nd isotope analysis of shales. Earth Planet. Sci. Lett. 67, 19-34.

Anhaeusser, C.R. (1971) Cyclic volcanicity and sedimentation in the evolutionary development of Archean greenstone belts of shield areas. Geol. Soc. Aust. Spec. Pub. 3, 57-70.

----- (1973) The evolution of the early Precambrian crust of southern Africa. Royal Soc. London Philos. Trans., A., 273, 359-388.

----- (1981) The relationship of mineral deposits to early crustal evolution. In Econ. Geol. 75th Anniv. Vol. (ed. B.J. Skinner) The Economic Geology Publishing Company, El Paso, Texas pp. 42-62.

----- and Robb, L.J. (1981) Magmatic cycles and the evolution of the Archean granitic crust in the eastern Transvaal and Swaziland. Geol. Soc. Aust. Spec. Pub. 7, 457-467.

Armstrong, N.V., Hunter, D.H. and Wilson, A.H. (1982) Stratigraphy and petrology of the Archean Nsuze Group, northern Natal and southeastern Transvaal, South Africa. Precamb. Res. 19, 75-107.

-----, Wilson, A.H. and Hunter, D.H. (1986) The Nsuze Group, Pongola sequence, South Africa: Geochemical evidence for Archean volcanism in a continental setting. Precamb. Res. 34, 175-203.

Armstrong, R.A. Compston, W., Retief, E.A. and Welke, H.J. (1986) Ages and isotopic evolution of the Ventersdorp volcanics. Geocongress '86, Extended Abs., Geol. Soc. S. Afr., Johannesburg, pp. 89-92.

Armstrong, R.A. Compston, W., Dodson, M.H., Kronar, A. and Williams, I.S. (1987) Archean crustal history in southern Africa. In The Australian National University Research School of Earth Sciences Annual Report 1987. pp. 62-63.

Austin, G.S. (1987) X-Ray examination of clays. Unpub. laboratory manual, New Mexico Institute of Mining and Technology, Socorro, New Mexico.

Baer, A.J. (1981) A Grenvillian model of Proterozoic plate tectonics. In Precambrian Plate Tectonics. Developments in Precambrian Geology 4. (ed. A. Kroner) Elsevier, Amsterdam pp. 353-385.

Bailey, S.W. (1984) Crystal chemistry of the true micas. In Micas (ed. S.W. Bailey) Reviews in mineralogy, Mineral Soc. Amer., Vol. 13, Chapt. 2, pp. 13-60.

Balashov Y.A., Ronov, A.B., Migdisov, A.A. and Turankskaya N.V. (1964) The effect of climate and facies environment on the fractionation of the REE during sedimentation. Geochem. Intl. 5, 951-969.

----- and Khitrov, L.M. (1967) On the reserve of mobile rare earth elements in sedimentary rocks. Geochem. Intl., 4, 404-407.

Balistrieri, L.S. and Murray, J.M. (1984) Marine scavenging: Trace metal adsorption by interfacial sediment from MANOP site H. Geochim. Cosmochim. Acta 48, 921-929.

Ball, P.J. and Gilkes, R.J. (1987) The Mount Saddleback bauxite deposit, southwestern Australia. Chem. Geol. 60, 215-225.

Barker, O.B. (1976) The Soutpansberg trough (northern Transvaal)-An aulacogen. Discussion. Geol. Soc. S. Afr. Trans. 79, 146.

----- (1979) A contribution to the geology of the Soutpansberg Group, Watersberg Supergroup northern Transvaal. Unpub. Msc. thesis, Univ. Witwatersrand, Johannesberg, S. Afr. 116 p.

Barton, J.M (1979) The chemical compositions, Rb-Sr isotopic systematics and tectonic setting of certain post-kinematic mafic igneous rocks, Limpopo mobile belt, southern Africa. Precamb. Res. 9, 57-80.

----- (1983) Our understanding of the Limpopo Belt-a summary with proposals for future research. In The Limpopo Belt (eds. W.J. van Biljon and J.H. Legg) Geol. Soc. S. Afr. Spec. Pub. 8, 191-203.

-----, Fripp, R.E.P. and Horrocks, P. (1983) Rb-Sr ages and chemical composition of some deformed Archean mafic dykes, Central Zone, Limpopo Mobile Belt, southern Africa. In The Limpopo Mobile Belt (eds. W.J. van Biljon and J.H. Legg) Geol. Soc. S. Afr. Spec. Pub. 8, 27-37.

-----, Fripp, R.E.P., Horrocks, P. and McLean, N. (1977) The geology, age, and tectonic setting of the Messina layered intrusion, Limpopo Mobile Belt, southern Africa. Amer. J. Sci. 279, 1108-1134.

----- and Key, R.M. (1981) The tectonic development of the Limpopo Mobile Belt and the evolution of the Archean cratons in southern Africa. In Precambrian Plate Tectonics (ed. A. Kroner) pp. 185-212.

----- and McCourt, S (1983) Rb-Sr age for the Palala Granite Limpopo mobile belt. In The Limpopo Belt (eds. W.J. van Biljon and J.H. Legg) Geol. Soc. S. Afr. Spec. Pub. 8, 45-46.

-----, Robb, L.J., Anhaeusser, C.R. and Van Nierop, D.A. (1983) Geochronologic and Sr-isotopic studies of certain units in the Barberton granite-greenstone terrane, South Africa. In Contributions to the geology of the Barberton Mountain Land. Geol. Soc. S. Afr. Spec. Pub. 9, 63-72.

-----, Roering, C., Barton, E.S., Van Reenan, D.D. and Smit, C.A. (1986) The late Archean-early Proterozoic evolution of the Kaapvaal craton and its possible relationships to the Witwatersrand basin. Geocongress '86, Extended Abs., Geol. Soc. S. Afr., Johannesberg, 15-18.

----- and Ryan, B. (1977) A review of the geochronologic framework of the Limpopo Mobile Belt. Bull. Geol. Surv. Botswana 12, 183-200.

Beukes, N.J. (1973) Precambrian iron formations of southern Africa. Econ. Geol. 68, 960-1004.

Bhatia, M.R. (1983) Plate tectonics and geochemical composition of sandstones. J. Geol. 91, 611-627.

----- and Crook, K.A.W. (1986) Trace element characteristics of greywackes and tectonic setting discrimination of sedimentary basins. Cont. Mineral. Petrol. 92, 181-193.

Burke, K., Kidd, W.S. and Kusky, T.M. (1985a) The Pongola structure of southeastern Africa: The world's oldest preserved Rift? J. Geodynam. 2, 35-49.

-----, Kidd, W.S. and Kusky, T.M. (1985b) Is the Ventersdorp rift system of southern Africa related to a continental collision between the Kaapvaal and Zimbabwe Cratons at 2.64 Ga ago? Tectonophysics 115, 1-24.

-----, Kidd, W.S. and Kusky, T.M. (1986) Archean foreland basin tectonics in the Witwatersrand, South Africa. Tectonics 5, 439-456.

Button, A. (1973a) Depositional History of the Wolkberg proto-basin, Transvaal. Trans. Geol. Soc. S. Afr. 76, 15-25.

-----, (1973b) A regional study of the stratigraphy and development of the Transvaal basin in the eastern and northern Transvaal. Unpub. Ph.D. thesis, Univ. of Witwatersrand, Johannesburg, South Africa, 352 p.

-----, (1975) A paleocurrent study of the Dwaal Heuvel Formation, Transvaal Supergroup. Trans. Geol. Soc. S. Afr. 78, 173-183.

-----, (1981a) The cratonic environment, the Pongola Supergroup. In Precambrian of the Southern Hemisphere (ed. D.R. Hunter) Elsevier, Amsterdam, Chapt. 9, pp. 501-510.

-----, (1981b) The cratonic environment, the Transvaal Supergroup. In Precambrian of the Southern Hemisphere (ed. D.R. Hunter) Elsevier, Amsterdam, Chapt. 9, pp. 527-536.

-----, and Tyler N. (1981) The character and economic significance of Precambrian paleoweathering and erosion surfaces in southern Africa. Econ. Geol. 75, 676-699.

Callow, M.J. and Myers, R.E. (1986) A tectono-stratigraphic model for the development of the Welkom fan placer deposits: Orange Free State Goldfield. Geocongress '86, Extended Abs., Geol. Soc. S. Afr., Johannesberg, 89-92.

Cameron, E.M. and Garrels, R.M. (1980) Geochemical Compositions of some Precambrian shales from the Canadian Shield. Chem. Geol. 28, 181-197.

Chaudhuri, S. and Cullers, R.L. (1979) The distribution of rare-earth elements in deeply buried Gulf Coast sediments. Chem. Geol. 24, 327-338.

Cheney, E.S. and Twist, D. (1986) The Waterberg ''basin''-A reappraisal. Trans. Geol. Soc. S. Afr. 89, 353-360.

Clendenin, C.W., Charlesworth, E.G. and Maske, S. (1987) Tectonic style and mechanism of early Proterozoic successor basin development, southern Africa. Inform. Circ. 197, Econ. Geol. Res. Unit, Univ. Witwatersrand, Johannesburg, 26 p.

Coertze, F.J., Burger, A.J., Walraven, F., Marlow, A.G. and MacCaskie, D.R. (1978) The transition from the Transvaal sequence to the Waterberg Group. Trans. Geol. Soc. S. Afr. 81, 1-12.

-----, Button, A., Du Plessis, M.D., Eriksson, K.A., Jansen, H., Malherbe, S.J., Smit, P.J., Visser, J.N.J. and Walraven, F. (1980) Transvaal sequence. In Stratigraphy of South Africa (compiler, L.E. Kent) Handbook 8, part 1, pp. 187-210.

Condie, K.C. (1981) Archean Greenstone Belts, Developments in Precambrian Geology 3. Elsevier, Amsterdam 434 p.

-----, (1982) Plate-tectonics model for Proterozoic continental accretion in the southwestern U.S. Geol. 10, 37-42.

-----, Macke, J.E. and Reimer, T.O. (1970) Petrology and geochemistry of early Precambrian greywackes from the Fig Tree Group, South Africa. Geol. Soc. Amer. Bull. 81, 2759-2776.

-----, and Martell, C. (1983) Early Proterozoic metasediments from north-central Colorado: Metamorphism, provenance, and tectonic setting. Geol. Soc. Amer. Bull. 94, 1215-1224.

----- and Boryta, M. (1989) Geochemistry of the Beitbridge Group and its bearing on the evolution of the Limpopo Belt, southern Africa. Contrib. Mineral. Petrol. (In prep.)

----- and Wronkiewicz, D.J. (1989) A new look at the Archean-Proterozoic boundary: Sediments and the tectonic setting constraint. In Developments in Precambrian Geology-Series. Elsevier, Amsterdam. (in press).

Coney, P.J., Jones, D.L. and Monger, J.W.H. (1980) Cordilleran suspect terranes. Nature 288, 329-333.

Cornell, D.H. (1978) Petrologic studies at T'Kop: evidence for metamorphic and metasomatic alterations of volcanic formations beneath the Transvaal volcanosedimentary pile. Trans. Geol. Soc. S. Afr. 81, 261-270.

Crampton, D. (1974) A note on the age of the Matsap Formation of the northern Cape Province. Trans. Geol. Soc. S. Afr. 77, 71-72.

Crow, H.C. III (1988) Geochemistry and origin of late Archean-early Proterozoic volcanics of the Kaapvaal craton, South Africa. Unpub. Ph.D. thesis, New Mexico Institute of Mining and Technology, Socorro, New Mexico, USA. 363 p.

----- and Condie, K.C. (1987) Geochemistry and origin of late Archean volcanic rocks from the Rhenosterhoek Formation, Dominion Group, South Africa. Precamb. Res. 37, 217-229.

-----, Condie, K.C., Hunter, D.R. and Wilson, A.H. (1989) Geochemistry of volcanic rocks from the Nsuze Group, South Africa: Arc-like volcanics in a 3.0 Ga-old intracratonic rift. J. of Afr. Earth Sci., (In press).

Cullers, R.L. (1988) Mineralogical and chemical changes of soil and stream sediment formed by intense weathering of the Danberg granite, Georgia, U.S.A. Lithos 21, 301-314.

-----, Basu, A. and Suttner, L.J. (1988) Geochemical signature of provenance in sand-sized material in soils and stream sediments near the Tobacco Root Batholith, Montana, U.S.A. Chem. Geol. 70, 335-348.

-----, Yeh, L. and Chaudhuri, S. (1974) Rare earth elements in Silurian pelitic schists from NW Main. Geochim. Cosmochim. Acta 38, 389-400.

-----, Chaudhuri, S., Arnold, B., Lee, M. and Wolf, C.W.Jr. (1975) Rare earth distributions in clay minerals and in the clay-sized fraction of the lower Permian Havensville and Eskridge shales of Kansas and Oklahoma. Geochim. Cosmochim. Acta 39, 1691-1703.

-----, Chaudhuri, S., Kilbane, N. and Koch. (1979) Rare earths in size fractions and sedimentary rocks of Pennsylvanian-Permian age from the mid-continent of the USA. Geochim. Cosmochim. Acta 43, 1285-1302.

-----, Barrett T., Carlson R., and Robinson B. (1987) REE and mineralogic changes in Holocene soil and stream sediment: a case study in the Wet Mountains, Colorado, U.S.A. Chem. Geol. 63, 275-297.

Danchin, R.V. (1967) Chromium and nickel in the Fig Tree Shale from South Africa. Science 158, 261-262.

Davidson, C.F. (1957) On the occurrence of uranium in ancient conglomerates. Econ. Geol. 52, 668-693.

----- (1964) Review of uranium in ancient conglomerates. Econ. Geol. 59, 168-176.

Davies, R.D., Allsopp, H.L. Erlank, A.J. and Manton, W.I. (1969) Sr-isotopic studies on various layered mafic intrusions in southern Africa. In Symposium on the Bushveld Igneous Complex and Other Layered Intrusions. Geol. Soc. S. Afr. Spec. Pub. I pp. 576-593.

----- and Allsopp, H.L. (1976) Strontium isotopic evidence relating to the evolution of the lower Precambrian granitic crust in Swaziland. Geol. 4, 553-556.

De Villiers, S.B. (1967) Aanvoerrigtings van sedimente van die Sisteme Loskop en Waterberg in noord-Transvaal soos weerspieel deur kruisgelaagdheid: Ann. Geol. Opn. S. Afr. 6, 63-67.

De Vries, W.C.P. (1968) Stratigraphy of the Waterberg system in the southern Waterberg area, northwestern Transvaal. S. Afr. Geol. Surv. Annals 7, 43-56.

Dickinson, W.R. (1970) Interpreting detrital modes of greywacke and arkose. J. Sed. Petrol. 40, 695-707.

----- and Snyder, W.S. (1978) Plate tectonics of the Laramide orogeny. Geol. Soc. Amer. Mem. 151, pp. 355-366.

----- and Suczek, C.A. (1979) Plate tectonics and sandstone compositions. Amer. Assoc. Petroleum Geol. Bull. 63, 82-86.

-----, Beard, L.S., Brakenridge, G.R., Erjavec, J.L. Ferguson, R.C., Inman, K.F., Knepp, R.A., Lindberg, F.A. and Ryberg, P.T. (1983) Provenance of North American Phanerozoic sandstones in relation to tectonic setting. Geol. Soc. Amer. Bull. 94, 222-235.

Dissanayake, C.B. (1987) Metals in a lateritic peat deposit-A case study from Sri Lanka. Chem. Geol. 60, 137-143.

Dix, O.R. (1984) Early Proterozoic braided stream, shelf and tidal deposition in the Pongola sequence, Zululand. Trans. Geol. Soc. S. Afr. 87, 1-10.

Duebendorfer, E.M. and Houston, R.S. (1987) Proterozoic accretionary tectonics at the southern margin of the Archean Wyoming craton. Geol. Soc. Amer. Bull. 98, 554-568.

Du Toit, M.C., Van Reenan, D.D. and Roering, C. (1983) Some aspects of the geology, structure, and metamorphism of the Southern Marginal Zone of the Limpopo Metamorphic Complex. In The Limpopo Mobile Belt (eds. W.J. van Biljon and J.H. Legg) Geol. Soc. S. Afr. Spec. Pub. 8, 121-141.

Els, B.G. (1988) Pebble morphology of an ancient conglomerate: The Middelvle gold placer, Witwatersrand, South Africa. J. Sed. Petrol. 58, 894-901.

Engel, A.E.J., Itson, S.P., Engel, C.G., Stickney, D.M. and Cray, E.J. (1975) Crustal evolution and global tectonics: A petrogenic view. Geol. Soc. Amer. Bull. 85, 843-858.

Eriksson, K.A. (1977) Tidal deposits from the Archean Moodies Group, Barberton Mountain Land, South Africa. Sed. Geol. 18, 255-281.

----- (1978) Alluvial and destructive beach facies from the Archean Moodies Group, Barberton Mountain Land, South Africa and Swaziland. In Fluvial Sedimentology (ed. A.D. Miall) Can. Soc. Petrol. Geol. Mem., 5, 287-311.

----- (1979) Marginal marine depositional processes from the Archean Moodies Group, Barberton Mountain Land, South Africa: Evidence and significance. Precamb. Res. 8, 153-182.

----- (1980) Transitional sedimentation styles in the Moodies and Fig Tree Groups, Barberton Mountain Land, South Africa: Evidence favoring an Archean continental margin. Precamb. Res. 12, 141-160.

----- and Voss, R.G. (1979) A fluvial fan depositional model for middle Proterozoic red beds from the Waterberg Group, South Africa. Precamb. Res. 9, 169-188.

-----, Turner, B.R. and Vos, R.G. (1981) Evidence of tidal processes from the lower part of the Witwatersrand Supergroup, South Africa. Sed. Geol. 29, 309-325.

----- and Soegaard, K. (1985) The petrography and geochemistry of Archean and Early Proterozoic sediments: Implications for crustal compositions and surface processes. Geol. Surv. Finland. 331, 7-32.

Evensen, N.M., Hamilton, P.J. and O'Nions, R.K. (1978) Rare-earth abundances in chondritic meteorites. Geochim. Cosmochim. Acta 42, 1199-1212.

Feather, C.E. and Koen G.M. (1973) The significance of the mineralogical and surface characteristics of gold grains in the recovery process. J. S. Afr. Inst. Min. Metall. 73, 223-233.

----- and Koen, G.S. (1975) The mineralogy of the Witwatersrand Reefs. Minerals Sci. Engn. 7, 189-224.

Fleet, A.J. (1984) Aqueous and sedimentary geochemistry of the rare earth elements. In Rare Earth Element Geochemistry (ed. P. Henderson), Elsevier, Amsterdam. Chapt. 10, pp. 343-373.

Frey, M. (1970) The step from diagenesis to metamorphism in pelitic rocks during Alpine orogenesis. Sedimentology 15, 261-279.

----- (1978) Progressive low grade metamorphism of a black shale formation, central Swiss Alps, with special reference to pyrophyllite- and margerite-bearing assemblages. J. Petrol. 19, 95-135.

-----, Haskin, L.A., Poetz, J. and Haskin, M.A. (1968) Rare earth abundances in some basic rocks. J. Geophys. Res. 73, B3, 6085-6098.

Fritz, S.J. (1988) A comparitive study of gabbro and granite weathering. Chem. Geol. 68, 275-290.

Fuller, A.O., Camden-Smith, P. Sprague, A.R.G., Waters, D.J. and Willis, J.P. (1981) Geochemical signature of shales from the Witwatersrand Supergroup. S. Afr. J. Sci. 77, 379-381.

Gebauer, D. and Grunenfelder, M. (1974) Rb-Sr whole-rock dating of late diagenetic to anchimetamorphic, Paleozoic sediments in southern France (Montagne Noire). Cont. Mineral. Petrol. 47, 113-130.

Gibbs, R.J. (1968) Clay mounting techniques for X-ray diffraction analyses, a discussion: J. Sed. Petrol. 38, 242-244.

----- (1977) Clay mineral segregation in the marine environment. J. Sed. Petrol. 47, 237-243.

Gibbs, A.K., Montgomery, C.W., O'Day, P.A. and Erslev, E.A. (1986) The Archean-Proterozoic transition: Evidence from the geochemistry of metasedimentary rocks of Guyana and Montana. Geochim. Cosmochim. Acta. 50, 2125-2141.

Gibson, I.L. and Jagam P. (1980) Instrumental neutron activation analysis of rocks and minerals. In Short Course in Neutron Activation Analyses in the Geosciences. Mineral. Assoc. Can. (ed. G.K. Muecke) pp. 109-131.

Giusti, L. (1988) U-Pb isotopic data for sulfides of the Varkenskraal granite (western Transvaal, South Africa) and their bearing on the age and origin of uranium mineralization in the Witwatersrand. Chem. Geol. (Isotope Geosci. Sec.) 72, 311-328.

Gladney, E.S., Burns, C.E. and Roelandts, I. (1983) 1982 compilation of elemental concentrations in eleven United States Geological Survey rock standards. Geostds. Newsletter 7, 3-226.

----- and Roelandts, I. (1988) 1987 compilation of elemental concentration data for USGS BIR-1, DNC-1 and W-2. Geostds. Newsletter 12, 63-118.

Goldich, S. (1938) A study in rock-weathering. J. Geol. 46, 17-58.

Goldman, R.N. and Weinberg, J.S. (1985) The correlation coefficient. In Statistics an Introduction. (ed. P.J. Martinac) Prentice-Hall, Inc., New Jersey. Sect. 2.2, pp. 82-91.

Goldstein, S.J. and Jacobson, S.J. (1988) Nd and Sr isotopic systematics of river water suspended material: implications for crustal evolution. Earth Planet. Sci. Lett. 87, 249-265.

Golightly, J.P. (1981) Nickeliferous Laterite Deposits. Econ. Geol. 75th Anniv. Vol. (ed. B.J. Skinner) Econ. Geol. Pub. Co., El Paso, Texas, pp. 710-735.

Govett, G.J.S. (1983) Handbook of exploration geochemistry, Vol. 3, Rock geochemistry in mineral exploration (ed. G.J.S. Govett) Elsevier, Amsterdam 461 p.

Grandstaff, D.E., Edelman, M.J., Foster, R.W., Zbinden, E. and Kimberley, M.M. (1986) Chemistry and mineralogy of Precambrian paleosols at the base of the Dominion and Pongola Groups, South Africa. Precamb. Res. 32, 97-132.

Gromet, L.P., Dymek,R.F., Haskin,L.A. and Korotev, R.L. (1984) The ''North American Shale Composite:'' Its compilation , major and trace element characteristics. Geochim. Cosmochim. Acta 48, 2469-2482.

Hallbauer, D.K. and Joughin, N.C. (1972) An investigation into the distribution size and shape of gold particles in some Witwatersrand reefs and their effects on sampling procedures. Johannesburg Chamber of Mines S. Afr. Res. Rep. 43, 72.

----- and Joughin, N.C. (1973) The size distribution and morphology of gold particles in Witwatersrand reefs and their crushed products. J. S. Afr. Inst. Min. Metall., 73, 395-405.

Hamilton, J. (1977) Sr isotope and trace element studies of the Great Dyke and Bushveld mafic phase and their relation to early Proterozoic magma genesis in southern Africa. J. Petrol. 18, 24-52.

Hegner, E., Tegtmeyer, a. and Kroner, A. (1981) Geochemie und petrogenese archaischer Vulkanite der Pongola-Gruppe in Natal. Chem. Erde 40, 23-57.

-----, Kroner, A. and Hofmann, A.W. (1984) Age and isotope geochemistry of the Archean Pongola and Usushwana suites in Swaziland, southern Africa: A case for crustal contamination of mantle-derived magma. Earth Planet. Sci. Lett. 70, 267-279.

Hemley, J.J. (1967) Stability relations of pyrophyllite, andalusite, and quartz at elevated pressures and temperatures. (abs.) Amer. Geophys. Union Trans. 48, 224.

Hirdes, W. and Saager, R. (1983) The Proterozoic Kimberley Reef placer in the Evander Goldfield Witwatersrand, South Africa. Monograph Series on Mineral Deposits, no. 20. Gebruder Borntraeger, Berlin. 100 p.

Hirst, D.M. (1962) The geochemistry of modern sediments from the Gulf of Paria-II. The location and distribution of trace elements. Geochim. Cosmochim. Acta. 26, 1147-1187.

Holland, H.H. (1978) The Chemistry of the Atmosphere and Oceans. John Wiley and Sons, New York, New York, 351 p.

---- (1984) The Chemical Evolution of the Atmosphere and Oceans. Princeton University Press, Princeton, New Jersey, 582 p.

Honnorez, J. (1983) Basalt-seawater exchange: A perspective from an experimental viewpoint. In Hydrothermal Processes at Seafloor Spreading Centers (eds. P.A. Rona, K. Bostrom, L. Laubier and K.L. Smith Jr.) Plenum Press, New York pp. 169-176.

Humphris, S.E. and Thompson, G. (1978) Trace element mobility during hydrothermal alteration of oceanic basalts. Geochim. Cosmochim. Acta 42, 127-136.

Hunter, D.R. (1963) The Mozaan series in Swaziland. Swaziland Geol. Survey, Bull. 3, 5-16.

-----, (1973) Geochemistry of granitic and associated rocks in the Kaapvaal Craton. Inform. Circ. 81, Econ. Geol. Res. Unit, Univ. of Witwatersrand, Johannesburg, 19 p.

-----, (1974) Crustal development in the Kaapvaal craton II. The Proterozoic. Precamb. Res. 1, 295-326.

-----, Barker, F. and Millard, H.T.Jr. (1978) The geochemical nature of the Archean Ancient Gneiss Complex and granodiorite suite, Swaziland: A preliminary study. Precamb. Res. 7, 105-127.

Hutchison, R.W. and Viljoen, R.P. (1986) Re-evaluation of gold source in Witwatersrand ores. Geocongress '86, Extended Abs., Geol. Soc. S. Afr., Johannesberg, 145-148.

----- (1987) Metallogeny of Precambrian gold deposits: Space time relationships. Econ. Geol. 82, 1993-2007.

Ingersol, R.V., Bullard, T.F., Ford, R.L., Grimm., J.P., Pickle, J.D. and Sares, S.W. (1984) The effect of grain size on detrital modes: A test of the Gazzi-Dickinson point counting method. J. Sed. Petrol. 54, 103-116.

Jansen, H (1975) The Soutpansberg trough (northern Transvaal)-An aulacogen. Trans. Geol. Soc. S. Afr. 78, 129-136.

----- (1976a) Precambrian basins on the Transvaal Craton and their sedimentalogical and structural features. Trans. Geol. Soc. S. Afr. 78, 25-33.

-----, (1976b) The Soutpansberg trough (Northern Transvaal) an aulacogen. Trans. Geol. Soc. S. Afr. 78, 129-136.

-----, (1981) The cratonic environment, the Waterberg and Soutpansburg Groups. In Precambrian of the Southern Hemisphere (ed. D.R. Hunter) Elsevier, New York. Chapt. 9, pp. 536-556.

Kent, L.E. (1980a) Dominion Group. In Stratigraphy of South Africa (compiler, L.E. Kent), Handbook 8, part 1, sect. 3.1, pp. 95-102.

----- (1980b) Witwatersrand Supergroup and Venterpost Coglomerate Formation. In Stratigraphy of South Africa (compiler, L.E. Kent), Handbook 8, part 1, sect. 3.2, pp. 103-118.

----- (1980c) Ventersdorp Supergroup. In Stratigraphy of South Africa (compiler, L.E. Kent), Handbook 8, part 1, sect. 3.3, pp. 121-135.

----- (1980d) Waterberg Group. In Stratigraphy of South Africa (compiler, L.E. Kent), Handbook 8, part 1, sect. 5.4, pp. 335-345.

-----, Brandl, G. and Jantsky, J.G. (1980) Intrusives of Randian Age. In Stratigraphy of South Africa (compiler, L.E. Kent), Handbook 8, part 1, sect. 3.12, pp. 181-183.

----- and Jansen, H. (1980) Soutpansberg Group. In Stratigraphy of South Africa (compiler, L.E. Kent), Handbook 8, part 1, sect. 5.3, pp. 327-333.

----- and Matthews, P.E. (1980) Pongola sequence. In Stratigraphy of South Africa (compiler, L.E. Kent), Handbook 8, part 1, sect. 2.5, pp. 103-120.

Kerrick, D.M. (1968) Experiments on the upper stability limit of pyrophyllite at 1.8 kilobars and 3.9 kilobars water pressure. Amer. J. Sci. 266, 204-214.

Kimberley, M.M. and Grandstaff, D.E. (1986) Profiles of elemental concentrations in Precambrian paleosols on basaltic and granitic parent materials. Precamb. Res. 32, 133-154.

Klemd, R. and Hallbauer, D.K. (1987) Hydrothermally altered peraluminous Archean granites as a provenance model for Witwatersrand sediments. Mineral. Deposita 22, 227-235.

Kluth, C.F. and Coney, P.J. (1981) Plate tectonics of the Ancestral Rocky Mountains. Geol. 9, 10-15.

Koppel, V.H. and Saager, R. (1974) Lead isotope evidence on the detrital origin of Witwatersrand pyrites and its bearing on the provenance of the Witwatersrand gold. Econ. Geol. 69, 318-331.

Kronberg, B.I., Fyfe, W.S., Leonards, O.H. Jr. and Santos, A.M. (1979) The chemistry of some brazilian soils: Element mobility during intense weathering. Chem. Geol. 24, 211-229.

-----, Nesbitt, H.W. and Lam, W.W. (1986) Upper Pleistocene Amazon deep-sea fan muds reflect intense chemical weathering of their mountainous source lands. Chem. Geol. 54, 283-294.

Kroner, A. and Compston, W. (1988) Ion microprobe ages of zircons from early Archean granite pebbles and greywacke, Barberton greenstone belt, southern Africa. Precamb. Res. 38, 367-380.

----- and Todt, W. (1988) Single zircon dating constraining the maximum age of the Barberton Greenstone Belt, southern Africa. J. Geophys. Res. 93, B12, 15,329-15,337.

Laskowski, N. and Kroner, A. (1985) Geochemical characteristics of Archean and Late Proterozoic to Paleozoic fine-grained sediments from Southern Africa and significance for the evolution of the continental crust. Geologische Rundschau 74, 1-9.

Lawton, T.F. (1986) Compositional trends within a clastic wedge adjacent to a fold-thrust belt: Indianola Group, central Utah, USA. Spec. Pub. Int. Assoc. Sed. Vol. 8, 411-423.

Layer, P.W., Kroner, A., McWilliams, M. and Clauer, N. (1988) Regional magnetic overprinting of the Witwatersrand Supergroup sediments, South Africa. J. Geophys. Res. 93, B3, 2191-2200.

Li, Y.H. (1981) Ultimate removal mechanism of elements from the ocean. Geochim. Cosmochim. Acta 45, 1659-1664.

Light, M.P.R. (1982) The Limpopo Mobile Belt: A result of continental collision. Tectonics 1, 325-342.

Lindstrom, D.J. and Korotev, R.L. (1982) TEABAGS: computer programs for instrumental neutron activation analyses. Radioanalyt. Chem. 70, 439-458.

Ludden, J., Gelinas, L. and Trudel, P. (1982) Archean metavolcanics from the Rouyn-Noranda district, Abitibi greenstone belt, Quebec. 2. Mobility of trace elements and petrogenetic constraints. Can. J. Earth Sci. 19, 2276-2287.

Manceau, A. and Calas, G. (1986) Nickel-bearing clay minerals: II. Intracrystalline distribution of nickel: An X-ray absorption study. Clay Mineral. 21, 341-360.

Martin, J.M. and Meybeck, M. (1979) Elemental mass-balance of material carried by major world rivers. Mar. Chem. 7, 173.

Matthews, P.E. (1967) The pre-Karroo formations of the Wit Umfolozi inlier, northern Natal. Trans. Geol. Soc. S. Afr. 70, 39-63.

----- and Scharrer, R.H. (1968) A graded unconformity at the base of the early Precambrian Pongola system. Trans. Geol. Soc. S. Afr. 71, 257-271.

McElhinny, M.W. and McWilliams, M.O. (1977) Precambrian geodynamics-A paleomagnetic view. Tectonophysics 40, 137-159.

McIver, J.R., Cawthorn, R.G. and Wyatt, B.A. (1981) The Ventersdorp Supergroup-The youngest komatiitic sequence in South Africa. In Komatiites (eds. E.G. Nesbitt and N.T. Arndt) Allen and Unwin, London, pp. 81-90.

McLennan, S.M., Nance, W.B. and Taylor, S.R. (1980) Rare earth element-thorium correlations in sedimentary rocks, and the composition of the continental crust. Geochim. Cosmochim. Acta. 44, 1833-1839.

----- and Taylor (1982) Geochemical constraints on the growth of continental crust. J. Sed. Geol. 90, 347-361.

-----, Taylor, S.R. and Kroner, A. (1983) Geochemical evolution of Archean shales from South Africa. I. The Swaziland and Pongola Supergroups. Precamb. Res. 22, 93-124.

----- and Taylor, S.R. (1988) Crustal evolution: Comments on ''The Archean-Proterozoic transition: Evidence from the geochemistry of metasedimentary rocks from Guyana and Montana'' by A.K. Gibbs, C.W. Montgomery, P.A. O'Day and E.A. Erslev. Geochim. Cosmochim. Acta 52, 785-787.

Meinster, B. and Tickell, S.J. (1976) Precambrian aeolian deposits in the Waterberg Supergroup. Trans. Geol. Soc. S. Afr. 78, 191-199.

Merriman, R.J., Bevins, R.E. and Ball, T.K. (1986) Petrological and geochemical variations within the Tal y Fan intrusion: A study of element mobility during low-grade metamorphism with implications for petrogenetic modeling. J. Sed. Petrol. 27, 1409-1436.

Meyer, M., Robb, L.J. and Anhaeusser, C.R. (1986) Uranium and thorium contents of Archean granitoids from the Barberton Mountain Land, South Africa. Precam. Res. 33, 303-321.

Middelburg, J.J., Van der Weijden, C.H. and Woittiez, J.R.W. (1988) Chemical processes affecting the mobility of major, minor and trace elements during weathering of granitic rocks. Chem. Geol. 68, 253-273.

Miller, R.G. and O'Nions, R.K. (1985) Source of Precambrian clastic sediments. Nature 314, 325-330.

Minter, W.E.L. (1978) A sedimentological synthesis of placer gold, uranium and pyrite concentrations in Proterozoic Witwatersrand sediments. In Fluvial Sedimentology (ed. A.D. Midall) Mem. Can. Soc. Petrol. Geol. 5, 801-829.

-----, Feather, C.E. and Glatther, C.W. (1988) Sedimentological and mineralogical aspects of the newly discovered Witwatersrand placer deposit that reflect Proterozoic weathering, Welkom Gold Field, South Africa. Econ. Geol. 83, 481-491.

Mottl, M.J., Holland, H.D. and Corr, R.F. (1979) Chemical exchange during hydrothermal alteration of basalt by seawater, II. Experimental results for Fe, Mn and sulfur species. Geochim. Cosmochim. Acta 43, 869-884.

Nance, W.B. and Taylor, S.R. (1976) Rare earth element patterns and crustal evolution-I. Australian post-Archean sedimentary rocks. Geochim. Cocmochim. Acta 40, 1539-1551.

Narayanaswamy and Gosh, S.K. (1987) Lateritisation of gabbro-granophyre rock units of the Ezhimala Complex of north Kerala, India. Chem. Geol. 60, 251-257.

Nesbitt, E.G. (1987) The Young Earth. An Introduction to Archean Geology. Allen and Unwin, Boston. 402 p.

-----, Wilson J.F. and Bickle, M.J. (1981) The evolution of the Rhodesian craton and adjacent Archean terrain: Tectonic models. In Precambrian Plate Tectonics. Developments in Precambrian Geology 4 (ed. A. Kroner) Elsevier, Amsterdam pp. 161-183.

Nesbitt, H.W. (1979) Mobility and fractionation of rare earth elements during weathering of a granodiorite. Nature 279, 206-210.

-----, Markovics, G. and Price, R.C. (1980) Chemical processes affecting alkalies and alkaline earths during continental weathering. Geochim. Cosmochim. Acta 44, 1659-1666.

-----, and Young, G.M. (1982) Early Proterozoic climates and plate motions inferred from major element chemistry of lutites. Nature 299, 715-717.

-----, and Young, G.M. (1988) Limits to chemical differentiation of clastic silicate sediments by physical processes. Geol. (In press.).

Nicolaysen, L.O., Burger, A.J. and Liebenberg, W.R. (1962) Evidence for the extreme age of certain minerals from the Dominion Reef conglomerates and the underlying granite in the western Transvaal. Geochim. Cosmochim. Acta 26, 15-23.

Norrish, K. and Chappel, B.W. (1977) X-ray fluorescense spectrometry. In Physical Methods in Determinative Mineralogy (ed. J. Zussman) Academic Press, New York. pp. 235-237 and 257-262.

Oosthuyzen, E.J. and Burger, A.J. (1964) Radiometric Dating of intrusives associated with the Waterberg system. S. Afr. Geol. Surv. Annals 3, 87-106.

Ogura, Y., Murata, K., and Iwai, M. (1987) Relation between chemical composition and particle-size distribution of ores in the profile of nickeliferous laterite deposits of the Rio Tuba Mine, Phillippines. Chem. Geol. 60, 259-271.

Perry, E.A.,Jr. and Turekian, K.K. (1974) The effects of diagenesis on the redistribution of strontium isotopes in shales. Geochim. Cosmochim. Acta 38, 929-935.

Pettijohn, F.J., Potter, P.E. and Siever, R. (1973) Sand and Sandstones. Springer-Verlag, New York. 618 p.

Phillips, G.N. (1986a) Metamorphism of shales in the Witwatersrand goldfields. Inform. Circ. 192, Econ. Geol. Res. Unit, Univ. Witwatersrand, Johannesburg, 25 p.

----- (1986b) Metamorphism of the Witwatersrand-Fact or fiction? Geocongress '86, Extended Abs., Geol. Soc. S. Afr., Johannesberg, 167-170.

----- (1986c) Geology and alteration in the Golden Mile, Kalgoorlie. Econ. Geol. 81, 779-808.

----- (1987) Anomalous gold in Witwatersrand shales. Econ. Geol. 82, 2179-2186.

-----, Myers, R.E. and Palmer, J.A. (1987) Problems with the placer model for Witwatersrand gold. Geol. 15, 1027-1030.

Piper, J.D.A. (1976) Paleomagnetic evidence for a Proterozoic supercontinent. Royal Soc. London Philos. Trans., A, 280, 469-490.

Pretorius, D.A. (1974) The geology of the Central rand goldfields. In The Geology of Some Ore Deposits of Southern Africa. (ed S.H. Haugten) Geol. Soc. S. Afr., Johannesburg, vol. 1, pp. 63-108.

----- (1976) The nature of the Witwatersrand gold-uranium deposits. Handbook of Stratabound and Stratiform Ore Deposits (ed. K.H. Wolf) Elsevier, Amsterdam, vol. 7, pp. 29-88.

----- (1981a) Gold and Uranium in quartz-pebble conglomerates. Econ. Geol. 75th Anniv. Vol. (ed. B.J. Skinner) Econ. Geol. Pub. Co., El Paso, Texas, pp. 117-138.

----- (1981b) The cratonic environment, the Witwatersrand Supergroup. In Precambrian of the Southern Hemisphere (ed. D.R. Hunter) Elsevier, Amsterdam. Chapt. 9, pp. 511-519.

Reed, J.R. and Condie K.C. (1987) Geochemical constraints on the composition of sandstone matrix and the interpretation of detrital modes. Geologie en Mijnbouw 66, 327-332.

Reid, A.M., le Roex, A.P. and Minter, W.E. (1988) Composition of gold grains in the Vaal placer, Klerksdorp, South Africa. Mineral. Deposita 23, 211-217.

Reimer, T.O. (1984) Alternative model for the derivation of gold in the Witwatersrand Supergroup. J. Geol. Soc. London 141, 263-272.

----- (1985) Volcanic rocks and weathering in the Early Proterozoic Witwatersrand Supergroup, South Africa. Geol. Surv. Finland Bull. 331, 33-49.

-----, Condie, K.C., Schneider, G. and Georgi, A. (1985) Petrography and geochemistry of granitoid and metamorphite pebbles from the early Archean Moodies Group, Barberton Mountainland/South Africa. Precamb. Res. 29, 383-404.

----- (1987) The late-Archean Dominion conglomerates (South Africa): new aspects of their derivation and their relationship with those of the Witwatersrand. Nues Jahr. Mineral. Abh. 158, 13-46.

Roaldset, E. (1983) Rare earth elements in Quaternary clays of the Numedal area, southern Norway. Lithos 6, 349-372.

Robb, L.J. and Meyer, M. (1985) The nature of the Witwatersrand hinterland: Conjectures on the source-area problem. Inform. Circ. 178, Econ. Geol. Res. Unit, Univ. Witwatersrand, Johannesburb, 25 p.

----- and Meyer, M. (1987) The nature of the Archean basement in the hinterland of the Witwatersrand basin: I. The Rand Anticline between Randfontein and Rysmierbult. S. Afr. Tydskr. Geol. 90, 44-63.

Roberts, R.G. (1987) Ore deposits models #11. Archean lode gold deposits. Geosci. Can. 14, 37-52.

Roering, C. (1986) Aspects of thrust faulting on the northern margin of the Witwatersrand basin. Geocongress '86, Extended Abs., Geol. Soc. S. Afr., Johannesberg, 59-62.

Ronov, A.B., Balashov, Y.A. and Migdisov, A.A. (1967) Geochemistry of the rare earths in the sedimentary cycle. Trans. Geokhimiya 1, 3-19.

-----, and Migdisov, A.A. (1971) Geochemical history of the crystalline basement and sedimentary cover of the Russian and North American platforms. Sedimentology 16, 137-185.

Roser, B.P. and Korsch, R.J. (1986) Determination of tectonic setting of sandstone-mudstone suites using SiO2 content and K2O/Na2O3 ratio. J. Geol. 94, 635-650.

Saager, R. (1969) The relationship of silver and gold in the basal reef of the Witwatersrand system, South Africa. Mineral. Deposita 4, 93-113.

Sales, J.K. (1968) Crustal mechanics of Cordilleran foreland deformation: A regional and scale-model approach. Amer. Ass. Petrol. Geologist Bull. 52, 2016-2044.

Schau, M. and Henderson, J.B. (1983) Archean chemical weathering at three localities on the Canadian Shield. Precamb. Res. 20, 189-224.

Schidlowski, M. (1968) The gold fraction of the Witwatersrand conglomerates from the Orange Free State Goldfield (South Africa). Mineral. Deposita 3, 344-363.

Schieber, J. (1988) Redistribution of rare-earth elements during diagenesis of carbonate rocks from the mid-Proterozoic Newland Formation, Montana, USA. Chem. Geol. 69, 111-126.

Schwab, F.L. (1986) Sedimentary 'signatures ' of foreland basin assemblages: Real or counterfit? Spec. Pub. Int. Assoc. Sed. 8, 395-410.

Schweitzer, J. and Kroner, A. (1985) Geochemistry and petrogenesis of early Proterozoic intracratonic volcanic rocks of the Ventersdorp Supergroup, South Africa. Chem. Geol. 51, 1151-1166.

Seyfried, W.E. Jr. and Mottl, M.J. (1982) Hydrothermal alteration of basalt by seawater under seawater-dominated conditions. Geochim. Cosmochim. Acta 46, 985-1002.

Shackleton, R.M. (1986) Precambrian collision tectonics in Africa. In Collision Tectonics (eds. M.P. Coward and A.C. Ries) Geol. Soc. Spec. Pub. 19, pp.329-349.

Shaw, D.M (1954) Trace elements in pelitic rocks. Part I. Geol. Soc. Amer. Bull. 65, 1151-1166.

----- (1956) Geochemistry of pelitic rocks. Part III. Major elements and general geochemistry. Geol. Soc. Amer. Bull. 67, 919-934.

Silver, L.T., Anderson, C.A., Crittenden, M. and Robertson, J.M. (1977) Chronostratigraphic elements of Precambrian rocks of the southwestern and far western United States. Geol. Soc. Amer. Abst. 9, 1176.

Stanley, O.J. and Liyanage, A.N. (1986) Clay-mineral variations in the northeastern Nile Delta, as influenced by decompositional processes. Mar. Geol. 73, 263-283.

Stannistreet, I.G., McCarthy, T.S. Charlesworth, E.G., Meyers, R.E. and Armstrong, R.A. (1986) Pre-Transvaal wrench tectonics along the northern margin of the Witwatersrand basin, South Africa. Tectonophysics 131, 53-74.

Tankard, A.J., Jackson, M.P.A., Eriksson, K.A., Hobday, D.K., Hunter, D.R. and Minter, W.E.L. (1982) Crustal Evolution of Southern Africa, Springer-Verlag, New York, 523 p.

Taylor, S.R. (1965) The application of trace element data to problems in petroloy. In Physics and Chemistry of the Earth. (eds. L.H. Ahrens, F. Press, S.K. Runcorn and H.C. Urey) Peramen Press, New York. Vol. 6, pp. 133-213.

----- and McLennan, S.M. (1981) The composition and evolution of the continental crust: rare earth element evidence from sedimentary rocks. Royal Soc. London Phil. Trans., A., 301, 381-399.

----- and McLennan, S.M. (1983) Geochemistry of early Proterozoic sedimentary rocks and the Archean/Proterozoic boundary. Geol. Soc. Amer. Mem. 161, 119-131.

----- and McLennan, S.M. (1985) The Continental Crust: Its Composition and Evolution. Blackwell, Oxford, 312 p.

------, Rudnick, R.L., McLennan, S.M. and Eriksson, K.A. (1986) Rare earth element patterns in Archean high-grade metasediments And their tectonic significance. Geochim. Cosmochim. Acta 50, 2267-2279.

Tegtmeyer, A.R. and Kroner, A. (1987) U-Pb zircon ages bearing on the nature of early Archean greenstone belt evolution, Barberton Mountainland, southern Africa. Precamb. Res. 36, 1-20.

Thompson, A.B. (1970) A note on the kaolinite-pyrophyllite equilibrium. Amer. J. Sci. 268, 454-458.

Topp, S.E., Salbu, B., Roaldset, E. and Jorgensen, P (1984) Vertical distribution of trace elements in laterite soil (Suriname). Chem. Geol. 47, 159-174.

Trocine, R.P. and Trefry, J.H. (1988) Distribution and chemistry of suspended particles from an active hydrothermal vent site on the Mid-Atlantic Ridge at 26 N. Earth Planet. Sci. Lett. 88, 1-15.

Tyler, N. (1979) Stratigraphy, geochemistry and correlation of the Ventersdorp Supergroup in the Derdepoort area, west central Transvaal. Trans. Geol. Soc. S. Afr., 82, 133-147.

Van Der Plas, L., and Tobi, A.C. (1965) A chart for judging the reliability of point counting results. Amer. J. Sci. 263, 87-90.

Van Niekerk, C.B. and Burger, A.J. (1969) Lead isotopic data relating to the age of the Dominion Reef lava. Trans. Geol. Soc. S. Afr. 72, 37-45.

-----, and Burger, A.J. (1978) A new age for the Ventersdorp acidic lavas. Trans. Geol. Soc. S. Afr. 81, 155-163.

Van Reenen, D.D., Barton, J.M.Jr., Roering, C., Smith, C.A. and Van Schalkwyk, J.F. (1987) Deep crustal response to continental collision: The Limpopo belt of southern Africa. Geol. 15, 11-14.

-----, Roering, C., Smit, C.A., Van Schalkwyk, J.F. and Barton, J.M.Jr. (1988) Evolution of the northern high-grade margin of the Kaapvaal craton, South Africa. J. Geol. 96, 549-560.

Van Schmus, W.R. and Bickford, M.E. (1981) Proterozoic chronology and evolution of the mid-continent region; North America. In Precambrian Plate Tectonics. Developments in Precambrian Geology 4. (ed. A. Kroner) Elsevier, Amsterdam, Chapt. 11, pp. 261-296.

Veizer, J. (1979) Secular variations in chemical composition of sediments: A review. In The Origin and Evolution of the Elements. (ed. L.H. Ahrens) Pergamon Press, London, pp. 269-278.

----- and Jansen, S.L. (1979) Basement and sedimentary recycling and continental evolution. J. Geol. 87, 341-370.

Viljoen, R.P., Saager, R. and Viljoen, M.J. (1970) Some thoughts on the origin and processes responsible for the concentration of gold in the early Precambrian of southern Africa. Mineral. Deposita 5, 164-180.

Viljoen, E.A. (1971) An electron-microprobe analyses of gold in the Witwatersrand blanket and in ores from the Barberton Mountain Land. Johannesburg, Natl. Inst. Metall., Res. Rep. no. 1361, 7 p.

Visser, D.J.L. (1984) Geological map of the Republics of South Africa, Transkei, Bophuthatswana, Venda and Ciskei and the Kingdoms of Lesotho and Swaziland.

Von Brunn, V. and Hobday, D.K. (1976) Early Precambrian tidal sedimentation in the Pongola Supergroup of South Africa. J. Sed. Petrol. 46, 670-679.

----- and Mason, T.R. (1977) Siliclastic-carbonate tidal deposits from the 3000 m.y. Pongola Supergroup, South Africa. Sed. Geol. 18, 245-255.

Von Rahden, H.V.R. and Hiemstra, S.A. (1967) The mineralogy of uranium in Western Areas ores. Johannesburg Natl. Inst. Metall., Res. Rept. no. 237.

Voss, R.G. and Eriksson, K.A. (1977) An embayment model for tidal and wave-swash deposits occurring within a fluvially-dominated Proterozoic sequence in South Africa. Sed. Geol. 18, 161-173.

Walraven, F., Burger, A.J. and Allsopp, H.L. (1983) Summary of age determinations carried out during the period April 1980 to March 1981. S. Afr. Geol. Surv. Annals 16, 107-114.

Watchorn, M.B. (1978) Sedimentology of the Mozaan Group in the south-eastern Transvaal and northern Natal. Unpub. M.Sc. thesis, Univ. Natal, Pietermaritzburg, South Africa.

----- (1980a) Fluvial and tidal sedimentation in the 3000 Ma Mozaan basin, South Africa. Precamb. Res. 13, 27-42.

----- (1980b) The stratigraphic and sedimentological development of the Witwatersrand West Rand basin in the Klerksdorp area. Inform. Circ. 148, Econ. Geol. Res. Unit, Univ. Witwatersrand, Johannesberg, 9 p.

----- (1981) Continental sedimentation and volcanism in the Dominion Group of the western Transvaal: a review. Trans. Geol. Soc. S. Afr. 84, 67-73.

----- and Armstrong, N.V. (1980) Contemporaneous sedimentation and volcanism at the base of the Early Precambrian Nsuze Group, South Africa. Trans. Geol. Soc. S. Afr. 83, 231-238.

Watkeys, M.K. (1981) Limpopo Excursion Guidebook (ed. J.M. Barton) Geol. Soc. S. Afr. 134 p.

----- and Armstrong, R.A. (1985) The importance of being alkaline-deformed late Archean lamprophyric dykes, central zone, Limpopo Belt. Trans. Geol. Soc. S. Afr. 88, 195-206.

-----, Light, M.P.R. and Broderick, T.J. (1983) A retrospective view of the Central Zone of the Limpopo Belt, Zimbabwe. In The Limpopo Mobile Belt (eds. W.J. van Biljon and J.H. Legg) Spec. Pub. Geol. Soc. S. Afr. 8, pp. 65-80.

Weaver, C.E. and Beck, K.C. (1971) Clay-water diagenesis during burial: How mud becomes gneiss: Geol. Soc. Amer. Spec. Paper 134. 96 p.

----- and Pollard, L.D. (1973) The chemistry of clay minerals: Developments in Sedimentology, 15, Elsevier, Amsterdam, 213 p.

-----, and Tarney (1984) Empirical approach to estimating the composition of the continental crust. Nature 310, 575-577.

Webber, B.N. (1972) Supergene nickel deposits. Trans. Soc. of Mining Engn., AIME 252, 333-347.

Wheelwright, E.J., Spedding, F.H. and Schwarzenbach, G. (1953) The stability of the rare earth complexes with ethylene-diaminetetraacetic acid. J. Assoc. Chem. Soc. 75, 4196-4201.

White, E.W. and Johnson, G.G.Jr. (1970) X-Ray absorption wavelengths and two-theta tables. Amer. Soc. for testing and materials-Data series DS 37A, 2nd ed., 293 p.

Whiteside, H.C.M. (1970) Volcanic rocks of the Witwatersrand Triad. In African Magmatism and Tectonics (eds. T.N. Clifford and I.G. Gass) Oliver and Boyd, Edinburgh pp. 78-87.

-----, Glasspool, K.R., Hiemstra, S.A., Pretorius, D.A. and Antrobus, E.S.A. (1976) Gold in the Witwatersrand Triad. In Mineral Resources of the Republic of South Africa (ed. C.B. Coetzee M.Sc., Ph.D.) Department of Mines, Fifth Ed., Handbook 7, pp. 39-73.

Wildeman, T.R. and Haskin, L.A. (1973) Rare earths in Precambrian sediments. Geochim. Cosmochim. Acta 37, 419-438.

Wilson, J.F., Bickle, M.J., Hawkesworth, C.J., Martin, A., Nesbitt, E.G. and Orpen, J.L. (1978) Granite-greenstone terrains of the Rhodesian Archean craton. Nature 271, 23-27.

-----, The granitic-gneiss greenstone shield, B. Zimbabwe. In Precambrian of the Southern Hemisphere (ed. D.R. Hunter) Elsevier, New York. Chapter 8, pp. 454-488.

Wronkiewicz, D.J. and Condie, K.C. (1987) Geochemistry of Archean shales from the Witwatersrand Supergroup, South Africa: Source-area weathering and provenance. Geochim. Cosmochim. Acta 51, 2401-2416.

----- and Condie, K.C. (1989a) Geochemistry of sediments from the Pongola Supergroup, South Africa: Evidence for a 3.0 Ga contenintal craton. Geochim. Cosmochim. Acta (In press).

----- and Condie, K.C. (1989b) Geochemistry and mineralogy of sediments from the Ventersdorp and Transvaal Supergroups, South Africa: Cratonic evolution during the early Proterozoic. Geochim. Cosmochim. Acta (In press).

----- and Condie, K.C. (1989c) Evolution of the Kaapvaal craton in southern Africa: Constraints from the chemical composition of sediments. 28th International Geological Congress, extended abs. (In press).

York, D. (1988) Coherent and incoherent light on old rocks. Chem. Geol. 70, 149.

Zeissink, H.E. (1971) Trace element behavior in two nickeliferous laterite profiles. Chem. Geol. 7, 25-36.

This thesis is accepted on behalf of the faculty of the Institute by the following committee:

Adviser

4 April, 1989

4/10/89

Date